

# REHABILITATION OF RC RESIDENTIAL HOUSES ON GRAVITY COLUMNS OVER SLOPE TERRAIN

By

Yvonne González Avellanet

A dissertation submitted in partial fulfillment of the requirements for the degree of

DOCTOR OF PHILOSOPHY  
in  
CIVIL ENGINEERING

UNIVERSITY OF PUERTO RICO  
MAYAGÜEZ CAMPUS  
2015

Approved by:

---

José O. Guevara, Ph.D.  
Member, Graduate Committee

---

Date

---

Ricardo R. López Rodríguez, Ph.D.  
Member, Graduate Committee

---

Date

---

Luis E. Suárez Colche, Ph.D.  
Member, Graduate Committee

---

Date

---

José A. Martínez Cruzado, Ph.D.  
President, Graduate Committee

---

Date

---

Ismael Pagán Trinidad, M.S.C.E  
Chairperson of the Department

---

Date

---

Elizabeth Vanacore, Ph.D.  
Representative of Graduate School

---

Date

## **ABSTRACT**

It is well known that Puerto Rico is exposed to the risk of experiencing strong earthquakes, since it is located in an earthquake prone region. It is a fact that in Puerto Rico there are many houses that are built over hilly terrain, and combined with poor construction practice, these types of houses are at a high seismic risk. Residences built over slope terrain are different from those in plains, i.e., they are very irregular and unsymmetrical in both horizontal and vertical structural planes. Due to site conditions, residences on hill slope are characterized by unequal column heights within a story, which results in variation in stiffness of columns of the same story. Furthermore, typically these residences have a retaining wall constructed on one side of the residence to support the slopes of earth masses on the higher side of the slope (uphill). These walls are often constructed of masonry block walls or reinforced concrete. The presence of this retaining wall induces an unsymmetrical distribution of mass and rigidity in the residences, since the wall is located only at one side of the house.

Because of the imminent risk of being affected by a strong earthquake, it is important to study the behavior and performance of these structures. Although these structures have been studied in the past, it is important to consider the particular feature of the differences in column elevations, torsional effects and propose rehabilitation techniques for the hilly terrain conditions. These structures need a rehabilitation system that fit the needs of the owners and meet the construction practice in the Island. The analytical models proposed are three-dimensional idealized models, based on the characteristic of these types of residences from a field survey. The objectives of this research are to determine the collapse mechanism of the three-dimensional models using a static nonlinear pushover analysis and nonlinear time history analysis and propose rehabilitation strategies for improving seismic the behavior of these structures.

The global performance of the models was established based on the performance point obtained through the Capacity Spectrum Method (ATC 40). At the performance point

global and local behavior of the frame elements were evaluated based on their damage limit state. The plastic hinge pattern of the models was studied to determine the collapse mechanism of these residences. After performing the analysis, the results showed that these residences cannot withstand the seismic demand imposed by the Uniform Building Code 1997 for Seismic Zone 3 and Soil Type Sd. The RC shear wall rehabilitation strategy was proven to be effective in increasing the capacity of the models.

## RESUMEN

Es de conocimiento general que Puerto Rico está expuesto a sufrir un terremoto de gran intensidad, ya que está localizado en una zona de alta peligrosidad sísmica. Es un hecho que en Puerto Rico hay muchas residencias que se construyen sobre terreno inclinado y, combinado con la pobre práctica de la construcción, este tipo de casas se encuentran en alto riesgo sísmico. Residencias construidas sobre terreno inclinado son diferentes a las que se encuentran en terreno plano. Estas residencias son irregulares y asimétricas tanto en el plano horizontal como en el vertical. Debido a las condiciones del terreno estas residencias se caracterizan por tener columnas de diferente altura en un mismo nivel, lo cual produce cambios en rigidez entre las columnas. Además, por lo general estas residencias tienen un muro de contención construido en un solo lado de la residencia para contener las masas de tierra en la pendiente. Estos muros se construyen a menudo con paredes de bloques de mampostería u hormigón armado. La presencia de estos muros de contención induce una distribución asimétrica en la masa pero principalmente en la rigidez de la planta de las residencias, ya que la pared se encuentra en un solo lado de la casa.

Debido al riesgo inminente de ser afectado por un fuerte terremoto, es importante estudiar el comportamiento y el desempeño de estas residencias. Aunque estas estructuras se han estudiado en el pasado, es importante considerar la característica particular de las diferencias en las elevaciones de columna, efectos de torsión y proponer técnicas de rehabilitación adecuadas para las condiciones del terreno inclinado. Estas estructuras necesitan un sistema de rehabilitación que se ajuste a las necesidades de los propietarios y a la práctica de la construcción en la Isla. Basado en las características de este tipo de residencias mediante un estudio de campo, se propusieron varios modelos tridimensionales idealizados para ser estudiados. Los objetivos principales de esta investigación son determinar el mecanismo de colapso de los modelos propuestos utilizando un análisis no lineal estático (pushover) y no lineal

dinámico, y desarrollar una estrategia de rehabilitación para mejorar el comportamiento sísmico de las mismas.

El desempeño global de los modelos se estableció basado en el punto obtenido a través del Método del Espectro de Capacidad (ATC 40). Este método utiliza la curva de capacidad de la estructura (curva pushover) y una reducción del espectro de respuesta para evaluar el desempeño de una estructura. En el punto de intersección se evaluó el comportamiento global y local de los elementos en función de su estado límite de daño. Se estudió el patrón de formación de articulaciones plásticas de los modelos para determinar el mecanismo de colapso. Después de haber realizado los análisis los resultados mostraron que estas residencias no pueden resistir la demanda sísmica impuesta por el Código UBC-1997, para la Zona Sísmica 3 y un tipo de suelo Sd. La estrategia de rehabilitación de muros de corte demostró ser eficaz en el aumento de la capacidad de los modelos.

© Yvonne González Avellanet 2015

*This dissertation is dedicated to my father, Efraín González Avellanet, his endless love and support is every reason for where I am and what I am.*

## **ACKNOWLEDGMENTS**

I would like to express my gratitude to God for giving me knowledge and strength in the most difficult moments of this research. Thanks God for holding me in your arms in every step of the way.

I express sincere appreciation to my advisor Dr. José A. Martínez Cruzado for his guidance, support and insight throughout the research.

Appreciation is also expressed to Dr. Luis Suárez, Dr. Ricardo López and Dr. José Guevara, my thesis committee members, whose comments on my dissertation greatly helped and improved the quality of my work.

Special thanks to the Puerto Rico Strong Motion Program for providing financial support to this research.

I would like to thank my friend Jairo Agudelo for his friendship during my graduate life.

I would like to thank Ariel Marrero for carrying out the concrete compressive strength laboratory test for this study.

My family deserves my deepest gratitude for their endless love. I would like to thank my father for his support and for always believing in me. Words cannot describe how proud I am for being his daughter. Thanks to my stepmother, Minerva, sister, Nicole and brother, Efraín, for their love and support with my sons. Thanks to my sons, Joel and Cristian, they make me strong and encourage me to never give up.



# TABLE OF CONTENTS

<b>CHAPTER 1. INTRODUCTION.....</b>	<b>1</b>
1.1 PURPOSE OF THE STUDY .....	1
1.2 OBJECTIVES.....	5
1.3 SUMMARY OF THE METHODOLOGY.....	5
1.4 PREVIOUS WORK.....	7
1.5 SUMMARY OF THE CHAPTERS.....	10
 <b>CHAPTER 2. FIELD SURVEY OF STRUCTURES OVER HILLY TERRAIN .....</b>	 <b>12</b>
2.1 INTRODUCTION.....	12
2.1.1 FIELD SURVEY OF TYPICAL STRUCTURES .....	12
2.1.1.1 OTHER RESIDENCES .....	26
2.1.2 FIELD SURVEY OF TYPICAL RESIDENCES (VAZQUEZ 2002) .....	28
 <b>CHAPTER 3. THREE DIMENSIONAL MODELS .....</b>	 <b>30</b>
3.1 INTRODUCTION.....	30
3.2 DEFINITION OF THE ANALYTICAL MODELS.....	30
3.2.1 GENERAL CHARACTERISTICS OF THE PROTOTYPE MODELS.....	30
3.2.2 MODELING THE RETAINING WALL.....	36
3.2.3 MODELING MASONRY WALLS AS DIAGONAL STRUT ELEMENTS.....	38
3.2.4 DEAD AND LIVE LOADS .....	40
3.2.5 ANALYTICAL MODELS 1 .....	41
3.2.6 ANALYTICAL MODELS 2 .....	46
3.2.7 ANALYTICAL MODELS 1.1 WITH VARIATION.....	48
3.2.8 COLUMNS BEAMS AND RC SHEAR WALL.....	51
3.3 GENERAL DETAILS OF THE ANALYTICAL MODELS .....	54
3.3.1 MATERIAL PROPERTIES.....	54
3.3.2 ADDITIONAL MODELING CONSIDERATIONS.....	55
 <b>CHAPTER 4. NONLINEAR ANALYSIS METHODS.....</b>	 <b>56</b>
4.1 INTRODUCTION.....	56
4.2 NONLINEAR PUSHOVER ANALYSIS.....	56

4.2.1	PUSHOVER ANALYSIS BACKGROUND .....	56
4.2.2	PUSHOVER ANALYSIS WITH SAP2000.....	58
4.2.2.1	DEFINING NONLINEAR MATERIAL BEHAVIOR .....	59
4.2.2.1.1	DEFAULT HINGES .....	61
4.2.2.1.2	USER DEFINED FLEXURAL (M3)/ AXIAL PLUS FLEXURAL HINGES (PM2M3) .....	62
4.2.2.1.2.1	SECTION DESIGNER MATERIAL STRESS –STRAIN RELATIONSHIP .....	62
4.2.2.1.2.2	SAP2000 MOMENT – CURVATURE ANALYSIS.....	66
4.2.2.1.3	SHEAR HINGES.....	72
4.2.2.2	HINGE UNLOADING .....	74
4.2.2.3	DEFINING LATERAL LOAD PATTERN.....	75
4.2.2.4	PERFORMING THE ANALYSIS .....	76
4.3	NONLINEAR TIME HISTORY ANALYSIS .....	82
4.4	NONLINEAR TIME HISTORY ANALYSIS WITH SAP2000.....	82
4.4.1	DAMPING.....	83
4.4.2	NONLINEAR MATERIAL BEHAVIOR.....	83
4.5	EARTHQUAKE GROUND MOTION RECORD SELECTION .....	84
<b>CHAPTER 5.</b>	<b>RESIDENCE SEISMIC PERFORMANCE .....</b>	<b>92</b>
5.1	INTRODUCTION.....	92
5.2	CAPACITY SPECTRUM METHOD (ATC 40) .....	93
<b>CHAPTER 6.</b>	<b>NONLINEAR ANALYSIS RESULTS .....</b>	<b>107</b>
6.1	LINEAR DYNAMIC ANALYSIS .....	107
6.1.1	DYNAMIC ANALYSIS RESULTS: MODEL 1.1 .....	107
6.1.2	DYNAMIC ANALYSIS RESULTS: MODEL 1.1 VS. MODEL 1.2 / MODEL 1.3 / MODEL 1.4.....	111
6.1.3	DYNAMIC ANALYSIS RESULTS: MODEL 1.1 VS 2.1: INCREASE IN NUMBER OF STORIES .....	114
6.1.4	DYNAMIC ANALYSIS RESULTS: MODEL 1.1b VS MODEL 1.1by - CHANGE IN COLUMNS ORIENTATION .....	116
6.1.5	DYNAMIC ANALYSIS RESULTS: MODEL 1.1 VS MODEL 1.1.2 / 1.1.3 / 1.1.4 CHANGE IN COLUMNS SIZE .....	117
6.2	NONLINEAR PUSHOVER RESULTS.....	118

6.2.1	PUSHOVER ANALYSIS RESULTS: MODEL 1.1b (BARE FRAME) VS. MODEL 1.1c / MODEL 1.1d (RETAINING WALL) .....	122
6.2.1.1	MODEL 1.1b: BARE FRAME .....	123
6.2.1.2	MODEL 1.1c: MASONRY BLOCK WALL .....	135
6.2.1.3	MODEL 1.1d: SHEAR WALL .....	140
6.2.2	PUSHOVER ANALYSIS RESULTS FOR MODEL 1.1 VS MODEL 1.2/ MODEL 1.3 / MODEL 1.4: DIFFERENCE IN BAY LENGTH .....	144
6.2.2.1	MODEL 1.2 .....	144
6.2.2.2	MODEL 1.3 .....	153
6.2.2.3	MODEL 1.4 .....	159
6.2.3	PUSHOVER ANALYSIS RESULTS: TWO LEVELS (MODELS 1) VS. THREE LEVELS (MODELS 2) .....	167
6.2.3.1	MODEL 1.1 VS MODEL 2.1 .....	167
6.2.3.2	MODEL 1.2 VS MODEL 2.2 .....	177
6.2.3.3	MODEL 1.3 VS MODEL 2.3 .....	184
6.2.3.4	MODEL 1.4 VS MODEL 2.4 .....	190
6.2.4	PUSHOVER ANALYSIS RESULTS: CHANGE IN COLUMNS ORIENTATION .....	197
6.2.4.1	MODEL 1.1 VS MODEL 1.1y .....	197
6.2.5	PUSHOVER ANALYSIS RESULTS: CHANGE IN COLUMNS SECTION ....	204
6.2.5.1	MODEL 1.1 VS MODEL 1.1.2 .....	205
6.2.5.2	MODEL 1.1 VS MODEL 1.1.3 .....	209
6.2.5.3	MODEL 1.1 VS MODEL 1.1.4 .....	216
6.2.6	PUSHOVER ANALYSIS SUMMARY RESULTS .....	221
6.3	NONLINEAR TIME HISTORY ANALYSIS RESULTS .....	225
6.3.1	NONLINEAR TIME HISTORY ANALYSIS RESULTS FOR MODEL 1.1b ....	226
6.3.1.1	RESULTS FOR THE PARKFIELD EARTHQUAKE: MODEL 1.1b .....	226
6.3.1.2	RESULTS FOR THE NORTHRIDGE EARTHQUAKE: MODEL 1.1b ..	230
6.3.1.3	RESULTS FOR THE SAN SALVADOR IGN EARTHQUAKE: MODEL 1.1b .....	233
6.3.1.4	RESULTS FOR THE SAN SALVADOR CIG EARTHQUAKE: MODEL 1.1b .....	237
6.3.2	NONLINEAR TIME HISTORY ANALYSIS RESULTS FOR MODEL 1.1c ....	240
6.3.2.1	RESULTS FOR THE SAN SALVADOR IGN EARTHQUAKE: MODEL 1.1c .....	241

6.3.2.2	RESULTS FOR THE SAN SALVADOR CIG EARTQUAKE: MODEL 1.1c .....	243
6.3.3	NONLINEAR TIME HISTORY ANALYSIS RESULTS FOR MODEL 1.1d ....	245
6.3.3.1	RESULTS FOR THE SAN SALVADOR CIG EARTHQUAKE: MODEL 1.1d.....	245
6.3.4	NONLINEAR TIME HISTORY ANALYSIS RESULTS FOR MODEL 1.4b ....	247
6.3.4.1	RESULTS FOR THE SAN SALVADOR IGN EARTHQUAKE: MODEL 1.4b.....	248
6.3.4.2	RESULTS FOR THE SAN SALVADOR CIG EARTHQUAKE: MODEL 1.4b.....	250
6.3.5	NONLINEAR TIME HISTORY ANALYSIS RESULTS FOR MODEL 1.4c ....	252
6.3.5.1	RESULTS FOR THE SAN SALVADOR IGN EARTHQUAKE: MODEL 1.4c.....	252
6.3.5.2	RESULTS FOR THE SAN SALVADOR CIG EARTQUAKE: MODEL 1.4c .....	254
6.3.6	NONLINEAR TIME HISTORY ANALYSIS RESULTS FOR MODEL 2.1b ....	256
6.3.6.1	RESULTS FOR THE SAN SALVADOR IGN EARTHQUAKE: MODEL 2.1b.....	256
6.3.6.2	RESULTS FOR THE SAN SALVADOR CIG EARTQUAKE: MODEL 2.1b .....	257
6.3.7	NONLINEAR TIME HISTORY ANALYSIS RESULTS FOR MODEL 2.1c ....	259
6.3.7.1	RESULTS FOR THE SAN SALVADOR CIG EARTHQUAKE: MODEL 2.1c.....	259
6.3.8	NONLINEAR TIME HISTORY ANALYSIS RESULTS FOR MODEL 1.1.3 ...	261
6.3.8.1	RESULTS FOR THE SAN SALVADOR CIG EARTHQUAKE: MODEL 1.1.3b.....	261
6.3.8.2	RESULTS FOR THE SAN SALVADOR CIG EARTQUAKE: MODEL 1.1.3c.....	265
6.3.9	SUMMARY OF TIME HISTORY ANALYSIS RESULTS.....	267
<b>CHAPTER 7.</b>	<b>PROPOSED RESIDENCES REHABILITATION.....</b>	<b>269</b>
7.1	INTRODUCTION .....	269
7.2	PUSHOVER ANALYSIS RESULTS FOR REHABILITATED MODELS.....	271
7.2.1	DISSCUSION OF RESULTS .....	283
7.2.2	NONLINEAR TIME HISTORY ANALYSIS REHABILITATED MODELS .....	284
7.2.3	DISCUSSION OF THE RESULTS.....	287

7.3	STRUCTURAL REHABILITATION WITH RC SHEAR WALL .....	287
7.3.1	GENERAL STRUCTURAL CONSIDERATIONS .....	288
7.3.2	LIMITATIONS .....	290
<b>CHAPTER 8.</b>	<b>CONCLUSIONS.....</b>	<b>292</b>
8.1	SUMMARY .....	292
8.2	CONCLUSIONS .....	293
8.2.1	LINEAR DYNAMIC ANALYSIS RESULTS .....	293
8.2.2	NONLINEAR PUSHOVER ANALYSIS RESULTS.....	294
8.2.3	NONLINEAR TIME HISTORY ANALYSIS RESULTS.....	296
8.2.4	REHABILITATION RESULTS .....	299
8.3	FUTURE WORK.....	299
<b>REFERENCES</b> .....		<b>299</b>
<b>Appendix A.</b>	ATC 40 / FEMA 356 HINGE PROPERTIES .....	307
<b>Appendix B.</b>	SUPPORTING MATERIAL FOR STEEL CONSTITUTIVE MODELS .....	309
<b>Appendix C.</b>	SUPPORTING MATERIAL FOR CONCRETE CONSTITUTIVE MODELS ..	310
<b>Appendix D.</b>	AXIAL LOAD CALCULATION .....	315
<b>Appendix E.</b>	SHEAR STRENGTH CAPACITY CALCULATION.....	323
<b>Appendix F.</b>	STRUCTURAL SYSTEMS .....	327
<b>Appendix G.</b>	DESIGN BASE SHEAR CALCULATION.....	328

# LIST OF FIGURES

<b>Figure 1-1.</b> Fault Map of Puerto Rico (Prentice and Mann, 2005) .....	2
<b>Figure 1-2.</b> Drawing of Typical Hilly Residences.....	4
<b>Figure 2-1.</b> Residence 1 in Aguada .....	13
<b>Figure 2-2.</b> Residence 1 Aguada. (a) Plan View. (b) Frame Elevation .....	14
<b>Figure 2-3.</b> Residence 2 in San Germán .....	15
<b>Figure 2-4.</b> San Germán Residence 2. (a) Plan View (b) Frame Elevation: Side View.....	15
<b>Figure 2-5.</b> Residence 3 in San Sebastian .....	17
<b>Figure 2-6.</b> San Sebastian Residence 3. (a) Plan View (b) Frame Elevation: Side View.....	18
<b>Figure 2-7.</b> Residence 4 in San Sebastian .....	19
<b>Figure 2-8.</b> Residence 4 in San Sebastian. (a) Footing Plan View. (b) Side view .....	20
<b>Figure 2-9.</b> Residence 4 in San Sebastian: Footing and Columns Structural Details .....	21
<b>Figure 2-10.</b> Residence 4 in San Sebastian: Beams Structural Details.....	22
<b>Figure 2-11.</b> Residence 4 in San Sebastian: Retaining Wall Structural Details .....	22
<b>Figure 2-12.</b> Residence 5 in Hormigueros .....	23
<b>Figure 2-13.</b> Residence 5 in Hormigueros. (a) Footing Plan View. (b) Side View.....	24
<b>Figure 2-14.</b> Residence 6 in Hormigueros .....	25
<b>Figure 2-15.</b> Residence 6 in Hormigueros. (a) Footing Plan View. (b) Side View.....	25
<b>Figure 2-16.</b> Residence with Exposed Rebar .....	26
<b>Figure 2-17.</b> Residences with Vertical Irregularities.....	27
<b>Figure 2-18.</b> Residences with Poor Constructions Details .....	27
<b>Figure 3-1.</b> Typical Model Type 1: 2 Story Residence .....	32
<b>Figure 3-2.</b> Typical Model Type 2: 3 Story Residence .....	33
<b>Figure 3-3.</b> (a) Plan View for Model 1.1 / 2.1, (b) Plan View for Model 1.2 / 2.2, .....	33
<b>Figure 3-4.</b> (c) Plan View for Model 1.3 / 2.3, (d) Plan View for Model 1.4 / 2.4 .....	34
<b>Figure 3-5.</b> Elevation at Frames A, B and C for Models 1 .....	34
<b>Figure 3-6.</b> Elevation at Frames 1, 2 and 3 for Models 1 .....	35
<b>Figure 3-7.</b> Elevation at Frames A, B and C for Models 2 .....	35
<b>Figure 3-8.</b> Elevation at Frames 1, 2 and 3 for Models 2 .....	36
<b>Figure 3-9.</b> (a) Residence with Masonry Block Wall. (b) Residence with Shear Wall .....	37
<b>Figure 3-10.</b> Typical Plan View. ....	37
<b>Figure 3-11.</b> (b) Side View Model type “b” Analyzed as Frame (c). Side View Model Type “c” Analyzed with Masonry Block Walls. (d) Model Type “d” Analyzed with Shear Walls .....	38
<b>Figure 3-12.</b> Diagonal Strut Model.....	39
<b>Figure 3-13.</b> Cross Section of Columns. (a) Column 16”x 6” (b) Column 12”x 6” (c) Column 16”x 8” (d) Column 12”x12” .....	52
<b>Figure 3-14.</b> Cross Section of Beam.....	53
<b>Figure 3-15.</b> Cross Section of RC Shear Wall .....	53
<b>Figure 4-1.</b> Typical Pushover Curve (ATC 40). ....	58
<b>Figure 4-2.</b> Generalized Force vs. Displacement or Moment vs. Rotation relationship. (CSI Manual) .....	60
<b>Figure 4-3.</b> Park Steel Stress Strain Model.....	63

<b>Figure 4-4.</b> Mander Concrete Confined Stress Strain Model.....	65
<b>Figure 4-5.</b> Beam Moment-Curvature Analysis. (a) Comparison SAP2000 Section Designer and CUMBIA. (b) Idealized Curve .....	67
<b>Figure 4-6.</b> Backbone Curve for Beam Hinge Assignment.....	68
<b>Figure 4-7.</b> Moment-Curvature Analysis for Column 16" X 6: Comparison between SAP2000 Section Designer and CUMBIA. Axial Load = 12 kips. (a) Strong Axis. (b) Weak Axis .....	69
<b>Figure 4-8.</b> Moment-Curvature Analysis for Column 12" X 12": Comparison between SAP2000 Section Designer and CUMBIA. Axial Load = 12 kips.....	70
<b>Figure 4-9.</b> Idealized Moment-Curvature Curve for Column 16" x 6": Strong Axis.....	71
<b>Figure 4-10.</b> Backbone Curve for Column 16"x 6":Strong Axis .....	71
<b>Figure 4-11.</b> Column 16x6 Moment – Curvature Analysis Strong Axis.....	72
<b>Figure 4-12.</b> Column 16x6 Moment – Curvature Analysis Weak Axis .....	72
<b>Figure 4-13.</b> SAP2000 Typical 3D Model.....	77
<b>Figure 4-14.</b> Column Element.....	78
<b>Figure 4-15.</b> Beam Element.....	79
<b>Figure 4-16.</b> User Graphics Interface for SAP2000 Load Case Data for Initial Pushover Analysis .....	80
<b>Figure 4-17.</b> Load Case Data for Lateral Pushover Analysis .....	81
<b>Figure 4-18.</b> Pushover Load Cases .....	81
<b>Figure 4-19.</b> Seismic Source Zones in the Region of Puerto Rico. Irizarry (1999) .....	85
<b>Figure 4-20.</b> Parkfield Earthquake Record.....	87
<b>Figure 4-21.</b> Parkfield 5% Damping Response Spectra.....	87
<b>Figure 4-22.</b> Northridge -Rollhill Earthquake Record .....	88
<b>Figure 4-23.</b> Northridge 5% Damping Response Spectra .....	88
<b>Figure 4-24.</b> San Salvador IGN Earthquake Record .....	89
<b>Figure 4-25.</b> San Salvador IGN 5% Damping Response Spectra .....	89
<b>Figure 4-26.</b> San Salvador CIG Earthquake Record .....	90
<b>Figure 4-27.</b> San Salvador CIG 5% Damping Response Spectra .....	90
<b>Figure 4-28.</b> Probabilistic Seismic Hazard Assessment for Puerto Rico. (USGS 2003) .....	91
<b>Figure 5-1.</b> Pushover Curve .....	94
<b>Figure 5-2.</b> Fundamental Mode Shape: X direction .....	96
<b>Figure 5-3.</b> Capacity Spectrum Curve .....	97
<b>Figure 5-4.</b> UBC-97 Demand Response Spectrum for $S_d$ Soil Type.....	98
<b>Figure 5-5.</b> UBC-97 Demand Response Spectrum for $S_d$ soil type. (a)Traditional Response Spectrum (b) ADRS Response Spectrum .....	100
<b>Figure 5-6.</b> Family of Reduced Response Spectrum for $S_d$ soil type. (a) Family of Reduced Response Spectrum Traditional Format ( $S_a$ vs $T$ ). (b) Family of Reduced Response Spectrum in ADRS Format ( $S_a$ vs $S_d$ ) .....	102
<b>Figure 5-7.</b> Bilinear Representation of Capacity Spectrum .....	103
<b>Figure 5-8.</b> Performance Point – Capacity Spectrum Solution .....	106
<b>Figure 6-1.</b> Deformed Mode Shape for Model 1.1b. (a) Mode 1 (b) Mode 2 (c) Mode 3.....	108
<b>Figure 6-2.</b> Deformed Mode Shape for Model 1.1c. (a) Mode 1 (b) Mode 2 (c) Mode 3.....	108
<b>Figure 6-3.</b> Deformed Mode Shape for Model 1.1d. (a) Mode 1 (b) Mode 2 (c) Mode 3.....	108

<b>Figure 6-4.</b> Location of Center of Mass (CM) and Center of Stiffness (CS) for Model 1.1b, Model 1.1c and Model 1.1d.....	110
<b>Figure 6-5.</b> Definition of the Ductility Demand ( $\mu_d$ ).....	121
<b>Figure 6-6.</b> Pushover Curves for Model 1.1b Push X (a) Different Load Patterns. (b) Direction Downhill (-X) and Uphill (X).(c) Fix vs. Pin Connection.....	124
<b>Figure 6-7.</b> Mode and Uniform Load Pattern Deformed Shape in the X Direction. ....	125
<b>Figure 6-8.</b> Deformed Shape. (a) Pushed Uphill. (b) Pushed Downhill .....	126
<b>Figure 6-9.</b> Pushover Deformed Shape and Hinge Formation for Model 1.1b: Push -X .....	127
<b>Figure 6-10.</b> Performance Point for Model 1.1b: Push -X.....	128
<b>Figure 6-11.</b> Ductility Demand for Mode 1.1b: Push -X.....	129
<b>Figure 6-12.</b> Pushover Curves for Model 1.1b: Push Y. (a) Different Load Pattern. (b) Design Base Shear vs. Capacity Curve.....	132
<b>Figure 6-13.</b> Pushover Deformed Shape and Hinge Formation for Model 1.1b: Push Y .....	133
<b>Figure 6-14.</b> Performance Point for Model 1.1b: Push Y.....	134
<b>Figure 6-15.</b> Comparison Pushover curves for Model 1.1b and 1.1c: Push -X .....	135
<b>Figure 6-16.</b> Pushover Curves for Different Load Patterns for Model 1.1c: Push Y.....	136
<b>Figure 6-17.</b> Comparison Pushover Curves for Model 1.1b and 1.1c: Push Y .....	137
<b>Figure 6-18.</b> Pushover Deformed Shape and Hinge Formation for Model 1.1c: Push Y.....	138
<b>Figure 6-19.</b> Performance Point for Model 1.1c: Push Y.....	139
<b>Figure 6-20.</b> Comparison pushover curves for Models 1.1b, Model 1.1c and Model 1.1d: Push Y .....	141
<b>Figure 6-21.</b> Pushover Deformed Shape and Hinge Formation for Model 1.1d: Push Y .....	142
<b>Figure 6-22.</b> Performance Point for Model 1.1d: Push Y.....	142
<b>Figure 6-23.</b> Comparison Pushover Curves for Model 1.1 in the X and Y direction.....	143
<b>Figure 6-24.</b> Comparison Pushover Curves for Model 1.1b and Model 1.2b: Push -X .....	145
<b>Figure 6-25.</b> Performance Point for Model 1.2b: Push X.....	146
<b>Figure 6-26.</b> Comparison Pushover Curves for Model 1.1b and Model 1.2b: Push Y.....	147
<b>Figure 6-27.</b> Performance Point for Model 1.2b: Push Y.....	148
<b>Figure 6-28.</b> Comparison Pushover Curves for Model 1.1c and Model 1.2c: Push Y .....	149
<b>Figure 6-29.</b> Pushover Deformed Shape and Hinge Formation for Model 1.2c: Push Y.....	150
<b>Figure 6-30.</b> Performance Point for Model 1.2c: Push Y .....	150
<b>Figure 6-31.</b> Comparison Pushover curves for Model 1.1d and Model 1.2d: Push Y .....	151
<b>Figure 6-32.</b> Pushover Deformed Shape and Hinge Formation for Model 1.2d:Push Y .....	152
<b>Figure 6-33.</b> Performance Point for Model 1.2d: Push Y.....	152
<b>Figure 6-34.</b> Comparison Pushover Curves for Model 1.1b and Model 1.3b: Push -X .....	154
<b>Figure 6-35.</b> Performance Point for Model 1.3b: Push X.....	154
<b>Figure 6-36.</b> Comparison Pushover Curves for Model 1.1b and Model 1.3c: Push Y.....	155
<b>Figure 6-37.</b> Pushover Deformed Shape and Hinge Formation for Model 1.3b: Push -X .....	156
<b>Figure 6-38.</b> Performance Point for Model 1.3c: Push Y .....	156
<b>Figure 6-39.</b> Comparison Pushover Curves for Model 1.1b and Model 1.3d: Push Y.....	157
<b>Figure 6-40.</b> Pushover Deformed Shape and Hinge Formation for Model 1.3d: Push Y .....	158
<b>Figure 6-41.</b> Performance Point for Model 1.3d: Push Y.....	158
<b>Figure 6-42.</b> Comparison Pushover Curves for Model 1.1b and 1.4b: Push -X .....	160
<b>Figure 6-43.</b> Performance Point for Model 1.4b: Push -X .....	160



<b>Figure 6-44.</b>	Comparison Pushover Curves for Models 1.1b and 1.4b: Push Y .....	162
<b>Figure 6-45.</b>	Performance Point for Model 1.4b: Push Y.....	162
<b>Figure 6-46.</b>	Comparison Pushover Curves for Models 1.1c and 1.4c: Push Y.....	163
<b>Figure 6-47.</b>	Pushover Deformed Shape and Hinge Formation for Model 1.4c: Push Y.....	164
<b>Figure 6-48.</b>	Performance Point for Model 1.4c: Push Y.....	164
<b>Figure 6-49.</b>	Comparison Pushover Curves for Models 1.1d and 1.4d: Push Y .....	165
<b>Figure 6-50.</b>	Pushover Deformed Shape and Hinge Formation for Model 1.4d: Push Y .....	166
<b>Figure 6-51.</b>	Performance Point for Model 1.4d: Push Y.....	166
<b>Figure 6-52.</b>	Comparison Pushover Curves for Model 1.1b and Model 2.1b: Push X.....	168
<b>Figure 6-53.</b>	Pushover Deformed Shape and Hinge Formation for Model 2.1: Push -X .....	169
<b>Figure 6-54.</b>	Performance Point for Model 2.1b: Push -X.....	170
<b>Figure 6-55.</b>	Comparison Pushover Curves for Model 1.1b and Model 2.1b: Push Y.....	171
<b>Figure 6-56.</b>	Pushover Deformed Shape and Hinge Formation for Model 2.1b: Push Y .....	172
<b>Figure 6-57.</b>	Performance Point for Model 2.1b: Push Y.....	172
<b>Figure 6-58.</b>	Comparison Pushover Curves for Model 1.1c and Model 2.1c: Push Y.....	173
<b>Figure 6-59.</b>	Pushover Deformed Shape and Hinge Formation for Model 2.1c: Push Y.....	174
<b>Figure 6-60.</b>	Performance Point for Model 2.1c: Push Y.....	174
<b>Figure 6-61.</b>	Comparison Pushover Curves for Model 1.1d and Model 2.1d: Push Y.....	175
<b>Figure 6-62.</b>	Pushover Deformed Shape and Hinge Formation for Model 2.1d: Push Y .....	176
<b>Figure 6-63.</b>	Performance Point for Model 2.1d: Push Y.....	176
<b>Figure 6-64.</b>	Performance Point for Model 2.2b: Push X.....	178
<b>Figure 6-65.</b>	Performance Point for Model 2.2b: Push Y.....	179
<b>Figure 6-66.</b>	Comparison Pushover Curves for Model 1.2c and Model 2.2c: Push Y .....	180
<b>Figure 6-67.</b>	Pushover Deformed Shape and Hinge Formation for Model 2.2c: Push Y.....	180
<b>Figure 6-68.</b>	Performance Point for Model 2.2c: Push Y.....	181
<b>Figure 6-69.</b>	Comparison Pushover Curves for Model 1.2d and Model 2.2d.....	182
<b>Figure 6-70.</b>	Pushover Deformed Shape and Hinge Formation for Model 2.2d: Push Y .....	183
<b>Figure 6-71.</b>	Performance Point for Model 2.2d: Push Y.....	183
<b>Figure 6-72.</b>	Comparison Pushover Curves for Model 1.3b and Model 2.3b: Push -X.....	185
<b>Figure 6-73.</b>	Performance Point for Model 2.3b: Push -X.....	185
<b>Figure 6-74.</b>	Comparison Pushover Curves for Model 1.3c and Model 2.3c: Push Y .....	186
<b>Figure 6-75.</b>	Pushover Deformed Shape and Hinge Formation for Model 2.3c: Push Y.....	187
<b>Figure 6-76.</b>	Performance Point for Model 2.3c: Push Y.....	187
<b>Figure 6-77.</b>	Comparison Pushover Curves for Model 1.3d and Model 2.3d: Push Y.....	188
<b>Figure 6-78.</b>	Pushover Deformed Shape and Hinge Formation for Model 2.3d: Push Y .....	189
<b>Figure 6-79.</b>	Performance Point for Model 2.3d: Push Y.....	189
<b>Figure 6-80.</b>	Comparison Pushover Curves for Model 1.4b and Model 2.4b: Push -X.....	191
<b>Figure 6-81.</b>	Performance Point for Model 2.4b: Push X.....	191
<b>Figure 6-82.</b>	Performance Point for Model 2.3b: Push Y.....	192
<b>Figure 6-83.</b>	Comparison Pushover Curves for Model 1.4c and Model 2.4c: Push Y .....	193
<b>Figure 6-84.</b>	Pushover Deformed Shape and Hinge Formation for Model 2.4c: Push Y.....	194
<b>Figure 6-85.</b>	Performance Point for Model 2.4c: Push Y.....	194
<b>Figure 6-86.</b>	Comparison Pushover Curves for Model 1.4d and Model 2.4d: Push Y.....	195
<b>Figure 6-87.</b>	Pushover Deformed Shape and Hinge Formation for Model 2.4d: Push Y .....	196

<b>Figure 6-88.</b> Performance Point for Model 2.4d: Push Y .....	196
<b>Figure 6-89.</b> Comparison Pushover Curves for Model 1.1b and Model 1.1yb: Push -X.....	198
<b>Figure 6-90.</b> Pushover Deformed Shape and Hinge Formation for Model 1.1yb: Push -X .....	198
<b>Figure 6-91.</b> Performance Point for Model 1.1yb: Push -X.....	199
<b>Figure 6-92.</b> Comparison Pushover Curves for Model 1.1b and Model 1.1yb: Push Y.....	200
<b>Figure 6-93.</b> Pushover Deformed Shape and Hinge Formation for Model 1.1yb: Push Y.....	201
<b>Figure 6-94.</b> Performance Point for Model 1.1yb: Push Y .....	201
<b>Figure 6-95.</b> Comparison Pushover Curves for Model 1.1b and Model 1.1yc: Push Y .....	202
<b>Figure 6-96.</b> Pushover Deformed Shape and Hinge Formation for Model 1.1yc: Push Y .....	203
<b>Figure 6-97.</b> Performance Point for Model 1.1yc: Push Y .....	204
<b>Figure 6-98.</b> Comparison Pushover Curves for Model 1.1b and Model 1.1.2b: Push Y.....	206
<b>Figure 6-99.</b> Performance Point for Model 1.1.2b: Push Y.....	207
<b>Figure 6-100.</b> Comparison Pushover Curves for Model 1.1b and Model 1.1.2c: Push Y.....	208
<b>Figure 6-101.</b> Performance Point for Model 1.1.2c: Push Y .....	209
<b>Figure 6-102.</b> Comparison Pushover Curves for Model 1.1b and Model 1.1.3b: Push -X.....	210
<b>Figure 6-103.</b> Performance Point for Model 1.1.3b: Push -X.....	211
<b>Figure 6-104.</b> Comparison Pushover Curves for Model 1.1b and Model 1.1.3b: Push y .....	212
<b>Figure 6-105.</b> Comparison Pushover Curves for Model 1.1b and Model 1.1.3b: Push Y.....	213
<b>Figure 6-106.</b> Performance Point for Model 1.1.3b: Push Y .....	214
<b>Figure 6-107.</b> Comparison Pushover Curves for Model 1.1b and Model 1.1.3c: Push Y .....	215
<b>Figure 6-108.</b> Performance Point for Model 1.1.3c: Push Y .....	216
<b>Figure 6-109.</b> Comparison Pushover Curves for Model 1.1b and Model 1.1.4b: Push -X.....	217
<b>Figure 6-110.</b> Performance Point for Model 1.1.4b: Push -X.....	218
<b>Figure 6-111.</b> Comparison Pushover Curves for Model 1.1b and Model 1.1.4c: Push Y .....	219
<b>Figure 6-112.</b> Performance Point for Model 1.1.4c: Push Y .....	220
<b>Figure 6-113.</b> Joint label for Model 1.1b .....	226
<b>Figure 6-114.</b> Displacement Time History of Top Joint for Model 1.1b: Parkfield EQ in the X direction .....	227
<b>Figure 6-115.</b> Base Shear Time History Model 1.1b: Parkfield EQ X direction.....	227
<b>Figure 6-116.</b> Hinge Formation for Model 1.1b: Parkfield EQ X Direction .....	228
<b>Figure 6-117.</b> Displacement Time History of Top Joint for Model 1.1b: Parkfield EQ in the Y Direction.....	228
<b>Figure 6-118.</b> Base Shear Time History Model 1.1b: Parkfield EQ Y Direction .....	229
<b>Figure 6-119.</b> Hinge Formation for Model 1.1b: Parkfield EQ Y Direction .....	229
<b>Figure 6-120.</b> Displacement Time History of Top Joint for Model 1.1b: Northridge EQ in the X Direction.....	231
<b>Figure 6-121.</b> Base Shear Time History Model 1.1b: Northridge EQ X Direction .....	231
<b>Figure 6-122.</b> Displacement Time History of Top Joint for Model 1.1b: Northridge EQ in the Y Direction.....	232
<b>Figure 6-123.</b> Base Shear Time History Model 1.1b: Northridge EQ Y Direction .....	232
<b>Figure 6-124.</b> Hinge Formation for Model 1.1b: Northridge EQ Y Direction .....	233
<b>Figure 6-125.</b> Displacement Time History of Top joint for Model 1.1b: San Salvador IGN EQ in the X Direction .....	234
<b>Figure 6-126.</b> Base Shear Time History Model 1.1b: San Salvador IGN EQ X Direction .....	234

<b>Figure 6-127.</b> Hinge Formation for Model 1.1b: San Salvador IGN EQ X Direction .....	235
<b>Figure 6-128.</b> Displacement Time History of Top Joint for Model 1.1b: San Salvador IGN EQ in the Y Direction .....	235
<b>Figure 6-129.</b> Base Shear Time History Model 1.1b: San Salvador IGN EQ Y Direction .....	236
<b>Figure 6-130.</b> Hinge Formation for Model 1.1b: San Salvador IGN EQ Y Direction .....	236
<b>Figure 6-131.</b> Displacement Time History of Top Joint for Model 1.1b: San Salvador CIG EQ in the X Direction .....	237
<b>Figure 6-132.</b> Base Shear Time history Model 1.1b: San Salvador CIG EQ X Direction .....	238
<b>Figure 6-133.</b> Hinge Formation for Model 1.1b: San Salvador CIG EQ X Direction .....	238
<b>Figure 6-134.</b> Displacement Time History of Top joint for Model 1.1b: San Salvador CIG EQ in the Y Direction .....	239
<b>Figure 6-135.</b> Base Shear Time History Model 1.1b: San Salvador CIG Y Direction .....	239
<b>Figure 6-136.</b> Hinge Formation for San Salvador CIG EQ Y Direction.....	240
<b>Figure 6-137.</b> Joint Label for Model 1.1c .....	241
<b>Figure 6-138.</b> Displacement Time History of Top Joint for Model 1.1c: San Salvador IGN EQ in the Y Direction .....	241
<b>Figure 6-139.</b> Base Shear Time History Model 1.1c: San Salvador IGN Y Direction.....	242
<b>Figure 6-140.</b> Hinge Formation for Model 1.1c: San Salvador IGN EQ Y Direction.....	242
<b>Figure 6-141.</b> Displacement Time History of Top Joint for Model 1.1c: San Salvador CIG EQ in the Y Direction .....	244
<b>Figure 6-142.</b> Base Shear Time history Model 1.1c: San Salvador CIG Y Direction .....	244
<b>Figure 6-143.</b> Hinge Formation for Model 1.1c: San Salvador CIG EQ Y Direction.....	245
<b>Figure 6-144.</b> Displacement Time History of Top Joint for Model 1.1d: San Salvador CIG EQ in the Y Direction .....	246
<b>Figure 6-145.</b> Base Shear Time History Model 1.1d: San Salvador CIG Y Direction .....	246
<b>Figure 6-146.</b> Hinge Formation for Model 1.1d: San Salvador IGN EQ Y Direction .....	247
<b>Figure 6-147.</b> Comparison Displacement Time History of Top Joint for Model 1.1b and Model 1.4b: San Salvador IGN EQ in the X Direction .....	248
<b>Figure 6-148.</b> Comparison Base Shear Time History Model 1.1b and Model 1.4b: San Salvador IGN X Direction .....	249
<b>Figure 6-149.</b> Hinge Formation for Model 1.4b: San Salvador IGN EQ X Direction .....	249
<b>Figure 6-150.</b> Comparison Displacement Time History of Top Joint for Model 1.1b and Model 1.4b: San Salvador CIG EQ in the X Direction .....	250
<b>Figure 6-151.</b> Comparison Base Shear Time History Model 1.1b and Model 1.4b: San Salvador CIG X Direction .....	251
<b>Figure 6-152.</b> Hinge Formation for Model 1.4b: San Salvador CIG EQ X Direction .....	251
<b>Figure 6-153.</b> Comparison Displacement Time History of Top Joint for Model 1.1b and Model 1.4b: San Salvador IGN EQ in the Y Direction .....	252
<b>Figure 6-154.</b> Comparison Base Shear Time History for Model 1.1c and Model 1.4c: San Salvador IGN Y Direction .....	253
<b>Figure 6-155.</b> Hinge Formation for Model 1.4c: San Salvador IGN EQ Y Direction.....	253
<b>Figure 6-156.</b> Comparison Displacement Time history of Top Joint for Model 1.1b and Model 1.4b: San Salvador CIG EQ in the Y Direction .....	254

<b>Figure 6-157.</b> Comparison Base Shear Time History Model 1.1b and Model 1.4b: San Salvador CIG Y Direction .....	255
<b>Figure 6-158.</b> Hinge Formation for Model 1.4c: San Salvador CIG EQ Y Direction.....	255
<b>Figure 6-159.</b> Comparison Displacement Time history of Top Joint for Model 1.1b and Model 2.1b: San Salvador IGN EQ in the Y Direction .....	256
<b>Figure 6-160.</b> Comparison Base Shear Time History Model 1.1b and Model 2.1b: San Salvador IGN X Direction .....	257
<b>Figure 6-161.</b> Hinge Formation for Model 2.1b: San Salvador IGN EQ X Direction .....	257
<b>Figure 6-162.</b> Comparison Displacement Time history of Top Joint for Model 1.1b and Model 1.4b: San Salvador CIG EQ in the X Direction .....	258
<b>Figure 6-163.</b> Comparison Base Shear Time History Model 1.1b and Model 1.4b: San Salvador CIG X Direction .....	258
<b>Figure 6-164.</b> Hinge Formation for Model 2.1b: San Salvador CIG EQ X Direction .....	259
<b>Figure 6-165.</b> Comparison Displacement Time history of Top Joint for Model 1.1c and Model 2.1c: San Salvador CIG EQ in the Y Direction.....	260
<b>Figure 6-166.</b> Comparison Base Shear Time History Model 1.1b and Model 1.4b: San Salvador CIG Y Direction .....	260
<b>Figure 6-167.</b> Hinge Formation for Model 2.1c: San Salvador CIG EQ Y Direction.....	261
<b>Figure 6-168.</b> Displacement Time history of Top Joint for Model 1.1.3b: San Salvador CIG EQ in the X Direction.....	262
<b>Figure 6-169.</b> Base Shear Time History Model 1.1.3b: San Salvador CIG X Direction.....	262
<b>Figure 6-170.</b> Hinge Formation for Model 1.1.3b: San Salvador CIG EQ X Direction .....	263
<b>Figure 6-171.</b> Displacement Time history of Top Joint for Model 1.1.3b: San Salvador CIG EQ in the Y Direction.....	263
<b>Figure 6-172.</b> Base Shear Time History Model 1.1.3b: San Salvador CIG Y Direction.....	264
<b>Figure 6-173.</b> Hinge Formation for Model 1.1.3b: San Salvador CIG EQ Y Direction .....	264
<b>Figure 6-174.</b> Displacement Time history of Top Joint for Model 1.1.3c: San Salvador CIG EQ in the Y Direction.....	265
<b>Figure 6-175.</b> Base Shear Time History Model 1.1.3c Salvador CIG Y Direction .....	266
<b>Figure 6-176.</b> Hinge Formation for Model 1.1.3c: San Salvador CIG EQ Y Direction.....	266
<b>Figure 7-1.</b> Analytical Model with RC Shear Walls location.....	272
<b>Figure 7-2.</b> Comparison Pushover Curves with Rehabilitation for Model 1.3c: Push Y .....	273
<b>Figure 7-3.</b> Comparison Performance Point for Model 1.3c: Push Y. (a) Without Rehabilitation. (b) With Rehabilitation.....	274
<b>Figure 7-4.</b> Comparison Pushover Curves with Rehabilitation for Model 1.4b: Push -X.....	275
<b>Figure 7-5.</b> Comparison Performance Point for Model 1.4b: Push -X. ((a) Without Rehabilitation. (b) With Rehabilitation.....	275
<b>Figure 7-6.</b> Comparison Pushover Curves with Rehabilitation for Model 1.4c: Push Y .....	276
<b>Figure 7-7.</b> Comparison Performance Point for Model 1.4c: Push Y. (a) Without Rehabilitation. (b) With Rehabilitation.....	277
<b>Figure 7-8.</b> Comparison Pushover Curves with Rehabilitation for Model 2.4b: Push -X.....	278
<b>Figure 7-9.</b> Comparison Performance Point for Model 2.4b: Push -X. (a) Without Rehabilitation. (b) With Rehabilitation.....	278
<b>Figure 7-10.</b> Comparison Pushover Curves with Rehabilitation for Model 2.4c: Push Y .....	279

<b>Figure 7-11.</b> Comparison Performance Point for Model 2.4c: Push Y. (a) Without Rehabilitation. (b) With Rehabilitation.....	280
<b>Figure 7-12.</b> Comparison Pushover Curves with Rehabilitation for Model 1.1yb: Push -X .....	281
<b>Figure 7-13.</b> Comparison Performance Point for Model 1.1yb: Push -X. (a) Without Rehabilitation. (b) With Rehabilitation.....	281
<b>Figure 7-14.</b> Comparison Pushover Curves with Rehabilitation for Model 1.1.5c: Push Y .....	282
<b>Figure 7-15.</b> Comparison Performance Point for Model 1.1.5c: Push Y. (a) Without Rehabilitation. (b) With Rehabilitation.....	283
<b>Figure 7-16.</b> Displacement Time History of Top Joint for Model 1.4b: San Salvador CIG EQ in the X Direction .....	285
<b>Figure 7-17.</b> Displacement Time History of Top Joint for Model 1.4c: San Salvador CIG EQ in the Y Direction .....	285
<b>Figure 7-18.</b> Displacement Time History of Top Joint for Model 2.4: San Salvador CIG EQ in the X Direction .....	286
<b>Figure 7-19.</b> Displacement Time History of Top Joint for Model 1.4c: San Salvador CIG EQ in the Y Direction .....	286
<b>Figure 7-20.</b> Displacement Time History of Top Joint for Model 1.1yb: San Salvador CIG EQ in the Y Direction .....	287
<b>Figure 7-21.</b> New RC Shear Wall Structural Detail .....	290

## LIST OF TABLES

<b>Table 2-1.</b> Summary of Structural Parameters of Residence 1 .....	13
<b>Table 2-2.</b> Summary of Structural Parameters of Residence 2 .....	14
<b>Table 2-3.</b> Summary of Structural Parameters of Residence 3 .....	16
<b>Table 2-4.</b> Summary of Structural Parameters of Residence 4 .....	19
<b>Table 2-5.</b> Residence 4 in San Sebastian: Footing and Columns Structural Details.....	21
<b>Table 2-6.</b> Summary of Structural Parameters of Residence 5 .....	23
<b>Table 2-7.</b> Summary of Structural Parameters of Residence 6 .....	24
<b>Table 2-8.</b> Summary of the Residences Columns Height. Vázquez (2002) .....	28
<b>Table 2-9.</b> Summary of the Column Sections. Vázquez (2002).....	28
<b>Table 2-10.</b> Summary of Residences Spans. Vázquez (2002) .....	28
<b>Table 3-1.</b> Summary of Analytical Models.....	31
<b>Table 3-2.</b> Equivalent Masonry Strut's Material Properties.....	40
<b>Table 3-3.</b> Parameters for Model 1.1 .....	42
<b>Table 3-4.</b> Parameters for Model 1.2 .....	43
<b>Table 3-5.</b> Parameters for Model 1.3 .....	44
<b>Table 3-6.</b> Parameters for Model 1.4 .....	45
<b>Table 3-7.</b> Parameters for Model 2.1 .....	46
<b>Table 3-8.</b> Parameters for Model 2.2 .....	47
<b>Table 3-9.</b> Parameters for Model 2.3 .....	47
<b>Table 3-10.</b> Parameters for Model 2.4 .....	48
<b>Table 3-11.</b> Parameters for Model 1.1y.....	49
<b>Table 3-12.</b> Parameters for Model 1.1.2 .....	49
<b>Table 3-13.</b> Parameters for Model 1.1.3 .....	50
<b>Table 3-14.</b> Parameters for Model 1.1.4 .....	50
<b>Table 3-15.</b> Minimum Longitudinal Reinforcement for Columns .....	51
<b>Table 3-16.</b> 7 and 28 days Compression Test Results 7 and 28 .....	54
<b>Table 4-1.</b> Maximum Expected Earthquake Magnitude and Maximum Depth for Each Seismic Zone Fault. Irizarry (1999).....	85
<b>Table 4-2.</b> Epicentral Distances Used for the Earthquake Record Search. Irizarry (1999) .....	85
<b>Table 4-3.</b> Characteristics of the Dominant Earthquake in the Response Spectra Envelope for Mayagüez and Ponce (Irizarry 1999) .....	86
<b>Table 4-4.</b> Characteristics of the Dominant Earthquake in the Response Spectra Envelope for San Juan (Irizarry 1999).....	86
<b>Table 5-1.</b> Data to Convert Pushover Curve to Capacity Spectrum Curve .....	96
<b>Table 5-2.</b> UBC-97 Design Spectrum Data, for Soil Type <i>S<sub>d</sub></i> .....	98
<b>Table 5-3.</b> UBC-97 Demand Spectrum Data in ADRS Format for Soil Type <i>S<sub>d</sub></i> .....	100
<b>Table 5-4.</b> Structural Behavior Type (ATC 40) .....	102
<b>Table 5-5.</b> Values for Damping Modification Factor, $\kappa$ (ATC-40) .....	104
<b>Table 5-6.</b> Demand Curve Calculation .....	106
<b>Table 6-1.</b> Dynamic Properties: Model 1.1 .....	107
<b>Table 6-2.</b> Dynamic Properties: Model 1.2: .....	112

<b>Table 6-3.</b> Dynamic Properties: Model 1.3: .....	112
<b>Table 6-4.</b> Dynamic Properties: Model 1.4 .....	112
<b>Table 6-5.</b> Dynamic Properties: Model 2.1 .....	114
<b>Table 6-6.</b> Dynamic Properties: Model 2.2 .....	114
<b>Table 6-7.</b> Dynamic Properties: Model 2.3: .....	115
<b>Table 6-8.</b> Dynamic Properties: Model 2.4: .....	115
<b>Table 6-9:</b> Dynamic Properties: Model 1.1yb. Column Orientation .....	116
<b>Table 6-10.</b> Dynamic Properties: Model 1.1.2. Columns 16 X 8 .....	117
<b>Table 6-11.</b> Dynamic Properties: Model 1.1.3. Columns 12 X 12 .....	117
<b>Table 6-12.</b> Dynamic Properties: Model 1.1.4. Columns 12 X 6 .....	117
<b>Table 6-13.</b> UBC 97 Soil Profile Type .....	120
<b>Table 6-14.</b> Model 1.1b: Tabular Data for Pushover Curve for Model 1.1b: Push -X .....	123
<b>Table 6-15.</b> Response Modification Factors (R) as per UBC 97 .....	130
<b>Table 6-16.</b> Response Modification Factor (R) and Ductility factors ( $R\mu$ ) .....	131
<b>Table 6-17.</b> Tabular Data for Pushover Curve for Model 1.1b: Push Y .....	131
<b>Table 6-18.</b> Tabular Data for Pushover Curve for Model 1.1c: Push Y .....	136
<b>Table 6-19.</b> Tabular Data for Pushover Curve for Model 1.1d: Push Y .....	140
<b>Table 6-20.</b> Tabular Data for Pushover Curve for Model 1.2b Push -X .....	145
<b>Table 6-21.</b> Tabular Data for Pushover Curve for Model 1.2b: Push Y .....	147
<b>Table 6-22.</b> Tabular Data for Pushover Curve for Model 1.2c: Push Y .....	149
<b>Table 6-23</b> Tabular Data for Pushover Curve for Model 1.2d: Push Y .....	151
<b>Table 6-24.</b> Tabular Data for Pushover Curve for Model 1.3b: Push -X .....	153
<b>Table 6-25.</b> Tabular Data for Pushover Curve for Model 1.3c: Push Y .....	155
<b>Table 6-26.</b> Tabular Data for Pushover Curve for Model 1.3d: Push Y .....	157
<b>Table 6-27</b> Tabular Data for Pushover Curve for Model 1.4b: Push -X .....	159
<b>Table 6-28.</b> Tabular Data for Pushover Curve for Model 1.4b: Push Y .....	161
<b>Table 6-29.</b> Tabular Data for Pushover Curve. for Model 1.4b: Push Y .....	163
<b>Table 6-30.</b> Tabular Data for Pushover Curve for Model 1.4d: Push Y .....	165
<b>Table 6-31.</b> Tabular Data for Pushover Curve for Model 2.1b: Push -X .....	168
<b>Table 6-32.</b> Tabular Data for Pushover Curve for Model 2.1b: Push Y .....	171
<b>Table 6-33.</b> Tabular Data for Pushover Curve. for Model 2.1c: Push Y .....	173
<b>Table 6-34.</b> Tabular Data for Pushover Curve for Model 2.1d: Push Y .....	175
<b>Table 6-35.</b> Tabular Data for Pushover Curve for Model 2.2b: Push -X .....	177
<b>Table 6-36.</b> Tabular Data for Pushover Curve for Model 2.2c: Push Y .....	179
<b>Table 6-37.</b> Tabular Data for Pushover Curve for Model 2.2d: Push Y .....	182
<b>Table 6-38.</b> Tabular Data for Pushover Curve for Model 2.3b: Push -X .....	184
<b>Table 6-39.</b> Tabular Data for Pushover Curve for Model 2.3c: Push Y .....	186
<b>Table 6-40.</b> Tabular Data for Pushover Curve for Model 2.3d: Push Y .....	188
<b>Table 6-41.</b> Tabular Data for Pushover Curve for Model 2.4b: Push -X .....	190
<b>Table 6-42.</b> Tabular Data for Pushover Curve for Model 2.4c: Push X .....	193
<b>Table 6-43.</b> Tabular Data for Pushover Curve for Model 2.4d: Push Y .....	195
<b>Table 6-44.</b> Tabular Data for Pushover Curve for Model 1.1yb: Push -X .....	197
<b>Table 6-45.</b> Tabular Data for Pushover Curve for Model 1.1yb: Push Y .....	200
<b>Table 6-46.</b> Tabular Data for Pushover Curve for Model 1.1yc: Push Y .....	202

<b>Table 6-47.</b> Tabular Data for Pushover Curve for Model 1.1.2b: Push Y.....	205
<b>Table 6-48.</b> Tabular Data for Pushover Curve for Model 1.1.2c: Push Y.....	207
<b>Table 6-49.</b> Tabular Data for Pushover Curve for Model 1.1.3b: Push -X.....	210
<b>Table 6-50.</b> Tabular Data for Pushover Curve for Model 1.1.3b: Push Y.....	212
<b>Table 6-51.</b> Tabular Data for Pushover Curve for Model 1.1.3c: Push Y.....	215
<b>Table 6-52.</b> Tabular Data for Pushover Curve for Model 1.1.4b: Push -X.....	217
<b>Table 6-53.</b> Tabular Data for Pushover Curve for Model 1.1.4c: Push Y.....	219
<b>Table 6-54.</b> Summary Results Pushover Analysis Models 1 .....	221
<b>Table 6-55.</b> Summary Results Pushover Analysis Models 2 .....	222
<b>Table 6-56.</b> Summary Results Pushover Analysis Models 1.1 with Variation .....	223
<b>Table 6-57.</b> Summary Results Nonlinear Time History Analysis .....	267
<b>Table 7-1.</b> Tabular Data for Pushover Curve for Model 1.3c: Push Y Rehabilitation .....	273
<b>Table 7-2.</b> Tabular Data for Pushover Curve for Model 1.4b: Push -X Rehabilitation .....	274
<b>Table 7-3.</b> Tabular Data for Pushover Curve for Model 1.4c: Push Y Rehabilitation .....	276
<b>Table 7-4.</b> Tabular Data for Pushover Curve for Model 2.4b: Push -X Rehabilitation .....	277
<b>Table 7-5.</b> Tabular Data for Pushover Curve for Model 2.4d: Push Y Rehabilitation .....	279
<b>Table 7-6.</b> Tabular Data for Pushover Curve for Model 1.1yb: Push –X Rehabilitation.....	280
<b>Table 7-7.</b> Tabular Data for Pushover Curve for Model 1.1.5c: Push Y Rehabilitation.....	282
<b>Table 7-8.</b> Shear Strength on New RC Shear Wall .....	289
<b>Table 7-9.</b> Reinforcement and Spacing Requirements for 6 inch Wall .....	289
<b>Table. A-1.</b> Default Hinges Properties for Reinforced Concrete Beam (FEMA 356).....	309
<b>Table A-2.</b> Default Hinges Properties for Reinforced Concrete Columns (FEMA 356).....	310
<b>Table D-3.</b> Axial Load Calculation Model 1.1.....	317
<b>Table D-2.</b> Axial Load Calculation Model 1.2.....	318
<b>Table D-3.</b> Axial Load Calculation Model 1.3.....	319
<b>Table D-4.</b> Axial Load Calculation Model 1.4.....	320
<b>Table D-5.</b> Axial Load Calculation Model 2.1.....	321
<b>Table D-6.</b> Axial Load Calculation Model 2.2.....	322
<b>Table D-7.</b> Axial Load Calculation Model 2.3.....	323
<b>Table D-8.</b> Axial Load Calculation Model 2.4.....	324
<b>Table E-4.</b> Shear Strength Capacity Calculations: Column 16" X 6".....	325
<b>Table E-5.</b> Shear Strength Capacity Calculations: Column 16" X 8".....	326
<b>Table E-6.</b> Shear Strength Capacity Calculations: Column 12" X 6".....	327
<b>Table E-7.</b> Shear Strength Capacity Calculations: Column 12" X 12".....	328
<b>Table F-8.</b> Response Modification Factors R Proposed by UBC-97.....	329
<b>Table G-9.</b> Design Base Shear for Model 1.1.....	330
<b>Table G-10.</b> Summary Design Base Shear.....	330



# CHAPTER 1. INTRODUCTION

---

## 1.1 PURPOSE OF THE STUDY

It is well known that Puerto Rico is exposed to the hazard of experiencing strong earthquakes, since it is located in an earthquake prone region. Puerto Rico is located on a microplate inserted between the North American and Caribbean plates. Figure 1-1 shows the principal seismic faults for the area of Puerto Rico. The major tectonic fault lines surrounding the Island are the boundaries of the microplate. The Puerto Rico Trench and the Muertos Trench form the north and south borders of the microplate. The Anegada Trough and the Mona Canyon are two normal fault system that form the eastern and western borders of the microplate, respectively. The main sources of seismic activity in the region are at the boundaries of the microplate (Clinton et al., 2006). Therefore, current seismic hazard assessments primarily consider only the impact of offshore seismic faults because onshore fault hazard is unknown (Prentice and Mann, 2005). However, recent studies demonstrated a Holocene surface rupture on a previously undocumented fault in southwestern Puerto Rico (Lajas Valley Fault). This fault may be part of a larger fault zone that extends from the western end of the Lajas Valley toward Ponce, the second largest city in Puerto Rico (Prentice and Mann, 2005). This 50-km long inland fault segment can produce M7.0 events (LaForge and McCann, 2003)

At the south, the Great Southern Puerto Rico Fault Zone (GSPRFZ) crosses the Island from the west to the southern coast (Irizarry, 1999). The Great Northern Puerto Rico Fault Zone (GNPRFZ) runs from east coast to the central mountains of Puerto Rico.

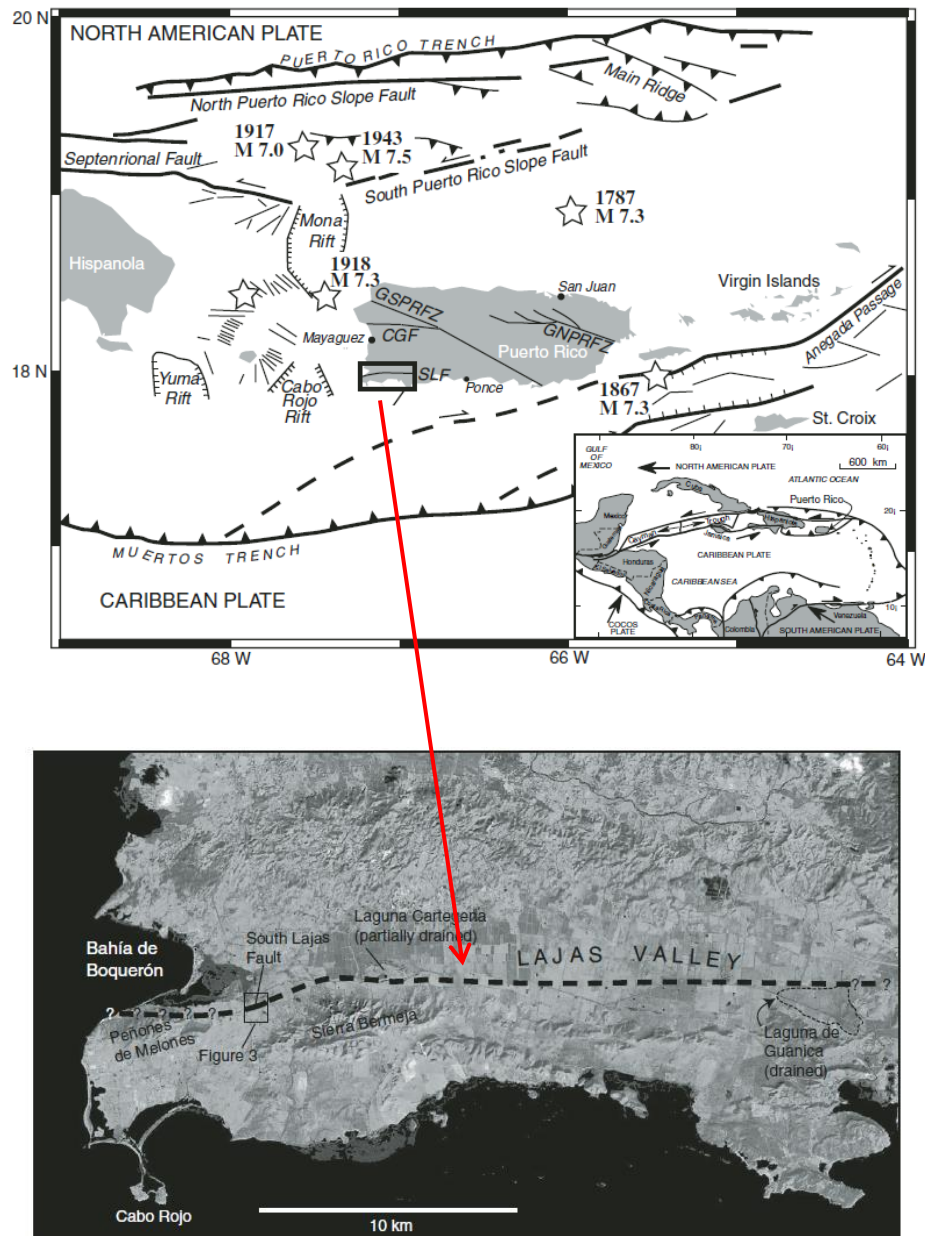


**Figure 1-1. Fault Map of Puerto Rico (Prentice and Mann, 2005)**

It has been close to 100 years since the last major earthquake stroke the island in 1918. It was generated at the Mona Canyon, about 50 km to the northwest of the Island, with a magnitude of 7.3, and was accompanied by a tsunami which got up to 6 meters (19.5 feet) high. Damage was concentrated in the western area of the Island because this was the closest zone to the earthquake epicenter. According to the National Earthquake Information Center, 116 people died in the 1918 event, and the economic loss was

calculated at four million dollars, two times the annual budget for the whole island at the time.

There is evidence of three other major earthquakes that affected the island since the beginning of the colonization. The first strong earthquake, whose magnitude has not been determined, occurred in August 15, 1670, significantly affecting the area of the San German District. The second one occurred on May 2, 1787 in which damage and destruction were reported from all areas of the island except in the south. The magnitude of this earthquake was at least 8.0 according to the National Earthquake Information Center and the epicenter was possibly located in the Northern Puerto Rico Trench. The third earthquake was reported on November 17, 1867 with an estimated magnitude of 7.3 and affected the eastern zone of Puerto Rico. Based on the recorded seismic history it is very likely that an event greater than M7.0 will jerk the Island.

If an earthquake of similar magnitude occurred today, the consequences would be devastating causing considerable loss of life and properties. The seismic performance evaluation and retrofitting of existing residences pose a great challenge. The risk, measured in both lives and dollars, is high. Equally high is the uncertainty of where, when, and how intense future earthquakes will strike.

The threat of experiencing strong earthquakes is increased by the topography of Puerto Rico. From the study of damages during past earthquakes, it has been shown that the surface topography on the site of the structure can considerably amplify the ground motions. Ridges and hills produce a scattering, reflection and diffraction of the seismic waves causing amplification and, in some cases, attenuation of the ground acceleration.

Furthermore, this problem is more troublesome due to the common practice in Puerto Rico to build reinforced concrete frames for residential houses in hillsides and hilly terrains and supporting them on slender columns (Figure 1-2). There is a scarcity of plane ground in hilly areas which obligates the construction of residences on slopes.

Because of the imminent risk of being affected by a strong earthquake, it is important to study the behavior and damage vulnerability of these structures.

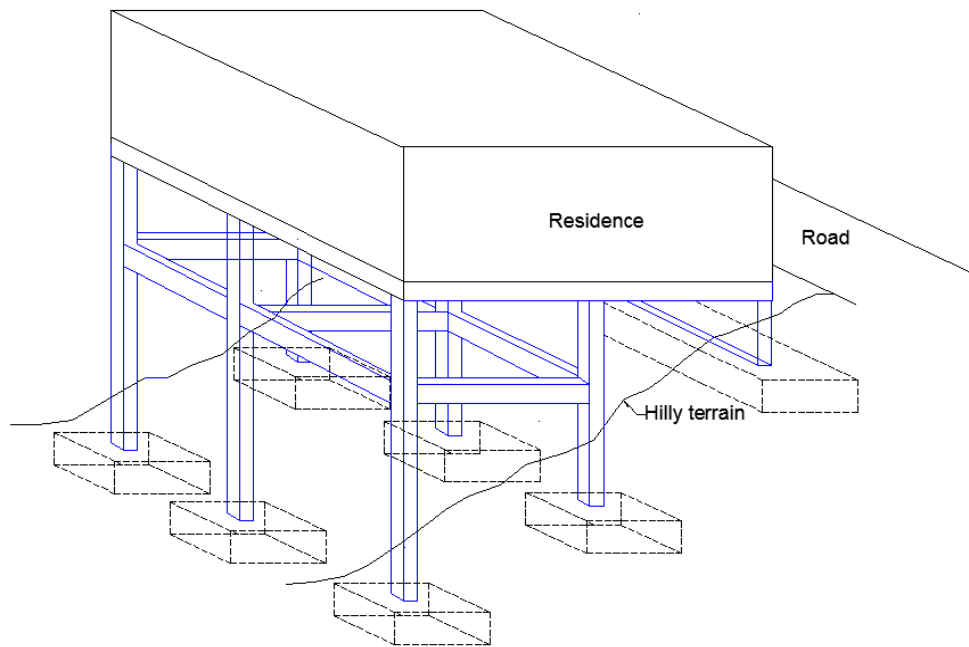


**Figure 1-2.** Drawing of Typical Hilly Residences

It is a fact that in Puerto Rico there are many houses that are built over hilly terrain and combined with poor construction practices, these types of structures are at a high seismic risk. Recent studies have indicated the vulnerability of these structures to seismic events, especially when the loading is amplified to account for the site topography (Vázquez, 2002). These structures need rehabilitation systems that fit the needs of the owners and meet the construction practices in the Island. Although these structures have been studied in the past, the particular feature of the differences in column elevations and the design of rehabilitation techniques adapted for the hilly terrain conditions needs to be evaluated with more attention.

## 1.2 OBJECTIVES

The goal of this research is to analytically evaluate the performance of typical residential structures located at hillsides and hilly terrain, focusing in modeling the difference in length of the gravity columns due to hilly terrain conditions. Specifically, the objectives are to:

- Determine the typical construction details of residences built on hilly terrain in Puerto Rico from the survey of actual construction site visits to characterize the difference in length of the gravity columns due to the terrain conditions.
- Determine the collapse mechanism of three dimensional models using a static nonlinear pushover and nonlinear time history analysis.
- Develop rehabilitation strategies for improving the seismic behavior based on the pushover analysis results.

## 1.3 SUMMARY OF THE METHODOLOGY

The methodology of this research work is briefly described here. A more detailed explanation is found in each of the following chapters:

1. Perform a field survey across the island to define the typical parameters of residences on hilly terrain. Preliminary evaluation involves acquisition of typical residences data, i.e. the number of spans, size of columns, size of beams, number of stories, story height, and slope of hilly terrain. The most important parameters to be searched for are the difference in length of the gravity columns due to the terrain conditions. Vázquez (2002) survey will be also used.

2. With the parameters acquired in the field survey and from structures previously studied, typical analytical models in 3 dimensions will be defined.
3. The residences response will be obtained with nonlinear analyses. Several studies indicate that this is the best approach to obtain information about the structures in the inelastic range. Elastic analysis can predict the elastic capacity of structure and indicate where the first yielding will occur. However, they do not predict failure mechanisms. Non Linear Static Pushover is a commonly used approximate method to determine the nonlinear behavior of structures. The structure is subjected to a monotonically increasing pattern of lateral loads. Nonlinear time history analysis is the “most” accurate method to examine the nonlinear behavior of building structures. In this method, the structure is subjected to real ground motion records (horizontal component).
4. Several criteria like collapse mechanism, maximum capacity and maximum rotation of the structural elements will be used to establish the collapse criteria. The pushover and time history analysis will be performed on the prototype models utilizing the structural analysis program SAP2000. The analyses to be performed are:
  - Nonlinear static pushover analysis of the models in three dimensions in the direction perpendicular to the road.
  - Nonlinear static pushover analysis of the models in three dimensions in the direction parallel to the road.
  - Nonlinear time history analysis of selected models in three dimensions in the direction perpendicular to the road.
  - Nonlinear time history analysis of selected models in three dimensions in the direction parallel to the road.

5. After the nonlinear analyses, similar analyses will be performed integrating a rehabilitation system to increase the seismic capacity of the analytical models. Reinforced concrete structural walls were chosen as the rehabilitation system. The reinforced concrete structural walls increase both the stiffness and the capacity of the structure.

## 1.4 PREVIOUS WORK

According to Arroyo (2001) the geography of Puerto Rico makes many regions prone to topographic seismic amplifications. The problem is aggravated by many residential structures located on hills and slopes that are constructed with weak first stories consisting of slender columns. Arroyo studied the effect of surface topography irregularities like hills and escarpments on the amplification of seismic waves based on a peak acceleration comparison. For the study, Arroyo varied the slope of the escarpments and also the ratio between the length of the base and the height of the hills when subjected to ground motions. She performed a two dimensional finite element analysis with the finite element program QUAD4M for plane soil structures subjected to a horizontal earthquake excitation at the base. Four soil profiles defined in the UBC 97 were used to define the material properties. The seismic input was the acceleration time history of the El Centro and San Salvador earthquakes. The nonlinear behavior of the soil was taken into account with the Equivalent Linear Method. A series of equations was created to relate the amplification factor to the topography as well to the location of the structure along the hill or escarpment. Arroyo concluded from the two dimensional nonlinear analyses that the amplification factor varies from a range of 1 to 2.35. The amplification factor obtained in the investigation was based on absolute peak ground accelerations.

In the dissertation “Seismic Behavior and Retrofitting of Hillside and Hilly Terrain R/C Houses Raised on Gravity Columns” by Vázquez (2002), he utilized the results of the ground amplifications factors found by Arroyo (2001) to analyze their effect on actual

residential structures in Puerto Rico. Vázquez conducted a field survey in five municipalities and a total of 24 residences were evaluated and measured. The parameters considered were the height of the columns, the cross-sectional properties, the span length of beams, the steel reinforcement, and the number of stories. Vázquez analyzed two dimensional frames from the surveyed homes, all consisting in two stories and two spans frames, varying the story height, span length and steel reinforcement in six prototypes. Since each model was analyzed in the strong and weak direction, the total number of cases analyzed increased to twelve.

In his analysis Vázquez performed nonlinear static pushovers and nonlinear dynamic transient analyses for the seismic vulnerability evaluation. In the first part of the investigation a Nonlinear Static Pushover was performed. The Capacity Spectrum Method was used to study the behavior of the structures in the non-linear range. At first the residences were evaluated without topographic amplification. Vázquez concluded from this preliminary analysis that the structural integrity of almost all the residences was compromised when subjected to strong motions similar to the ones considered in the study (i.e., described by the response spectrum UBC-97 for soil profile *Sb*).

Next in the research Vázquez designed residences with current seismic zone requirements and studied their behavior. The residences were designed using the most typical sizes and parameters found in the field survey but satisfying all seismic zone requirements of the UBC – 97 and the ACI 318-99. The residences were evaluated with and without topographic amplification, considering an amplification factor of 2 developed by Arroyo (2001). Since the analysis were based on the Capacity Spectrum Method and the amplification factors were based on the peak ground acceleration, it was necessary to establish how the amplification factors will be applied to the corresponding spectrum. The amplification factors obtained by Arroyo were defined in terms of the peak ground acceleration, which means that these factors can be applied directly to the seismic coefficient  $C_a$  of the UBC- 97. First the seismic coefficients  $C_a$  and  $C_v$  for a particular soil profile were obtained. The ratio between the coefficients  $C_a$  and  $C_v$  was then calculated. Finally the amplification factor from the Arroyo report was applied to the



seismic coefficient  $C_a$  and to the corresponding seismic coefficient  $C_v$  using the ratio previously obtained. After the amplified response spectra were obtained, Capacity Demand plots were generated. The designed residences presented a very good behavior when compared with the capacity demand without an amplification factor. The Capacity Demand plot showed that all the residences resisted the demand almost linearly. However, none of the residences were able to withstand earthquakes described by the amplified spectra. Vázquez concluded that it is essential to include the topographic amplification effects in the seismic design provisions in order to obtain residences that will survive under amplified motions.

The last part of the Vázquez study consisted of a Nonlinear Time History Analysis or Non-linear Dynamic Transient Analysis. All the typical residences studied collapsed when subjected to an earthquake record compatible with the UBC-97 for  $S_b$  soil type with topographic amplification. All the designed residences were capable of resisting the  $S_b$  and  $S_e$  soil type earthquake. However, none of the designed residences were capable of resisting the  $S_e$  soil type amplified earthquake. The results of the analyses were used to select a seismic rehabilitation technique. Vázquez recommended that the most practical rehabilitation system to take care of the deficiencies of the typical residences is the reinforced concrete structural walls.

González (2007) in his thesis “Retrofitting of R/C Structures on Gravity Columns using inverted Y Steel Bracings” examined the use of inverted-Y steel bracing system as a retrofitting measure. The system performance was evaluated against shear wall retrofits which was the option suggested by Vázquez. González analyzed the structures previously studied by Vázquez and compared the results. To test the structural integrity of the structures, he used four earthquakes with and without amplification to emulate the hillside conditions. The selected earthquake records were a synthetic accelerogram developed for the Mayagüez area, a Northridge (1994) record, a Kobe (1995) record and an Uzbekistan (1976) record. The results showed that most models suffered extensive damage and collapse when subjected to earthquakes without amplification and they collapsed in all cases when the amplification factor was utilized. He concluded

that all structures needed retrofitting to prevent extensive damage in earthquakes without amplification and to prevent collapse when subjected to amplified earthquakes. The building prototypes were retrofitted with the inverted Y-shape steel frame and numerically analyzed in order to develop design guidelines. The size and placement of retrofits were found to be a function of geometric and topographic properties such as the building footprints, column heights, number of bays, and whether or not the earthquake is amplified. He concluded that the inverted-Y retrofit is more cost effective compared to the shear walls. According to González, in the aftermath of an earthquake, only the shear links will most likely need to be replaced. Easy reparability is an added cost benefit of these systems over the shear wall retrofits.

## **1.5 SUMMARY OF THE CHAPTERS**

This dissertation is composed of eight chapters. A brief account of their contents is provided next:

Chapter 1 presents the purpose of the study, objectives, methodology and previous works.

Chapter 2 contains a description of typical residential houses built over hilly terrain based on present and past inventory.

Chapter 3 explained the criteria used to propose the three dimensional analytical models. It introduces the general modeling details and geometry of the models.

Chapter 4 presents a brief background of nonlinear analysis. The main points for conducting pushover and time history analysis with SAP2000 are discussed. It presents the nonlinear properties (material, moment curvature relations for beams and columns). The description of the earthquake ground motions records selected as input for the nonlinear time history analysis is presented.

Chapter 5 explains the Capacity Spectrum Method (CSM) used to establish the residences seismic performance.

Chapter 6 presents the results of the nonlinear pushover and time history analyses.

Chapter 7 analyses a selection of models with the proposed rehabilitation strategy.

Chapter 8 presents significant conclusions from this study and future scope of research in the area.

## CHAPTER 2. FIELD SURVEY OF STRUCTURES OVER HILLY TERRAIN

---

### 2.1 INTRODUCTION

In order to investigate the seismic behavior of typical residences built over slope terrain, several three dimensional analytical models were proposed in this study, based on a field survey.

In hilly regions, construction is constrained by local topography resulting in the adoption of unequal column heights within a story, which results in drastic variation in stiffness of the columns of the same story. The short, stiff columns on uphill side attract much higher lateral forces and thus they are prone to damage. It must be noted that the dynamic characteristics of residences over slope terrain are different from those on flat topography; as the former are irregular and unsymmetrical in both horizontal and vertical directions.

Residential houses built over hilly terrain are normally older structures that consist of an essentially complete gravity frame system assembly of reinforced concrete columns and beams. The house is mostly located at the road level and in the underside are located the gravity columns supporting the main structure. Depending on the hilly characteristics of the terrain, residences may have 1 to 3 levels of gravity columns.

#### 2.1.1 FIELD SURVEY OF TYPICAL STRUCTURES

##### Residence 1

The first residence visited is located in the municipality of Aguada (Figure 2-1). The residence was built during 1975. There are 3 bays in the X direction and 2 bays in the Y

direction, where the X direction is perpendicular to the road and the Y direction is parallel to the road (Figure 2-2a). The columns in the Y and X direction are separated 13 ft. and 12 ft. respectively. The total floor area is 936 ft<sup>2</sup>. Columns dimensions are 12" x 12" and the beams dimension are 12" X 18". Originally the structure did not have an intermediate slab and the owner explained that it was decided later to build a slab to interrupt the height of the columns (Figure 2-2b). To support the earth pressure from the slope, the residence have a masonry block wall (Figure 2-2a). A summary of the structural parameters of residence 1 is shown in Table 2-1. The slope of the terrain was measured between the highest and lowest point of the columns at ground level.

**Table 2-1.** Summary of Structural Parameters of Residence 1

<b># span Y</b>	2	
span length (ly)	13	ft
total length (Ly)	26	ft

<b># span X</b>	3	
span length (lx)	12	ft
Total length (Lx)	36	ft

<b>Total floor area =</b>	936	ft <sup>2</sup>
---------------------------	-----	-----------------

<b># stories</b>	3	
Residence height	9	ft
story 2	8.5	ft
story 1	2 to 7.5	ft

<b>Columns</b>	12 x 12	in
<b>beams</b>	6 x 16	in
<b>Slope</b>	13°	



**Figure 2-1.** Residence 1 in Aguada

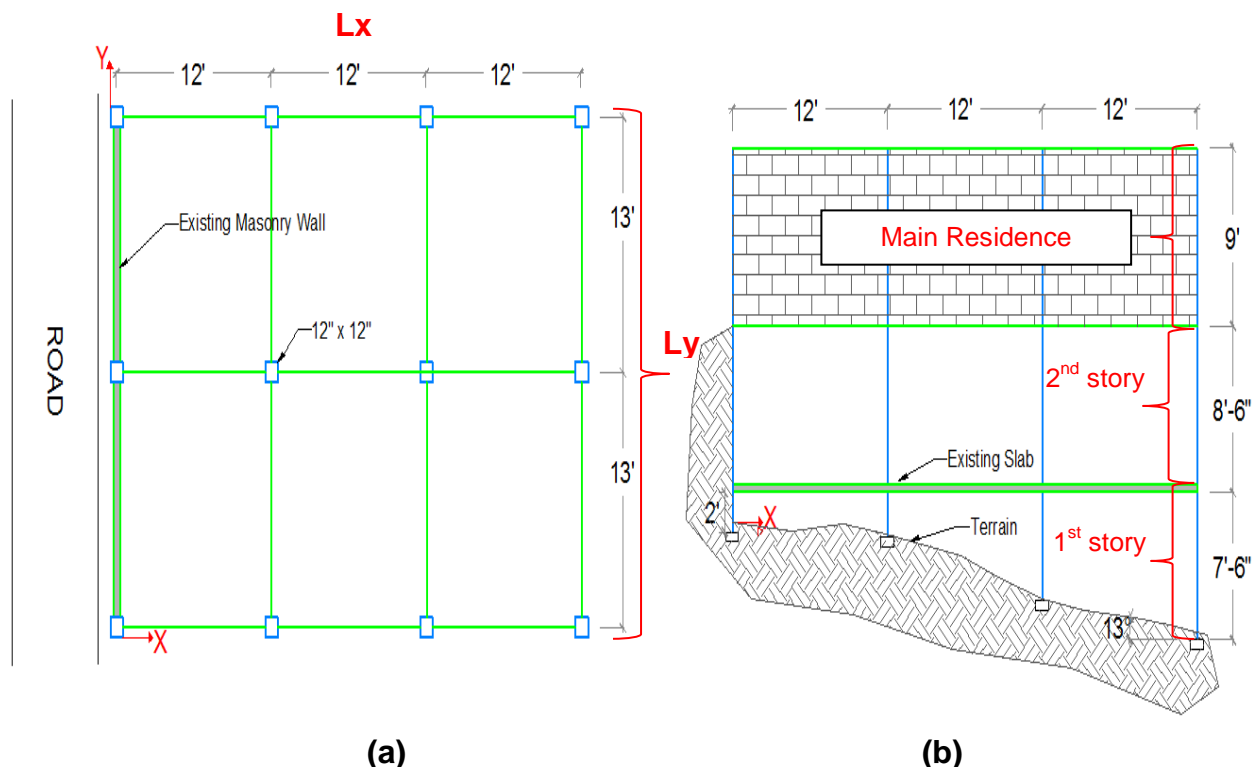


**Figure 2-2.** Residence 1 Aguada. (a) Plan View. (b) Frame Elevation

## Residence # 2

This residence is in the municipality of San Germán (Figure 2-3). It was built over 20 years ago. The columns in the Y and X direction are separated 14.5 ft. and 8.5 ft. respectively. There are 2 bays in both the X and Y direction. The floor area is 493 ft<sup>2</sup>. The columns dimensions are 16" x 6" and the beams dimension are 6" X 16". The retaining wall is a masonry block wall. A summary of the structural parameters of residence 2 is shown in Table 2-2.

**Table 2-2.** Summary of Structural Parameters of Residence 2

<b># span Y</b>	2	
span length (ly)	14.5	ft
total length (Ly)	29	ft

<b># span X</b>	2	
span length (lx)	8.5	ft
Total length (Lx)	17	ft

<b>Total floor area =</b>	493	ft <sup>2</sup>
---------------------------	-----	-----------------

<b># stories</b>	2	
Residence height	9	ft
story 1	6.5 to 11.5	ft

<b>Columns</b>	16 x 6	in
<b>beams</b>	6 x 16	in
<b>Slope</b>	16°	



**Figure 2-3.** Residence 2 in San Germán

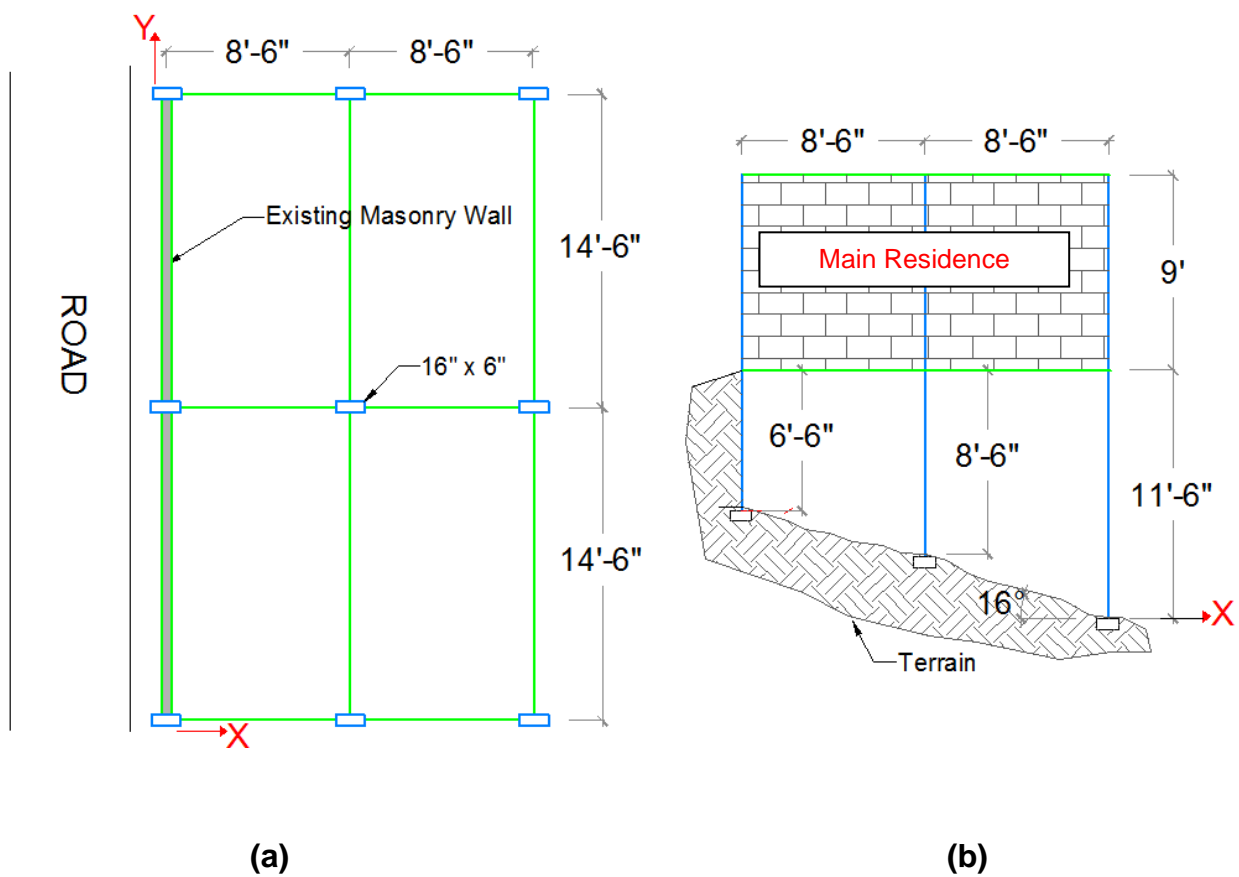


**Figure 2-4.** San Germán Residence 2. (a) Plan View (b) Frame Elevation: Side View

### **Residence 3**

The third residence visited is located in the municipality of San Sebastian (Figure 2-5). The residence was built 15 years ago. The columns dimensions are 8" x 16" and beams dimension are 21" X 6". There are 3 bays in the Y direction (parallel to the road) and 3 bays in the X direction (perpendicular to the road). The columns in the Y and X direction are separated 11 ft. and 15 ft. respectively. The floor area is 1485 ft<sup>2</sup>. It can be observed that the residence did not have beams in the weak direction (Figure 2-5). A summary of the structural parameters of residence 3 is shown in Table 2-3.

**Table 2-3.** Summary of Structural Parameters of Residence 3

<b># span Y</b>	3	
span length (ly)	15	ft
total length (Ly)	45	ft

<b># span X</b>	3	
span length (lx)	11	ft
Total length (Lx)	33	ft

<b>Total floor area =</b>	1485	ft <sup>2</sup>
---------------------------	------	-----------------

<b># stories</b>	3	
Residence height	9	ft
story 2	8.5	ft
story 1	0 to 6	ft

<b>Columns</b>	21 x 6	in
<b>beams</b>	8 x 16	in
<b>Slope</b>	20°	





**Figure 2-5.** Residence 3 in San Sebastian

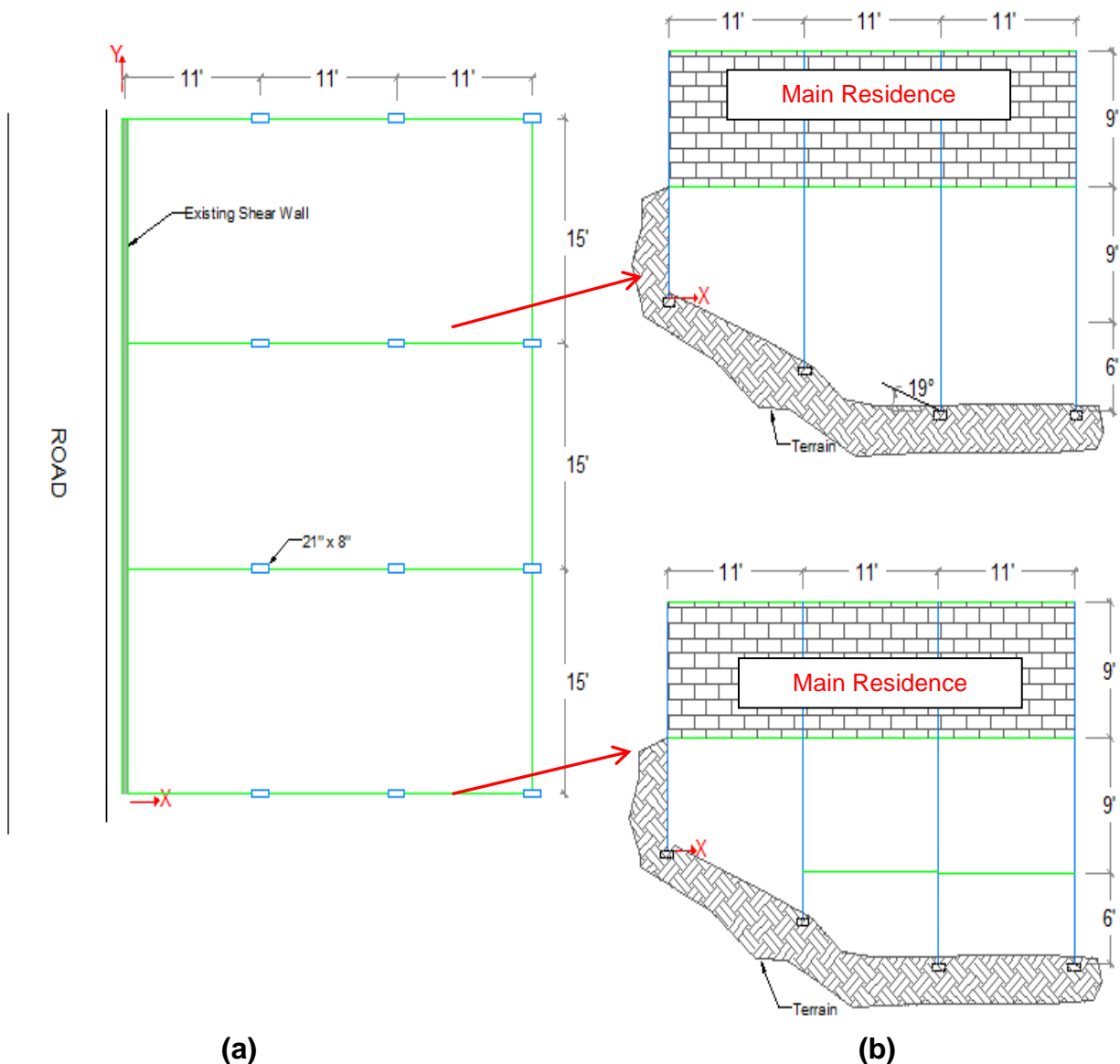


**Figure 2-6.** San Sebastian Residence 3. (a) Plan View (b) Frame Elevation: Side View

#### **Residence 4**

This residence is located in the municipality of San Sebastian (Figure 2-7). The residence was built approximately 15 years ago. The structural drawings were provided and some were re-drawn for clarity purposes. Figure 2-8a presents the footing plan view. It can be noticed that the columns orientations vary. There are 4 bays in the Y direction (parallel to the road) and 2 bays in the X direction (perpendicular to the road) of the residence covering a total floor plan of 1440 ft<sup>2</sup>. The floor slab is 5.5 inches thick.

The first floor (main structure) is 9 ft high and the remaining floor height varies as shown in Figure 2-8b. The footings and columns sizes and reinforcement are given in Table 2-5. Figure 2-9 shows the structural detail layout for the footings and columns referred to in Table 2-5. Figure 2-10 shows the structural details for the retaining wall. A summary of the structural parameters of residence 4 is shown in Table 2-4.

**Table 2-4.** Summary of Structural Parameters of Residence 4

<b># span Y</b>	2	
span length (ly)	10 to 15	ft
total length (Ly)	45	ft

<b># span X</b>	2	
span length (lx)	13 to 15	ft
Total length (Lx)	29.67	ft

<b>Total floor area =</b>	1335.15	ft <sup>2</sup>
---------------------------	---------	-----------------

<b># stories</b>	2	
Residence height	9	ft
story 2	9	ft
story 1	0 to 4.5	ft

<b>Columns</b>		in
C-1	18 x 8	
C-2	21 x 8	
C-3	30 x 8	
<b>beams</b>	6 x 16	in
<b>Slope</b>	23°	

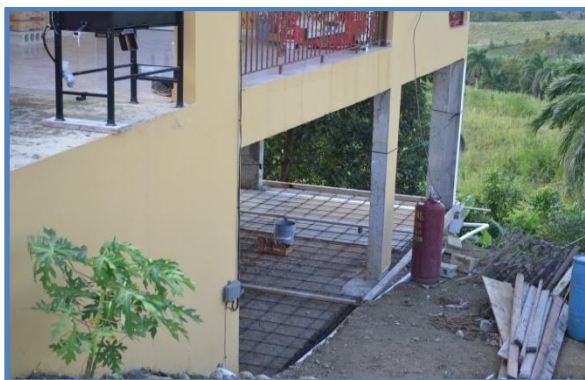
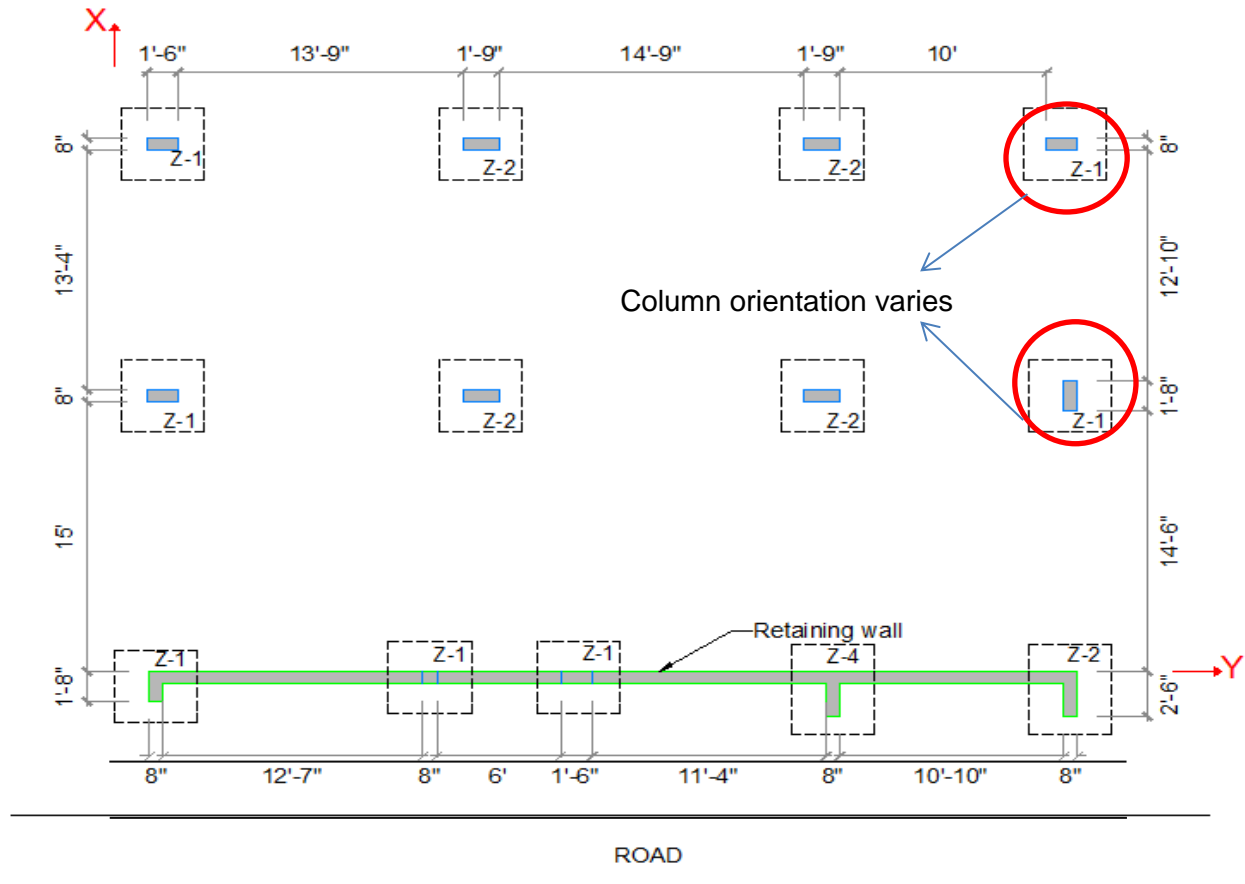
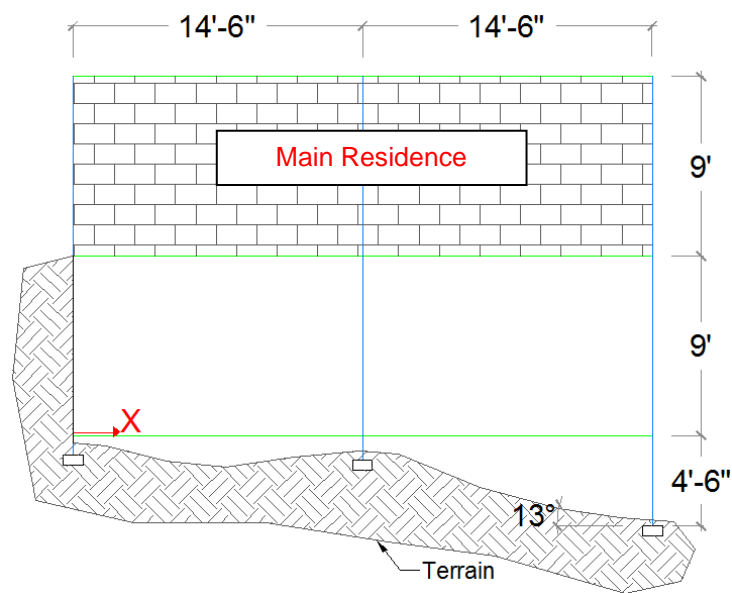


**Figure 2-7.** Residence 4 in San Sebastian



(a)



(b)

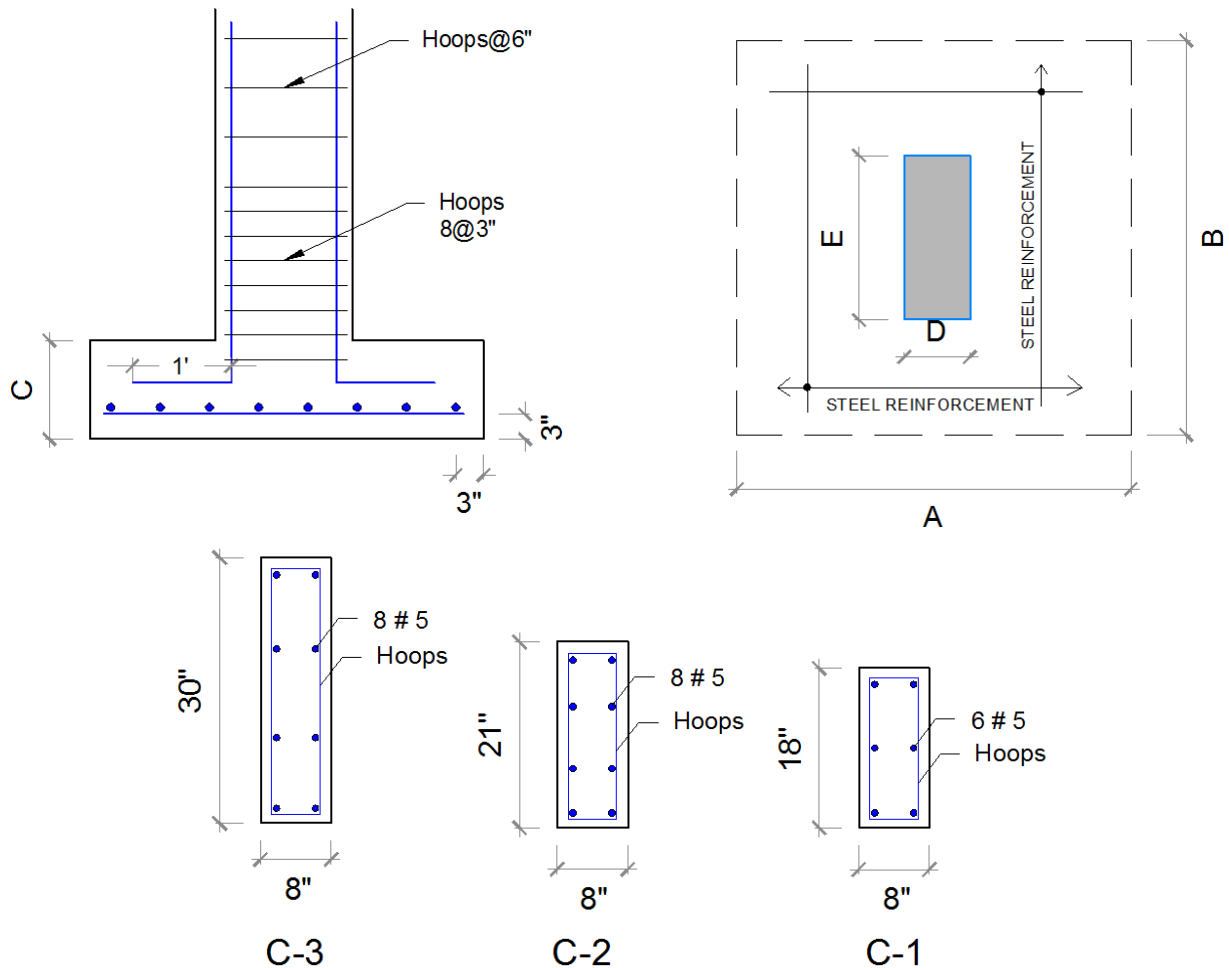
**Figure 2-8.** Residence 4 in San Sebastian. (a) Footing Plan View. (b) Side view

**Table 2-5.** Residence 4 in San Sebastian: Footing and Columns Structural Details

Footing #	A	B	C	Reinforcement	Column #	D	E	Reinforcement
Z-1	4'-0"	4'-0"	12"	# 5 @ 6"	C-1	8"	18"	6 # 5
Z-2	4'-0"	4'-0"	12"	# 5 @ 6"	C-2	8"	21"	8 # 5
Z-3	4'-0"	4'-0"	12"	# 5 @ 6"	C-3	8"	30"	8 # 5
Z-4	4'-0"	5'-0"	12"	# 5 @ 6"				

**Footings dimension  
and rebar reinforcement  
(Figure 2-9)**

**Columns dimension  
and rebar reinforcement  
(Figure 2-9)**



Hoops @ 3" ends of columns, @ 6" rest

**Figure 2-9.** Residence 4 in San Sebastian: Footing and Columns Structural Details

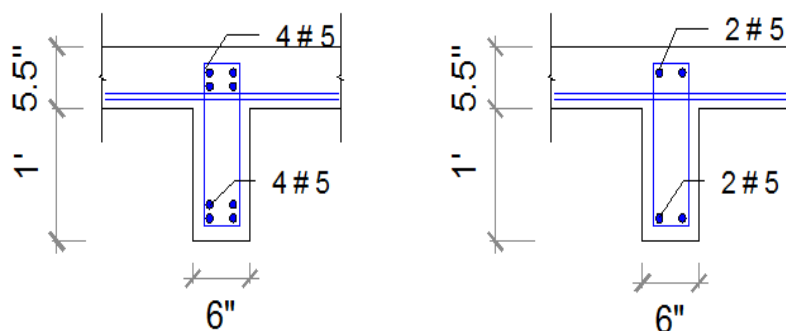


**Figure 2-10.** Residence 4 in San Sebastian: Beams Structural Details

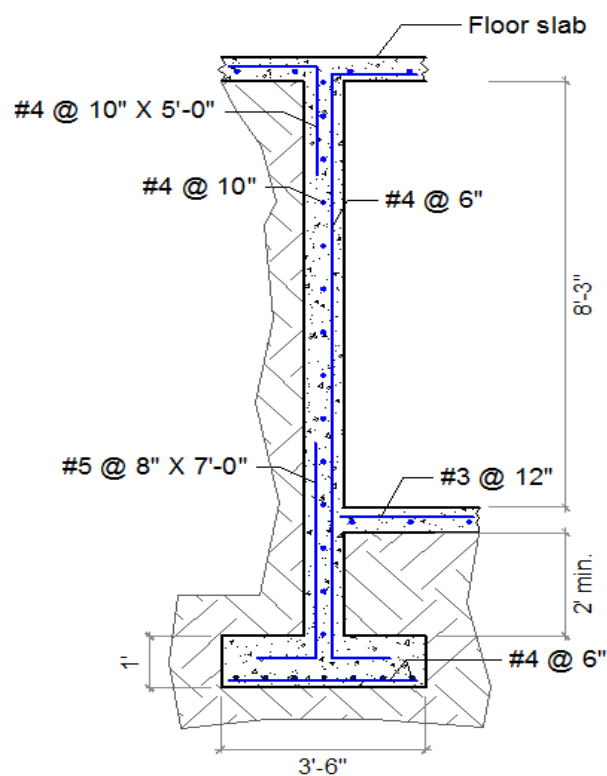


**Figure 2-11.** Residence 4 in San Sebastian: Retaining Wall Structural Details

### **Residence 5**

This residence is located in the municipality of Hormigueros (Figure 2-12). The residence was built approximately 40 years ago. There are 3 bays in each direction (X and Y) the columns in the Y and X direction are separated 12 ft. The floor area is 1296 ft<sup>2</sup>. The columns dimensions are 10" x 10" and the beam dimensions are 10" X 16". To



support the earth pressure from the slope, the residence has a concrete wall. A summary of the structural parameters of residence 5 is shown in Table 2-6.

**Table 2-6.** Summary of Structural Parameters of Residence 5

<b># span Y</b>	3	
span length (ly)	12	ft
total length (Ly)	36	ft

<b># span X</b>	3	
span length (lx)	12	ft
Total length (Lx)	36	ft

<b>Total floor area =</b>	1296	ft <sup>2</sup>
---------------------------	------	-----------------

<b># stories</b>	3	
Residence height	9	ft
story 2	9	ft
story 1	0 to 6	ft

<b>Columns</b>	10 x 10	in
<b>beams</b>	6 x 16	in
<b>Slope</b>	24°	



**Figure 2-12.** Residence 5 in Hormigueros

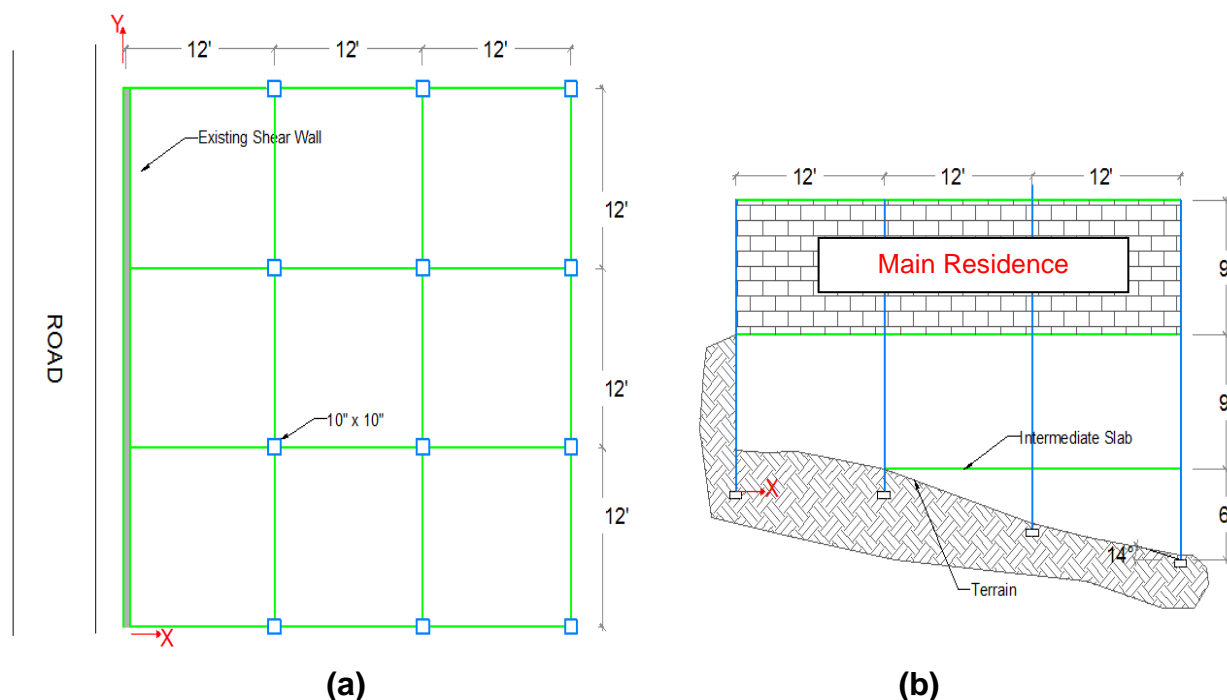


**Figure 2-13.** Residence 5 in Hormigueros. (a) Footing Plan View. (b) Side View

## **Residence 6**

This residence is located in the municipality of Hormigueros. The residence was built 15 years ago. The owner did not allow to visit the area underside near the gravity columns; however some structural details were provided and pictures were taken. As it can be observed from Figure 2-14, the house has 2 stories of gravity columns. There are 3 bays in each both X and Y direction (Figure 2-15). To support the earth pressure from the slope the residence has a reinforced concrete wall. A summary of the structural parameters of residence 6 is shown in Table 2-7.

**Table 2-7.** Summary of Structural Parameters of Residence 6

<b># span Y</b>	3	
span length (ly)	14	ft
total length (Ly)	45	ft

<b># spans X</b>	4	
span length (lx)	12	ft
Total length (Lx)	48	ft

<b>Total floor area =</b>	2160	ft <sup>2</sup>
---------------------------	------	-----------------

<b># stories</b>	4	
Residence height	9	ft
story 3	8	ft
story 2	8	ft
story 1	0 to 3.5	ft

<b>Columns</b>	16 x 6	in
<b>beams</b>	6 x 16	in
<b>Slope</b>	20°	





**Figure 2-14.** Residence 6 in Hormigueros

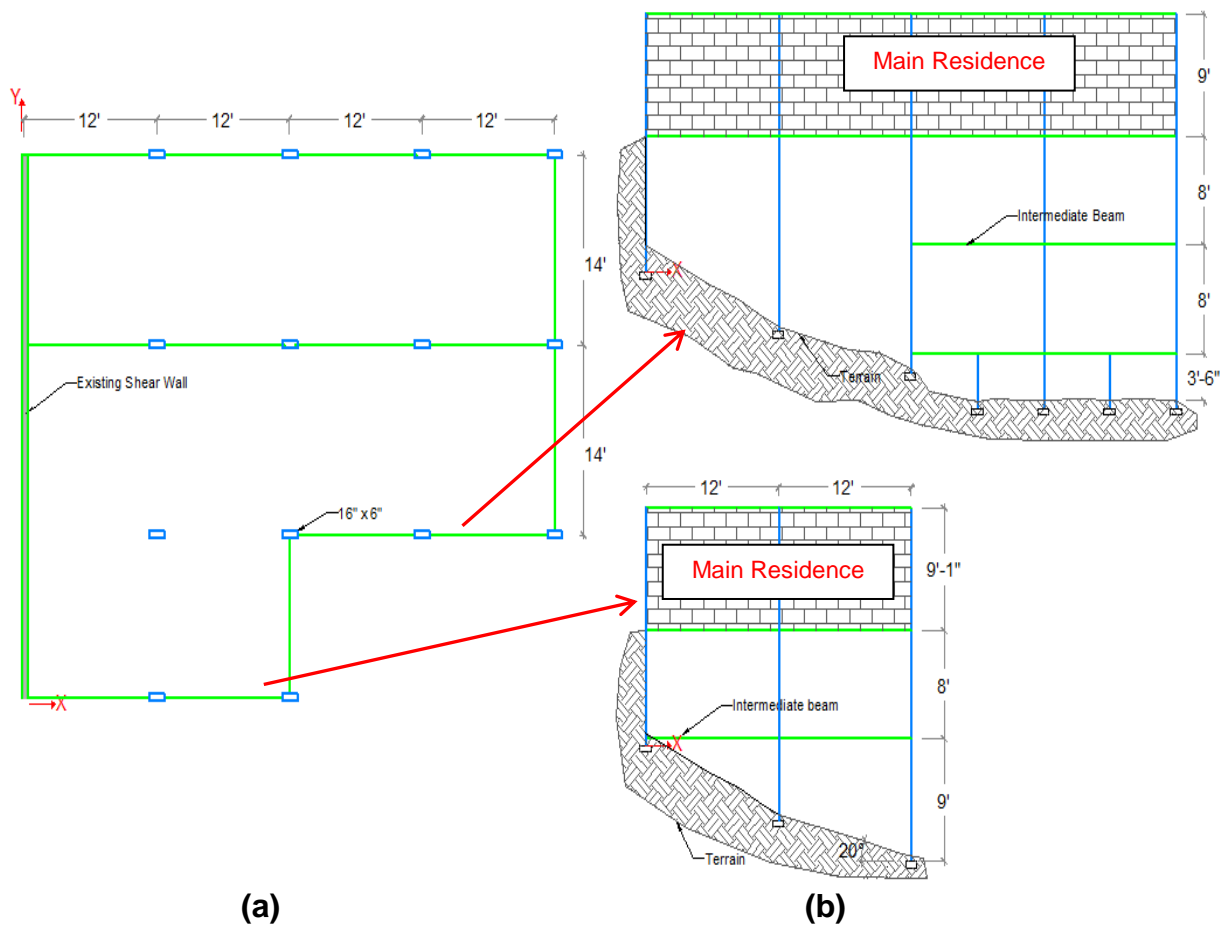


**Figure 2-15.** Residence 6 in Hormigueros. (a) Footing Plan View. (b) Side View

### 2.1.1.1 OTHER RESIDENCES

Below is a compilation of other residences around the Island constructed over hilly terrain. Not enough structural parameters were obtained for these residences however, some important structural deficiencies were observed. The study of these structural deficiencies is not part of the scope of this investigation. However, it is important to keep in mind that the construction of these residences has serious deficiencies that make them even more vulnerable. Figure 2-16 shows a residence with exposed rebar and stirrups along the length of the beams.



**Figure 2-16.** Residence with Exposed Rebar

Figure 2-17 shows examples of residences with vertical irregularities created by uneven vertical distribution of mass and stiffness between floors that may result in concentration of force at certain levels.





**Figure 2-17.** Residences with Vertical Irregularities

Figure 2-18 shows example of residences with poor construction details.



**Figure 2-18.** Residences with Poor Constructions Details

### 2.1.2 FIELD SURVEY OF TYPICAL RESIDENCES (VAZQUEZ 2002)

Residential structural characteristics were collected from the field data survey conducted by Vázquez (2000) and the survey conducted for this study. Vázquez reported a total of 24 houses around Puerto Rico, from 5 municipalities, namely Jayuya, Cabo Rojo, Hormigueros, Yauco and Arecibo. All relevant structural data were documented including column heights, bay lengths, cross-sectional dimensions and steel reinforcements. A summary of these structural parameters for the 24 residences is shown in Tables 2-8 to 2-10.

**Table 2-8.** Summary of the Residences Columns Height. Vázquez (2002)

Height [ft]	From	To	From	To	From	To	Over 20
	8	12	12	16	16	20	
# of Residences	12		6		3		3

**Table 2-9.** Summary of the Column Sections. Vázquez (2002)

Section [in]	From	To	From	To	Exactly
	6X12	6X18	8X12	10X10	12X12
# of Residences	7		8		9

**Table 2-10.** Summary of Residences Spans. Vázquez (2002)

Span [ft] cc.	From	To	From	To	
	8	12	12	16	over 16
# of Residences	12		11		1

The height range is between 8 and 20 ft., where the dominant height was between 8 to 12 feet because these are the practical heights for most residences. The span length of the residences varies from 8 feet to a maximum of 16 feet. The other two parameters considered by Vázquez were the steel reinforcement and the number of stories. He found that basically the two stories is the most common case, since only one structure in the entire inventory has three stories. The steel reinforcement parameter was not found in all the residences because the residences were old and the owners did not have the construction drawings. However, according to the owners, in almost all the cases they used 6 bars size #4 and #5 in the beams and columns. The predominant

configurations were the six #4 bars and six #5 bars for the columns and 6 #4 bars for the beams.

## **CHAPTER 3. THREE DIMENSIONAL MODELS**

---

### **3.1 INTRODUCTION**

The procedures followed to generate the analytical models of three dimensional residential houses are explained in detail in this chapter, including the basic assumptions, the geometry, and the structural parameters.

### **3.2 DEFINITION OF THE ANALYTICAL MODELS**

For buildings with complex configurations or which are susceptible to torsion, pushover models should be three-dimensional (with push force applied along the principal axes) (HAZUS,1997).Two dimensional computer models may be a good approximation for investigating these system. However, due to the vertical irregular geometries of hillside houses the use of three dimensional models is essential, in order to take into consideration torsional effects as well as the structural behavior caused by of the difference in column heights among frames.

#### **3.2.1 GENERAL CHARACTERISTICS OF THE PROTOTYPE MODELS**

Based on the information presented in Chapter 2 a total of 32 prototype models were analyzed. The analytical models were divided into 3 main groups. Table 3-1 presents a summary of the principal characteristics of the cases analyzed. Detailed structural sizes and drawings are discussed and shown below.

**Table 3-1. Summary of Analytical Models**

Model	# stories	X-bay (ft)	Y-bay (ft)	Columns	Beams
<b>Model Group 1</b>					
1.1b	2	10	10	16" x 6"	16" x 6"
1.1c		10	10		
1.1d		10	10		
1.2b		10	15		
1.2c		10	15		
1.2d		10	15		
1.3b		15	10		
1.3c		15	10		
1.3d		15	10		
1.4b		15	15		
1.4c		15	15		
1.4d	↓	15	15	↓	↓
<b>Model Group 2</b>					
2.1b	3	10	10	16" x 6"	16" x 6"
2.1c		10	10		
2.1d		10	10		
2.2b		10	15		
2.2c		10	15		
2.2d		10	15		
2.3b		15	10		
2.3c		15	10		
2.3d		15	10		
2.4b		15	15		
2.4c		15	15		
2.4d	↓	15	15	↓	↓
<b>Model Group 1 with variation</b>					
1.1yb	2	10	10	6" x 16"	16" x 6"
1.1yc				6" x 16"	
1.1.2b				16" x 8"	
1.1.2c				16" x 8"	
1.1.3b				12" x 12"	
1.1.3c				12" x 12"	
1.1.4b				12" x 6"	
1.1.4c	↓	↓	↓	12" x 6"	↓

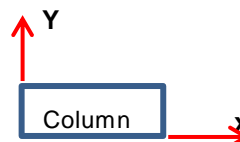
X direction = perpendicular to the road

Y direction = parallel to the road

b = bare frame

c = masonry wall

d = shear wall



Group models 1 have only 2 stories as shown in Figure 3-1; the upper level is where the house stands and the lower level where the gravity columns stand. Group models 2

have 3 stories as shown in Figure 3-2; the upper level is where the house stands and there are 2 levels of gravity columns. For models 1 and 2, the strong direction refers to the direction in which the moment of inertia of the columns is larger (X direction). For models 1 and 2, the span length varies from 10 to 15 feet in each direction. To distinguish between the models 1 and 2 with different span length, the numbers 1 to 4 were added to the names of the cases. Figures 3-3 and 3.4 show the plan view for the different span length arrangements. Only two bays in each orthogonal direction were considered. Model 1.1 with variation has the same span lengths and story levels as model 1.1 but the columns orientation and columns dimensions were changed in order to investigate their effect in the results.

The house height level is 9 feet for all analytical models. For model group 2 the slope terrain considered varies from 15 to 25 degrees approximately. For model group 1 the slope terrain considered varies from 9 to 14 degrees approximately. Figure 3-5 to 3-8 shows the elevation of each frame. When the bay length was increased, the length of the columns did not change, only the slope of the terrain changed.

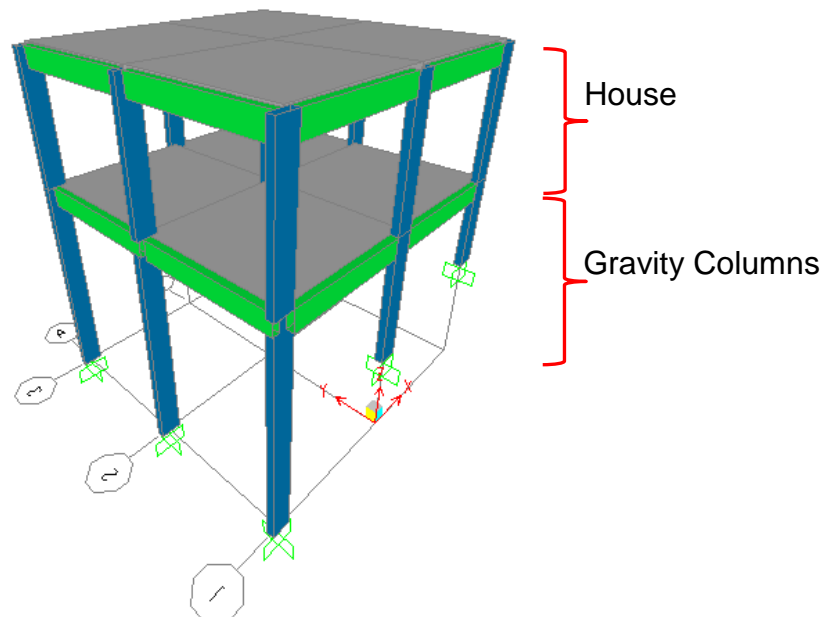


**Figure 3-1.** Typical Model Type 1: 2 Story Residence



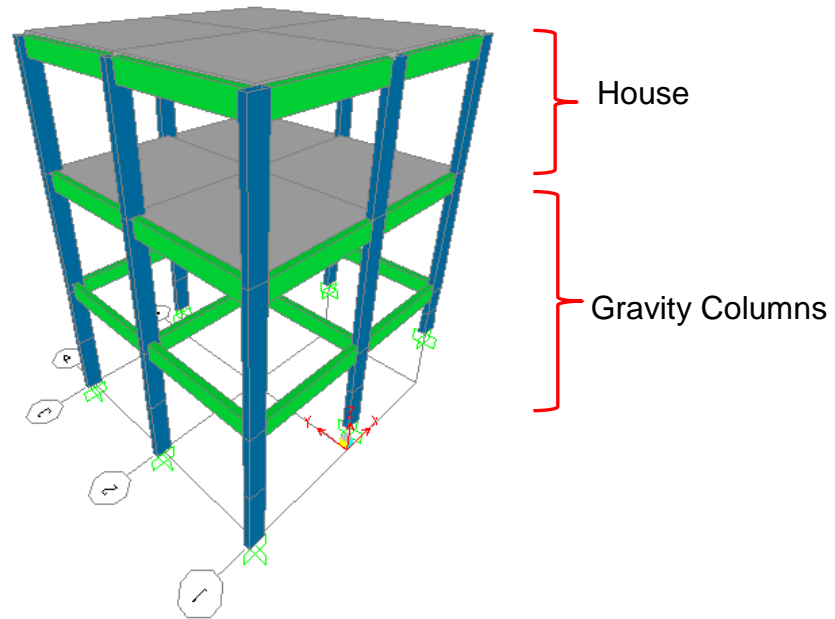


**Figure 3-2.** Typical Model Type 2: 3 Story Residence

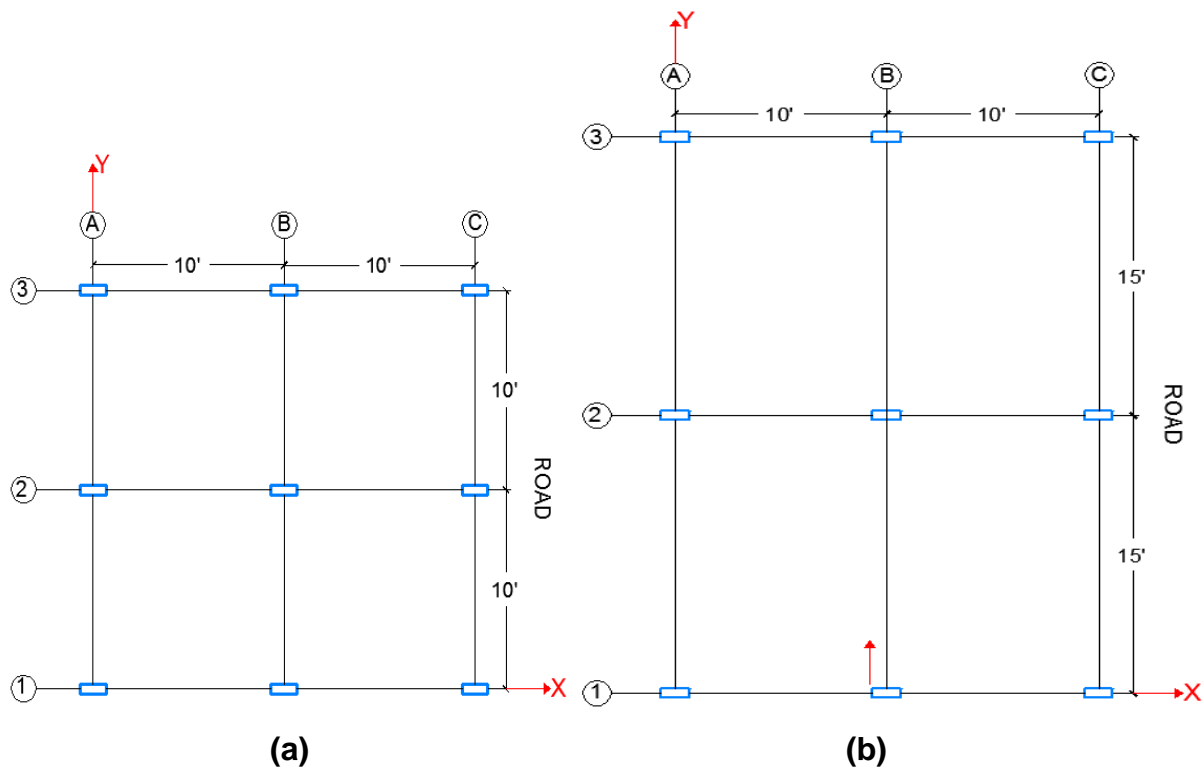


**Figure 3-3.** (a) Plan View for Model 1.1 / 2.1, (b) Plan View for Model 1.2 / 2.2,

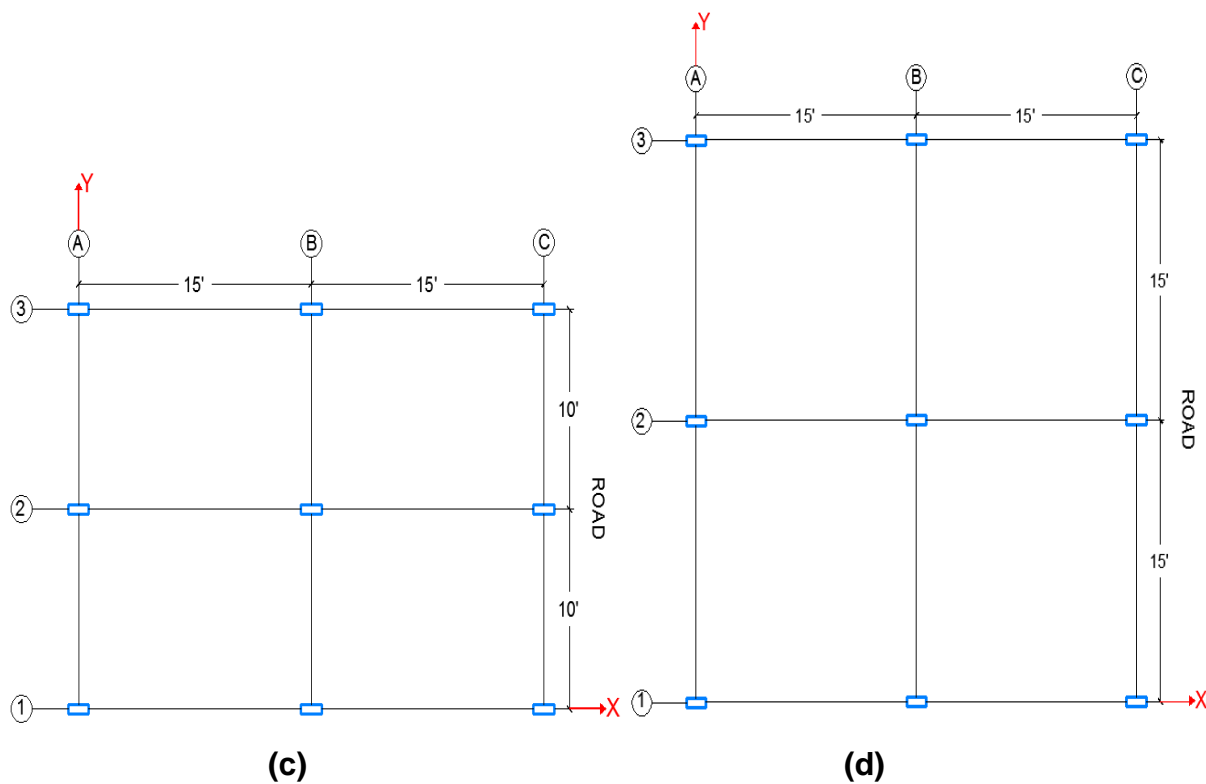


**Figure 3-4.** (c) Plan View for Model 1.3 / 2.3, (d) Plan View for Model 1.4 / 2.4

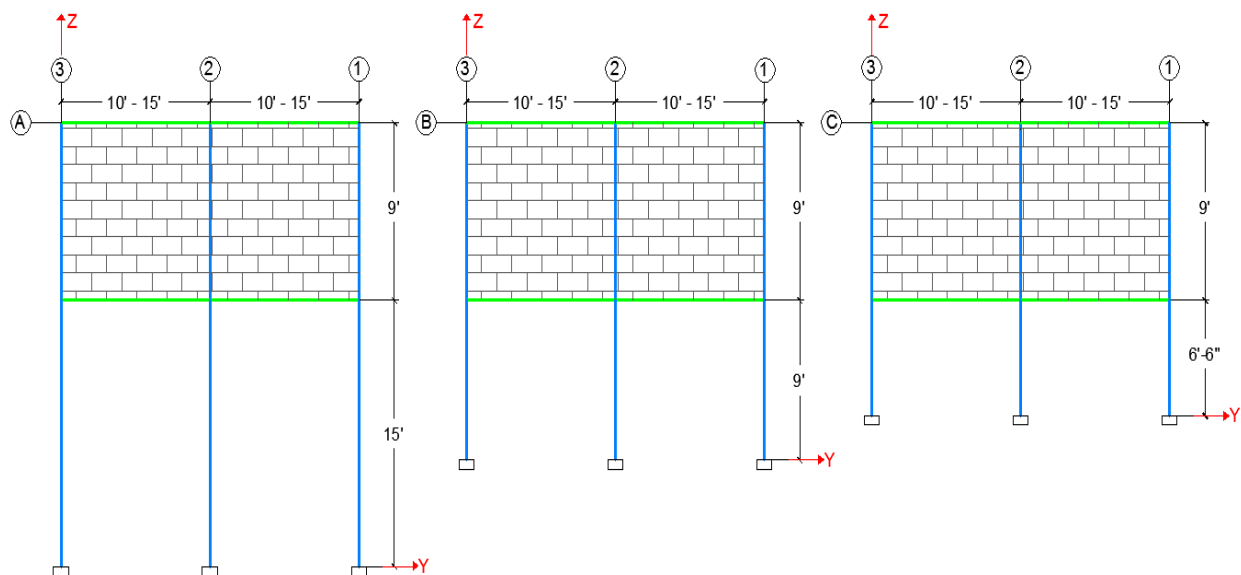


**Figure 3-5.** Elevation at Frames A, B and C for Models 1

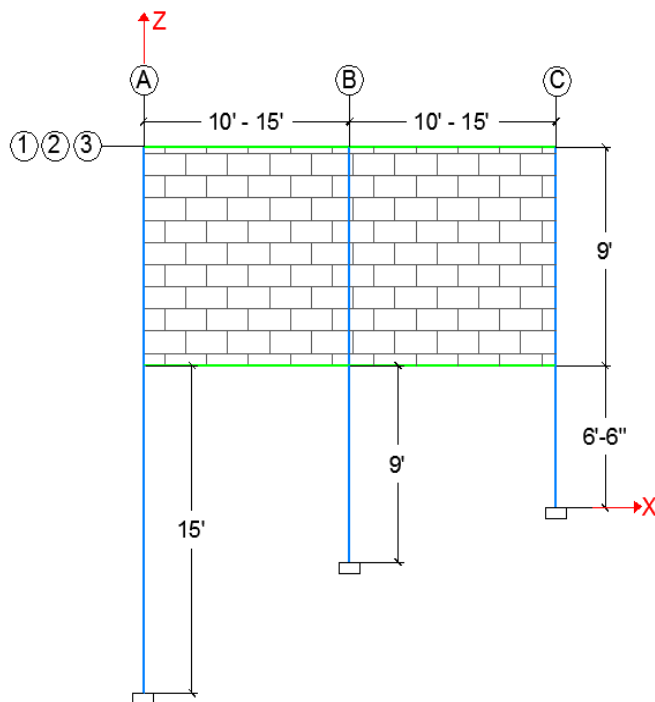


**Figure 3-6.** Elevation at Frames 1, 2 and 3 for Models 1

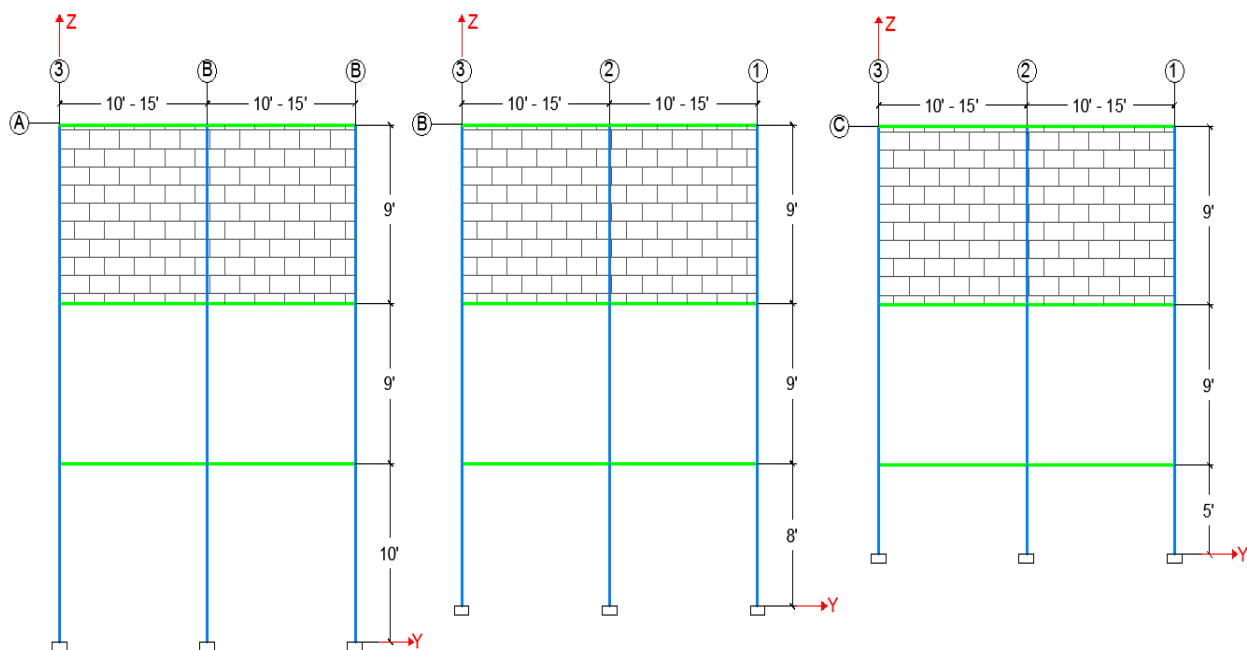


**Figure 3-7.** Elevation at Frames A, B and C for Models 2

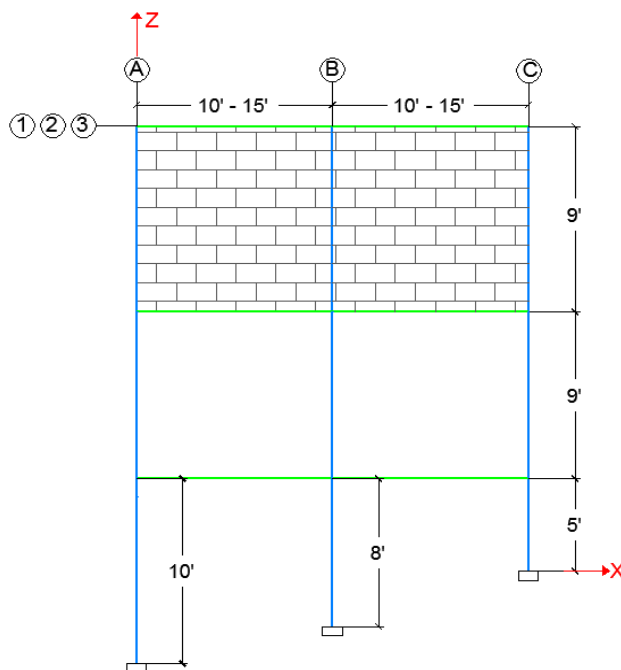


**Figure 3-8. Elevation at Frames 1, 2 and 3 for Models 2**

### 3.2.2 MODELING THE RETAINING WALL

Typically these residences have a retaining wall constructed to support the earth pressure. These walls are often constructed of masonry block walls or reinforced concrete as shown in Figure 3-8. The presence of a retaining wall contributes to an unsymmetrical distribution of mass and stiffness in the residences, since this unique wall is located at an edge frame as shown in Figure 3-9a. One of the main sources for the torsional response of structures is the unsymmetrical distribution of mass or lateral load resisting elements in the plan of the structure which is usually referred to mass or stiffness eccentricity (Mansuri, 2009). This study evaluated this effect on the residences as shown in Figures 3-10 and 3.11. The letters “b”, “c”, and “d” were added to the names of the cases, “b” stands for models analyzed only as frames without considering retaining walls, “c” indicates models analyzed with masonry block walls, and “d” identifies the models analyzed with RC shear walls.



(a)



(b)

**Figure 3-9.** (a) Residence with Masonry Block Wall. (b) Residence with Shear Wall

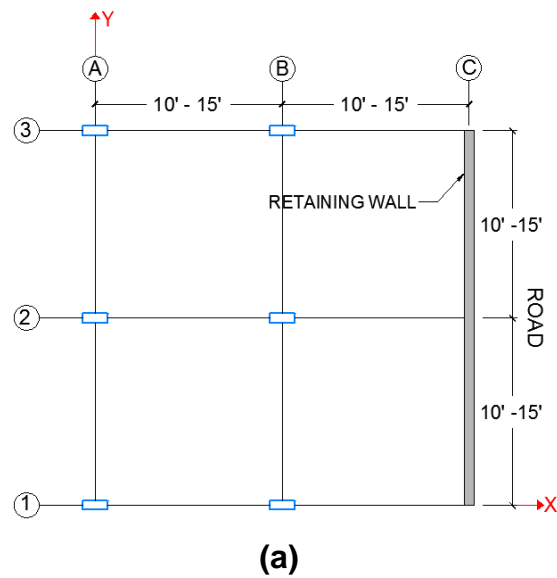


**Figure 3-10.** Typical Plan View.

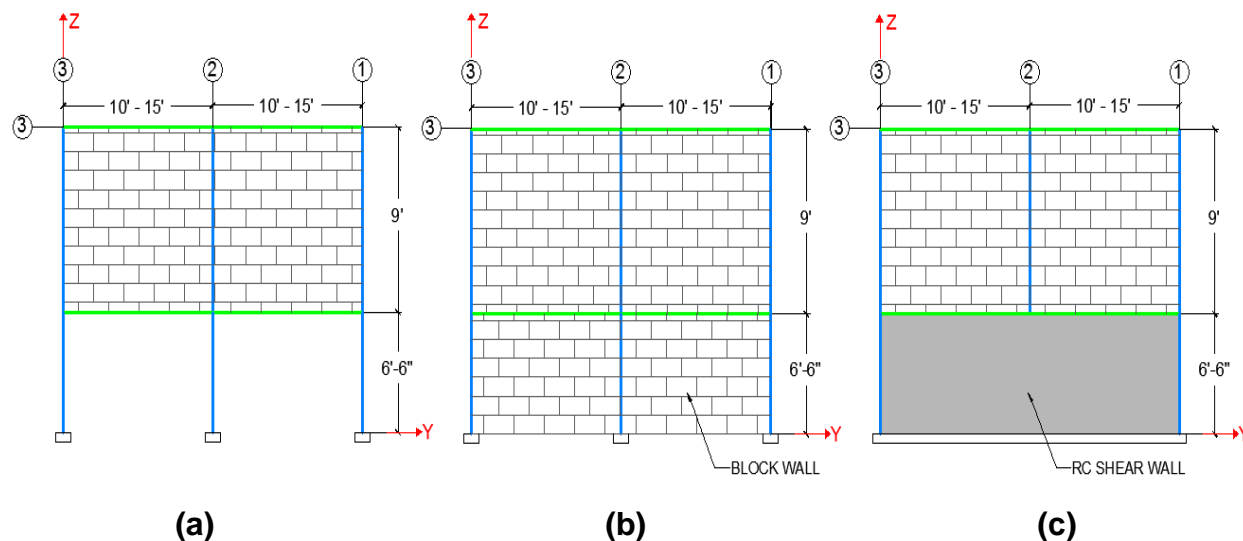


**Figure 3-11.** (b) Side View Model type “b” Analyzed as Frame (c). Side View Model Type “c” Analyzed with Masonry Block Walls. (d) Model Type “d” Analyzed with Shear Walls

### 3.2.3 MODELING MASONRY WALLS AS DIAGONAL STRUT ELEMENTS

Masonry infill walls are widely used as partitions in Puerto Rico residential construction. The design philosophy considers these masonry walls as partitions, not as structural walls (Vélez, 2007). However, despite often being considered as non-structural elements, they affect both the structural and non-structural performance of a structure. Masonry infill walls have a considerable stiffness and strength and they have significant effect on the seismic response of the structural system. Because of the potential negative consequences of ignoring the structural role of masonry infill walls, proper consideration of infill walls is essential in any structural analysis of RC frame structures with masonry infill walls. The most common method of modeling masonry infill walls is to use the equivalent diagonal compression struts (Figure 3-12).

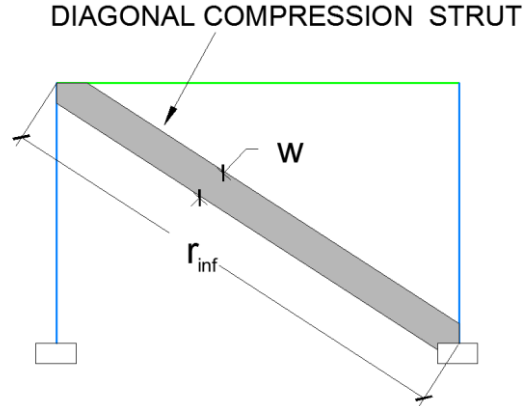


**Figure 3-12.** Diagonal Strut Model

Different effective widths ( $w$ ) of the equivalent diagonal strut in a solid infill wall has been proposed by researchers. A high value of  $w$  will result in a stiffer structure, and therefore potentially higher seismic response (Paulay and Priestley, 1991). Paulay and priestley suggested a conservative value of:

$$w = \frac{r_{inf}}{4} \quad (3-1)$$

where:

$r_{inf}$  : length of the diagonal strut.

The effect of infilled frames with openings (doors and windows) is not considered in equation 3-1. The experimental results obtained by Velez (2007) showed that an infilled frame with a 25 % area of opening reduces the stiffness of the infill wall by 34 to 40% as compared with that of a similar infilled frame with a solid panel. Based on experimental and analytical research it was found that an infilled frame with an opening of size 20%–30% of the wall area on either of the loaded diagonal reduces the stiffness by 85 to 90% as compared with that of a similar infilled frame with a solid panel (Mallick and Garg, 1971). FEMA 356 (2000) indicates that it is possible to evaluate the local effect of the perforated infill panel using multiple compression struts. However, for the purpose of this investigation the effect of openings on the lateral stiffness of the infilled frame was

represented by a diagonal strut of reduced width. A reduction factor of 50 % of equation 3-1 for the effective width of the diagonal strut was used, as shown in equation (3-2).

$$w = \frac{r_{inf}}{8} \quad (3-2)$$

The thickness of the equivalent strut is same as the masonry wall's thickness ( $t = 6$  inch). The masonry infill panel material properties to calculate the equivalent strut capacity were based on Velez (2007) experimental work. Table 3-2 shows the material properties for the equivalent diagonal strut.

**Table 3-2.** Equivalent Masonry Strut's Material Properties

Description	Value
Compressive strength ( $f'_m$ )	1500 psi
Modulus of Elasticity ( $E_m$ )	1125 psi
Specific Weight ( $\gamma$ )	130 lb/ft <sup>3</sup>
Thickness ( $t$ )	6 in

### 3.2.4 DEAD AND LIVE LOADS

Gravity loads consisting of dead loads and 20% of live loads were considered in pushover and nonlinear time history analyses. The structure load consists of dead loads which are the masonry block wall (partition), slab weight, beam and column weight, and live load. A slab thickness of 5 inches was considered for the floor and roof. Additional weight from topping and floor tiles were considered by increasing the floor slab 0.5 inches. The weight of the main structural components of beams and columns (frame members) and slabs (area sections) was accounted for by using the self-weight option in SAP2000. The structure self-weight is automatically computed based on element volume and material density. A specific weight of 150 lb/ft<sup>3</sup> was used for reinforced concrete. ASCE recommends using 44 psf for hollow concrete masonry blocks, and in order to consider surface finishing a dead weight of 50 psf for the masonry block walls (partitions) was used. The dead weight of the masonry block was assumed to act as a uniformly distributed load on the beam. The live load on the floor was 40 psf and the live

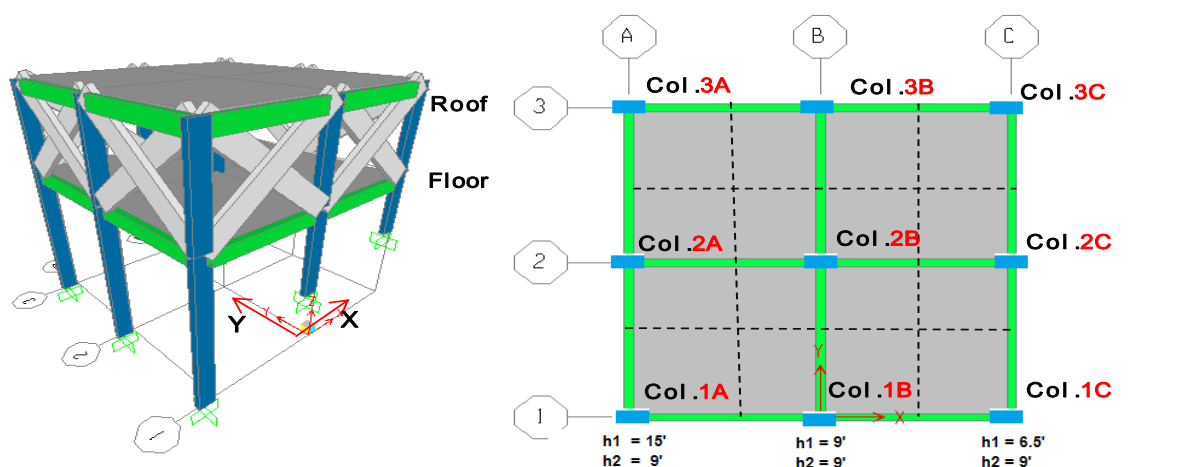


load on the roof was 20 psf. Live loads were assigned as uniform area load on the slab elements.

Sections 3.2.5 to 3.2.7 describe in detail the geometry, section dimensions and other structural parameters for each model.

### **3.2.5 ANALYTICAL MODELS 1**

Tables 3-3 to 3-6 present the geometry, cross section dimension, applied loads and mass calculation assigned to each node at the roof and floor level for group Model 1. As mentioned before, the mass calculation for the roof and floor levels only include the weight of the partitions (masonry block walls) and reduced live load. Included in these tables are the screen shot of the 3D models directly from SAP2000.

**Table 3-3. Parameters for Model 1.1**

Story	Height (ft)	Span X (ft)	Span Y (ft)	Cross section		Reinforcement	
				beam (in)	column (in)	beam	column
1	15 - 6.5	10	10	6 x 16	16 x 6	6 # 4	6 # 4
2	9	10	10	6 x 16	16 x 6	6 # 4	6 # 4

X-bay	2	<i>strong axis</i>
Y-bay	2	

Floor Load		
Wslab	0.063	ksf
20% Live	0.008	ksf
Partitions	0.050	ksf

Roof Load		
Wslab	0.063	ksf
20% Live	0.004	ksf

\*\* 5.5 inch slab was used in the program to account for: topping and tiles

### Masonry Block Wall - Distributed Load Calculation

Partitions	0.375	k/ft	in 7.5 ft height
Partitions	0.225	k/ft	40 % reduction window/ door openings

### Mass Distribution - tributary area

*Mass Floor (Partitions + Live) added to model*

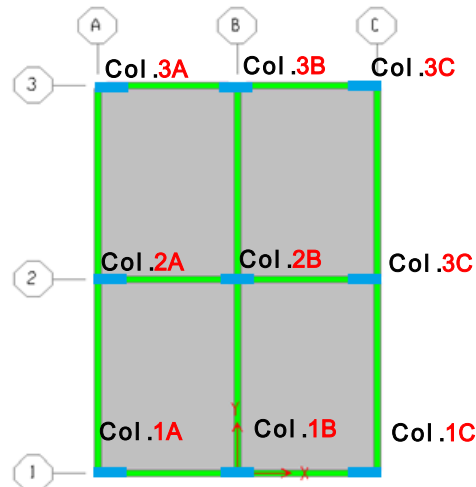
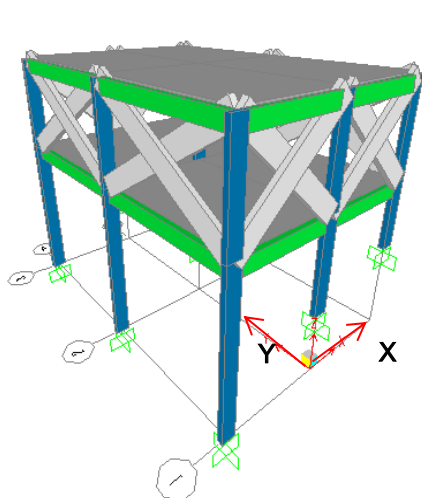
Columns	lx(ft)	ly(ft)	W (kips)	m (k-s <sup>2</sup> /ft)
3A 3C 1A 1C	5	5	2.450	0.076
2B	10	10	5.300	0.165
3B 1B	10	5	3.775	0.117
2A 2C	5	10	3.775	0.117

mass added to the nodes of the models in SAP2000. Area / frame element masses is automatically add by the program

*Mass Roof (Live) added to model*

Columns	lx(ft)	ly(ft)	W (kips)	m (k-s <sup>2</sup> /ft)
3A 3C 1A 1C	5	5	0.100	0.003
2B	10	10	0.400	0.012
3B 1B	10	5	0.200	0.006
2A 2C	5	10	0.200	0.006

mass added to the nodes of the models in SAP2000. Area / frame element masses is automatically add by the program

**Table 3-4.** Parameters for Model 1.2

Story	Height (ft)	Span X (ft)	Span Y (ft)	Cross section		Reinforcement	
				beam (in)	column (in)	beam	column
1	15 - 6.5	10	15	6 x 16	16 x 6	6 # 4	6 # 4
2	9	10	15	6 x 16	16 x 6	6 # 4	6 # 4

X - bay	2	<i>strong axis</i>
Y - bay	2	

Floor Load		
Wslab	0.063	ksf
Live	0.008	ksf
Partitions	0.225	k/ft

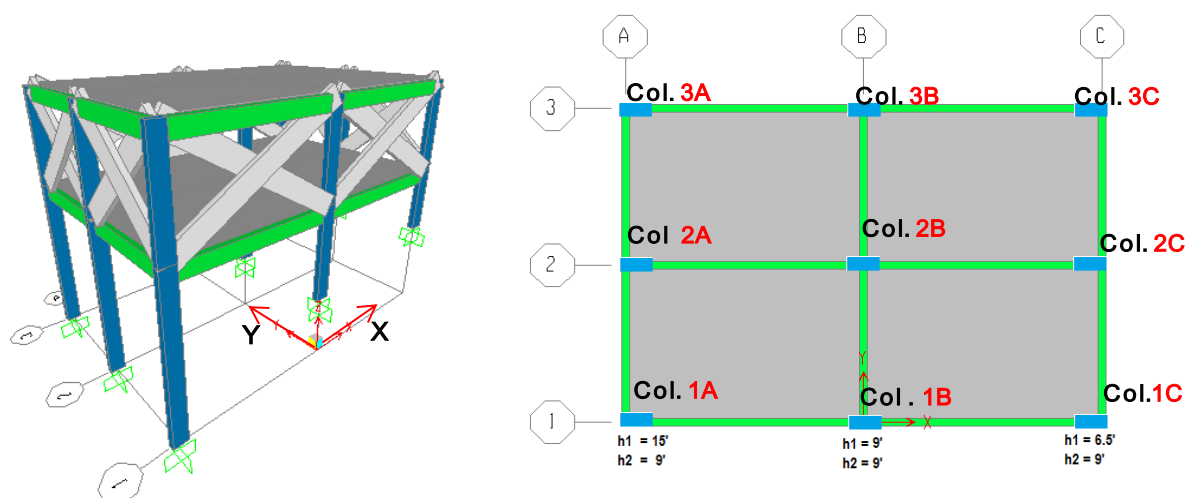
Roof Load		
Wslab	0.0625	ksf
Live	0.0040	ksf

**Mass Distribution - tributary area***Mass Floor (Partitions + Live) added to model*

Columns	lx(ft)	ly(ft)	W (kips)	m (k-s <sup>2</sup> /ft)
3A 3C 1A 1C	5	7.5	3.113	0.097
2B	10	15	6.825	0.212
3B 1B	10	7.5	4.538	0.141
2A 2C	5	15	5.100	0.158

*Mass Roof ( Live ) added to model*

Columns	lx(ft)	ly(ft)	W (kips)	m (k-s <sup>2</sup> /ft)
3A 3C 1A 1C	5	7.5	0.150	0.005
2B	10	15	0.600	0.019
3B 1B	10	7.5	0.300	0.009
2A 2C	5	15	0.300	0.009

**Table 3-5. Parameters for Model 1.3**

Story	Height (ft)	Span X (ft)	Span Y (ft)	Cross section		Reinforcement	
				beam (in)	column (in)	beam	column
1	15 - 6.5	15	10	6 x 16	16 x 6	6 # 4	6 # 4
2	9	15	10	6 x 16	16 x 6	6 # 4	6 # 4

X-bay	2	<i>strong axis</i>
Y-bay	2	

Floor Load		
Wslab	0.063	ksf
20% Live	0.008	ksf
Partitions	0.225	k/ft

Roof Load		
Wslab	0.063	ksf
20% Live	0.004	ksf

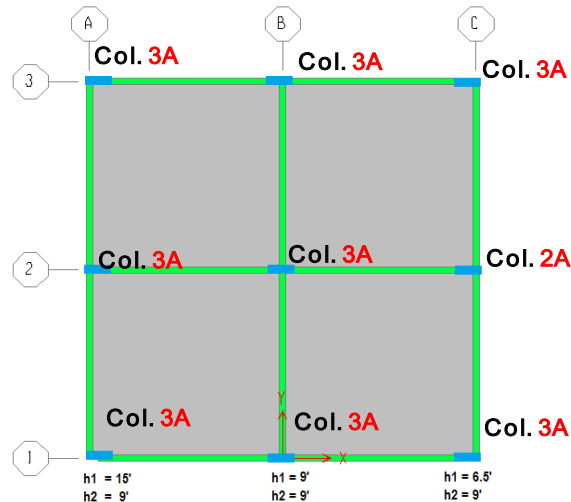
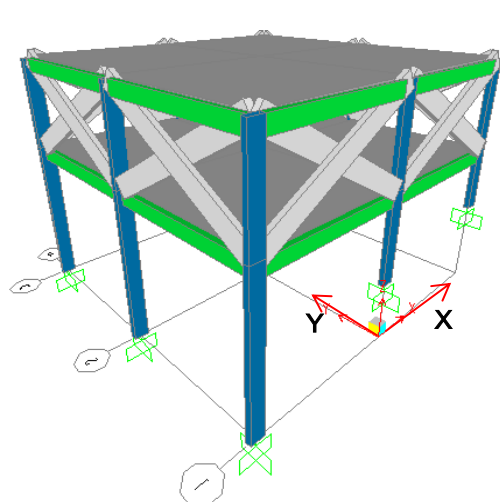
### Mass Distribution - tributary area

*Mass Floor (Partitions + Live) added to model*

Columns	lx(ft)	ly(ft)	W (kips)	m (k-s <sup>2</sup> /ft)
3A 3C 1A 1C	7.5	5	3.113	0.097
2B	15	10	6.825	0.212
3B 1B	15	5	5.100	0.158
2A 2C	7.5	10	4.538	0.141

*Mass Roof (Live) added to model*

Columns	lx(ft)	ly(ft)	W (kips)	m (k-s <sup>2</sup> /ft)
3A 3C 1A 1C	7.5	5	0.150	0.005
2B	15	10	0.600	0.019
3B 1B	15	5	0.300	0.009
2A 2C	7.5	10	0.300	0.009

**Table 3-6. Parameters for Model 1.4**

Story	Height (ft)	Span X (ft)	Span Y (ft)	Cross section		Reinforcement	
				beam (in)	column (in)	beam	column
1	15 - 6.5	15	15	6 x 16	16 x 6	6 # 4	6 # 4
2	9	15	15	6 x 16	16 x 6	6 # 4	6 # 4

X - bay	2	<i>strong axis</i>
Y - bay	2	

Floor Load		
Wslab	0.063	ksf
Live	0.008	ksf
Partitions	0.225	ksf

Roof Load		
Wslab	0.063	ksf
Live	0.004	ksf

### Mass Distribution - tributary area

*Mass Floor (Partitions + Live) added to model*

Columns	lx(ft)	ly(ft)	W (kips)	m (k-s <sup>2</sup> /ft)
3A 3C 1A 1C	7.5	7.5	3.825	0.119
2B	15	15	8.550	0.266
3B 1B	15	7.5	5.963	0.185
2A 2C	7.5	15	5.963	0.185

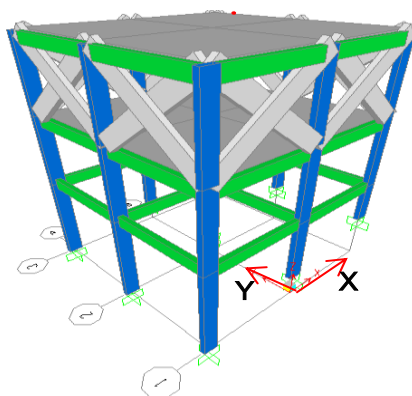
*Mass Roof (Live) added to model*

Columns	lx(ft)	ly(ft)	W (kips)	m (k-s <sup>2</sup> /ft)
3A 3C 1A 1C	7.5	7.5	0.225	0.007
2B	15	15	0.900	0.028
3B 1B	15	7.5	0.450	0.014
2A 2C	7.5	15	0.450	0.014

### 3.2.6 ANALYTICAL MODELS 2

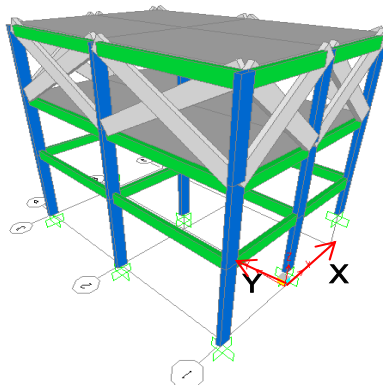
Tables 3-7 to 3-11 show the geometry and cross section dimension of the prototype Models 2. Mass calculations for the roof and floor level are the same as for prototype model 1, since these levels are not affected with the addition of the third story.

**Table 3-7.** Parameters for Model 2.1



Story	Height (ft)	Span X (ft)	Span Y (ft)	Cross section		Reinforcement	
				beam (in)	column (in)	beam	column
1	10 - 5	10	10	6 x 16	16 x 6	6 # 4	6 # 4
2	9	10	10	6 x 16	16 x 6	6 # 4	6 # 4
3	9	10	10	6 x 16	16 x 6	6 # 4	6 # 4

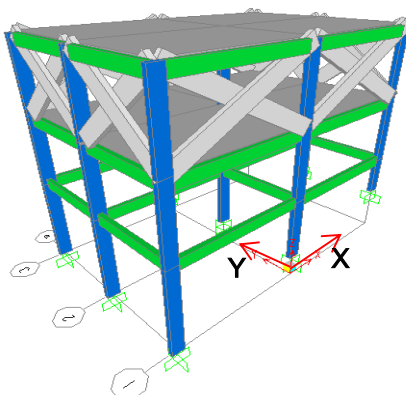
X - bay	2	<i>strong axis</i>
Y - bay	2	

**Table 3-8.** Parameters for Model 2.2

Story	Height (ft)	Span X (ft)	Span Y (ft)	Cross section		Reinforcement	
				beam (in)	column (in)	beam	column
1	10 - 5	10	15	6 x 16	16 x 6	6 # 4	6 # 4
2	9	10	15	6 x 16	16 x 6	6 # 4	6 # 4
3	9	10	15	6 x 16	16 x 6	6 # 4	6 # 4

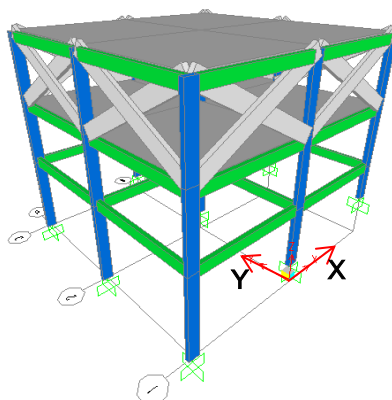
X-bay	2	<i>strong axis</i>
Y-bay	2	

**Table 3-9.** Parameters for Model 2.3

Story	Height (ft)	Span X (ft)	Span Y (ft)	Cross section		Reinforcement	
				beam (in)	column (in)	beam	column
1	10 - 5	15	10	6 x 16	16 x 6	6 # 4	6 # 4
2	9	15	10	6 x 16	16 x 6	6 # 4	6 # 4
3	9	15	10	6 x 16	16 x 6	6 # 4	6 # 4

X - bay	2	<i>strong axis</i>
Y - bay	2	

**Table 3-10.** Parameters for Model 2.4

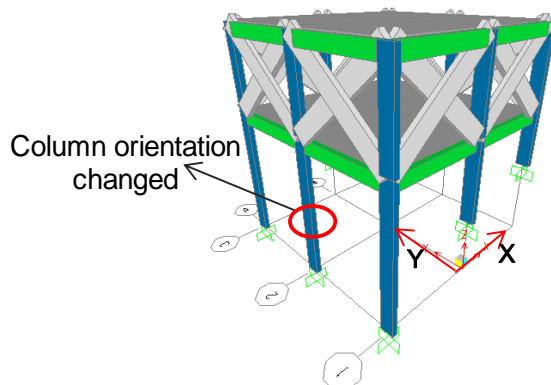
Story	Height (ft)	Span X (ft)	Span Y (ft)	Cross section		Reinforcement	
				beam (in)	column (in)	beam	column
1	10 - 5	15	15	6 x 16	16 x 6	6 # 4	6 # 4
2	9	15	15	6 x 16	16 x 6	6 # 4	6 # 4
3	9	15	15	6 x 16	16 x 6	6 # 4	6 # 4

X-bay	2	<i>strong axis</i>
-------	---	--------------------

### 3.2.7 ANALYTICAL MODELS 1.1 WITH VARIATION

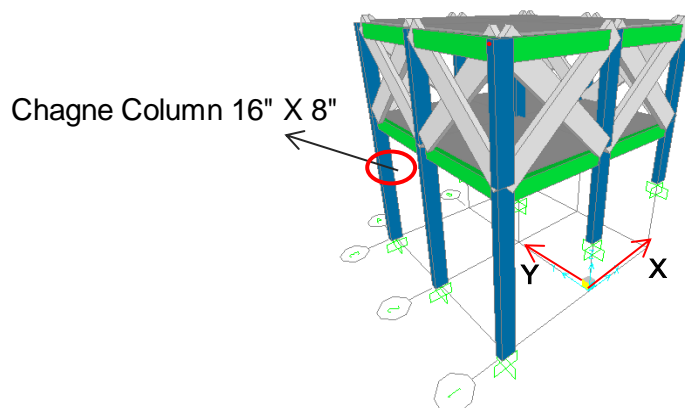
Models 1.1 with variation are equal to Model 1.1 in terms of the span length, column height and beam dimension. The differences for this group of prototype models consist in a change on the column orientation and columns dimensions. For example Model 1.1y is same as Model 1.1; however in this case the strong axis is in the “y” direction. Tables 3-11 to 3-14 show the geometry, cross section dimension and the applied loads and masses.



**Table 3-11.** Parameters for Model 1.1y

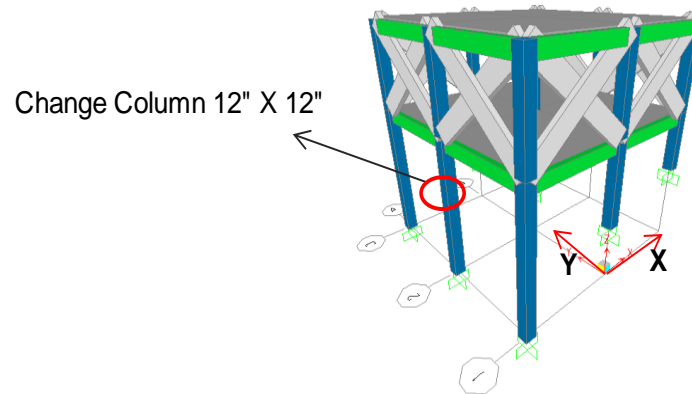
Story	Height (ft)	Span X (ft)	Span Y (ft)	Cross section		Reinforcement	
				beam (in)	column (in)	beam	column
1	15 - 6.5	10	10	6 x 16	6 x 16	6 # 4	4 # 4
2	9	10	10	6 x 16	6 x 16	6 # 4	4 # 4

X - bay	2	
Y - bay	2	<b>strong axis</b>

**Table 3-12.** Parameters for Model 1.1.2

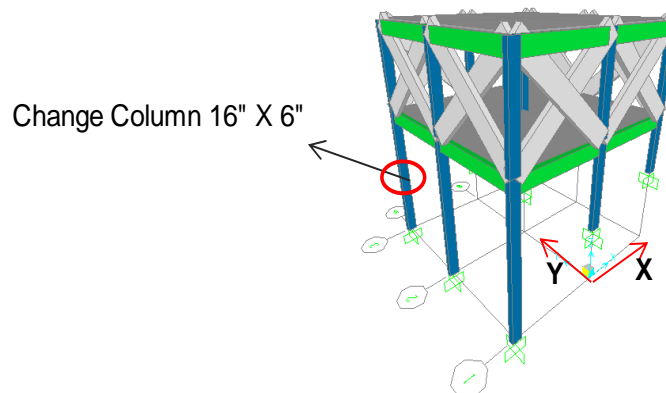
Story	Height (ft)	Span X (ft)	Span Y (ft)	Cross section		Reinforcement	
				beam (in)	column (in)	beam	column
1	15 - 6.5	10	10	6 x 16	16 x 8	6 # 4	4 # 4
2	9	10	10	6 x 16	16 x 8	6 # 4	4 # 4

X - bay	2	<i>strong axis</i>
Y - bay	2	

**Table 3-13.** Parameters for Model 1.1.3

Story	Height (ft)	Span X (ft)	Span Y (ft)	Cross section		Reinforcement	
				beam (in)	column (in)	beam	column
1	15 - 6.5	10	10	6 x 16	12 x 12	6 # 4	4 # 4
2	9	10	10	6 x 16	12 x 12	6 # 4	4 # 4

X - bay	2	
Y - bay	2	

**Table 3-14.** Parameters for Model 1.1.4

Story	Height (ft)	Span X (ft)	Span Y (ft)	Cross section		Reinforcement	
				beam (in)	column (in)	beam	column
1	15 - 6.5	10	10	6 x 16	12 x 6	6 # 4	4 # 4
2	9	10	10	6 x 16	12 x 6	6 # 4	4 # 4

X - bay	2	<i>strong axis</i>
Y - bay	2	

### 3.2.8 COLUMNS BEAMS AND RC SHEAR WALL

This section presents the dimensions and minimum reinforcement used for the columns and beams. The nonlinear properties of the frame elements (columns and beams) are explained in Chapter 4. The retaining wall for models type d (RC shear wall) was analyzed with linear elastic properties using shell elements.

#### Columns

Due to the lack of reliable information about the reinforcement details in the columns it was determined to use minimum reinforcement requirements as per ACI 318-11 (10.9.2). Vázquez (2002) in his study also found that the steel reinforcement parameter were not available in the residences because the residences were old and the owners did not have the construction drawings. The minimum longitudinal reinforcement ( $\rho_t$ ) ratio is 0.01. The minimum longitudinal steel area ( $A_{st}$ ) is calculated as:

$$A_{st} = \rho_{t*} A_g \quad (3-3)$$

where:

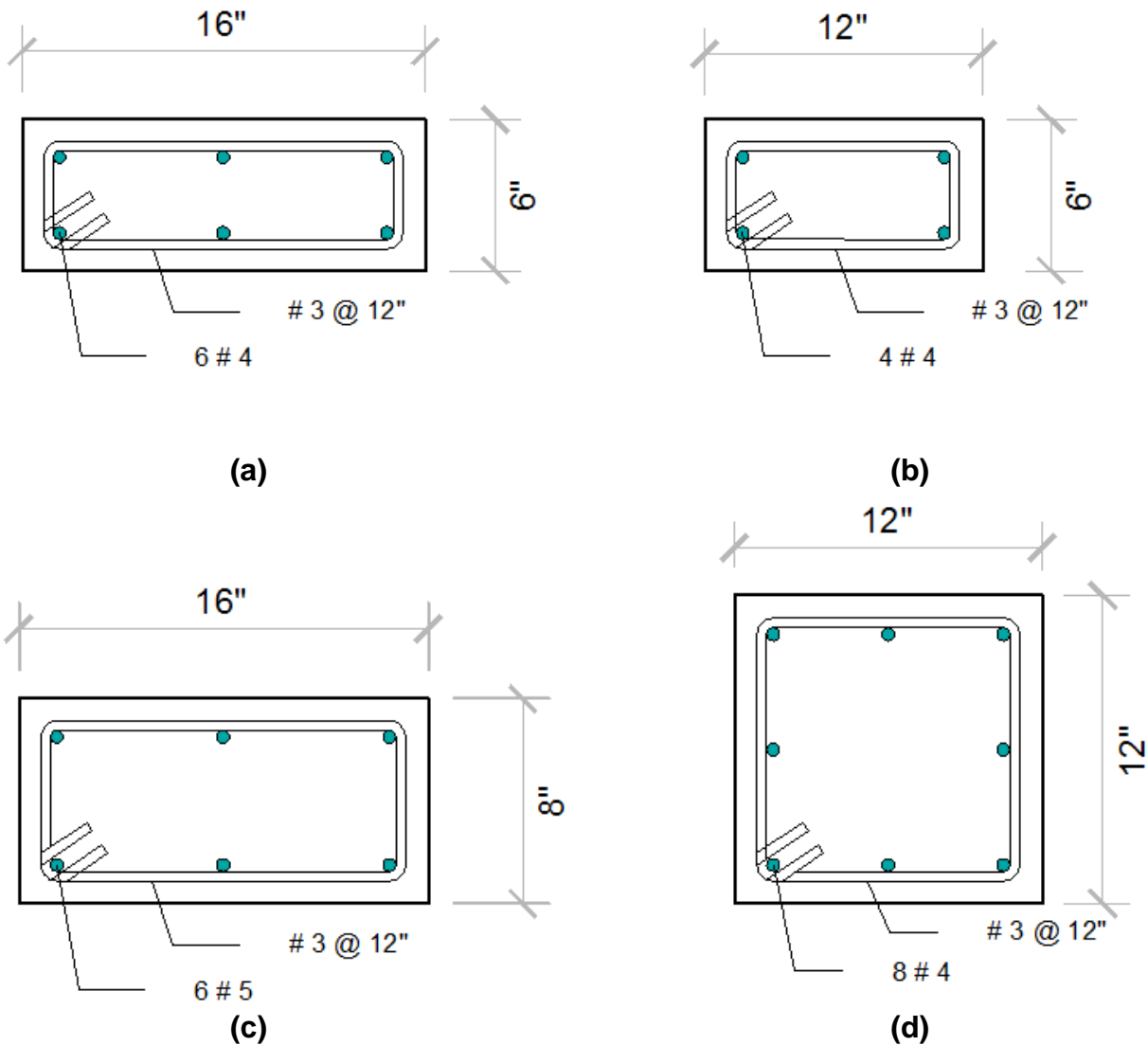
$A_g$  :cross sectional area of the column [in<sup>2</sup>].

Table 3-15 shows the longitudinal reinforcement provided for each column section.

**Table 3-15.** Minimum Longitudinal Reinforcement for Columns

Columns	Ast (req) (in <sup>2</sup> )	Bar	Ast (provided) (in <sup>2</sup> )
16 x 6	0.96	6 # 4	1.18
16 x 8	1.28	6 # 5	1.84
12 x 6	0.72	4 # 4	0.79
12 x 12	1.44	8 # 4	1.57

In absence of sufficient transverse reinforcement, the confinement considered for the concrete core was # 3 bars close ties separated uniformly 12 inches along the member. The detailing of columns is illustrated in Figure 3-13.



**Figure 3-13.** Cross Section of Columns. (a) Column 16"x 6" (b) Column 12"x 6" (c) Column 16"x 8" (d) Column 12"x12"

### **Beams**

For all beams the reinforcement provided was 6 # 4 (3 # 4 top and 3 #4 bottom). This provisions were verified with the minimum reinforcement required as per ACI 318-11

The detailing of beam is illustrated in Figure 3-14.

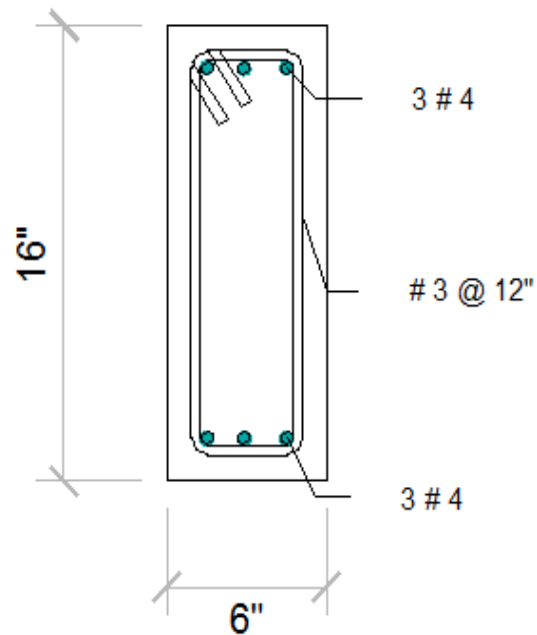


**Figure 3-14.** Cross Section of Beam

### **RC SHEAR WALL**

The thickness of the RC shear wall is 6 inch. The cross section of the RC shear wall is illustrated in Figure 3-15.

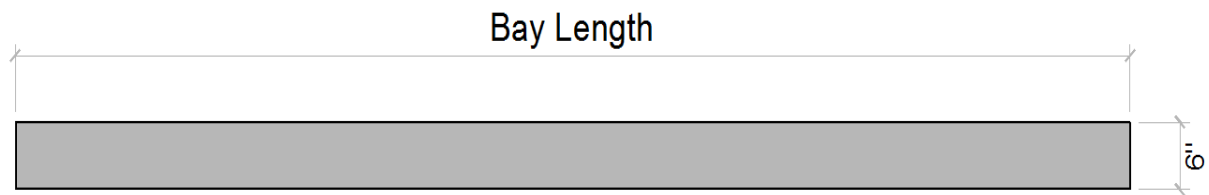


**Figure 3-15.** Cross Section of RC Shear Wall

### 3.3 GENERAL DETAILS OF THE ANALYTICAL MODELS

#### 3.3.1 MATERIAL PROPERTIES

All models have the same material properties: modulus of elasticity of concrete  $E=2850$  ksi, modulus of elasticity of steel  $E=29000$  ksi and reinforcing bars yield strength  $f_y=60$  ksi.

#### **CONCRETE COMPRESSIVE STRENGTH ( $f'_c$ )**

The compressive strength of concrete ( $f'_c$ ) used was 2,500 psi based on the laboratory tests done for this investigation with the assistance of graduate student Ariel Irizarry. It was considered common construction practice for concrete mix, in order to investigate the concrete strength. Mostly these types of houses were built without the supervision of a civil / structural engineer and concrete mix does not include any design basis. Typically home owners used a concrete mix named (3, 2, 1) which contains 3 pails of  $\frac{3}{4}$ " coarse aggregate, 2 pails of fine aggregate, 1 pail of Portland cement and  $\frac{1}{2}$  pail of water, which generates a water cement ratio of 0.50. Other common concrete mix used is named (2, 2, 1) which contains 2 pails of  $\frac{3}{4}$ " coarse aggregate, 2 pails of fine aggregate, 1 pail of Portland cement and  $\frac{1}{2}$  pail of water, which also generates a water cement ratio of 0.50. Table 3-16 shows the results obtained from the compression tests.

**Table 3-16.** 7 and 28 days Compression Test Results 7 and 28

Mix	$f'_c$ (7days) (psi)	$f'_c$ (28 days) (psi)
(3, 2, 1)	1638	2363
(2, 2, 1)	1630	2553

### **3.3.2 ADDITIONAL MODELING CONSIDERATIONS**

The rigid floors were modeled with floor shell elements. A lumped mass modeling strategy was adopted, in which masses were lumped at the nodal points according to its tributary area. Soil structure interaction was not considered. The columns were assumed fixed at the base. However, for the purpose of comparison one model will be analyzed with the base pinned. According to ACI 318 for column elements, cracked section was assumed with an effective stiffness equal to 70% of the gross section and for beam elements, cracked section was assumed with an effective stiffness equal to 35 % of gross section.

## **CHAPTER 4. NONLINEAR ANALYSIS METHODS**

---

### **4.1 INTRODUCTION**

This study will consist of nonlinear analysis. The elastic analysis can predict the elastic capacity of structure and indicate where the first yielding will occur. However, they do not predict failure mechanisms. The nonlinear behavior of reinforced concrete (RC) sections leads to a redistribution of moments and shear forces, resulting in an increased load demand in some structural members of the structure. As the applied load is increased, hinges start forming in succession at locations where the hinge moment capacity is reached. With further increase in the applied load the structure forms a collapse mechanism resulting in failure.

### **4.2 NONLINEAR PUSHOVER ANALYSIS**

#### **4.2.1 PUSHOVER ANALYSIS BACKGROUND**

Pushover analysis has been developed over the past twenty years and has become the preferred analysis procedure for design and seismic performance evaluation purposes as the procedure is relatively simple and considers postelastic behavior (Oguz, 2005). Pushover Analysis is defined in the Federal Emergency Management Agency document FEMA 273 as a nonlinear static approximation of the response a structure will undergo when subjected to dynamic earthquake loading. The main purpose of the pushover analysis is to compare the strength and deformation capacity with the demands at the corresponding performance level. While nonlinear time history analysis is the most rigorous procedure to compute seismic demands, current structural engineering practice uses the nonlinear static procedure (NSP) or pushover analysis. Compared with nonlinear dynamic analysis, the pushover analysis is relatively simple and much less time consuming. Because the procedure involves certain approximations and



simplifications that some amount of variation is always expected to exist in seismic demand prediction of pushover analysis (Oguz, 2005). However, the approach used in this investigation is supposed to give a reasonable idea of this behavior of the models.

During a pushover analysis the magnitude of the loading is incrementally increased in accordance with a certain predefined pattern until a target displacement is reached. The pushover curve is very sensitive to the choice of lateral load distribution. The lateral load patterns commonly used in pushover analysis are proportional to the story masses, elastic first mode, and "code" distributions. These lateral load patterns are based on the assumption that the response is controlled by the fundamental mode and that the mode shape remains unchanged after the structure yields (Chopra and Goel, 2001). The limited capability to predict higher mode effects in postelastic range have led many researchers to propose adaptive load patterns which consider the changes in inertia forces with the level of inelasticity. The underlying approach of this technique is to redistribute the lateral load shape with the extent of inelastic deformations. Although some improved predictions have been obtained from adaptive load patterns, they make pushover analysis computationally demanding and conceptually complicated. The scale of improvement has been a subject of discussion and thus simple invariant load patterns are widely preferred at the expense of accuracy (Oguz, 2001).

A typical pushover curve (Figure 4-1) represents the behavior of the building structure under increasing base shear forces. As the capacities of the members exceed their yield limits during the increasing of the lateral forces, the slope of the force-deformation curve will be reduced, and hence the nonlinear behavior can be represented.

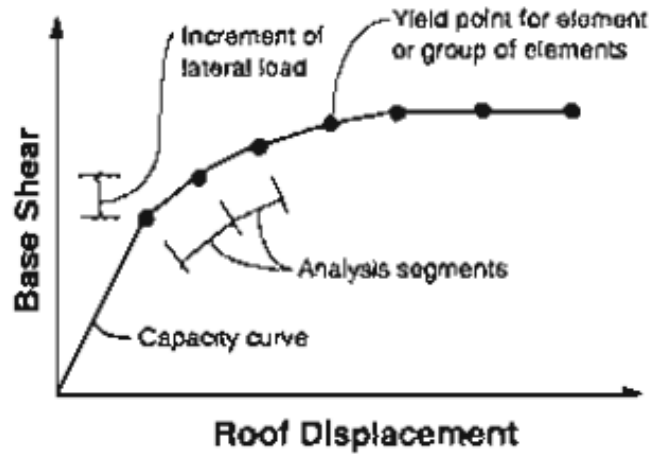


**Figure 4-1.** Typical Pushover Curve (ATC 40).

The internal forces and deformations computed at the target displacements are used as estimates of the strength and deformation demands, which need to be compared to the available capacities. Based on the desired Building Performance Level, the Response Spectrum for the design earthquake may be determined. The Response Spectrum gives the Spectral Acceleration, a single degree of freedom structure is likely to experience under the design ground shaking given the structure's fundamental period of vibration. The pushover analyses are performed using the analytical models in order to investigate the inelastic behavior using SAP2000.

#### **4.2.2 PUSHOVER ANALYSIS WITH SAP2000**

SAP2000 is a comprehensive analysis package from Computers and Structures Inc. for structural analysis and design. It is probably the most widely used analysis tool among immediately and easily available analysis software (Güner, 2007). Nonlinear static pushover analysis is a very powerful feature offered in the nonlinear version 14 of SAP2000. The main points for conducting pushover analysis can be summarized as follows:

- Defining nonlinear material behavior
- Hinge unloading method
- Defining lateral load pattern
- Performing the analysis

Sections 4.2.2.1 through 4.2.2.4 cover in detail the above aspects and is based on CSI Analysis Reference Manual.

#### **4.2.2.1 DEFINING NONLINEAR MATERIAL BEHAVIOR**

In SAP2000, a frame element is modeled as a line element having linearly elastic properties. Yielding and post-yielding behavior can be modeled using discrete hinges. There are several types of hinges, such as flexural, shear, axial and axial plus flexural which yields based on the interaction of axial force and bending moments at the hinge location. The main types of hinge properties in SAP2000 are default hinge properties and user-defined hinge properties. A generalized force-displacement curve characteristic of hinge properties in SAP2000 is shown in Figure 4-2. When these hinge properties (default or user-defined) are assigned to a frame element, the program automatically creates a new generated hinge property for each hinge. User defined moment-rotation characteristics of plastic hinges were utilized to perform pushover analyses.

In this study, flexural hinges (M3) were used for beams, while axial plus flexural (PM2M3) hinges were used for columns. Also shear hinges were introduced for columns (V2V3) due to the fact that short and tall columns exist within the same story level as a consequence of the hilly terrain. During earthquake shaking all columns move horizontally along with the floor slab at a particular level and the short columns attract larger earthquake force and get more damaged compared to taller ones. Furthermore, most of these types of residences are old (more than 30 years old) with low concrete strength and insufficient amount of transverse steel. Therefore shear, failures of members were taken into consideration.

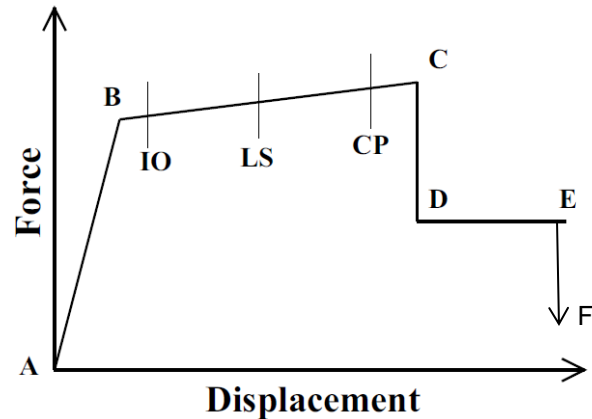


**Figure 4-2.** Generalized Force vs. Displacement or Moment vs. Rotation relationship.  
(CSI Manual)

The main points in the force - displacement curve shown in the Figure 4-2 can be defined as follows:

- **Point A** corresponds to unloaded condition.
- **Point B** represents yielding of the element. Prior to reaching point B, all deformation is linear elastic and occurs in the frame element itself, not the hinge. Plastic deformation beyond point B occurs in the hinge in addition to any elastic deformation that may occur in the element. When the hinge unloads elastically, it does so without any plastic deformation.
- **Point C** corresponds to the deformation at which significant strength degradation begins. The drop from C to D represents the initial failure of the element and resistance to lateral loads beyond point C is usually unreliable.
- **Point D** represents the residual strength; from point D to E the frame elements sustain gravity loads.
- **Point E** represents total failure. Beyond point E the hinge load will drop down. The gravity load can no longer be sustained.

In this curve, points marked as IO, LS and CP represent the structure performance level. These points of performance level describe a limiting damage condition which may be considered satisfactory for a given building with specific ground motion. The values assigned to each of these points vary depending on the type of member as well as many other parameters defined in the ATC-40 and FEMA-273 documents. The descriptions of each performance level based on the ATC-40 and FEMA-273 for primary concrete frame elements are:

- **Immediate Occupancy IO:** damage is relatively limited; the structure retains a significant portion of its original stiffness and most if not all of its strength. Minor hairline cracking. No crushing (concrete strain below 0.003).
- **Life Safety level LS:** substantial damage has occurred to the structure, and it may have lost a significant amount of its original stiffness. However, a substantial margin remains for additional lateral deformation before collapse would occur.
- **Collapse prevention CP:** at this level the building has experienced extreme damage, if laterally deformed beyond this point; the structure can experience instability and collapse.

#### 4.2.2.1.1 DEFAULT HINGES

When default hinge properties are used, the program combines its built-in default criteria with the defined section properties for each element to generate the final hinge properties. SAP2000 default hinge properties are provided based on ATC-40 (1996) and FEMA-356 (FEMA, 2000) criteria. The default-hinge properties based on FEMA-356 are shown on Appendix A.

#### **4.2.2.1.2 USER DEFINED FLEXURAL (M3)/ AXIAL PLUS FLEXURAL HINGES (PM2M3)**

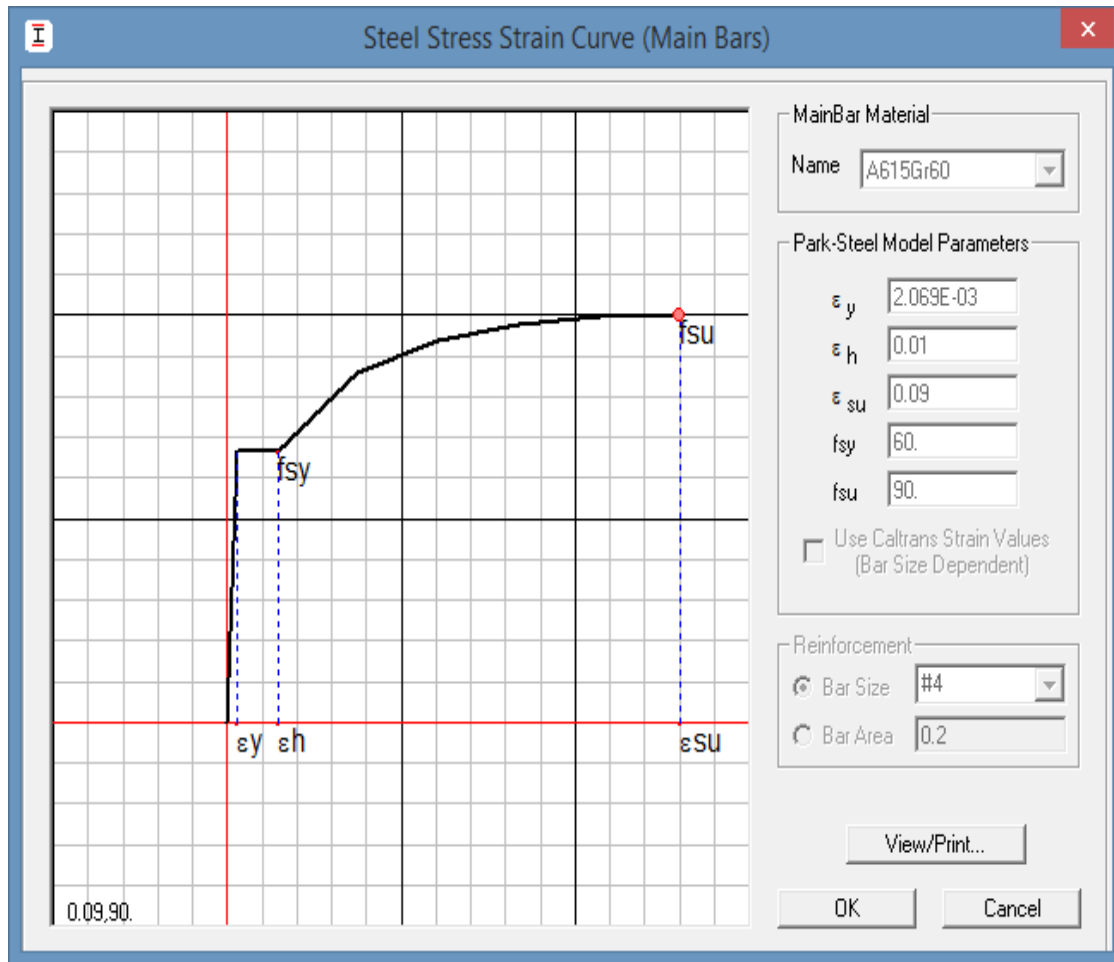
The definition of user-defined hinge properties requires a moment–curvature analysis of each element. The Section Designer SD module of SAP2000 was utilized to determine moment-curvature relationships of members. The moment-curvature relation is a basic tool in nonlinear analysis to model plastic hinge behavior. Moment-curvature relationships of beams and columns and interaction diagrams of columns were calculated based on the section and material properties previously defined in Chapter 3.

##### **4.2.2.1.2.1 SECTION DESIGNER MATERIAL STRESS –STRAIN RELATIONSHIP**

Moment-curvature analysis in Section Designer is a method to accurately determine the load-deformation behavior of a concrete section using nonlinear material stress-strain relationships. Researchers emphasized that accuracy of results obtained from pushover analysis are strongly influenced by basic inputs like: (1) stress-strain relationship of constitutive materials; as well as (2) P-M yield interaction (Chandrasekara et. al, 2010). Point C (Figure 4-2) occurred when the concrete strain in the core exceeded the maximum concrete compressive strain ( $\epsilon_{cu}$ ), the steel bar exceeded the maximum tension steel strain ( $\epsilon_{su}$ ) or there is a sudden loss of strength.

#### **Rebar**

The Park stress-strain curve was used for this study. The maximum steel strain  $\epsilon_{su}$  is dependent on rebar size. Typically for bars # 10 or smaller  $\epsilon_{su}$  is 0.09. Figure 4-3 shows the steel material definition from SAP2000 Section Designer. The parameters that define the stress-strain curve for rebar material are located in Appendix B.



### Steel Properties

$\epsilon_{sy}$  = yield strain of steel = 0.002069

$f_{sy}$  = yield stress of steel = 60 ksi

$\epsilon_{sh}$  = longitudinal steel strain for strain steel hardening = 0.01

$\epsilon_{su}$  = ultimate / maximum steel strain = 0.09

$f_{su}$  = ultimate stress capacity of steel = 90 ksi

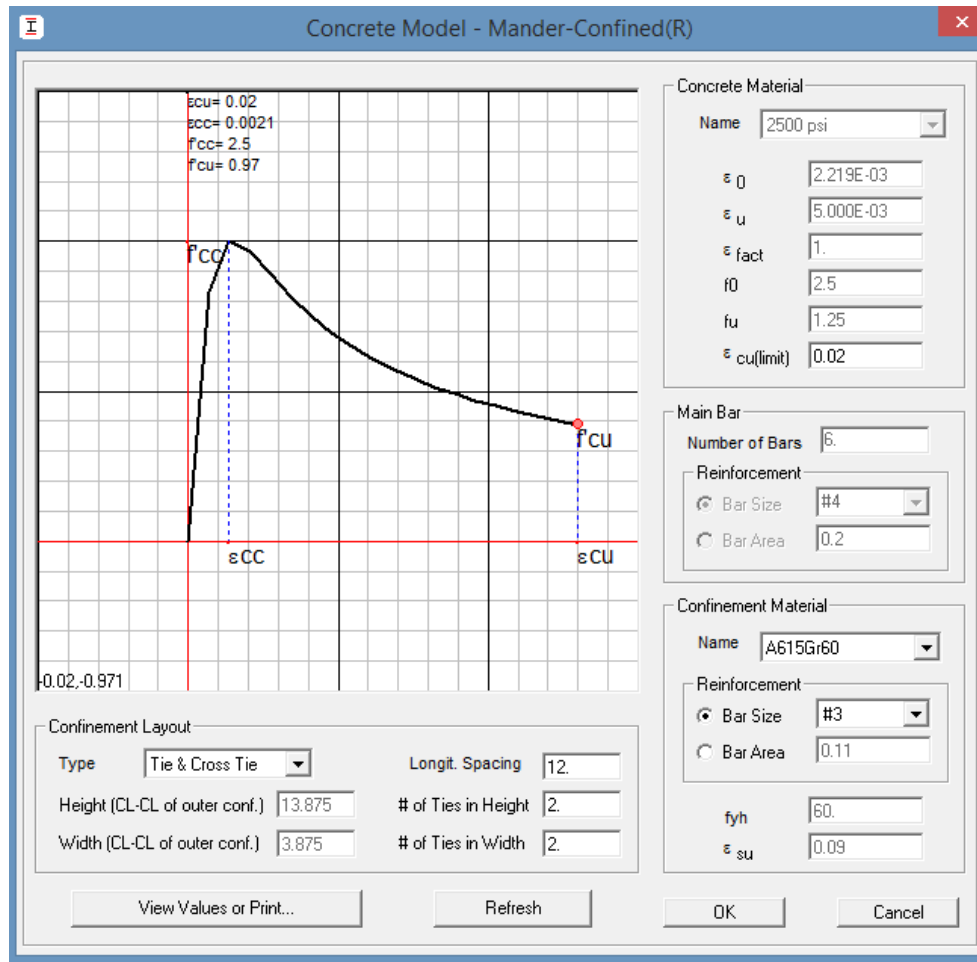
**Figure 4-3.** Park Steel Stress Strain Model

## **Concrete**

For concrete material the Section Designer module uses Mander (1988) stress – strain curve. The Mander unconfined concrete model was used for the outer concrete material and the Mander confined concrete model was used for the core. Figure 4-4 shows the confined concrete material definition from SAP2000 Section Designer. The deficiency of minimal transverse reinforcement at members represents a critical aspect that must be considered. The ACI-318 defines the strain deformation of 0.003 as the strain where an unconfined concrete fails. However, it is recalled that this strain is for design considerations, hence assuming no confinement reinforcement would be overly conservative. The concrete outside the core (unconfined or concrete cover) generally commence to spall when the unconfined compressive strength is reached, hence having characteristics of unconfined concrete up to a maximum concrete strain (spalling). A maximum / ultimate unconfined strain deformation  $\varepsilon_u$  of 0.005 at spalling was permitted (FEMA 273). FEMA 273 established that larger strains are permitted for the confined concrete (concrete inside the core) but shall not exceed 0.02. The parameters that define the stress-strain curve for unconfined and confined concrete material are located in Appendix C

.





### Unconfined concrete properties

$f'_c = f'_0$  = compressive strength of unconfined concrete = 2.5 ksi

$\epsilon_0$  = concrete strain at  $f'_c$  = 0.002

$\epsilon_{sp}$  = concrete spalling strain

$\epsilon_{sp} = \epsilon_u$

$\epsilon_u$  = maximum / ultimate concrete strain for unconfined concrete,  $\epsilon_{u(lim)} = 0.005$

### Confined concrete properties

$f'_{cc}$  = compressive strength of confined concrete

$\epsilon_{cu}$  = ultimate / maximum concrete strain for confined concrete,  $\epsilon_{cu(lim)} = 0.02$

**Figure 4-4.** Mander Concrete Confined Stress Strain Model

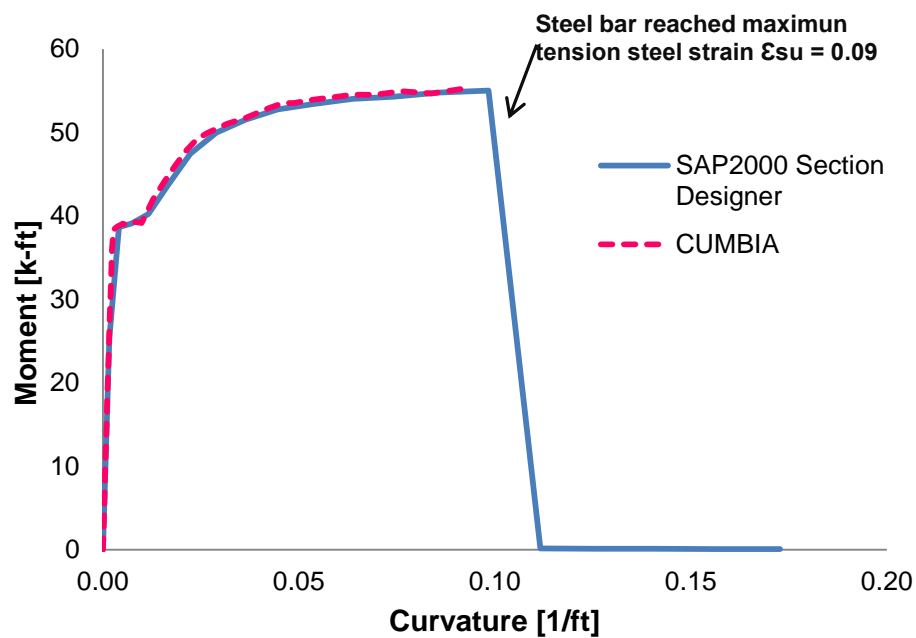
#### 4.2.2.1.2.2 SAP2000 MOMENT – CURVATURE ANALYSIS

The moment-curvature properties were calculated using SAP2000 built-in features, described in the previous section. The cross sections of the beam and columns defined to analyze the nonlinear properties of the models were presented in Chapter 3

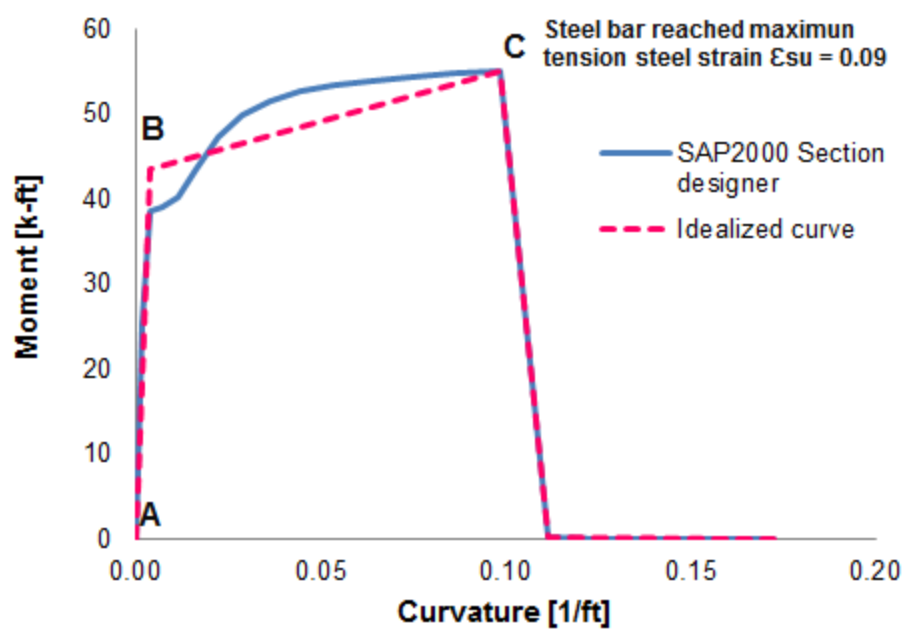
##### **Beam**

In order to verify the SAP2000 moment-curvature output, the program CUMBIA (Montejo and Kowalsky, 2007) was used to compare the results for the beam. For beams the axial load is assumed to be zero. As shown in Figure 4-5a, the moment curvature obtained by CUMBIA stopped when the tension steel strain reaches the maximum value specified. On the other side, SAP2000 Section Designer modelled the strength loss after reaching the maximum steel strain. It can be noticed that reinforcement yields before the concrete is crushed in compression. After the steel bars reaches the maximum tension strain  $\varepsilon_{su} = 0.09$ , the section rapidly lost all strength capacity. The moment-curvature relationship from the original analyses was idealized to approximate the backbone curve (Figure 4-5b).

In SAP2000 the input required is the moment-rotation relationship. The curvature was multiplied by the plastic hinge length (equal to half the section depth) to obtain the rotation. Figure 4-6 shows the idealized moment-rotation backbone curve used as input for the beam hinge assignment.



(a)



(b)

**Figure 4-5.** Beam Moment-Curvature Analysis. (a) Comparison SAP2000 Section Designer and CUMBIA. (b) Idealized Curve

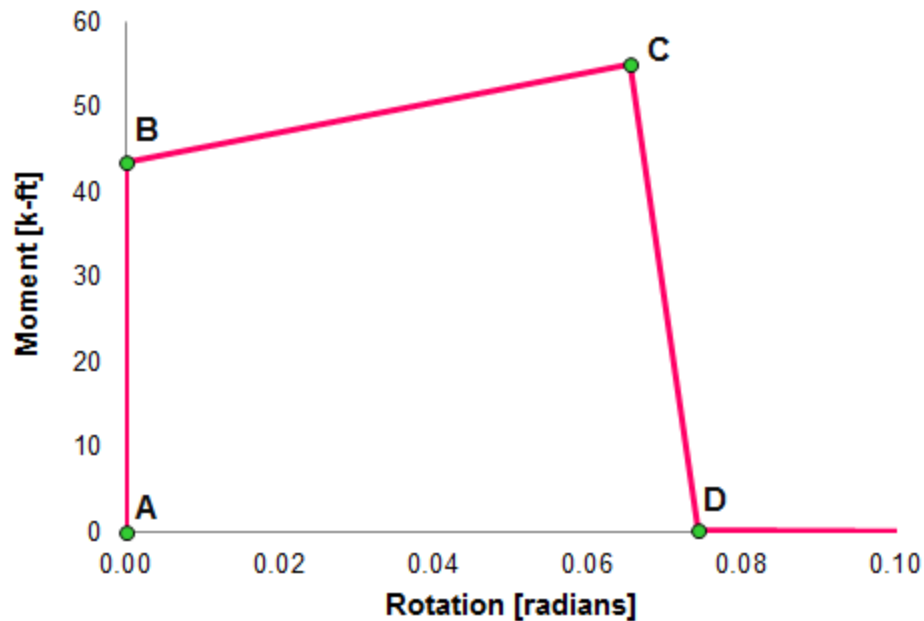


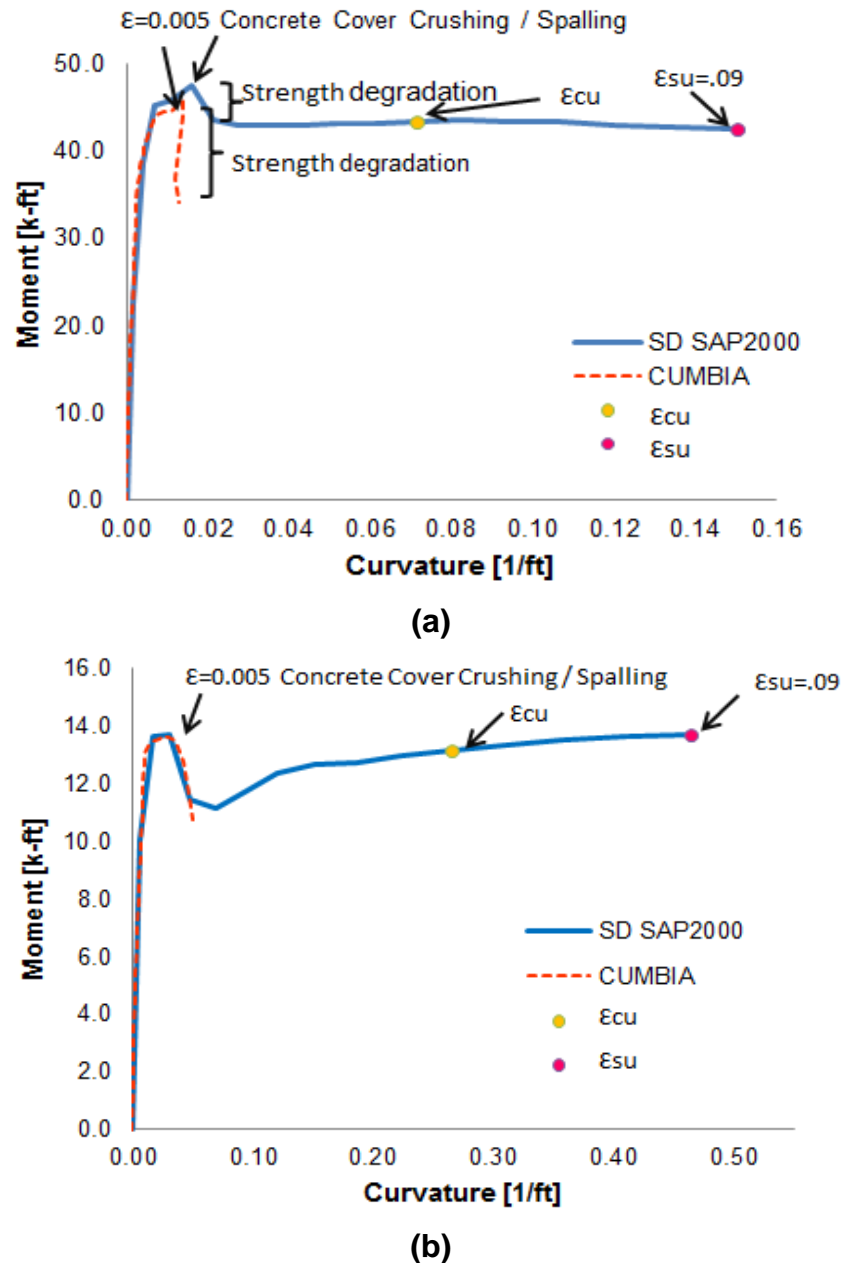
**Figure 4-6.** Backbone Curve for Beam Hinge Assignment

### Columns

Because plastic hinge behavior for columns depends on the axial force on the cross section, a separate hinge model was defined for each column to account for different axial loads. The axial loads were calculated manually based on the dead load and 20 % live load per tributary area assigned to each column. For the column bottom, the column self-weight is included as well. Since the difference between the axial load at the column top and bottom is very small, a further simplification was made by assuming the same axial load for both locations. Appendix D presents the calculation to obtain the axial load.

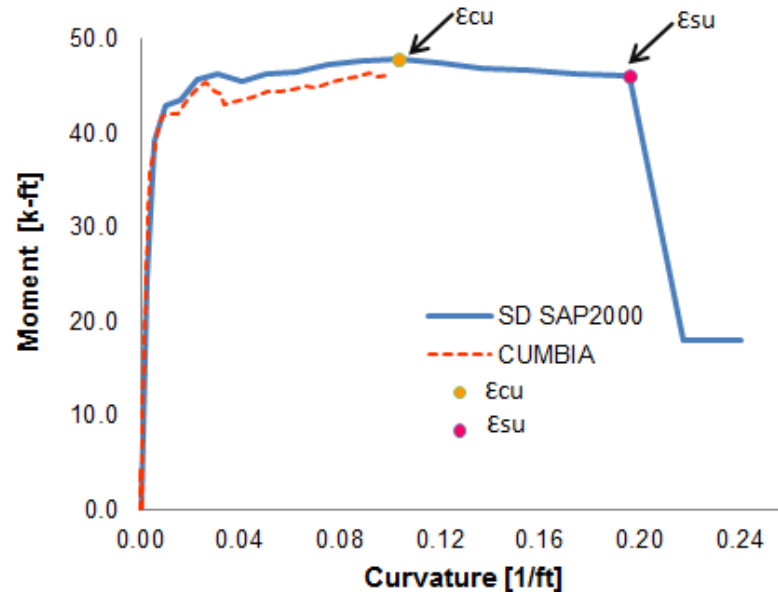
Figure 4-7 shows results for the moment-curvature analysis for column 16"x 6" strong and weak axis with an axial load of 12 kips, obtained with SD and CUMBIA. The discrepancy between the curves is primarily due to the failure criteria used by each program. It can be noticed that CUMBIA stops when there is a sudden loss of strength. Also CUMBIA uses a different equation to calculate the confined compressive strength, based on suggestions by King (1986). SD calculates the confined compressive strength

using a chart for the multiaxial failure criterion in terms of two lateral confining stresses (Mander et al, 1984). The strength degradation occurred when the concrete cover started to spall off, thus the capacity that remains is less. Eventually a compression failure occurred when  $\epsilon_{cu}$  reached a maximum value resulting in crushing of the concrete core. After this point the longitudinal rebar buckles outward between the ties.



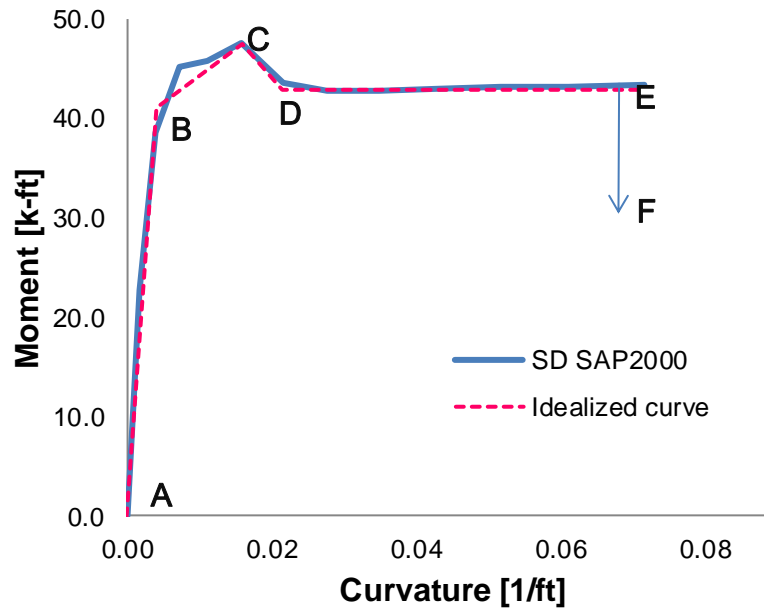
**Figure 4-7.** Moment-Curvature Analysis for Column 16" X 6: Comparison between SAP2000 Section Designer and CUMBIA. Axial Load = 12 kips. (a) Strong Axis. (b) Weak Axis

Figure 4-8 shows the results of the moment-curvature analysis for column 12"x12 with an axial load of 12 kips, executed with SD and CUMBIA. It can be noticed that CUMBIA stopped when the concrete strain  $\epsilon_{cu}$  exceeded its maximum value. SD continued the analysis until the steel bars reaches the maximum tension strain  $\epsilon_{su} = 0.09$ ; after this point the section rapidly lost strength capacity.



**Figure 4-8.** Moment-Curvature Analysis for Column 12" X 12": Comparison between SAP2000 Section Designer and CUMBIA. Axial Load = 12 kips

Figure 4-9 shows the idealized moment-curvature curve for column 16"x 6" strong axis. When a hinge unloads, the program must find a way to remove the load that the hinge was carrying and possibly redistribute it to the rest of the structure. Hinge unloading occurs whenever the moment-curvature curve shows a drop in capacity, such as is occurred from point C to point D (Figure 4-9). Such unloading along a negative slope may be unstable in the analysis and very difficult to model. A solution is not always mathematically guaranteed. SAP2000 reference manual recommends avoiding specifying sudden strength loss or negative slope. Therefore, the idealized moment-rotation curve adopted for this study used a relationship with no strength loss as shown in Figure 4-10. The same analysis was applied for the weak axis and other column sections.



**Figure 4-9.** Idealized Moment-Curvature Curve for Column 16" x 6": Strong Axis

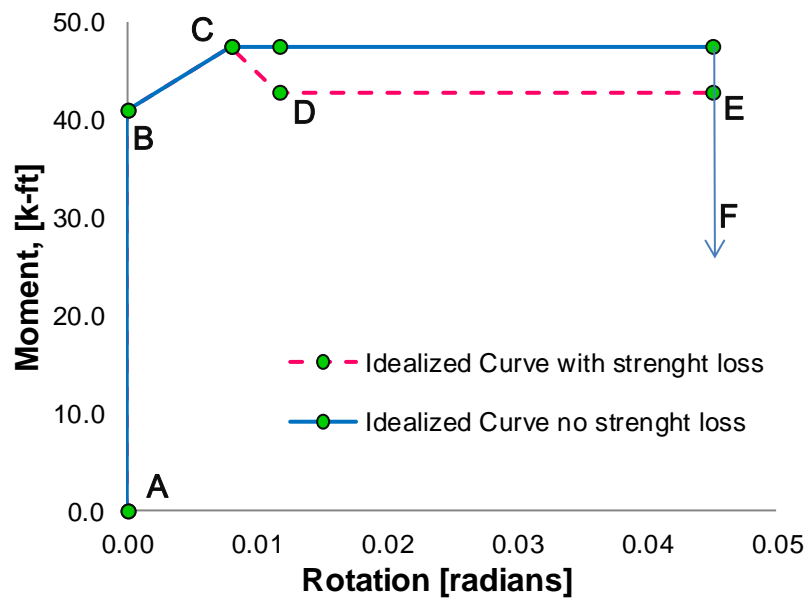


**Figure 4-10.** Backbone Curve for Column 16"x 6":Strong Axis

Figures 4-11 to 4-12 present the variation of the moment curvature under different axial loads for column 16" x 6" in the strong and weak direction, respectively. It can be observed that the column axial capacity increases with axial load.

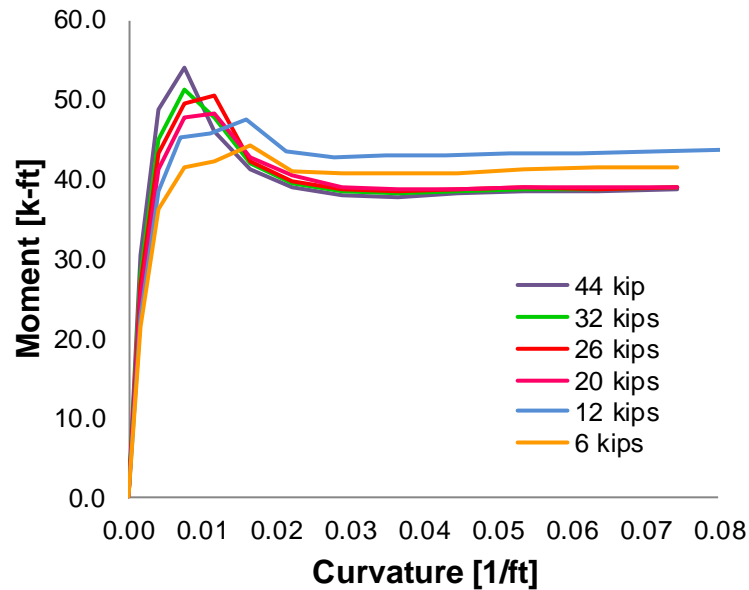


**Figure 4-11.** Column 16x6 Moment – Curvature Analysis Strong Axis

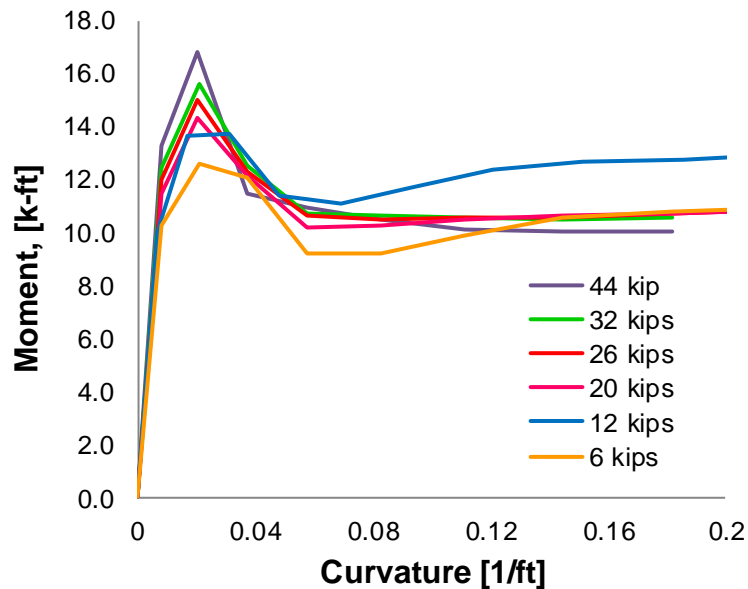


**Figure 4-12.** Column 16x6 Moment – Curvature Analysis Weak Axis

#### 4.2.2.1.3 SHEAR HINGES

Because of the brittle failure of concrete in shear, no ductility was considered for this type of hinge. Shear hinges in all columns elements were considered force-controlled. Shear hinge properties are defined such that, when the shear force in the member reaches its strength, the member fails immediately. The total shear capacity of a



reinforced concrete column depends on the shear capacity of the concrete,  $V_c$  and the shear capacity carried by the transverse reinforcement,  $V_s$ .

The shear strength of each member ( $V_n$ ) was calculated according to ACI-318 as follows:

$$V_n = V_c + V_s \quad (4-1)$$

where:

$V_c$  : shear strengths provided by concrete in accordance with equation 4-2, and

$V_s$  : shear strength provided by reinforcement in accordance with equations 4-3

$$V_c = 2 \left( 1 + \frac{N}{2000A_g} \right) \sqrt{f'_c} b d \quad (4-2)$$

$$V_s = \frac{A_v f_{yh} d}{s} \quad (4-3)$$

where:

$N$  : applied axial load [lb],

$B$  : is the section width [in],

$s$  : transverse reinforcement spacing [in],

$d$  : effective depth [in],

$A_g$  : gross area of member cross section [in<sup>2</sup>],

$A_v$  : area of the transverse reinforcement [in<sup>2</sup>], and

$f_{yh}$  : yield strength of the transverse reinforcement [psi].

Appendix E contains the shear capacity calculation for each column used in this study.

#### 4.2.2.2 HINGE UNLOADING

While performing a nonlinear static pushover analysis to a model, the structural members are expected to exceed their capacities and hence the redistribution of the loads on these members to the rest of the structure becomes an important issue. As mentioned before, when a member reaches its capacity, the program must find a way to remove the load that the structural element was carrying and possibly redistribute it to the rest of the structure. Hinge unloading occurs whenever the force-deformation or moment-rotation curve shows a sudden drop in force or moment, such as it is often assumed when the hinge reaches a negative-sloped portion in its force-displacement curve during pushover analysis. Such unloading along a negative slope is unstable in a static analysis and a unique solution is not always mathematically guaranteed. SAP2000 provides three different member unloading methods to remove the load that the hinge was carrying and to redistribute it to the rest of the structure.

1. **Unload Entire Structure:** When a hinge reaches a negative slope portion of the force - displacement curve (point C at Figure 4-2), the program continues to try to increase the applied load. If this results in increased lateral deformation the analysis proceeds. If not, the program instead reverses the load on the whole structure until the hinge is fully unloaded to the next segment on the force - displacement curve (point D). At this point the program reverts to increasing the load on the structure. Other parts of the structure may now pick up the load that was removed from the unloading hinge. If hinge unloading requires large reductions in the applied lateral load and two hinges compete to unload, i.e., where one hinge requires the applied load to increase while the other requires the load to decrease, the method fails.
2. **Apply Local Redistribution:** This method is similar to the first method, except that instead of unloading the entire structure, only the element containing the hinge is unloaded. If the program proceeds by reducing the base shear when a hinge reaches point C, the hinge unloading is performed by applying a temporary, localized, self-equilibrating, internal load that unloads the element. Once the hinge is

unloaded, the temporary load is reversed, transferring the removed load to the neighboring elements. This method will fail if two hinges in the same element compete to unload, i.e., where one hinge requires the temporary load to increase while the other requires the load to decrease.

3. **Restart Using Secant Stiffness:** Whenever any hinge reaches point C on the force-displacement curve, all hinges that have become nonlinear are reformed using secant stiffness properties, and the analysis is restarted. This method may fail when the stress in a hinge under gravity load is large enough that the secant stiffness is negative. On the other hand, this method may also give solutions where the other two methods fail due to hinges with small (nearly horizontal) negative slopes.

#### 4.2.2.3 DEFINING THE LATERAL LOAD PATTERN

In pushover analysis the model of the structure is pushed with a specific load distribution pattern along the height of the building. The magnitude of the total force is increased but the pattern of the loading remains the same until the end of the process. Pushover analysis results are very sensitive to the load pattern as mentioned previously. The lateral load patterns should approximate the inertial forces expected in the building during an earthquake. The distribution of lateral inertial forces determines the relative magnitudes of shears, moments, and deformations within the structure. The distribution of these forces will vary continuously during the earthquake response as the members yield and stiffness characteristics change. It also depends on the type and magnitude of earthquake ground motion. There are three different methods of describing the distribution of load on the structure for a pushover load case in SAP2000.

1. **Proportional to the mass at each node:** a uniform acceleration is applied in the appropriate direction; a lateral force is applied at each node that is proportional to the mass tributary to that node.

2. **Mode load pattern:** This load pattern applies a lateral force that is proportional to the product of a specified mode shape times the mass tributary to that node.
3. **Static load pattern:** FEMA 356 (2000) recommends the following load patterns.
  - Code-based vertical distribution of lateral forces used in equivalent static analysis (permitted only when more than 75% of the total mass participates in the fundamental mode in the direction under consideration).
  - A vertical distribution proportional to the shape of the fundamental mode in the direction under consideration (permitted only when more than 75% of the total mass participates in this mode).
  - A vertical distribution proportional to the story shear distribution calculated by combining modal responses from a response spectrum analysis of the building (a sufficient number of modes to capture at least 90% of the total building mass is required to be considered).

For this investigation the proportional to the mass and mode shape load patterns were used. The advantages of these methods are that the program automatically calculated the load pattern selected. On the other hand, static load patterns need to be calculated by hand and given as input. It is expected that the results will be very similar, since the vertical code distribution is proportional to the fundamental mode.

#### **4.2.2.4 PERFORMING THE ANALYSIS**

Pushover analysis is numerically demanding and may cause numerical difficulties for SAP2000 to run the analysis. Simplifying the model as much as possible is helpful, and therefore several cases were executed to evaluate the effect of various parameters that influence the run and reduce the run time. In this study, linear area elements like shells

to model slabs were modeled with the least possible amount of meshing. The run time significantly reduced when a less dense mesh was used to model floors.

The following general sequence of steps was involved in performing the pushover analysis:

1. A three dimensional computer model was created (Figure 4-13). Material properties, frame sections and shell elements were defined for all the models as explained in Chapter 3.

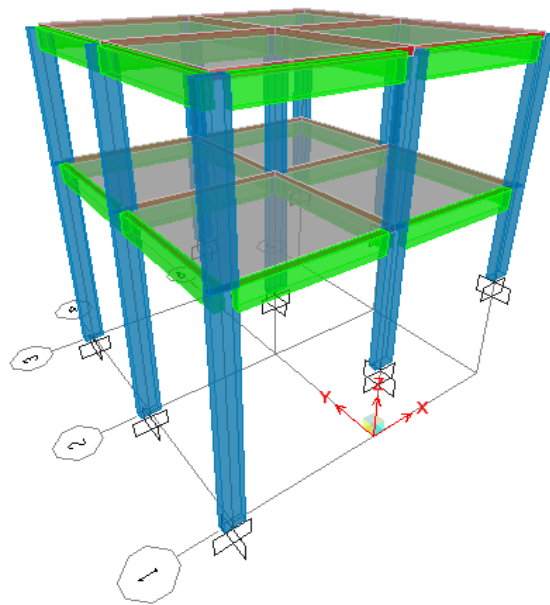


**Figure 4-13.** SAP2000 Typical 3D Model

2. Load and masses were applied to the model.
  - **Dead load:** the weights of the frame and shell elements were considered by the program. Additional dead loads like masonry wall load shave been calculated and assigned as uniformly distributed loads over the beams.

- **Live Load:** live load was added to the slab system as an uniform area load over the shell in the gravity direction
  - **Mass:** the mass is obtained from the elements using the mass density of the material and the volume of the element. The program automatically produces lumped masses from the elements at the joints. Additional mass from the masonry block walls was also assigned to the joints.
3. Hinges were assigned to the frame elements. It is commonly assumed that the locations where the plastic hinges formed, in RC beams and columns is generally at the ends. The cracking process takes place, in those locations since the bending moments are more intense and as consequence, those are the sections where the nonlinear deformations exists because of the inelastic behavior of the materials
- **Columns:** flexural hinges types P-M2-M3 were assigned at the columns faces of the joint. Shear hinges were assigned at the columns mid high (Figure 4-14).

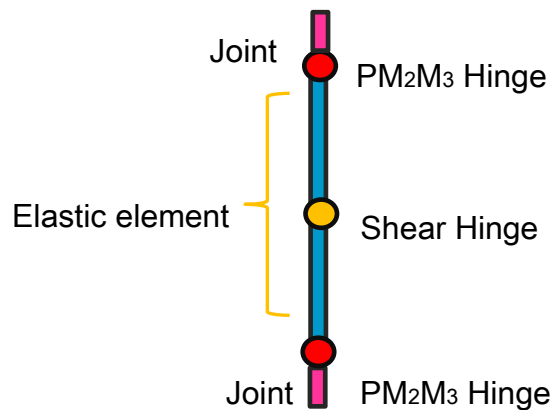


**Figure 4-14.** Column Element

- **Beams:** flexural hinges types M3 were assigned to the beams ends (Figure 4-15).

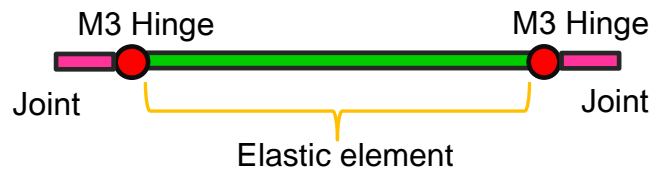


**Figure 4-15.** Beam Element

4. Static nonlinear load cases were defined. SAP2000 has two distinctly different types of control available for applying the load. Each analysis case can use a different type of load control.

- **Force control:** The full load combination is applied as specified. Force control should be used when the load is known (such as gravity load), and the structure is expected to be able to support the load in the elastic range.
- **Displacement control:** The magnitude of the load combination is increased or decreased as necessary until the control displacement reaches a value that the user specified. Displacement control should be used when the magnitude of the applied load is not known in advance.

Two nonlinear cases were defined, one for gravity load and another for lateral forces.

- **Gravity:** An initial force controlled loading was applied to the model. This case is composed of the dead loads and reduced live loads (Figure 4-16).
- **Lateral Push:** A displacement controlled pushover case was defined starting from the initial gravity pushover case. In the analyses, two different load patterns (uniform mass and mode shape) are applied on the structural systems. Figure 4-17 shows the load type selection cases as uniform acceleration and mode

pattern. For the uniform mass case the lateral force is applied at each node proportional to the tributary mass to that node. For the mode shape case the lateral load force is applied proportional to the specified mode. Pushover analyses were performed in each orthogonal direction as shown in Figure 4-18. Due to symmetry only one case was necessary in the Y direction, however for the X direction a pushover case uphill and downhill was initially considered. The pushover cases were named as: push Y, push -X (downhill) and push X (uphill), in addition the name “uniform” or “mode” was used to differentiate among the lateral load pattern used.

Load Case Name: NLD [Set Def Name] Notes: [Modify/Show...]

Initial Conditions:

- ☒ Zero Initial Conditions - Start from Unstressed State
- ☐ Continue from State at End of Nonlinear Case [ ]

Important Note: Loads from this previous case are included in the current case

Modal Load Case:

All Modal Loads Applied Use Modes from Case: MODAL [ ]

Loads Applied:

Load Type	Load Name	Scale Factor
Load Pattern	DEAD	1.
Load Pattern	DEAD	1.
Load Pattern	liveroof	0.2
Load Pattern	livelfloor	0.2
Load Pattern	bloque	1.

[Add] [Modify] [Delete]

**Figure 4-16.** User Graphics Interface for SAP2000 Load Case Data for Initial Pushover Analysis



Load Case Name:

Notes:

Initial Conditions:

☐ Zero Initial Conditions - Start from Unstressed State

☒ Continue from State at End of Nonlinear Case

Important Note: Loads from this previous case are included in the current case

Modal Load Case

All Modal Loads Applied Use Modes from Case:

Loads Applied

Load Type	Load Name	Scale Factor
Accel	UX	-1.
Accel	UX	-1.

Load Case Name:

Notes:

Initial Conditions:

☐ Zero Initial Conditions - Start from Unstressed State

☒ Continue from State at End of Nonlinear Case

Important Note: Loads from this previous case are included in the current case

Modal Load Case

All Modal Loads Applied Use Modes from Case:

Loads Applied

Load Type	Load Name	Scale Factor
Mode	1	-1.
Mode	1	-1.

**Figure 4-17.** Load Case Data for Lateral Pushover Analysis

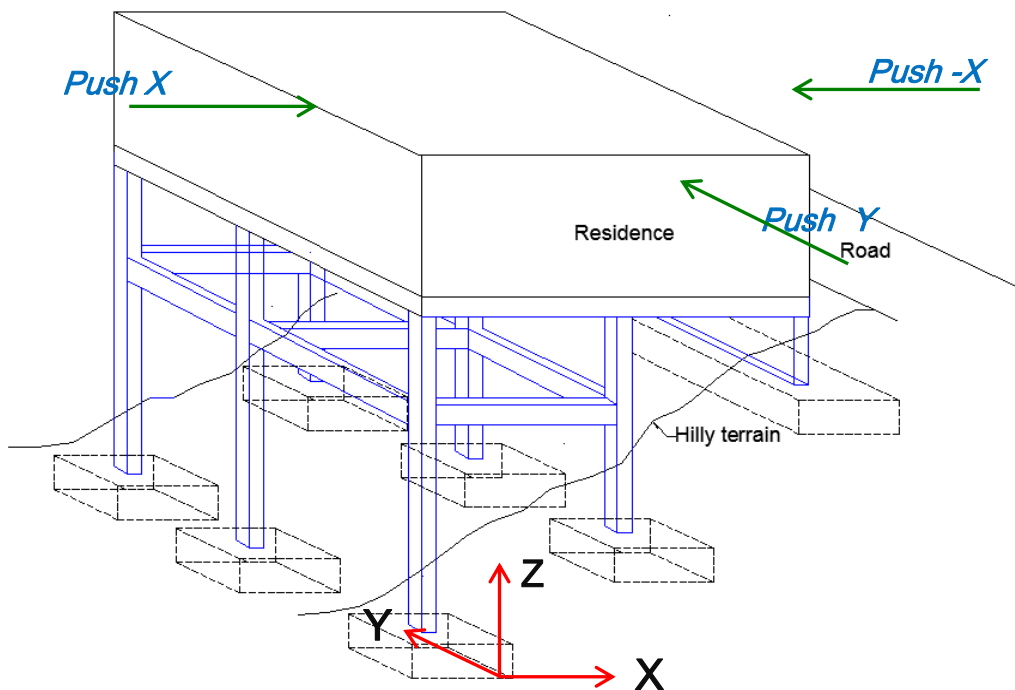


**Figure 4-18.** Pushover Load Cases

5. The analysis was then run and pushover curves were obtained. The results are presented in Chapter 6.

### **4.3 NONLINEAR TIME HISTORY ANALYSIS**

In order to examine more accurately nonlinear behavior of structures, nonlinear time history analysis has to be carried out. In this method, the structure is subjected to real ground motion records. This makes this analysis method quite different from all the other approximate methods as the inertial forces are directly determined from the ground motions and the response of the structure is calculated as a function of time, considering the dynamic properties of the structure. The appropriate selection of ground motions is a difficult task in earthquake engineering practice because of uncertainties exist on their nature (Themelis, 2008). The calculated response can be very sensitive to the characteristics of the ground motion used as seismic input. Therefore, in this study a set of worldwide earthquake record similar to those expected in the Puerto Rico region were used. The selected records were used by Irizarry (1999) to develop seismic design spectra for the main cities of Puerto Rico. Specific details about earthquake record selection are provided in section 4.5.

There are two methods to perform a nonlinear time history analysis of a structure in SAP2000: Modal Time History and Direct Integration. The modal time history method has shown to give results faster with a good degree of accuracy; however the nonlinearity is restricted to the Link elements. On the other hand, the direct integration method includes all types of nonlinearity (Hinge, link, etc.) and it seems to be a better approach for a nonlinear dynamic analysis. In this study the nonlinear time history analysis was performed using the direct integration method.

### **4.4 NONLINEAR TIME HISTORY ANALYSIS WITH SAP2000**

Direct integration of the full equations of motion without the use of modal superposition is available in SAP2000. Direct integration methods are used to solve an initial value problem using step-by-step integration in time. Direct integration results are extremely sensitive to time step size, and therefore the analysis should usually be repeated with

varying time steps until convergence is achieved. The time-integration methods available in SAP2000 include the Newmark, Wilson, Hilber-Hughes-Taylor, Collocation and Chung and Hulbert techniques. The “Hilber-Hughes-Taylor alpha” (HHT) method was used, which was recommended in the SAP2000 reference manual for poorly converging nonlinear time-history cases. Hilber-Hughes-Taylor is an implicit method that can handle numerical damping without degrading the order of accuracy. In direct integration time history analysis, the damping in the structure is modeled using a full damping matrix. This allows for coupling between the modes to be considered. For each direct integration time history analysis case, proportional damping coefficients that apply to the structure as a whole were specified.

A nonlinear direct integration time history analysis can be initiated from zero initial conditions (unloaded structure) or continued from a nonlinear static analysis or another direct integration time history nonlinear analysis. The vertical loads that correspond to dead loads and 20% of live loads are taken as the initial analysis case.

#### **4.4.1 DAMPING**

The damping model used by SAP2000 for time history analysis via direct integration is called mass and stiffness proportional damping coefficients. For the analysis, the damping ratio was specified as 5%. Using specified first and second periods the program calculates the mass proportional and stiffness proportional coefficients.

#### **4.4.2 NONLINEAR MATERIAL BEHAVIOR**

Material nonlinearity was defined in the models for pushover analysis thru plastic hinges. The same criteria will be considered in the nonlinear direct integration time history analysis. The energy dissipation which occurs during time history analysis may be modeled using hysteretic links. Links are useful for capturing dynamic loading and unloading because of their multi-axial response. However, hinges dissipated energy

thru the use of isotropic dissipation. For isotropic hysteresis, hinges unload elastically, parallel to the initial stiffness tangent (A-B slope, Figure 4-2), while for other hysteresis types, unloading follows a more complex nonlinear relationship.

## **4.5 EARTHQUAKE GROUND MOTION RECORD SELECTION**

This section describes the earthquake ground motions records selected as input for the nonlinear time history analysis. Data of historical earthquakes in Puerto Rico is scarce and no strong motion records of those events exists (Irizarry, 1999). In the absence of local strong earthquake records, the selections of ground motion records were based in the work done by Irizarry (1999).

Irizarry suggested maximum probable design earthquakes and design spectra for Puerto Rico's main municipalities of Mayagüez, Ponce, and San Juan. The proposed design earthquakes and design spectra were developed considering the geologic conditions of the Island and past earthquake records from a worldwide database. The parameters used in the search for past earthquake records were earthquake magnitude, focal depth, epicentral distance, site's geology and structure type. Irizarry divided the Puerto Rico region in ten seismic sources zones as shown in Figure 4-19. For each seismic source zone the maximum expected magnitude and maximum focal depth were established from the literature and data from the Puerto Rico Seismic Network (PRSN), and are shown in Table 4-1.

Irizarry calculated the range of epicentral distances as the difference of the coordinates between the farthest and closet point of each seismic source zone relative to each considered city (Table 4-2).

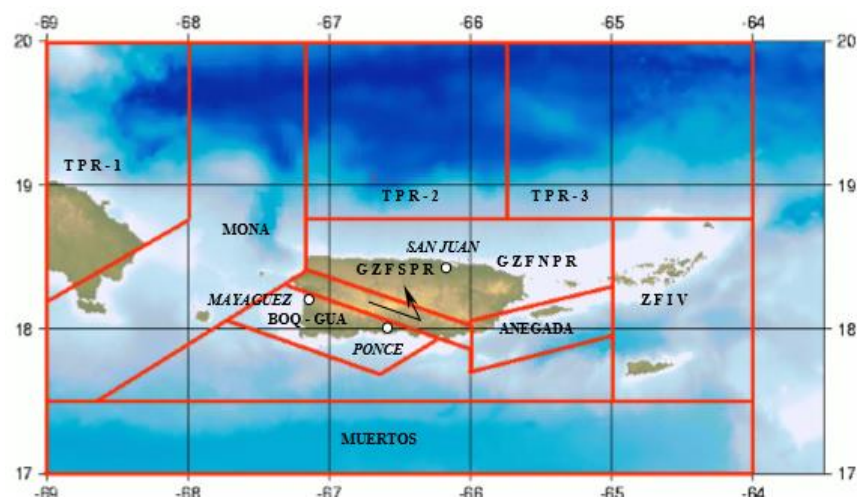


**Figure 4-19.** Seismic Source Zones in the Region of Puerto Rico. Irizarry (1999)

**Table 4-1.** Maximum Expected Earthquake Magnitude and Maximum Depth for Each Seismic Zone Fault. Irizarry (1999)

Seismic Source Zone	Maximum Magnitude	Maximum Depth (km)
Puerto Rico Trench I	8.0	150
Puerto Rico Trench II	8.0	150
Puerto Rico Trench III	8.0	150
Mona Canyon	7.5	200
Great Northern Puerto Rico Fault	6.5	40
Great Southern Puerto Rico Fault	6.5	40
Anegada Trough	7.5	30
Boquerón-Guánica Fault	6.5	40
Muertos Trough	7.5	50
Virgin Islands	7.5	50

**Table 4-2.** Epicentral Distances Used for the Earthquake Record search. Irizarry (1999)

Epicentral Distance, km						
City	San Juan		Ponce		Mayagüez	
Fault Zone	Min.	Max.	Min.	Max.	Min.	Max.
PRTI	202	353	167	339	107	283
PRTII	32	207	81	243	59	253
PRTIII	50	285	122	357	160	392
GSPRFZ	44	137	20	93	20	136
BOQ-GNC	64	179	0	124	0	100
ANEGADA	46	135	64	175	123	232
MONA	109	380	41	331	19	296
MUERTOS	107	349	56	302	78	363
GNPRFZ	0	128	20	193	21	239
VIFZ	118	252	170	291	227	345

With the data from Tables 4-1 and 4-2 and considering free field records in competent soils, Irizarry selected all records that comply with the above conditions. For each record, Irizarry developed the response spectra. Tables 4-3 and 4-4 show the dominant earthquake obtained by Irizarry. Four earthquake records were selected from these tables with a range of periods similar to the period of the analytical models. The selected earthquake records are: San Salvador CIG, San Salvador IGN, Parkfield (Usaca) and Northridge (Rollhill). The selected ground motion records represent the potential earthquake hazards for Puerto Rico. Figures 4-20 to 4-27 show the four time histories of acceleration and spectral acceleration used in this investigation.

**Table 4-3.** Characteristics of the Dominant Earthquake in the Response Spectra Envelope for Mayagüez and Ponce (Irizarry 1999)

Period Range	Fault Zone	Filename	EPI (Km)	Depth (km)	Magnitude	Earthquake
0-0.4	BOQ-GNC	CIG.EW	4.3	8	5.4	San Salvador
0.4-1.3	BOQ-GNC	IGN.EW	5.7	8	5.4	San Salvador
1.3-1.6	BOQ-GNC	CIG.EW	4.3	8	5.4	San Salvador
1.6-1.8	Mona	Castaicn.v2	4.1	18	6.7	Northridge
1.8-3.0	BOQ-GNC	CIG.EW	4.3	8	5.4	San Salvador

**Table 4-4.** Characteristics of the Dominant Earthquake in the Response Spectra Envelope for San Juan (Irizarry 1999)

Period Range	Fault Zone	Filename	EPI (Km)	Depth (km)	Magnitude	Earthquake
0-.05	GNPRFZ	Usaca01.109	27	6	5.5	Parkfield
.05-.10	PRT II	Mex03.112	83	20	7.6	Michoacan Aft
..10-.16	GNPRFZ	Mtwilson l.v2	24	11	5.8	Sierra Madre
.16-.18	GNPRFZ	Usaca38.061	31	6	5.3	Humbolt
.1-.20	GNPRFZ	Jap03.104	103	31	6.4	Japanese EQ
.20-.50	GNPRFZ	Usaca01.109	27	6	5.5	Parkfield
.50-.70	Group	Rollhill 1v.2	50	18	6.7	Northridge
.70-.80	Group	pacoimaw.v2	43	9	6.1	Whittier
.80-1.2	Group	Usaca66.001	62	11	7.1	Loma Prieta
1.2-1.3	Group	Jap03.120	90	40	5.1	Japanese EQ
1.3-3	Group	Usaca66.001	62	11	7.1	Loma Prieta

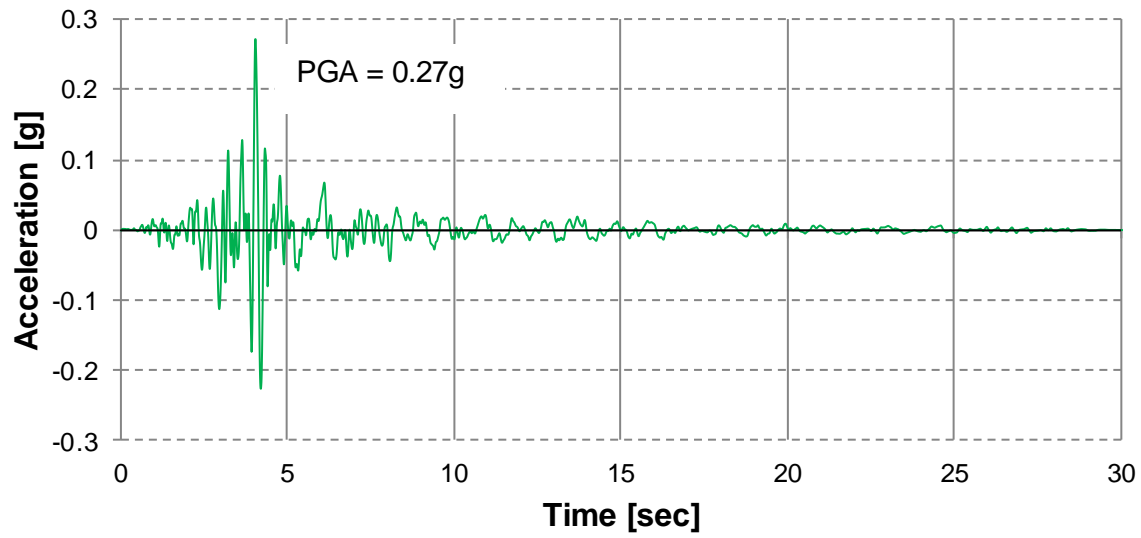


**Figure 4-20.** Parkfield Earthquake Record

The peak ground acceleration (PGA) is 0.27 g and it occurred at 4.04 seconds.

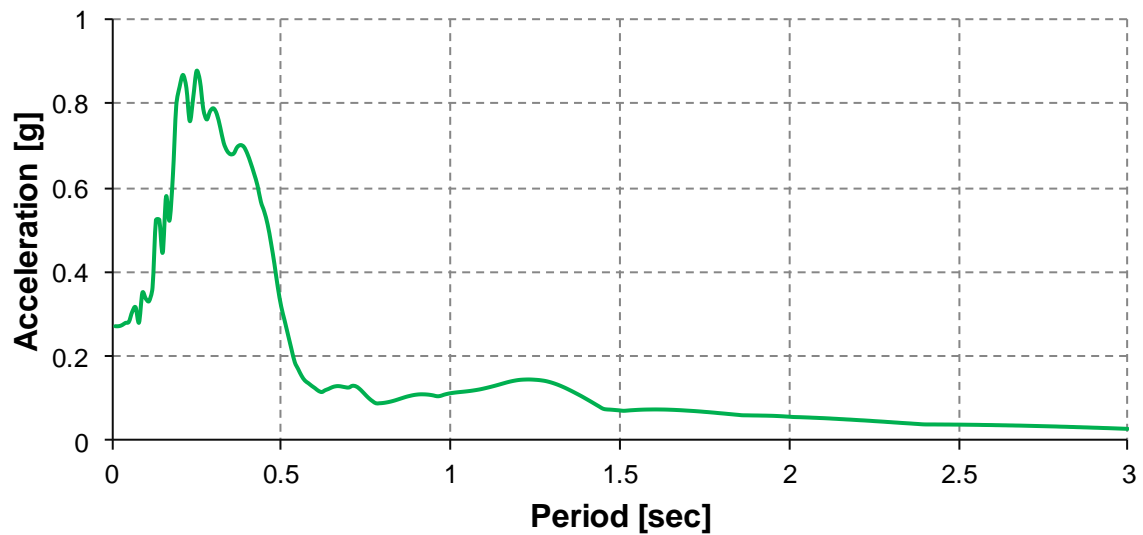


**Figure 4-21.** Parkfield 5% Damping Response Spectra

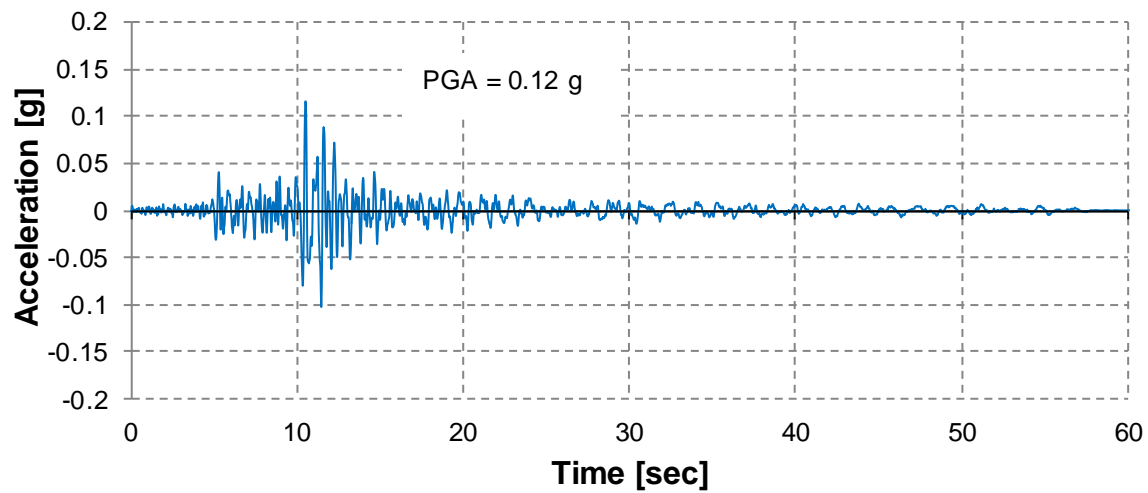


**Figure 4-22.** Northridge -Rollhill Earthquake Record

The peak ground acceleration (PGA) is 0.12 g and it occurred at 4.04 seconds.

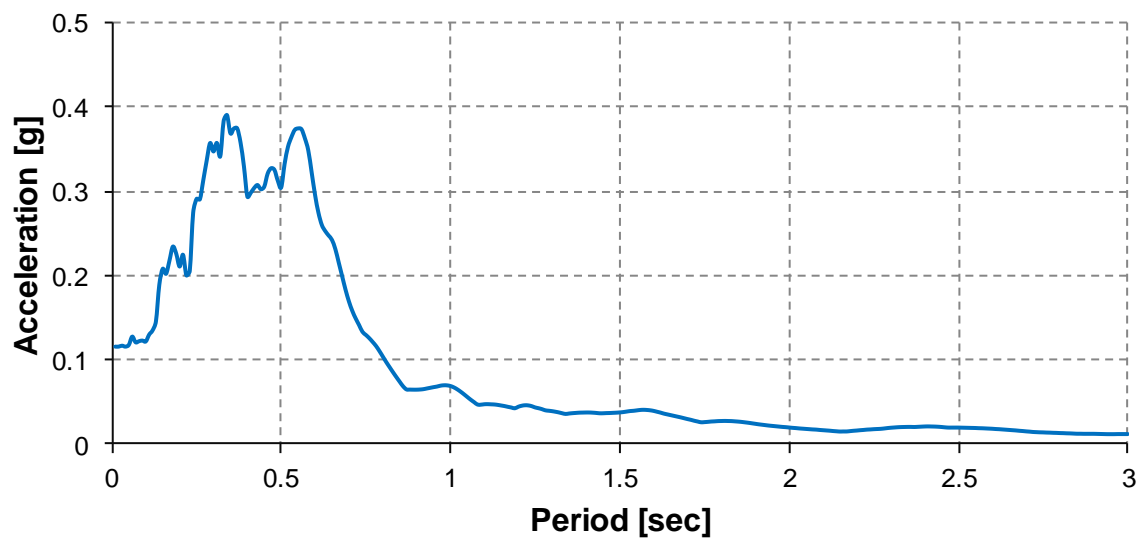


**Figure 4-23.** Northridge 5% Damping Response Spectra



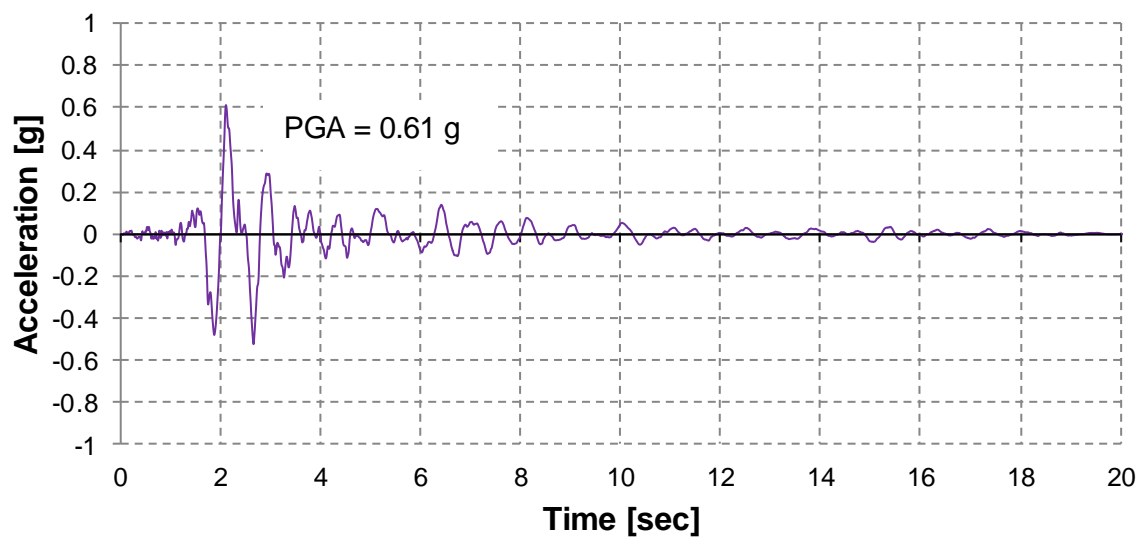


**Figure 4-24.** San Salvador IGN Earthquake Record

The peak ground acceleration (PGA) is 0.61 g and it occurred at 2.1 seconds.

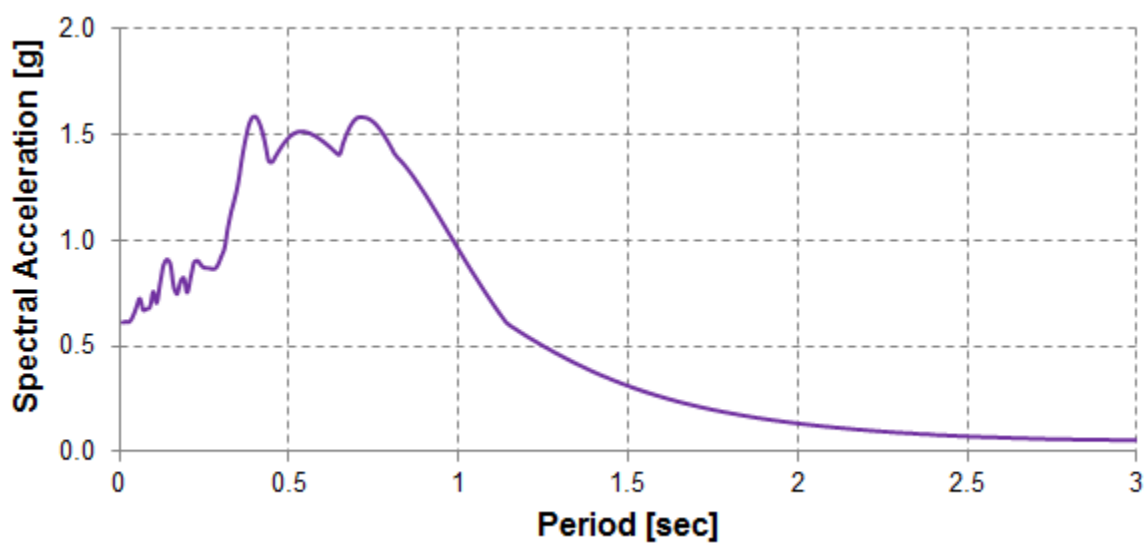


**Figure 4-25.** San Salvador IGN 5% Damping Response Spectra

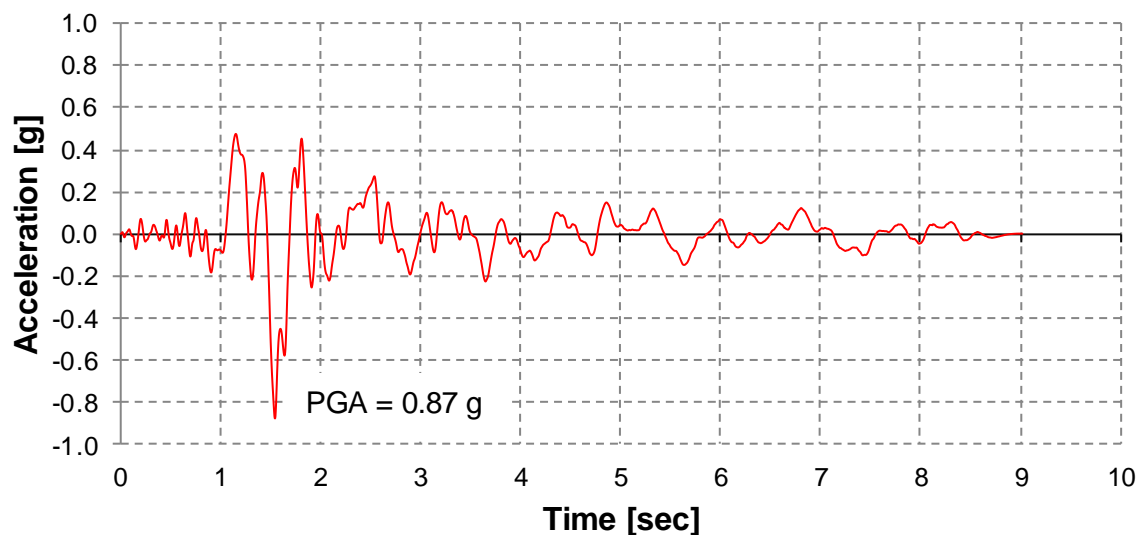


**Figure 4-26.** San Salvador CIG Earthquake Record

The peak ground acceleration (PGA) is 0.87 g and it occurred at 1.54 seconds.

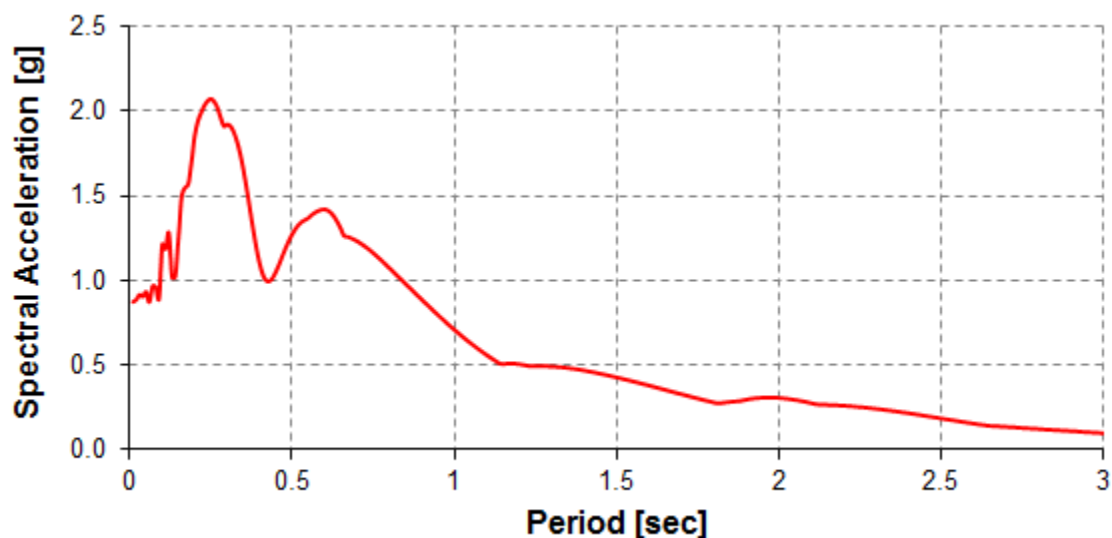


**Figure 4-27.** San Salvador CIG 5% Damping Response Spectra

In order to support the scenario where an earthquake of a peak ground acceleration PGA of 0.6 g or higher may occur, Figure 4-27 presents the probabilistic seismic hazard assessment for Puerto Rico based on a study performed by the U.S Geological Survey (USGS 2003). The study applied the probabilistic hazard methodology developed by the USGS as described by Frankel et. al (1996, 2002), and presents maps of probabilistic

ground motions: peak ground acceleration (PGA), 1.0-second spectral response, and 0.2-second spectral response, with 2% and 10% probability of exceedance in 50 years, corresponding to return periods of approximately 2500 and 500 years, respectively (Mueller et al, 2003). From Figure 4-28 it can be noticed that the peak ground acceleration map for Puerto Rico shows values between 0.30 and 0.60 g. The map shows that the maximum PGA is expected for the west area of the Island, specifically for the municipalities of Cabo Rojo and Lajas. In addition, from the study of damages during past earthquakes, it has been shown that the surface topography on the site of the structure can considerably amplify the ground motions. Arroyo (2001) concluded that that the amplification factor for the PGAs varies in a range of 1 to 2.35.

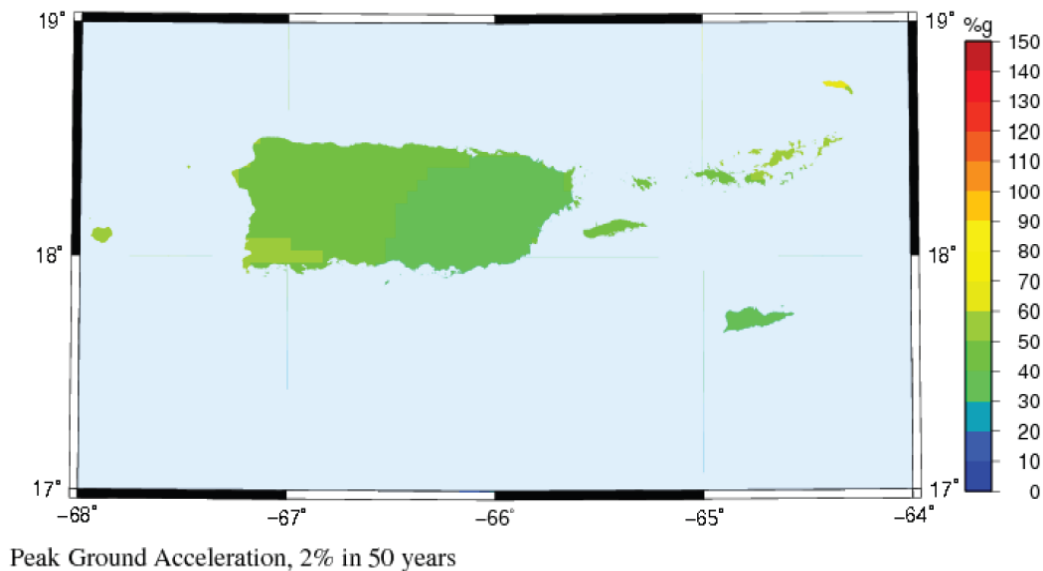


**Figure 4-28.** Probabilistic Seismic Hazard Assessment for Puerto Rico. (USGS 2003)

## CHAPTER 5. RESIDENCE SEISMIC PERFORMANCE

---

### 5.1 INTRODUCTION

The seismic performance of a structure is measured as the result of the state of damage under a certain level of seismic loading. The state of damage is quantified by the drift of the roof and the displacement of the structural elements. As discussed in the previous chapter pushover analysis gives an insight into the maximum base shear that the structure is capable of resisting. The purpose is to give a realistic assessment of how a structure will perform when subjected to earthquake ground motion

The Capacity Spectrum Method (CSM) is a procedure to evaluate the nonlinear static response of a structure. The CSM was developed by Freeman et al. (1975). The objective is to estimate the maximum displacement that the structure can achieve. Inelastic displacements increase damping and reduce demand. The CSM reduces the demand to find an intersection with the capacity spectrum, where the displacement is consistent with the implied damping. This intersection point of the capacity spectrum and demand spectrum, where the capacity equals the demand, is known as the performance point. It corresponds to the state that the structure is expected to reach under the considered earthquake. The performance point is the inelastic displacement that the structure is going to experience for the given level of earthquake. This is a very important parameter in pushover analysis because the global and local component responses (forces and displacement) of the building at the target displacement are compared with the desired performance limit state to know the building performance.

The Capacity Spectrum Method is recommended by ATC-40 as a displacement-based design and assessment tool for structures. The method has gone through several modifications since its development. The most recent three versions (Procedures A, B and C) of CSM are presented in detail in ATC-40. The CSM requires that both the pushover curve and the demand response spectrum curve be represented in format

known as ADRS. Section 5.2 summarizes the Capacity Spectrum Method according to ATC-40.

## 5.2 CAPACITY SPECTRUM METHOD (ATC 40)

The Capacity Spectrum Method reduces the elastic response spectrum to intersect the pushover curve in spectral coordinates to find a performance point. The vulnerability of the residences will be evaluated using the performance point. SAP2000 calculates performance point of the structure using CSM (ATC 40).

The procedure to estimate the performance point as per ATC 40 is given below. In order to verify the SAP2000 output results, the following steps include a detailed example with verification calculation.

1. **Obtain the Pushover Curve:** A capacity curve (base shear versus roof displacement) of the analytical model was obtained by means of a pushover analysis. Figure 5-1 shows a typical pushover curve obtained with SAP2000. The curve corresponds to a pushover case performed with a load pattern proportional to the floor masses.

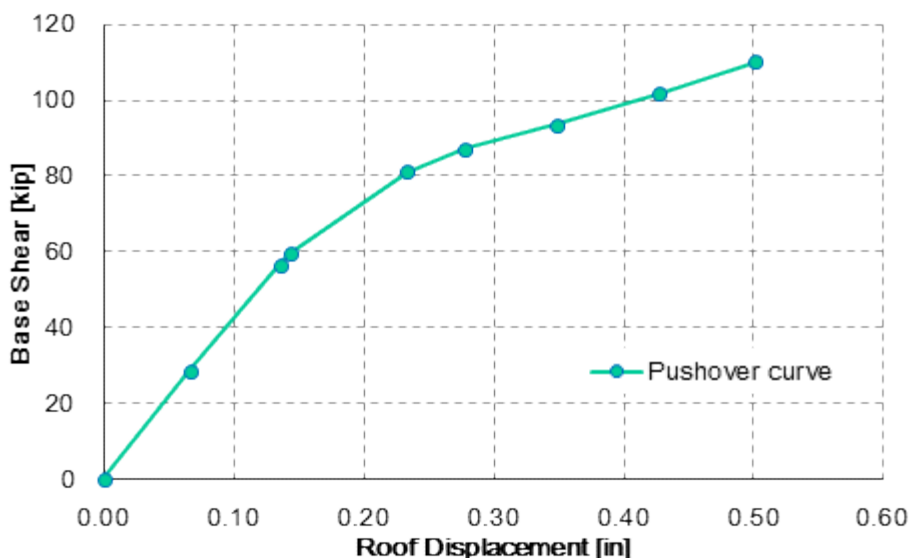


**Figure 5-1. Pushover Curve**

2. **Convert the pushover curve to ADRS format:** As mentioned before, CSM requires that both the pushover curve and the demand response spectrum curves be plotted in the spectral acceleration ( $S_a$ ) vs. spectral displacement ( $S_d$ ) domain (ADRS format). In order to convert the pushover curve into a capacity spectrum which is a representation of the capacity curve in ( $S_a$ ) vs. ( $S_d$ ) format, it is necessary to do a point by point conversion to first fundamental mode spectral coordinates. Any point (Base Shear ( $V_i$ ) vs. Roof displacement ( $U_{ri}$ )) on the capacity curve (Figure 5-1) is converted to the corresponding point ( $S_a, S_d$ ) on the capacity spectrum. The required equations to make the transformation are the equations (5-1) to (5-4). The example was done with the X direction. The fundamental mode shape in the X orthogonal direction is shown in Figure 5-2. Conversion data of the pushover curve into capacity spectrum is shown in Table 5-1. Figure 5-3 shows comparison of the Capacity spectrum obtained directly by the program and by calculating the points using the formulas (5-1) to (5-4). SAP2000 automatically convert pushover curves to capacity curves using the following formulas.

$$S_a = \frac{V_i/W}{\alpha_i} \quad (5-1)$$

$$S_d = \frac{U_{ri}}{PF_1 \phi_{1,r}} \quad (5-2)$$

$$PF_1 = \frac{\sum_{j=1}^n w_i \phi_i}{\sum_{i=1}^n w_i \phi_i^2} \quad (5-3)$$

$$\alpha_1 = \frac{[\sum_{j=1}^n w_i \phi_i]^2}{\sum_{i=1}^n w_i \sum_{i=1}^n w_i \phi_i^2} \quad (5-4)$$

where:

- $W$  : total weight of the residence [kip],  
 $w_i$  : weight at any level [kip],  
 $V_i$  : base shear at a step [kip],  
 $U_{ri}$  : roof displacement at a step [in],  
 $\alpha_1$  : modal mass coefficient for the fundamental mode,  
 $PF_1$  : modal participation factor for the fundamental mode [k-s<sup>2</sup>],  
 $\phi_{1,r}$  : amplitude of the fundamental mode at roof level,  
 $S_a$  : spectral acceleration [g], and  
 $S_d$  : spectral displacement [in].

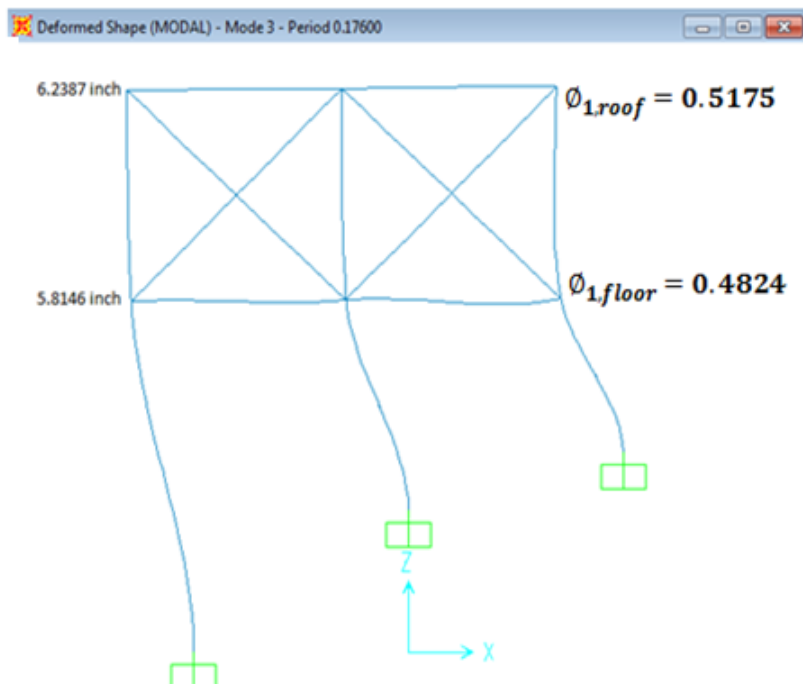


**Figure 5-2.** Fundamental Mode Shape: X direction

**Table 5-1.** Data to Convert Pushover Curve to Capacity Spectrum Curve

	$\phi$	<b>W</b> (kip)
<b>roof</b>	0.518	82.70
<b>floor</b>	0.482	57.05

$$W = 139.75$$

$$PF_1 = \frac{82.70 * 0.518 + 57.05 * 0.482}{82.70 * 0.518^2 + 57.05 * 0.482^2} = 2.011 \text{ k-s}^2$$

$$\alpha_1 = 0.973 \text{ (obtained from SAP200)}$$

PUSH X Uniform mass			Capacity Curve hand calculation		Capacity Curve SAP2000	
Step	$U_{ri}$ (in)	$V_i$ (kip)	<b>Sd</b> (in)	<b>Sa</b> (g)	<b>Sd</b> (in)	<b>Sa</b> (g)
0	0.00	0.00	0.00	0.00	0.00	0.00
1	0.07	28.59	0.06	0.21	0.07	0.22
2	0.14	56.66	0.13	0.42	0.13	0.43
3	0.14	59.88	0.14	0.44	0.14	0.46
4	0.23	81.12	0.22	0.60	0.22	0.62
5	0.28	87.27	0.27	0.64	0.27	0.66
6	0.35	93.63	0.33	0.69	0.34	0.71
7	0.43	101.64	0.41	0.75	0.41	0.77
8	0.50	110.21	0.48	0.81	0.47	0.77



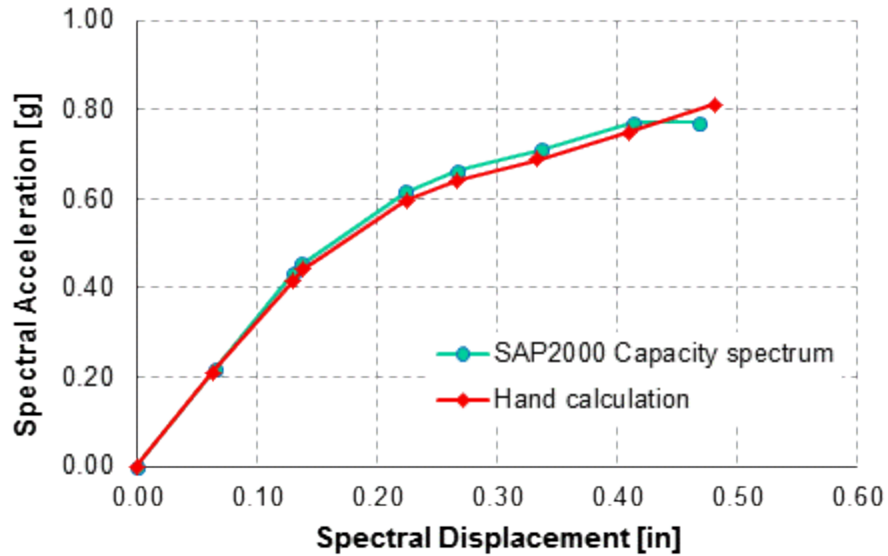


**Figure 5-3. Capacity Spectrum Curve**

3. **Define the Earthquake demand response spectrum:** The UBC 97 design demand spectrum ( $S_a$  vs  $T$ ) for soil profile type  $S_d$  (Figure 5-4) was used. Chapter 6 explains in detail the earthquake demand spectrum used to evaluate the performance of the analytical models under different events. The data to generate soil type  $S_d$  response spectrum are shown in Table 5-2. When the capacity spectrum option is chosen, the program calculates the response spectrum automatically based on the input data seismic coefficient  $C_A$  and the seismic coefficient  $C_V$ . The seismic coefficients depend on the seismic zone ( $Z$ ) and soil profile type. The user can also upload any earthquake response spectrum from a file.

**Table 5-2.** UBC-97 Design Spectrum Data, for Soil Type  $S_d$ Soil profile =  $S_d$ 

" when soil properties are unknown"

Seismic Zone = 3

Zone factor ( $Z$ ) = 0.3 $C_A = 0.36$  seismic coefficient, table 16-Q UBC 97 $C_V = 0.54$  seismic coefficient, table 16-R UBC 97

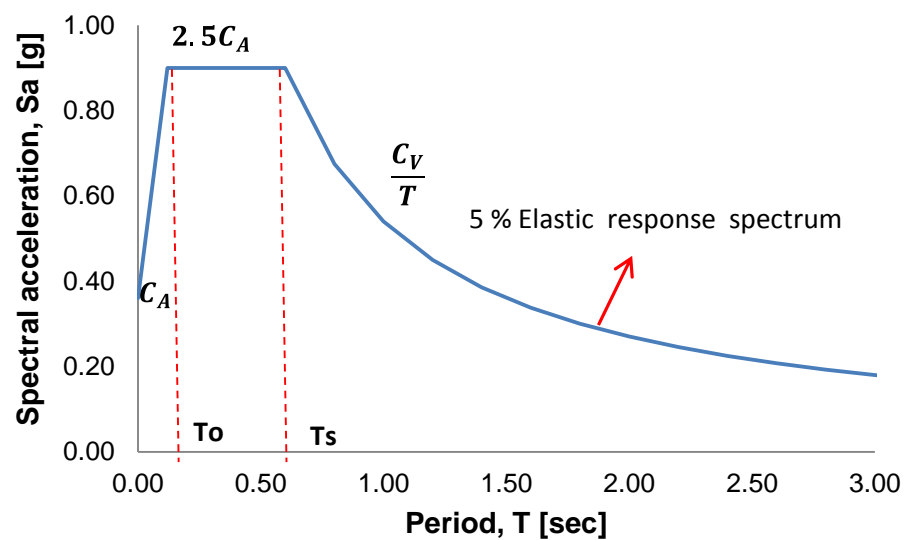
$$T_s = \frac{C_V}{2.5C_A} = 0.6 \text{ sec}$$

$$T_0 = 0.2T_s = 0.12 \text{ sec}$$

 $S_a$  = pseudo spectral acceleration

T = Period

<b>Sa (g)</b>	<b>T(sec)</b>
0.36	0.00
0.90	0.12
0.90	0.60
0.90	0.60
0.68	0.80
0.54	1.00
0.45	1.20
0.39	1.40
0.34	1.60
0.30	1.80
0.27	2.00
0.25	2.20
0.23	2.40
0.21	2.60
0.19	2.80
0.18	3.00
0.17	3.20

**Figure 5-4.** UBC-97 Demand Response Spectrum for  $S_d$  Soil Type

4. **Convert the demand response spectrum to ADRS format:** Convert design demand spectrum ( $S_a$  vs  $T$ ) into acceleration – displacement ( $S_a$  vs  $S_d$ ) response spectrum (ADRS) format. Every point on the demand response spectrum curve has associated a unique spectral acceleration, spectral velocity, spectral displacement and natural period ( $T$ ). To convert a spectrum from standard to ADRS format, it is necessary to determine the value at each point on the curve. The line radiating from the origin to a point on the curve represents the natural period. The spectral displacement is related to spectral acceleration and time period as given in equation (5-2). The data to generate the demand spectrum for soil type  $S_d$  in ADRS format is shown in Table 5-3. Figure 5-2 shows the design spectrum for  $S_d$  soil type in ADRS format. The graphical representation of the response spectrum in the traditional and in ADRS format is shown in Figure 5-6. The program SAP2000 automatically calculates the spectrum in the ADRS format.

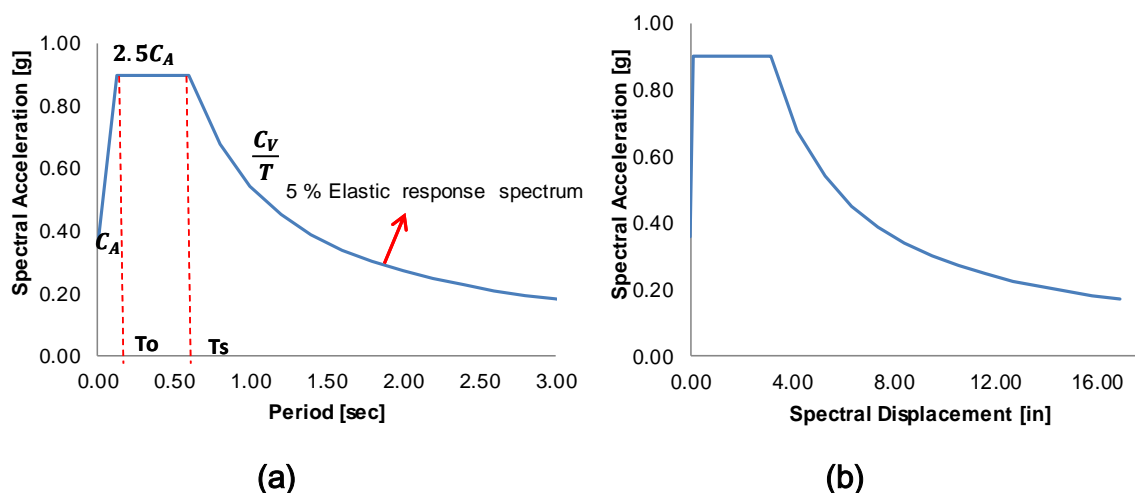
$$S_d = \frac{T^2}{4\pi^2} S_a g \quad (5-5)$$

where:

$S_a$  : spectral acceleration [g],  
 $S_d$  : spectral displacement [in], and  
 $g$  : constant gravity [in/s<sup>2</sup>].

**Table 5-3.** UBC-97 Demand Spectrum Data in ADRS Format for Soil Type  $S_d$ 

$T, (\text{sec})$	$S_a, g$	$S_d(\text{in})$
0.00	0.36	0.00
0.12	0.90	0.13
0.60	0.90	3.17
0.60	0.90	3.17
0.80	0.68	4.23
1.00	0.54	5.29
1.20	0.45	6.34
1.40	0.39	7.40
1.60	0.34	8.46
1.80	0.30	9.51
2.00	0.27	10.57
2.20	0.25	11.63
2.40	0.23	12.68
2.60	0.21	13.74
2.80	0.19	14.80
3.00	0.18	15.86
3.20	0.17	16.91

**Figure 5-5.** UBC-97 Demand Response Spectrum for  $S_d$  soil type. (a) Traditional Response Spectrum (b) ADRS Response Spectrum

5. **Draw a family of reduced response spectrum:** The total effective damping ( $\beta_{\text{eff}}$ ) that occurs when the structure is pushed into the inelastic range can be viewed as a combination of viscous and hysteretic damping. A 5 % viscous damping inherent in the structure was assumed. The hysteretic damping is related to the area inside the

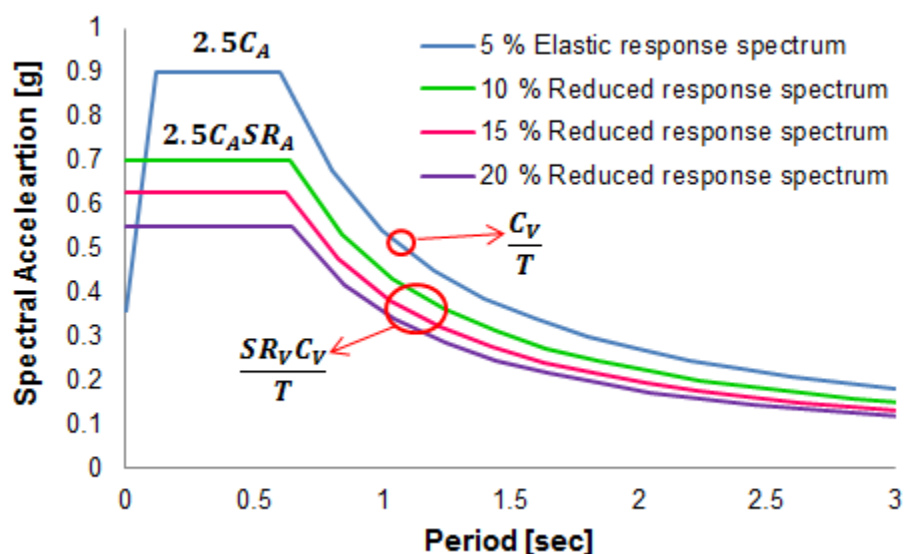
loops that are formed when the base shear is plotted against the structure displacement. The hysteretic damping is directly related to the structure ability to dissipate energy. A damping modification factor ( $\kappa$ ) take into consideration the structural behavior of the building in terms of it ability to dissipate energy base of the lateral resisting system and current code ductility requirements. Further discussion about the hysteretic damping and the damping modification factors are given in step 7. The family of reduced response spectra to be considered corresponds to effective damped values ( $\beta_{eff}$ ) ranging from 5 percent to the maximum value allowed for the building's structural behavior type (Table 5-4). Type A represents buildings whose primary elements make up an essentially new lateral system and little strength or stiffness is contributed by noncomplying elements. Type B denotes buildings whose primary elements are combination of existing and new elements. Type C represents buildings whose primary elements make up noncomplying lateral force system with poor or unreliable behavior. The residences analyzed in this investigation were considered as Type C. The maximum value  $\beta_{eff}$  for a type C building is 20 %, thus in addition to the elastic (5 % damped) demand spectrum; spectra for 10 % 15 % and 20 % were developed. For different values of  $\beta_{eff}$  the spectral reduction factors ( $SR_A, SR_V$ ) are calculated with equations (5-6) and (5-7). The spectral reduction factors are used to reduce the elastic 5% damped design response spectrum to account for yielding, i.e. hysteric effects. The reduced spectra curves were plotted in Figure 5-6.

$$SR_A = \frac{3.21 - .68 \ln(\beta_{eff})}{2.12} \quad (5-6)$$

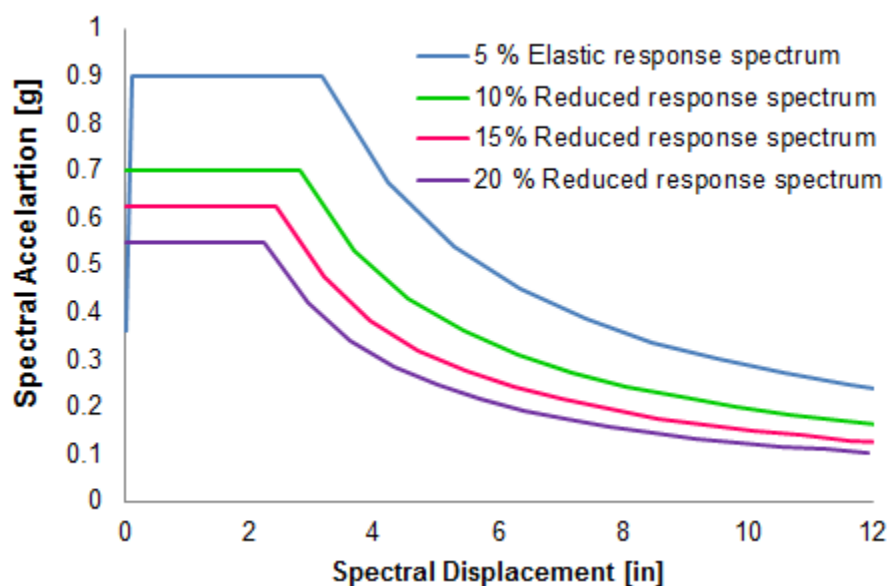
$$SR_V = \frac{2.31 - 0.41 \ln(\beta_{eff})}{1.65} \quad (5-7)$$

**Table 5-4.** Structural Behavior Type (ATC 40)

Shaking Duration	Essentially New Building	Essentially Existing Buildings	Poor Existing Building
short	Type A	Type A	Type C
long	Type B	Type B	Type C



(a)



(b)

**Figure 5-6.** Family of Reduced Response Spectrum for  $S_d$  soil type. (a) Family of Reduced Response Spectrum Traditional Format ( $S_a$  vs  $T$ ). (b) Family of Reduced Response Spectrum in ADRS Format ( $S_a$  vs  $S_d$ )

6. **Estimate trial performance point:** A trial performance point  $a^*$ ,  $d^*$  is selected. This may be done using the equal displacement approximation (Figure 5-7) or on the basis of engineering judgment. The initial slope of the bilinear curve is equal to the initial stiffness of the residences. The post yield segment of the bilinear representation should be run through the capacity spectrum at a displacement equal to the spectral displacement of the 5 percentage damped spectrum of the initial pre - yield stiffness (equal displacement rule) point  $a^*$ ,  $d^*$ . The post-yield segment should then be rotated around this point to balance the areas A1 and A2. The intent of setting A1 equal to A2 is to have equal energy associated with each curve. The area A1 was approximate by equal to the area A2 using an iterative procedure rotating the green line around the fixed point  $(a^*, d^*)$ .

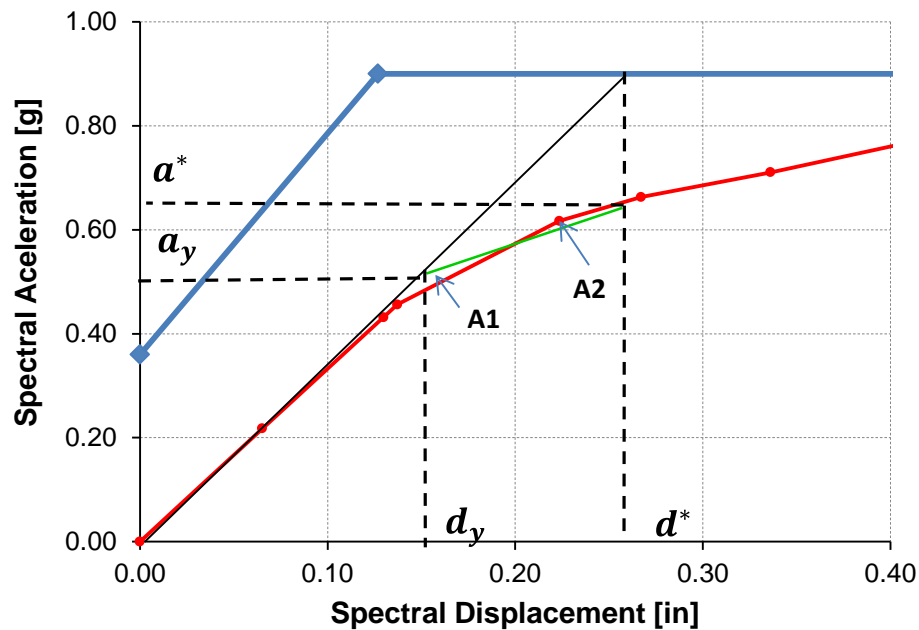


**Figure 5-7.** Bilinear Representation of Capacity Spectrum

7. **Calculate the Performance point:**

Table 5-6 summarizes the calculations to obtain the performance point.

- Calculate the effective damping ( $\beta_{eff}$ ) for various displacements near point  $a^*$  and  $d^*$  (Figure 5-7).  $\beta_{eff}$  is defined as:

$$\beta_{eff} = \frac{63.7\kappa (a_y d_{pi} - d_y a_{pi})}{a_{pi} d_{pi}} \quad (5-8)$$

The  $\kappa$  factor is a damping modification factor and it depends on the structural behavior of the building, which depends on quality of the seismic resisting system. As discussed in step 5, the residences analyzed in this investigation were considered as Type C. The range and limits of the  $\kappa$  factor for the three structural systems are shown in Table 5.5.

**Table 5-5.** Values for Damping Modification Factor,  $\kappa$  (ATC-40)

<b>Structural Behavior Type <sup>1</sup></b>	<b><math>\beta_0</math> (percent)</b>	<b><math>\kappa</math></b>
Type A <sup>2</sup>	$\leq 16.25$	1.0
	$> 16.25$	$1.13 - \frac{0.51(a_y d_{pi} - d_y a_{pi})}{a_{pi} d_{pi}}$
Type B	$\leq 25$	0.67
	$> 25$	$0.845 - \frac{0.446(a_y d_{pi} - d_y a_{pi})}{a_{pi} d_{pi}}$
Type C	Any value	0.33

- Calculate  $T_s$ , the period where the 5% damped spectrum changes from the constant acceleration range to the constant velocity range, with equation (5-9):

$$T_s = \frac{C_V}{2.5C_A} \quad (5-9)$$

- For each  $d_{pi}$  value, calculate the corresponding period as:



$$T = 2\pi \left( \frac{d_{pi}}{a_{pi}} \right) \quad (5-10)$$

- For each  $T$  calculate for the corresponding spectral acceleration on the 5% damped spectrum ( $S_{a5\%}$ ) as:

$$S_{a5\%} = 2.5C_A \quad \text{if } T \leq T_s \quad (5-11)$$

$$S_{a5\%} = \frac{C_V}{T} \quad \text{if } T > T_s \quad (5-12)$$

- For each  $S_{a5\%}$  calculate the corresponding spectral displacement on the 5% damped spectrum ( $S_{d5\%}$ ) as

$$S_{d5\%} = S_{a5\%} \left( \frac{T}{2\pi} \right) \quad (5-13)$$

- For each  $d_{pi}$ , if  $T \leq T_s$ , calculate the spectral reduction factors  $SR_A$  using equation (5-6). If  $T > T_s$ , calculate the spectral reduction factor  $SR_V$  using equation (5-7)
- For each  $d_{pi}$ , the spectral acceleration ( $S_a$ ) and spectral displacement ( $S_d$ ) are calculated as

$$S_a = SR_A \text{ or } V S_{a5\%} \quad (5-14)$$

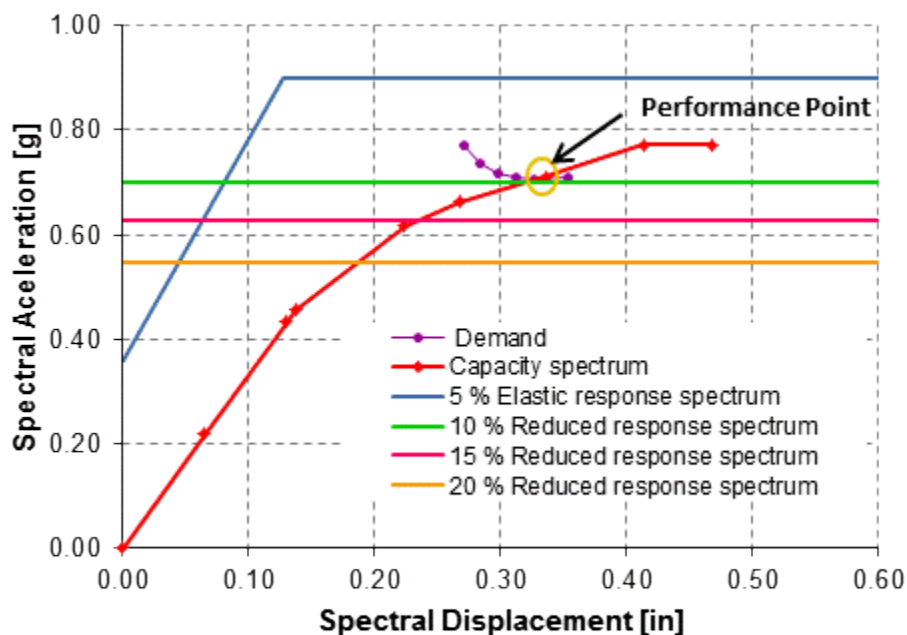
$$S_d = SR_A \text{ or } V S_{d5\%} \quad (5-15)$$

**Table 5-6.** Demand Curve Calculation**From Figure 5-7**

$$\begin{aligned}
 d_y &= 0.15 \text{ in} \\
 a_y &= 0.50 \text{ g} \\
 a^* &= 0.66 \text{ g} \\
 d^* &= 0.27 \text{ in}
 \end{aligned}$$

$d_{pi}$ (in)	$a_{pi}$ (g)	$\beta_{eff}$	$T$ (sec)	$SR_A$	$SR_V$	$T_s$ (sec)	$S_{a5\%}$ (g)	$S_{d5\%}$ (in)	$S_a$ (g)	$S_d$ (in)
0.15	0.50	5.00	0.18	1.00	1.00	0.60	0.90	0.27	0.90	0.27
0.20	0.57	7.78	0.19	0.86	0.89	0.60	0.90	0.32	0.77	0.27
0.24	0.62	8.81	0.20	0.82	0.86	0.60	0.90	0.35	0.73	0.28
0.28	0.67	9.35	0.21	0.80	0.84	0.60	0.90	0.37	0.72	0.30
0.32	0.73	9.61	0.21	0.79	0.84	0.60	0.90	0.40	0.71	0.31
0.36	0.78	9.72	0.22	0.78	0.83	0.60	0.90	0.42	0.71	0.33
0.45	0.90	9.67	0.23	0.79	0.84	0.60	0.90	0.45	0.71	0.35

8. **Plot the results:** The resulting  $S_a$  and  $S_d$  demand points from step 7 are plotted on the same chart as the capacity spectrum. The intersection of the line with the capacity spectrum defines the performance point. Figure 5-8 shows the demand curve obtained by SAP2000 and the verification calculations.

**Figure 5-8.** Performance Point – Capacity Spectrum Solution

## CHAPTER 6. NONLINEAR ANALYSIS RESULTS

### 6.1 LINEAR DYNAMIC ANALYSIS

The vibration modes were obtained to identify the initial dynamic properties of the models. A linear dynamic analysis is a useful tool to provide a preliminary understanding of the behavior of the structure. The participation factor shows how strongly a given mode contributes to the response of the structure when subjected to earthquake acceleration in a given direction.

#### 6.1.1 DYNAMIC ANALYSIS RESULTS: MODEL 1.1

Tables 6-1 shows the natural periods of Model 1.1b, Model 1.1c and Model 1.1d with the corresponding modal mass participation ratio. In the table, UX and UY represent the perpendicular to the road and parallel to the road translations respectively and RZ represents the rotation (torsion) about the Z axis normal to the structure plan. As mentioned before, the models were analyzed considering the effect of modeling the retaining wall. The letter “b” refers to pure frame, the letter “c” refers to masonry blocks and the letter “d” refers to shear walls. Figure 6-1 to 6-3 shows the plan view for the first, second and third mode shape for Model 1.1b, Model 1.1.c and Model 1.1d.

**Table 6-1. Dynamic Properties: Model 1.1**

Mode	Model 1.1b				Model 1.1c				Model 1.1d			
	Period (sec)	Modal participating mass ratio			Period (sec)	Modal participating mass ratio			Period (sec)	Modal participating mass ratio		
		UX	UY	RZ		UX	UY	RZ		UX	UY	RZ
1	0.47	0.00	0.97	0.07	0.31	0.00	0.51	0.50	0.33	0.00	0.48	0.51
2	0.21	0.00	0.03	0.93	0.19	1.00	0.00	0.00	0.18	1.00	0.00	0.00
3	0.19	1.00	0.00	0.00	0.05	0.00	0.43	0.44	0.04	0.00	0.20	0.19

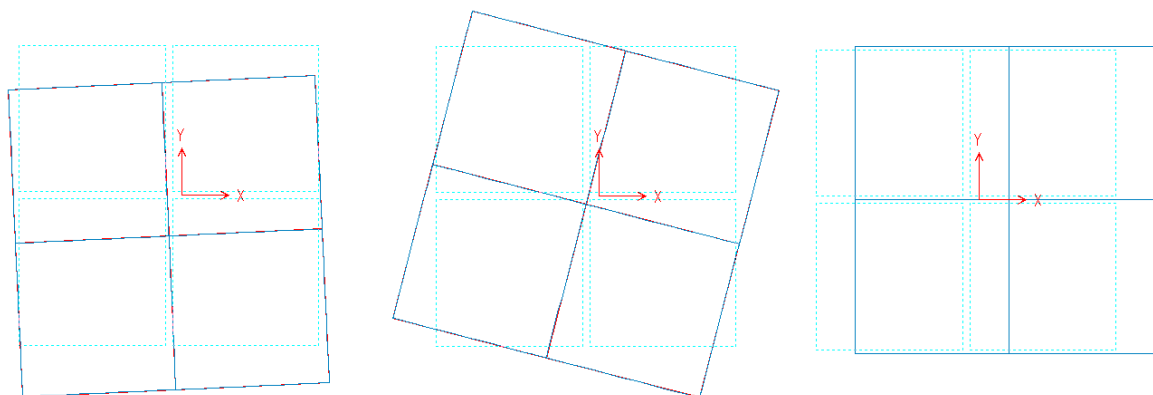


**Figure 6-1.** Deformed Mode Shape for Model 1.1b. (a) Mode 1 (b) Mode 2 (c) Mode 3

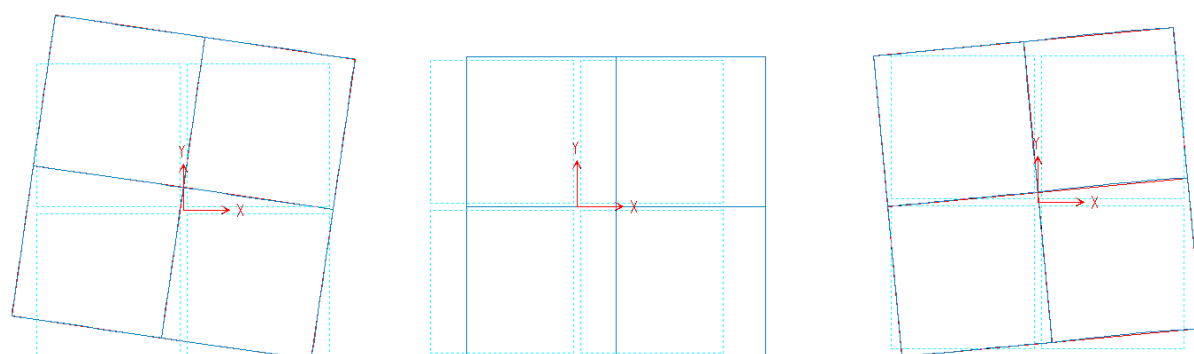


**Figure 6-2.** Deformed Mode Shape for Model 1.1c. (a) Mode 1 (b) Mode 2 (c) Mode 3

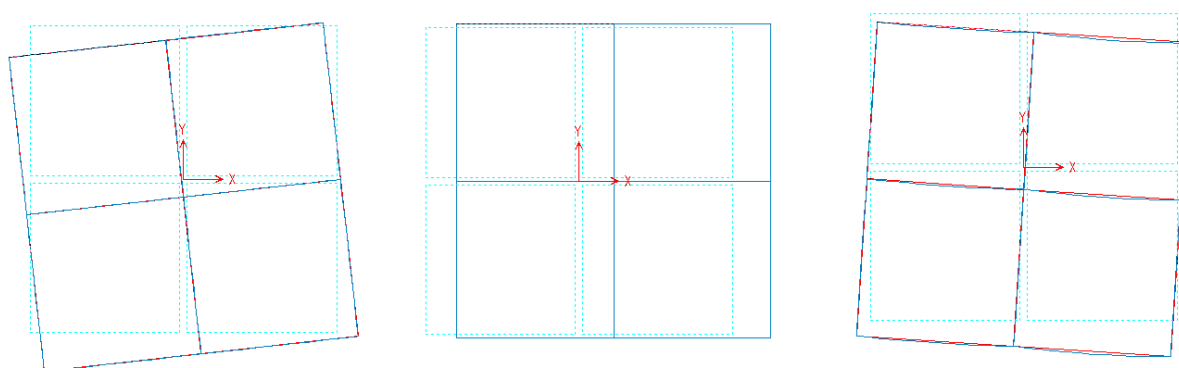


**Figure 6-3.** Deformed Mode Shape for Model 1.1d. (a) Mode 1 (b) Mode 2 (c) Mode 3

From Table 6-1 it can be noticed that for Model 1.1b the first mode is predominantly translational in the Y direction (UY) with a period and modal mass participating ratio of 0.47 seconds and 0.96 respectively. Also, there is a small translation (UY) – rotational (RZ) coupling effect (Figure 6-1a), mainly because the frames in the Y direction are not symmetric due to the change in columns length, causing a shift of the centers of stiffness with respect to the center of mass. The edge frame close to the road has the shortest columns. The stiffness of a column is inversely proportional to the cubic length. When the length of a column decreases, the stiffness ( $K_{col}$ ) increases as shown in the following relation.

$$K_{col} = \frac{12EI}{L^3} \quad (6-1)$$

where:

$E$  :modulus of elasticity,

$I$  :inertia, and

$L$  :length of the column.

The second mode, with a period of 0.21 seconds, is almost purely torsional (Figure 6-1b). The third mode is predominantly in the X direction (UX) (Figure 6-1c) with a period and modal mass participating ratio of 0.19 seconds and 0.99, respectively. It can be noted that the period in the Y direction is higher than in the X direction. The Y direction is more flexible, since it is the weak axis of the column orientations, so the period is expected to be higher.

When the models include a retaining wall (Model 1.1c and Model 1.1d) the first and third modes are characterized by floor translation (UY) and rotation (RZ) as it can be seen in Figure 6-2a and Figure 6-3a. The model modal participating mass ratio for the first mode in the Y direction is approximately 0.50. The coupling effect is more significant as it was observed for Model 1.1b, mainly because the edge frame now contains the

retaining wall affecting the Y direction even more and as a consequence the shift of the centers of stiffness with respect to the center of mass is larger. Figure 6.4 shows the location of the center of mass (CM) and center of stiffness (CS) for Model 1.1b, Model 1.1c and Model 1.1d. The center of stiffness was calculated based on linear 3-D analyses for a unit lateral load.

The location of the center of mass is assumed to be the geometric center of the floor for all models. The distribution of the floor masses is almost symmetric. It was verified that the effect of the retaining wall at the edge frame had a minimal effect in the location of the center of mass; in contrast the location of the center of stiffness is moved significantly as it can be observed in Figure 6.4

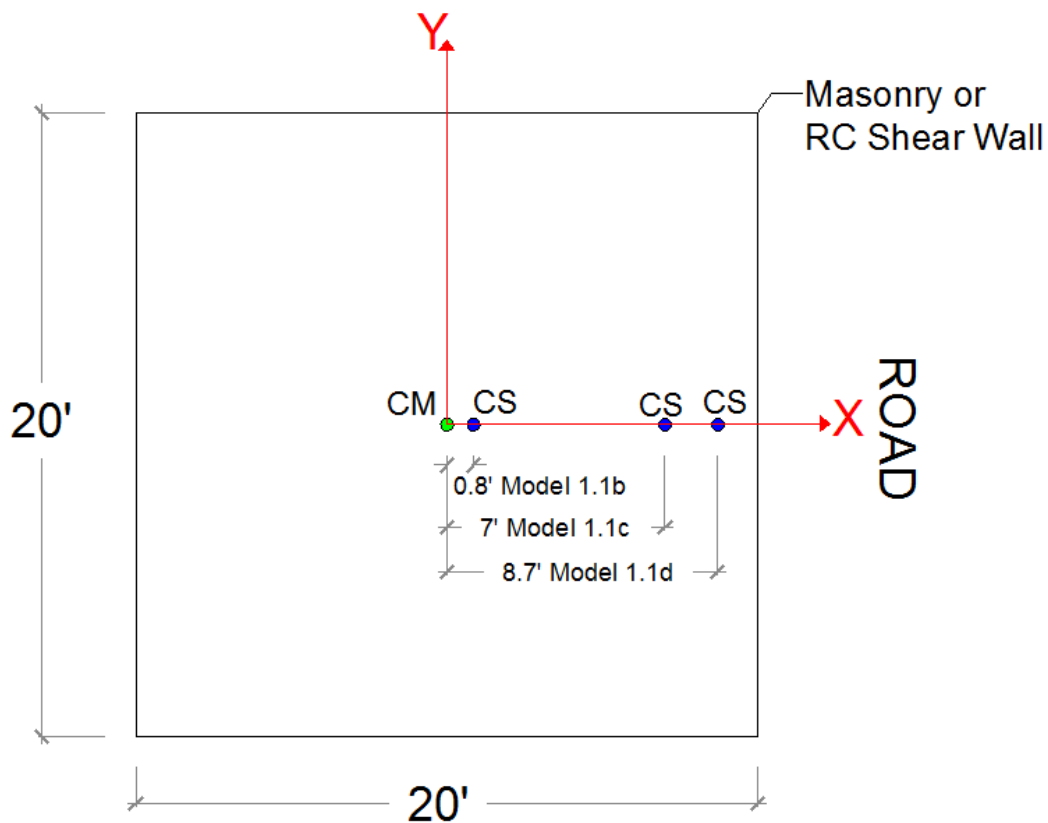


**Figure 6-4.** Location of Center of Mass (CM) and Center of Stiffness (CS) for Model 1.1b, Model 1.1c and Model 1.1d

The first natural period for Model 1.1c and Model 1.1d in the Y direction is 0.31 and 0.33 seconds, respectively. It can be observed (Table 6-1) that due to the presence of the retaining wall the model becomes stiffer in the Y direction and the period decreases. It is known that period of a single degree of freedom structure is related to both mass and stiffness. When the mass increases the period increases and when the stiffness increases the period decreases, as shown in the relation.

$$T = \frac{2\pi}{\omega}; \omega = \sqrt{\frac{K}{m}} \rightarrow T \propto \sqrt{m} \text{ and } T \propto \sqrt{\frac{1}{K}} \quad (6-2)$$

where:

$T$  : structure natural period,

$m$  : structure mass, and

$K$  : structure stiffness.

The second mode is predominant translational in the X direction with a modal participating mass ratio of approximately 0.99 (Figure 6-2b and Figure 6-3b). The period in the X direction for Model 1.1c and Model 1.1d is 0.19 and 0.18 seconds, respectively, similar that it was for Model 1.1b, this value was expected since the X direction is less affected while including a retaining wall.

### **6.1.2 DYNAMIC ANALYSIS RESULTS: MODEL 1.1 VS. MODEL 1.2 / MODEL 1.3 / MODEL 1.4**

This section compares the effect in the dynamic properties of the analytical models when the bay length is increased in the X and Y direction. Tables 6-2 to 6-4 show the periods of Model 1.2, Model 1.3 and Model 1.4 with the corresponding modal participating mass ratio in the UX and UY directions and rotation about RZ axis.

**Table 6-2. Dynamic Properties: Model 1.2:**

Mode	Model 1.2b				Model 1.2c				Model 1.2d			
	Period (sec)	Modal participating mass ratio			Period (sec)	Modal participating mass ratio			Period (sec)	Modal participating mass ratio		
		UX	UY	RZ		UX	UY	RZ		UX	UY	RZ
1	0.54	0.00	0.99	0.01	0.29	0.00	0.41	0.60	0.29	0.00	0.37	0.63
2	0.22	0.00	0.01	0.99	0.22	1.00	0.00	0.00	0.19	1.00	0.00	0.00
3	0.22	1.00	0.00	0.00	0.07	0.00	0.56	0.38	0.04	0.00	0.25	0.15

**Table 6-3. Dynamic Properties: Model 1.3:**

Mode	Model 1.3b				Model 1.3c				Model 1.3d			
	Period (sec)	Modal participating mass ratio			Period (sec)	Modal participating mass ratio			Period (sec)	Modal participating mass ratio		
		UX	UY	RZ		UX	UY	RZ		UX	UY	RZ
1	0.59	0.00	0.91	0.09	0.48	0.00	0.58	0.43	0.51	0.00	0.57	0.43
2	0.28	0.00	0.09	0.91	0.23	1.00	0.00	0.00	0.22	1.00	0.00	0.00
3	0.23	1.00	0.00	0.00	0.06	0.00	0.35	0.49	0.04	0.00	0.14	0.19

**Table 6-4. Dynamic Properties: Model 1.4**

Mode	Model 1.4b				Model 1.4c				Model 1.4d			
	Period (sec)	Modal participating mass ratio			Period (sec)	Modal participating mass ratio			Period (sec)	Modal participating mass ratio		
		UX	UY	RZ		UX	UY	RZ		UX	UY	RZ
1	0.65	0.00	0.97	0.03	0.44	0.00	0.51	0.49	0.44	0.00	0.49	0.51
2	0.30	0.00	0.03	0.97	0.26	1.00	0.00	0.00	0.23	1.00	0.00	0.00
3	0.26	1.00	0.00	0.00	0.07	0.00	0.45	0.47	0.05	0.00	0.00	0.00

For Model 1.2b, Model 1.3b and Model 1.4b the results show that the first mode is translational in the Y direction, while the predominant translational mode in the X direction is the third mode. The second mode corresponds to the torsional mode. For models that include a retaining wall, Models 1.2c/d, Models 1.3c/d and Models 1.4c/d, the first and third modes are translational in the Y direction and rotational, the second mode is predominant by translational in the X direction.

It can be noticed that when the span was increased from 10 feet to 15 feet in the Y or X direction the natural period increased. The additional mass due to larger bay lengths increase the period, also with an increase in bay length the frame becomes more flexible. The case where the highest periods were obtained was in the Y direction, since this is also the weak columns orientation. It can be noticed that for Model 1.3b where the span in Y remains the same as for Model 1.1b, the period in the Y direction



increased: this occurred because the increase in the length of the span in the X direction adds more mass to the model in each direction. As mentioned before, an increase in the mass of the model increases its natural period.

For Model 1.2c/d the periods decreased with respect to Model 1.2b where no retaining wall was considered, because the retaining wall makes the model stiffer. However when the periods are compared with Model 1.1c/d it can be seen from Table 6-2 to 6-4 that the period is slightly higher in the X direction and lower in the Y directions. This can be explained because the increase in span length in the Y direction add more mass to the model in both directions and at the same time adds more stiffness in the Y direction. Therefore it is expected that the period increased in the X direction and decrease in the Y direction.

For Model 1.3c/d the span in the X direction was increased, it can be noted that the period increased in both directions when compared with Model 1.1c/d and Model 1.2c/d. In this case more mass was added to the model in both directions, but the length of the retaining wall length was not increased. Also the increase in span length makes the model more flexible.

For Model 1.4c the spans were increased from 10 feet to 15 feet in both Y and X directions, providing more floor mass in both directions but only more stiffness in the Y direction. The periods of Models 1.2c/d were lower than for Model 1.4c/d since the Y direction was stiffened with the implementation of the retaining wall but less floor mass is added. Also it can be noticed that for Model 1.4d higher modes contribute to the response of the structure in the Y direction.

In terms of the torsional effect it can be observed that in all the models that include the retaining wall (models type c/d), the Y direction is affected drastically, the modal mass participation ratio is between 0.37 and 0.50. In general, these models exhibited high torsional issues. This phenomenon was expected since the location of the walls is

extremely asymmetric in plan; basically the stiffness of the residences is concentrated in one side only as it was observed in Figure 6.4.

### 6.1.3 DYNAMIC ANALYSIS RESULTS: MODEL 1.1 VS 2.1: INCREASE IN NUMBER OF STORIES

This section compares the effect in the dynamic properties of the analytical models when the number of stories is increased. Tables 6-5 to 6-8 shows the period of Model 2.1, Model 2.2, Model 2.3 and Model 2.4 with the corresponding modal mass participation ratio in each UX and UY translation directions and rotation about RZ axis.

**Table 6-5. Dynamic Properties: Model 2.1**

Mode	Model 2.1b				Model 2.1c				Model 2.1d			
	Period (sec)	Modal participating mass ratio			Period (sec)	Modal participating mass ratio			Period (sec)	Modal participating mass ratio		
		UX	UY	RZ		UX	UY	RZ		UX	UY	RZ
1	0.66	0.00	0.95	0.02	0.44	0.00	0.51	0.47	0.45	0.00	0.45	0.46
2	0.32	0.00	0.01	0.93	0.29	0.94	0.00	0.00	0.29	0.92	0.00	0.00
3	0.29	0.94	0.00	0.00	0.14	0.00	0.02	0.00	0.14	0.00	0.02	0.00
4					0.10	0.00	0.04	0.03	0.10	0.00	0.02	0.01
5					0.08	0.00	0.40	0.43	0.05	0.00	0.00	0.00
6									0.05	0.00	0.04	0.14
7									0.05	0.07	0.00	0.00
8									0.05	0.00	0.24	0.18

**Table 6-6. Dynamic Properties: Model 2.2**

Mode	Model 2.2b				Model 2.2c				Model 2.2d			
	Period (sec)	Modal participating mass ratio			Period (sec)	Modal participating mass ratio			Period (sec)	Modal participating mass ratio		
		UX	UY	RZ		UX	UY	RZ		UX	UY	RZ
1	0.80	0.00	0.96	0.00	0.43	0.00	0.41	0.57	0.43	0.00	0.34	0.57
2	0.34	0.00	0.00	0.94	0.34	0.95	0.00	0.00	0.33	0.92	0.00	0.00
3	0.34	0.95	0.00	0.00	0.15	0.00	0.03	0.00	0.15	0.00	0.02	0.00
4					0.11	0.00	0.08	0.04	0.11	0.00	0.01	0.00
5					0.10	0.00	0.46	0.34	0.06	0.00	0.00	0.00
6									0.05	0.00	0.02	0.11
7									0.05	0.06	0.00	0.00
8									0.05	0.01	0.00	0.00
9									0.05	0.00	0.29	0.14

**Table 6-7. Dynamic Properties: Model 2.3:**

		Model 2.3b			Model 2.3c				Model 2.3d			
Mode	Period (sec)	Modal participating mass ratio			Period (sec)	Modal participating mass ratio			Period (sec)	Modal participating mass ratio		
		UX	UY	RZ		UX	UY	RZ		UX	UY	RZ
1	0.81	0.00	0.92	0.05	0.67	0.00	0.57	0.41	0.68	0.00	0.53	0.39
2	0.46	0.00	0.04	0.90	0.37	0.95	0.00	0.00	0.37	0.94	0.00	0.00
3	0.37	0.95	0.00	0.00	0.16	0.00	0.01	0.01	0.16	0.00	0.01	0.00
4					0.14	0.00	0.03	0.01	0.14	0.00	0.02	0.01
5					0.09	0.00	0.35	0.50	0.06	0.00	0.00	0.00
6									0.06	0.00	0.04	0.12
7									0.05	0.06	0.00	0.00
8									0.05	0.00	0.19	0.20

**Table 6-8. Dynamic Properties: Model 2.4:**

		Model 2.4b			Model 2.4c				Model 2.4d			
Mode	Period (sec)	Modal participating mass ratio			Period (sec)	Modal participating mass ratio			Period (sec)	Modal participating mass ratio		
		UX	UY	RZ		UX	UY	RZ		UX	UY	RZ
1	0.96	0.00	0.96	0.02	0.66	0.00	0.50	0.48	0.66	0.00	0.45	0.46
2	0.49	0.00	0.01	0.94	0.44	0.96	0.00	0.00	0.41	0.94	0.00	0.00
3	0.44	0.96	0.00	0.00	0.17	0.00	0.01	0.00	0.17	0.00	0.01	0.00
4					0.14	0.00	0.03	0.01	0.14	0.00	0.02	0.00
5					0.11	0.00	0.43	0.46	0.06	0.00	0.00	0.00
6									0.06	0.00	0.00	0.00
8									0.06	0.00	0.02	0.10
9									0.05	0.06	0.00	0.00
10									0.05	0.00	0.20	0.16

In general Models 2 have the same tendency in terms of the effect when the bay length was increased and the effect of a retaining wall as Models 1. Also, it can be noticed that for Models 2 type c and d higher modes contribute to the response of the structure in the Y direction. On the other side with the increase in number of stories the period also increased. Since there is an increase in column length of the model, the stiffness will be significantly reduced increasing the natural time period. It has been observed that due to the increase of number of stories the building becomes more flexible with less stiffness. For example, for Model 1.1b the period in the Y and X direction was 0.46 and 0.19 seconds respectively, while the period for the Model 2.1b in the Y and X direction was 0.66 and 0.29 seconds, respectively. The highest period was 0.96 seconds for Model 2.4b in the Y direction; this model is obviously the most flexible.

#### 6.1.4 DYNAMIC ANALYSIS RESULTS: MODEL 1.1b VS MODEL 1.1by - CHANGE IN COLUMNS ORIENTATION

This section compares the effect in the dynamic properties of the analytical models when the column orientation is changed. Table 6-9 shows the periods of Model 1.1yb, with the corresponding modal mass participation ratio in each UX and UY translation directions and rotation about RZ axis.

**Table 6-9: Dynamic Properties: Model 1.1yb. Column Orientation**

Mode	Model 1.1.yb				Model 1.1.yc				Model 1.1.yd			
	Period (sec)	Modal participating mass ratio			Period (sec)	Modal participating mass ratio			Period (sec)	Modal participating mass ratio		
		UX	UY	RZ		UX	UY	RZ		UX	UY	RZ
1	0.44	1.00	0.00	0.00	0.43	1.00	0.00	0.00	0.28	0.00	0.48	0.51
2	0.33	0.00	0.42	0.59	0.28	0.00	0.49	0.52	0.22	1.00	0.00	0.00
3	0.15	0.00	0.58	0.41	0.05	0.00	0.44	0.42	0.04	0.00	0.20	0.20

Model 1.1y is equal to Model 1.1; the only difference is that the column orientation was changed, so currently the Y direction is the strong axis. The results show that for Model 1.1yb the first mode is predominantly translational in the X direction with a period and modal mass participating ratio of 0.44 seconds and 1.0, respectively. Comparing the results with Model 1.1b, the period increased from 0.19 seconds to 0.44 seconds in the X direction, mainly because now the X direction is significantly more flexible as it is the weak axis. In the Y direction, the period was reduced, however significant coupling between translation in Y and rotation is observed for both modes 2 and 3. The dimension of the column in the Y direction now is 16 inches, for instance the center of stiffness is closer to the edge frame beside the road, increasing the eccentricity in the model. For example, the center of stiffness for Model 1.1b was located at 0.80 feet from the center of mass, for Model 1.1by the center of stiffness is located at 5 feet from the center of mass. Same conclusion can be made for Model 1.1cy and Model 1.1dy.

### 6.1.5 DYNAMIC ANALYSIS RESULTS: MODEL 1.1 VS MODEL 1.1.2 / 1.1.3 / 1.1.4 CHANGE IN COLUMNS SIZE

This section compares the effect in the dynamic properties of the analytical models when the column dimension changed, as explained in section 3.2.7. Tables 6-10 to 6-12 shows the period of Model 1.1.2, Model 1.1.3 and Model 1.1.4 with the corresponding modal mass participation ratio in each UX and UY translation directions and rotation about RZ axis.

**Table 6-10. Dynamic Properties: Model 1.1.2. Columns 16 X 8**

Mode	Model 1.1.2b				Model 1.1.2c				Model 1.1.2d			
	Period (sec)	Modal participating mass ratio			Period (sec)	Modal participating mass ratio			Period (sec)	Modal participating mass ratio		
		UX	UY	RZ		UX	UY	RZ		UX	UY	RZ
1	0.33	0.00	0.91	0.09	0.27	0.00	0.51	0.50	0.30	0.00	0.48	0.52
2	0.18	0.00	0.09	0.91	0.17	1.00	0.00	0.00	0.18	1.00	0.00	0.00
3	0.17	1.00	0.00	0.00	0.05	0.00	0.44	0.45	0.04	0.00	0.21	0.21

**Table 6-11. Dynamic Properties: Model 1.1.3. Columns 12 X 12**

Mode	Model 1.1.3b				Model 1.1.3c				Model 1.1.3d			
	Period (sec)	Modal mass participation ratio			Period (sec)	Modal mass participation ratio			Period (sec)	Modal mass participation ratio		
		UX	UY	RZ		UX	UY	RZ		UX	UY	RZ
1	0.27	0.00	0.65	0.37	0.26	0.00	0.50	0.51	0.29	0.00	0.48	0.50
2	0.20	1.00	0.00	0.00	0.20	1.00	0.00	0.00	0.22	0.98	0.00	0.00
3	0.15	0.00	0.35	0.63	0.05	0.00	0.45	0.44	0.04	0.00	0.24	0.24

**Table 6-12. Dynamic Properties: Model 1.1.4. Columns 12 X 6**

Mode	Model 1.1.4b				Model 1.1.4c				Model 1.1.4d			
	Period (sec)	Modal participating mass ratio			Period (sec)	Modal participating mass ratio			Period (sec)	Modal participating mass ratio		
		UX	UY	RZ		UX	UY	RZ		UX	UY	RZ
1	0.55	0.00	0.93	0.08	0.42	0.00	0.50	0.51	0.38	0.00	0.48	0.51
2	0.28	0.00	0.07	0.92	0.26	1.00	0.00	0.00	0.20	1.00	0.00	0.00
3	0.26	1.00	0.00	0.00	0.05	0.00	0.42	0.42	0.04	0.00	0.19	0.18

For Model 1.1.2 the columns size was increase in the weak Y axis form 6 to 8 inches. The period in the X and Y directions decreased when compared to Model 1.1. Larger member sections stiffened the model and it is expected the period to decrease.

For Model 1.1.3, with square columns 12" x 12", the period in the Y direction decreased from 0.47 to 0.27 seconds in comparison to Model 1.1. However for Model 1.1b the mode in the Y direction was almost purely translational, on the other hand for Model 1.1.3b significant coupling between translation in Y and rotation is observed for both modes 1 and 3. The same conclusion as for the case of Model 1.1by can be made in terms of the increase in the dimension of the column in the Y direction moving the center of stiffness closer to the edge frame beside the road. In the X direction a small increase in the period is observed mainly because the reduction in the columns dimension from 16 inches to 12 inches reduced the stiffness of the frames.

For Model 1.1.4 the columns size was decreased in the strong axis X direction from 16 inches to 12 inches. In the X direction the period increased, since the model is more flexible with smaller columns sections.

## **6.2 NONLINEAR PUSHOVER RESULTS**

One of the most important tasks in the seismic evaluation of the residences is to obtain the capacity (pushover) curve of the analytical models. From the dynamic analysis significant torsional effects in the orthogonal Y direction were observed. It was mentioned earlier that pushover analysis is very sensitive to the lateral load pattern used especially in irregular structures. To overcome these limitations, two different load patterns were considered in this study, namely: uniform, and mode shape. From section 6.1 the mode shape in the Y direction corresponds to translation UY and rotation UZ, therefore for models type c and d, the mode shape load pattern corresponds to the torsional mode. The development of multiple pushover curves is essential to evaluate the different modes of response and failure of the building under different loading patterns.

As explained in Chapter 5, the seismic performance of the models is evaluated using the capacity spectrum method to obtain the performance point or maximum seismic

displacement demands of the residences. The displacement at the performance point is intended to represent the maximum displacement likely to be experienced by the structure under a selected seismic hazard level. The structural performance level will be verified at the performance point. As explained in Chapter 4 section 4.2.2.1 the force displacement curve (Figure 4-2) is associated with a structural performance level in order to quantify the damage in the element (Hinge). In summary the structural performance levels as per ATC 40 are:

- **Point B to C**

**Immediate Occupancy:** limited structural damage had occurred

**Life Safety:** significant damage to the structure had occurred, but some margin against partial or total collapse remains. It is expected that extensive structural repair will likely be necessary prior to the reoccupation of the building.

**Collapse Prevention:** at this level the building has experienced extreme damage. If laterally deformed beyond this point, the structure can experience instability and collapse.

- **Point C to D:** significant strength degradation, initial failure of the component.
- **D to E:** represents the residual strength
- **E to F:** total failure

In order to investigate the performance of the models under extreme load conditions that exceeded the displacement at the performance point, the analysis was carried out further beyond this point until the program stop due to structural instability, numerical issues or a predefined displacement was achieved.

To obtaining the performance point of the model, the only loading pattern considered was the mode shape load pattern. The performance point is the point where the capacity curve crosses the demand curve according to ATC-40. In order to account for nonlinear inelastic behavior of the structural system, effective viscous damping ( $\beta_{eff}$ ) values were applied to linear elastic response spectra to approximate the reduction in structural response due to the increasing levels of damage. The elastic and inelastic response spectra provide the basis for calculating the target displacements of any structural systems being studied using pushover analysis.

An important step to obtain the linear elastic response spectrum is to identify the soil type. The UBC 97 code classifies the soil in six soil types ( $S_A, S_B, S_C, S_D, S_E$  and  $S_F$ ). Table 6-13 presents the soil type classification as per UBC 97. The response spectrum utilized in this investigation was the UBC spectrum for unknown soil type (Soil profile  $S_D$ ) (Figure 4-2). UBC 97 recommends using soil profile type  $S_D$  when soil properties are not known. The data to generate the soil type  $S_D$  spectrum were shown in Chapter 5 (Table 5-2)

**Table 6-13. UBC 97 Soil Profile Type**

<b>Soil Profile Type</b>	<b>Soil Profile Description</b>
$S_A$	Hard rock
$S_B$	rock
$S_C$	Very dense soil and soft rock
$S_D$	Stiff soil profile
$S_E$	Soft soil profile
$S_F$	Soil require Site-specific evaluation

With the information obtained from the pushover (capacity) curve and the Capacity Spectrum Method it is possible to calculate the ductility demand ( $\mu_d$ ) imposed by the earthquake. The ductility demand was obtained using the performance point as the ultimate displacement. The system ductility demand is estimated as the ratio of the yield displacement to the ultimate displacement (Figure 6-5).

$$\mu_d = \frac{d_{pp}}{d_y} \quad (6-3)$$



where:

$d_{pp}$  :displacement at the performance point [in], and

$d_y$  :yield displacement obtained from a bilinear representation of the capacity curve [in].

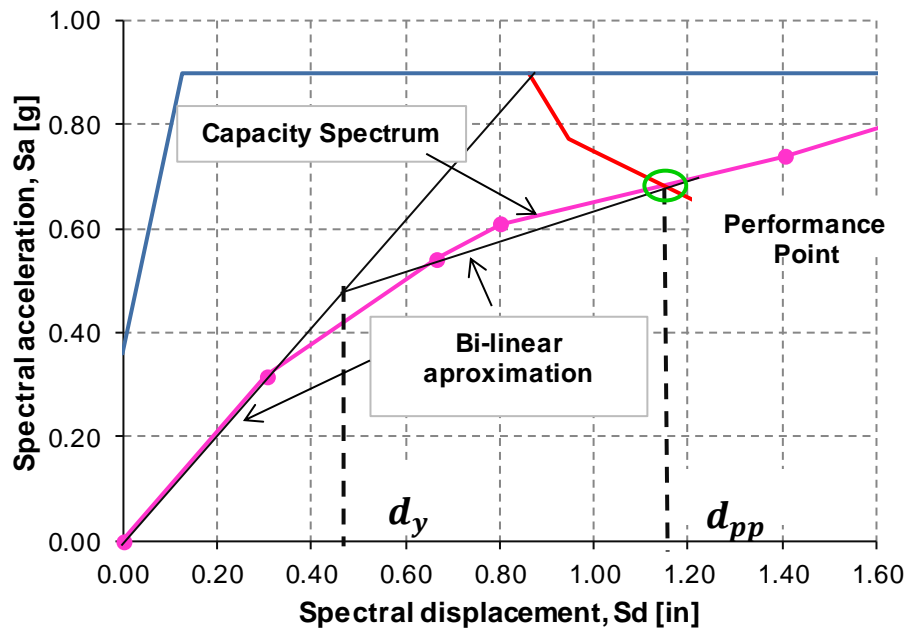


**Figure 6-5.** Definition of the Ductility Demand ( $\mu_d$ )

The results of the static pushover analysis are presented and discussed as follows:

- Section 6.2.1 compares the effect of including a retaining wall in the analytical models either as a masonry block wall (model type c) or a RC shear wall (model type d) with the bare frame model (type b)
- Section 6.2.2 compares the effect of increasing the bay length in the Y direction (Model 1.2), in the X direction (Model 1.3) and in both X and Y direction (Model 1.4).
- Section 6.2.3 compares the effect of increasing the number of stories from two to three levels.
- Section 6.2.4 compares the effect of changing the column orientation.

- Section 6.2.5 compares the effect of changing the column size.
- Section 6.2.6 presents a summary of the results and conclusions obtained from the pushover analysis.

The results of the pushover analysis use the following nomenclature to define the model and the analysis type case.

b = bare frame

c = masonry block wall

d = RC shear wall

Push X = Pushover analysis case uphill, perpendicular to the road

Push - X = Pushover analysis case downhill, perpendicular to the road

Push Y = Pushover analysis case parallel to the road

Uniform = lateral load pattern uniform to mass

Mode = lateral load pattern proportional to the first mode shape

### **6.2.1 PUSHOVER ANALYSIS RESULTS: MODEL 1.1b (BARE FRAME) VS. MODEL 1.1c / MODEL 1.1d (RETAINING WALL)**

The following sections will compare the effect of including a retaining wall in the analytical models either as a masonry block wall (model type c) or a RC shear wall (model type d).

### 6.2.1.1 MODEL 1.1b: BARE FRAME

#### Model 1.1b: -X direction

Table 6-14 includes the tabular data to generate the pushover curves for Model 1.1b for the mode load pattern. The table summarizes the number of hinges in each state: Immediate Occupancy (IO), Life Safety (LS), Collapse Prevention (CP), Collapse (C), D, E and F. The definition of each performance state was provided in Chapter 4 and summarized in section 6.2.1. The step where the performance occurs is in bold. Figure 6-6a shows a comparison of the force displacement plots (pushover curves) for different load patterns. Figure 6-6b shows a comparison for the pushover curves uphill and downhill. Figure 6-6c shows a comparison of the pushover curves for different base connections (fixed and pin)

**Table 6-14. Model 1.1b: Tabular Data for Pushover Curve for Model 1.1b: Push -X**

PUSH -X Mode			Hinge Sequence								Shear
Step	Disp. (in)	Base Force (Kip)	A to B	B to IO	IO to LS	LS to CP	CP to C	C to D	D to E	E to F	
0	0.00	0.00	102	0	0	0	0	0	0	0	
1	-0.17	49.02	100	2	0	0	0	0	0	0	
<b>2</b>	<b>-0.34</b>	<b>74.45</b>	<b>94</b>	<b>5</b>	<b>3</b>	<b>0</b>	<b>0</b>	<b>0</b>	<b>0</b>	<b>0</b>	
<b>3</b>	<b>-0.55</b>	<b>83.33</b>	<b>90</b>	<b>3</b>	<b>6</b>	<b>3</b>	<b>0</b>	<b>0</b>	<b>0</b>	<b>0</b>	
4	-0.76	88.71	90	0	5	4	1	1	1	0	
5	-0.80	90.23	90	0	5	4	0	3	0	0	
6	-1.00	94.70	88	2	2	1	2	7	0	0	
7	-1.25	97.60	87	0	3	2	0	6	4	0	
8	-1.42	99.27	85	2	3	1	1	3	7	0	
9	-1.69	101.09	84	1	5	0	0	3	9	0	
10	-2.11	104.94	84	0	3	3	0	0	12	0	
11	-2.40	106.89	84	0	3	1	0	2	12	0	

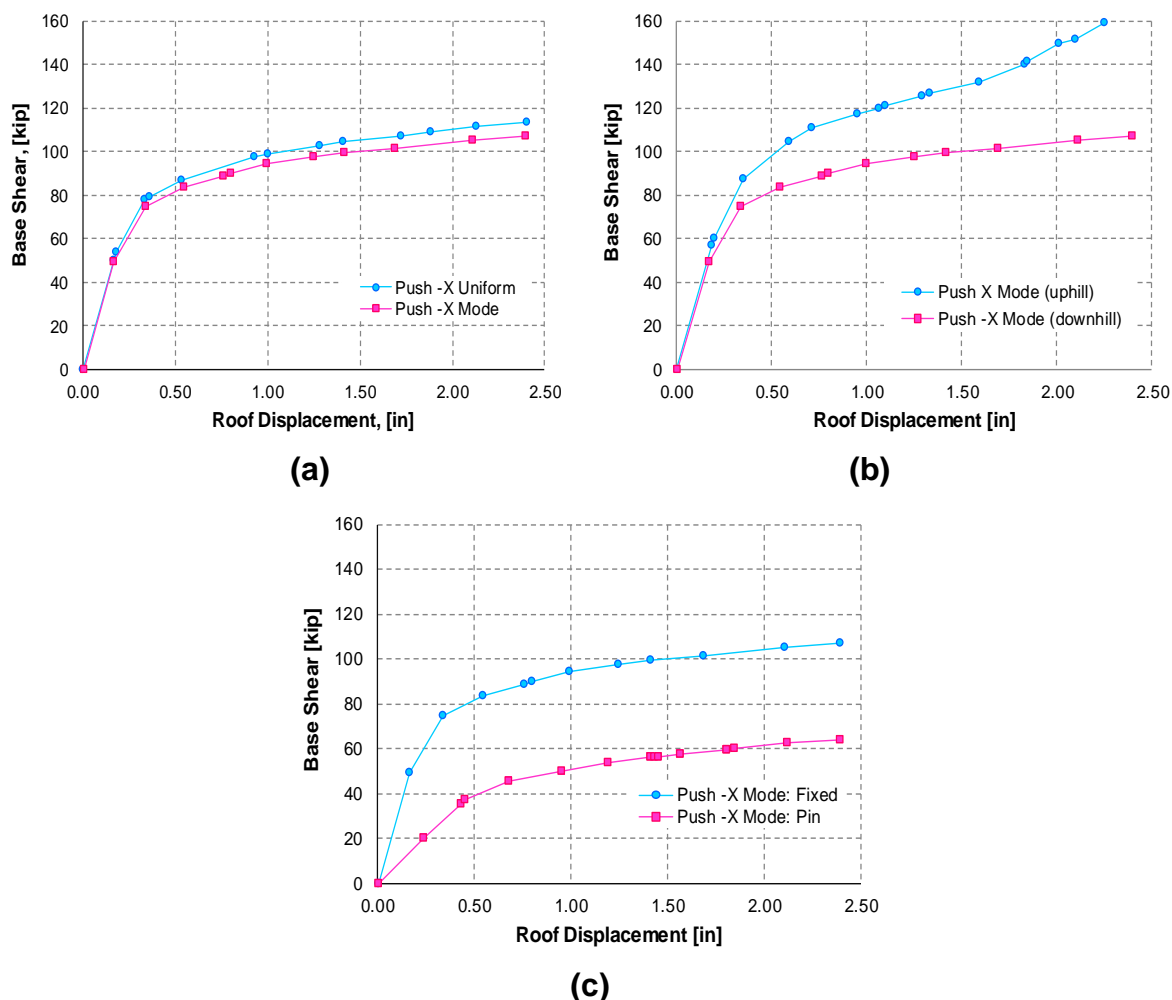


**Figure 6-6.** Pushover Curves for Model 1.1b Push X (a) Different Load Patterns. (b) Direction Downhill (-X) and Uphill (X). (c) Fix vs. Pin Connection

The curves in Figure 6-6 are initially linear but start to deviate from linearity as the columns undergo inelastic actions. When the model is pushed into the inelastic range, the curves become linear again but with a smaller slope.

The model behaves completely elastically up to approximately 50 kips for the uniform and mode load patterns (Figure 6-6a). Plot profiles for both the uniform and mode shape load patterns are very similar indicating a comparable response in these directions. This is reasonable because the model in the X direction is symmetric in geometry, mass and stiffness. It is expected that the uniform load pattern produce a similar deformed shape as its fundamental mode. The uniform load pattern is

proportional to the mass at each floor level and it is considered to be equivalent to the first mode shape of the structure. For example the mass of the residences is concentrated at the house level while the lower levels are very flexible with little mass producing a deformed shape in the X direction as shown in Figure 6-7.

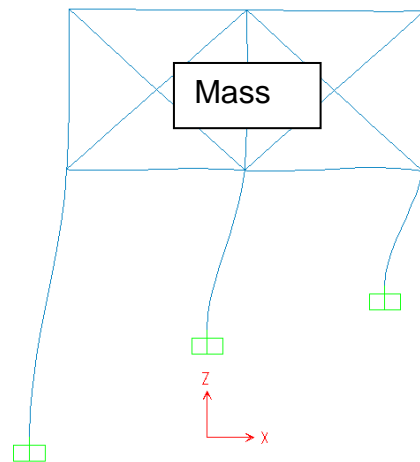


**Figure 6-7.** Mode and Uniform Load Pattern Deformed Shape in the X Direction.

Plot profiles (Figure 6-6 b) for the pushover applied in the positive and negative X direction shows that the capacity downhill is less than uphill. The model is perfectly symmetric in the X direction and the decrease in capacity can be explained using Figure 6-8. When the model is pushed uphill, short columns are in compression and slender columns are in tension (Figure 6-8a). When the model is pushed downhill, short columns are in tension and slender columns are in compression (Figure 6-8b). The capacity of a column is irrespective of its length under primary stresses. Long columns develop secondary stresses (moments) associated with column deformations (P- $\Delta$  effect), especially if they are not braced laterally. Consequently, slender columns resist lower axial loads than short columns having the same cross-section.

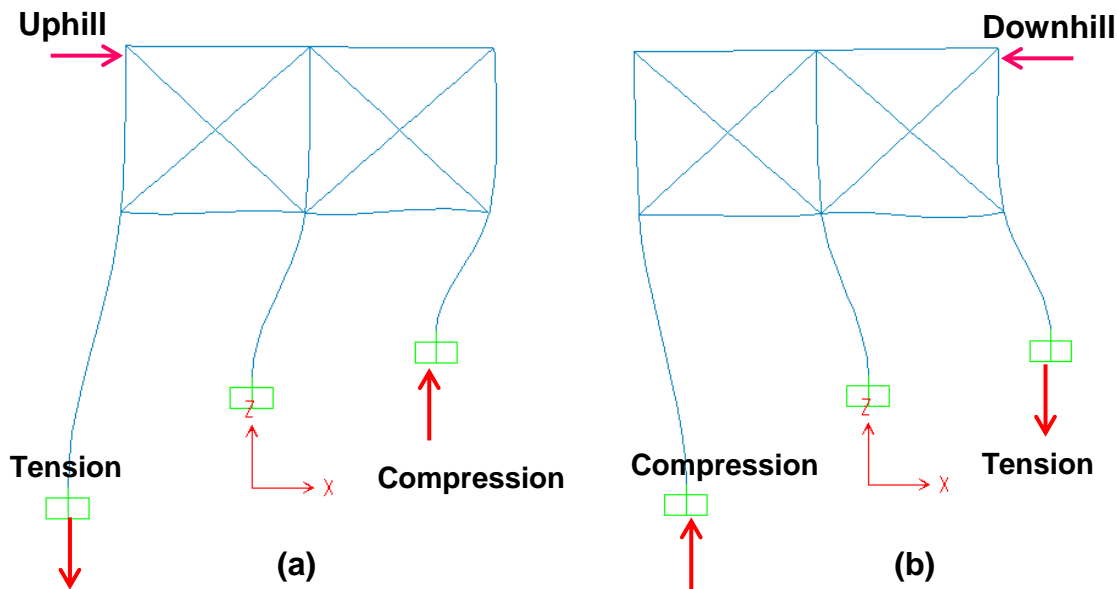


**Figure 6-8.** Deformed Shape. (a) Pushed Uphill. (b) Pushed Downhill

In Figure 6-6c it can be noticed that analyzing the models with a pin connection at the base reduced the capacity by approximately 40 percent. The evaluation of the interaction of the connection between the footing and column and interaction of the footing with the soil was out of the scope of this investigation. Probably the actual base condition is not completely fixed or completely pinned. The actual condition is possibly something in between. Considering a pin connection will be overly conservative and detrimental for the models. Therefore, in order to not penalize the results significantly all the cases were analyzed with a fixed base end condition.

Only Model 1.1b was analyzed considering the pushover analysis case in the X direction, downhill and uphill. The other cases were only analyzed in the negative X direction (downhill), since the results shows that the pushover case downhill was the critical condition.

A graphical representation of the hinge sequence formation and the plot of performance point are presented in Figure 6-9 to 6-11 for mode the load pattern.

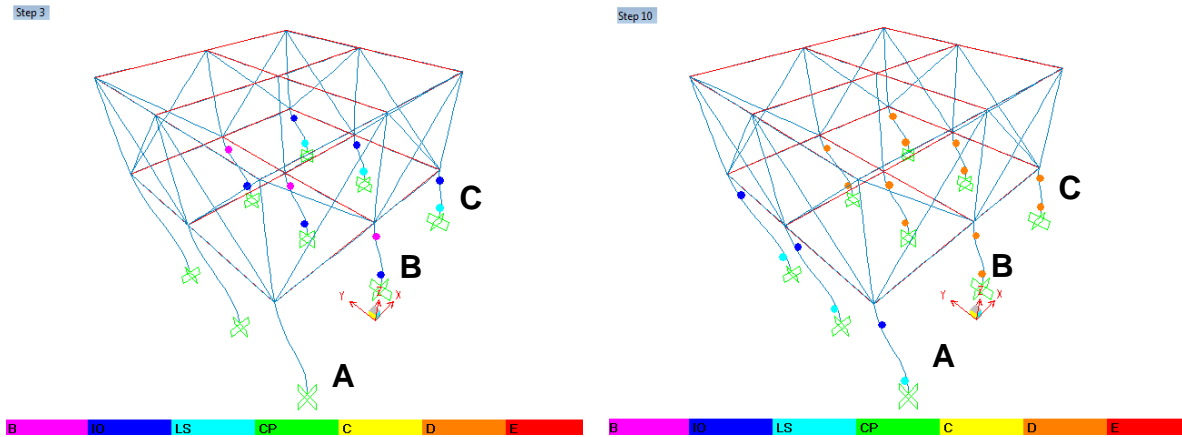


**Figure 6-9.** Pushover Deformed Shape and Hinge Formation for Model 1.1b: Push -X

From Figure 6-9 it can be observed that there is no hinge formation at the upper story. It is important to understand why the first story columns are more prone to suffer damage when subject to lateral loads in these type of structures. These models have structural vertical irregularity since the mass and stiffness of the first story is significantly more than the mass and stiffness of the lower story. The walls in the first story force the structure above it to act as a rigid body, and thus most of the seismic forces and deformations shift to the columns of the lowest story where the inelastic action take place.

Plastic hinges formation at the lower story starts at frame C where the shortest columns are. Then propagates to frames B and A down-hill. Short columns attract much higher lateral forces, so they are prone to suffer more damage. Also, it can be noted that no hinges form in the beams: this illustrate a weak column strong beam behavior. At step 10 of the pushover analysis several hinges are beyond the Collapse (C) limit state. The stage from C to D represents the initial failure of the element and resistance to lateral loads beyond point C is usually unreliable. Specifically point D represents the residual strength due to gravity load.

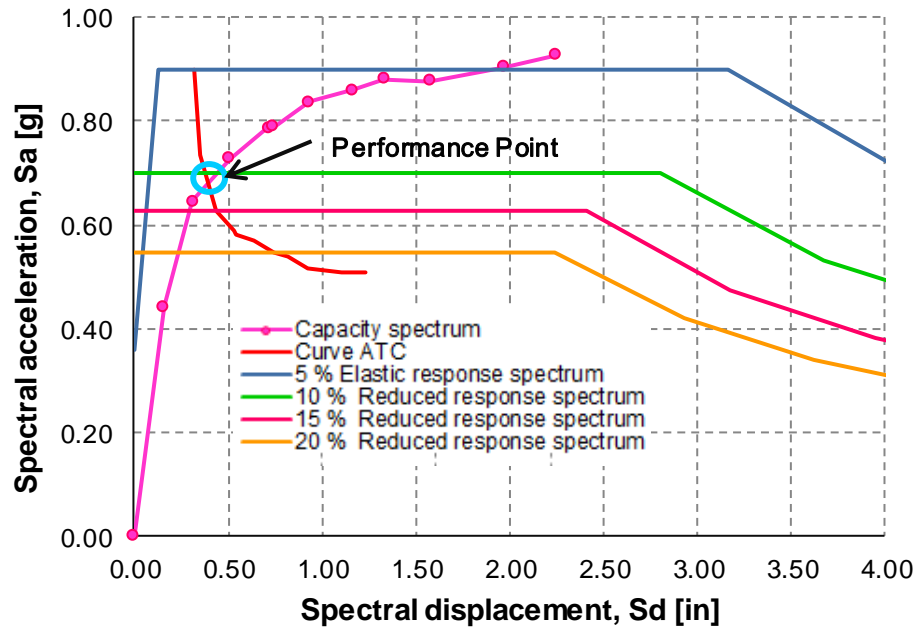


**Figure 6-10.** Performance Point for Model 1.1b: Push -X

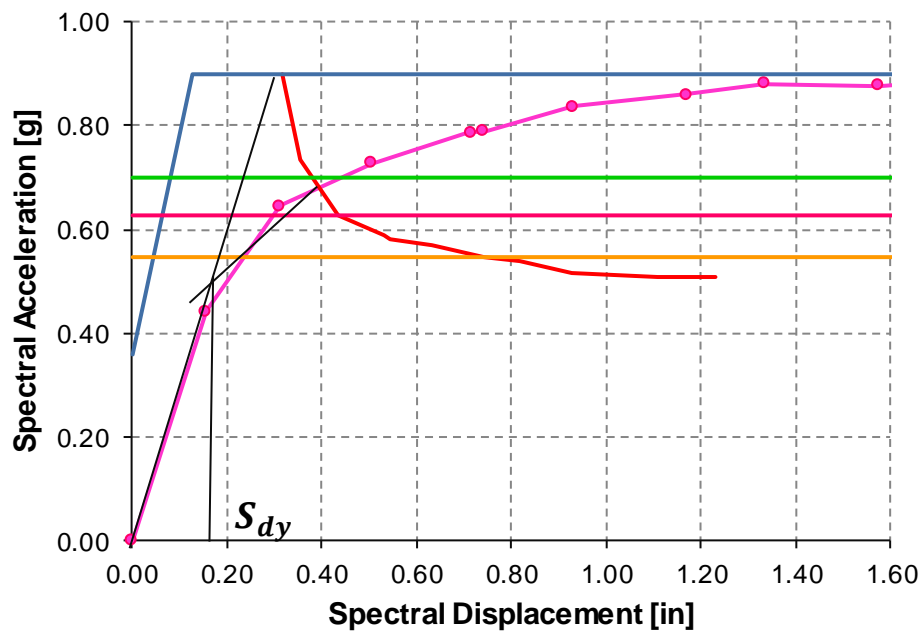
The demand response spectrum for  $\beta_{eff} = 5\%$ , 10%, 15%, and 20% are shown in Figure 6-10. To obtaining the performance point of the model, the only load pattern considered was the mode shape load pattern. The pink curve represents the capacity spectrum, and the red line defines the locus of points as defined by ATC-40. The intersection of the red line (demand) and the pink curve (capacity) is the performance point. At the performance point the spectral displacement ( $S_d$ ) and spectral acceleration ( $S_a$ ) are 0.37 in. and 0.71 g respectively.

From Table 6-14 it is shown that the demand curve intersects the capacity curve (step 2 and 3) between the point B and C i.e. Life Safety and Collapse Prevention performance level. At step 3 bottom hinges at frame C (Figure 6-9) are at Life Safety limit state. According to ATC 40, Life Safety means that significant damage to the structural element has occurred, but some margin against either partial or total structural collapse remains. Structural elements are severely damaged, but this has not resulted in large falling debris hazards. At frame B bottom hinges are at Immediate Occupancy performance level. Immediate Occupancy means limited structural damage has occurred. Minor cracking at the bottom of columns of frame B is expected.



Note that the elastic limit of the capacity curve does not reach the 5 percent elastic demand spectrum; therefore, the elastic demand exceeds the elastic capacity and the structure will displace into the inelastic range. Specifically, it can be noticed that at the performance point the model intersects a reduced response spectrum with 10 % of damping ratio approximately.

Figure 6-11 shows the ductility demand ( $\mu_d$ ) graphic computation.



$V_{pp}$	=	77.67	k	Base shear at performance point
$D_{pp}$	=	0.42	in	Displacement at performance point
$S_{app}$	=	0.68	g	Spectral acceleration at performance point
$S_{dpp}$	=	0.38	in	Spectral displacement at performance point
$S_{dy}$	=	0.18	in	Spectral yield displacement (bilinear approximation)
$\mu_d$	=	2.11		Ductility demand

**Figure 6-11.** Ductility Demand for Mode 1.1b: Push -X

From Figure 6-11 the ductility demand ( $\mu_d$ ) is 2.11. It is expected that these residences may develop a ductility between 1.25 and 2.32. This conclusion is made based on the relation of the response modification factor ( $R$ ). The response modification factor ( $R$ ) reflects the capacity of structure to dissipate energy through inelastic behavior (Patel

and Shah, 2010). Commonly, the response modification factor is expressed as a function of various parameters of the structural system, such as strength, ductility, damping and redundancy. Hence, the  $R$  factor as per ATC-19 is defined by equation 6-4:

$$R = R_o R_\mu R_\xi R_R \quad (6-4)$$

where:

$R_o$  : overstrength factor,

$R_\mu$  : ductility factor,

$R_\xi$  : damping factor, and

$R_R$  : redundancy factor.

The lateral force resisting system of these residences can be classified as one of the three lateral systems described in the UBC -97. Table 6-15 shows the lateral system and the corresponding  $R$  values. Appendix F shows a complete table with the  $R$  values as per UBC 97.

**Table 6-15.** Response Modification Factors ( $R$ ) as per UBC 97

Lateral Force Resisting Frame	R
Ordinary Moment Resisting Fram (OMRF)	3.5
Shear Wall with (OMRF)	6.5
Masonry Wall (OMRF)	4.2

The overstrength factor ( $R_o$ ) is a measure of the built-in overstrength in the structural system. The UBC-97 recommends a  $R_o$  value of 2.8.

The damping factor ( $R_\xi$ ) is intended to account for the influence of supplemental viscous damping devices (Mondal et. al, 2013). Without such devices, the damping

factor is generally assigned a value equal to 1.0 (Whittaker, 1999). Following the conservative suggestion of ASCE7, a redundancy factor ( $R_R$ ) of 1.0 is used in this study. Substituting these values in equation 6-4 and solving for the ductility factor ( $R_\mu$ ) for different values of  $R$  gives the results shown in Table 6-16.

**Table 6-16.** Response Modification Factor ( $R$ ) and Ductility factors ( $R_\mu$ )

$R$	$R_\mu$
3.5	1.25
6.5	2.32
4.2	1.50

### **Model 1.1b: Y direction**

Table 6-17 and Figure 6-12 includes the tabular data to generate the pushover curve and pushover curve respectively for Model 1.1b.

**Table 6-17.** Tabular Data for Pushover Curve for Model 1.1b: Push Y

PUSH Y Mode			Hinge Sequence								Shear
Step	Disp. (in)	Base Force (Kip)	A to B	B to IO	IO to LS	LS to CP	CP to C	C to D	D to E	E to F	
0	0.00	0.00	102	0	0	0	0	0	0	0	
1	0.14	7.35	100	2	0	0	0	0	0	0	
2	0.23	9.97	94	5	3	0	0	0	0	0	
3	0.31	10.92	91	2	9	0	0	0	0	0	
4	0.55	12.25	89	1	4	6	1	1	0	0	
5	0.62	12.47	87	3	3	5	2	2	0	0	
6	0.72	12.67	84	3	5	2	5	3	0	0	
7	1.10	13.02	84	0	6	0	8	3	1	0	
8	1.33	13.23	84	0	1	5	5	5	2	0	
9	1.55	13.42	84	0	0	2	7	5	4	0	
10	1.55	13.42	84	0	0	2	7	5	4	0	
11	1.84	13.60	84	0	0	0	4	9	5	0	
12	2.17	13.77	84	0	0	0	4	5	9	0	
13	2.32	13.86	84	0	0	0	4	4	10	0	
14	2.39	13.92	84	0	0	0	2	3	13	0	

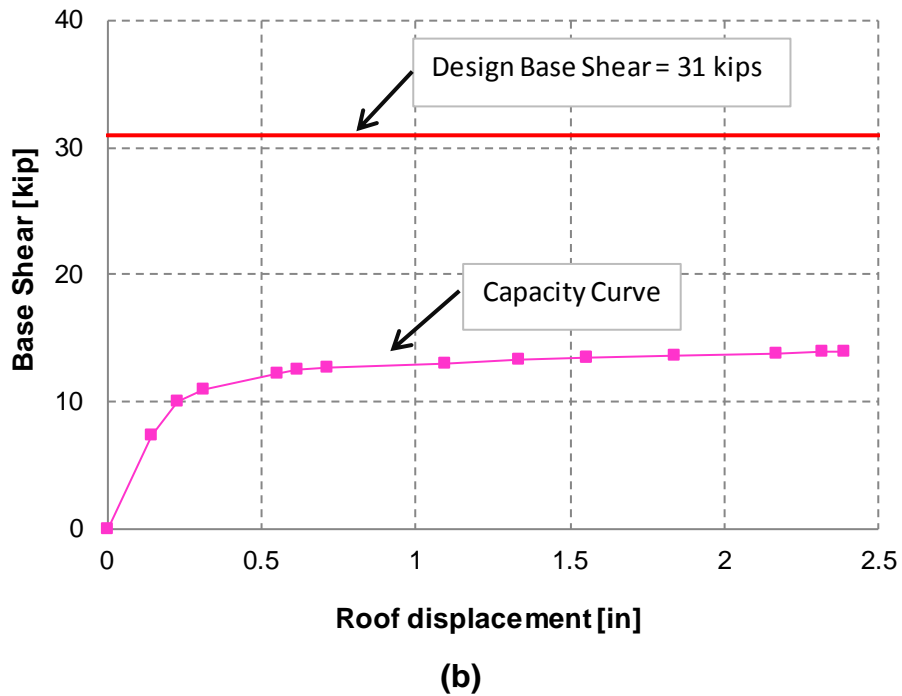
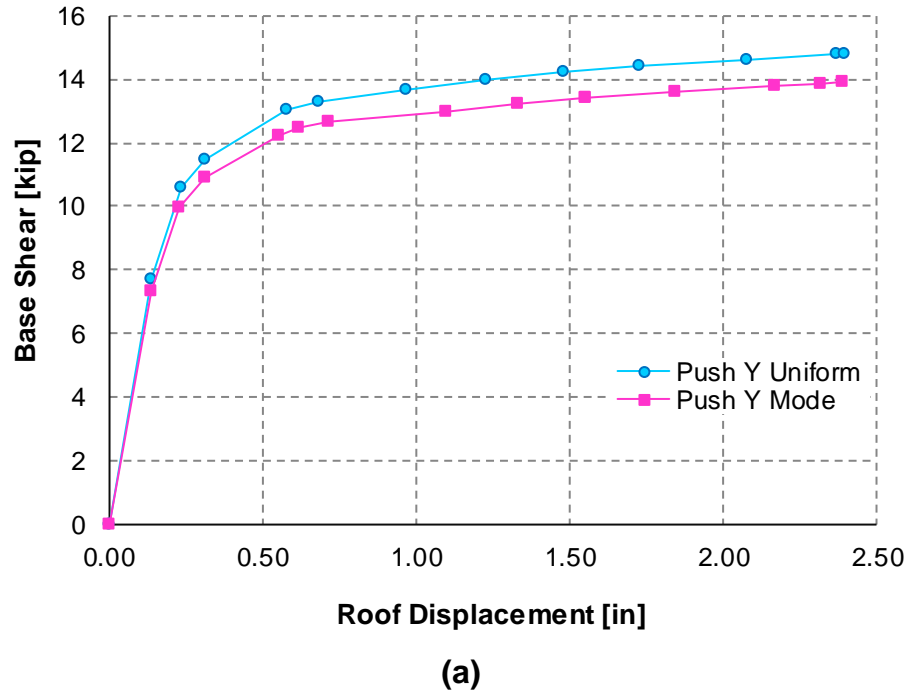


**Figure 6-12.** Pushover Curves for Model 1.1b: Push Y. (a) Different Load Pattern. (b) Design Base Shear vs. Capacity Curve

From Figure 6-12a it can be observed that the capacity is slightly lower when the mode shape load pattern was used. The difference is not significant as the model have no

irregularities in mass; the irregularity in stiffness is due to the change in columns length in the frames. Therefore the capacity curves are very similar for both load pattern used. From Figure 6-12b it can be noticed that the maximum base shear value due to the pushover analysis is much less than the design base shear ( $V_y$ ). The design base shear calculation is shown in Appendix G. Basically in the Y direction the capacity curve is not able to meet the design requirements.

The maximum base shear in the X and Y direction, was 106 (Table 6-14) and 14 (Table 6-17) kips, respectively. The capacity in the Y direction is about 85 % less than in the X direction.

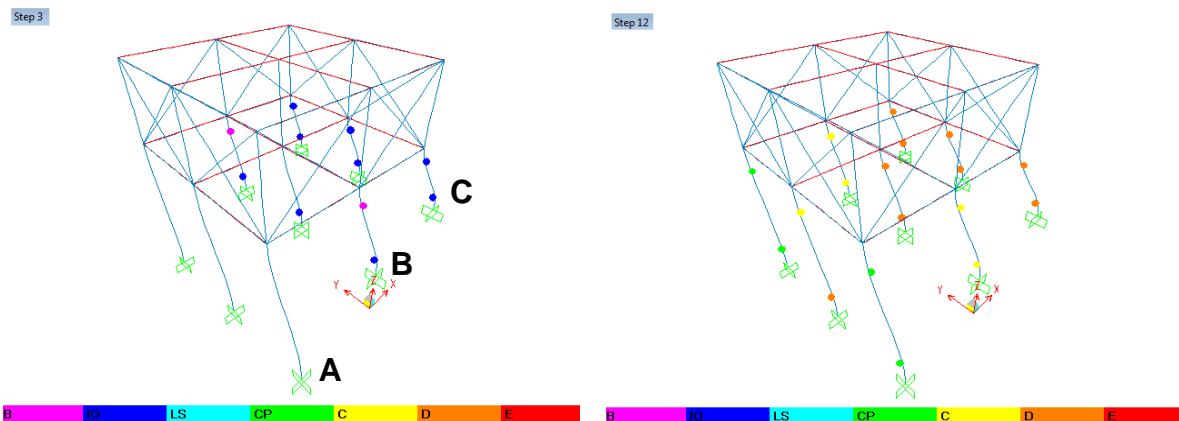


**Figure 6-13.** Pushover Deformed Shape and Hinge Formation for Model 1.1b: Push Y

Similar as it was observed in X direction the upper story don't form any hinges (Figure 6-13). Plastic hinges formation starts with the frame including the shortest columns of the lower story then propagates to the frames down-hill. In other words, the side way failure mechanism caused by top and bottom column hinging is very likely to occur.

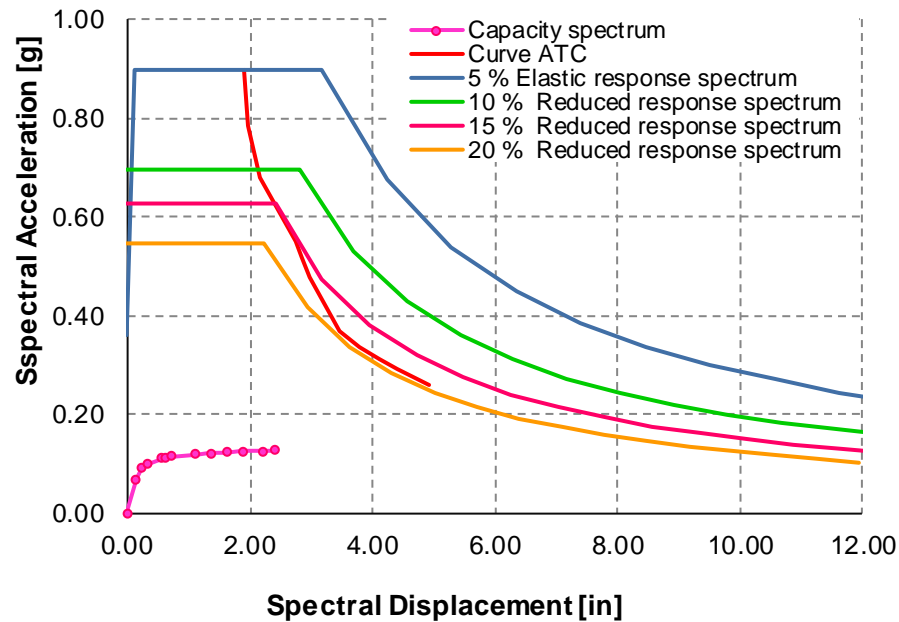


**Figure 6-14.** Performance Point for Model 1.1b: Push Y

From Figure 6-14 it is observed that no performance point was reached. The capacity spectrum curves lay substantially below the reduced response spectrums. In other words, the model is not able to satisfy the demand. From Table 6-17 it is observed that at the end of the analysis 13 elements have exceeded the Collapse limit level (between D to E). These results indicate that failure in the Y direction had or is next to occurring. The stage between D to E represents the residual resistance; elements have lost most of their lateral resistance and only are capable of sustaining gravity loads. It was mentioned before that when a hinge state is beyond the Collapse limit level it represents the initial failure of the element. It is associated with fracture of longitudinal reinforcement and spalling of concrete. Little residual stiffness and strength remains in the structural element if any. From a structural repair point of view, elements with this level of damage are nor repairable and the structure must be demolished.

### 6.2.1.2 MODEL 1.1c: MASONRY BLOCK WALL

#### Model 1.1c: – X direction

Figure 6-15 shows the comparison pushover curves in the –X direction for Model 1.1b and Model 1.1c.

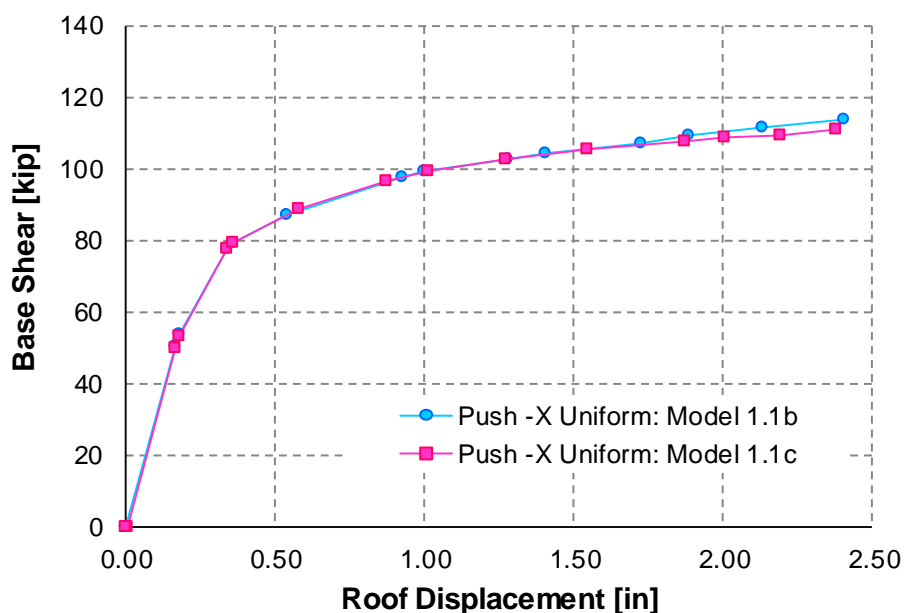


**Figure 6-15.** Comparison Pushover curves for Model 1.1b and 1.1c: Push –X

As can be seen in Figure 6-15 the X direction was not affected due to the presence of the modeling of the retaining wall, the pushover curves were basically the same for Model 1.1b and 1.1c. For the following analyses the analytical models type c and d were only analyzed in the Y direction.

#### Model 1.1c: Y direction

The tabular data for pushover curve mode shape load pattern is shown in Table 6-18. Force displacement plot for the pushover analysis case for mode shape and uniform load patterns are presented in Figure 6.20. For the purpose of comparison the pushover plots for Model 1.1b and Model 1.1c have also been included (Figure 6-17). The graphic

representation of the hinge sequence formation and performance point are presented in Figures 6-18 to 6-19.

**Table 6-18.** Tabular Data for Pushover Curve for Model 1.1c: Push Y

PUSH Y Mode			Hinge Sequence								Shear
Step	Disp. (in)	BaseForce (Kip)	A to B	B to IO	IO to LS	LS to CP	CP to C	C to D	D to E	E to F	
0	0.00	0.00	102	0	0	0	0	0	0	0	
1	0.16	18.41	102	0	0	0	0	0	0	0	
2	0.34	29.55	92	1	9	0	0	0	0	0	
3	0.64	38.21	86	0	6	8	1	1	0	0	
4	0.77	41.09	85	1	2	7	3	4	0	0	
5	0.79	41.64	85	1	2	8	2	4	0	0	
6	0.93	44.62	85	1	0	2	8	4	2	0	
7	0.97	46.20	85	1	0	1	8	5	2	0	1
8	0.98	46.62	84	2	0	1	8	5	2	0	1
9	1.22	51.43	83	0	2	0	4	8	4	1	1
10	1.29	53.29	83	0	2	0	5	5	6	1	1
11	1.54	56.26	83	0	2	0	2	4	10	1	1
12	1.67	57.61	83	0	2	0	4	2	10	1	1
13	1.69	58.04	83	0	1	0	4	3	10	1	1

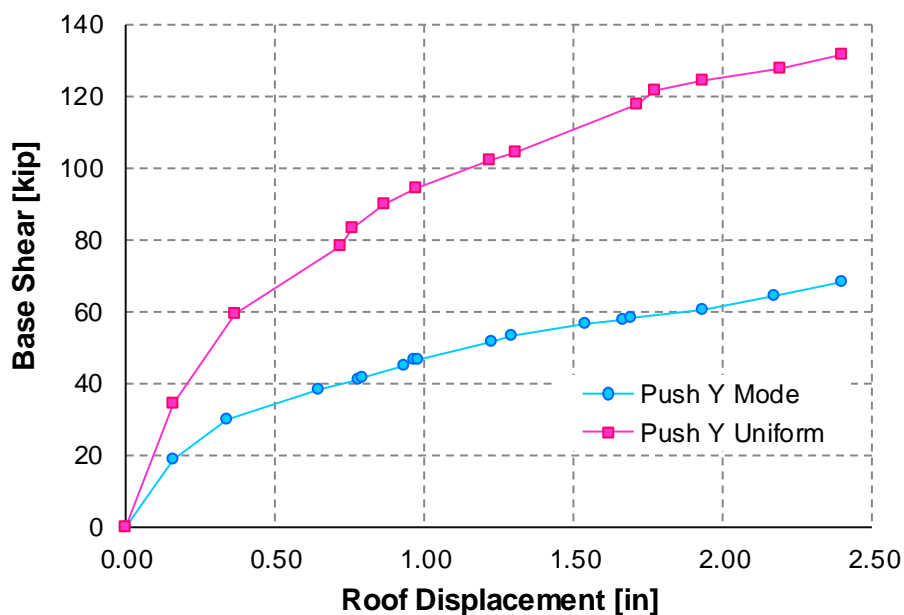


**Figure 6-16.** Pushover Curves for Different Load Patterns for Model 1.1c: Push Y



As it can be seen in Figure 6-16 that the pushover curves for Models type c with different load patterns shows significant difference since important torsional effects were observed. For all the curves presented so far the same trend can be observed, when the mode shape is used as the load pattern to perform the pushover analysis, the curves tend to be the critical case. For the rest of the models only the mode shape load pattern was used, as this was proven to be the critical case.

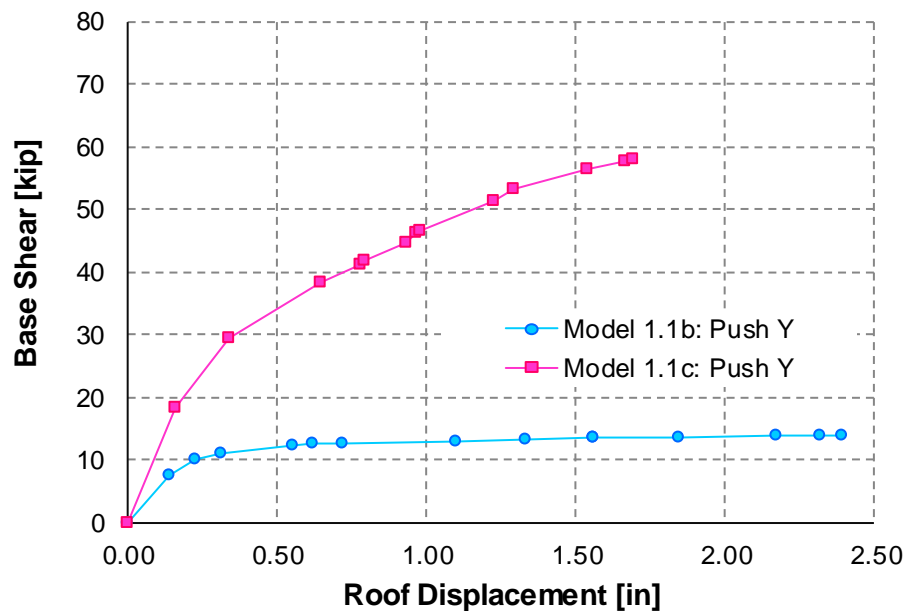


**Figure 6-17.** Comparison Pushover Curves for Model 1.1b and 1.1c: Push Y

It can be observed from Figure 6-17 that when the residences have a retaining wall modeled as a masonry block wall the capacity and stiffness of the residence improves significantly. The maximum base shear obtained from the pushover analysis for Model 1.1b and Model 1.1c are 13.92 kip and 71.71 kip, respectively. Existence of the masonry block walls basically provides higher stiffness and strength for the frame. The masonry block walls also cause severe irregularities in stiffness and strength in the residence's elevation and plan. Still, even if the capacity of the models increases due to the presence of walls the asymmetric location produce torsional problems and this effect is not desirable for the models.

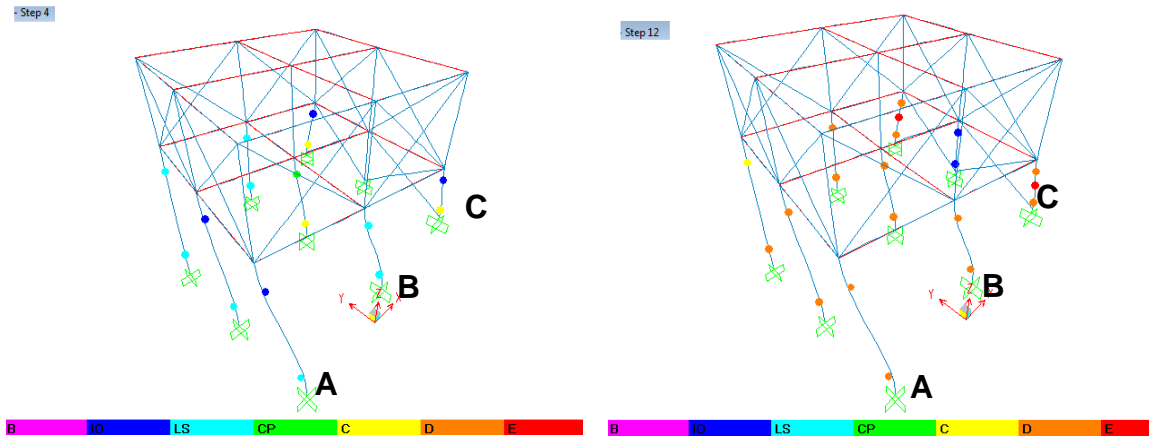
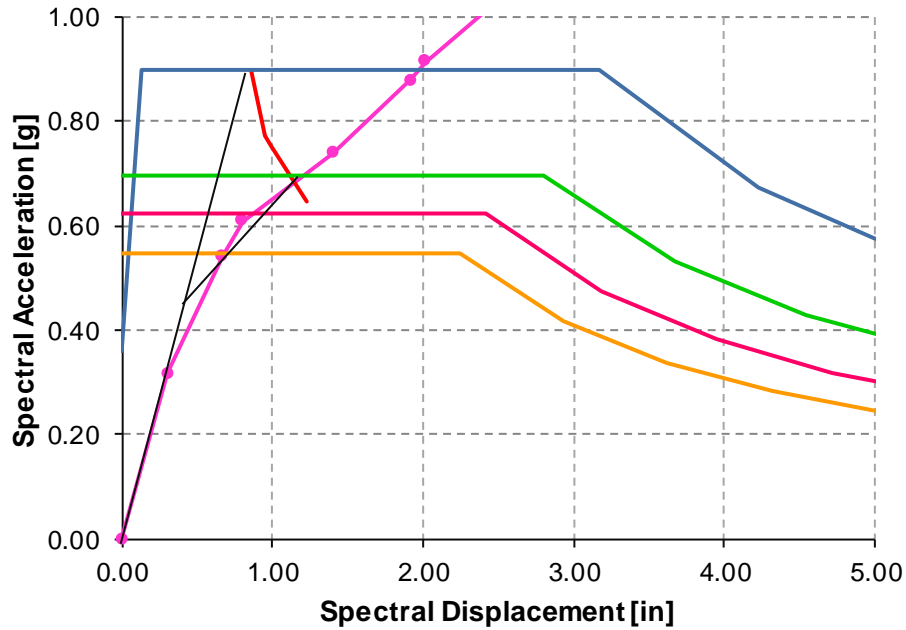


**Figure 6-18.** Pushover Deformed Shape and Hinge Formation for Model 1.1c: Push Y

Figure 6-18 shows how the model deforms in a twisting form due to the presence of modeling the retaining wall. The retaining wall makes frame C stiffer than frames A and B, therefore this frames are more flexible. Recall that for Model 1.1b (without retaining wall) in the Y direction the deformed shape of the building was uniform in the Y direction. Hinges can be observed at the columns between the block walls (frame C), this is not so likely to occur in the Y direction since the columns are confined between the block walls. However this hinges forms due to the moment ( $M_3$ ) in the X direction that is produced due to the torsion the model experiments.



$$\begin{aligned}
 S_{app} &= 0.68 \text{ g} & V_{pp} &= 36.40 \text{ k} \\
 S_{dpp} &= 1.11 \text{ in} & D_{pp} &= 0.57 \text{ in} \\
 S_{dy} &= 0.46 \text{ in} \\
 \mu_d &= 2.41
 \end{aligned}$$

**Figure 6-19.** Performance Point for Model 1.1c: Push Y

From Figure 6-19 at the performance point the spectral displacement ( $S_d$ ) and spectral acceleration ( $S_a$ ) are 1.11 inches and 0.68 g respectively. The ductility demand is 2.41. The demand curve intersects the capacity curve between the point of Life Safety (LS) and Collapse Prevention (CP). In conclusion even when the presence of a retaining wall increases the capacity of the model, still several columns are at Collapse Prevention or Collapse stage at the performance point. It is expected that columns at frames A and B suffer extensive damage.

### 6.2.1.3 MODEL 1.1d: SHEAR WALL

#### Model 1.1d: Y direction

Models type d (RC shear wall) were only analyzed using mode shape load pattern. The tabular data for pushover curve is shown in Table 6-19. Pushover curve is presented in Figure 6.20. For the purpose of comparison the pushover curve for Model 1.1b and Model 1.1c have also been included. The graphic representation of the hinge sequence formation and performance point are presented in Figures 6-21 to 6-22

**Table 6-19.** Tabular Data for Pushover Curve for Model 1.1d: Push Y

PUSH Y Mode			Hinge Sequence								Shear
Step	Disp. (in)	BaseForce (Kip)	A to B	B to IO	IO to LS	LS to CP	CP to C	C to D	D to E	E to F	
0	0.00	0.00	86	0	0	0	0	0	0	0	
1	0.16	13.88	84	2	0	0	0	0	0	0	
2	0.57	38.71	74	0	6	5	0	1	0	0	
3	0.85	52.53	74	0	0	1	7	4	0	0	
4	1.15	64.96	74	0	0	0	6	5	1	0	
5	1.44	77.03	74	0	0	0	1	6	5	0	
6	1.69	86.91	74	0	0	0	1	2	9	0	
7	2.10	103.40	72	1	1	0	0	0	12	0	
8	2.34	113.23	72	0	2	0	0	3	9	0	
9	2.40	115.76	71	1	2	0	0	2	10	0	

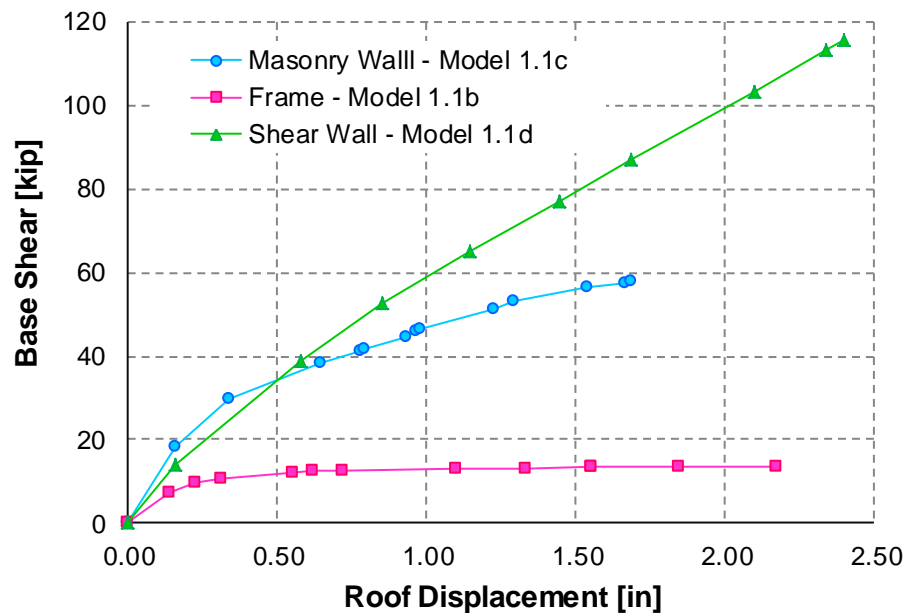


**Figure 6-20.** Comparison pushover curves for Models 1.1b, Model 1.1c and Model 1.1d:  
Push Y

It can be inferred from Figure 6-20 that when the residences have a retaining wall built as RC shear wall the capacity of the model is higher than when it was modeled as a masonry block wall or bare frame. The initial slope from the pushover curves is much steeper for Model 1.1c/d compared with Model 1.1b, meaning that the model is able to sustain higher base shear forces in the elastic range. RC shear walls are stiffer than masonry block walls, however it can be notice form Figure 6-20 that between the first 2 steps the slope for Model 1.1c (masonry block) is stepper that Model 1.1d (RC shear wall) this can be attributed to the diagonal strut model of the masonry block walls. The diagonal strut model is a simplified model that involved modeling simplification techniques, such as the equivalent width of the diagonal strut. The RC shear walls were modeled as elastic shell elements. Therefore, exactitude in the results may vary since both the masonry block wall and RC shear wall were modeled considering different approaches.

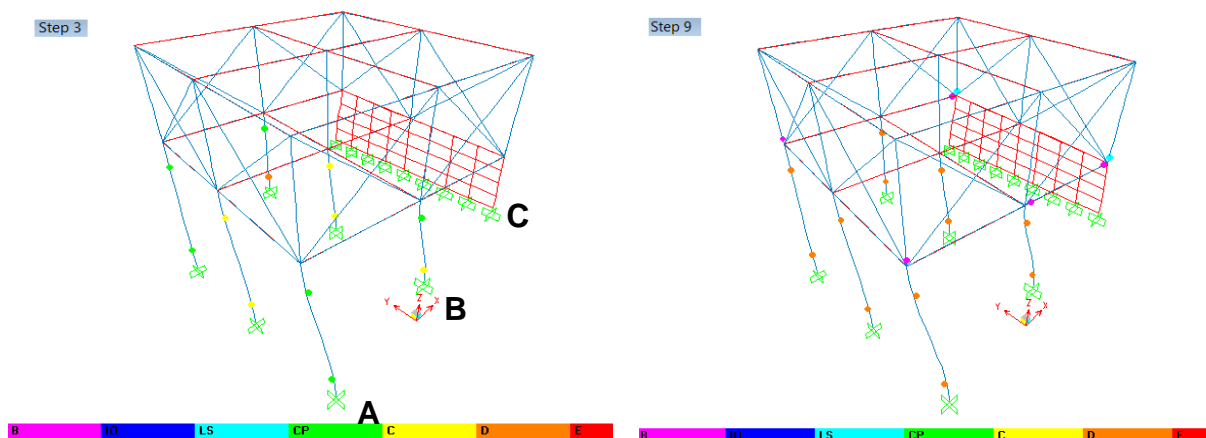
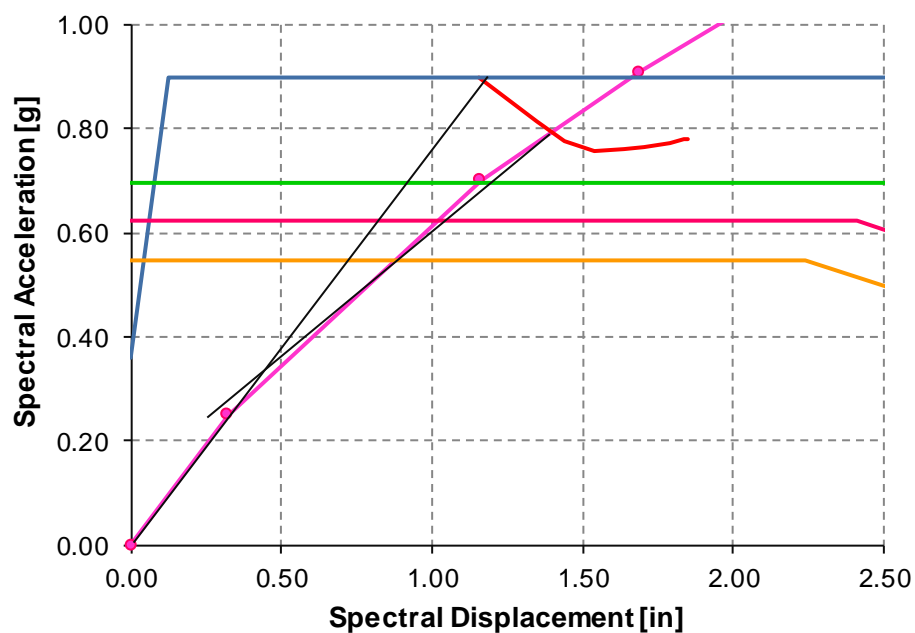


**Figure 6-21.** Pushover Deformed Shape and Hinge Formation for Model 1.1d: Push Y

In terms of the hinging pattern, the same conclusion made for Model 1.1c can be reached. It can be observed that columns standing alone (frame A and B) without lateral support forms hinges at the top and bottom. Figure 6-22 shows how the model deforms in a twisting form due to the presence of the retaining wall.



$$\begin{aligned}
 S_{app} &= 0.79 \text{ g} & V_{pp} &= 44.16 \text{ k} \\
 S_{dpp} &= 1.39 \text{ in} & D_{pp} &= 0.69 \text{ in} \\
 S_{dy} &= 0.40 \text{ in} \\
 \mu_d &= 3.48
 \end{aligned}$$

**Figure 6-22.** Performance Point for Model 1.1d: Push Y

From Figure 6-22 at the performance point the spectral displacement ( $S_d$ ) and spectral acceleration ( $S_a$ ) are 1.09 in. and 0.83 g respectively. From Table 6-20 it is shown that the demand curve intersects the capacity curve between the point (step 2 and 3) of Life Safety (LS) and Collapse (C). It can be concluded that the shear wall increase the capacity of the model drastically, however when verifying the formation of hinges it can be observed that center column at frame B is beyond collapse limit state at the performance point. After step 3, all lower level columns rapidly go beyond collapse limit state.

### **Model 1.1 Summary**

For the purpose of comparison the pushover plots in the X and Y direction for Model 1.1b, Model 1.1c and Model 1.1d are shown in Figure 6-23.

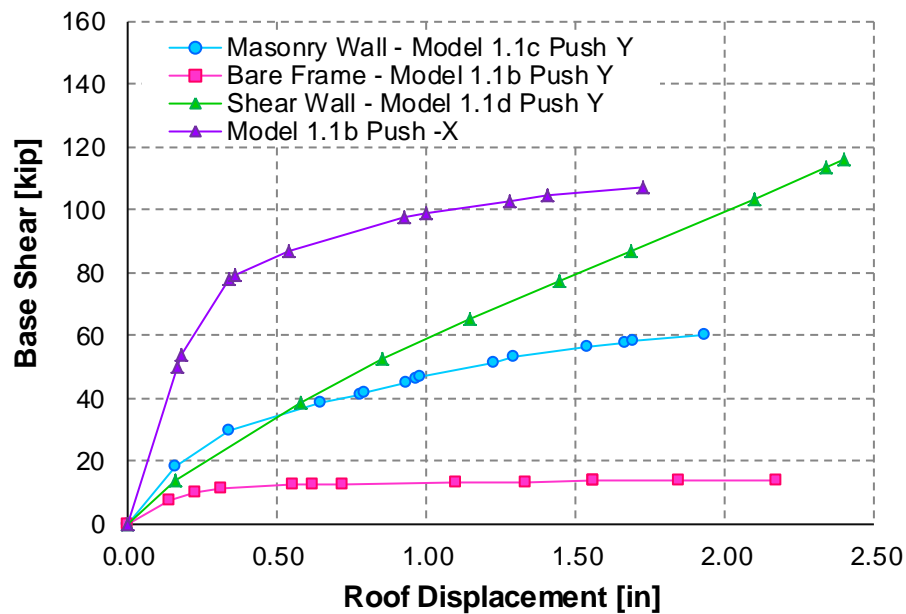


**Figure 6-23.** Comparison Pushover Curves for Model 1.1 in the X and Y direction

As can be seen in Figure 6-24 Model 1.1b is much stiffer in the X direction, which can be attributed in part to column strong axis orientation. It is apparent that the addition of masonry walls or shear walls stiffens the response of the structure in the Y direction.

## **6.2.2 PUSHOVER ANALYSIS RESULTS FOR MODEL 1.1 VS MODEL 1.2/ MODEL 1.3 / MODEL 1.4: DIFFERENCE IN BAY LENGTH**

The following sections will study the effect of increasing the bay length in Y direction (Model 1.2), in the X directions (Model 1.3) and in both X and Y direction (Model 1.4).

For the remaining cases hinge sequence graphic representation is not presented for models type b in the X and Y directions. The hinging sequence follow the same pattern as presented and discussed in Model 1.1b.

### **6.2.2.1 MODEL 1.2**

For Model 1.2 the bay in the Y direction was increased from 10 to 15 feet. The tabular data for pushover, pushover curves, hinge sequences (only for Models c/d) and performance point are presented in Tables 6-20 to 6-22 and Figures 6-24 to Figure 6-35.

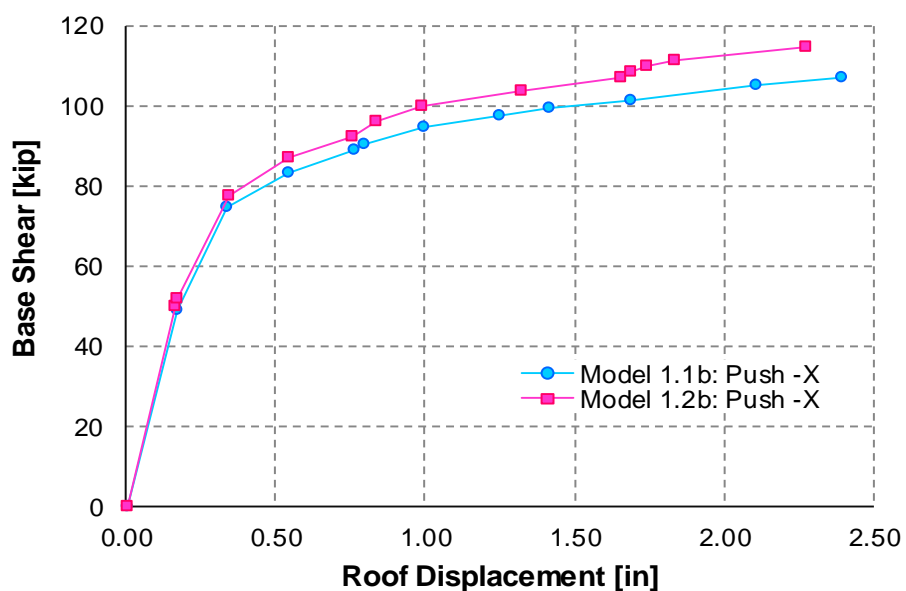
#### **Model 1.2b: -X direction**

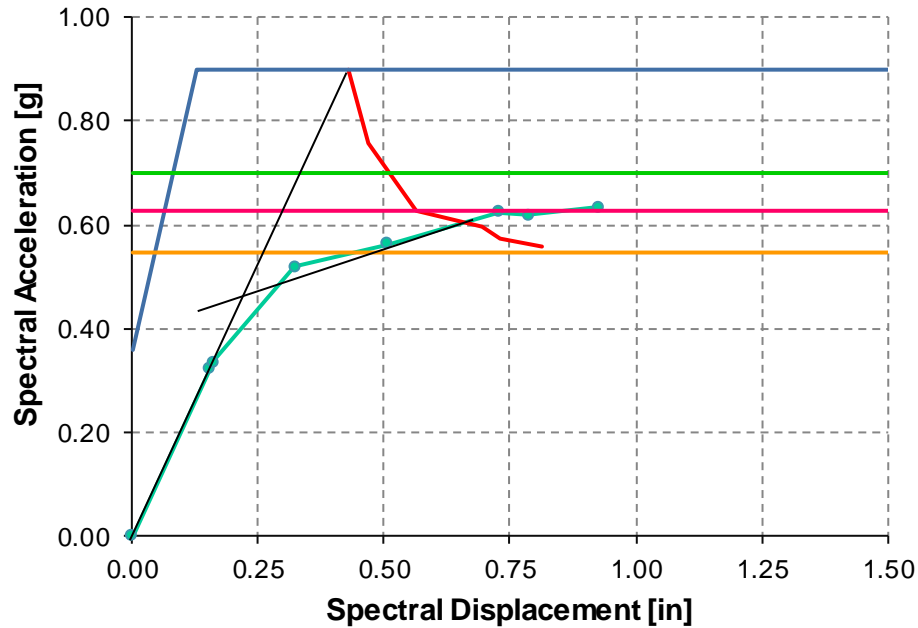
The pushover curve is very similar as for Model 1.1b (Figure 6-24). It is expected, that the effect on the pushover curve due to the increase in bay length in the Y direction is minimal in the X direction. On the other hand, it was observed that the effect in the performance point was significant; therefore the tabular data for pushover, pushover curves, and performance point are presented for further discussion.



**Table 6-20.** Tabular Data for Pushover Curve for Model 1.2b Push -X

PUSH -X Mode			Hinge Sequence								Shear
Step	Disp. (in)	BaseForce (kip)	A to B	B to IO	IO to LS	LS to CP	CP to C	C to D	D to E	E to F	
0	0.00	0.00	102	0	0	0	0	0	0	0	
1	-0.17	49.90	102	0	0	0	0	0	0	0	
2	-0.17	51.62	100	2	0	0	0	0	0	0	
3	-0.34	77.46	94	5	3	0	0	0	0	0	
4	<b>-0.54</b>	<b>86.97</b>	<b>90</b>	<b>3</b>	<b>5</b>	<b>2</b>	<b>1</b>	<b>1</b>	<b>0</b>	<b>0</b>	
5	<b>-0.76</b>	<b>92.27</b>	<b>90</b>	<b>0</b>	<b>2</b>	<b>4</b>	<b>1</b>	<b>4</b>	<b>1</b>	<b>0</b>	
6	-0.84	96.25	90	0	2	2	2	6	0	0	
7	-0.99	99.76	88	2	0	2	1	8	1	0	
8	-1.33	103.88	87	0	3	0	0	7	5	0	
9	-1.65	106.88	84	1	4	1	0	2	10	0	
10	-1.69	108.46	84	1	4	1	0	3	9	0	
11	-1.74	109.69	84	1	4	1	0	2	10	0	
12	-1.84	111.13	84	0	5	0	0	2	11	0	
13	-2.27	114.52	84	0	2	3	0	1	12	0	
14	-2.40	115.99	84	0	2	1	1	2	12	0	

**Figure 6-24.** Comparison Pushover Curves for Model 1.1b and Model 1.2b: Push -X



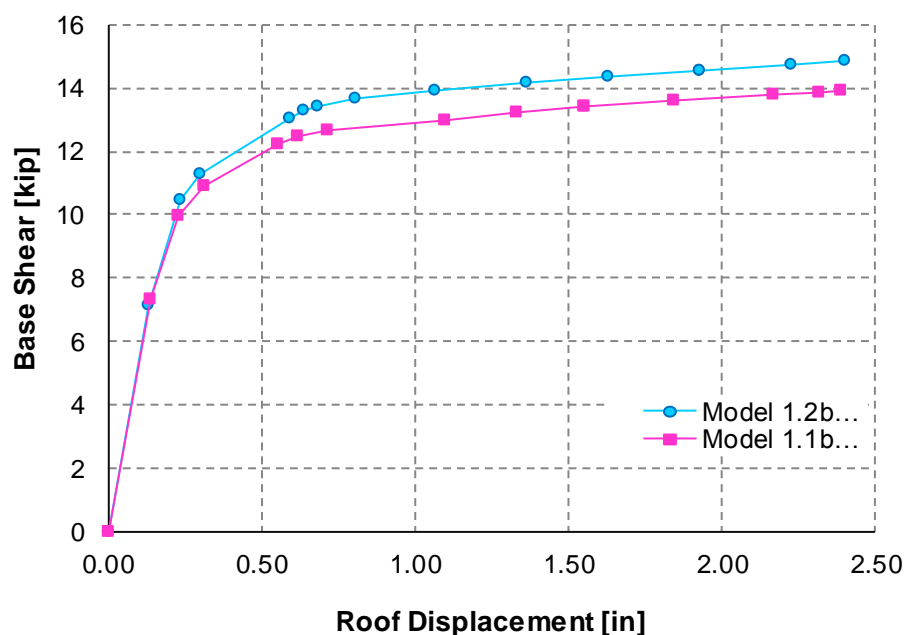
$$\begin{aligned}
 S_{app} &= 0.60 \quad \text{g} & V_{pp} &= 90.29 \quad \text{k} \\
 S_{dpp} &= 0.65 \quad \text{in} & D_{pp} &= 0.68 \quad \text{in} \\
 S_{dy} &= 0.21 \quad \text{in} \\
 \mu_d &= 3.07
 \end{aligned}$$

**Figure 6-25.** Performance Point for Model 1.2b: Push X

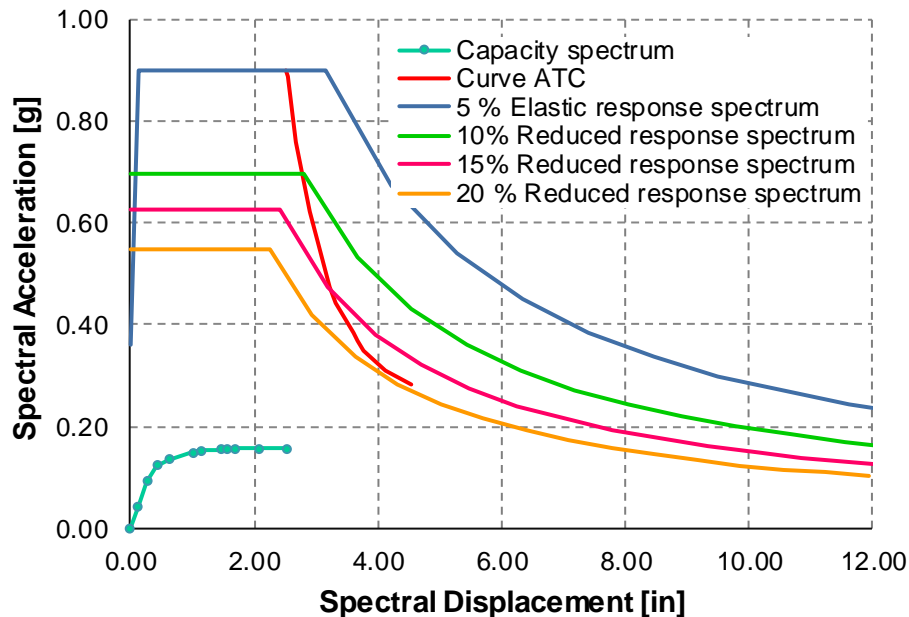
From Figure 6-25 it can be noticed that the variation in the curves between Model 1.1b and Model 1.2c is minimal. However, comparing Figures 6-11 and 6-25 the effect in the performance point is more significant. The spectral displacement increased from 0.37 inch for Model 1.1b to 0.65 inch for Model 1.2b. The ductility demand increased from 2.20 for Model 1.1b to 2.80 for Model 1.2b. This occurred due to the increase in floor mass when the bay is increased affecting both X and Y directions. Also, this implies that at the performance point columns have suffered more damage. It can also be noticed from Table 6-20 that at the performance point (between steps 4 and 5) approximately 4 columns are beyond Collapse limit state, while at the performance point (between step 2 and 3) for Model 1.1b hinges were between Immediate Occupancy and Life safety limit state.

**Model 1.2b: Y direction****Table 6-21.** Tabular Data for Pushover Curve for Model 1.2b: Push Y

PUSH Y Mode			Hinge Sequence								Shear
Step	Disp. (in)	BaseForce (kip)	A to B	B to IO	IO to LS	LS to CP	CP to C	C to D	D to E	E to F	
0	0.00	0.00	102	0	0	0	0	0	0	0	
1	0.13	7.16	101	1	0	0	0	0	0	0	
2	0.24	10.45	95	4	3	0	0	0	0	0	
3	0.30	11.28	92	2	7	1	0	0	0	0	
4	0.59	13.07	90	0	2	3	4	3	0	0	
5	0.64	13.27	88	2	0	4	5	3	0	0	
6	0.68	13.42	86	4	0	2	7	3	0	0	
7	0.81	13.65	84	2	4	0	8	4	0	0	
8	1.07	13.93	84	0	5	1	4	7	1	0	
9	1.37	14.19	84	0	1	3	0	12	2	0	
10	1.63	14.36	84	0	0	1	3	8	6	0	
11	1.93	14.56	84	0	0	0	4	6	8	0	
12	1.93	14.56	84	0	0	0	4	6	8	0	
13	2.23	14.75	84	0	0	0	4	5	9	0	

**Figure 6-26.** Comparison Pushover Curves for Model 1.1b and Model 1.2b: Push Y

From Figure 6-26 it can be observed that the increase in bay length in the Y direction has the effect of increasing the capacity slightly. The hinge sequence follows the same pattern than for Model 1.1b.

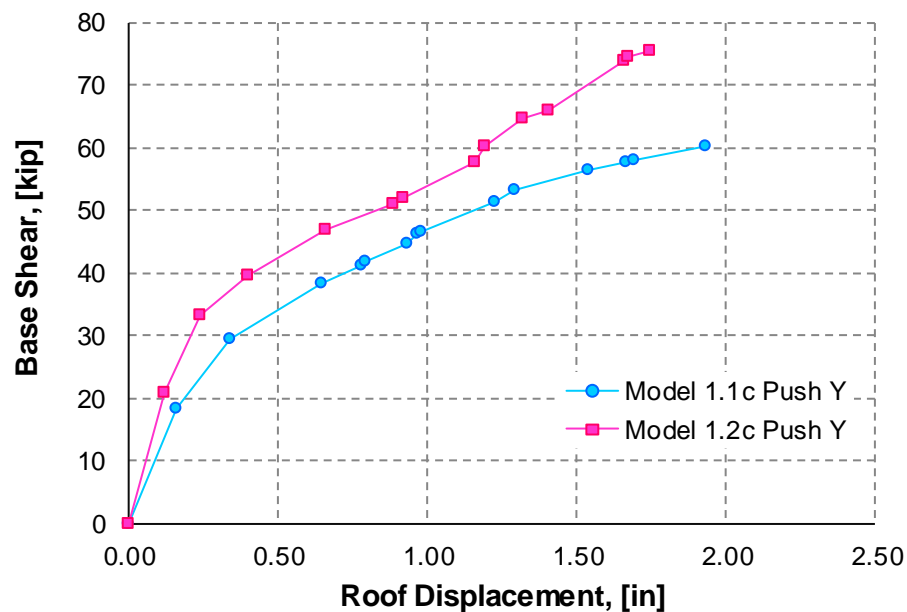


**Figure 6-27.** Performance Point for Model 1.2b: Push Y

From Figure 6-27 it is observed that no performance point was reached, same as it occurred for Model 1.1b. It can be concluded that when the models were modeled as bare frame (type b) the capacity spectrum curves lay substantially below the reduced response spectrums, due to the weak orientation of the column in the Y direction. When comparing models 1.1b and 1.2b to each other it is evident that their performance is similar.

**Model 1.2c: Y direction****Table 6-22.** Tabular Data for Pushover Curve for Model 1.2c: Push Y

PUSH Y Mode			Hinge Sequence								Shear
Step	Disp. (in)	BaseForce (kip)	A to B	B to IO	IO to LS	LS to CP	CP to C	C to D	D to E	E to F	
0	0.00	0.00	102	0	0	0	0	0	0	0	
1	0.12	20.92	101	1	0	0	0	0	0	0	
2	<b>0.24</b>	<b>33.07</b>	<b>96</b>	<b>2</b>	<b>4</b>	<b>0</b>	<b>0</b>	<b>0</b>	<b>0</b>	<b>0</b>	
3	<b>0.40</b>	<b>39.67</b>	<b>87</b>	<b>3</b>	<b>9</b>	<b>3</b>	<b>0</b>	<b>0</b>	<b>0</b>	<b>0</b>	
4	0.65	47.00	85	1	2	5	4	4	1	0	
5	0.88	50.87	85	0	1	0	4	8	4	0	
6	0.92	51.94	85	0	1	0	4	6	6	0	
7	1.16	57.72	83	0	2	0	2	6	8	1	1
8	1.19	60.28	82	0	2	0	3	5	8	2	2
9	1.32	64.56	82	0	2	0	3	5	8	2	2
10	1.40	66.10	82	0	2	0	1	6	9	2	2
11	1.66	73.99	81	1	2	0	0	8	8	2	2
12	1.67	74.48	81	1	2	0	0	7	9	2	2
13	1.75	75.47	81	1	2	0	0	4	11	3	3

**Figure 6-28.** Comparison Pushover Curves for Model 1.1c and Model 1.2c: Push Y

It can be observed from Figure 6-28 that the capacity for Model 1.2c is higher than for model 1.1c. Also, the stiffness increased reducing the displacement capacity. This is expected because as the bay length increase also the length of the masonry wall increase providing more stiffness to the model.

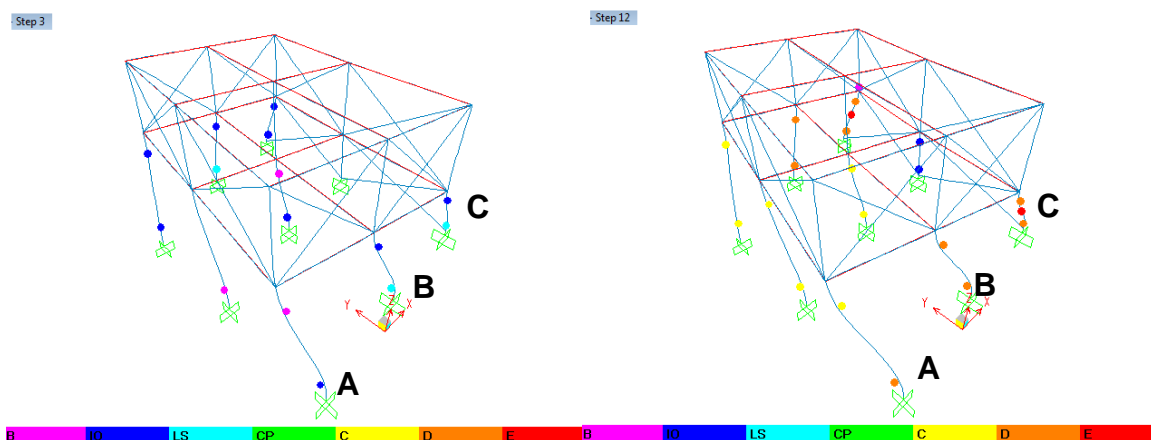
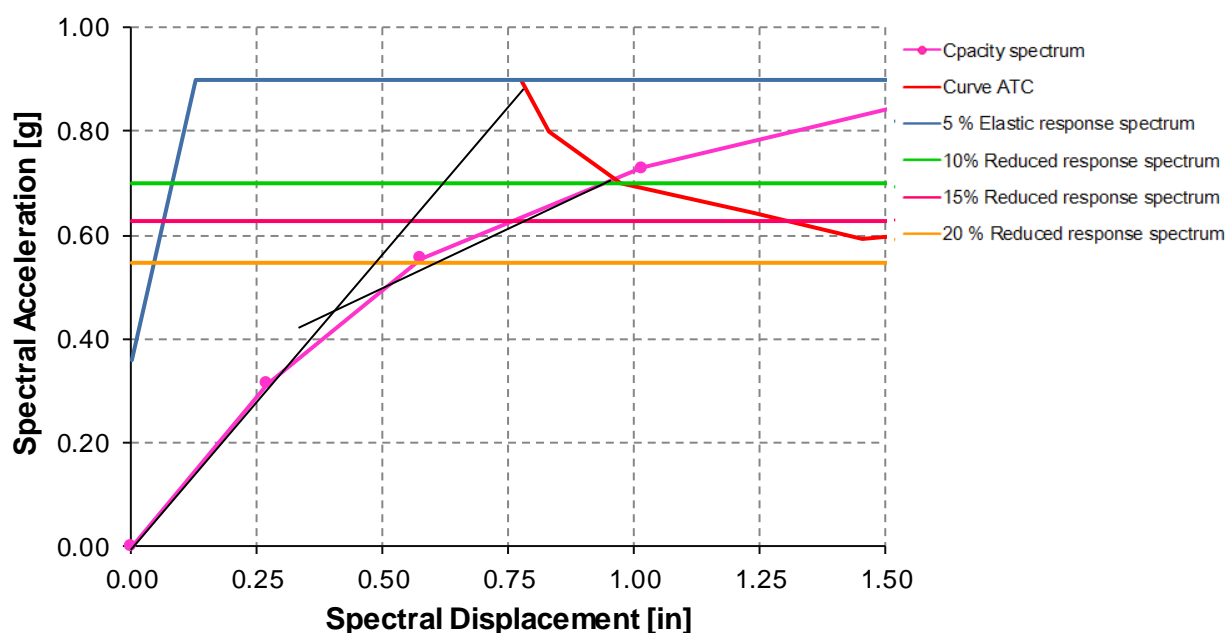


**Figure 6-29.** Pushover Deformed Shape and Hinge Formation for Model 1.2c: Push Y

Similar to Model 1.1c it can be observed that the model twists when the pushover analysis is carried out in the Y direction due to the presence of the masonry block wall.



$$\begin{aligned}
 S_{app} &= 0.70 \text{ g} & V_{pp} &= 38.71 \text{ k} \\
 S_{dpp} &= 0.95 \text{ in} & D_{pp} &= 0.37 \text{ in} \\
 S_{dy} &= 0.39 \text{ in} \\
 \mu_d &= 2.44
 \end{aligned}$$

**Figure 6-30.** Performance Point for Model 1.2c: Push Y

From Figure 6-30 at the performance point the spectral displacement ( $S_d$ ) and spectral acceleration ( $S_a$ ) are 0.95 in. and 0.70 g, respectively. The ductility demand is 2.44. The demand curve intersects the capacity curve between (steps 2 and 3) Immediate Occupancy (IO) and Life Safety (LS).

### Model 1.2d – Y direction

**Table 6-23** Tabular Data for Pushover Curve for Model 1.2d: Push Y

PUSH Y Mode			Hinge Sequence							Eto F	Shear
Step	Disp. (in)	BaseForce (kip)	B to IO	IO to LS	LS to CP	CP to C	C to D	D to E	E to F		
0	0.00	0.00	86	0	0	0	0	0	0	0	
1	0.14	19.39	85	1	0	0	0	0	0	0	
<b>2</b>	<b>0.40</b>	<b>47.01</b>	<b>75</b>	<b>1</b>	<b>8</b>	<b>2</b>	<b>0</b>	<b>0</b>	<b>0</b>	<b>0</b>	
3	0.64	66.70	74	0	1	5	1	5	0	0	
4	0.88	85.35	74	0	0	0	4	6	2	0	
5	1.15	107.38	73	1	0	0	2	6	4	0	
6	1.43	128.53	71	1	2	0	0	5	7	0	
7	1.68	147.24	70	2	2	0	1	2	9	0	
8	2.00	170.91	69	3	1	1	0	1	11	0	
9	2.35	196.72	68	2	2	1	0	2	11	0	
10	2.40	200.49	68	2	2	1	0	1	12	0	

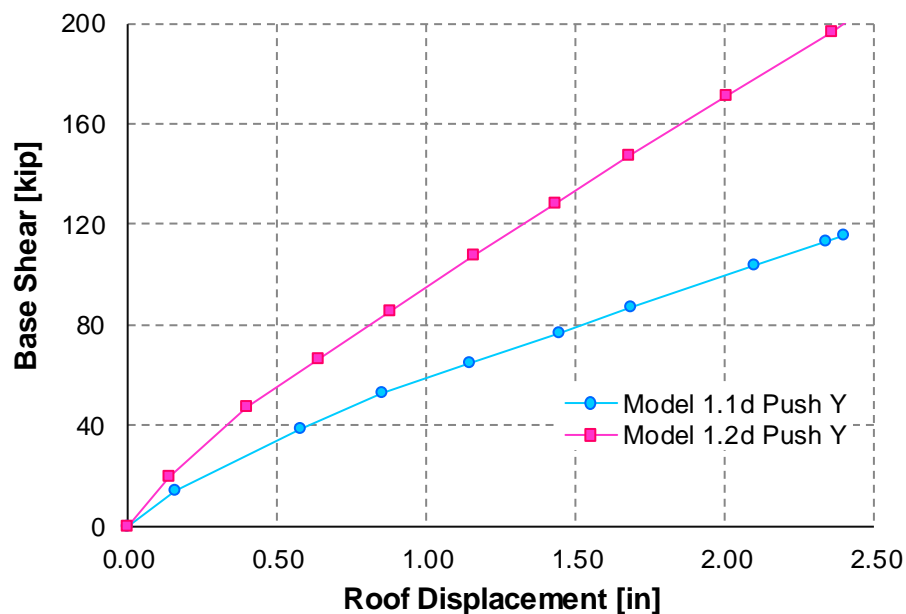


**Figure 6-31.** Comparison Pushover curves for Model 1.1d and Model 1.2d: Push Y

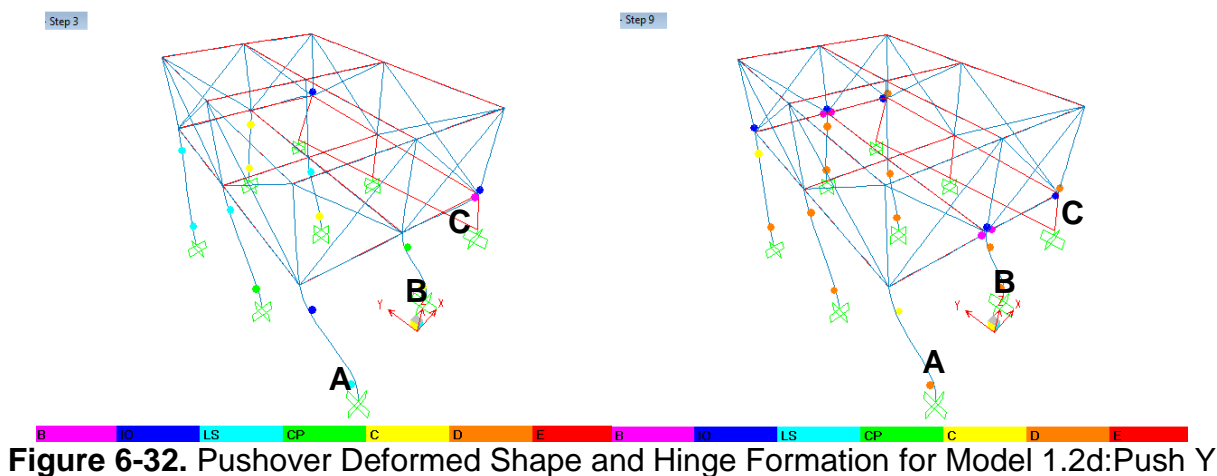
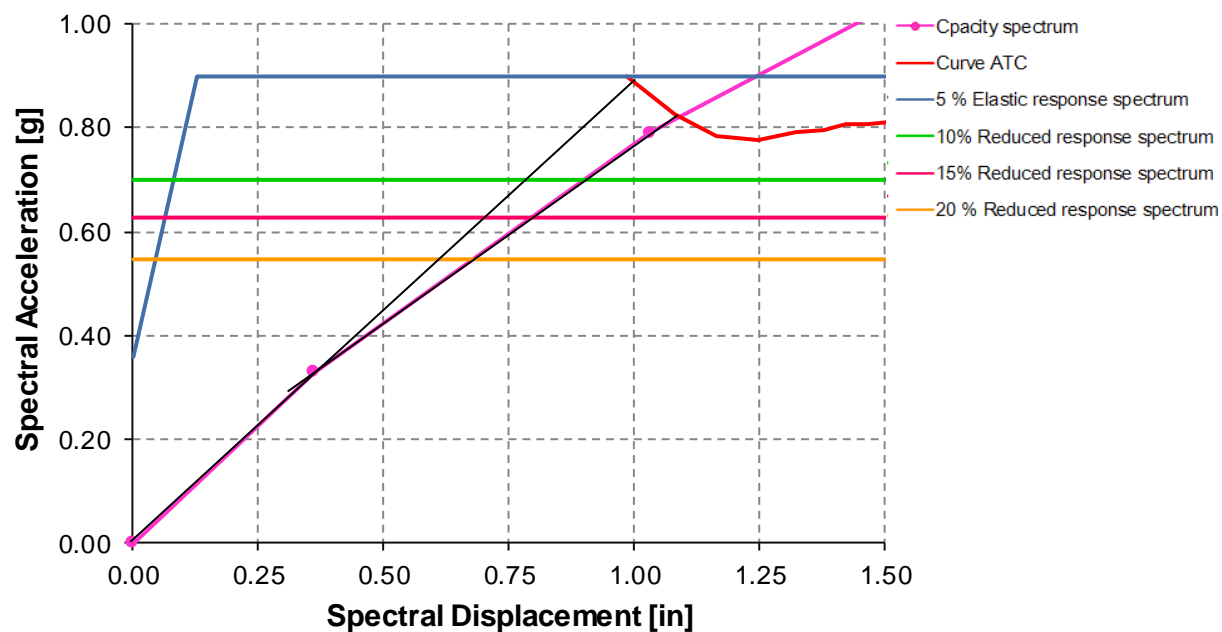


**Figure 6-32.** Pushover Deformed Shape and Hinge Formation for Model 1.2d:Push Y



$$\begin{aligned}
 S_{app} &= 0.82 \text{ g} & V_{pp} &= 48.78 \text{ k} \\
 S_{dpp} &= 1.09 \text{ in} & D_{pp} &= 0.42 \text{ in} \\
 S_{dy} &= 0.38 \text{ in} \\
 \mu_d &= 2.87
 \end{aligned}$$

**Figure 6-33.** Performance Point for Model 1.2d: Push Y

From Figure 6-33 at the performance point the spectral displacement ( $S_d$ ) and spectral acceleration ( $S_a$ ) are 0.78 in. and 0.82 g. The ductility demand is 1.12. The same conclusions as for Model 1.1d in the Y direction apply for this case. The shear wall increases the capacity of the model drastically, however when verifying the formation of



hinges it can be observed that several hinges at the columns are near Collapse Prevention (CP) limit at just the second step in the pushover analysis.

### 6.2.2.2 MODEL 1.3

For Model 1.3 the bay in the X direction was increased from 10 to 15 feet. The tabular data for pushover, pushover curves, hinge sequences (only for Models c/d) and performance point are presented in Tables 6-24 to 6-26 and Figures 6-36 to Figure 6-41. Results of Model 1.3b in the Y direction are not presented, the increase in the bay length was in the X direction, therefore it is expected that this case will suffer no major impact. On the other hand the results of Model 1.3c /d in the Y direction are presented because these models have demonstrated to be affected by torsion due to the presence of the retaining wall so any change in either X or Y direction will affect the results.

#### Model 1.3b: -X direction

**Table 6-24.** Tabular Data for Pushover Curve for Model 1.3b: Push -X

PUSH -X Mode			Hinge Sequence								Shear
Step	Disp. (in)	Base Force (Kip)	A to B	B to IO	IO to LS	LS to CP	CP to C	C to D	D to E	E to F	
0	0.00	0.00	102	0	0	0	0	0	0	0	
1	-0.18	50.77	102	0	0	0	0	0	0	0	
2	-0.20	54.23	99	3	0	0	0	0	0	0	
3	-0.38	80.52	96	3	3	0	0	0	0	0	
4	-0.40	82.48	93	4	4	1	0	0	0	0	
5	<b>-0.59</b>	<b>91.22</b>	<b>90</b>	<b>3</b>	<b>5</b>	<b>2</b>	<b>0</b>	<b>2</b>	<b>0</b>	<b>0</b>	
6	<b>-0.74</b>	<b>95.46</b>	<b>90</b>	<b>0</b>	<b>5</b>	<b>4</b>	<b>0</b>	<b>2</b>	<b>1</b>	<b>0</b>	
7	-0.75	95.96	90	0	5	4	0	3	0	0	
8	-1.02	102.40	87	3	0	2	2	7	1	0	
9	-1.30	105.61	87	0	3	0	1	7	4	0	
10	-1.55	108.31	84	2	3	1	0	5	7	0	
11	-1.98	111.99	84	0	3	2	0	1	12	0	
12	-2.02	113.02	84	0	3	2	0	2	11	0	
13	-2.26	115.83	84	0	2	2	0	2	12	0	
14	-2.41	116.95	84	0	2	0	1	3	12	0	

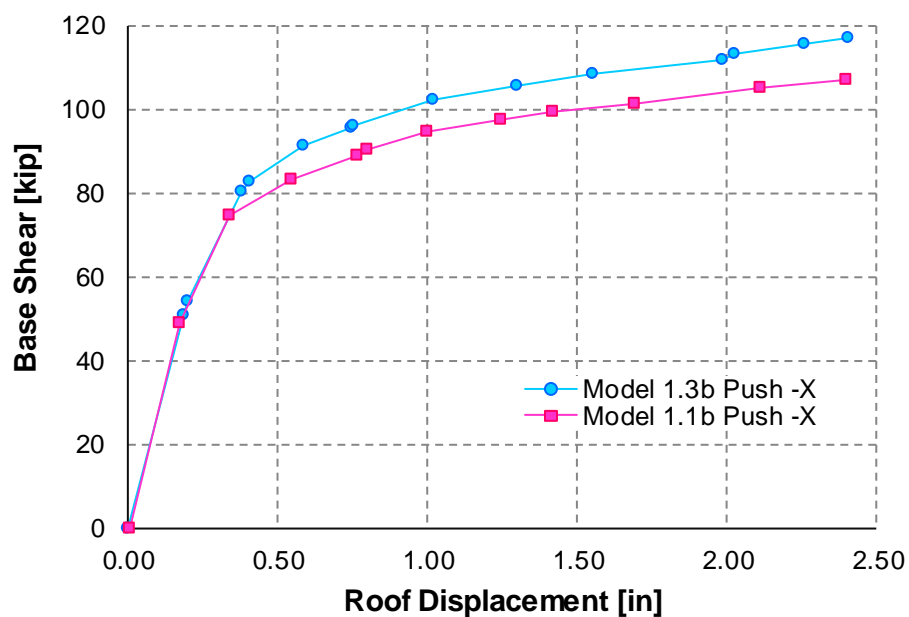
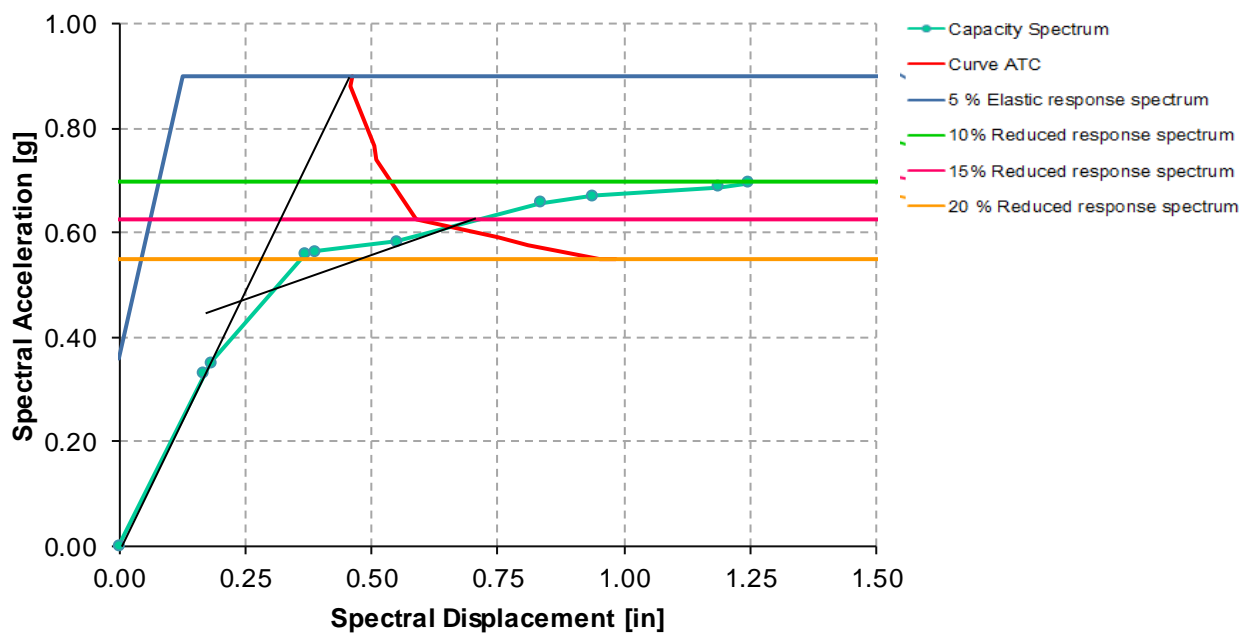


**Figure 6-34.** Comparison Pushover Curves for Model 1.1b and Model 1.3b: Push -X



$$\begin{aligned}
 S_{app} &= 0.61 \text{ g} & V_{pp} &= 94.94 \text{ k} \\
 S_{dpp} &= 0.68 \text{ in} & D_{pp} &= 0.725 \text{ in} \\
 S_{dy} &= 0.25 \text{ in} \\
 \mu_d &= 2.72
 \end{aligned}$$

**Figure 6-35.** Performance Point for Model 1.3b: Push X

From Figure 6-35 at the performance point the spectral displacement ( $S_d$ ) and spectral acceleration ( $S_a$ ) are 0.68 in. and 0.61. The ductility demand is 2.72. In terms of the performance point (step 5 and 6) it can be observed from Table 6-26 that two hinges are at Collapse (C) limit state. In general most of the hinges are between LS and CP limit state.

### Model 1.3c: Y direction

**Table 6-25.** Tabular Data for Pushover Curve for Model 1.3c: Push Y

PUSH Y Mode			Hinge Sequence								Shear
Step	Disp. (in)	Base Force (Kip)	A to B	B to IO	IO to LS	LS to CP	CP to C	C to D	D to E	E to F	
0	0.00	0.00	102	0	0	0	0	0	0	0	
1	0.20	13.48	100	2	0	0	0	0	0	0	
2	0.29	18.64	94	6	2	0	0	0	0	0	
3	0.60	26.51	87	1	7	4	3	0	0	0	
4	0.73	28.15	86	0	5	3	6	2	0	0	
5	0.99	32.11	86	0	2	1	6	7	0	0	
6	1.28	35.86	86	0	1	1	5	9	0	0	
7	1.55	40.69	85	1	0	0	4	10	2	0	
8	1.66	41.65	84	1	1	0	4	8	4	0	
9	1.72	42.43	84	1	1	0	3	6	7	0	
10	2.07	45.41	83	0	2	0	2	4	10	1	1
11	2.38	48.23	82	0	2	0	0	2	14	2	2

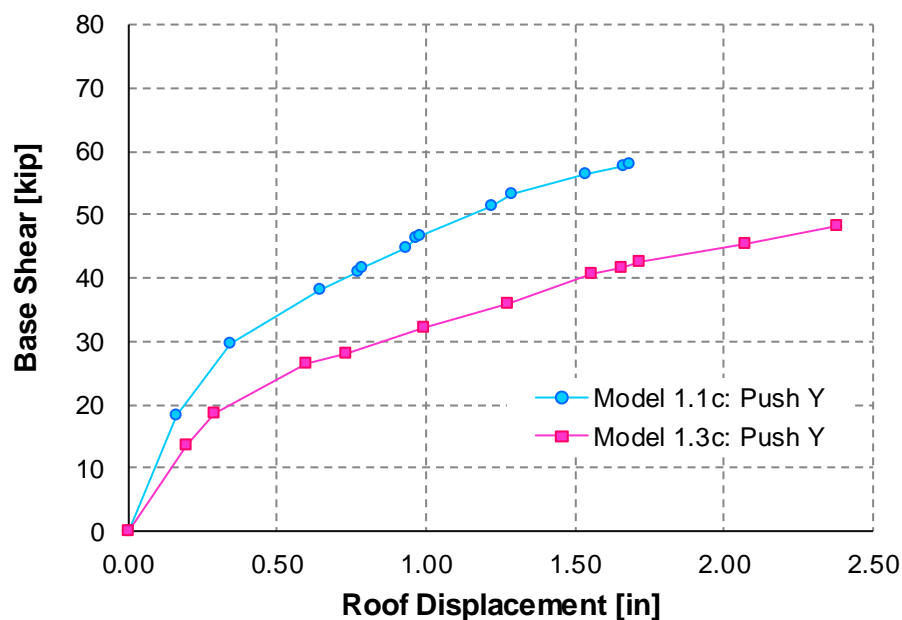


**Figure 6-36.** Comparison Pushover Curves for Model 1.1b and Model 1.3c: Push Y

From Figure 6-36 it can be observed that increasing the bay in the X direction, decreases the capacity in the Y direction of Model 1.3c. This effect was only observed when the model includes a retaining wall (model type c and d). In the case of Model 1.3b the Y direction suffers no impact while the bay length in X direction increases.

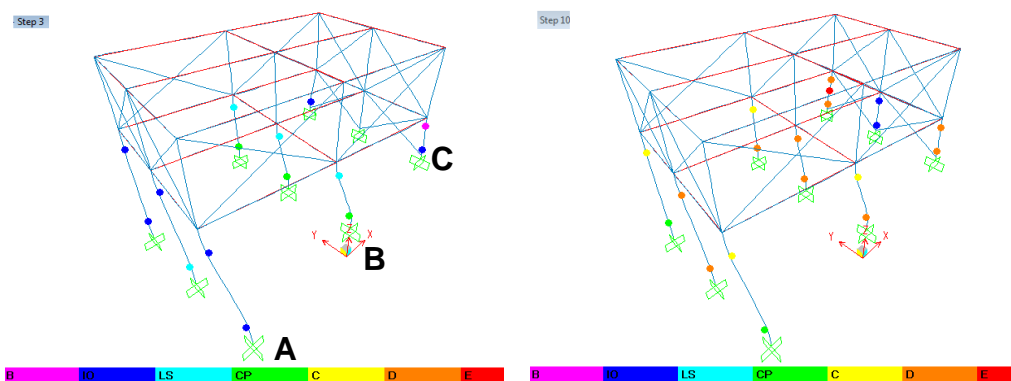
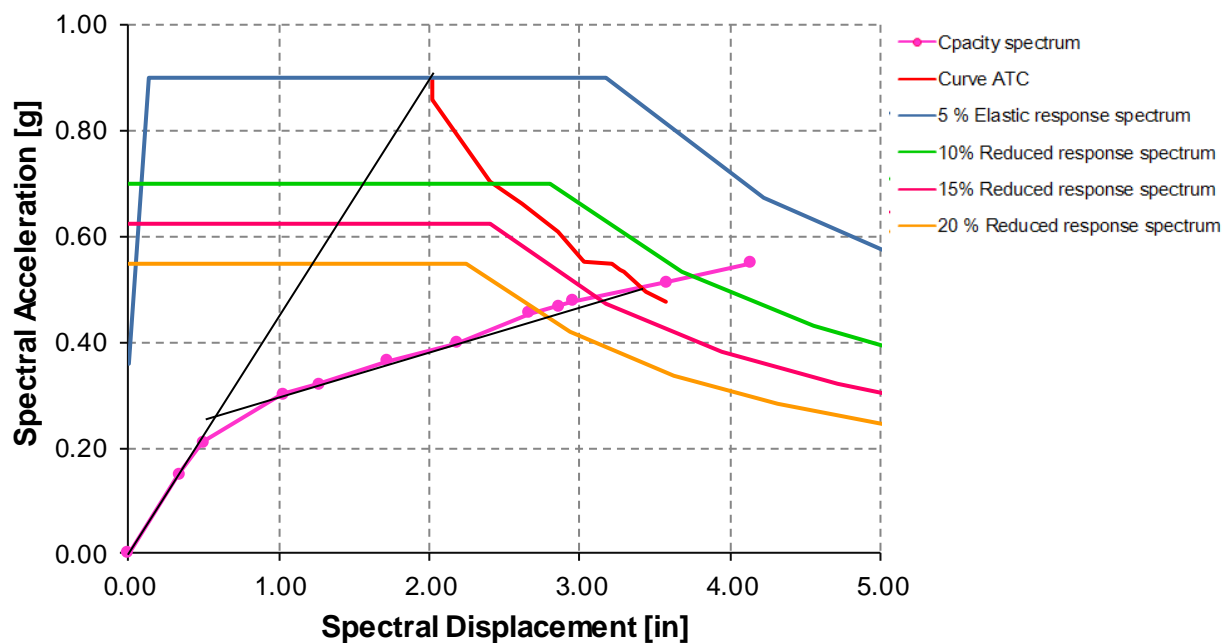


Figure 6-37. Pushover Deformed Shape and Hinge Formation for Model 1.3b: Push -X



$$\begin{aligned}
 S_{app} &= 0.50 \text{ g} & V_{pp} &= 44.6 \text{ k} \\
 S_{dpp} &= 3.40 \text{ in} & D_{pp} &= 1.97 \text{ in} \\
 S_{dy} &= 0.51 \text{ in} \\
 \mu_d &= 6.67
 \end{aligned}$$

Figure 6-38. Performance Point for Model 1.3c: Push Y

From Figure 6-38 at the performance point the spectral displacement ( $S_d$ ) and spectral acceleration ( $S_a$ ) are 3.40 in. and 0.50 g. The ductility demand is 5.86. At the performance point (between step 9 and 10) it can be observed from Table 6-25 that several hinges are beyond Collapse (C) limit state, including shear failure at the corner column at frame C (Figure 6-41).

### **Model 1.3d: Y direction**

**Table 6-26.** Tabular Data for Pushover Curve for Model 1.3d: Push Y

PUSH Y Mode			Hinge Sequence								Shear
Step	Disp. (in)	Base Force (Kip)	A to B	B to IO	IO to LS	LS to CP	CP to C	C to D	D to E	E to F	
0	0.00	0.00	86	0	0	0	0	0	0	0	
1	0.19	10.44	84	2	0	0	0	0	0	0	
2	0.60	25.26	74	0	4	5	2	1	0	0	
3	0.86	31.87	74	0	0	2	6	4	0	0	
4	1.17	39.31	74	0	0	0	6	6	0	0	
5	1.41	45.07	74	0	0	0	4	8	0	0	
6	1.68	51.80	74	0	0	0	3	3	6	0	
7	2.05	59.88	74	0	0	0	2	4	6	0	
8	2.43	68.66	72	2	0	0	0	3	9	0	
9	2.44	68.93	72	2	0	0	0	1	11	0	

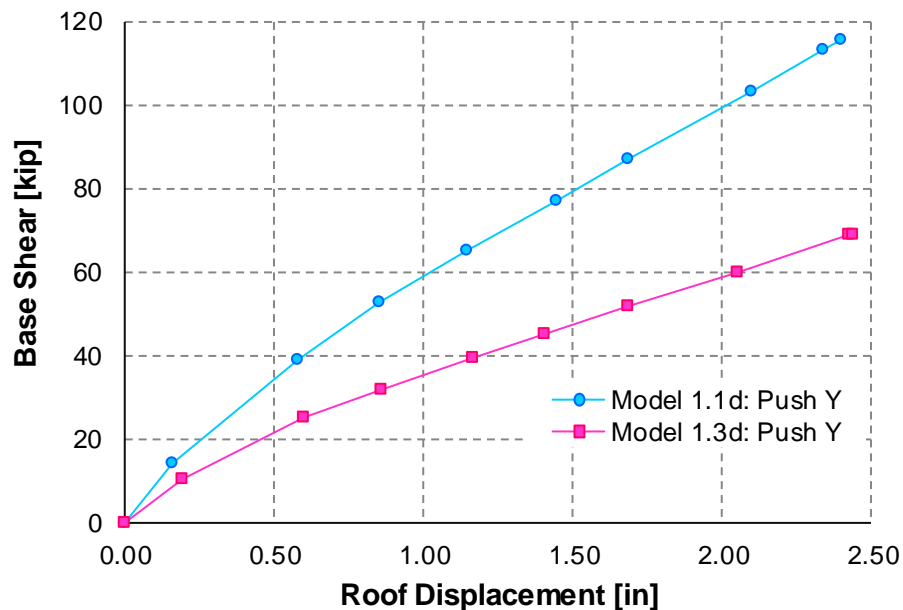


**Figure 6-39.** Comparison Pushover Curves for Model 1.1b and Model 1.3d: Push Y

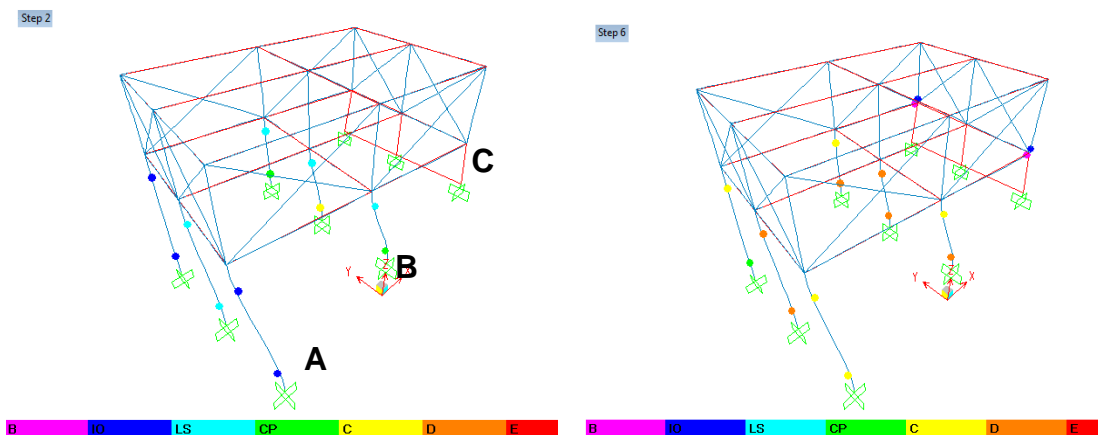
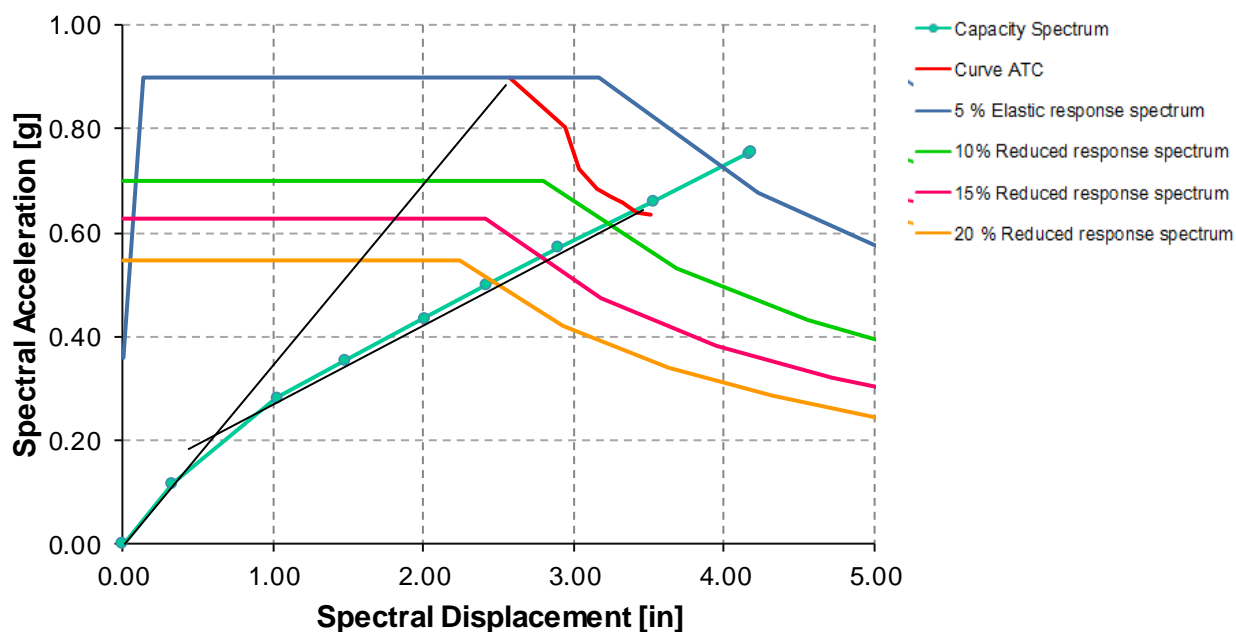


**Figure 6-40.** Pushover Deformed Shape and Hinge Formation for Model 1.3d: Push Y



$$\begin{aligned}
 S_{app} &= 0.64 \text{ g} & V_{pp} &= 58.23 \text{ k} \\
 S_{dpp} &= 3.40 \text{ in} & D_{pp} &= 1.98 \text{ in} \\
 S_{dy} &= 0.52 \text{ in} \\
 \mu_d &= 6.54
 \end{aligned}$$

**Figure 6-41.** Performance Point for Model 1.3d: Push Y

From Figure 6-41 at the performance point the spectral displacement ( $S_d$ ) and spectral acceleration ( $S_a$ ) are 3.40 in. and 0.64 g, respectively. The ductility demand is 6.54. At the performance point (step 5 and 6) it can be observed from Table 6-25 that several hinges are at and beyond Collapse (C) limit state.

### 6.2.2.3 MODEL 1.4

For Model 1.4 the bay in the X and Y directions were increased from 10 to 15 feet. The tabular data for pushover, pushover curves, hinge sequences (only for Models c/d) and performance point are presented in Tables 6-27 to 6-28 and Figures 6-42 to 6-51.

#### Model 1.4b: -X direction

**Table 6-27** Tabular Data for Pushover Curve for Model 1.4b: Push -X

PUSH -X Mode			Hinge Sequence								Shear
Step	Disp. (in)	Base Force (Kip)	A to B	B to IO	IO to LS	LS to CP	CP to C	C to D	D to E	E to F	
0	-0.01	0.00	102	0	0	0	0	0	0	0	
1	-0.19	53.39	102	0	0	0	0	0	0	0	
2	-0.39	84.84	96	3	3	0	0	0	0	0	
3	-0.40	86.30	93	6	2	1	0	0	0	0	
4	-0.54	94.11	93	0	5	2	0	2	0	0	
5	-0.61	99.03	90	2	5	4	0	1	0	0	
6	-0.86	106.56	90	0	2	3	0	7	0	0	
7	-1.00	110.29	88	2	1	2	0	8	1	0	
8	-1.25	113.79	87	0	3	0	0	9	3	0	
9	<b>-1.41</b>	<b>116.23</b>	<b>86</b>	<b>1</b>	<b>3</b>	<b>0</b>	<b>0</b>	<b>8</b>	<b>4</b>	<b>0</b>	
10	-1.70	119.24	84	1	4	1	0	5	7	0	
11	-1.85	121.15	84	0	4	1	0	5	8	0	
12	-2.05	122.58	84	0	2	3	0	3	10	0	
13	-2.15	123.88	84	0	2	3	0	3	10	0	
14	-2.21	124.39	84	0	2	2	1	2	11	0	

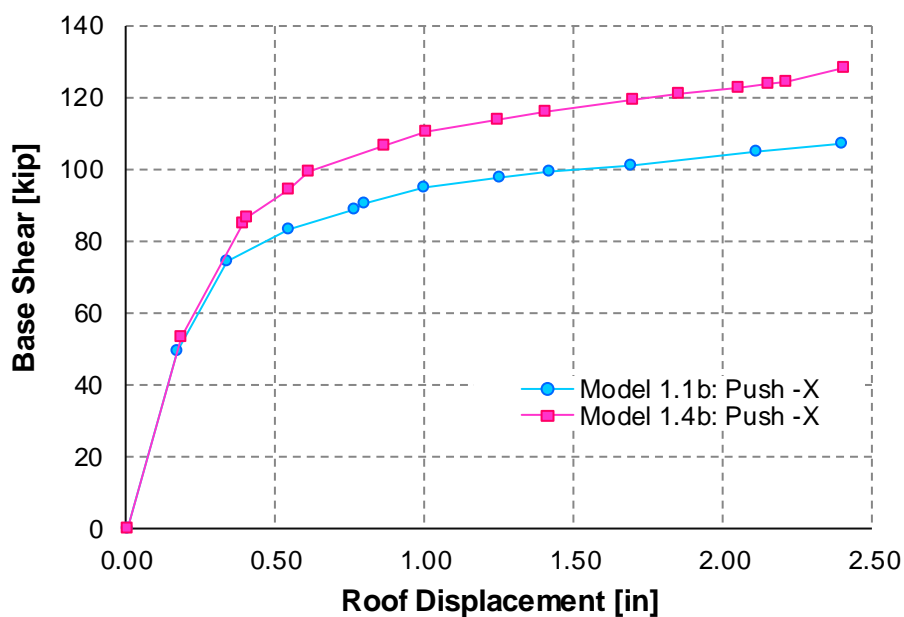
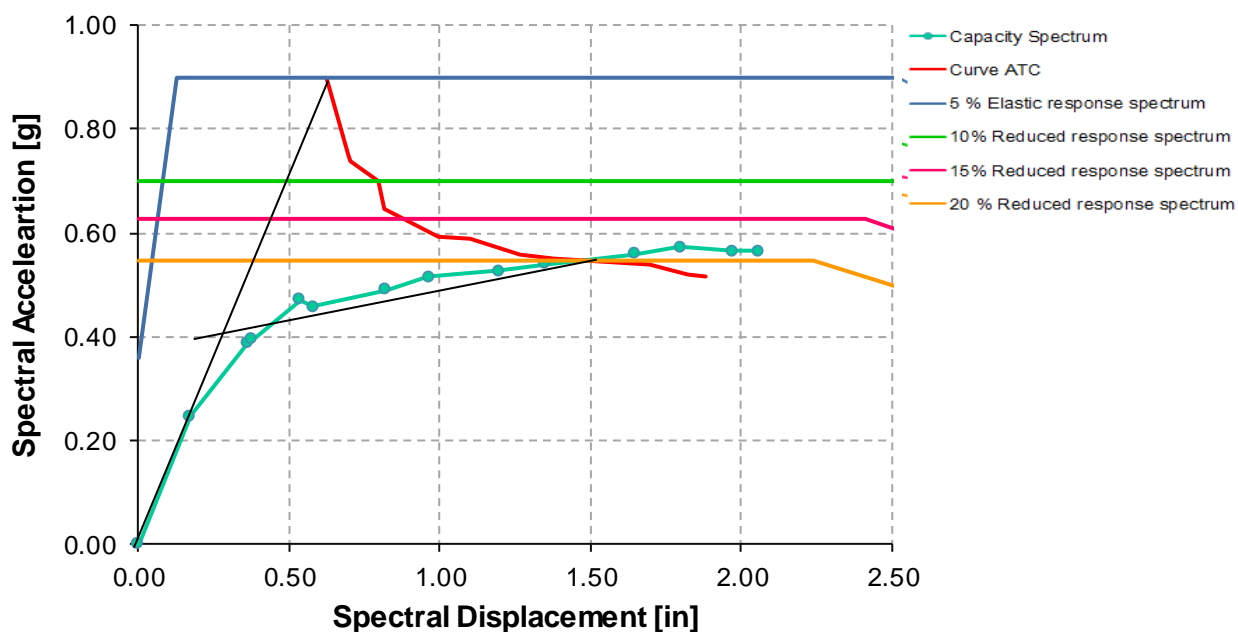


**Figure 6-42.** Comparison Pushover Curves for Model 1.1b and 1.4b: Push -X



$$\begin{aligned}
 S_{app} &= 0.55 \text{ g} & V_{pp} &= 117.3 \text{ k} \\
 S_{dpp} &= 1.45 \text{ in} & D_{pp} &= 1.51 \text{ in} \\
 S_{dy} &= 0.30 \text{ in} \\
 \mu_d &= 4.83
 \end{aligned}$$

**Figure 6-43.** Performance Point for Model 1.4b: Push -X

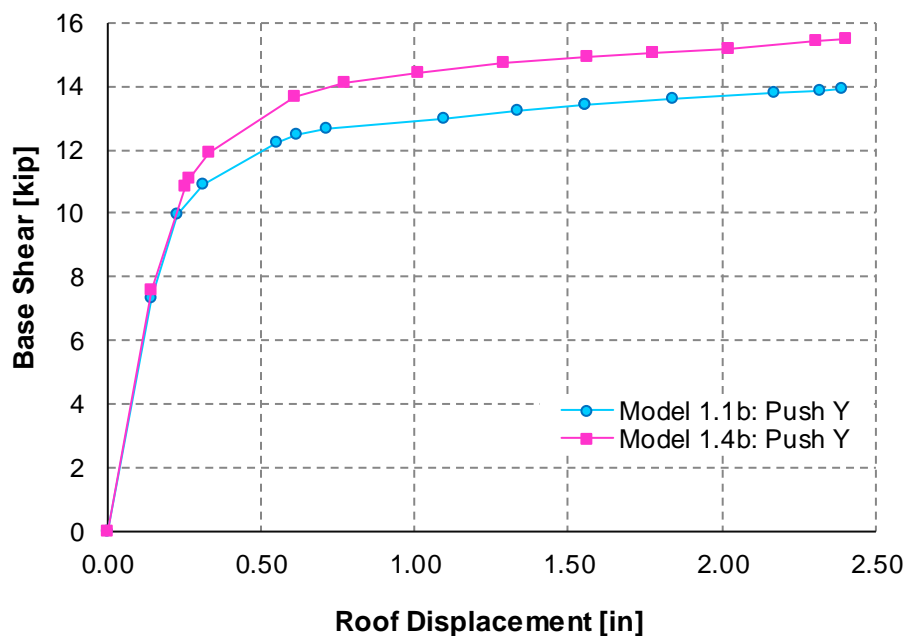


From Figure 6-43 at the performance point the spectral displacement ( $S_d$ ) and spectral acceleration ( $S_a$ ) are 1.45 in. and 0.55. The ductility demand is 4.83. At the performance point (step 9) it can be observed from Table 6-25 that eight hinges are beyond Collapse (C) limit state.

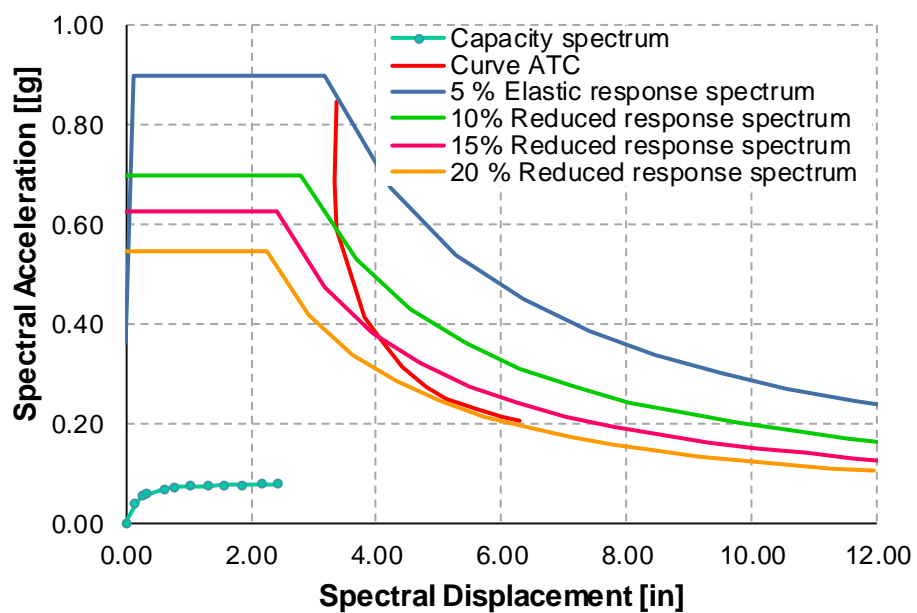
### **Model 1.4b: Y direction**

**Table 6-28.** Tabular Data for Pushover Curve for Model 1.4b: Push Y

PUSH Y Mode			Hinge Sequence								Shear
Step	Disp. (in)	Base Force (Kip)	A to B	B to IO	IO to LS	LS to CP	CP to C	C to D	D to E	E to F	
0	0.00	0.00	102	0	0	0	0	0	0	0	
1	0.15	7.57	101	1	0	0	0	0	0	0	
2	0.25	10.85	96	3	3	0	0	0	0	0	
3	0.26	11.12	94	5	3	0	0	0	0	0	
4	0.33	11.94	92	2	7	1	0	0	0	0	
5	0.61	13.70	88	2	2	4	5	1	0	0	
6	0.77	14.13	84	3	3	0	8	4	0	0	
7	1.01	14.43	84	0	5	1	8	4	0	0	
8	1.29	14.73	84	0	2	2	4	9	1	0	
9	1.56	14.91	84	0	0	2	2	12	2	0	
10	1.78	15.04	84	0	0	0	4	9	5	0	
11	1.78	15.04	84	0	0	0	4	9	5	0	
12	2.02	15.20	84	0	0	0	4	6	8	0	
13	2.02	15.20	84	0	0	0	4	6	8	0	
14	2.31	15.41	84	0	0	0	2	8	8	0	



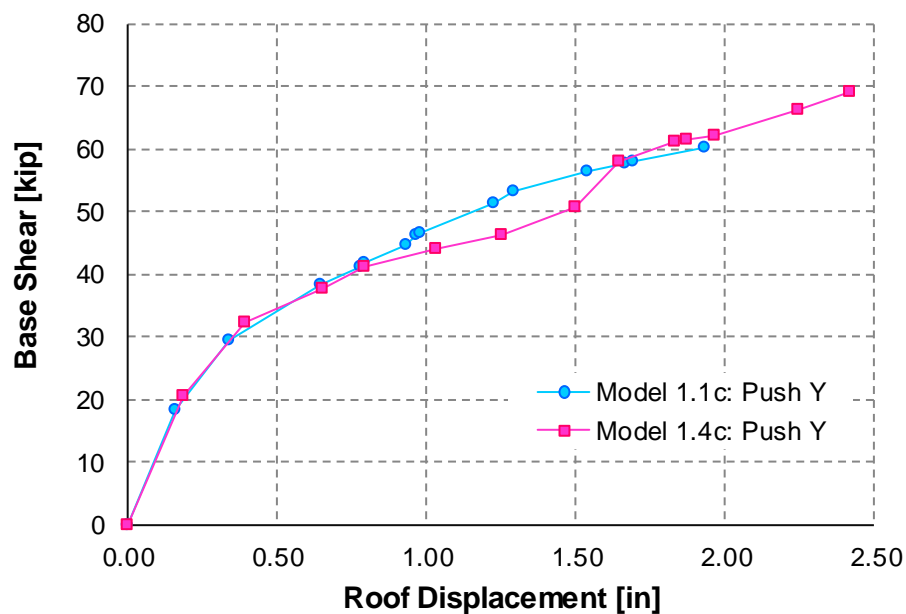
**Figure 6-44.** Comparison Pushover Curves for Models 1.1b and 1.4b: Push Y



**Figure 6-45.** Performance Point for Model 1.4b: Push Y

**Model 1.4c: Y direction****Table 6-29.** Tabular Data for Pushover Curve. for Model 1.4b: Push Y

PUSH Y Mode			Hinge Sequence								Shear
Step	Disp. (in)	BaseForce (Kip)	A to B	B to IO	IO to LS	LS to CP	CP to C	C to D	D to E	E to F	
0	0.00	0.00	102	0	0	0	0	0	0	0	
1	0.18	20.44	101	1	0	0	0	0	0	0	
2	0.39	32.42	90	3	7	2	0	0	0	0	
3	0.65	37.66	86	0	5	5	4	2	0	0	
4	0.79	41.16	86	0	2	4	6	4	0	0	
5	1.03	44.11	85	1	0	0	4	11	1	0	
6	1.25	46.38	84	1	0	0	4	8	4	1	
7	<b>1.49</b>	<b>50.56</b>	<b>84</b>	<b>0</b>	<b>1</b>	<b>0</b>	<b>4</b>	<b>7</b>	<b>5</b>	<b>1</b>	1
8	1.65	58.04	81	2	1	0	2	9	5	2	2
9	1.83	61.28	81	2	1	0	1	7	8	2	2
10	1.87	61.63	81	1	2	0	0	7	9	2	2
11	1.96	62.28	81	1	2	0	0	5	11	2	2
12	2.25	66.32	81	0	3	0	0	1	15	2	2
13	2.42	69.12	80	1	3	0	0	1	14	3	2

**Figure 6-46.** Comparison Pushover Curves for Models 1.1c and 1.4c: Push Y

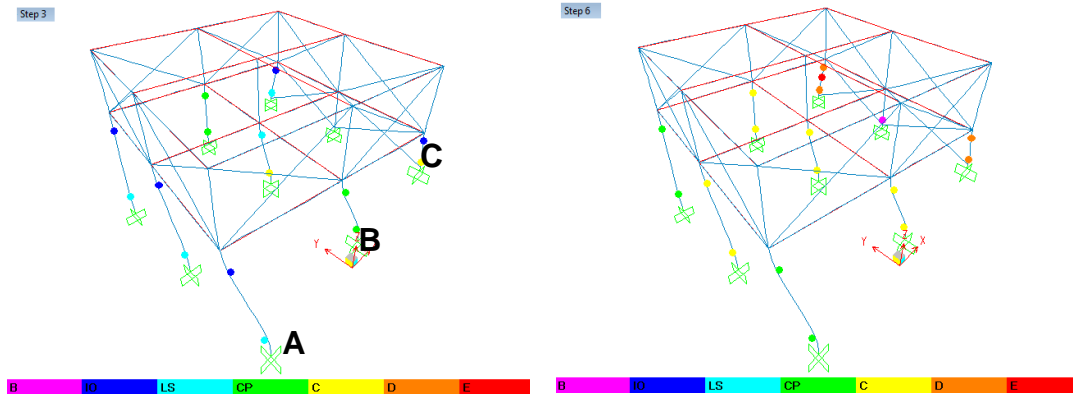
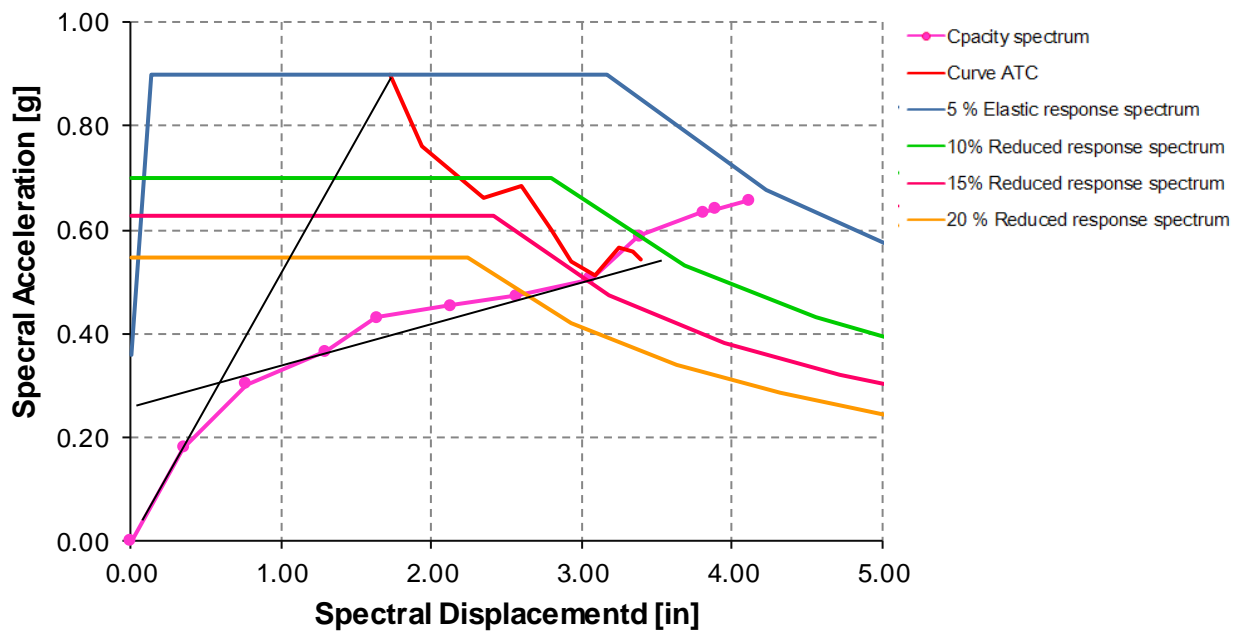


**Figure 6-47.** Pushover Deformed Shape and Hinge Formation for Model 1.4c: Push Y



$$\begin{aligned}
 S_{app} &= 0.52 \text{ g} & V_{pp} &= 51.99 \text{ k} \\
 S_{dpp} &= 3.12 \text{ in} & D_{pp} &= 1.52 \text{ in} \\
 S_{dy} &= 0.52 \text{ in} \\
 \mu_d &= 6.00
 \end{aligned}$$

**Figure 6-48.** Performance Point for Model 1.4c: Push Y

From Figure 6-48 at the performance point the spectral displacement ( $S_d$ ) and spectral acceleration ( $S_a$ ) are 3.12 in. and 0.52. The ductility demand is 6.00. At the performance point (step 7) it can be observed from Table 6-29 that seven hinges are beyond Collapse (C) limit state, including shear failure at the corner column (Figure 6-51). The shear failure occurs due to the shear forces exceeding the maximum shear capacity

specified in the X direction. As mentioned before the models in the Y direction with a retaining wall suffers high torsion that induces forces in both the X and Y direction.

### Model 1.4d: Y direction

**Table 6-30.** Tabular Data for Pushover Curve for Model 1.4d: Push Y

PUSH Y Mode			Hinge Sequence								Shear
Step	Disp. (in)	BaseForce (Kip)	A to B	B to IO	IO to LS	LS to CP	CP to C	C to D	D to E	E to F	
0	0.00	0.00	86	0	0	0	0	0	0	0	86
1	0.18	15.65	85	1	0	0	0	0	0	0	86
2	0.44	34.19	74	3	7	2	0	0	0	0	86
3	0.68	46.60	74	0	2	4	4	2	0	0	86
4	0.96	59.06	74	0	0	0	5	7	0	0	86
5	1.36	77.35	73	1	0	0	3	9	0	0	86
6	1.63	89.80	72	1	1	0	2	7	3	0	86
7	1.88	100.18	72	0	2	0	1	4	7	0	86
8	2.14	111.43	72	0	2	0	0	3	9	0	86
9	2.39	121.48	71	1	2	0	0	0	12	0	86
10	2.41	122.41	71	1	2	0	0	2	10	0	86

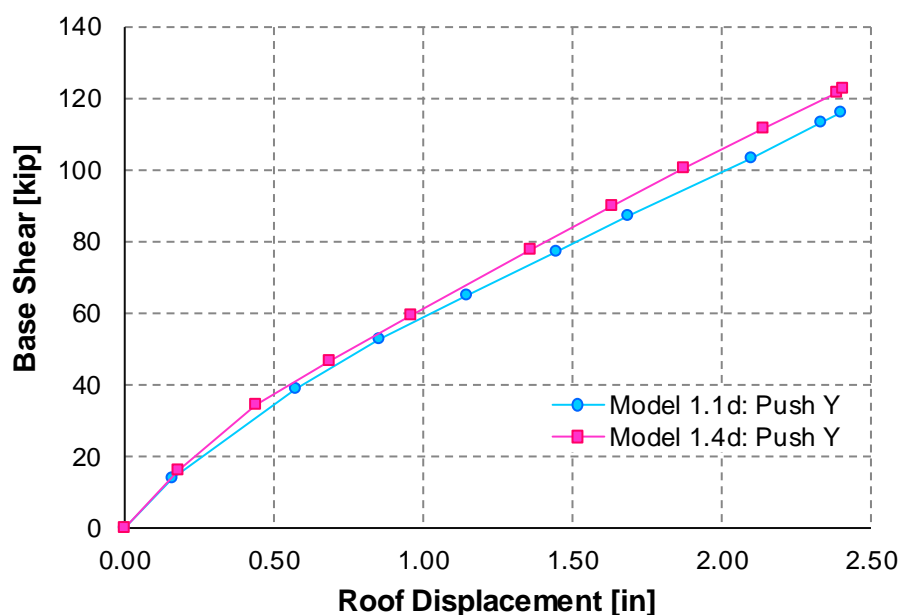


**Figure 6-49.** Comparison Pushover Curves for Models 1.1d and 1.4d: Push Y

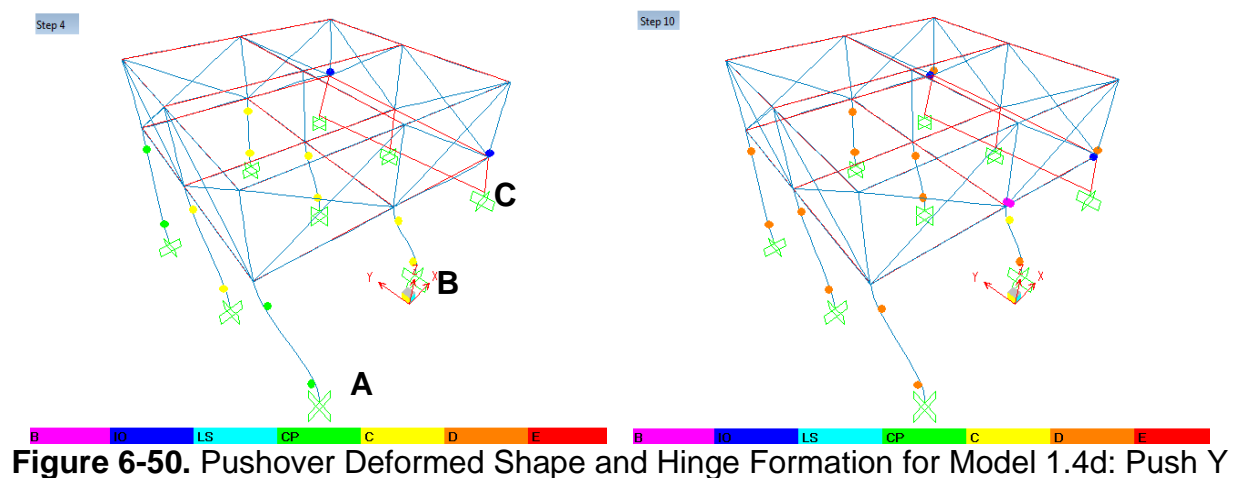


**Figure 6-50.** Pushover Deformed Shape and Hinge Formation for Model 1.4d: Push Y

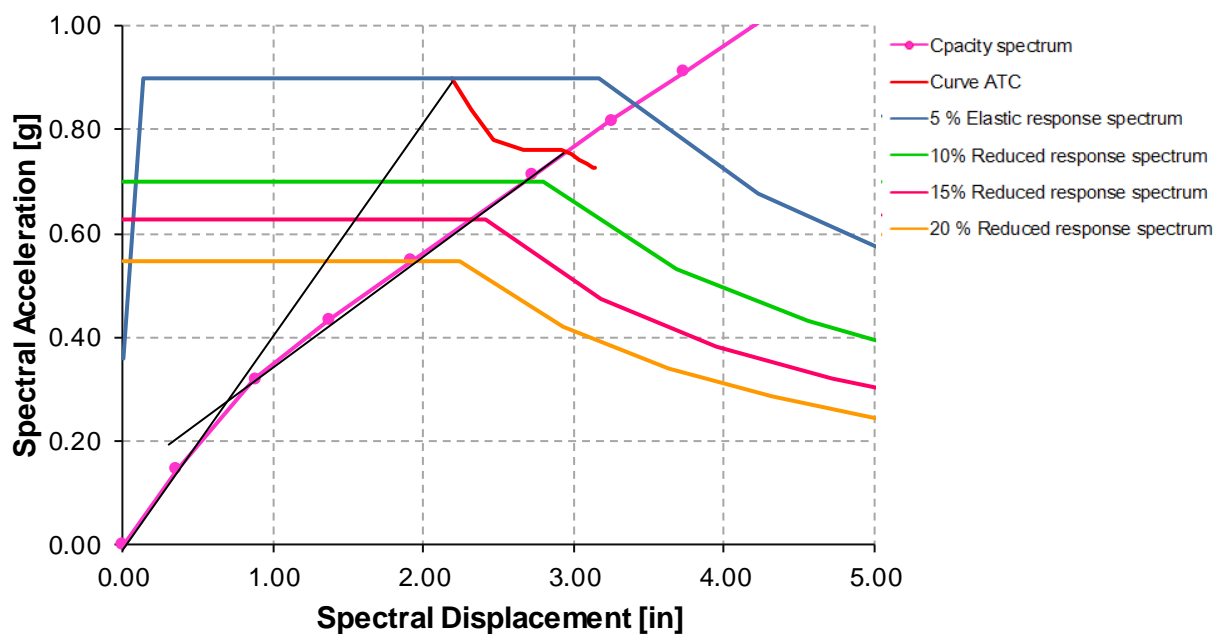


**Figure 6-51.** Performance Point for Model 1.4d: Push Y

$$\begin{aligned}
 S_{app} &= 0.76 \text{ g} & V_{pp} &= 82.6 \text{ k} \\
 S_{dpp} &= 2.95 \text{ in} & D_{pp} &= 1.47 \text{ in} \\
 S_{dy} &= 0.60 \text{ in} \\
 \mu_d &= 4.92
 \end{aligned}$$

From Figure 6-51 at the performance point the spectral displacement ( $S_d$ ) and spectral acceleration ( $S_a$ ) are 2.02 in. and 0.78. The ductility demand is 4.04. In terms of the performance point (step 5 and 6) it can be observed from Table 6-30 that nine hinges

are beyond Collapse (C) limit state. This model follows a similar pattern that the other models type d analyzed with a shear wall.

### **6.2.3 PUSHOVER ANALYSIS RESULTS: TWO LEVELS (MODELS 1) VS. THREE LEVELS (MODELS 2)**

The following sections will study the effect of increasing the story level from two to three levels. The results of the first case presented (Model 2.1) are discussed in detail. It is not necessary to discuss the remaining models with so much detail, as many of the conclusions are similar and repetitive among the models.

After the presentation and discussion of the results for Model 2.1, for Models 2.2, 2.3 and 2.3, hinge sequence graphic representation is not presented for models type b in the X and Y directions. Basically, the hinging sequence follow the same trend as presented for the previous cases. Also, the results so far indicated that no performance point is reached when the analysis is performed in the Y direction for models type b, therefore for these cases only the performance point curve is presented.

#### **6.2.3.1 MODEL 1.1 VS MODEL 2.1**

The tabular data for pushover, pushover curves, hinge sequences and performance point plot are presented in Tables 6-31 to 6-34 and Figures 6-52 to 6-63.

**Model 2.1b:– X direction****Table 6-31.** Tabular Data for Pushover Curve for Model 2.1b: Push -X

PUSH -X Mode			Hinge Sequence								Shear
Step	Disp. (in)	BaseForce (Kip)	A to B	B to IO	IO to LS	LS to CP	CP to C	C to D	D to E	E to F	
0	0.00	0.00	162	0	0	0	0	0	0	0	
1	-0.39	53.39	160	2	0	0	0	0	0	0	
2	-0.76	83.04	150	9	3	0	0	0	0	0	
3	<b>-0.95</b>	<b>88.47</b>	<b>139</b>	<b>11</b>	<b>10</b>	<b>2</b>	<b>0</b>	<b>0</b>	<b>0</b>	<b>0</b>	
4	-1.11	91.24	134	16	9	3	0	0	0	0	
5	-1.61	94.69	129	6	22	2	0	3	0	0	
6	-2.33	98.92	129	0	17	9	0	4	3	0	
7	-2.74	101.37	129	0	15	3	3	9	3	0	
8	-3.34	103.94	126	1	10	7	3	9	6	0	
9	-3.97	106.20	124	2	6	5	10	2	11	2	

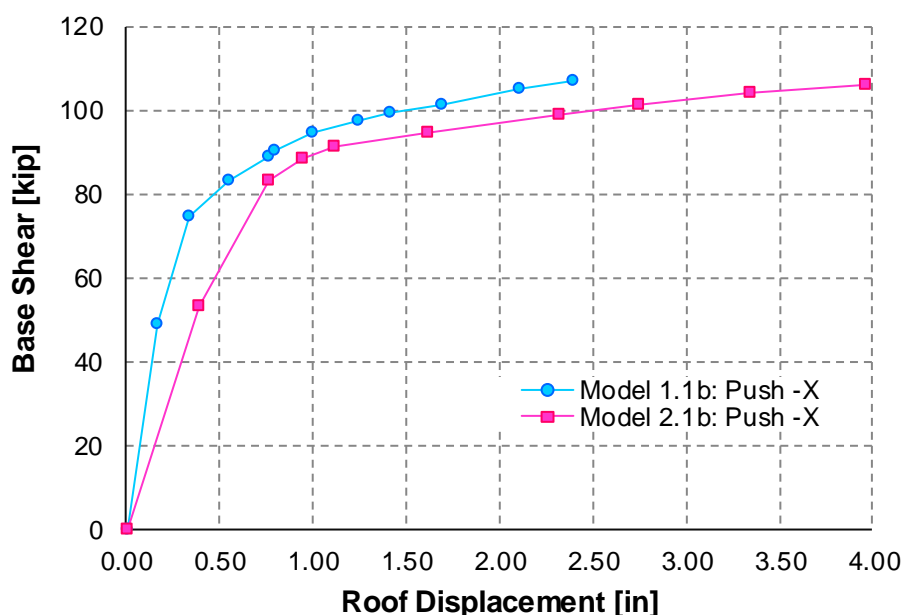
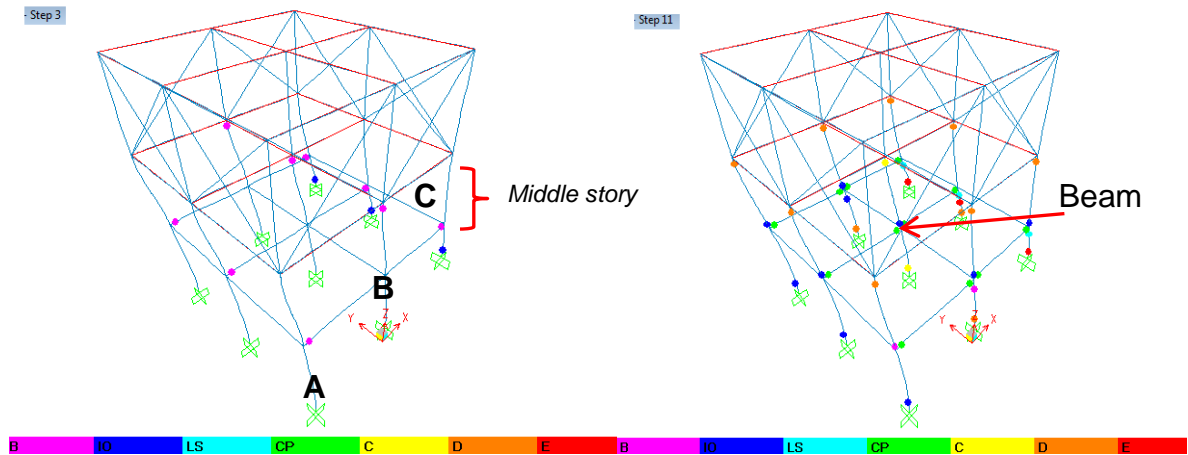
**Figure 6-52.** Comparison Pushover Curves for Model 1.1b and Model 2.1b: Push X

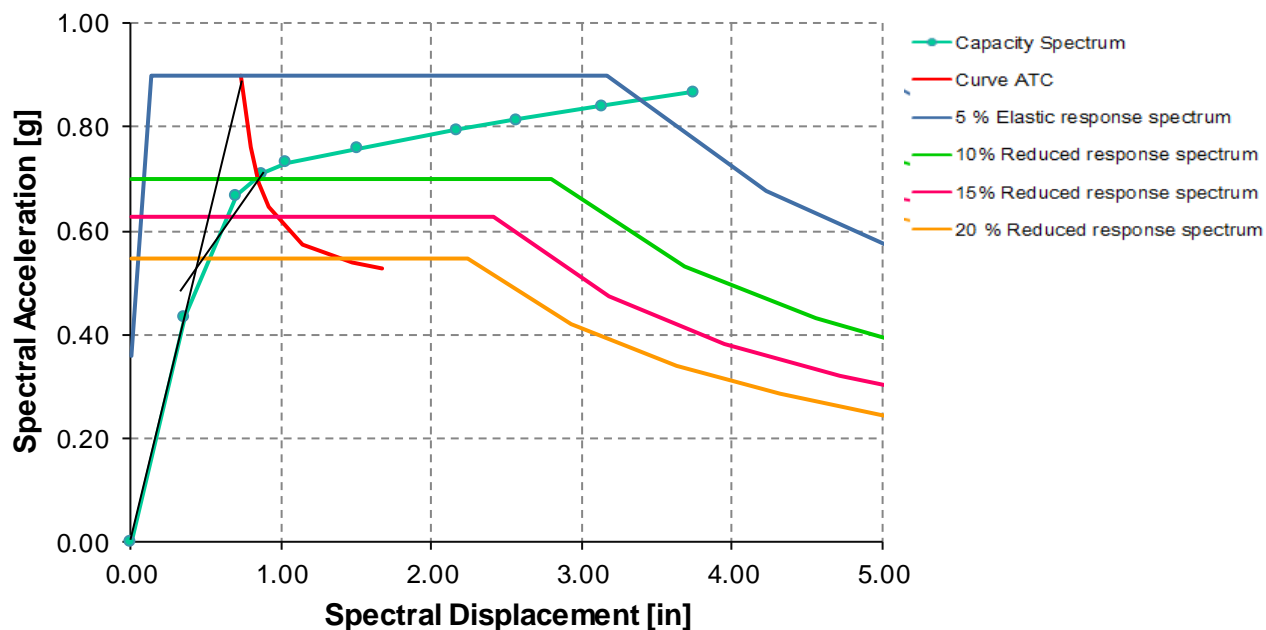
Figure 6-52 shows the Pushover curve for Model 1.1 and Model 2.1 in order to compare the effect of increasing the number of stories. It can be observed that the capacity of Model 2.1b in the X direction is lower than for Model 1.1b. Also the stiffness decreased and the displacement capacity increased.





**Figure 6-53.** Pushover Deformed Shape and Hinge Formation for Model 2.1: Push –X

From Figure 6-53 it can be observed that the upper story doesn't form any hinges same as it was for the case of Model 1.1. Plastic hinges formation starts at frame C including the shortest columns of the lower story, these columns takes more loads since shorter columns are stiffer and hence attract more load. Next some hinges forms at the beams, following the formation of hinges at the middle frame (B) in the middle level. While the analysis progress, hinges at the top of the columns in the middle level reaches D limit state.



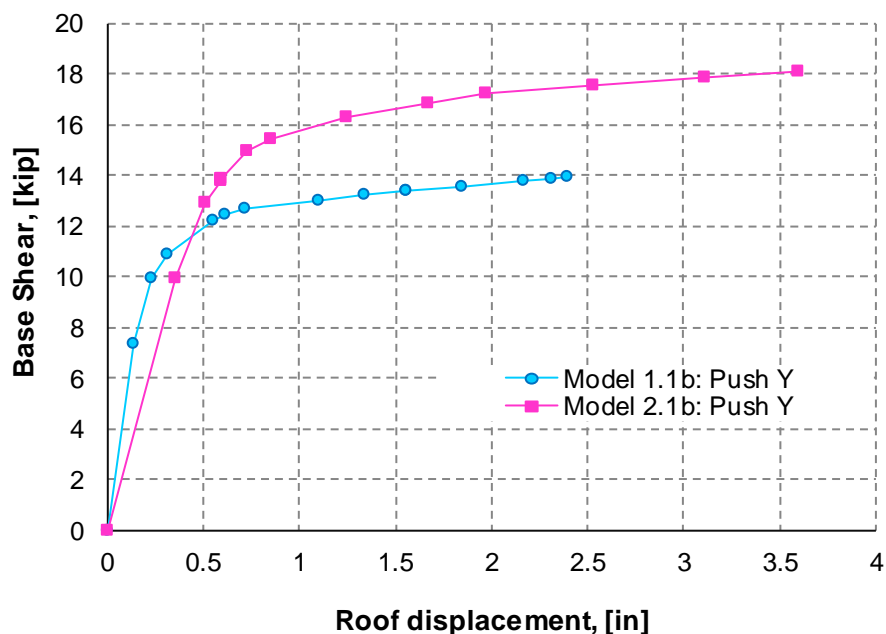
$$\begin{aligned}
 S_{app} &= 0.70 \text{ g} & V_{pp} &= 87.45 \text{ k} \\
 S_{dpp} &= 0.84 \text{ in} & D_{pp} &= 0.91 \text{ in} \\
 S_{dy} &= 0.40 \text{ in} \\
 \mu_d &= 2.11
 \end{aligned}$$

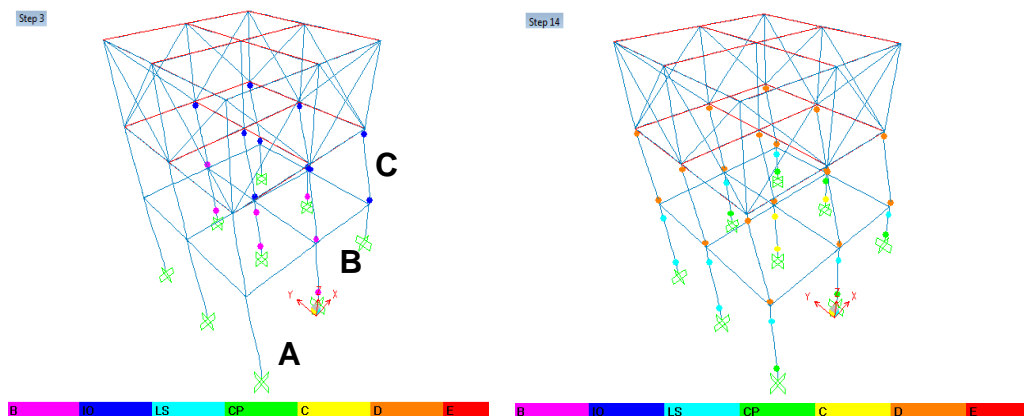
**Figure 6-54.** Performance Point for Model 2.1b: Push -X

From Figure 6-54 at the performance point the spectral displacement ( $S_d$ ) and spectral acceleration ( $S_a$ ) are 0.84 in. and 0.70 g, respectively. The ductility demand is 2.11. At the performance point (step 3) it can be observed from Table 6-31 that several hinges are between Life Safety (LS) and Collapse Prevention (CP) level.

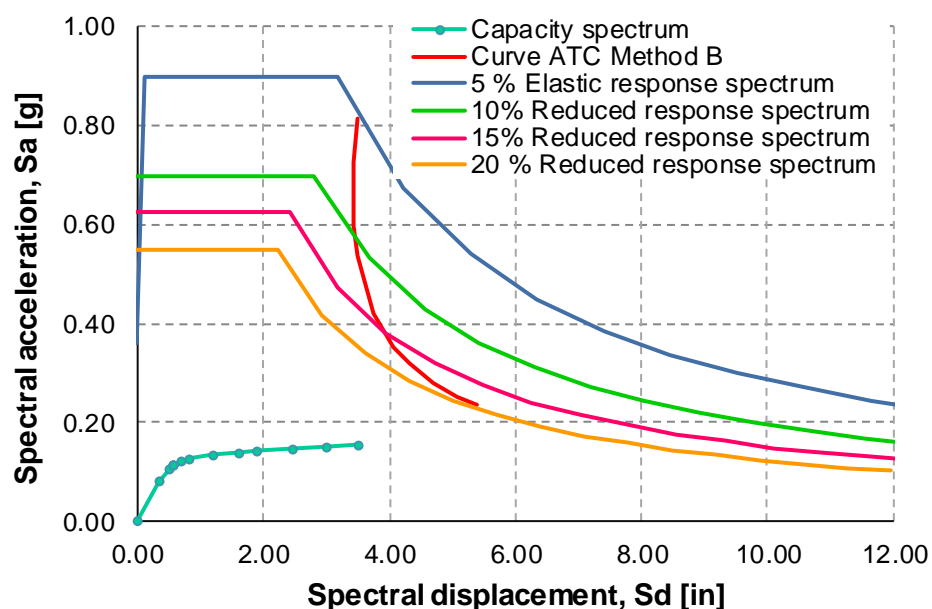
**Model 2.1b: Y direction****Table 6-32.** Tabular Data for Pushover Curve for Model 2.1b: Push Y

PUSH Y Mode			Hinge Sequence								Shear
Step	Disp. (in)	Base Force (Kip)	A to B	B to IO	IO to LS	LS to CP	CP to C	C to D	D to E	E to F	
0	0.00	0.00	162	0	0	0	0	0	0	0	
1	0.36	9.98	160	2	0	0	0	0	0	0	
2	0.51	12.94	152	4	6	0	0	0	0	0	
3	0.59	13.80	145	7	10	0	0	0	0	0	
4	0.59	13.80	145	7	10	0	0	0	0	0	
5	0.60	13.87	145	7	10	0	0	0	0	0	
6	0.60	13.87	145	7	10	0	0	0	0	0	
7	0.73	14.95	134	12	16	0	0	0	0	0	
8	0.85	15.42	129	10	15	8	0	0	0	0	
9	1.24	16.27	126	2	18	6	4	6	0	0	
10	1.67	16.85	126	0	16	2	8	8	2	0	
11	1.97	17.22	126	0	10	6	4	11	5	0	
12	2.53	17.56	126	0	4	12	0	9	11	0	
13	3.11	17.88	126	0	0	14	2	2	18	0	
14	3.60	18.15	126	0	0	9	6	3	18	0	

**Figure 6-55.** Comparison Pushover Curves for Model 1.1b and Model 2.1b: Push Y



**Figure 6-56.** Pushover Deformed Shape and Hinge Formation for Model 2.1b: Push Y

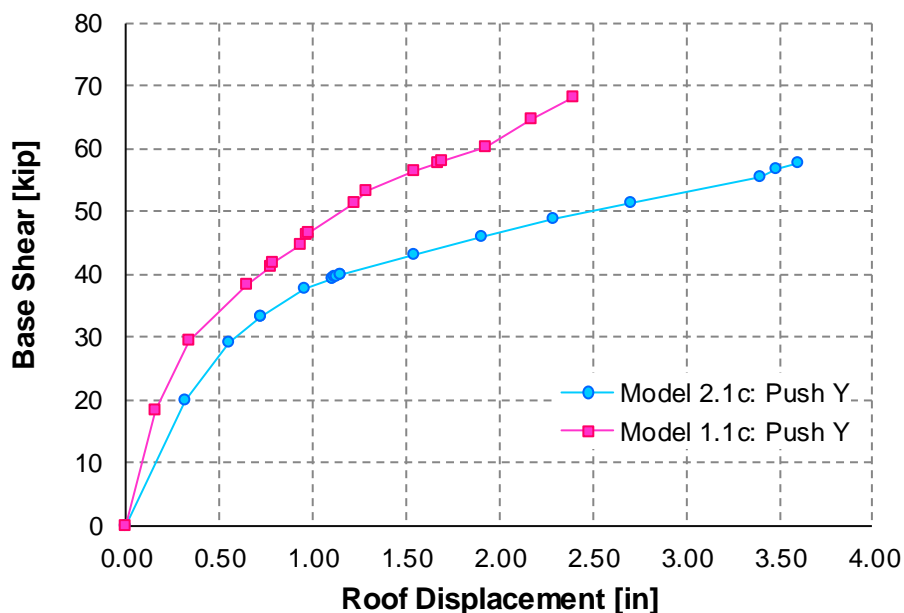


**Figure 6-57.** Performance Point for Model 2.1b: Push Y

From Figure 6-57 it can be observed that no performance point was reached, therefore the model is not able to satisfy the demand. From Figure 6-56 it can be noticed that the collapse mechanism formed at the middle story. Based on the hinge pattern sequence by the end of the analysis all hinges in the middle story are at point D. The results based on the hinge pattern sequence and performance state in the middle floor columns indicates that the entire floor may collapse.

**Model 2.1c: Y direction****Table 6-33.** Tabular Data for Pushover Curve. for Model 2.1c: Push Y

PUSH Y Mode			Hinge Sequence								Shear
Step	Disp. (in)	BaseForce (Kip)	A to B	B to IO	IO to LS	LS to CP	CP to C	C to D	D to E	E to F	
0	0.00	0.00	162	0	0	0	0	0	0	0	
1	0.32	19.90	161	1	0	0	0	0	0	0	
2	0.55	29.16	138	9	15	0	0	0	0	0	
3	0.72	33.32	136	2	16	8	0	0	0	0	
4	0.72	33.32	136	2	16	8	0	0	0	0	
5	0.96	37.59	131	5	13	5	4	4	0	0	
6	1.10	39.33	129	5	9	8	7	4	0	0	
11	1.11	39.38	129	5	9	8	7	4	0	0	
12	1.12	39.47	128	6	9	8	7	4	0	0	
14	1.12	39.57	127	7	9	8	7	4	0	0	
18	1.15	39.84	127	7	9	8	7	4	0	0	
<b>19</b>	<b>1.15</b>	<b>39.84</b>	<b>127</b>	<b>7</b>	<b>9</b>	<b>8</b>	<b>7</b>	<b>4</b>	<b>0</b>	<b>0</b>	
<b>20</b>	<b>1.54</b>	<b>43.05</b>	<b>126</b>	<b>5</b>	<b>9</b>	<b>3</b>	<b>12</b>	<b>5</b>	<b>2</b>	<b>0</b>	
21	1.91	45.99	125	1	10	4	10	9	3	0	
22	2.29	48.84	123	1	9	2	9	8	9	1	
23	2.70	51.47	122	2	7	2	7	5	16	1	
24	3.40	55.54	120	2	6	3	7	4	19	1	
25	3.48	56.67	119	2	5	4	6	4	20	2	
26	3.60	57.55	119	2	5	4	4	6	20	2	

**Figure 6-58.** Comparison Pushover Curves for Model 1.1c and Model 2.1c: Push Y

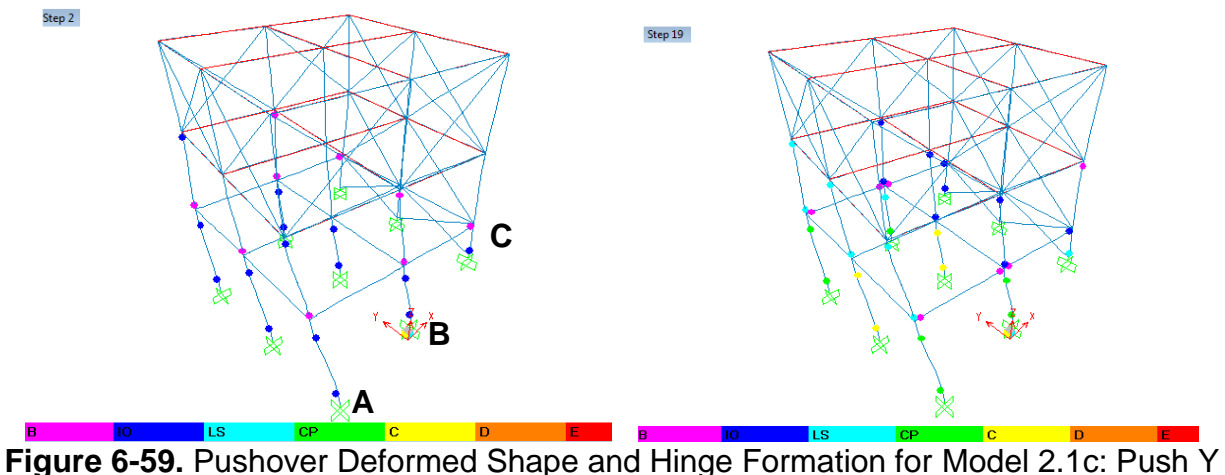
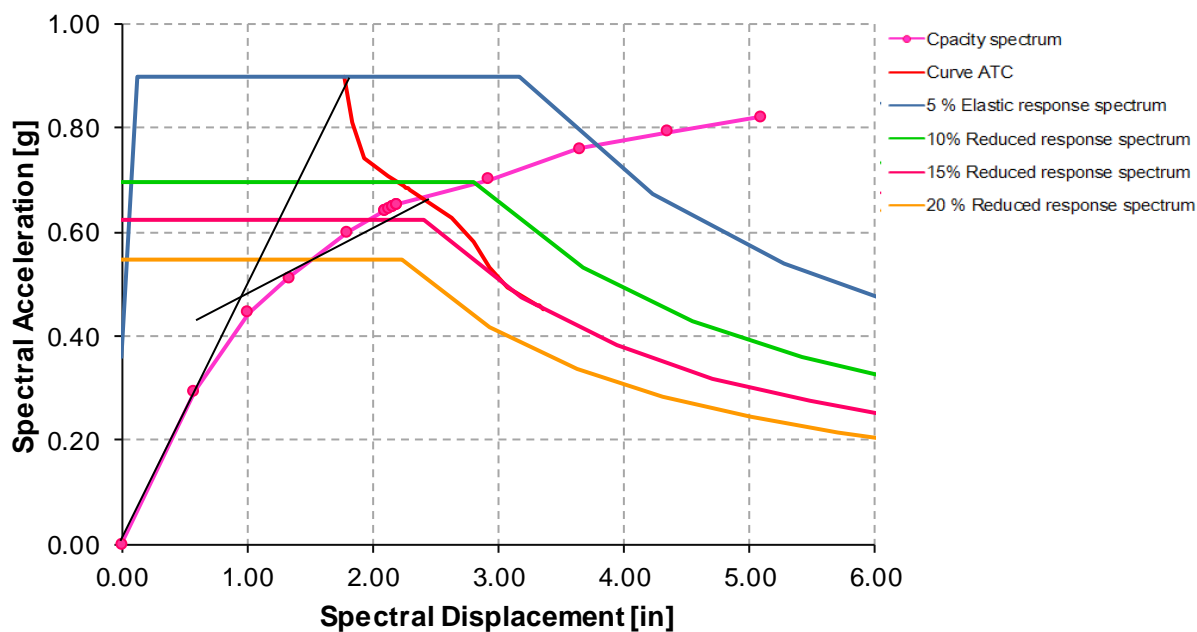


**Figure 6-59.** Pushover Deformed Shape and Hinge Formation for Model 2.1c: Push Y



$$\begin{aligned}
 S_{app} &= 0.67 \text{ g} & V_{pp} &= 41.07 \text{ k} \\
 S_{dpp} &= 2.37 \text{ in} & D_{pp} &= 1.24 \text{ in} \\
 S_{dy} &= 0.95 \text{ in} \\
 \mu_d &= 2.49
 \end{aligned}$$

**Figure 6-60.** Performance Point for Model 2.1c: Push Y

From Figure 6-60 at the performance point the spectral displacement ( $S_d$ ) and spectral acceleration ( $S_a$ ) are 2.37 in. and 0.67 g respectively. The ductility demand is 2.49. From Table 6-33 and Figure 6-59 it is shown that at the performance point (steps 19 and 20) central columns at frames A and B are beyond Collapse limit state. In comparison Model 1.2c suffered much less damage at the performance point, hinges were between

(IO) and (LS) limit state. It is evident that three-story models are more susceptible to suffer damage than the two-story models. This result is because as the number of stories increased the total height of the residence increased, thus the model becomes more flexible with less stiffness, therefore prone to more damage.

### Model 2.1d: Y direction

**Table 6-34.** Tabular Data for Pushover Curve for Model 2.1d: Push Y

PUSH Y Mode			Hinge Sequence								Shear
Step	Disp. (in)	BaseForce (Kip)	A to B	B to IO	IO to LS	LS to CP	CP to C	C to D	D to E	E to F	
0	0.00	0.00	130	0	0	0	0	0	0	0	
1	0.32	17.82	126	4	0	0	0	0	0	0	
2	0.76	34.86	108	0	12	9	0	1	0	0	
3	0.76	34.88	108	0	12	9	0	1	0	0	
4	0.78	35.64	107	1	12	7	2	1	0	0	
5	0.78	35.64	107	1	12	7	2	1	0	0	
6	1.18	43.51	98	8	6	3	11	4	0	0	
7	1.33	45.87	98	8	6	0	13	3	2	0	
8	1.73	52.00	98	3	5	3	11	8	2	0	
9	2.12	57.27	98	0	8	2	5	10	7	0	
10	2.29	59.70	98	0	8	0	6	8	10	0	
11	2.29	59.70	98	0	8	0	6	8	10	0	

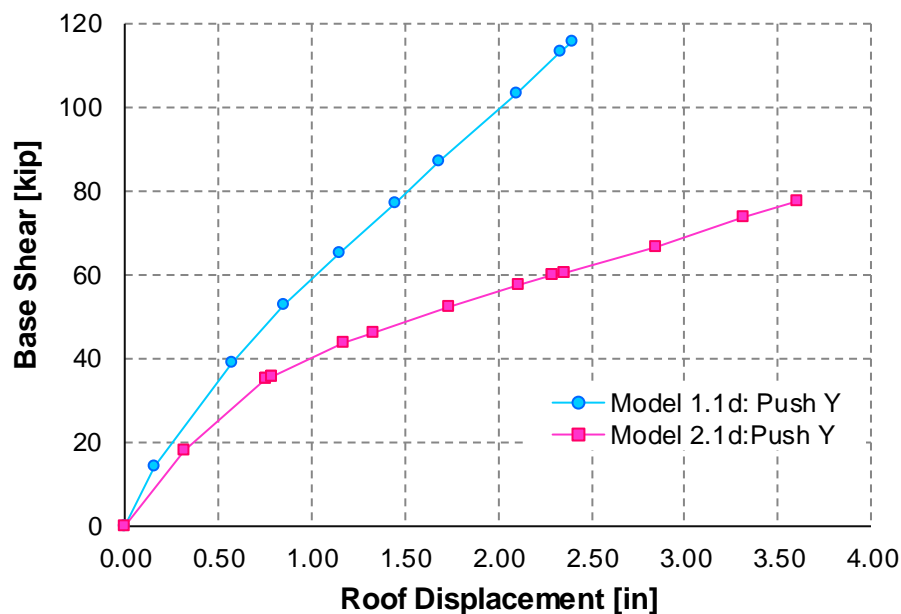


**Figure 6-61.** Comparison Pushover Curves for Model 1.1d and Model 2.1d: Push Y

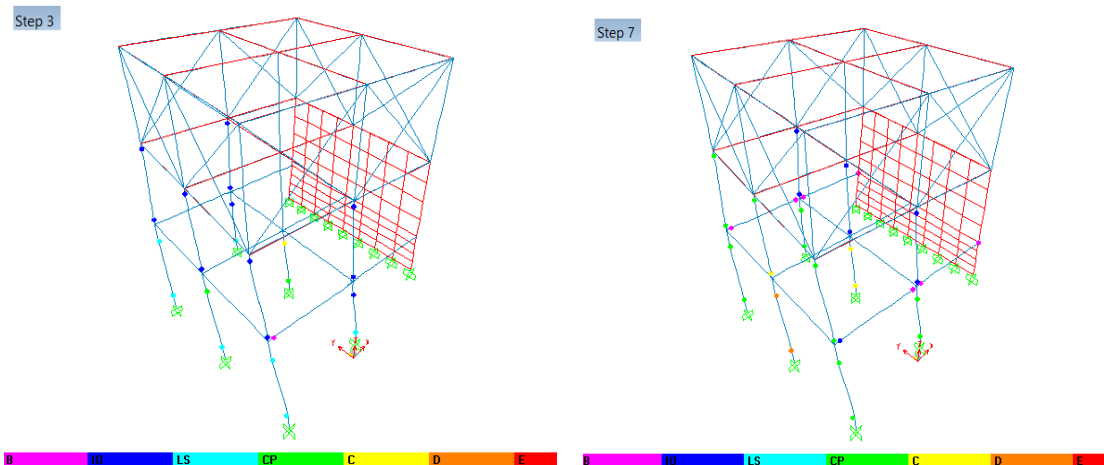
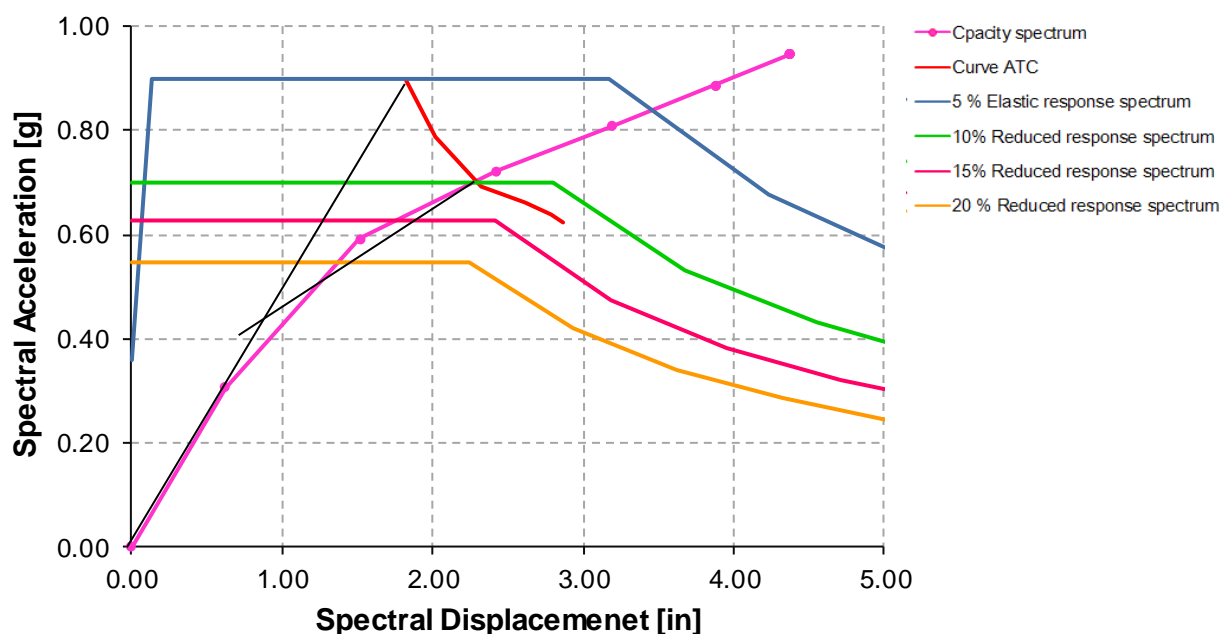


**Figure 6-62.** Pushover Deformed Shape and Hinge Formation for Model 2.1d: Push Y



$$\begin{aligned}
 S_{app} &= 0.69 \text{ g} & V_{pp} &= 45.93 \text{ k} \\
 S_{dpp} &= 2.54 \text{ in} & D_{pp} &= 1.34 \text{ in} \\
 S_{dy} &= 0.90 \text{ in} \\
 \mu_d &= 2.82
 \end{aligned}$$

**Figure 6-63.** Performance Point for Model 2.1d: Push Y

From Figure 6-63 at the performance point the spectral displacement ( $S_d$ ) and spectral acceleration ( $S_a$ ) are 2.27 in. and 0.70 g respectively. The ductility demand is 2.82. From Table 6-34 and Figure 6-62 at the performance point (steps 7) it can be observed



that 13 columns are reaching Collapse limit state, three hinges are beyond Collapse limit state and two are between D and E.

### 6.2.3.2 MODEL 1.2 VS MODEL 2.2

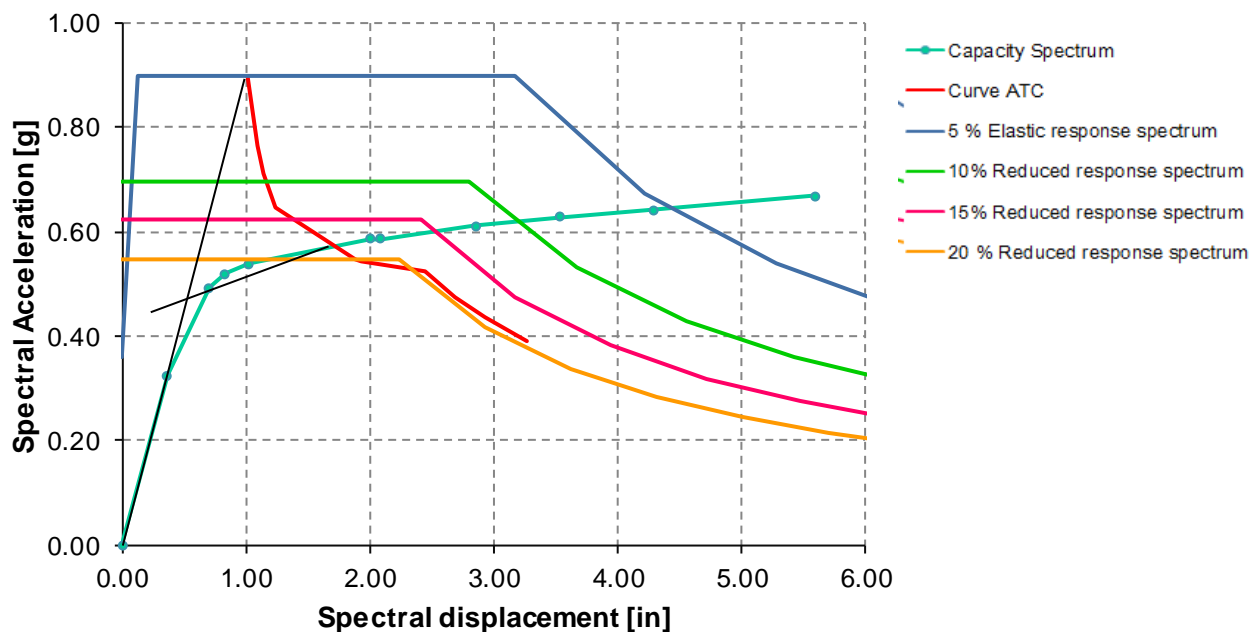
The tabular data for pushover, pushover curves, hinge sequences (only for Models c/d) and performance point are presented in Tables 6-35 to 6-38 and Figures 6-64 to 6-72.

#### **Model 2.2b:-X direction**

Pushover curve is not presented; the result is similar as for Model 2.1b. As explained before, the effect on the pushover curve due to the increase in bay length in the Y direction is minimal in the X direction. On the other hand, it was observed in the case of Model 1.2 that the effect in the performance point was significant.

**Table 6-35.** Tabular Data for Pushover Curve for Model 2.2b: Push -X

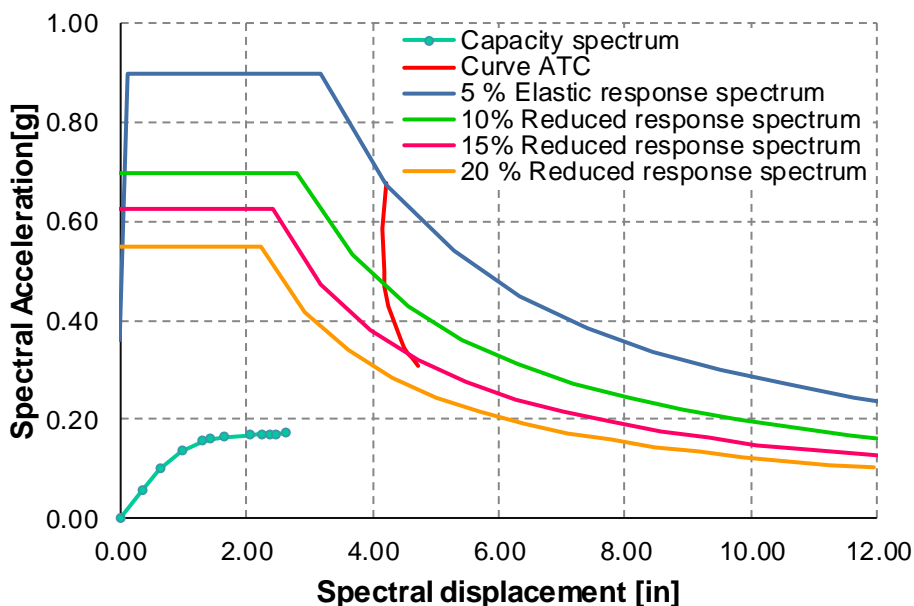
PUSH -X Mode			Hinge Sequence								
Step	Disp. (in)	BaseForce (Kip)	A to B	B to IO	IO to LS	LS to CP	CP to C	C to D	D to E	E to F	Shear
0	-0.01	0.00	162	0	0	0	0	0	0	0	
1	-0.39	54.75	160	2	0	0	0	0	0	0	
2	-0.76	83.66	151	11	0	0	0	0	0	0	
3	-0.90	88.56	143	13	6	0	0	0	0	0	
4	-1.11	92.19	136	20	5	1	0	0	0	0	
5	-2.12	99.08	130	5	20	0	0	6	1	0	
6	-2.23	100.11	130	5	16	4	0	6	1	0	
7	-3.04	104.54	128	7	6	7	3	8	3	0	
8	-3.77	107.33	126	8	1	6	6	11	4	0	
9	-4.57	109.66	123	6	6	0	12	5	10	0	
10	-5.94	113.79	123	0	8	3	12	1	13	2	



$$\begin{aligned}
 S_{app} &= 0.57 \text{ g} & V_{pp} &= 96.52 \text{ k} \\
 S_{dpp} &= 1.64 \text{ in} & D_{pp} &= 1.75 \text{ in} \\
 S_{dy} &= 0.60 \text{ in} \\
 \mu_d &= 2.73
 \end{aligned}$$

**Figure 6-64.** Performance Point for Model 2.2b: Push X

Comparing Figures 6-54 and 6-64 the effect in the performance point is more significant. The spectral displacement ( $S_d$ ) increased from 0.84 inch for Model 1.1b to 1.64 inch for Model 2.2b. The ductility demand increased from 2.11 for Model 2.1b to 2.73 for Model 2.2 b. From Table 6-35 at the performance point (between step 4 and 5) six hinges are beyond Collapse limit state.

**Model 2.2b Y direction****Figure 6-65. Performance Point for Model 2.2b: Push Y****Model 2.2c: Y direction****Table 6-36. Tabular Data for Pushover Curve for Model 2.2c: Push Y**

PUSH Y Mode			Hinge Sequence								Shear
Step	Disp. (in)	BaseForce (Kip)	A to B	B to IO	IO to LS	LS to CP	CP to C	C to D	D to E	E to F	
0	0.00	0.00	162	0	0	0	0	0	0	0	
1	0.27	23.48	162	0	0	0	0	0	0	0	
2	0.41	32.48	145	17	0	0	0	0	0	0	
3	0.62	40.04	135	18	9	0	0	0	0	0	
4	0.98	44.43	127	11	14	6	2	2	0	0	
5	1.36	48.16	126	3	13	3	10	7	0	0	
6	1.56	49.72	125	1	13	2	11	10	0	0	
7	1.62	50.43	124	1	12	4	12	7	1	1	1
8	2.05	53.82	123	2	6	3	12	10	5	1	1
9	2.42	56.58	122	3	2	4	11	10	9	1	1
10	2.59	57.51	122	3	2	3	11	11	9	1	1
11	2.70	58.61	122	3	1	3	11	12	9	1	1
12	3.09	60.85	120	4	0	2	10	10	14	2	2
13	3.20	61.72	120	4	0	2	8	11	15	2	2
14	3.49	63.17	120	4	0	0	11	7	18	2	2
15	3.60	64.29	120	4	0	0	10	9	17	2	2

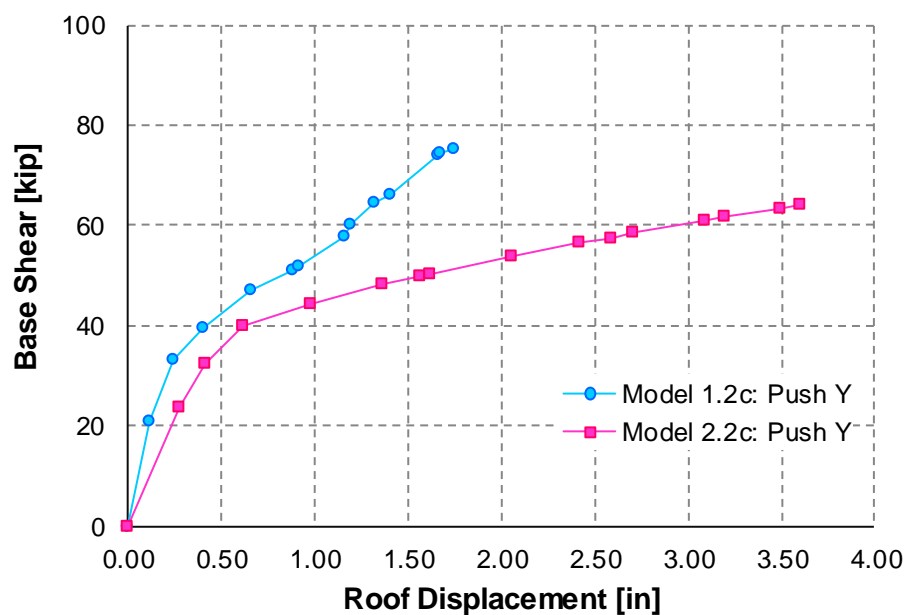


**Figure 6-66.** Comparison Pushover Curves for Model 1.2c and Model 2.2c: Push Y

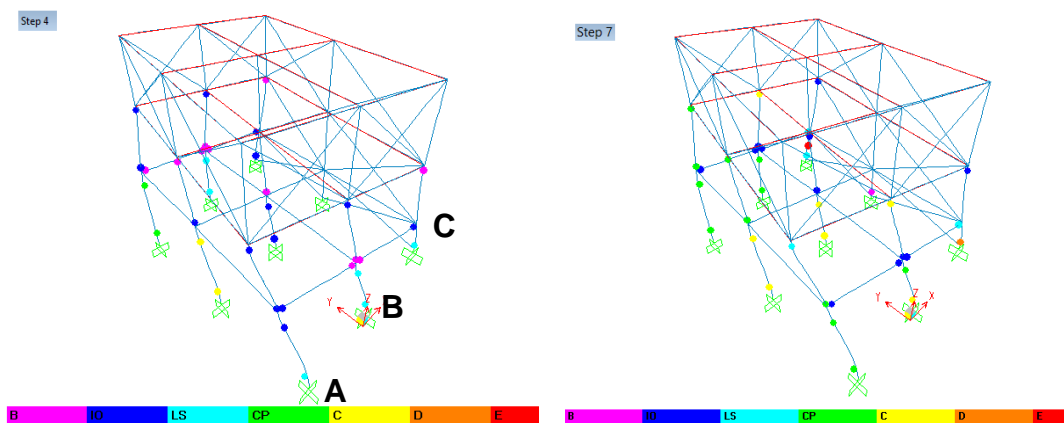
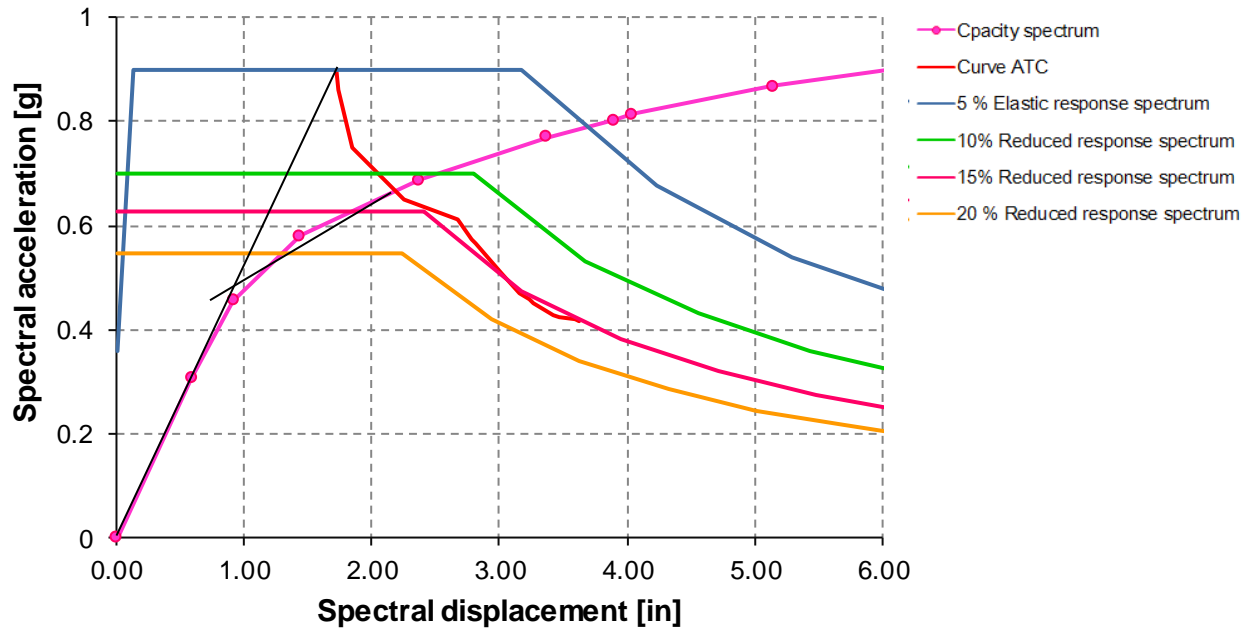


**Figure 6-67.** Pushover Deformed Shape and Hinge Formation for Model 2.2c: Push Y



$$\begin{aligned}
 S_{app} &= 0.66 \text{ g} & V_{pp} &= 43.41 \text{ k} \\
 S_{dpp} &= 2.17 \text{ in} & D_{pp} &= 0.89 \text{ in} \\
 S_{dy} &= 0.95 \text{ in} \\
 \mu_d &= 2.28
 \end{aligned}$$

**Figure 6-68.** Performance Point for Model 2.2c: Push Y

From Figure 6-68 at the performance point the spectral displacement ( $S_d$ ) and spectral acceleration ( $S_a$ ) are 2.16 in. and 0.66 g respectively. The ductility demand is 2.28. From Table 6-36 and Figure 6-67 at the performance point (step 7) it can be observed that seven hinges are beyond Collapse limit state. Model 1.2c suffered much less damage at the performance point most of the hinges were between (IO) and (LS) limit state.

### Model 2.2d Y direction

**Table 6-37.** Tabular Data for Pushover Curve for Model 2.2d: Push Y

PUSH Y Mode			Hinge Sequence								
Step	Disp. (in)	BaseForce (Kip)	A to B	B to IO	IO to LS	LS to CP	CP to C	C to D	D to E	E to F	Shear
0	0.00	0.00	130	0	0	0	0	0	0	0	
1	0.29	23.29	129	1	0	0	0	0	0	0	
2	0.50	37.49	108	21	1	0	0	0	0	0	
3	0.55	38.95	106	22	2	0	0	0	0	0	
4	0.68	42.98	102	20	8	0	0	0	0	0	
5	0.72	43.75	102	18	10	0	0	0	0	0	
6	0.73	43.86	102	17	11	0	0	0	0	0	
7	<b>0.90</b>	<b>47.56</b>	<b>100</b>	<b>9</b>	<b>15</b>	<b>4</b>	<b>0</b>	<b>2</b>	<b>0</b>	<b>0</b>	
8	0.93	48.06	99	8	16	5	0	2	0	0	
9	1.08	51.09	98	6	12	5	5	4	0	0	
10	1.50	58.89	98	1	9	1	9	12	0	0	
11	1.89	66.34	98	0	7	3	9	7	6	0	
12	2.28	73.95	98	0	5	1	7	13	6	0	
13	2.64	80.98	98	0	4	1	6	10	11	0	
14	3.14	90.97	97	1	1	3	6	9	13	0	
15	3.50	97.43	97	1	0	2	8	6	15	1	
16	3.60	99.29	97	1	0	2	8	5	16	1	

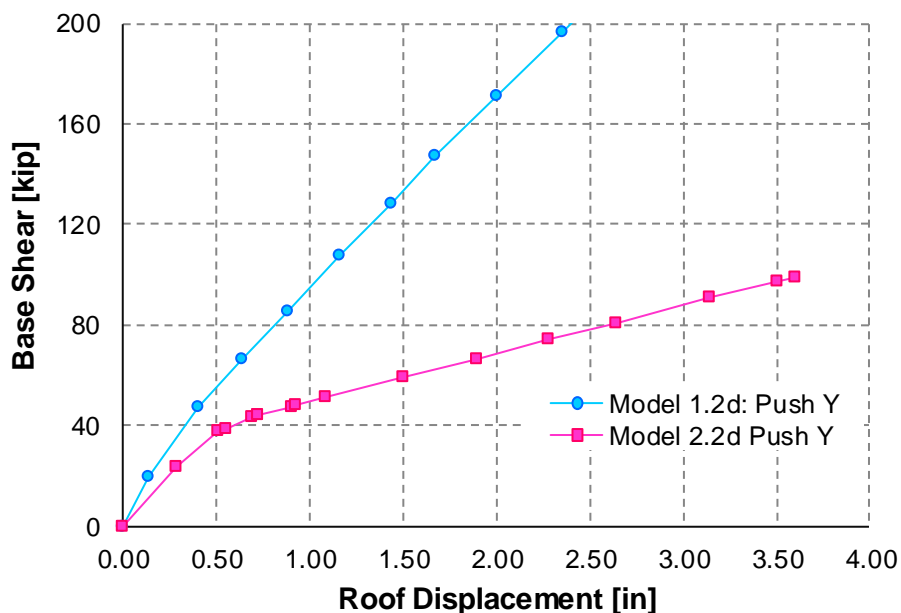


**Figure 6-69.** Comparison Pushover Curves for Model 1.2d and Model 2.2d

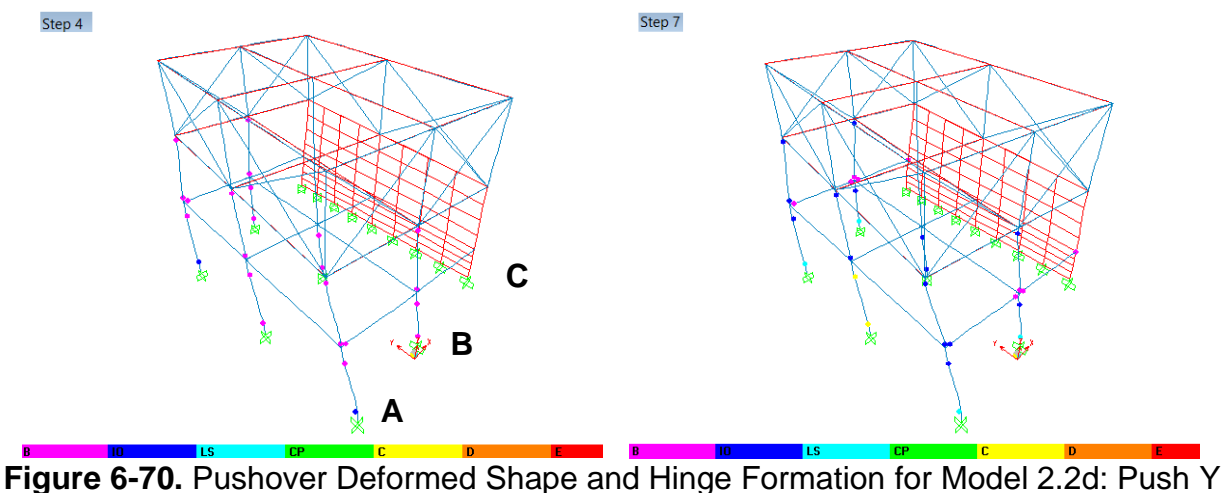
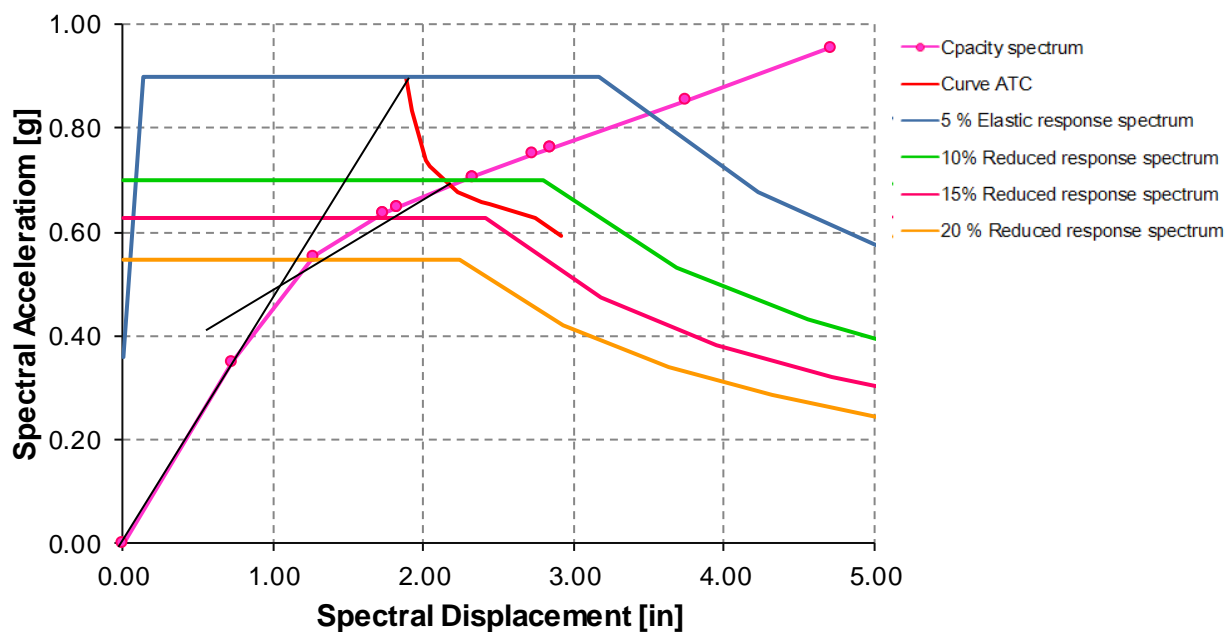


**Figure 6-70.** Pushover Deformed Shape and Hinge Formation for Model 2.2d: Push Y



$$\begin{aligned}
 S_{app} &= 0.70 \text{ g} & V_{pp} &= 46.69 \text{ k} \\
 S_{dpp} &= 2.17 \text{ in} & D_{pp} &= 0.86 \text{ in} \\
 S_{dy} &= 1.05 \text{ in} \\
 \mu_d &= 2.07
 \end{aligned}$$

**Figure 6-71.** Performance Point for Model 2.2d: Push Y

From Figure 6-71 at the performance point the spectral displacement ( $S_d$ ) and spectral acceleration ( $S_a$ ) are 2.17 in. and 0.70 g, respectively. The ductility demand is 2.07. From Table 6-37 and Figure 6-70 at the performance point (step 7) it can be observed, that several hinges are between Immediate Occupancy and Life Safety. Basically as

discussed before this means that significant damage to the structural element has occurred, but some margin against either partial or total structural collapse remains. Also two hinges are beyond Collapse limit state.

### 6.2.3.3 MODEL 1.3 VS MODEL 2.3

The tabular data for pushover, pushover curves, hinge sequences (only for Models c/d) and performance point are presented in Tables 6-38 to 6-40 and Figures 6-72 to 6-79.

#### **Model 2.3b: -X direction**

**Table 6-38.** Tabular Data for Pushover Curve for Model 2.3b: Push -X

PUSH -X Mode			Hinge Sequence								
Step	Disp. (in)	BaseForce (Kip)	A to B	B to IO	IO to LS	LS to CP	CP to C	C to D	D to E	E to F	Shear
0	0.00	0.00	162	0	0	0	0	0	0	0	
1	-0.36	42.38	162	0	0	0	0	0	0	0	
2	-0.47	54.38	160	2	0	0	0	0	0	0	
3	-0.88	84.60	153	6	3	0	0	0	0	0	
4	-0.90	85.65	148	11	3	0	0	0	0	0	
5	-1.14	91.02	138	18	5	1	0	0	0	0	
6	-1.33	93.27	135	21	5	0	1	0	0	0	
<b>7</b>	<b>-1.78</b>	<b>96.73</b>	<b>133</b>	<b>7</b>	<b>18</b>	<b>1</b>	<b>0</b>	<b>3</b>	<b>0</b>	<b>0</b>	
8	-2.17	99.50	132	3	20	2	0	5	0	0	
9	-2.74	103.20	132	3	11	6	0	8	2	0	
10	-3.13	105.59	129	6	6	5	3	10	3	0	
11	-3.60	107.69	126	9	0	6	6	11	4	0	



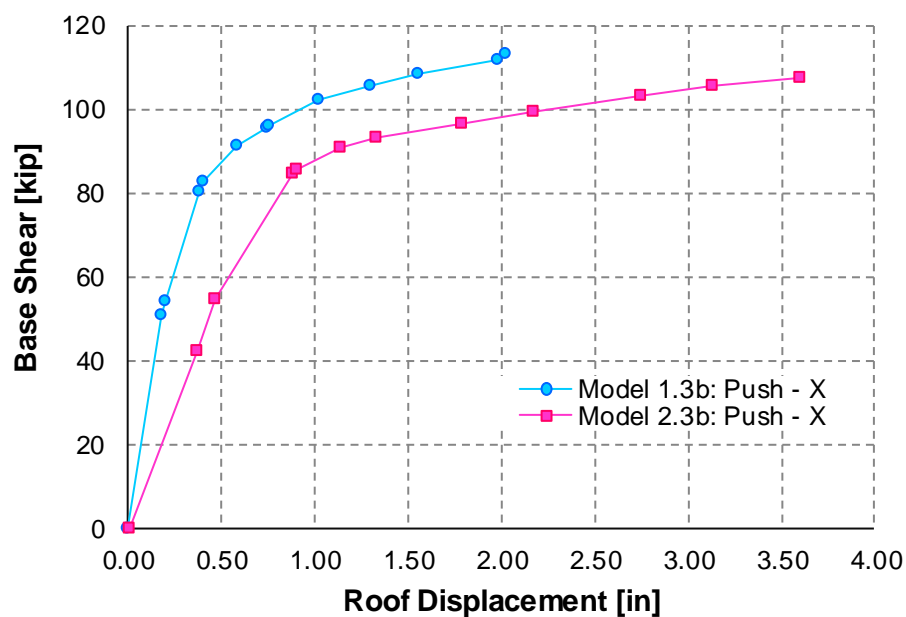
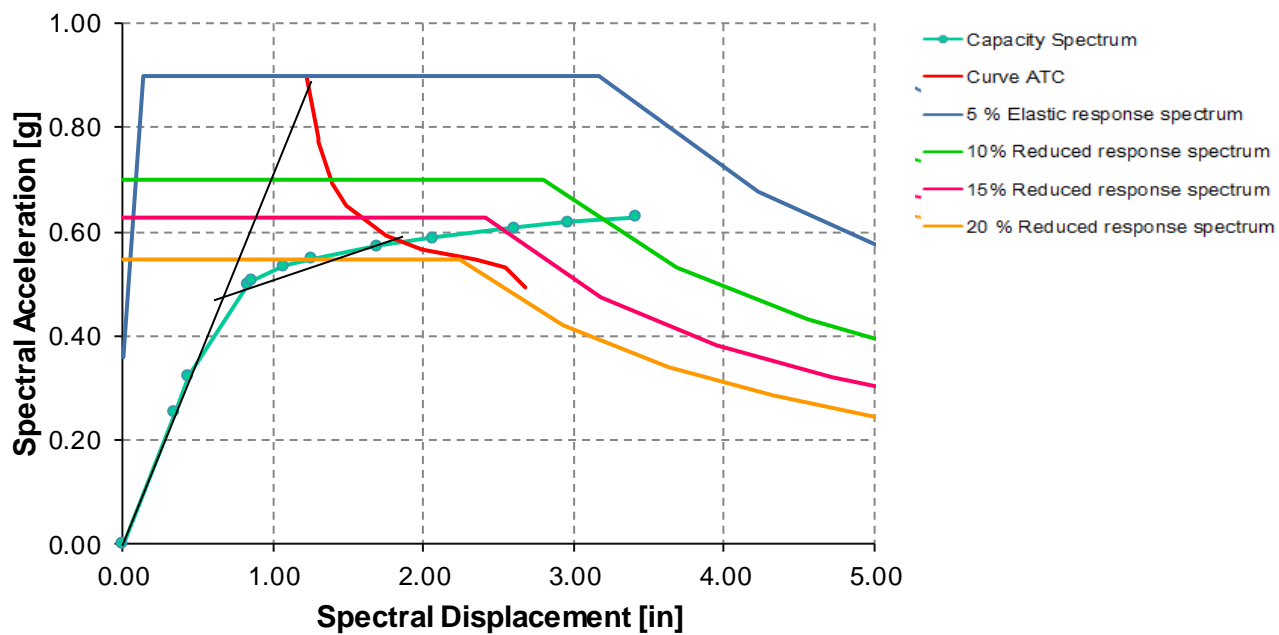


**Figure 6-72.** Comparison Pushover Curves for Model 1.3b and Model 2.3b: Push -X



$$\begin{aligned}
 S_{app} &= 0.58 \text{ g} & V_{pp} &= 97.99 \text{ k} \\
 S_{dpp} &= 1.86 \text{ in} & D_{pp} &= 1.96 \text{ in} \\
 S_{dv} &= 0.65 \text{ in}
 \end{aligned}$$

**Figure 6-73.** Performance Point for Model 2.3b: Push -X

From Figure 6-73 at the performance point the spectral displacement ( $S_d$ ) and spectral acceleration ( $S_a$ ) are 1.86 in. and 0.58 g, respectively. The ductility demand is 2.86. From Table 6-38 at the performance point (step 7) it can be observed that three hinges are beyond Collapse limit state.

### Model 2.3c: Y direction

**Table 6-39.** Tabular Data for Pushover Curve for Model 2.3c: Push Y

PUSH Y Mode			Hinge Sequence								
Step	Disp. (in)	BaseForce (Kip)	A to B	B to IO	IO to LS	LS to CP	CP to C	C to D	D to E	E to F	Shear
0	0.00	0.00	162	0	0	0	0	0	0	0	
1	0.33	12.73	159	3	0	0	0	0	0	0	
2	0.64	20.42	141	15	6	0	0	0	0	0	
3	0.66	20.76	139	17	3	3	0	0	0	0	
4	0.66	18.93	139	13	4	3	2	1	0	0	
5	0.73	21.27	139	13	4	3	2	1	0	0	
6	1.13	27.26	134	7	10	3	5	3	0	0	
7	1.49	30.92	134	5	2	2	13	6	0	0	
8	1.86	33.62	128	7	4	1	12	10	0	0	
9	2.27	35.60	126	8	3	2	12	7	4	0	
10	2.70	37.54	126	5	6	0	8	11	6	0	
11	3.09	39.24	126	1	9	1	6	10	9	0	
12	3.48	40.79	124	1	8	2	3	9	14	1	
13	3.60	41.22	124	1	8	2	3	8	15	1	

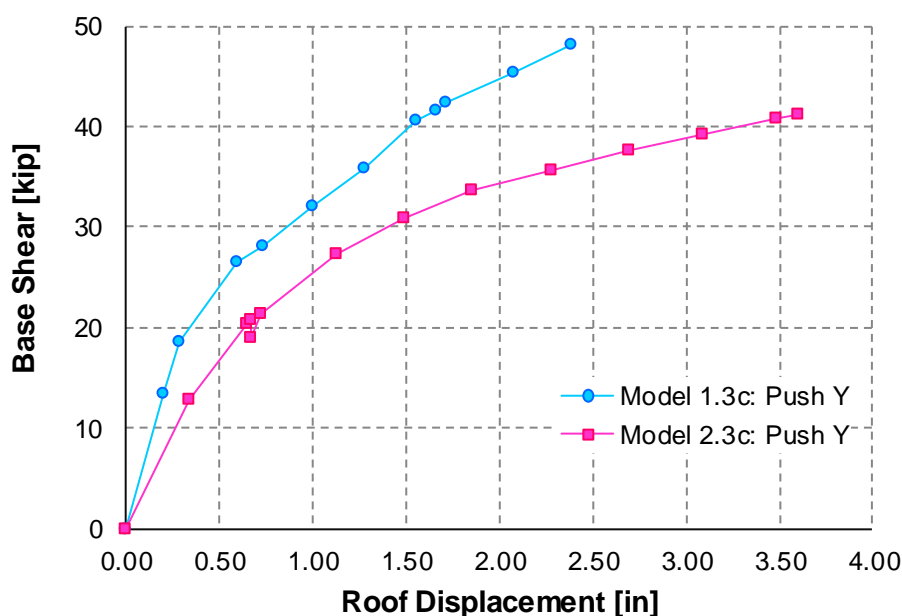


**Figure 6-74.** Comparison Pushover Curves for Model 1.3c and Model 2.3c: Push Y

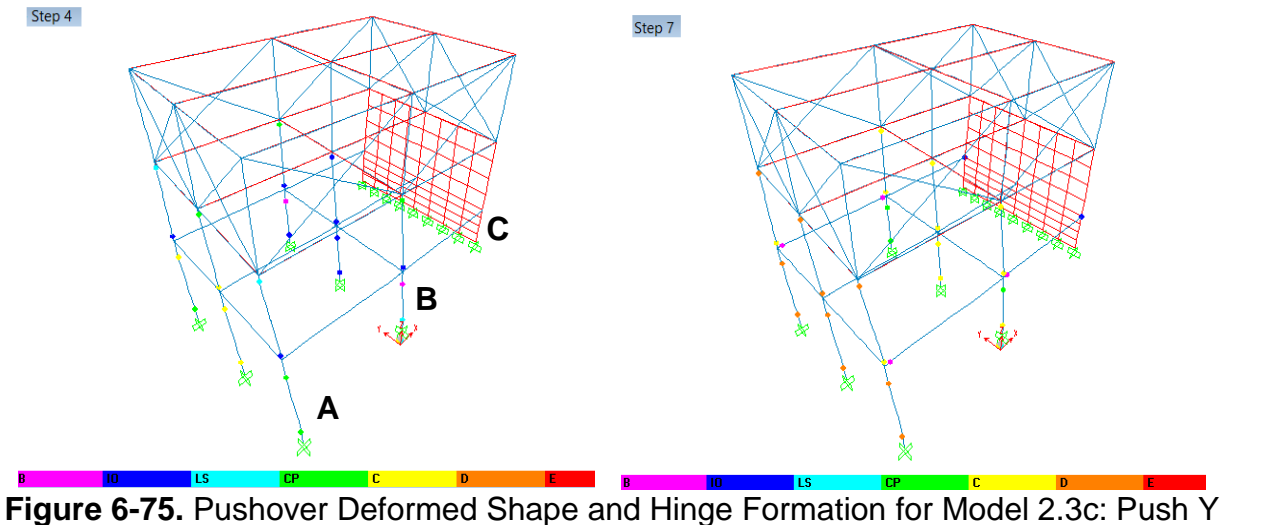
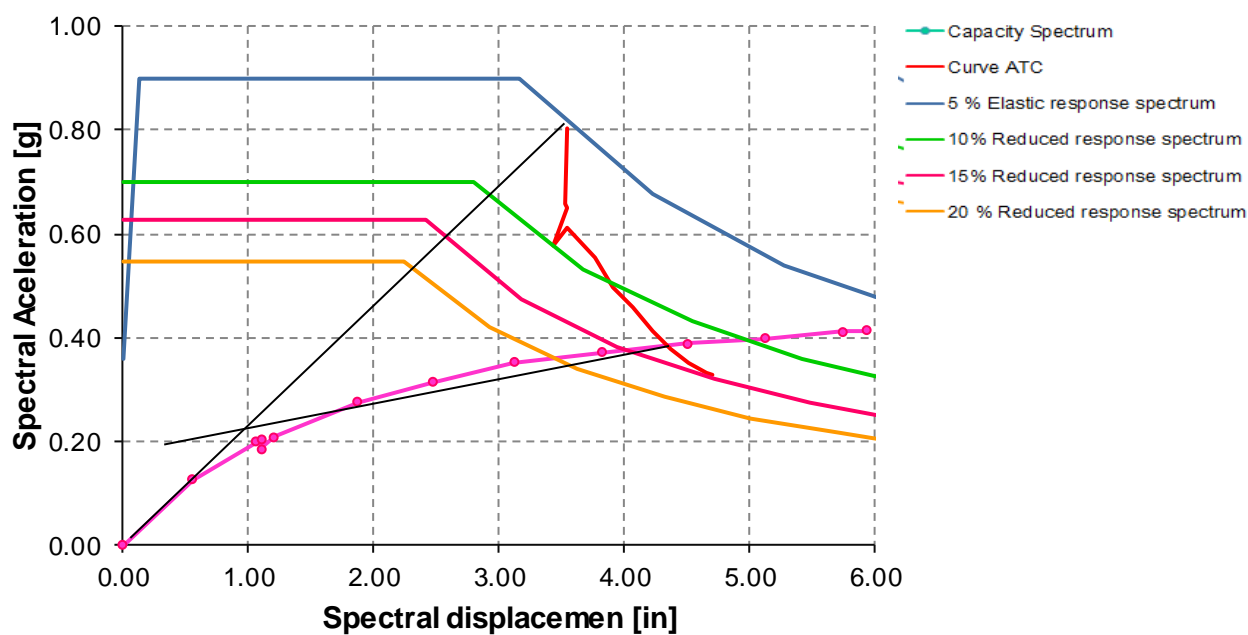


Figure 6-75. Pushover Deformed Shape and Hinge Formation for Model 2.3c: Push Y



$$\begin{aligned}
 S_{app} &= 0.38 \text{ g} & V_{pp} &= 37.05 \text{ k} \\
 S_{dpp} &= 4.34 \text{ in} & D_{pp} &= 2.6 \text{ in} \\
 S_{dy} &= 0.90 \text{ in} \\
 \mu_d &= 4.82
 \end{aligned}$$

Figure 6-76. Performance Point for Model 2.3c: Push Y

From Figure 6-76 at the performance point the spectral displacement ( $S_d$ ) and spectral acceleration ( $S_a$ ) are 1.87 in. and 0.70 g, respectively. The ductility demand is 4.82.

From Table 6-40 and Figure 6-75 at the performance point (step 10) it can be observed, that eleven hinges are beyond Collapse limit state.

### Model 2.3d: Y direction

**Table 6-40.** Tabular Data for Pushover Curve for Model 2.3d: Push Y

PUSH Y Mode			Hinge Sequence								Shear
Step	Disp. (in)	BaseForce (Kip)	A to B	B to IO	IO to LS	LS to CP	CP to C	C to D	D to E	E to F	
0	0.00	0.00	130	0	0	0	0	0	0	0	
1	0.48	17.02	130	0	0	0	0	0	0	0	
2	0.59	20.83	128	2	0	0	0	0	0	0	
3	1.01	30.41	114	10	0	4	0	2	0	0	
4	1.62	36.30	106	2	9	3	6	4	0	0	
5	2.18	40.59	102	4	1	1	11	11	0	0	
6	2.67	43.50	101	5	0	0	6	13	5	0	
7	3.16	46.17	100	4	2	0	3	11	10	0	
8	3.76	49.35	99	5	2	0	2	6	16	0	

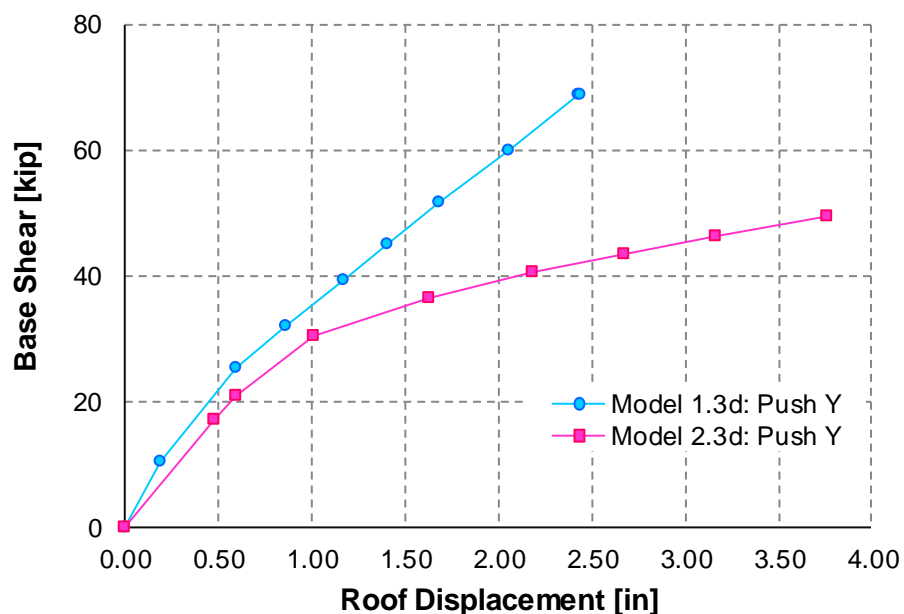


**Figure 6-77.** Comparison Pushover Curves for Model 1.3d and Model 2.3d: Push Y

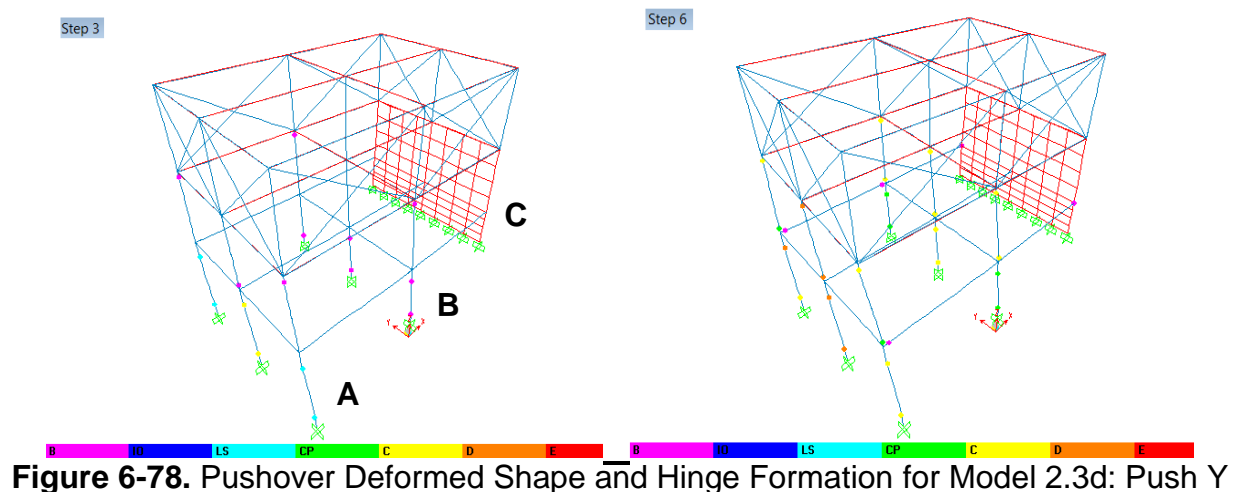
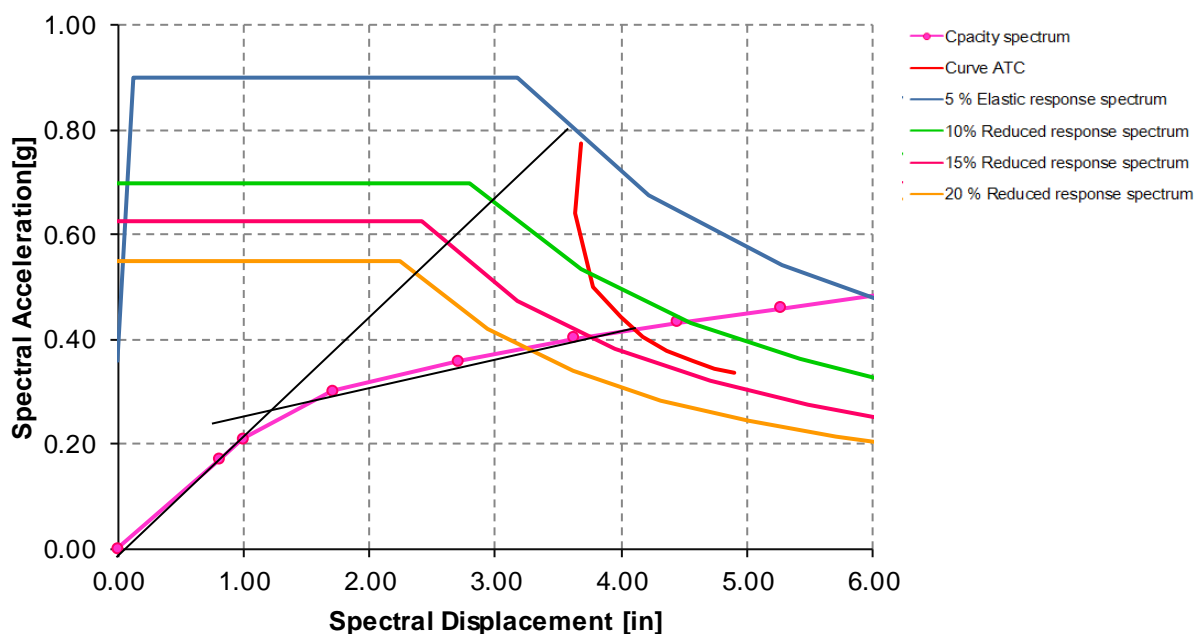


**Figure 6-78.** Pushover Deformed Shape and Hinge Formation for Model 2.3d: Push Y



$$\begin{aligned}
 S_{app} &= 0.43 \text{ g} & V_{pp} &= 42.24 \text{ k} \\
 S_{dpp} &= 4.10 \text{ in} & D_{pp} &= 2.46 \text{ in} \\
 S_{dy} &= 1.22 \text{ in} \\
 \mu_d &= 3.36
 \end{aligned}$$

**Figure 6-79.** Performance Point for Model 2.3d: Push Y

From Figure 6-79 at the performance point the spectral displacement ( $S_d$ ) and spectral acceleration ( $S_a$ ) are 4.10 in. and 0.43 g, respectively. The ductility demand is 3.36. From Table 6-40 and Figure 6-78 at the performance point (between step 6 and 7) it

can be observed, that thirteen hinges are beyond Collapse limit state. Most hinges at frame A have reached point D.

#### 6.2.3.4 MODEL 1.4 VS MODEL 2.4

The tabular data for pushover, pushover curves, hinge sequences (only for Models c/d) and performance point are presented in Tables 6-41 to 6-28 and Figures 6-80 to 6-89.

#### Model 2.4b: -X direction

**Table 6-41.** Tabular Data for Pushover Curve for Model 2.4b: Push -X

PUSH -X Mode			Hinge Sequence								
Step	Disp. (in)	BaseForce (Kip)	A to B	B to IO	IO to LS	LS to CP	CP to C	C to D	D to E	E to F	Shear
0	0.00	0.00	162	0	0	0	0	0	0	0	
1	-0.36	42.69	162	0	0	0	0	0	0	0	
2	-0.48	56.60	160	2	0	0	0	0	0	0	
3	-0.88	86.04	152	9	1	0	0	0	0	0	
4	-0.94	88.40	145	14	3	0	0	0	0	0	
5	-1.11	92.53	138	18	6	0	0	0	0	0	
6	-1.37	95.77	135	18	8	1	0	0	0	0	
7	-1.76	98.82	134	7	18	0	2	1	0	0	
8	-2.27	102.45	133	2	20	2	0	5	0	0	
9	-2.84	106.08	132	3	9	7	2	7	2	0	
<b>10</b>	<b>-3.26</b>	<b>108.55</b>	<b>129</b>	<b>6</b>	<b>4</b>	<b>6</b>	<b>4</b>	<b>10</b>	<b>3</b>	<b>0</b>	
11	-3.60	110.08	127	8	0	7	5	12	3	0	

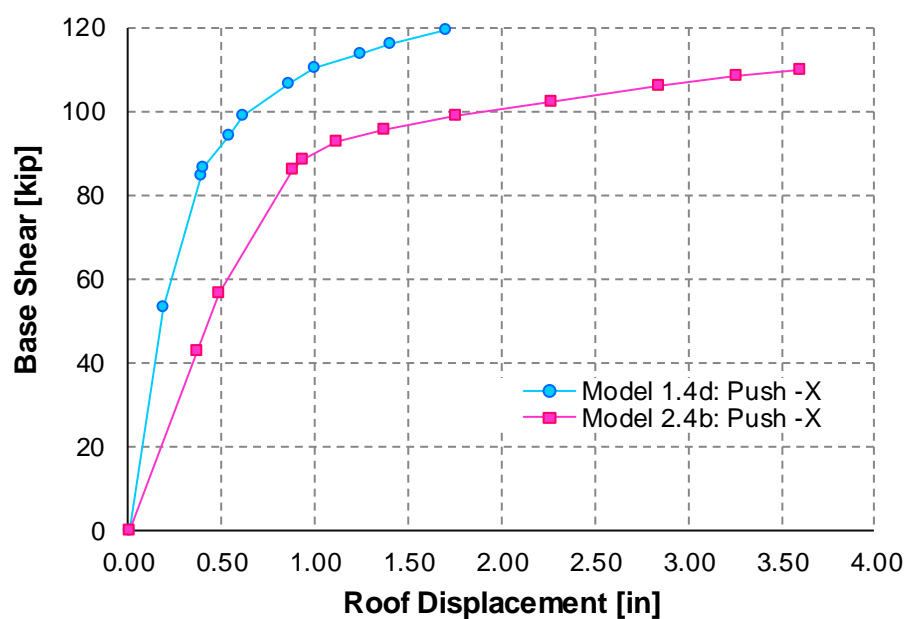
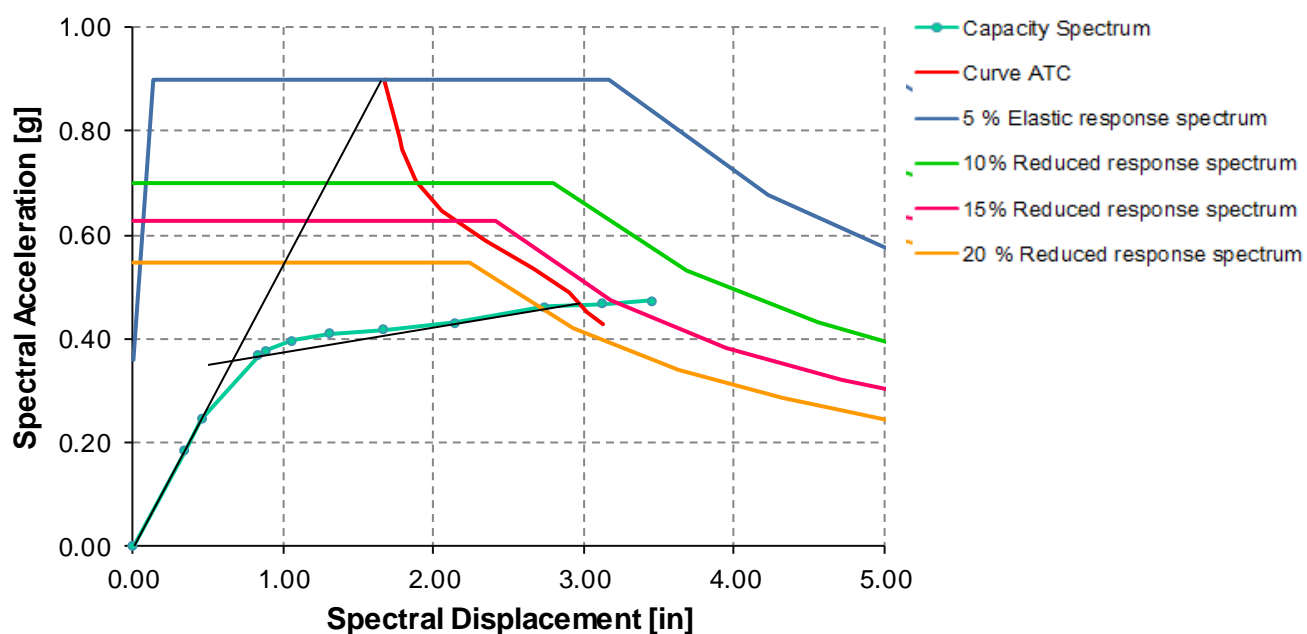


**Figure 6-80.** Comparison Pushover Curves for Model 1.4b and Model 2.4b: Push -X

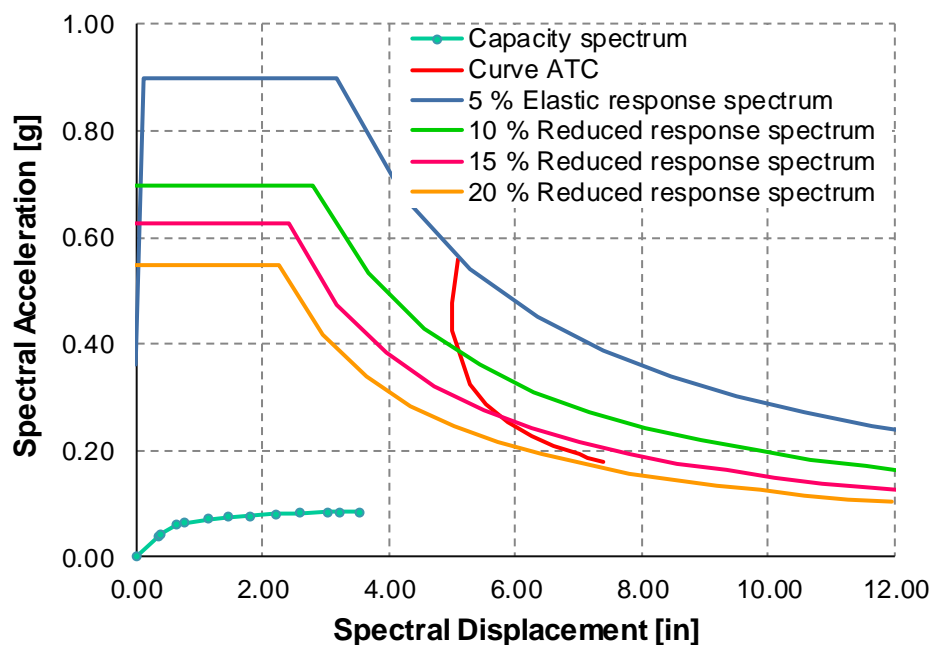


$$\begin{aligned}
 S_{app} &= 0.47 \text{ g} & V_{pp} &= 107.62 \text{ k} \\
 S_{dpp} &= 2.98 \text{ in} & D_{pp} &= 3.10 \text{ in} \\
 S_{dy} &= 0.65 \text{ in}
 \end{aligned}$$

**Figure 6-81.** Performance Point for Model 2.4b: Push X

From Figure 6-81 at the performance point the spectral displacement ( $S_d$ ) and spectral acceleration ( $S_a$ ) are 3.94 in. and 0.43 g, respectively. The ductility demand is 4.58. From Table 6-41 at the performance point (step 10) it can be observed that ten hinges are beyond Collapse limit state. Model 1.4b suffered also extensive damage at the performance eight hinges were beyond Collapse limit state.

### **Model 2.4b: Y direction**

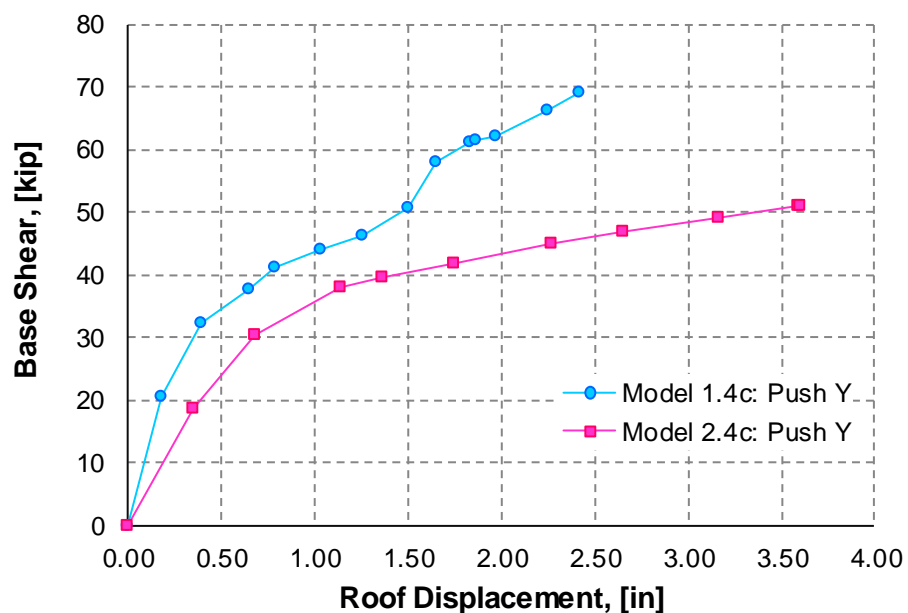


**Figure 6-82.** Performance Point for Model 2.3b: Push Y



**Model 2.4c: Y direction****Table 6-42.** Tabular Data for Pushover Curve for Model 2.4c: Push X

PUSH Y Mode			Hinge Sequence								Shear
Step	Disp. (in)	BaseForce (Kip)	A to B	B to IO	IO to LS	LS to CP	CP to C	C to D	D to E	E to F	
0	0.00	0.00	162	0	0	0	0	0	0	0	
1	0.35	18.60	161	1	0	0	0	0	0	0	
2	0.68	30.36	138	18	6	0	0	0	0	0	
3	1.13	37.95	131	8	12	3	4	4	0	0	
4	1.36	39.70	126	11	10	3	7	5	0	0	
5	1.75	41.93	126	6	9	3	11	7	0	0	
6	2.26	44.94	126	0	10	2	10	9	5	0	
7	2.65	46.72	125	0	8	2	6	15	5	1	
8	3.17	49.12	124	1	7	1	8	9	11	1	
9	3.59	51.00	123	1	5	1	5	10	15	2	
10	3.60	51.02	123	1	5	1	5	10	15	2	

**Figure 6-83.** Comparison Pushover Curves for Model 1.4c and Model 2.4c: Push Y

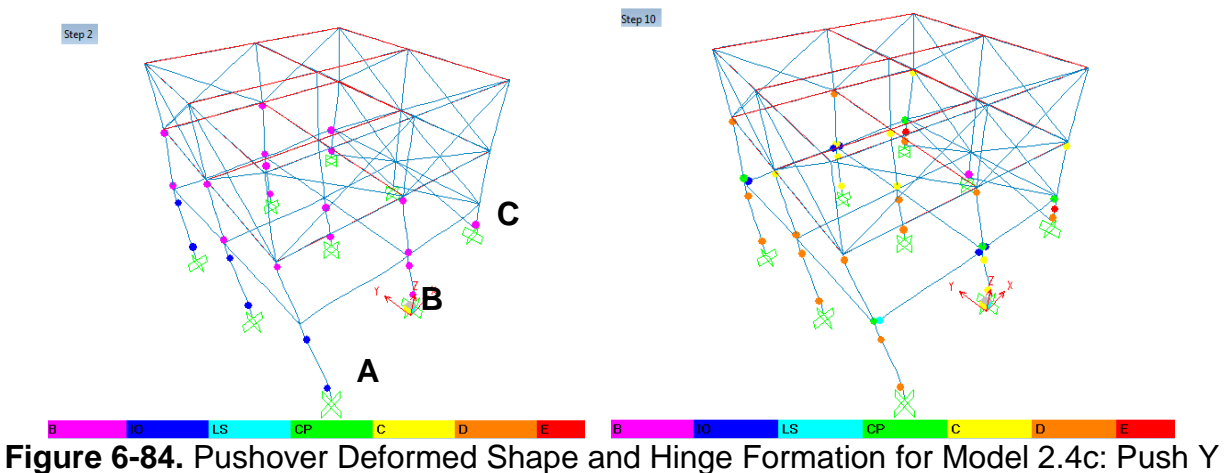
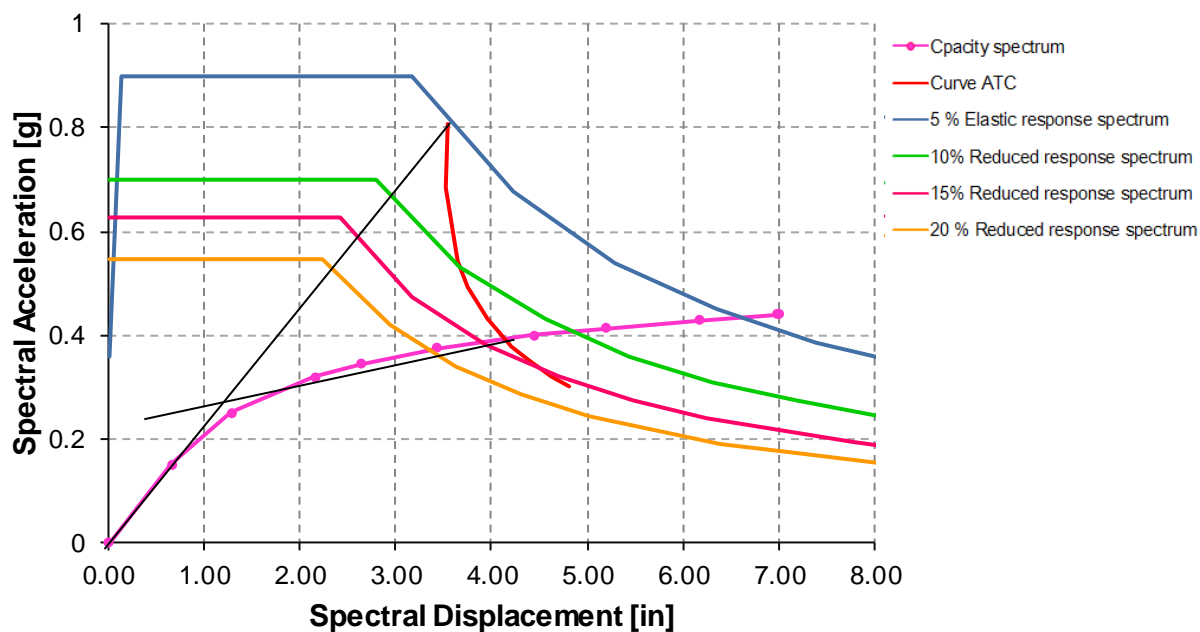


Figure 6-84. Pushover Deformed Shape and Hinge Formation for Model 2.4c: Push Y



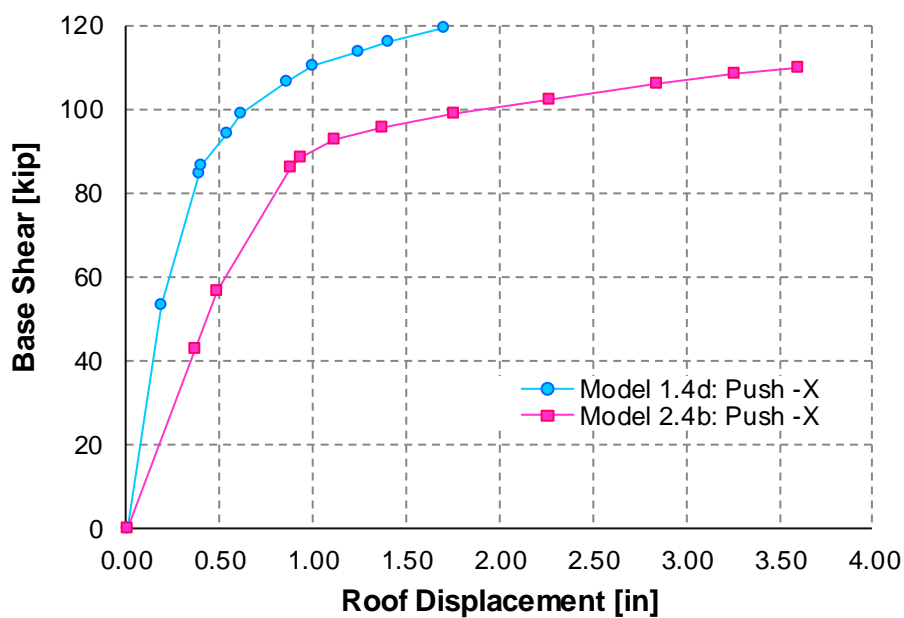
$$\begin{aligned}
 S_{app} &= 0.39 \text{ g} & V_{pp} &= 44.03 \text{ k} \\
 S_{dpp} &= 4.14 \text{ in} & D_{pp} &= 2.10 \text{ in} \\
 S_{dy} &= 1.10 \text{ in} \\
 \mu_d &= 3.76
 \end{aligned}$$

Figure 6-85. Performance Point for Model 2.4c: Push Y

From Figure 6-85 at the performance point the spectral displacement ( $S_d$ ) and spectral acceleration ( $S_a$ ) are 4.14 in. and 0.39 g respectively. The ductility demand is 3.76.

**Model 2.4d – Y direction****Table 6-43.** Tabular Data for Pushover Curve for Model 2.4d: Push Y

PUSH Y Mode			Hinge Sequence								Shear
Step	Disp. (in)	BaseForce (Kip)	A to B	B to IO	IO to LS	LS to CP	CP to C	C to D	D to E	E to F	
0	0.00	0.00	130	0	0	0	0	0	0	0	
1	0.36	17.85	130	0	0	0	0	0	0	0	
2	0.53	26.21	130	0	0	0	0	0	0	0	
3	0.79	36.07	117	13	0	0	0	0	0	0	
4	1.16	42.94	107	8	9	6	0	0	0	0	
5	1.56	47.76	101	8	4	5	6	6	0	0	
6	2.14	53.48	98	9	3	0	7	12	1	0	
7	2.72	59.22	98	2	9	1	4	10	6	0	
8	3.11	62.97	98	0	8	3	1	7	13	0	
9	3.51	66.83	98	0	6	2	2	6	16	0	
10	3.57	67.33	98	0	6	2	2	6	16	0	

**Figure 6-86.** Comparison Pushover Curves for Model 1.4d and Model 2.4d: Push Y

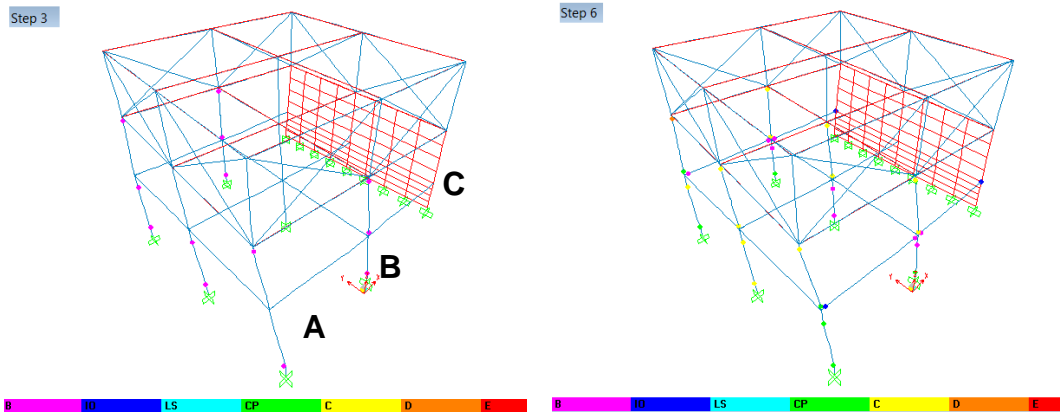
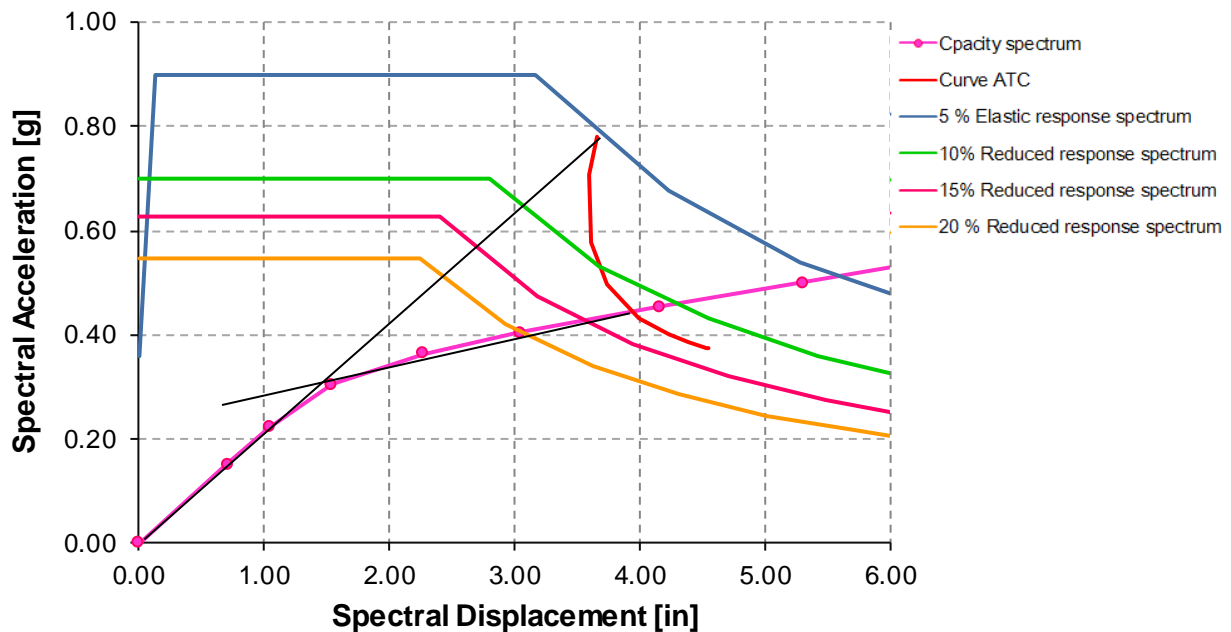


**Figure 6-87.** Pushover Deformed Shape and Hinge Formation for Model 2.4d: Push Y



$$\begin{aligned}
 S_{app} &= 0.44 \text{ g} & V_{pp} &= 52.31 \text{ k} \\
 S_{dpp} &= 3.94 \text{ in} & D_{pp} &= 2.02 \text{ in} \\
 S_{dy} &= 1.50 \text{ in} \\
 \mu_d &= 2.63
 \end{aligned}$$

**Figure 6-88.** Performance Point for Model 2.4d: Push Y

From Figure 6-88 at the performance point the spectral displacement ( $S_d$ ) and spectral acceleration ( $S_a$ ) are 3.94 in. and 0.44 g, respectively. The ductility demand is 2.63. From Table 6-43 and Figure 6-87 at the performance point (step 6) it can be observed, that eleven hinges are beyond Collapse limit state. Most of the damage is observed at

the middle floor. Model 1.4 also suffered a lot of damage at the performance point most of the hinges were beyond Collapse limit state.

## 6.2.4 PUSHOVER ANALYSIS RESULTS: CHANGE IN COLUMNS ORIENTATION

In this section the effect of changing the column orientation will be studied. The X direction is the strong axis of the columns in Model 1.1. Model 1.1y is equal to Model 1.1 in terms of geometry, story levels and bay length, the only difference is that the Y direction is the strong axis of the column instead of the X direction. Model type d is not considered.

### 6.2.4.1 MODEL 1.1 VS MODEL 1.1y

The tabular data for pushover, pushover curves, hinge sequences and performance point plot are presented in Tables 6-44 to 6-46 and Figures 6-89 to 6-97.

#### Model 1.1yb: -X direction

**Table 6-44.** Tabular Data for Pushover Curve for Model 1.1yb: Push -X

PUSH -X Mode			Hinge Sequence								Shear
Step	Disp. (in)	Base Force (Kip)	A to B	B to IO	IO to LS	LS to CP	CP to C	C to D	D to E	E to F	
0	0.00	0.00	102	0	0	0	0	0	0	0	
1	0.24	14.11	102	0	0	0	0	0	0	0	
2	0.27	16.24	99	3	0	0	0	0	0	0	
3	0.51	22.53	94	2	3	3	0	0	0	0	
4	0.68	24.14	91	2	3	3	0	3	0	0	
5	0.96	25.35	90	0	2	1	2	4	3	0	
6	1.32	26.75	88	2	0	0	0	6	6	0	
7	1.36	26.82	87	3	0	0	0	6	6	0	
8	1.61	27.08	84	3	3	0	0	4	8	0	
9	1.93	27.11	84	0	3	3	0	0	12	0	
10	2.17	27.14	84	0	3	0	3	0	12	0	
11	2.20	27.14	84	0	0	3	0	3	12	0	
12	2.40	27.15	84	0	0	3	0	3	12	0	

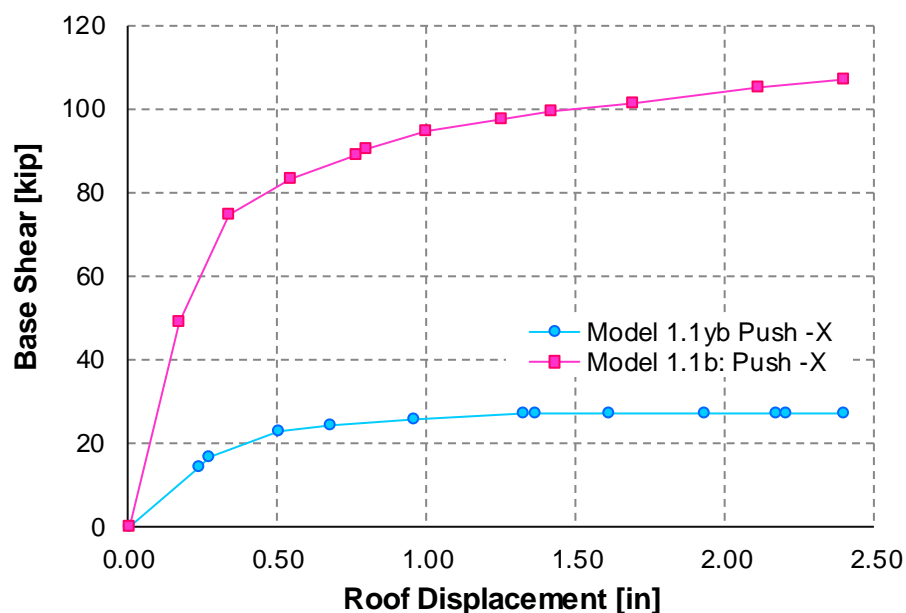
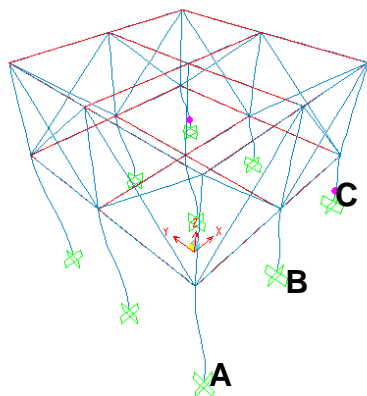


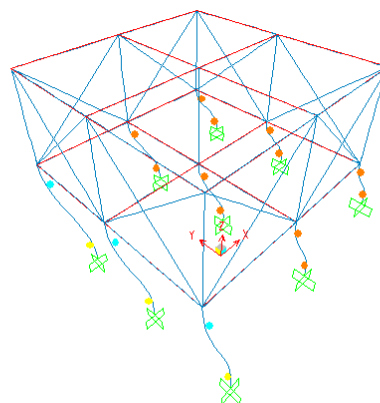
**Figure 6-89.** Comparison Pushover Curves for Model 1.1b and Model 1.1yb: Push -X

From Figure 6-89 it can be observed that the capacity in the X directions drops drastically due to the change in columns orientation. The maximum base shear obtained from the pushover analysis for Model 1.1b and Model 1.1cy are 106.89 and 27.15 kip, respectively. This numbers reflects a decrease in capacity of 75 %.

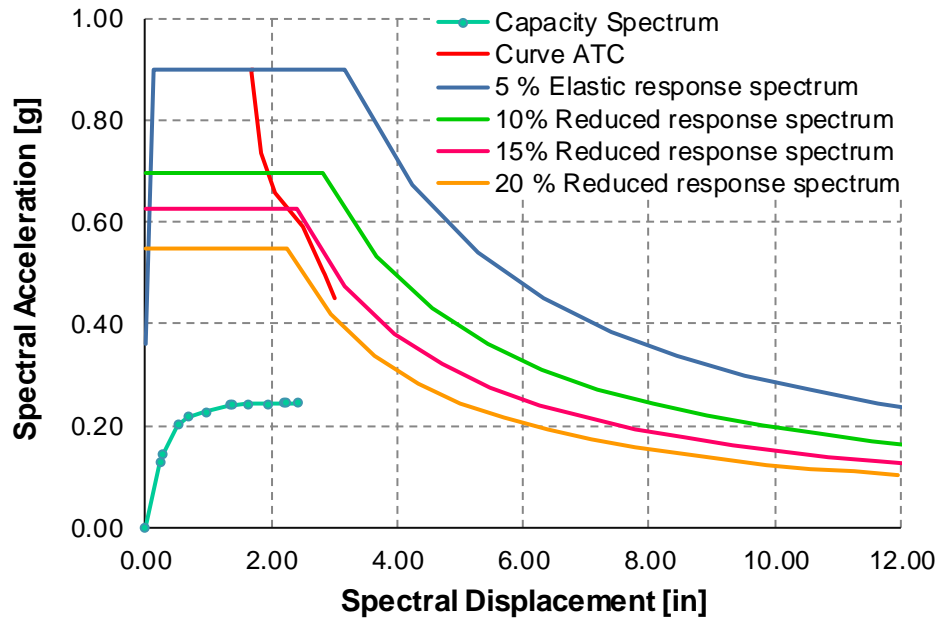
Step 2



Step 13



**Figure 6-90.** Pushover Deformed Shape and Hinge Formation for Model 1.1yb: Push -X

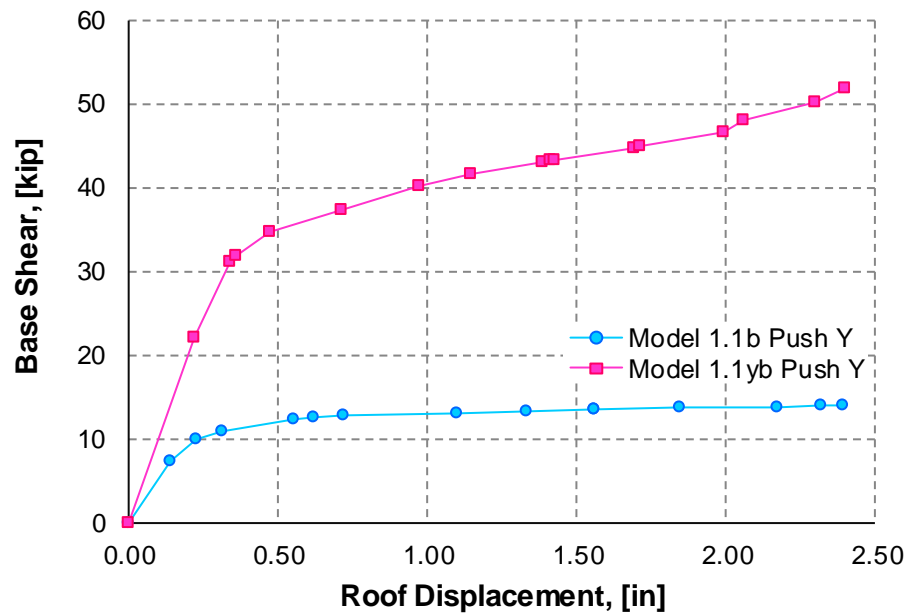


**Figure 6-91.** Performance Point for Model 1.1yb: Push -X

From Figure 6-91 it is observed that no performance point was reached. The capacity spectrum curves lay substantially below the reduced response spectrums. In other words the model is not able to satisfy the demand. By the end of the analysis 12 hinges are beyond Collapse limit state (D to E). The results show similar behavior as for Model 1.1b when the Y direction was the weak axis of the column. The models will fail in their weak direction, especially with columns of 6 inch wide. Typically residential houses in Puerto Rico have columns built 6 inch wide in their weak direction.

**Model 1.1yb: Y direction****Table 6-45.** Tabular Data for Pushover Curve for Model 1.1yb: Push Y

PUSH Y Mode			Hinge Sequence								
Step	Disp. (in)	Base Force (Kip)	A to B	B to IO	IO to LS	LS to CP	CP to C	C to D	D to E	E to F	Shear
0	0.00	0.00	102	0	0	0	0	0	0	0	
1	0.21	22.10	101	1	0	0	0	0	0	0	
2	0.34	31.19	94	4	4	0	0	0	0	0	
3	0.35	31.92	92	5	5	0	0	0	0	0	
4	<b>0.47</b>	<b>34.77</b>	<b>86</b>	<b>4</b>	<b>9</b>	<b>3</b>	<b>0</b>	<b>0</b>	<b>0</b>	<b>0</b>	
5	0.71	37.41	86	0	5	5	5	1	0	0	
6	0.97	40.17	85	1	0	5	7	4	0	0	
7	1.14	41.66	85	1	0	1	5	10	0	0	
8	1.38	42.96	85	0	1	0	1	10	5	0	
9	1.41	43.24	85	0	1	0	1	10	5	0	
10	1.43	43.36	85	0	1	0	1	9	6	0	
11	1.69	44.76	84	1	1	0	0	2	14	0	
12	1.71	44.96	84	1	1	0	0	2	14	0	
13	1.99	46.53	84	0	2	0	0	1	15	0	
14	2.05	47.97	84	0	2	0	0	0	16	0	
15	2.29	50.15	84	0	2	0	0	0	16	0	
16	2.40	51.80	84	0	2	0	0	0	16	0	

**Figure 6-92.** Comparison Pushover Curves for Model 1.1b and Model 1.1yb: Push Y



From Figure 6-92 it can be observed that the capacity in the Y directions for Model 1.1by increased due to the change columns orientation. The maximum base shear obtained from the pushover analysis for Model 1.1b and Model 1.1cy was 13.92 and 51.80 kip, respectively. This numbers reflects an increase in capacity of 73 %.

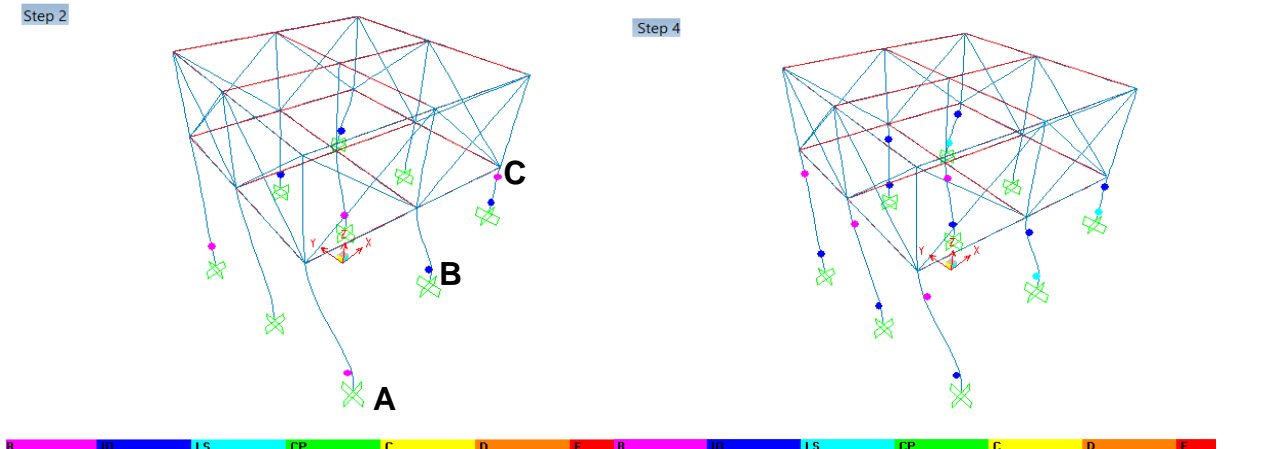
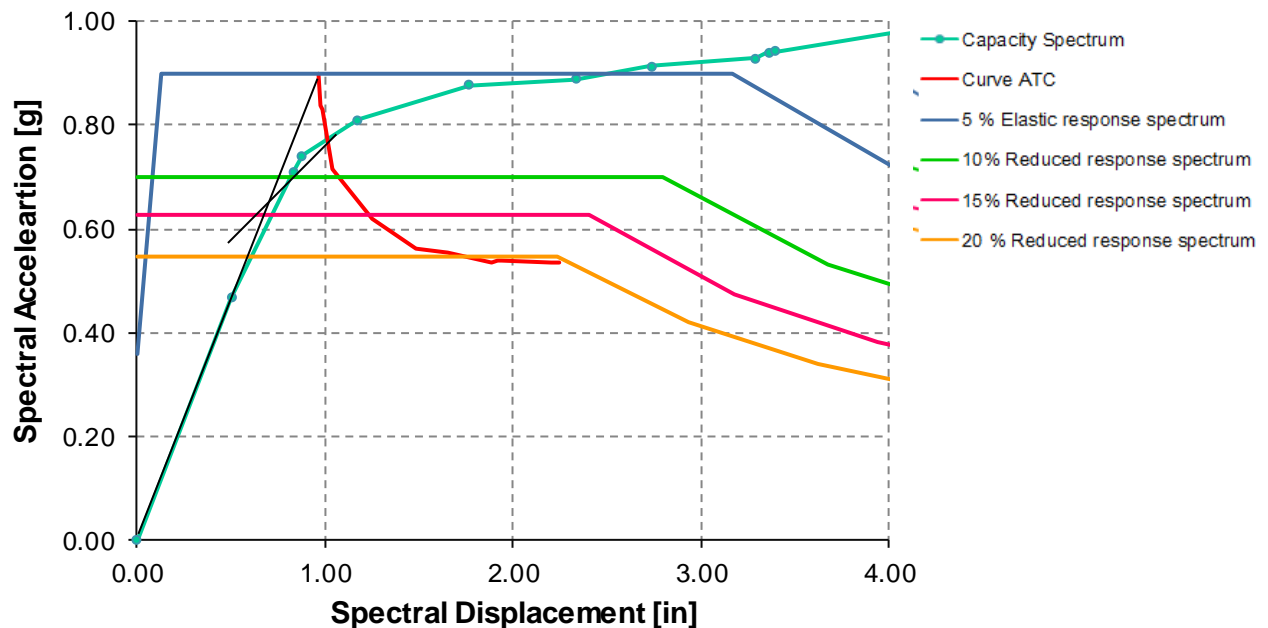


**Figure 6-93.** Pushover Deformed Shape and Hinge Formation for Model 1.1yb: Push Y



$$\begin{aligned}
 S_{app} &= 0.77 \text{ g} & V_{pp} &= 33.2 \text{ k} \\
 S_{dpp} &= 1.00 \text{ in} & D_{pp} &= 0.407 \text{ in} \\
 S_{dy} &= 0.70 \text{ in} \\
 \mu_d &= 1.43
 \end{aligned}$$

**Figure 6-94.** Performance Point for Model 1.1yb: Push Y

From Figure 6-94 at the performance point the spectral displacement ( $S_d$ ) and spectral acceleration ( $S_a$ ) are 1.00 in. and 0.77 g, respectively. The ductility demand is 1.43. In terms of the performance point (step 4) it can be observed from Table 6-45 that nine hinges are between IO and LS limit state.

### Model 1.1yc: Y direction

**Table 6-46.** Tabular Data for Pushover Curve for Model 1.1yc: Push Y

PUSH Y Mode			Hinge Sequence								Shear
Step	Disp. (in)	Base Force (Kip)	A to B	B to IO	IO to LS	LS to CP	CP to C	C to D	D to E	E to F	
0	0.00	0.00	102	0	0	0	0	0	0	0	
1	0.19	24.85	101	1	0	0	0	0	0	0	
2	0.28	33.60	95	4	3	0	0	0	0	0	
3	<b>0.38</b>	<b>37.12</b>	<b>90</b>	<b>3</b>	<b>9</b>	<b>0</b>	<b>0</b>	<b>0</b>	<b>0</b>	<b>0</b>	
4	0.41	37.68	87	5	10	0	0	0	0	0	
5	0.69	40.02	86	0	5	6	4	1	0	0	
6	0.71	40.47	86	0	4	6	5	1	0	0	
7	0.76	40.97	86	0	3	8	2	3	0	0	
8	1.02	42.65	86	0	0	2	2	11	1	0	
9	1.21	43.84	86	0	0	0	3	9	4	0	
10	1.51	46.74	86	0	0	0	0	2	14	0	
11	1.86	50.62	86	0	0	0	0	0	16	0	
12	2.10	54.09	86	0	0	0	0	0	16	0	
13	2.34	57.37	86	0	0	0	0	0	16	0	
14	2.40	58.76	86	0	0	0	0	0	15	1	

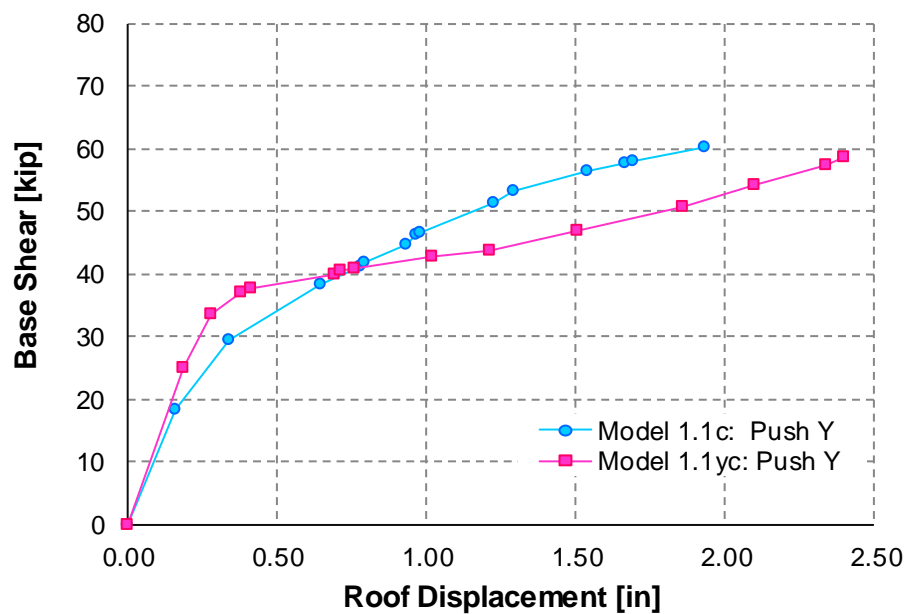


**Figure 6-95.** Comparison Pushover Curves for Model 1.1b and Model 1.1yc: Push Y

From Figure 6-95 it can be observed that initially the capacity for Model 1.1yc is higher than for Model 1.1c. The curve for Model 1.1yc has a steeper slope in the elastic range, as it starts to deviate into the inelastic range the slope is less steep in comparison to Model 1.1c. For Model 1.1yc the column orientation was changed, in other words, the dimension in the Y direction was increased from 6 to 16 inches and the dimension in the X direction was reduced from 16 to 6 inches. As it was mentioned before due to torsional issues any change in the X direction also affect the Y direction. As a consequence comparing the results with Model 1.1c initially it can be observed an increase in capacity however as the analysis progress the columns size reduction in the X direction start to affect the capacity.

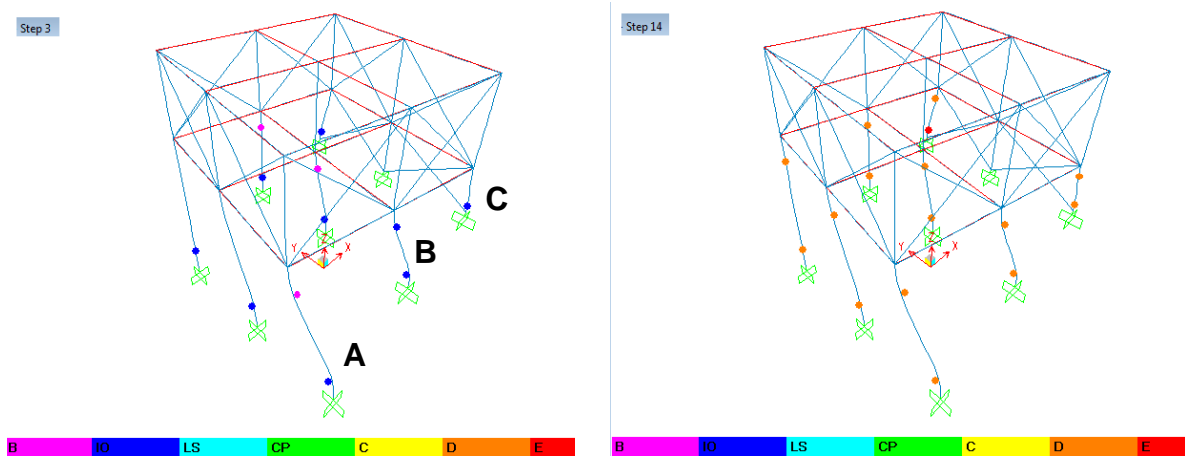


**Figure 6-96.** Pushover Deformed Shape and Hinge Formation for Model 1.1yc: Push Y

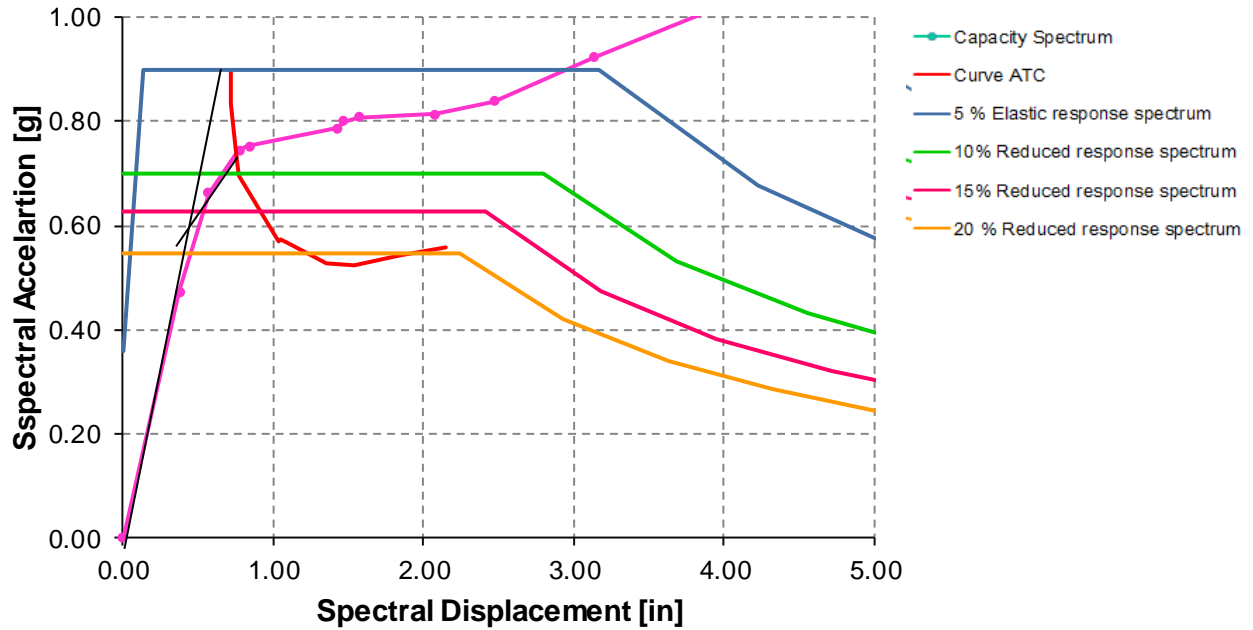


**Figure 6-97.** Performance Point for Model 1.1yc: Push Y

From Figure 6-97 at the performance point the spectral displacement ( $S_d$ ) and spectral acceleration ( $S_a$ ) are 0.75 in. and 0.74 g. The ductility demand is 1.67. In terms of the performance point (step 3) it can be observed from Table 6-46 that hinges are between Immediate Occupancy and Life Safety) limit state.

### 6.2.5 PUSHOVER ANALYSIS RESULTS: CHANGE IN COLUMNS SECTION

In this section the effect of changing the column size will be studied. As mentioned previously for Model 1.1.2 the column size is 16" x 8", for Model 1.1.3 the column size is 12" x 12" and for Model 1.1.5 the columns size is 12" x 6". Hinge sequence graphic representation is not presented. Model type d is not considered.

### 6.2.5.1 MODEL 1.1 VS MODEL 1.1.2

The results are only presented for the Y direction.

#### Model 1.1.2b: Y direction

**Table 6-47.** Tabular Data for Pushover Curve for Model 1.1.2b: Push Y

PUSH Y Mode			Hinge Sequence								Shear
Step	Disp. (in)	Base Force (Kip)	A to B	B to IO	IO to LS	LS to CP	CP to C	C to D	D to E	E to F	
0	0.00	0.00	102	0	0	0	0	0	0	0	
1	0.15	15.48	101	1	0	0	0	0	0	0	
2	0.22	19.87	96	3	3	0	0	0	0	0	
3	0.23	20.32	93	6	3	0	0	0	0	0	
4	0.30	21.50	90	3	9	0	0	0	0	0	
5	0.47	23.14	88	2	4	5	3	0	0	0	
6	0.49	23.26	87	3	3	6	3	0	0	0	
7	0.61	23.64	84	3	3	4	4	4	0	0	
8	0.63	23.67	84	3	3	3	2	7	0	0	
9	0.76	23.74	84	0	6	1	1	10	0	0	
10	0.89	23.78	84	0	6	0	0	12	0	0	
11	1.32	23.85	84	0	0	5	1	10	2	0	
12	1.52	23.88	84	0	0	3	1	6	8	0	
13	1.71	23.89	84	0	0	0	2	8	8	0	
14	1.73	23.89	84	0	0	0	1	9	8	0	
15	1.79	23.90	84	0	0	0	0	10	8	0	
16	1.87	23.90	84	0	0	0	0	9	9	0	
17	2.17	23.91	84	0	0	0	0	6	12	0	
18	2.41	23.92	84	0	0	0	0	6	12	0	
19	2.45	23.92	84	0	0	0	0	5	13	0	

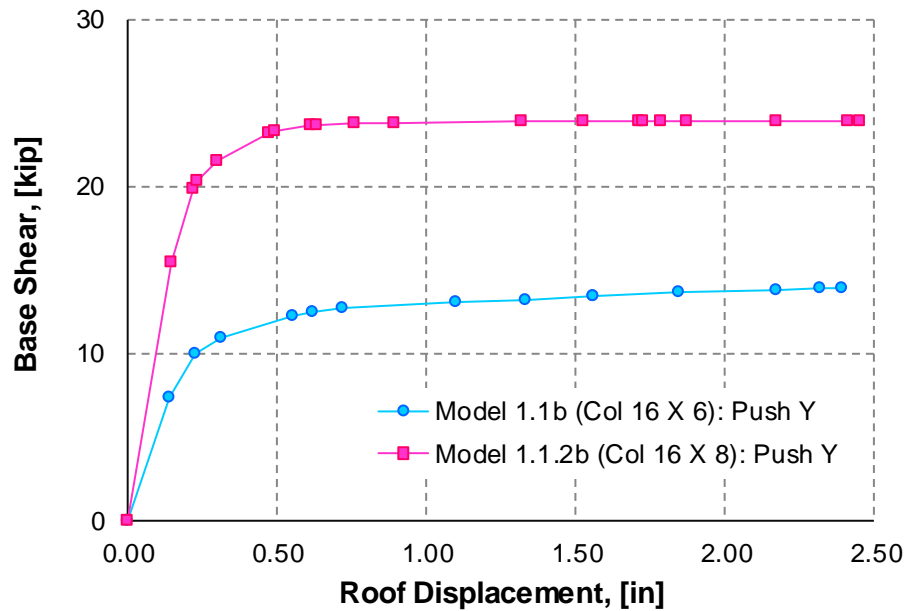


**Figure 6-98.** Comparison Pushover Curves for Model 1.1b and Model 1.1.2b: Push Y

From Figure 6-98 it can be observed that the capacity in the Y directions for Model 1.1.2b increased as columns dimension increased from 6 to 8 inch. The maximum base shear obtained from the pushover analysis for Model 1.1b and Model 1.1.2b was 13.92 and 23.92 kip, respectively. This numbers reflects an increase in capacity of 42 %. However, from Figure 6-99 it is observed that no performance point was reached, even with the increase in columns size the model failed in the Y direction.

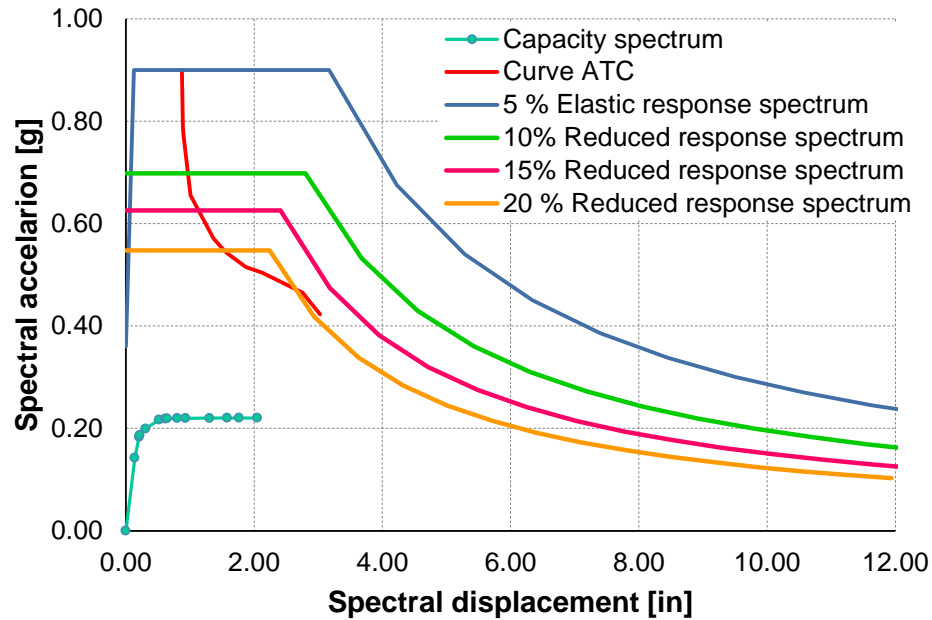
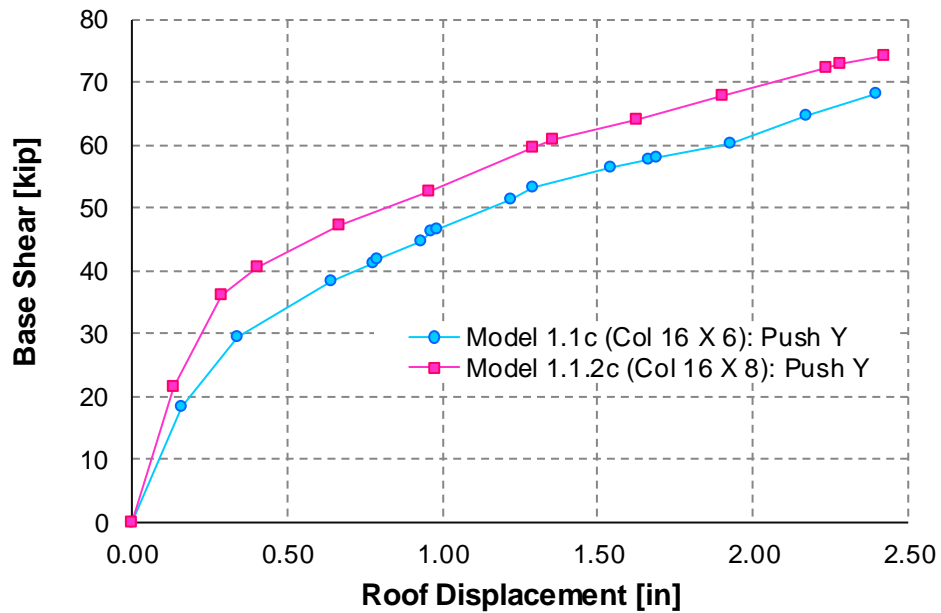


Figure 6-99. Performance Point for Model 1.1.2b: Push Y

### Model 1.1.2c – Y direction

Table 6-48. Tabular Data for Pushover Curve for Model 1.1.2c: Push Y

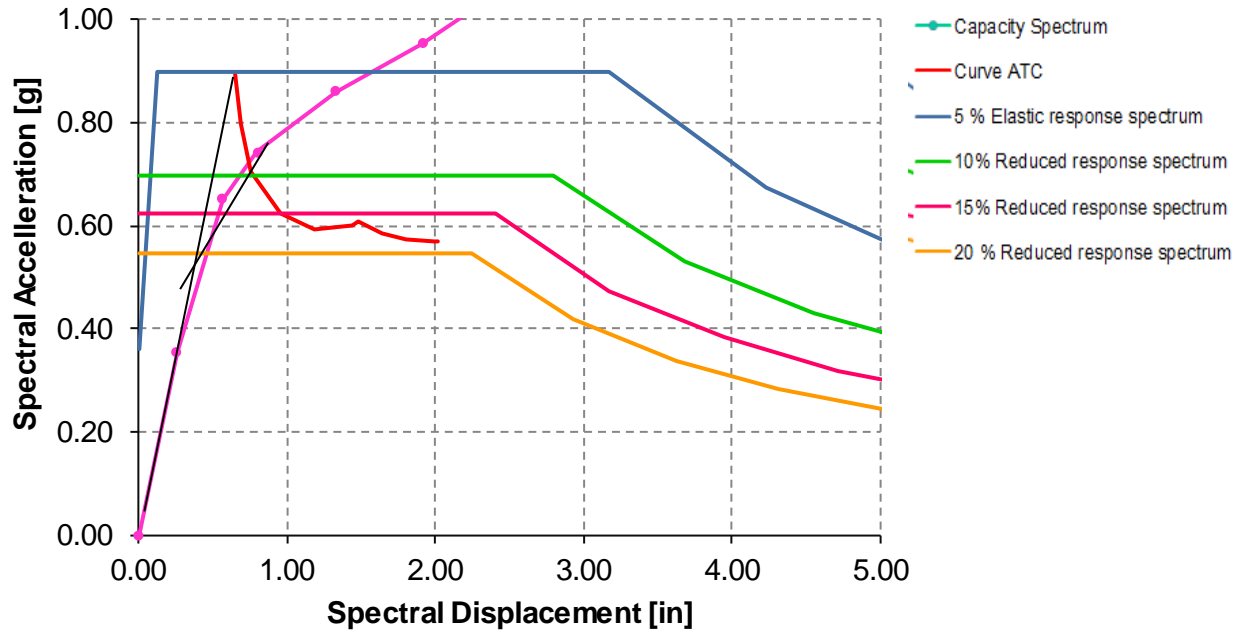
PUSH Y Mode			Hinge Sequence								Shear
Step	Disp. (in)	Base Force (Kip)	A to B	B to IO	IO to LS	LS to CP	CP to C	C to D	D to E	E to F	
0	0.00	0.00	102	0	0	0	0	0	0	0	
1	0.13	21.52	101	1	0	0	0	0	0	0	
2	0.29	35.92	91	6	3	1	0	1	0	0	
<b>3</b>	<b>0.40</b>	<b>40.40</b>	<b>86</b>	<b>1</b>	<b>10</b>	<b>2</b>	<b>0</b>	<b>3</b>	<b>0</b>	<b>0</b>	
4	0.67	47.12	86	0	1	2	3	10	0	0	
5	0.96	52.71	84	1	1	0	1	13	2	0	
6	1.29	59.45	83	0	2	0	0	10	6	1	
7	1.36	60.90	83	0	2	0	0	7	9	1	
8	1.63	64.18	83	0	1	0	0	3	14	1	
9	1.90	67.85	82	0	0	0	0	2	16	2	
10	2.24	72.22	82	0	0	0	0	1	17	2	
11	2.28	72.86	82	0	0	0	0	0	18	2	
12	2.42	74.31	82	0	0	0	0	0	18	2	



**Figure 6-100.** Comparison Pushover Curves for Model 1.1b and Model 1.1.2c: Push Y

From Figure 6-100 it can be observed that the capacity in the Y directions for Model 1.1.2c increased. The maximum base shear obtained from the pushover analysis for Model 1.1c and Model 1.1.2c was 68.14 and 74.31 kip, respectively. These numbers reflect an increase in capacity of 8 %.





$$\begin{aligned}
 S_{app} &= 0.84 \text{ g} & V_{pp} &= 39.29 \text{ k} \\
 S_{dpp} &= 0.74 \text{ in} & D_{pp} &= 0.37 \text{ in} \\
 S_{dy} &= 0.4 \text{ in} \\
 \mu_d &= 1.85
 \end{aligned}$$

**Figure 6-101.** Performance Point for Model 1.1.2c: Push Y

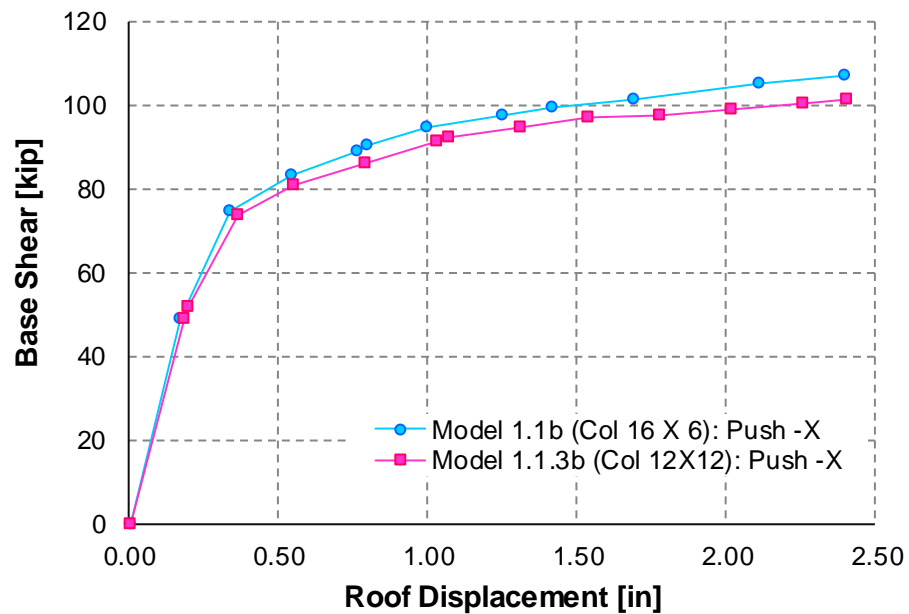
From Figure 6-101 at the performance point the spectral displacement ( $S_d$ ) and spectral acceleration ( $S_a$ ) are 0.74 in. and 0.84 g, respectively. In terms of the performance point (step 4) it can be observed from Table 6-48 that three hinges are beyond Collapse (C) limit state.

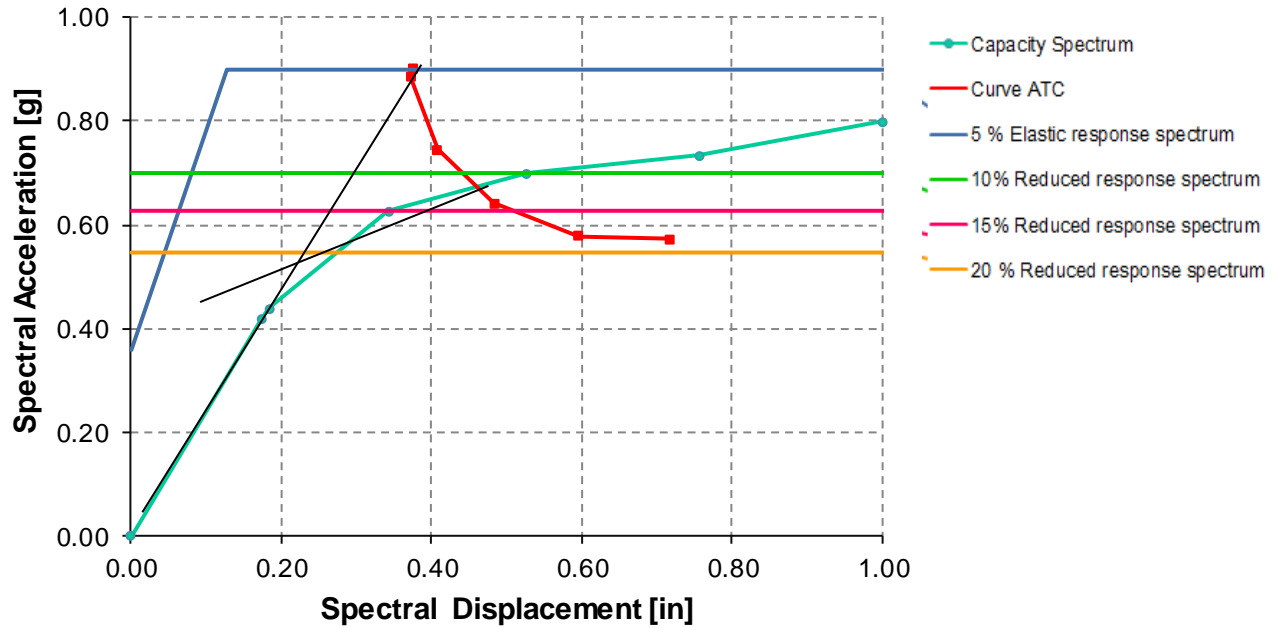
#### 6.2.5.2 MODEL 1.1 VS MODEL 1.1.3

The tabular data for pushover, pushover curves, hinge sequences and performance point plot are presented in Tables 6-49 to 6-51 and Figures 6-102 to 6-107.

**Model 1.1.3b: -X direction****Table 6-49.** Tabular Data for Pushover Curve for Model 1.1.3b: Push -X

PUSH X Mode			Hinge Sequence								Shear
Step	Disp. (in)	Base Force (Kip)	A to B	B to IO	IO to LS	LS to CP	CP to C	C to D	D to E	E to F	
0	0.00	0.00	102	0	0	0	0	0	0	0	
1	-0.18	48.93	102	0	0	0	0	0	0	0	
2	-0.20	51.53	99	3	0	0	0	0	0	0	
3	-0.36	73.61	94	8	0	0	0	0	0	0	
4	-0.55	80.89	90	9	3	0	0	0	0	0	
5	-0.79	85.96	90	3	9	0	0	0	0	0	
6	-1.03	91.49	89	1	12	0	0	0	0	0	
7	-1.07	92.32	87	3	12	0	0	0	0	0	
8	-1.31	94.71	87	3	12	0	0	0	0	0	
9	-1.54	96.79	84	6	12	0	0	0	0	0	
10	-1.78	97.51	84	3	15	0	0	0	0	0	
11	-2.02	98.69	84	3	12	3	0	0	0	0	
12	-2.26	100.12	84	2	10	6	0	0	0	0	
13	-2.40	101.35	84	0	12	6	0	0	0	0	

**Figure 6-102.** Comparison Pushover Curves for Model 1.1b and Model 1.1.3b: Push -X



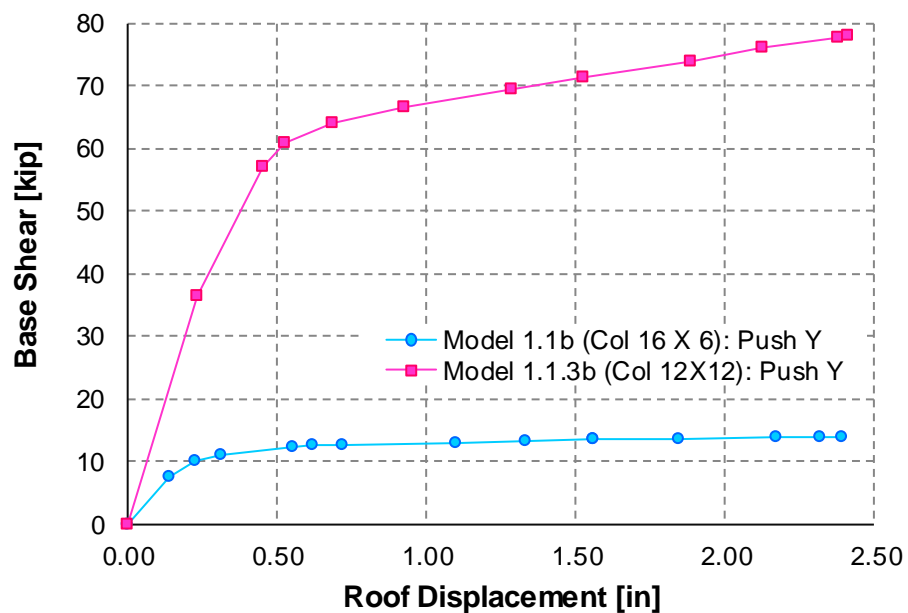
$$\begin{aligned}
 S_{app} &= 0.67 \text{ g} & V_{pp} &= 77.93 \text{ k} \\
 S_{dpp} &= 0.45 \text{ in} & D_{pp} &= 0.47 \text{ in} \\
 S_{dy} &= 0.22 \text{ in} \\
 \mu_d &= 2.06
 \end{aligned}$$

**Figure 6-103.** Performance Point for Model 1.1.3b: Push -X

From Figure 6-103 at the performance point the spectral displacement ( $S_d$ ) and spectral acceleration ( $S_a$ ) are 0.45 in. and 0.67 g respectively. The ductility demand is 2.06. In terms of the performance point (step 3 and 4) it can be observed from Table 6-49 that three hinges formed between the point of Immediate Occupancy (IO) and Life Safety (LS) limit level. In other word the model will suffer some minor repairable damage.

**Model 1.1.3b: Y direction****Table 6-50.** Tabular Data for Pushover Curve for Model 1.1.3b: Push Y

PUSH Y Mode			Hinge Sequence								Shear
Step	Disp. (in)	Base Force (Kip)	A to B	B to IO	IO to LS	LS to CP	CP to C	C to D	D to E	E to F	
0	0.00	0.00	102	0	0	0	0	0	0	0	
1	0.23	36.36	101	1	0	0	0	0	0	0	
2	0.45	57.21	93	9	0	0	0	0	0	0	
3	0.53	60.78	89	13	0	0	0	0	0	0	
4	0.68	64.00	86	12	4	0	0	0	0	0	
5	0.93	66.54	84	6	12	0	0	0	0	0	
6	1.29	69.32	84	1	17	0	0	0	0	0	
7	1.52	71.27	84	1	17	0	0	0	0	0	
8	1.88	73.99	84	0	18	0	0	0	0	0	
9	2.12	75.96	84	0	18	0	0	0	0	0	
10	2.37	77.77	84	0	18	0	0	0	0	0	
11	2.41	78.04	84	0	18	0	0	0	0	0	

**Figure 6-104.** Comparison Pushover Curves for Model 1.1b and Model 1.1.3b: Push y

From Figure 6-104 it can be observed that the capacity in the Y directions for Model 1.1.3b increased substantially as columns' dimension in the Y direction increased from 6 to 12 inch. The maximum base shear obtained from the pushover analysis for Model

1.1b and Model 1.1.3b was 13.92 and 78.04 kip, respectively. This numbers reflects an increase in capacity of 82 percentage.

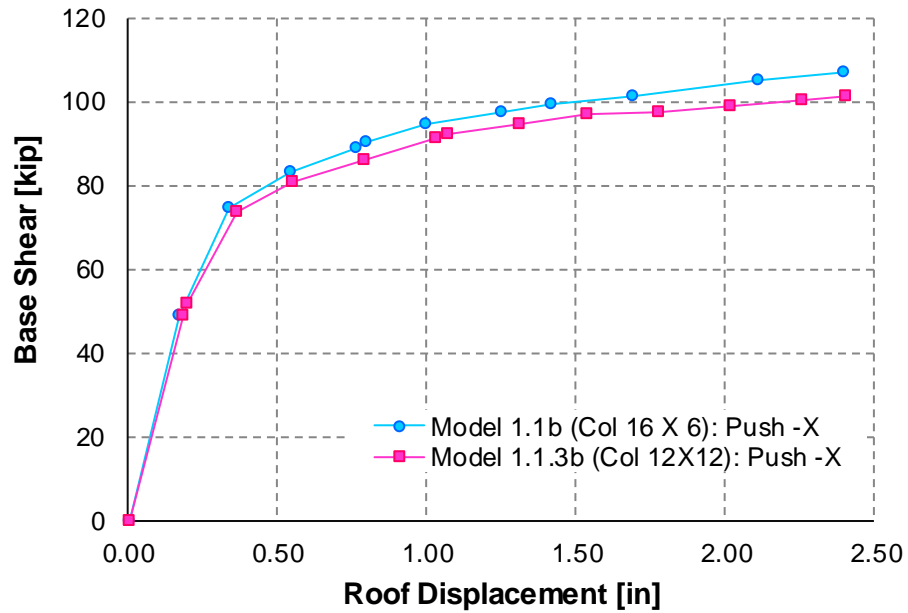
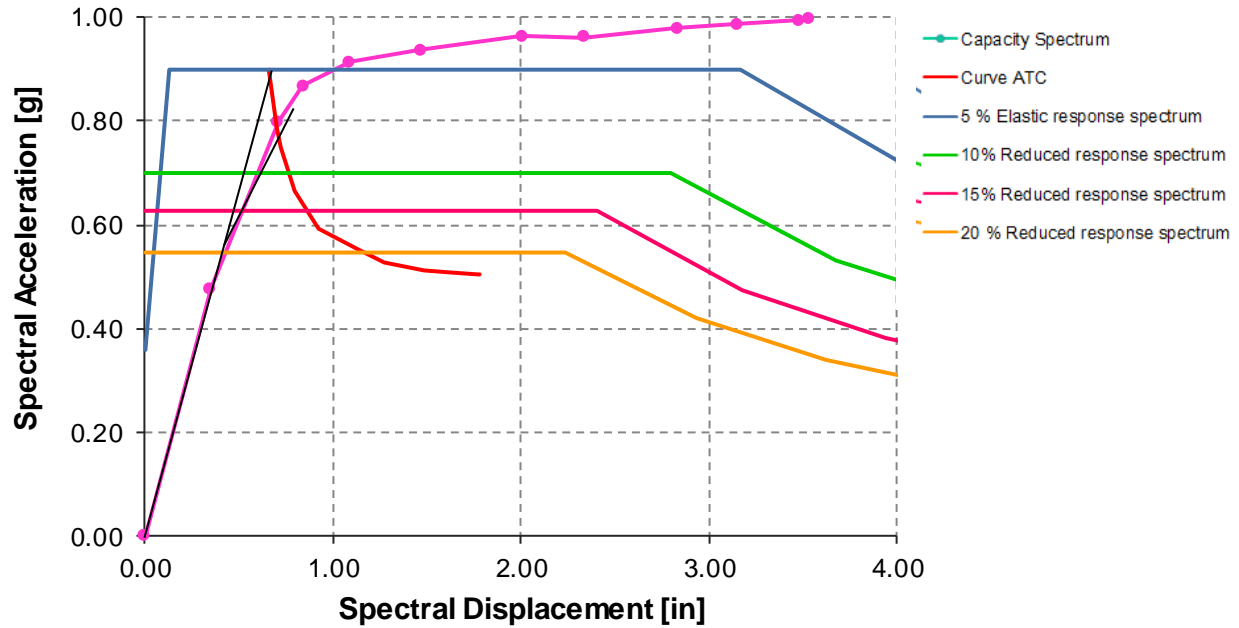


**Figure 6-105.** Comparison Pushover Curves for Model 1.1b and Model 1.1.3b: Push Y



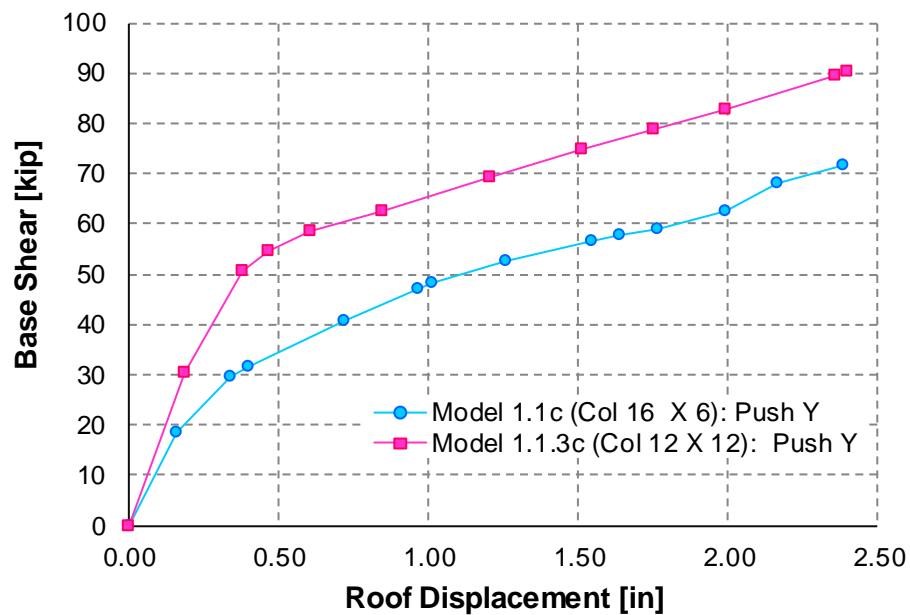
$$\begin{aligned}
 S_{app} &= 0.79 \text{ g} & V_{pp} &= 56.73 \text{ k} \\
 S_{dpp} &= 0.70 \text{ in} & D_{pp} &= 0.45 \text{ in} \\
 S_{dy} &= 0.42 \text{ in} \\
 \mu_d &= 1.67
 \end{aligned}$$

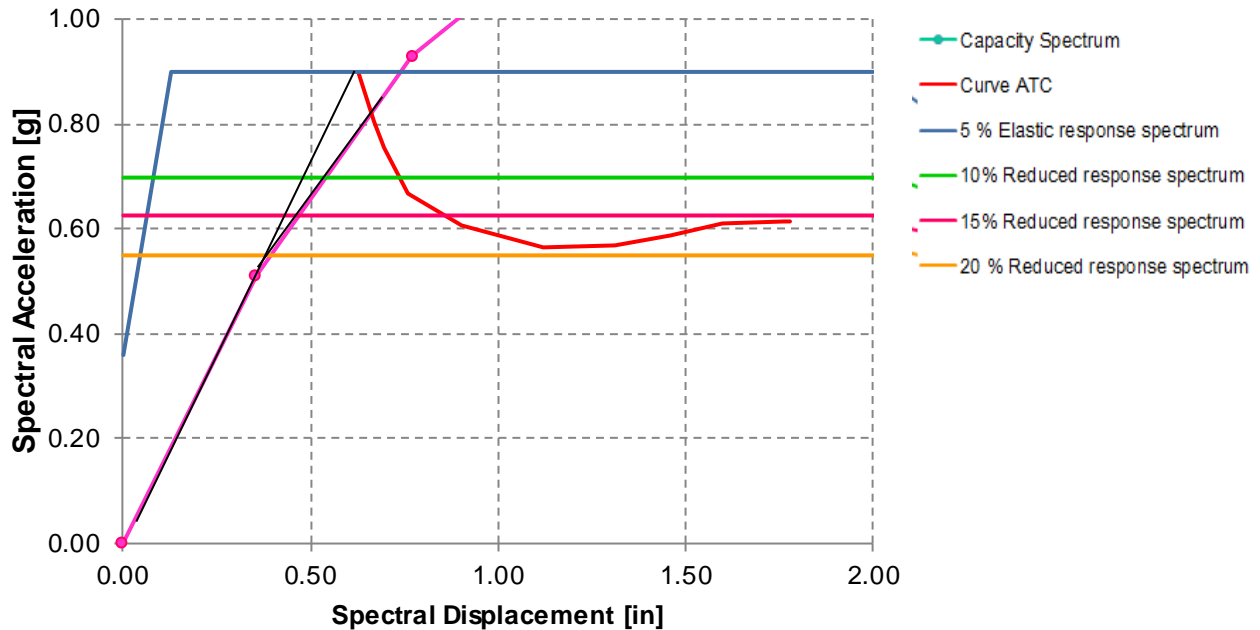
**Figure 6-106.** Performance Point for Model 1.1.3b: Push Y

From Figure 6-106 at the performance point the spectral displacement ( $S_d$ ) and spectral acceleration ( $S_a$ ) are 0.70 in. and 0.79 g, respectively. Recall that from Model 1.1b no performance point was reached. The behavior of the model improves when square 12" x 12" columns are used. The ductility demand is 1.67. In terms of the performance point (step 2) it can be observed from Table 6-50 that the demand curve intersects the capacity curve between the point B (yield) and immediate occupancy (IO) limit level. In other words the model performance is safe as no hinge have formed near or beyond collapse limit state.

**Model 1.1.3c : Y direction****Table 6-51.** Tabular Data for Pushover Curve for Model 1.1.3c: Push Y

PUSH Y Mode			Hinge Sequence								Shear
Step	Disp. (in)	Base Force (Kip)	A to B	B to IO	IO to LS	LS to CP	CP to C	C to D	D to E	E to F	
0	0.00	0.00	102	0	0	0	0	0	0	0	
1	0.18	30.43	102	0	0	0	0	0	0	0	
2	0.38	50.69	95	7	0	0	0	0	0	0	
3	0.46	54.78	90	11	1	0	0	0	0	0	
4	0.60	58.55	86	12	4	0	0	0	0	0	
5	0.84	62.43	86	4	12	0	0	0	0	0	
6	1.20	69.41	86	0	16	0	0	0	0	0	
7	1.51	74.73	84	2	16	0	0	0	0	0	
8	1.75	78.79	83	2	16	0	0	0	0	1	1
9	1.99	82.70	83	2	15	0	0	1	0	1	1
10	2.36	89.63	82	2	11	2	0	3	0	2	2
11	2.40	90.22	82	2	10	3	0	3	0	2	2

**Figure 6-107.** Comparison Pushover Curves for Model 1.1b and Model 1.1.3c: Push Y



$$\begin{aligned}
 S_{app} &= 0.82 \text{ g} & V_{pp} &= 45.11 \text{ k} \\
 S_{dpp} &= 0.66 \text{ in} & D_{pp} &= 0.32 \text{ in} \\
 S_{dy} &= 0.50 \text{ in} \\
 \mu_d &= 1.32
 \end{aligned}$$

**Figure 6-108.** Performance Point for Model 1.1.3c: Push Y

From Figure 6-108 at the performance point the spectral displacement ( $S_d$ ) and spectral acceleration ( $S_a$ ) are 0.66 in. and 0.82 g, respectively. In terms of the performance point (step 2) it can be observed from Table 6-51 that seven hinges are between the point B (yield) and immediate occupancy (IO) limit level. At the end of the pushover analysis 2 shear failures had occurred. At columns H57/H53 (edge columns at frame C) the maximum shear capacity was reached due to shear in the X direction ( $V_2$ ).

#### 6.2.5.3 MODEL 1.1 VS MODEL 1.1.4

The tabular data for pushover, pushover curves, hinge sequences and performance point plot are presented in Tables 6-52 to 6-53 and Figures 6-109 to 6-118.



### Model 1.1.4b: -X direction

Model 1.1.4b was only analyzed in the X direction. For Model 1.1b in the Y direction no performance point was reached, similar results are expected for Model 1.1.5b.

**Table 6-52.** Tabular Data for Pushover Curve for Model 1.1.4b: Push -X

PUSH-X Mode			Hinge Sequence								Shear
Step	Disp. (in)	Base Force (Kip)	A to B	B to IO	IO to LS	LS to CP	CP to C	C to D	D to E	E to F	
0	-0.01	0.00	102	0	0	0	0	0	0	0	
1	-0.12	17.65	100	2	0	0	0	0	0	0	
2	-0.24	26.23	94	5	3	0	0	0	0	0	
3	-0.29	27.65	93	1	8	0	0	0	0	0	
4	-0.41	29.56	90	3	5	4	0	0	0	0	
5	-0.72	32.37	87	3	2	0	2	8	0	0	
6	-0.93	32.94	85	2	3	0	1	10	1	0	
7	-0.97	33.00	84	3	3	0	0	11	1	0	
8	-1.52	33.44	84	0	3	0	3	4	8	0	
9	-1.58	33.54	84	0	2	1	2	5	8	0	
10	-1.94	33.86	84	0	0	0	2	4	12	0	
11	-2.33	34.12	84	0	0	0	0	6	12	0	
12	-2.69	34.80	84	0	0	0	0	6	12	0	
13	-2.82	35.05	84	0	0	0	0	6	12	0	
14	-2.95	35.18	84	0	0	0	0	3	13	2	

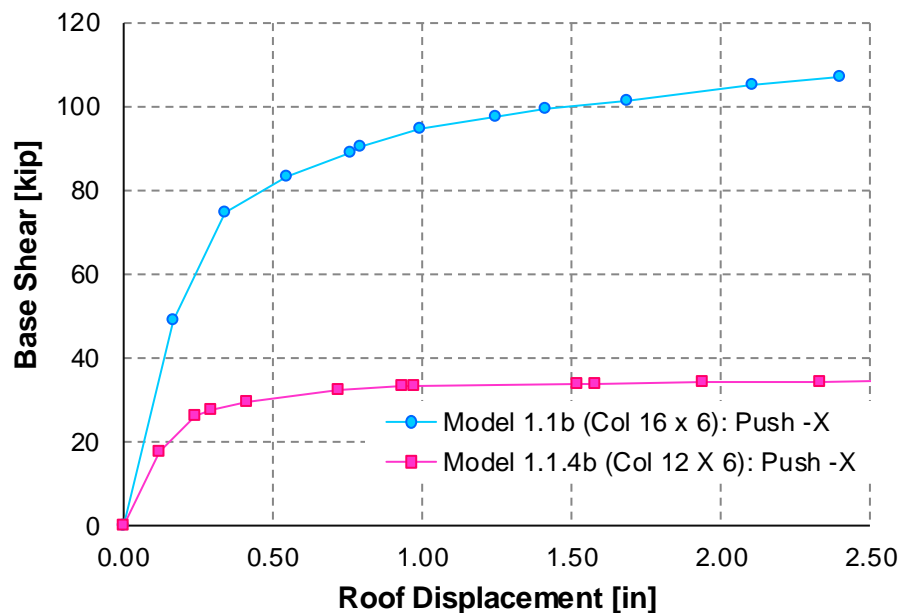


**Figure 6-109.** Comparison Pushover Curves for Model 1.1b and Model 1.1.4b: Push -X

From Figure 6-109 it can be observed that the capacity in the X direction for Model 1.1.4b drops as the column size decrease. The maximum base shear obtained from the pushover analysis for Model 1.1b and Model 1.1cy are 114.77 kip and 49 kip respectively.

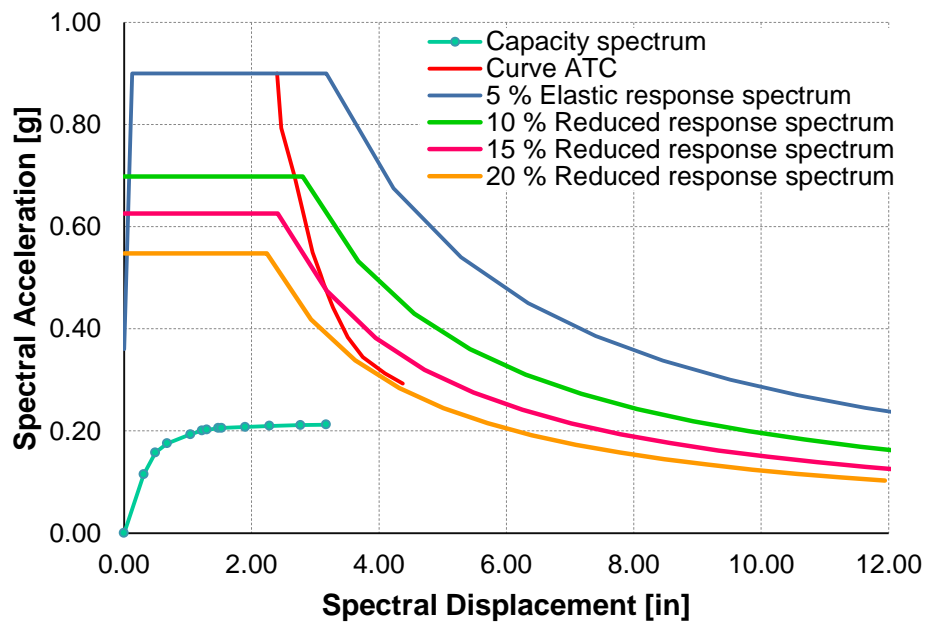


**Figure 6-110.** Performance Point for Model 1.1.4b: Push -X

### Model 1.1.4c: Y direction

For Model 1.1.4c the Y direction was considered since previous results have proven that when a retaining wall is considered in the analyses it affects both X and Y directions.

**Table 6-53.** Tabular Data for Pushover Curve for Model 1.1.4c: Push Y

PUSH Y Mode			Hinge Sequence								Shear
Step	Disp. (in)	Base Force (Kip)	A to B	B to IO	IO to LS	LS to CP	CP to C	C to D	D to E	E to F	
0	0.00	0.00	102	0	0	0	0	0	0	0	
1	0.09	5.44	102	0	0	0	0	0	0	0	
2	0.14	8.82	102	0	0	0	0	0	0	0	
3	0.14	8.82	102	0	0	0	0	0	0	0	
4	0.30	15.72	98	2	2	0	0	0	0	0	
5	0.57	20.81	91	3	4	2	1	1	0	0	
6	0.93	23.65	86	0	4	1	3	8	0	0	
7	1.21	25.17	84	2	0	1	2	10	3	0	
8	1.72	26.86	83	1	2	0	0	5	11	0	
9	2.10	28.68	82	2	1	1	0	3	13	0	
10	2.21	29.17	82	2	1	0	0	2	15	0	
11	2.21	29.18	82	2	0	0	0	3	15	0	
12	2.21	29.18	82	2	0	0	0	3	15	0	
13	2.62	30.64	82	2	0	0	0	0	18	0	
14	2.68	30.86	82	2	0	0	0	0	17	1	

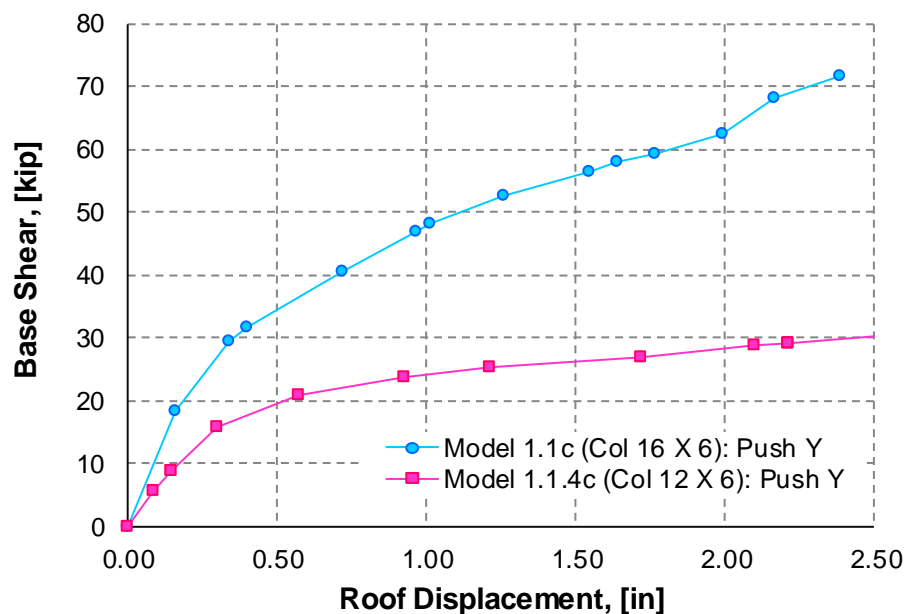
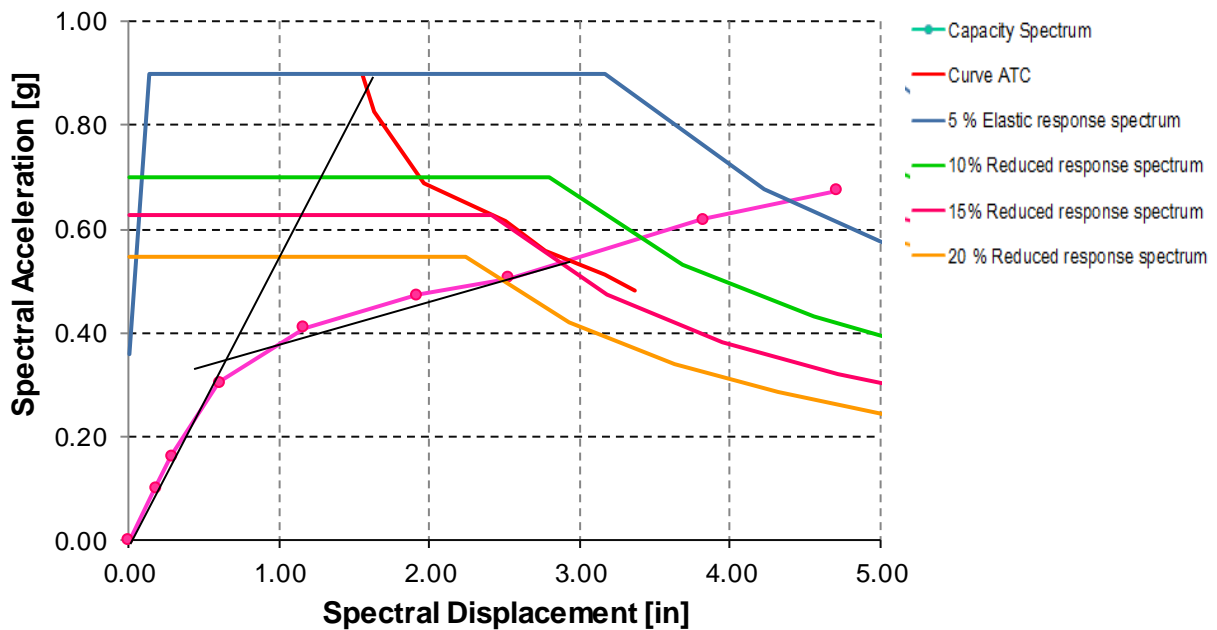


**Figure 6-111.** Comparison Pushover Curves for Model 1.1b and Model 1.1.4c: Push Y

From Figure 6-111 it can be observed that the capacity in the Y directions for Model 1.1.4b drops as the column size decrease. The maximum base shear obtained from the pushover analysis for Model 1.1c and Model 1.1.5c are 71.72 kip and 30.86 kip respectively. The drop in the capacity is due to the decrease in columns size in the X direction. It has been observed that due to the torsion the pushover analysis results are affected due to the interaction of both directions.



$$\begin{aligned}
 S_{app} &= 0.54 \text{ g} & V_{pp} &= 25.64 \text{ k} \\
 S_{dpp} &= 2.84 \text{ in} & D_{pp} &= 1.35 \text{ in} \\
 S_{dy} &= 0.60 \text{ in} \\
 \mu_d &= 4.73
 \end{aligned}$$

**Figure 6-112.** Performance Point for Model 1.1.4c: Push Y

From Figure 6-112 at the performance point the spectral displacement ( $S_d$ ) and spectral acceleration ( $S_a$ ) are 2.84 in. and 0.54 g respectively. The ductility demand is 4.73. In terms of the performance point (step 7) it can be observed from Table 6-53 that the demand curve intersects the capacity curve beyond collapse (C) limit level. In other word the model performance is not safe.

## 6.2.6 PUSHOVER ANALYSIS SUMMARY RESULTS

This section contains Tables 6-54 to 6-56 with a summary of the results obtained from the pushover analysis.

**Table 6-54.** Summary Results Pushover Analysis Models 1

Model	T	Direction	Performance Point						Ultimate Force	
			Force (k)	Disp. (in)	$S_{app}$ (g)	$S_{dpp}$ (in)	$S_{dy}$ (in)	$\mu_d$	Force (k)	Disp. (in)
1.1b	0.19	X	77.67	0.42	0.68	0.38	0.18	2.11	0.00	0.00
	0.47	Y	NR	NR	NR	NR	NR	NR	13.92	2.39
1.1c	0.19	X	76.64	0.40	0.70	0.37	0.21	1.78	117.87	2.24
	0.31	Y	36.40	0.57	0.68	1.11	0.46	2.41	68.14	2.40
1.1d	0.18	X	-	-	-	-	-	-	-	-
	0.33	Y	44.16	0.69	0.79	1.39	0.40	3.48	115.76	2.40
1.2b	0.22	X	-	-	-	-	-	-	-	-
	0.54	Y	NR	NR	NR	NR	NR	NR	13.92	2.39
1.2c	0.22	X	-	-	-	-	-	-	-	-
	0.29	Y	38.71	0.37	0.70	0.95	0.39	2.44	75.47	1.75
1.2d	0.19	X	-	-	-	-	-	-	-	-
	0.29	Y	48.78	0.42	0.82	1.09	0.38	2.87	200.49	2.40
1.3b	0.23	X	94.94	0.73	0.61	0.68	0.25	2.72	116.95	2.41
	0.59	Y	-	-	-	-	-	-	-	-
1.3c	0.23	X	-	-	-	-	-	-	-	-
	0.48	Y	44.56	1.97	0.50	3.40	0.51	3.40	48.23	2.38
1.3d	0.22	X	-	-	-	-	-	-	-	-
	0.51	Y	58.23	1.98	0.64	3.40	0.52	6.54	68.93	2.44
1.4b	0.26	X	117.30	1.51	0.55	1.45	0.30	4.83	127.97	2.41
	0.65	Y	NA	NA	NR	NR			15.04	1.78
1.4c	0.26	X	-	-	-	-	-	-	-	-
	0.44	Y	51.99	1.52	0.52	3.12	0.52	6.00	69.12	2.42
1.4d	0.23	X	-	-	-	-	-	-	-	-
	0.44	Y	82.60	1.47	0.76	2.95	0.60	4.92	122.41	2.41

NR = Performance Point Not Reached

Not Analyzed

**Table 6-55. Summary Results Pushover Analysis Models 2**

Model	T	Direction	Performance Point						Ultimate Force	
			Force (k)	Disp. (in)	$S_{app}$ (g)	$S_{dpp}$ (in)	$S_{dy}$ (in)	$\mu_d$	Force (k)	Disp. (in)
2.1b	0.29	X	87.45	0.91	0.70	0.84	0.40	2.11	106.20	3.97
	0.66	Y	NR	NR	NR	NR			18.15	3.60
2.1c	0.29	X	-	-	-	-	-	-	-	-
	0.44	Y	41.07	1.24	0.67	2.37	0.95	2.49	57.55	3.60
2.1d	0.29	X	-	-	-	-	-	-	-	-
	0.45	Y	66.69	73.63	0.69	2.54	0.90	2.82	59.70	2.29
2.2b	0.34	X	96.52	1.75	0.57	1.64	0.60	2.73	113.79	5.94
	0.80	Y	NR	NR	NR	NR	NR		18.96	3.60
2.2c	0.34	X	-	-	-	-	-	-	-	-
	0.43	Y	43.41	0.89	0.66	2.17	0.95	2.28	64.29	3.60
2.2d	0.33	X	-	-	-	-	-	-	-	-
	0.45	Y	46.69	0.86	0.70	2.17	1.05	2.07	51.09	1.08
2.3b	0.37	X	0.00	97.99	0.00	0.58	1.86	0.31	105.59	105.59
	0.81	Y	-	-	-	-	-	-	-	-
2.3c	0.37	X	-	-	-	-	-	-	-	-
	0.67	Y	37.05	2.60	0.38	4.34	0.90	4.82	41.22	3.60
2.3d	0.37	X	-	-	-	-	-	-	-	-
	0.68	Y	42.24	2.46	0.43	4.10	1.22	3.36	49.35	3.76
2.4b	0.37	X	0.00	107.62	0.00	0.47	2.98	0.16	108.55	3.26
	0.81	Y	NR	NR	NR	NR			18.65	2.64
2.4c	0.37	X	-	-	-	-	-	-	-	-
	0.67	Y	44.03	2.10	0.39	4.14	1.10	3.76	51.02	3.60
2.4d	0.37	X	-	-	-	-	-	-	-	-
	0.68	Y	52.31	2.02	0.44	3.94	1.50	2.63	67.33	3.57


NR = Performance Point Not Reached

 Not Analyzed

**Table 6-56.** Summary Results Pushover Analysis Models 1.1 with Variation

Model	T	Direction	Performance Point						Ultimate Force	
			Force (k)	Disp. (in)	$S_{app}$ (g)	$S_{dpp}$ (in)	$S_{dy}$ (in)	$\mu_d$	Force (k)	Disp. (in)
<b>1.1by</b>	0.19	<b>X</b>	NR	NR	NR	NR	NR		27.15	2.40
	0.47	<b>Y</b>	33.20	0.41	0.77	1.00	0.70	1.43	51.80	2.40
<b>1.1cy</b>	0.19	<b>X</b>	-	-	-	-	-	-	-	-
	0.18	<b>Y</b>	36.74	0.37	0.74	0.75	0.45	1.67	36.74	0.37
<b>1.1.2b</b>	0.17	<b>X</b>	81.21	0.33	0.70	0.30	0.20	1.50	103.46	-2.403
	0.33	<b>Y</b>	NR	NR	NR	NR	NR	NR	23.92	2.45
<b>1.1.2c</b>	0.17	<b>X</b>	-	-	-	-	-	-	-	-
	0.43	<b>Y</b>	39.29	0.37	0.84	0.74	0.40	1.85	74.31	2.42
<b>1.1.3b</b>	0.20	<b>X</b>	77.93	0.47	0.67	0.45	0.22	2.06	77.93	0.47
	0.27	<b>Y</b>	56.73	0.45	0.79	0.70	0.42	1.67	78.04	2.41
<b>1.1.3c</b>	0.20	<b>X</b>	-	-					-	-
	0.26	<b>Y</b>	45.11	0.32	0.82	0.66	0.50	1.32	90.22	2.40
<b>1.1.4b</b>	0.26	<b>X</b>	NR	NR	NR	NR	NR	NR	35.18	-2.95
	0.55	<b>Y</b>	NR	NR	NR	NR	NR	NR	15.45	3.02
<b>1.1.4c</b>	0.26	<b>X</b>	-	-	-	-	-	-	-	-
	0.42	<b>Y</b>	25.64	1.35	0.54	2.84	0.60	4.73	30.86	2.68

NR = Performance Point Not Reached

 Not Analyzed

The following general conclusions are derived from the pushover:

- The capacity predictions of the mode shape load pattern was observed to be the critical case, as the capacity curve leads to have less capacity. Therefore after the presentation of Model 1.1, only the mode shape load pattern was used.
- The models are relatively strong at the upper story, since the presence of column hinging was only observed at the lower levels. Plastic hinges formation starts with the frame including the shortest columns of the lower story then propagates to the frames down-hill.

- The models are very vulnerable when loaded in their weak direction. It was observed that the capacity of the models type b (without retaining wall) in the weak direction of the column is much less than in the strong direction of the column. Models 1 and 2 type b failed in the Y direction, no performance point was reached (Tables 6-57 to 6-60)
- When the analytical models had a retaining wall, built either as masonry block walls (type c) or as concrete wall (type d) the capacity of the residence improves significantly. It was observed that concrete shear walls had more stiffness/capacity than masonry block walls. Existence of the retaining wall basically provides higher stiffness and strength for the frames. Retaining wall also caused severe irregularities in stiffness and strength in the residence's elevation and plan. Poor distributions of walls had result in torsional irregular behavior of the residences. Therefore, even if the capacity of the models increases due to the presence of walls the asymmetric location produced torsional problems and this effect is not desirable for the models.
- For Model 2 (3 stories) It was observed that the middle story is more likely to collapse. Most of the damage was concentrated at the middle floor.
- When rectangular columns (16" x 8") were used no performance point was reached in the Y direction even with the increase in columns size for models type b.
- When square columns (12" x 12") were used the overall performance improved in the Y directions.
- When 12" x 6" columns were used it was observed that the capacity in the X directions for Model 1.1.5b drops as the column size decreases. The Y direction was also affected negatively even the column size remains the same dimension due to the torsional effect. It has been mentioned extensively that any modification in the X direction affects the Y direction. The behavior in the Y direction is not symmetric due



to the presence of the retaining wall and the difference in columns length in the frame.

- Overall failure in the models was in flexure and shear failure were not observed at the performance point.
- It was observed that columns are not stronger than beam, forcing initial yielding in these elements.
- Even though many models did not collapse the damages observed are beyond repair.

### **6.3 NONLINEAR TIME HISTORY ANALYSIS RESULTS**

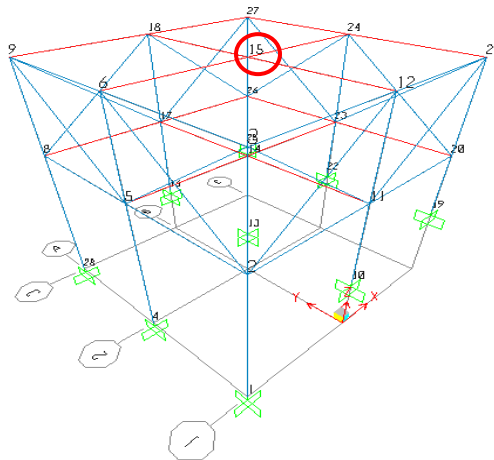
For the nonlinear dynamic response not all the cases were analyzed. The specific criteria for the selection of the models that will be analyzed are described below:

- The pushover analysis results give a preliminary estimate about the performance of the analytical models. Based on the pushover analysis results the models that showed the best performance will be analyzed. In general it can be expected that if these models are not capable of withstanding the earthquakes, the other models will not either. The pushover analysis results showed that the damage and ductility demand the analytical models presented increased when the bay length and number of stories increase. Therefore, Models 1.1 and Models 2.1 will be analyzed. Models 1.4 were also analyzed to compare the results with Model 1.1
- Model 1.1.3 had the best performance overall. Columns for this case were 12 x 12 square sections. Even without any retaining wall the model in the Y direction was able to reach the performance point, and all hinges were at acceptable limit states (Immediate Occupancy and Life Safety).

As discussed in Chapter 4, for the nonlinear time history analysis the models will be subjected to the earthquake records of Parkfield, Northridge, San Salvador IGN and San Salvador CIG.

### 6.3.1 NONLINEAR TIME HISTORY ANALYSIS RESULTS FOR MODEL 1.1b

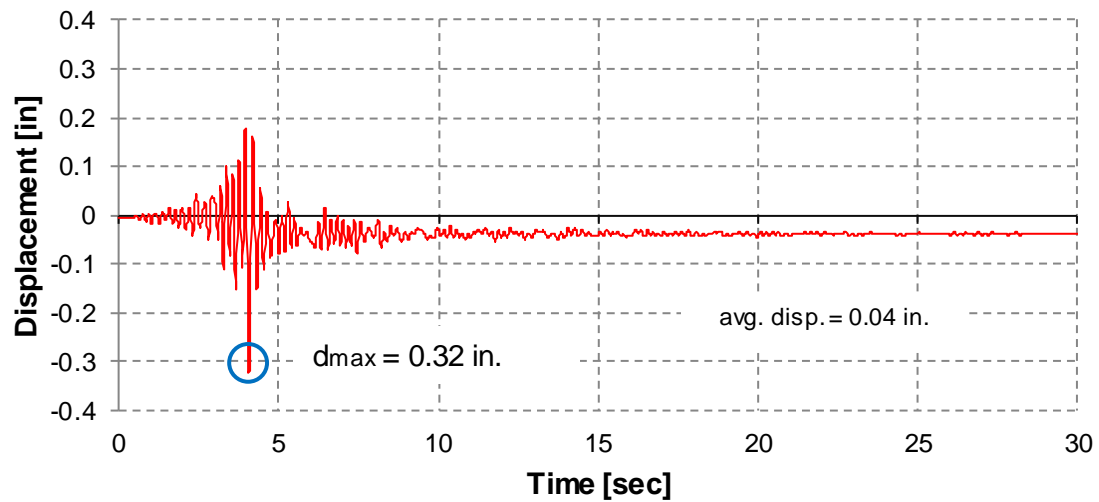
Model 1.1b was analyzed with all 4 records in the X and Y direction. Each section presents the results for the selected records in both directions. The displacement time histories were plotted for joint 15 (Figure 6-113). The maximum displacement and average residual displacement are marked at the displacement history plots. The maximum base shear is marked in the base shear time history plots.



**Figure 6-113.** Joint label for Model 1.1b

#### 6.3.1.1 RESULTS FOR THE PARKFIELD EARTHQUAKE: MODEL 1.1b

The displacement time history, base shear time history and hinge formation were plotted in Figures 6-114 to 6-119 for the earthquake record in the X and Y directions, respectively.

**Model 1.1b: X direction**

**Figure 6-114.** Displacement Time History of Top Joint for Model 1.1b: Parkfield EQ in the X direction

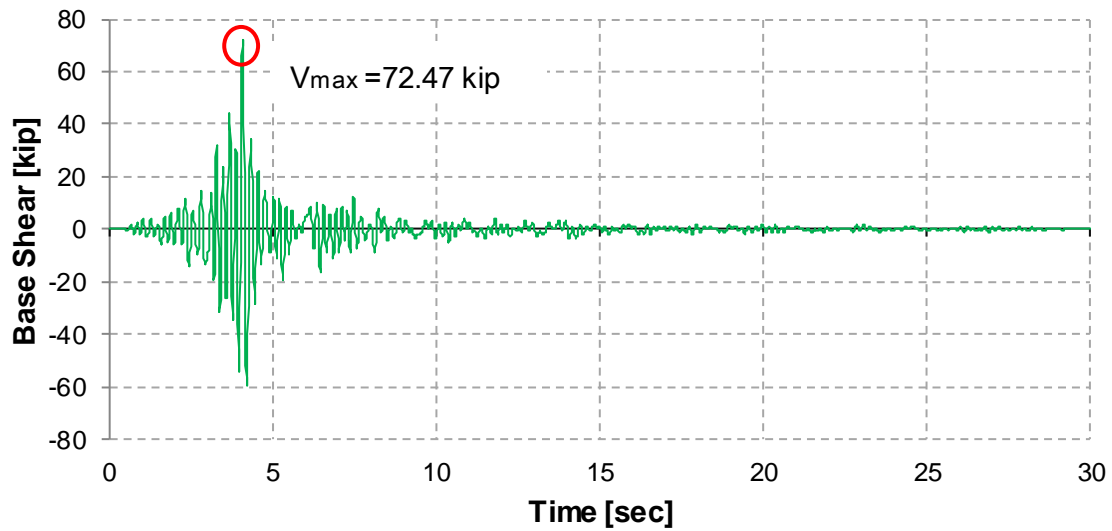


**Figure 6-115.** Base Shear Time History Model 1.1b: Parkfield EQ X direction

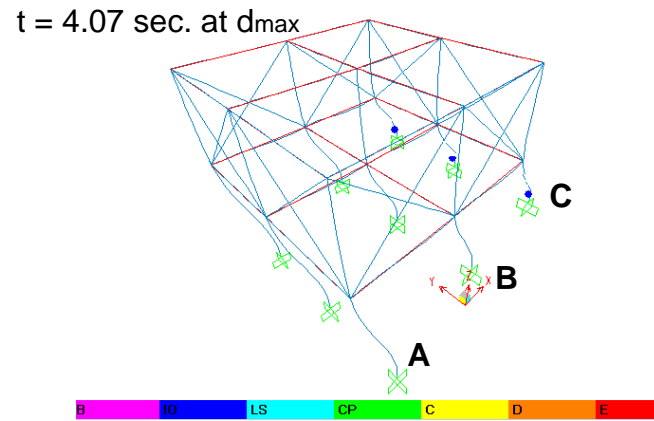


Figure 6-116. Hinge Formation for Model 1.1b: Parkfield EQ X Direction

### Model 1.1b: Y direction

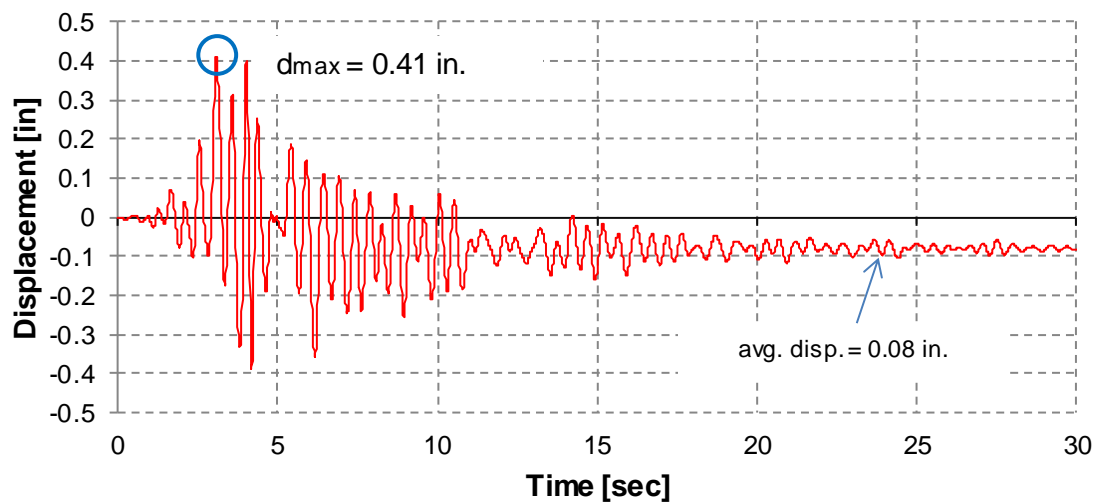
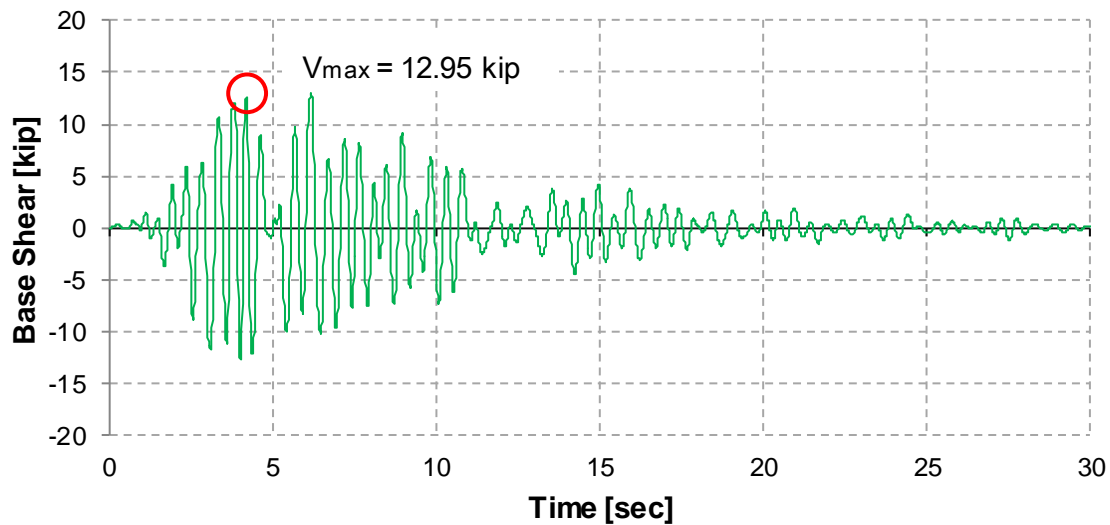
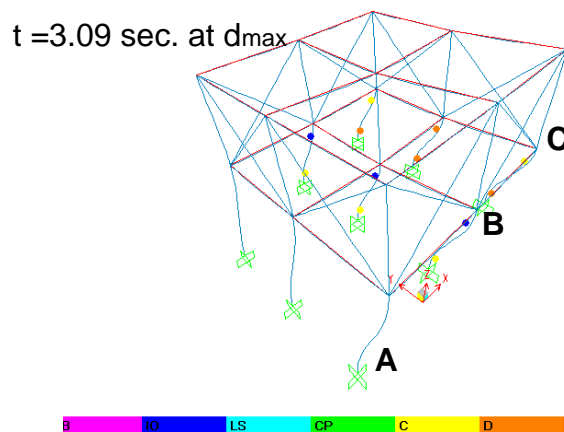


Figure 6-117. Displacement Time History of Top Joint for Model 1.1b: Parkfield EQ in the Y Direction



**Figure 6-118.** Base Shear Time History Model 1.1b: Parkfield EQ Y Direction



**Figure 6-119.** Hinge Formation for Model 1.1b: Parkfield EQ Y Direction

From Figures 6-114 and 6-115 it can be noticed that the maximum displacement and base shear in the X direction for Parkfield record was 0.32 inches and 72.45 kip, respectively. When the maximum displacement occurs at 4.07 seconds, plastic hinges were formed at the bottoms of the columns at frame C (Figure 6-116) all within the Immediate Occupancy (IO) limit state. This fact is also observed on Figure 6-113 where the displacement history is not oscillating around zero after 6.5 seconds approximately, indicating that a permanent damage is present in the model. The average residual displacement was approximately 0.04 inches. Based on the results the model is capable of withstanding the Parkfield earthquake, local damage was only observed at frame C bottom columns within the Immediate Occupancy limit level. This means the post-

earthquake structural damage is very limited, for example minor cracking at bottom of columns at frame C is expected.

From Figures 6-117 and 6-118 it can be noticed that the maximum displacement and base shear in the Y direction for Parkfield earthquake record was 0.41 inches and 12.95 kip respectively. The maximum displacement occurs at 3.09 seconds. From Figure 6-116 it can be noticed that at 10.70 seconds of the time history analyses present permanent deformation since the displacement traces were shifted from the origin. The residual displacement was approximately 0.08 inches. At 3.09 sec. of the analysis plastic hinges were formed at the bottoms and top of the columns at frame C and B (Figure 6-118). All three bottom hinges at frame C are beyond Collapse limit state. It was mentioned before that when a hinge state is beyond the Collapse limit level it represents the initial failure of the element. It is associated with fracture of longitudinal reinforcement and spalling of concrete. Little residual stiffness and strength remains in the structural element. Structural repair for elements with this level of damage is considered not feasible. Similar as it occurred in the pushover analysis, hinge sequence start with the shortest columns (frame C) and propagates downhill (frame B and A).

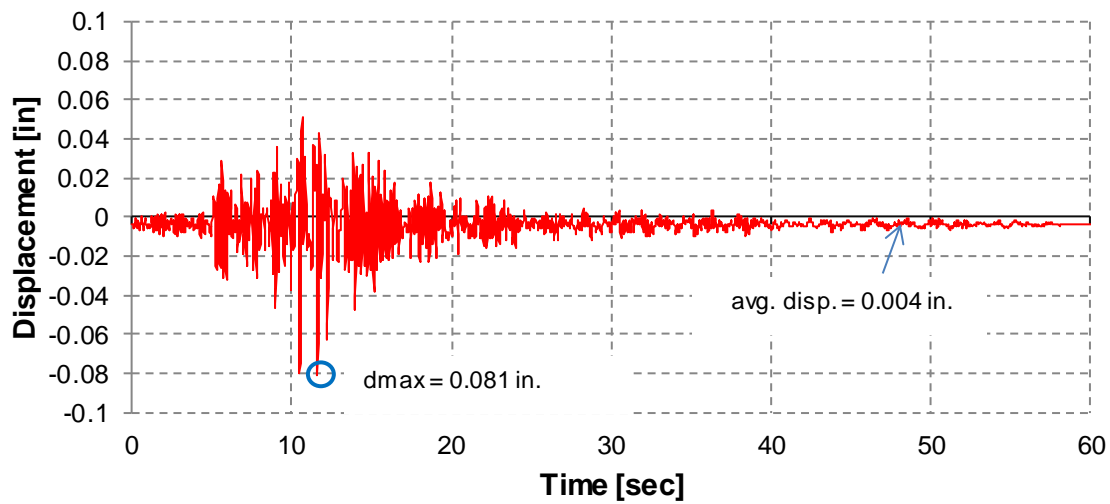
Comparing the results, the maximum response was observed in the Y direction where lateral displacement was 30.0 percent higher than those induced in the X direction. In terms of the damage state, the Y direction resulted with significant more damage. In the X direction all hinges were at Immediate Occupancy level, while in the Y direction hinges formed beyond Collapse limit state. This tendency also compares with the results from the pushover analysis; it was observed that Y is the critical direction due to its weak column orientation.

#### **6.3.1.2 RESULTS FOR THE NORTHRIDGE EARTHQUAKE: MODEL 1.1b**

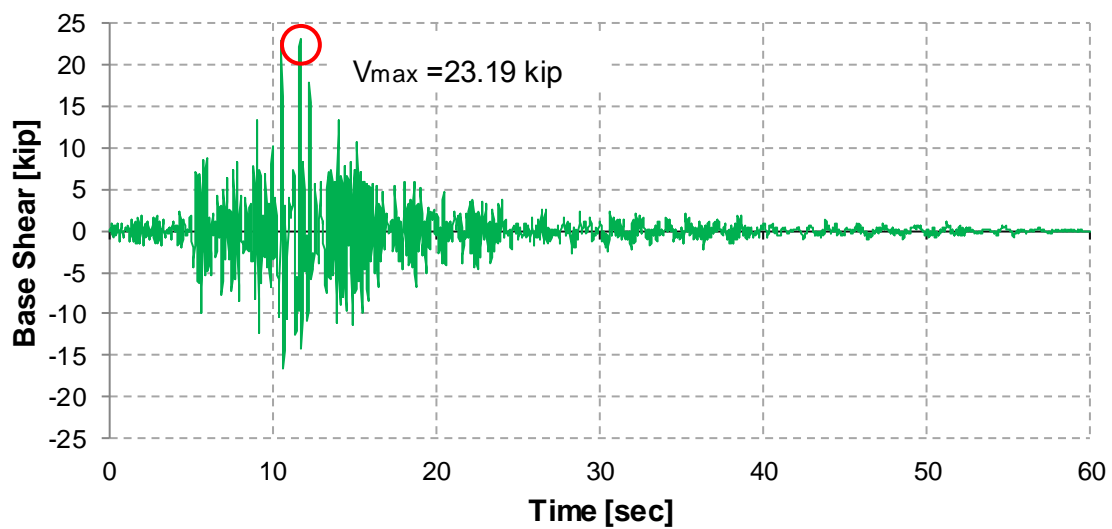
The displacement time history and base shear time history and hinge formation were plotted in Figures 6-120 to 6-124 for the earthquake in the X and Y directions,

respectively. A discussion of the above figures cited before is presented at the end of the section.

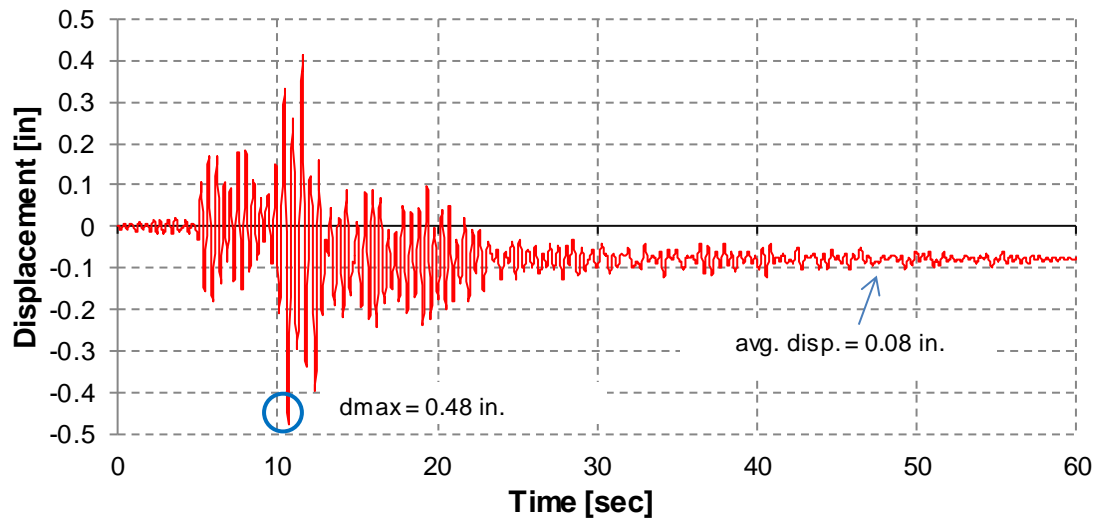
### **Model 1.1b: X direction**



**Figure 6-120.** Displacement Time History of Top Joint for Model 1.1b: Northridge EQ in the X Direction



**Figure 6-121.** Base Shear Time History Model 1.1b: Northridge EQ X Direction

**Model 1.1b: Y direction**

**Figure 6-122.** Displacement Time History of Top Joint for Model 1.1b: Northridge EQ in the Y Direction

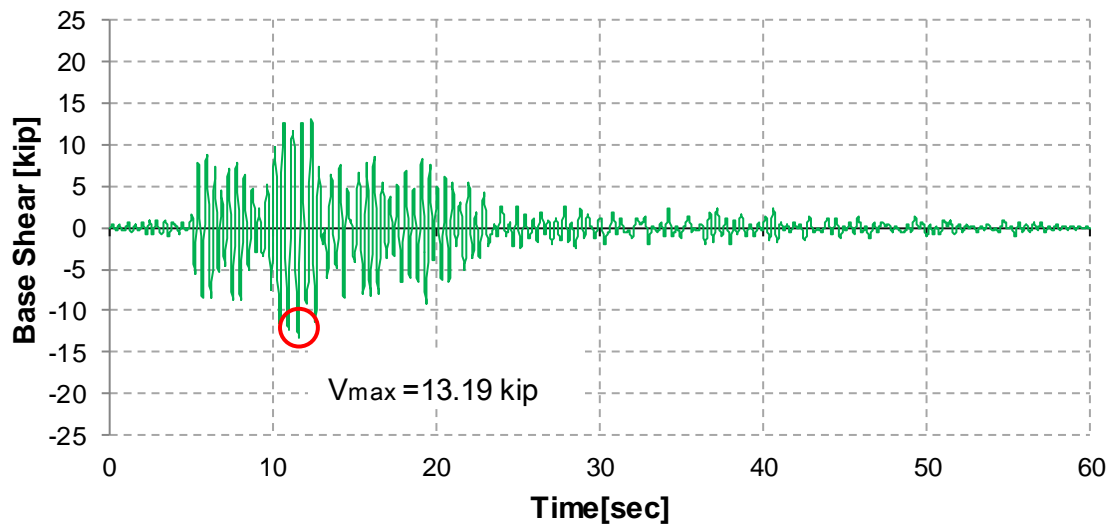


**Figure 6-123.** Base Shear Time History Model 1.1b: Northridge EQ Y Direction



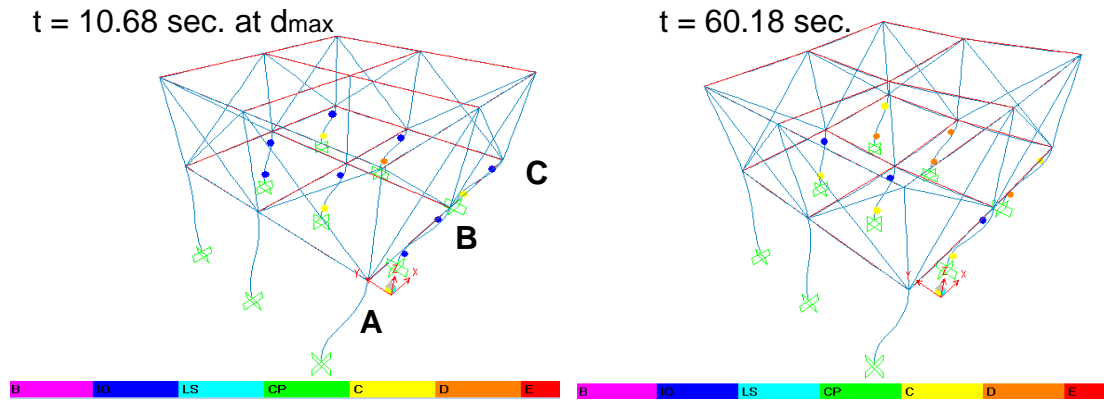


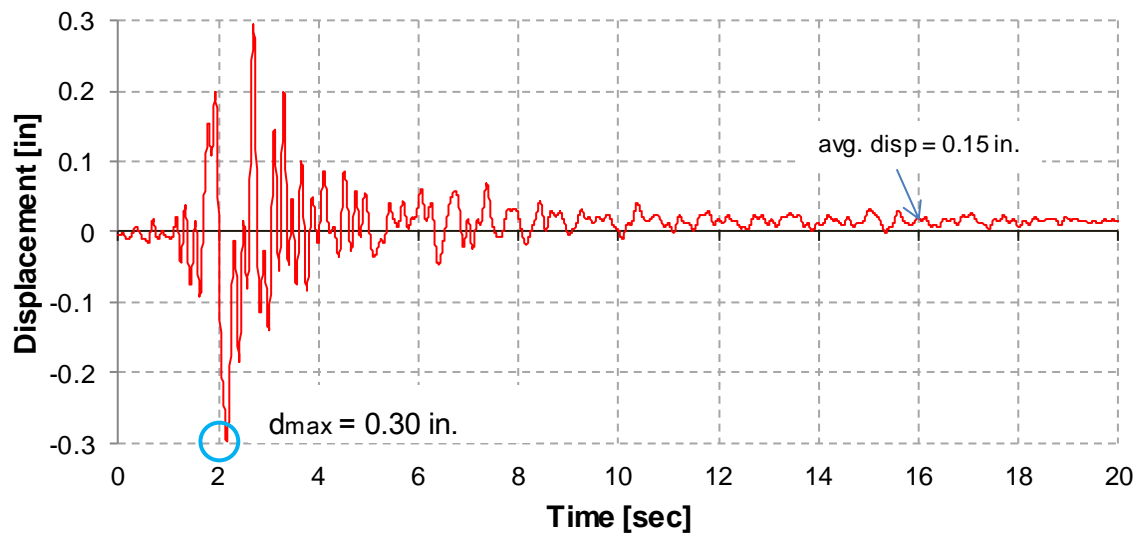
**Figure 6-124. Hinge Formation for Model 1.1b: Northridge EQ Y Direction**

The maximum displacement and base shear in the X direction for Northridge earthquake record was 0.081 inches and 23.19 kip, respectively. No plastic hinges were formed at the columns or beams during the analysis, meaning that the model is capable of withstanding the Northridge earthquake in the elastic range. The residual displacement was negligible, approximately 0.004 inches.

The maximum displacement and base shear in the Y direction for Northridge earthquake was 0.47 inches and 13.19 kip respectively. The displacement history show residual displacements due to the incursion in the nonlinear behavior. The average residual displacement was approximately 0.08 inches. At maximum displacement several hinges have formed at the top and bottom of the columns (Figure 6-124). At the end of the analysis plastic hinges were formed at the bottoms and top of the columns at frame C and B. Plastic hinges at frame C where all at or beyond collapse limit state. At frame B upper column hinges are within the Immediate Occupancy (IO) limit state and bottom hinges are at collapse limit state.

### 6.3.1.3 RESULTS FOR THE SAN SALVADOR IGN EARTHQUAKE: MODEL 1.1b

The displacement time history, base shear time history and hinge formation were plotted in Figures 6-125 to 6-130 for the earthquake in the X and Y directions, respectively. A discussion of the figures is presented at the end of the section

**Model 1.1b: X direction**

**Figure 6-125.** Displacement Time History of Top joint for Model 1.1b: San Salvador IGN EQ in the X Direction

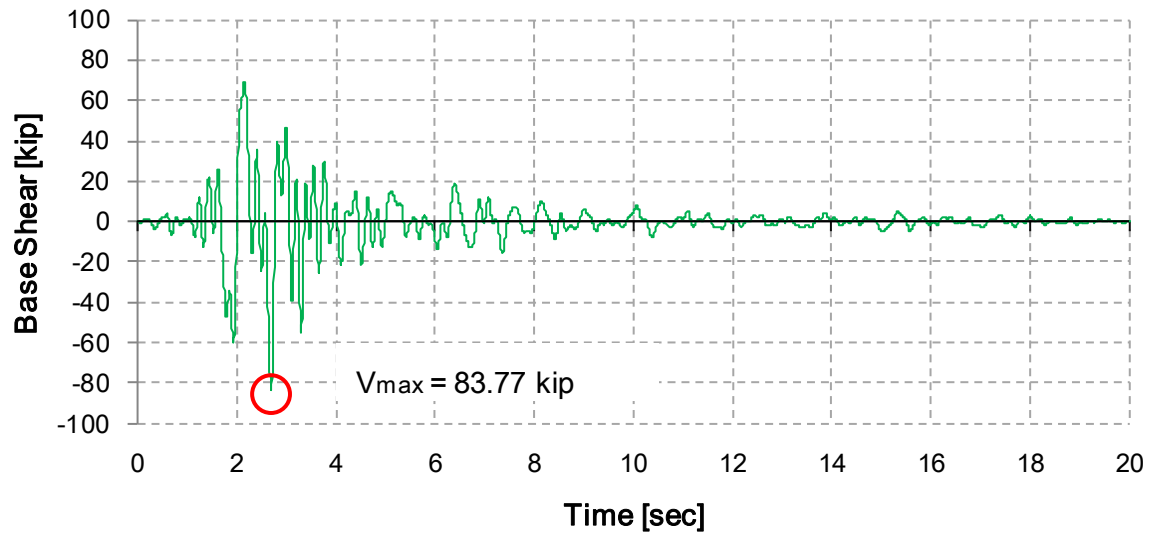


**Figure 6-126.** Base Shear Time History Model 1.1b: San Salvador IGN EQ X Direction

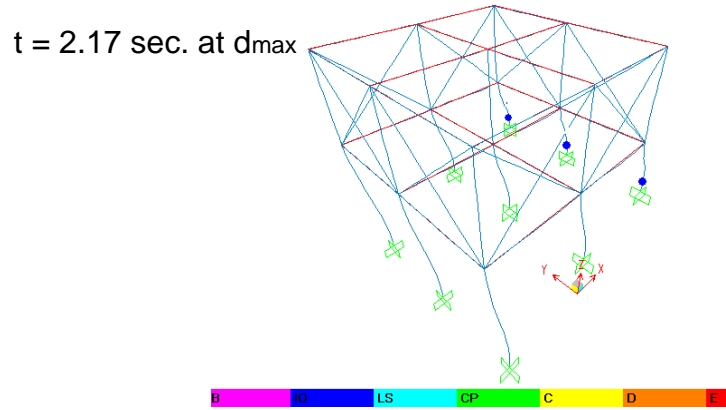


**Figure 6-127.** Hinge Formation for Model 1.1b: San Salvador IGN EQ X Direction

**Model 1.1b: Y direction**

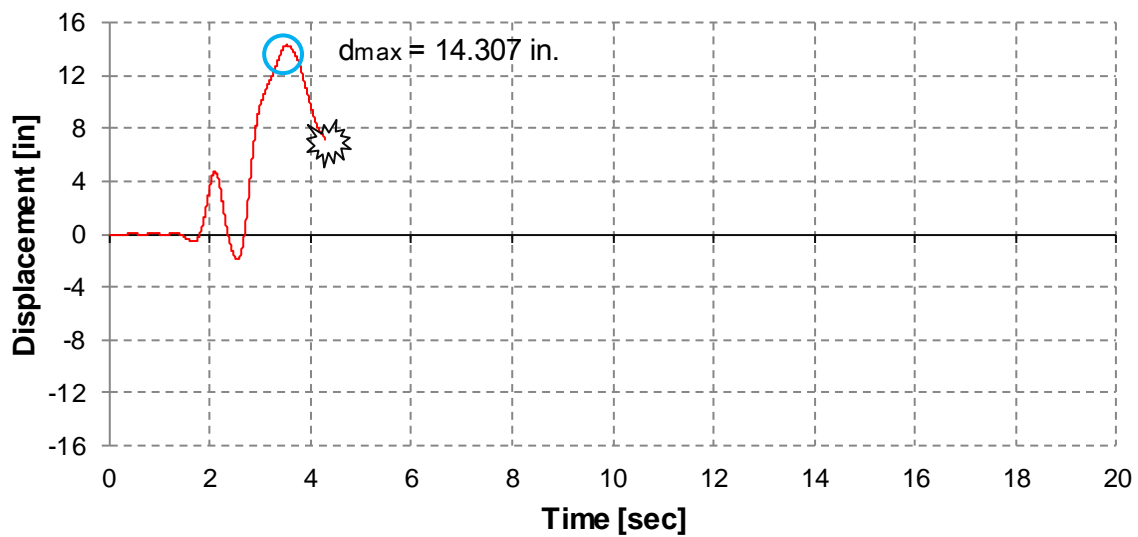


**Figure 6-128.** Displacement Time History of Top Joint for Model 1.1b: San Salvador IGN EQ in the Y Direction

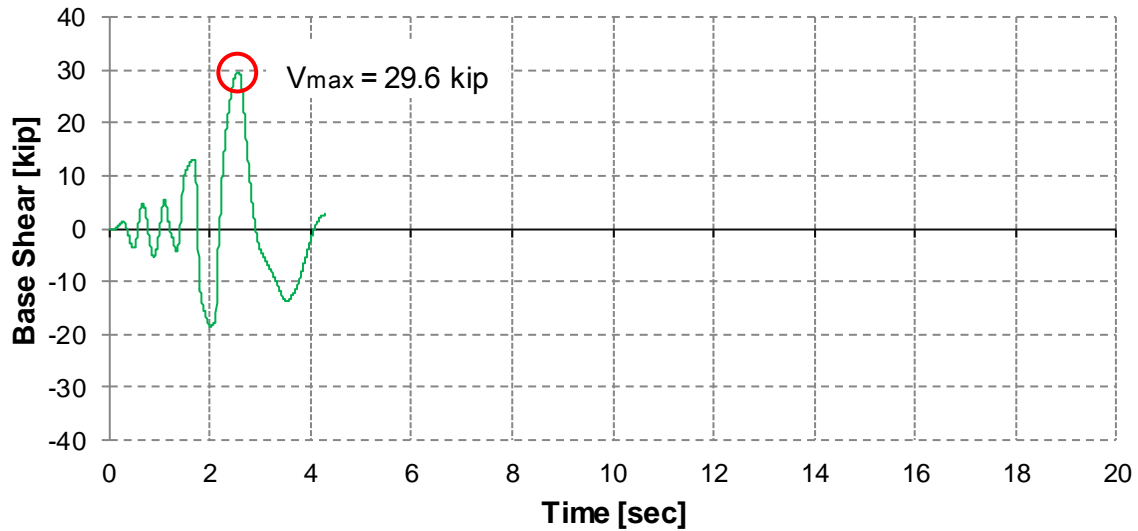


**Figure 6-129.** Base Shear Time History Model 1.1b: San Salvador IGN EQ Y Direction

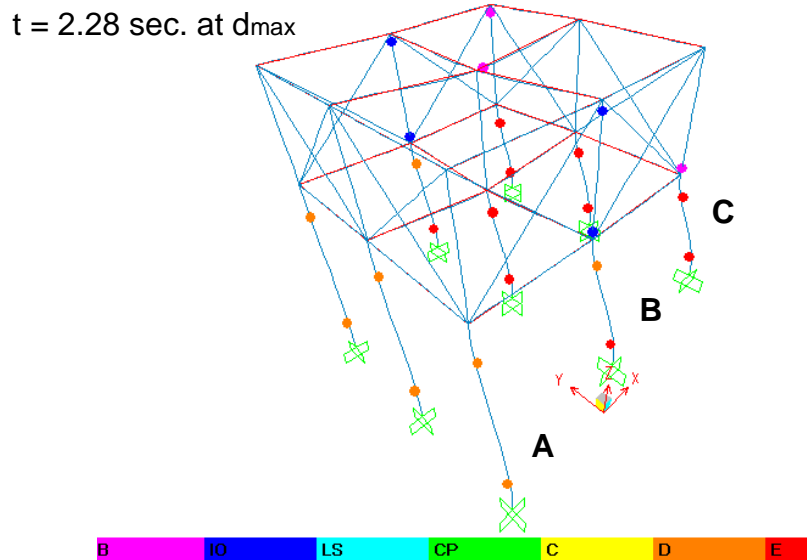


**Figure 6-130.** Hinge Formation for Model 1.1b: San Salvador IGN EQ Y Direction

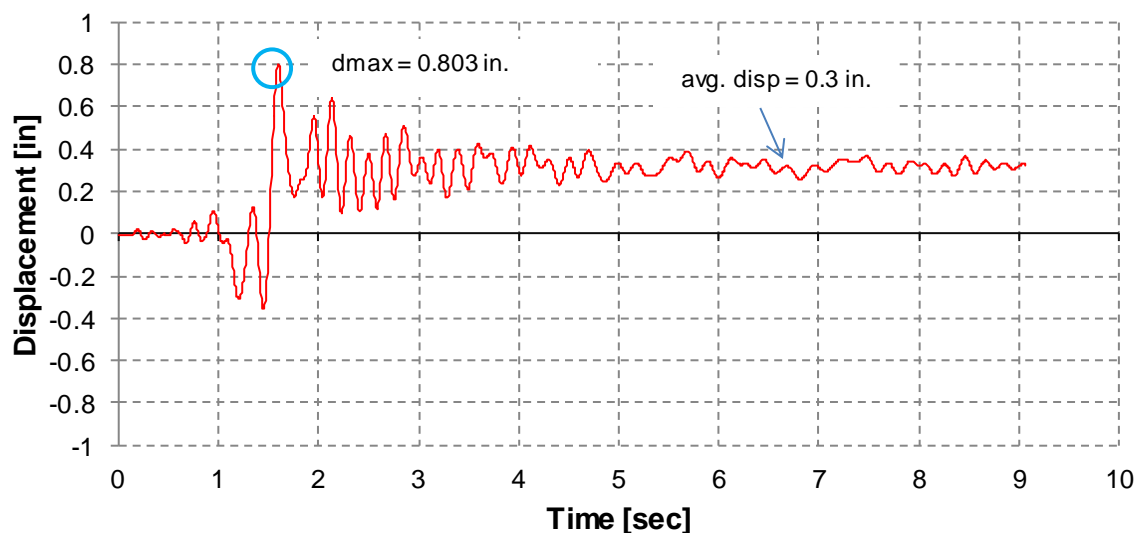
The maximum displacement and base shear in the X direction for San Salvador IGN earthquake was 0.29 inches and 83.77 kip respectively. The average residual displacement was approximately 0.15 inches. The maximum displacement occurs at 2.17 seconds; at this instance only at the bottom columns at frame C (Figure 6-127) hinge have formed all within Immediate Occupancy limit level.

The maximum displacement and base shear in the Y direction for San Salvador IGN earthquake was 14.03 inches and 29.6 kip respectively. So large displacement do not seem to be realistic, collapse is assumed to occur since a small increment in the ground motion intensity produces a large increase in the structural response (Figure 6-128). The analysis was stopped at 4.3 sec. The program failed to converge at this time steps, which can be linked to the unstable state of the model. When the maximum displacement occurs at 2.28 seconds, hinges at frame C have failed (E). At frame B, two hinges are at D limit state and 4 hinges are at E limit state, at frame A all column hinges have reached D limit state.

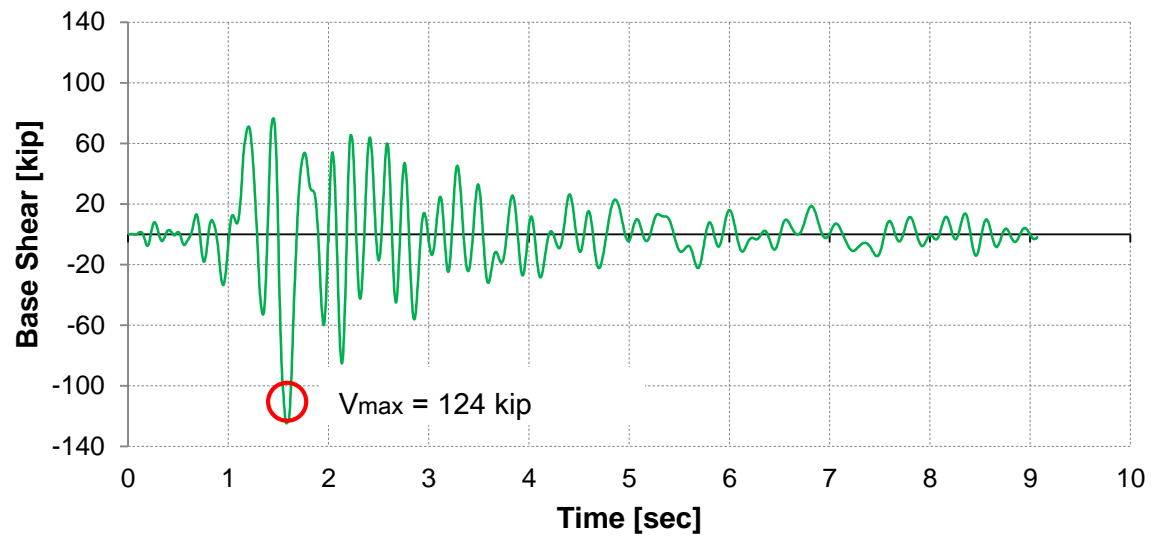
#### 6.3.1.4 RESULTS FOR THE SAN SALVADOR CIG EARTQUAKE: MODEL 1.1b

The displacement time history, base shear time history and hinge formation were plotted in Figures 6-131 to 6-136 for the earthquake in the X and Y directions, respectively. A discussion of the figures is presented at the end of the section.

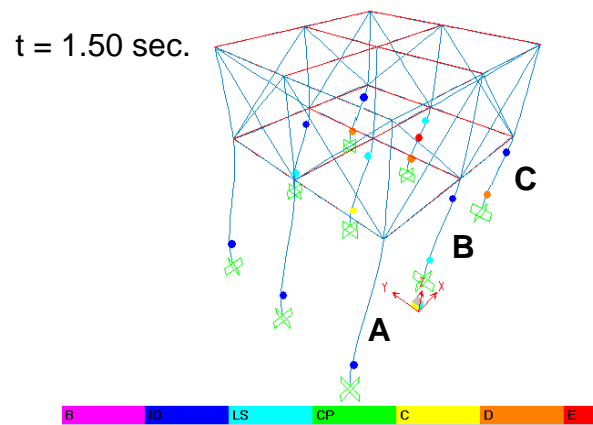
##### Model 1.1b: X direction



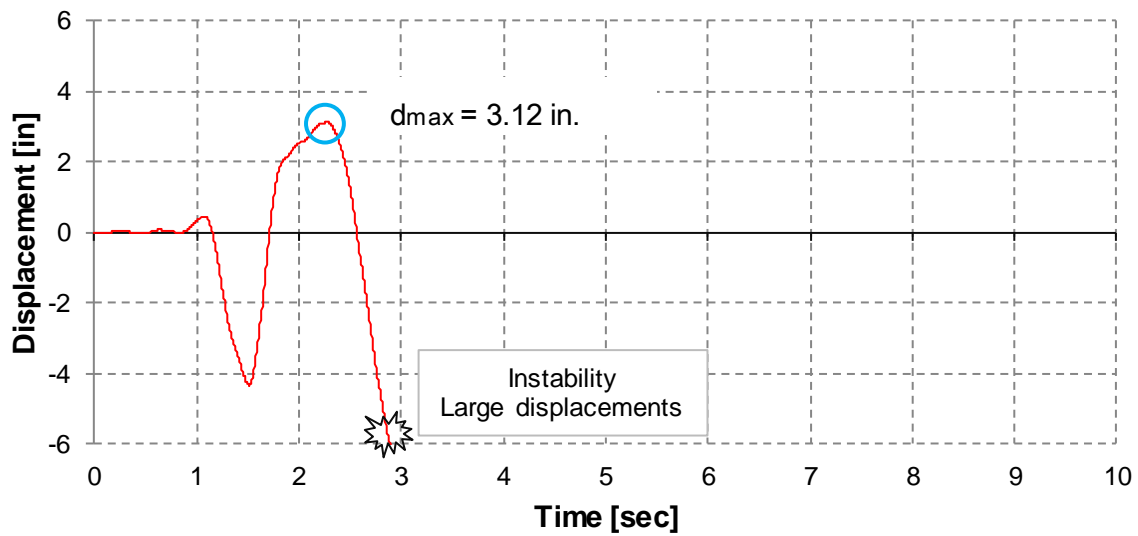
**Figure 6-131.** Displacement Time History of Top Joint for Model 1.1b: San Salvador CIG EQ in the X Direction



**Figure 6-132.** Base Shear Time history Model 1.1b: San Salvador CIG EQ X Direction



**Figure 6-133.** Hinge Formation for Model 1.1b: San Salvador CIG EQ X Direction

**Model 1.1b: Y direction**

**Figure 6-134.** Displacement Time History of Top joint for Model 1.1b: San Salvador CIG EQ in the Y Direction

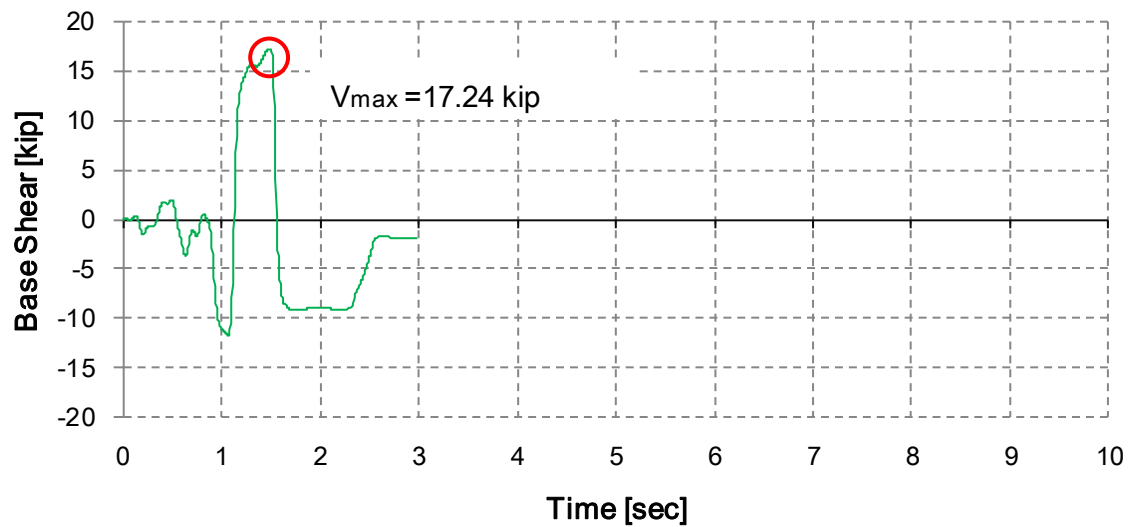


**Figure 6-135.** Base Shear Time History Model 1.1b: San Salvador CIG Y Direction

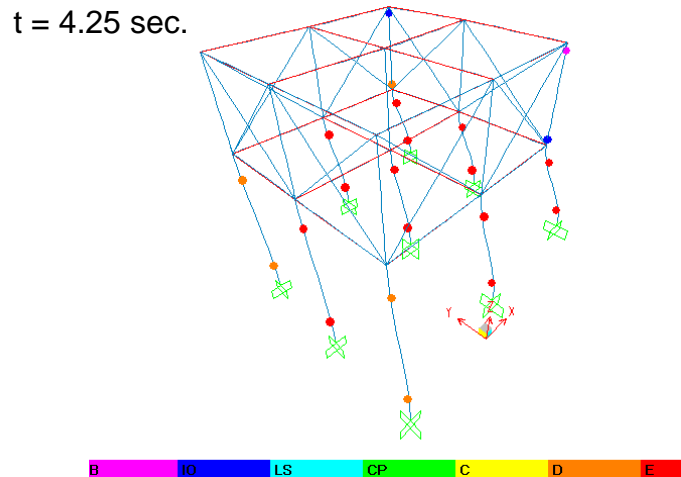


**Figure 6-136.** Hinge Formation for San Salvador CIG EQ Y Direction

The maximum displacement and base shear in the X direction for San Salvador CIG earthquake was 0.80 inches and 124 kip, respectively. The average residual displacement was approximately 0.30 inches. Hinge formed at the bottom of columns at frame C (Figure 6-133) are beyond Collapse limit state at 1.5 second when residual displacements started approximately. The middle column at frame C shows shear failure.

The maximum displacement and base shear in the Y direction for San Salvador CIG earthquake was 3.12 inches and 17.24 kip, respectively. The analysis was stopped at 4.25 seconds. Same as it was observed for the San Salvador IGN, collapse occurred. At 4.25 seconds, all columns at the lower story have failed (Figure 6-136).

### 6.3.2 NONLINEAR TIME HISTORY ANALYSIS RESULTS FOR MODEL 1.1c

For Model 1.1c the nonlinear time history analysis was only carried out for the two San Salvador records (IGN and CIG) in the Y direction. The displacements time histories were plotted for joint 15 and 9 (Figure 6-136). Joint 9 was expected to have higher displacements since the masonry wall induce higher deformation at the opposite edge of the residences.



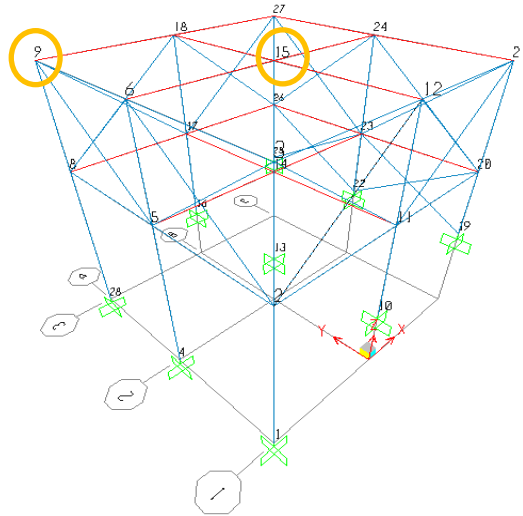


**Figure 6-137.** Joint Label for Model 1.1c

### 6.3.2.1 RESULTS FOR THE SAN SALVADOR IGN EARTQUAKE: MODEL 1.1c

The displacement time history, base shear time history and hinge formation were plotted in Figures 6-138 to 6-140 the earthquake in the Y direction. A discussion of the figures is presented at the end of the section.

#### Model 1.1c: Y direction

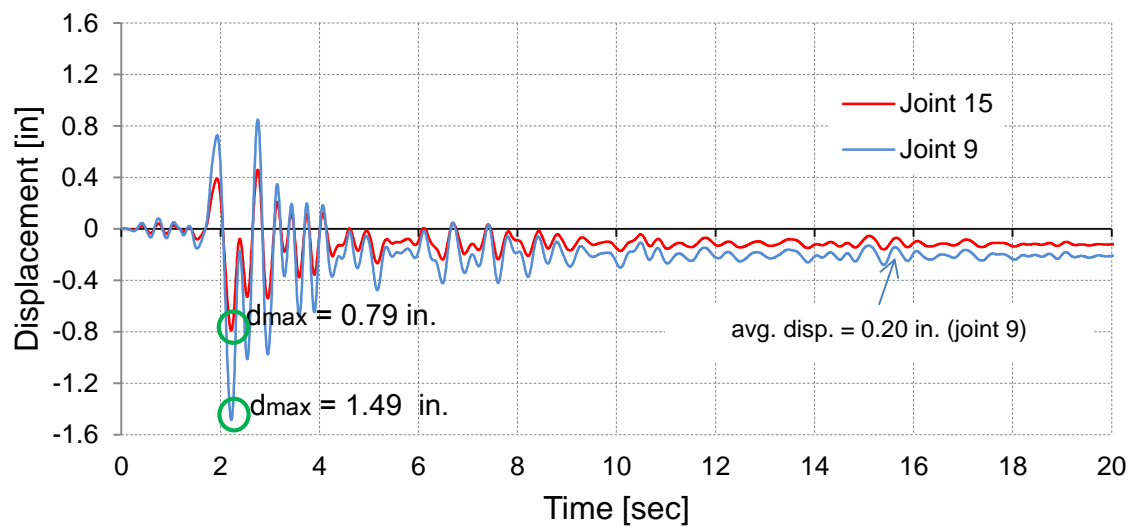


**Figure 6-138.** Displacement Time History of Top Joint for Model 1.1c: San Salvador IGN EQ in the Y Direction

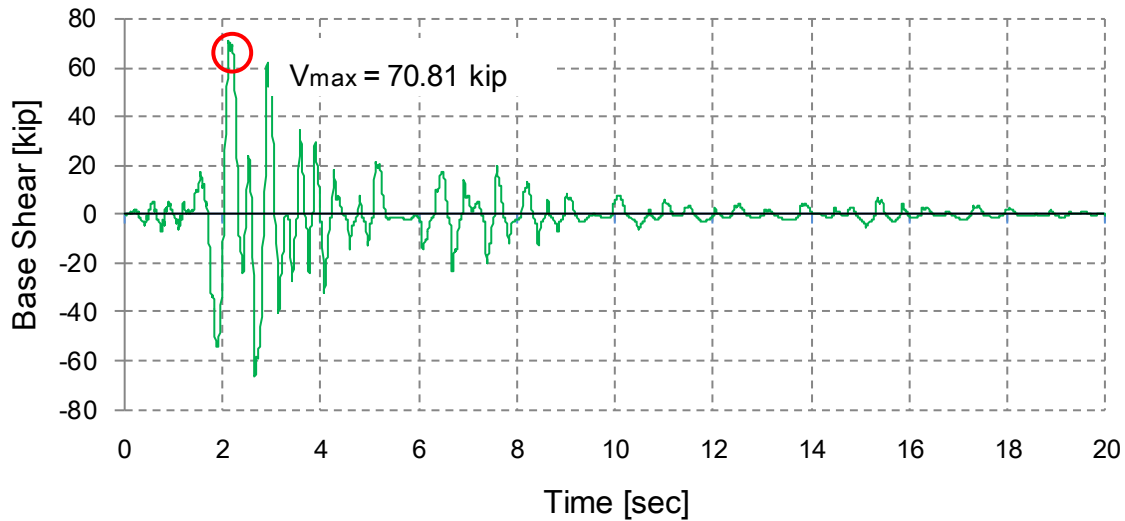


**Figure 6-139.** Base Shear Time History Model 1.1c: San Salvador IGN Y Direction

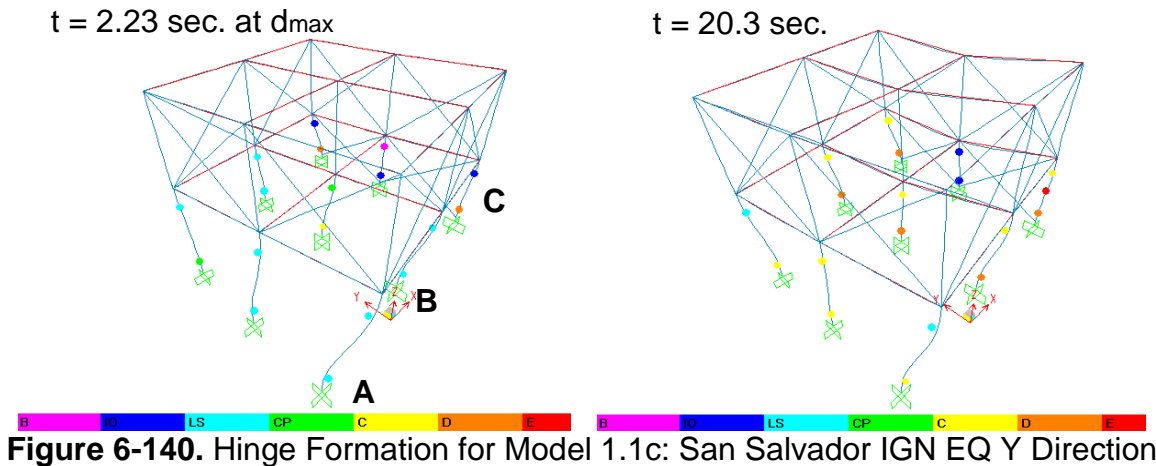


**Figure 6-140.** Hinge Formation for Model 1.1c: San Salvador IGN EQ Y Direction

It can be noticed from Figure 6-138 that at Joint 9 the maximum displacement was 1.49 inches, while for joint 15 the maximum displacement was 0.79 inches. The maximum base shear in the Y direction was 70.81 kip. The average residual displacement was approximately 0.20 inches. When the maximum displacement occurs at 2.23 seconds, plastic hinges are formed at the top and bottom of the columns at frame A, B and C (Figure 6-140). At frame A all hinges are at Life Safety limit state. At frame B top hinge at middle column is at Collapse Prevention limit state and bottom hinge is at Collapse limit state. At frame C, corner bottom hinges are beyond Collapse limit state. At the end of the analysis it can be noticed that six hinges are beyond collapse limit state. Also

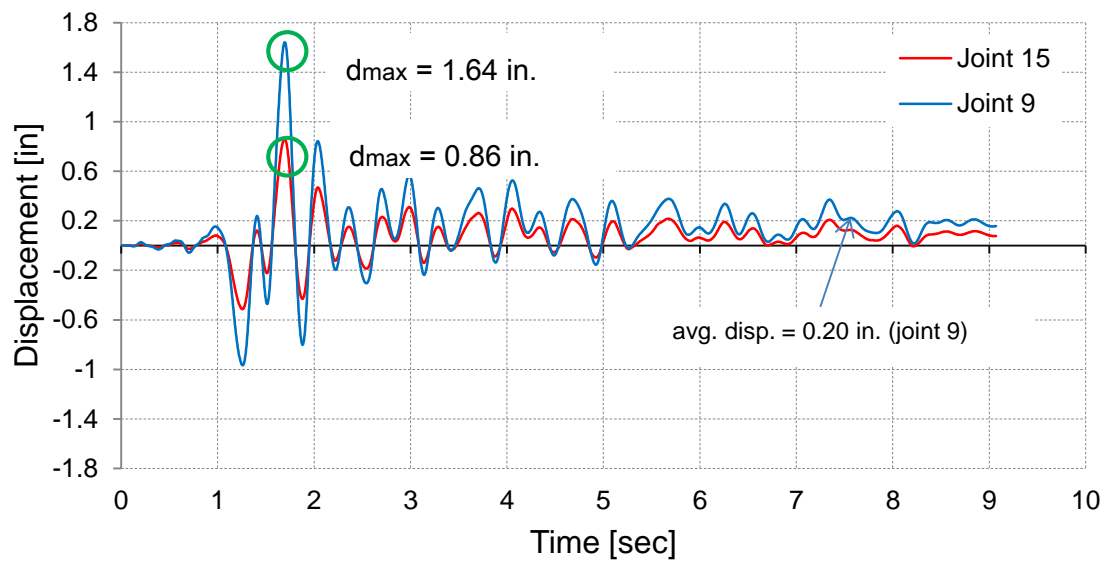
shear hinge formed at the corner column at frame C at 2.92 sec. The shear hinge formed in the (V2) X direction.

Comparing the displacement history with Model 1.1b in the Y direction it can be noticed that due to the presence of the retaining wall complete collapse and instability issues of the model is avoided, however hinges are beyond collapse limit state, meaning that they are no longer able to sustain lateral loads and the remaining capacity is due to the residual strength. In other words substantial damage to those elements has occurred, potentially including significant degradation in the stiffness and strength of the lateral force resisting system. In the aftermath of an earthquake the damage to this structural elements are not repairable and the structure may be needed to be demolished.

This conclusion is comparable with the pushover analysis. The pushover analysis showed that when the model including results from a retaining wall either as masonry wall or RC shear wall the overall capacity of the model increased significantly, however locally the columns at frames A and B suffered severe damage.

#### **6.3.2.2 RESULTS FOR THE SAN SALVADOR CIG EARTQUAKE: MODEL 1.1c**

The displacement time history, base shear time history and hinge formation were plotted in Figures 6-141 to 6-143 for the earthquake in the Y direction. A discussion of the figures is presented at the end of the section.

**Model 1.1c: Y direction**

**Figure 6-141.** Displacement Time History of Top Joint for Model 1.1c: San Salvador CIG EQ in the Y Direction

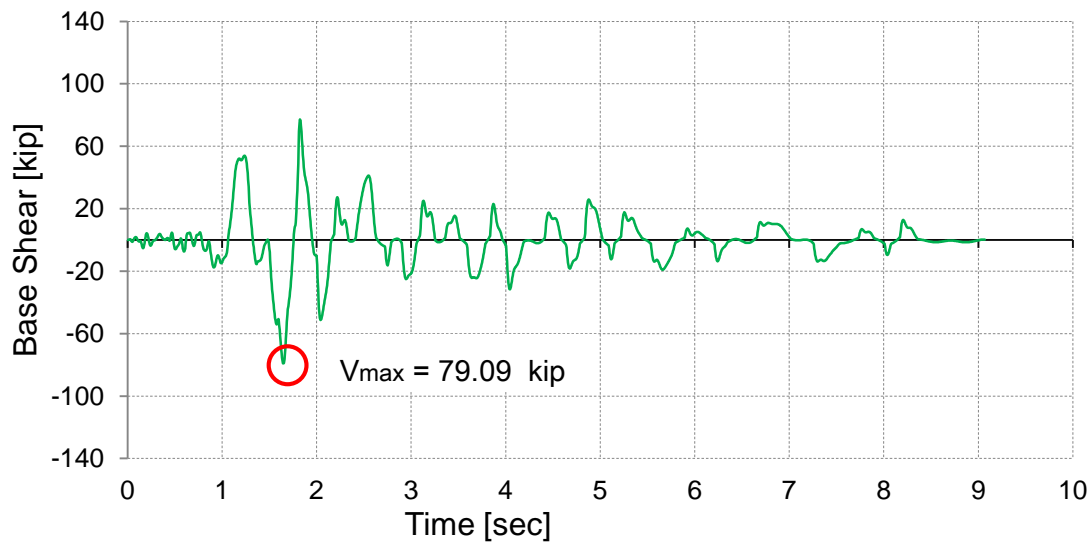


**Figure 6-142.** Base Shear Time history Model 1.1c: San Salvador CIG Y Direction

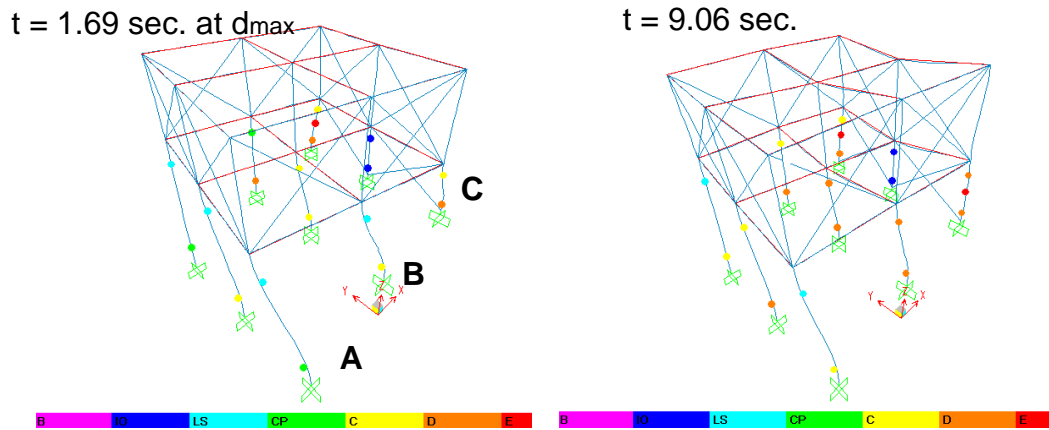


**Figure 6-143.** Hinge Formation for Model 1.1c: San Salvador CIG EQ Y Direction

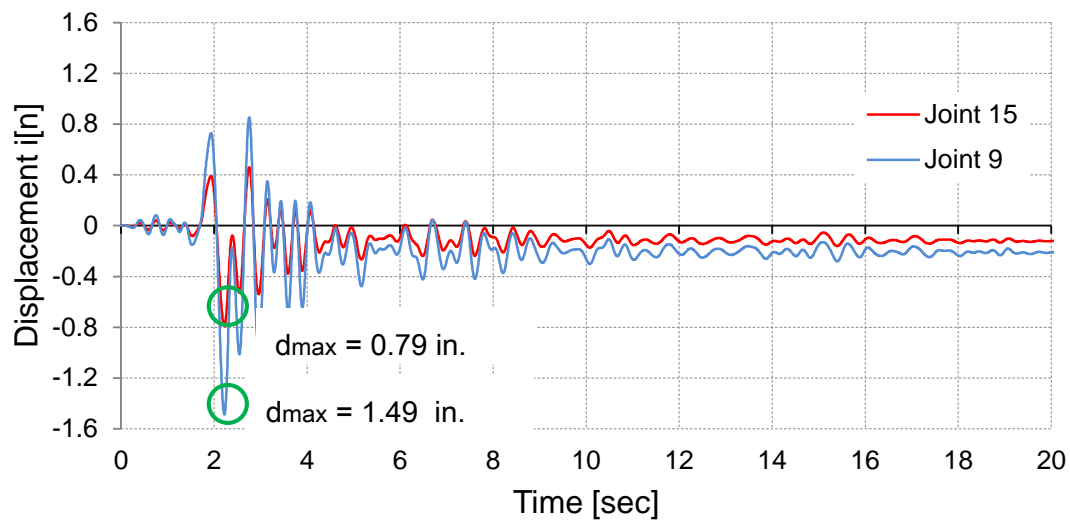
The maximum displacement and base shear in the Y direction at joint 9 for San Salvador IGN earthquake was 1.56 inches and 76.08 kip respectively. The maximum displacement occurs at 1.69 seconds. The average residual displacement for joint 9 was approximately 0.20 inches. It can be noticed that the displacements for the San Salvador CIG earthquakes are larger than for the San Salvador NGI earthquake. This is reasonable because the CIG record has a higher PGA, thus it is expected that the response is higher. At the end of the analysis it can be noticed that nine hinges are beyond collapse limit state, in addition two shear failures (Figure 6-143).

### 6.3.3 NONLINEAR TIME HISTORY ANALYSIS RESULTS FOR MODEL 1.1d

The pushover analysis results indicated that models type d tend to be the stiffest, therefore Model 1.1d was only analyzed for San Salvador CIG in the Y direction. The CIG record has shown to induce the maximum response in the models.

#### 6.3.3.1 RESULTS FOR THE SAN SALVADOR CIG EARTHQUAKE: MODEL 1.1d

The displacement time history, base shear time history and hinge formation were plotted in Figures 6-144 to 6-146 for the earthquake in the Y direction. A discussion of the figures is presented at the end of the section.

**Model 1.1d: Y direction**

**Figure 6-144.** Displacement Time History of Top Joint for Model 1.1d: San Salvador CIG EQ in the Y Direction

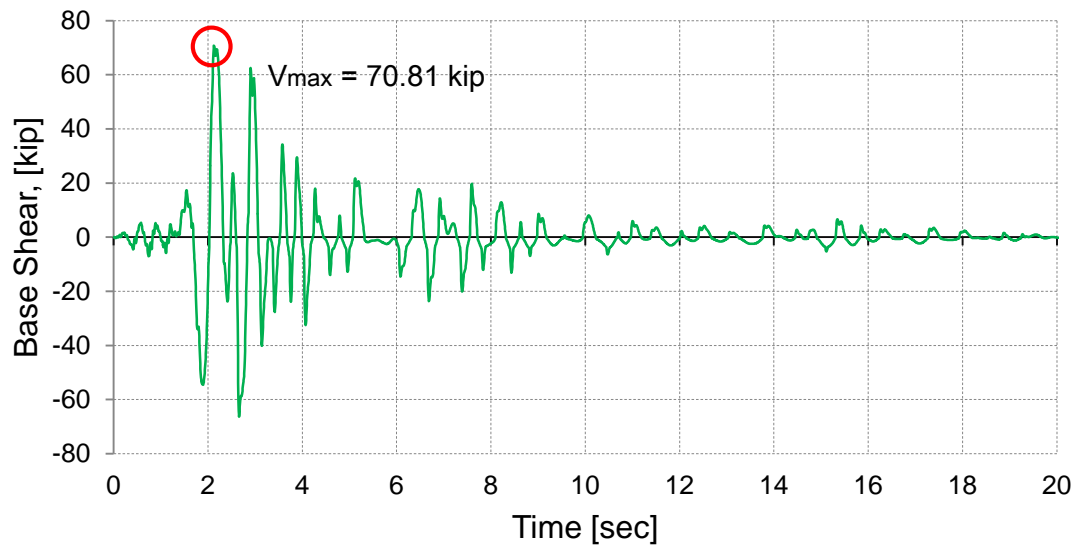


**Figure 6-145.** Base Shear Time History Model 1.1d: San Salvador CIG Y Direction

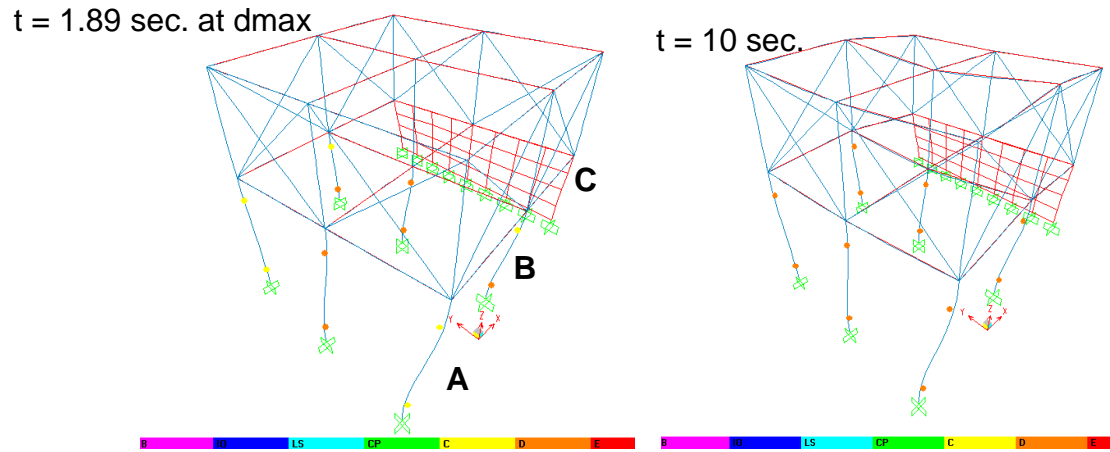


**Figure 6-146.** Hinge Formation for Model 1.1d: San Salvador IGN EQ Y Direction

The maximum displacement and base shear in the Y direction at joint 9 for San Salvador IGN earthquake was 1.49 inches and 70.81 kip respectively. The maximum displacement occurs at 1.89 seconds. From Figure 6-144 It can be observed that when the maximum displacements occurs, 6 hinges are beyond Collapse limit state. At the end of the analysis all lower story columns are beyond collapse limit state, specifically at point D. These elements have lost all ability to carry lateral load. The post-earthquake damage is extensive, possible the model have or is at the verge of experiencing partial or total collapse. As it has been mentioned due to the torsion the model experiment, results of the unsymmetrical location of the shear wall, the effect is significantly negative for the columns without lateral support (Frames A and B).

#### 6.3.4 NONLINEAR TIME HISTORY ANALYSIS RESULTS FOR MODEL 1.4b

For Model 1.4b the nonlinear time history analysis was only carried out for the two San Salvador records IGN and CIG in the X direction. It is not necessary to evaluate Model 1.4b in the Y direction because it was shown that Model 1.1b could not withstand the San Salvador records in the Y direction. However it worth to analyze Model 1.4b in the X direction, since the results for Model 1.1b for the San Salvador IGN record show damage in some members specially at the bottom of the shortest columns and at frame C and central column at frame B, but overall Model 1.1b was able to withstand the

records. Therefore the effect in performance due to the increase in the bay length during the San Salvador earthquakes records requires further study.

#### 6.3.4.1 RESULTS FOR THE SAN SALVADOR IGN EARTHQUAKE: MODEL 1.4b

The displacement time history, base shear time history and hinge formation were plotted in Figures 6-147 to 6-149 for the earthquake in the X directions. The results are compared with Model 1.1b. A discussion of the figures is presented at the end of the section.

##### Model 1.4b: X direction

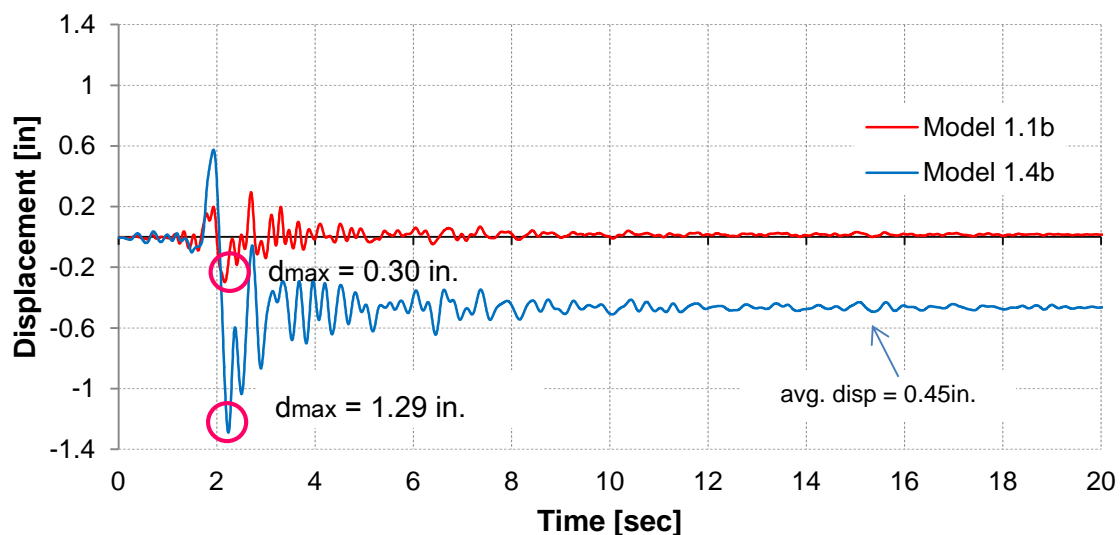


**Figure 6-147.** Comparison Displacement Time History of Top Joint for Model 1.1b and Model 1.4b: San Salvador IGN EQ in the X Direction



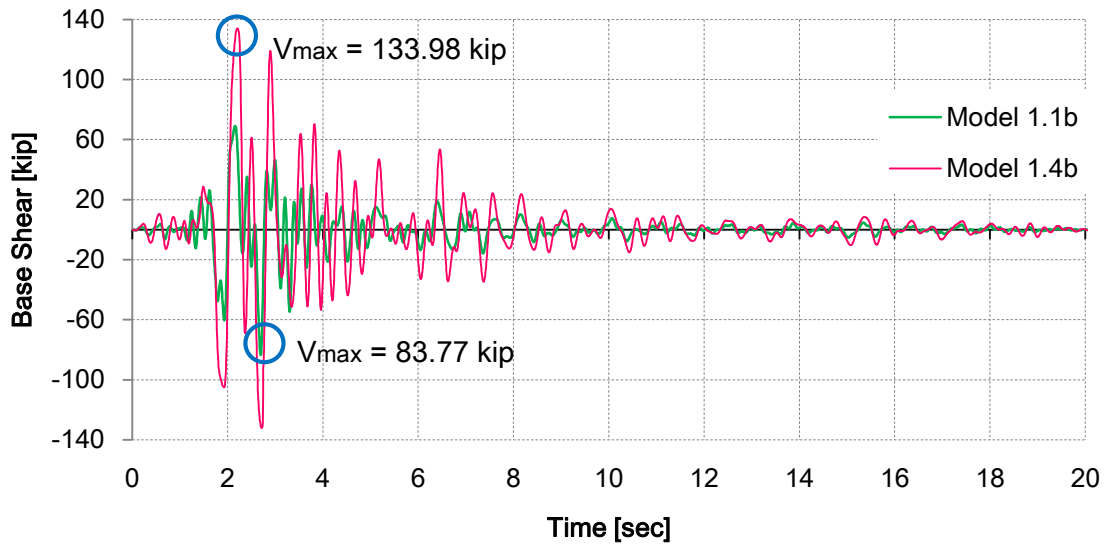


**Figure 6-148.** Comparison Base Shear Time History Model 1.1b and Model 1.4b: San Salvador IGN X Direction

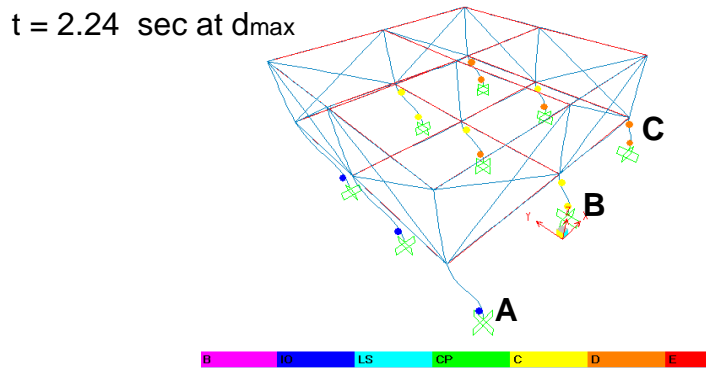


**Figure 6-149.** Hinge Formation for Model 1.4b: San Salvador IGN EQ X Direction

From Figures 6-147 and 6-148 it can be noticed that the displacement and base shear histories increase when compared with Model 1.1b. The maximum displacement was 0.30 and 1.29 inches for Model 1.1b and 1.4b, respectively. This represents an increase in displacement of 330 %. The maximum base shear was 83.77 and 133.98 kips for Model 1.1b and 1.4b, respectively. The average residual displacement was approximately 0.45 inches.

From Figure 6-149 it can be observed that at the maximum displacement, hinge have formed at the top and bottom of the columns. At frames C hinges are beyond Collapse limit state.

### 6.3.4.2 RESULTS FOR THE SAN SALVADOR CIG EARTHQUAKE: MODEL 1.4b

The displacement time history, base shear time history and hinge formation were plotted in Figures 6-150 to 6-155 for the earthquake in the X directions. The results are compared with Model 1.1b. A discussion of the figures is presented at the end of the section

#### Model 1.4b: X direction

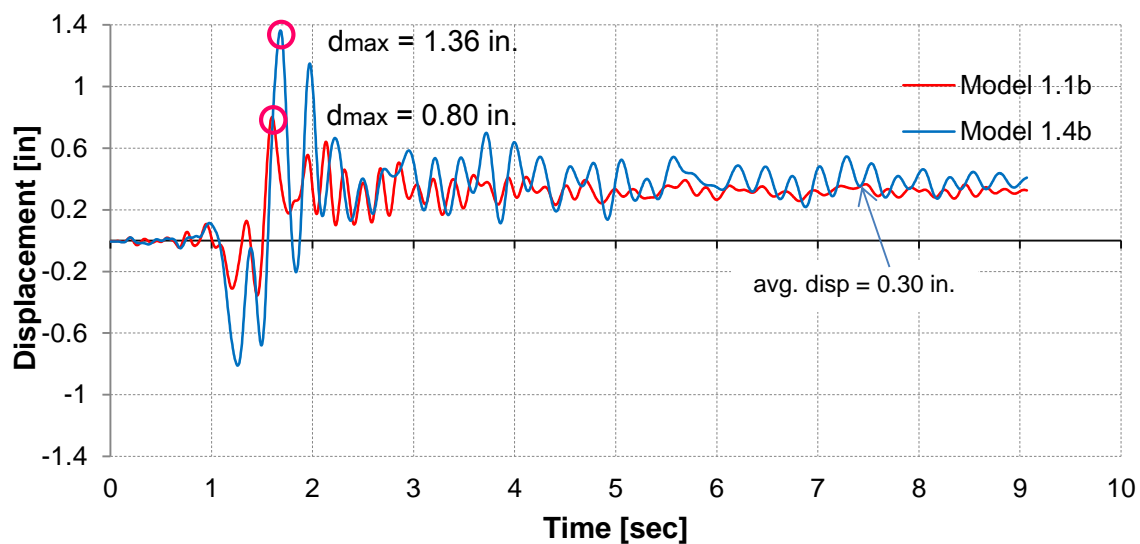


**Figure 6-150.** Comparison Displacement Time History of Top Joint for Model 1.1b and Model 1.4b: San Salvador CIG EQ in the X Direction

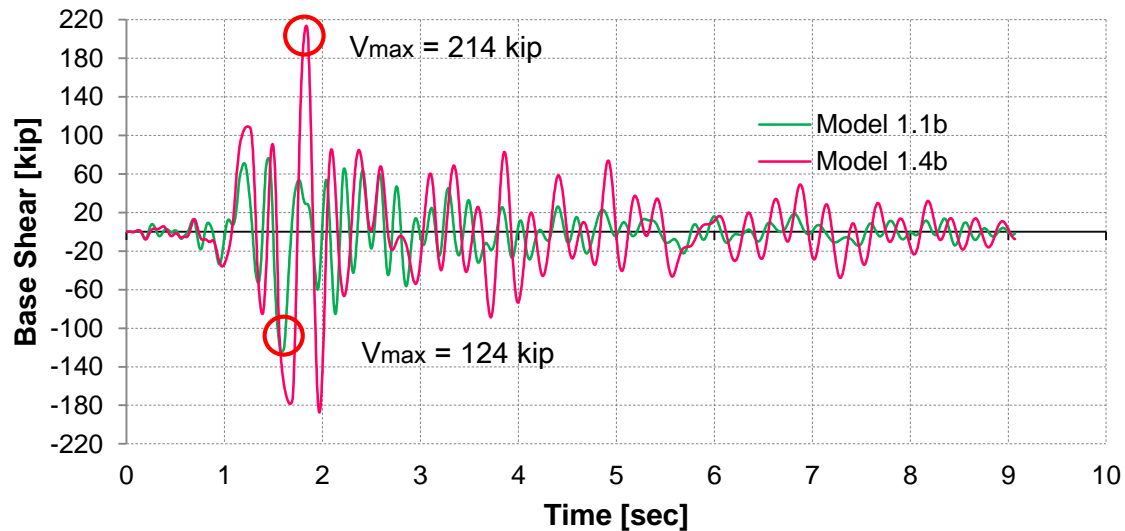


**Figure 6-151.** Comparison Base Shear Time History Model 1.1b and Model 1.4b: San Salvador CIG X Direction

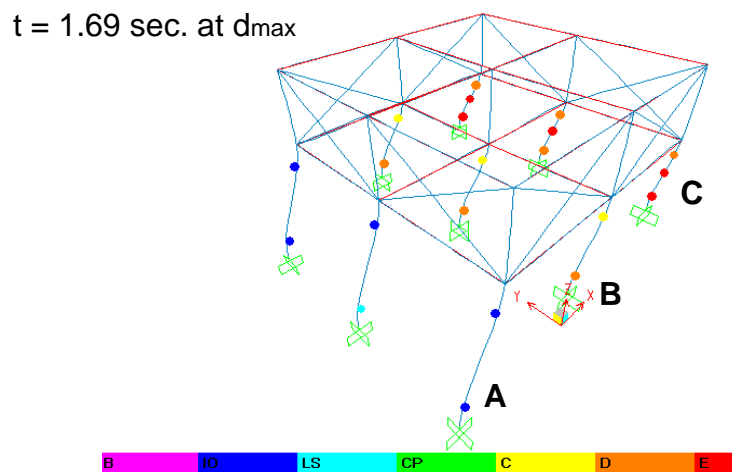


**Figure 6-152.** Hinge Formation for Model 1.4b: San Salvador CIG EQ X Direction

From Figures 6-150 and 6-151 it can be noticed that the displacement and base shear histories increase when compared with Model 1.1b. The maximum displacement was 0.80 and 1.36 inches for Model 1.1b and 1.4b, respectively. This represents an increase in displacement of 70 % approximately. The maximum base shear was 124 and 214 kips for Model 1.1b and 1.4b, respectively. This represents an increase in displacement of 72 %. The average residual displacement was approximately 0.30 inches.

From Figure 6-152 it can be observed that at the maximum displacement, hinge have formed at the top and bottom of the shortest columns at frame C are beyond Collapse limit state, also all columns at frame C have formed shear failure. In general it can be said that as the bay length increase, the model suffered extensive damage.

### 6.3.5 NONLINEAR TIME HISTORY ANALYSIS RESULTS FOR MODEL 1.4c

For Model 1.4c the nonlinear time history analysis was only carried out for the two San Salvador records IGN and CIG in the Y direction.

#### 6.3.5.1 RESULTS FOR THE SAN SALVADOR IGN EARTHQUAKE: MODEL 1.4c

The displacement time history, base shear time history and hinge formation were plotted in Figures 6-152 to 6-154 for the earthquake in the Y direction. A discussion of the above figures cited before is presented at the end of the section.

##### Model 1.4c: Y direction

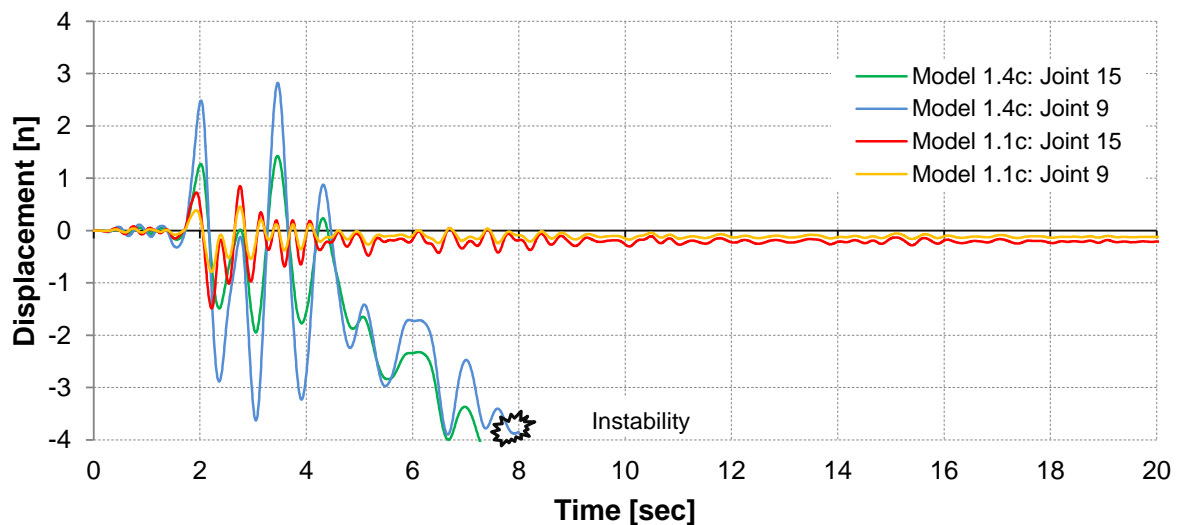


**Figure 6-153.** Comparison Displacement Time History of Top Joint for Model 1.1b and Model 1.4b: San Salvador IGN EQ in the Y Direction

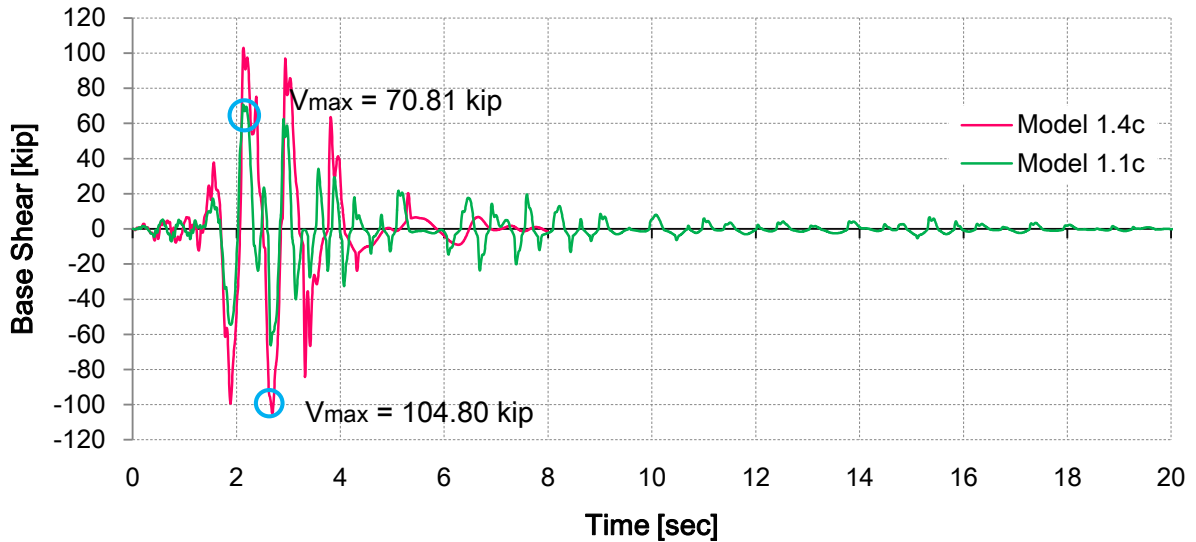


**Figure 6-154.** Comparison Base Shear Time History for Model 1.1c and Model 1.4c: San Salvador IGN Y Direction

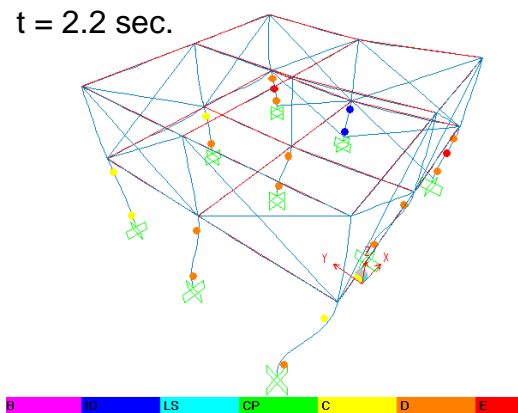


**Figure 6-155.** Hinge Formation for Model 1.4c: San Salvador IGN EQ Y Direction

The maximum displacement and base shear in the Y direction for San Salvador CIG earthquake was 11 inches and 105 kip respectively. As mentioned before so large displacements are not realistic. From Figure 6-153 it can be noticed that the response increase significantly for Model 1.4c when compared to Model 1.1c. From Figure 6-155 it can be observed that at 2.2 sec. the lower story is severely damaged, hinge have formed at the top and bottom column, twelve are beyond Collapse limit state (E).

### 6.3.5.2 RESULTS FOR THE SAN SALVADOR CIG EARTQUAKE: MODEL 1.4c

The displacement time history, base shear time history and hinge formation were plotted in Figures 6-156 to 6-158 for the earthquake in the Y direction. The results are compared with Model 1.1c. A discussion of the figures is presented at the end of the section.

#### Model 1.4c: Y direction

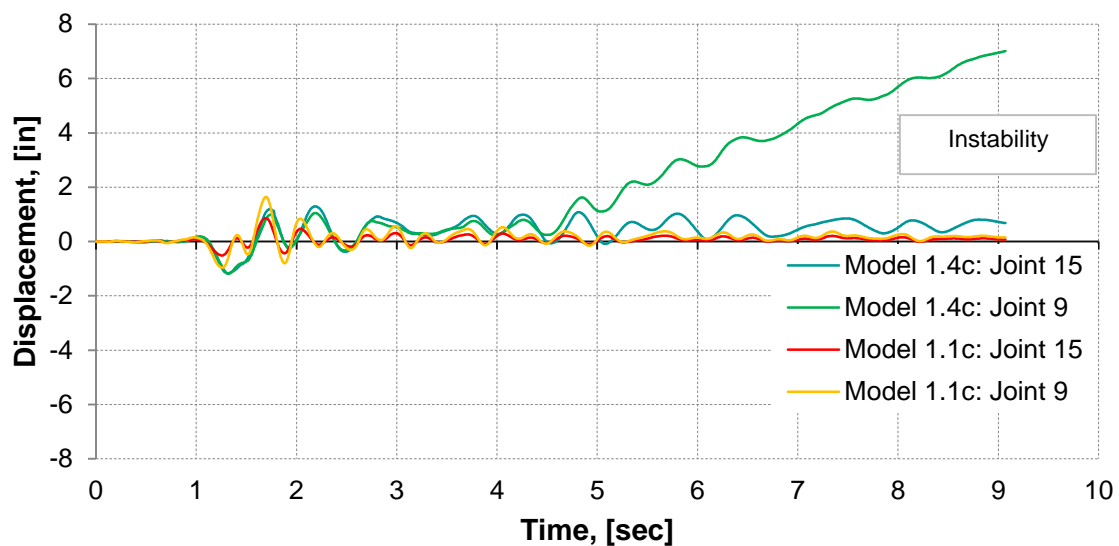


**Figure 6-156.** Comparison Displacement Time history of Top Joint for Model 1.1b and Model 1.4b: San Salvador CIG EQ in the Y Direction

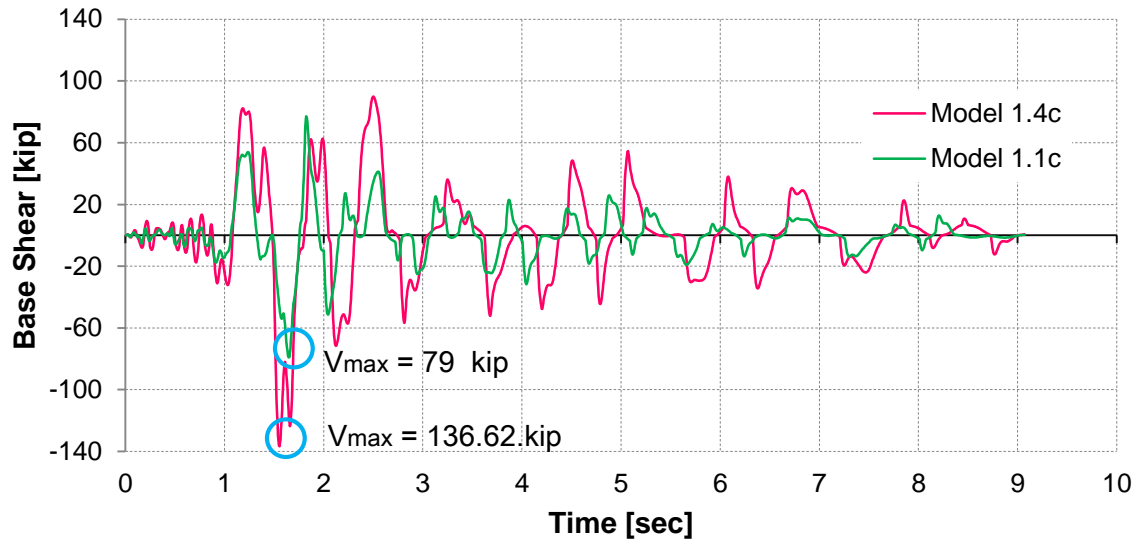


**Figure 6-157.** Comparison Base Shear Time History Model 1.1b and Model 1.4b: San Salvador CIG Y Direction

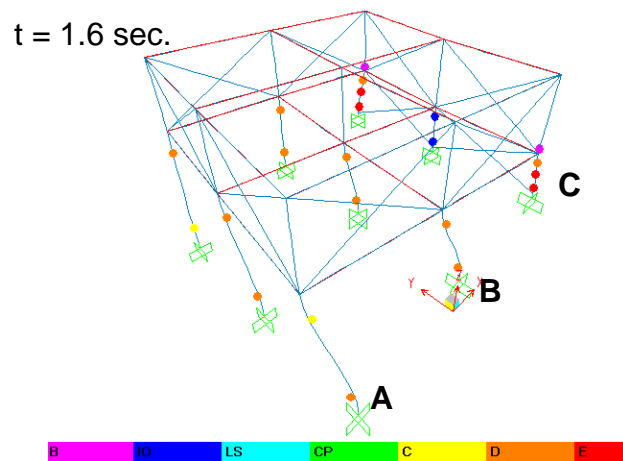


**Figure 6-158.** Hinge Formation for Model 1.4c: San Salvador CIG EQ Y Direction

The maximum displacement and base shear in the Y direction for San Salvador CIG earthquake was 7 inches and 136 kip respectively. From Figure 6-156 it can be observed that the displacements grow quite large at joint 9. Also it can be noticed that the displacement and base shear histories increase significantly when compared to model 1.1c. From Figure 6-158 it can be observed that at 1.6 seconds, ten hinges have formed at the top and bottom column, beyond Collapse limit state (E).

### 6.3.6 NONLINEAR TIME HISTORY ANALYSIS RESULTS FOR MODEL 2.1b

For Model 2.1b the nonlinear time history analysis was only carried out for the two San Salvador records IGN and CIG in the X direction.

#### 6.3.6.1 RESULTS FOR THE SAN SALVADOR IGN EARTHQUAKE: MODEL 2.1b

The displacement time history, base shear time history and hinge formation were plotted in Figures 6-159 to 6-160 for the earthquake in the X direction. The results are compared with Model 1.1b. A discussion of the figures is presented at the end of the section.

##### Model 2.1b: X direction

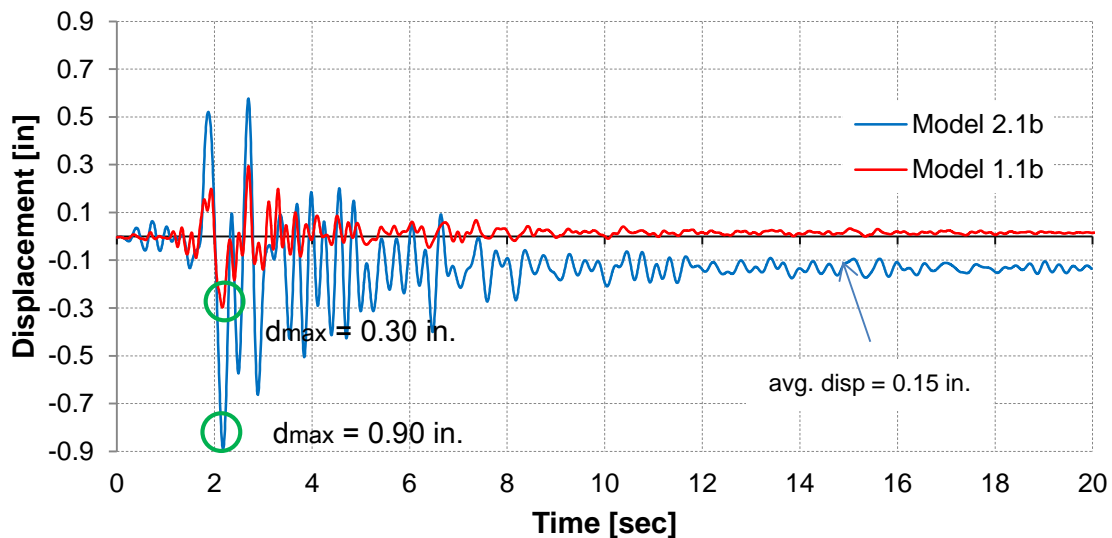


**Figure 6-159.** Comparison Displacement Time history of Top Joint for Model 1.1b and Model 2.1b: San Salvador IGN EQ in the Y Direction



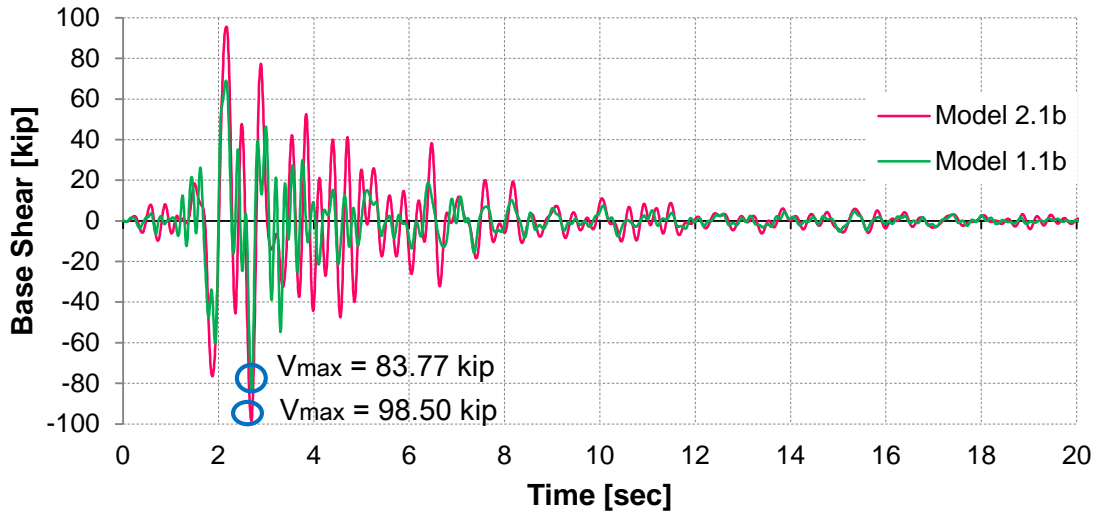


**Figure 6-160.** Comparison Base Shear Time History Model 1.1b and Model 2.1b: San Salvador IGN X Direction

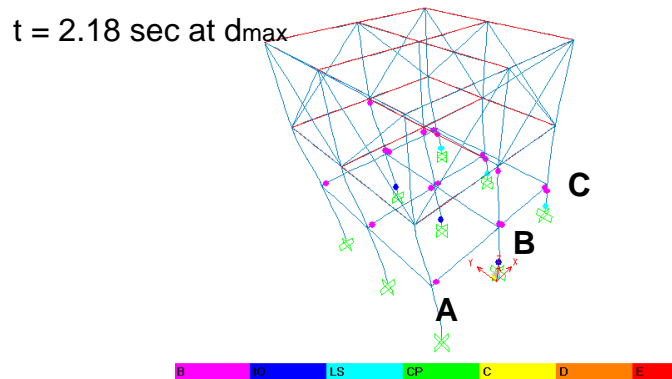


**Figure 6-161.** Hinge Formation for Model 2.1b: San Salvador IGN EQ X Direction

The maximum displacement and base shear in the X direction for San Salvador IGN earthquake was 0.89 inches and 98 kip respectively. From Figure 6-159 and 6-160 it can be noticed that the displacement and base shear histories increase when compared to model 1.1b. The displacement history show significant more residual displacements than Model 1.1b.

#### 6.3.6.2 RESULTS FOR THE SAN SALVADOR CIG EARTQUAKE: MODEL 2.1b

The displacement time history, base shear time history and hinge formation were plotted in Figures 6-162 to 6-164 for the earthquake in the X directions. The results are

compared with Model 1.1b. A discussion of the figures is presented at the end of the section.

### **Model 2.1b: X direction**

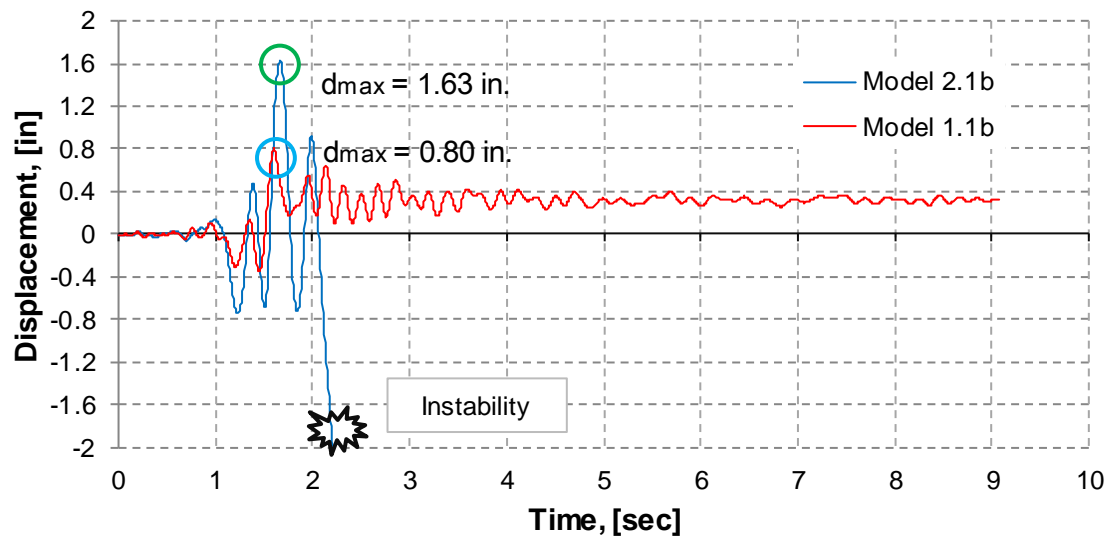


**Figure 6-162.** Comparison Displacement Time history of Top Joint for Model 1.1b and Model 1.4b: San Salvador CIG EQ in the X Direction

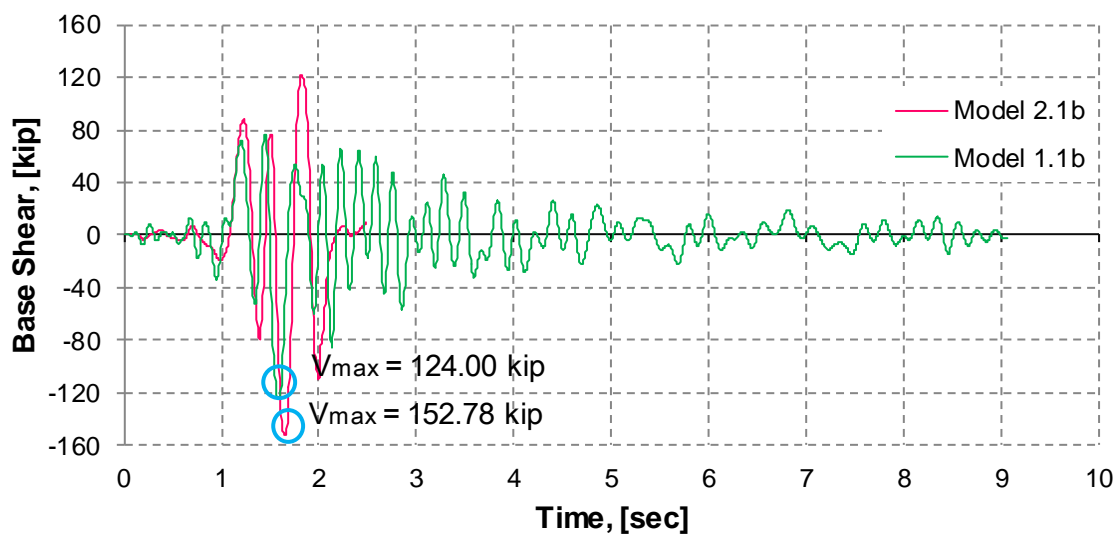


**Figure 6-163.** Comparison Base Shear Time History Model 1.1b and Model 1.4b: San Salvador CIG X Direction

$t = 2.10 \text{ sec.}$

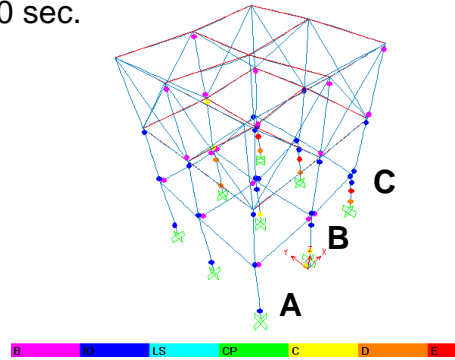


**Figure 6-164.** Hinge Formation for Model 2.1b: San Salvador CIG EQ X Direction

The maximum displacement and base shear in the X direction for San Salvador IGN earthquake was 1.63 inches and 153 kip respectively. From Figure 6-162 it can be noticed the San Salvador CIG analysis was stopped at 2.10 seconds. Columns at the lower story (frame C) failed in shear at 1.5 seconds (Figure 6-164).

### 6.3.7 NONLINEAR TIME HISTORY ANALYSIS RESULTS FOR MODEL 2.1c

For Model 2.1c the nonlinear time history analysis was only carried out for the two San Salvador CIG records in the Y direction.

#### 6.3.7.1 RESULTS FOR THE SAN SALVADOR CIG EARTHQUAKE: MODEL 2.1c

The displacement time history, base shear time history and hinge formation were plotted in Figures 6-165 to 6-167 for the earthquake in the Y directions. The results are compared with Model 1.1c. A discussion of the figures is presented at the end of the section.

### Model 2.1c: Y direction

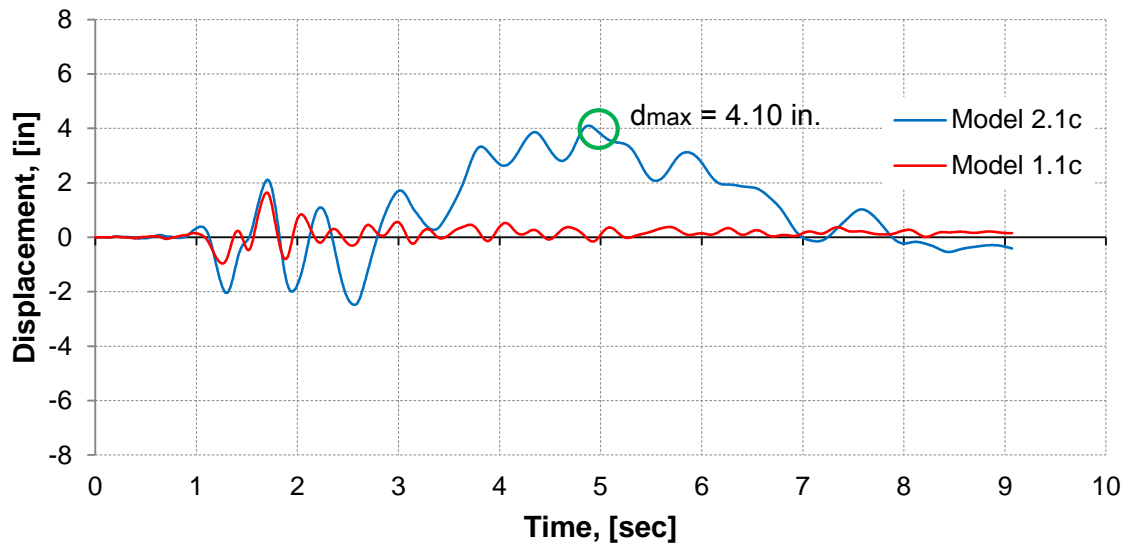


**Figure 6-165.** Comparison Displacement Time history of Top Joint for Model 1.1c and Model 2.1c: San Salvador CIG EQ in the Y Direction

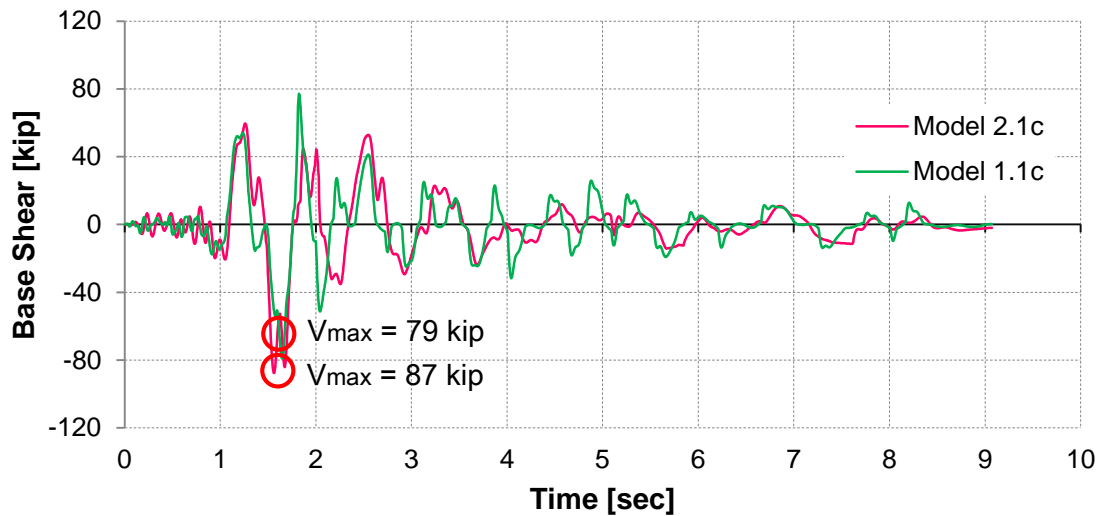


**Figure 6-166.** Comparison Base Shear Time History Model 1.1b and Model 1.4b: San Salvador CIG Y Direction

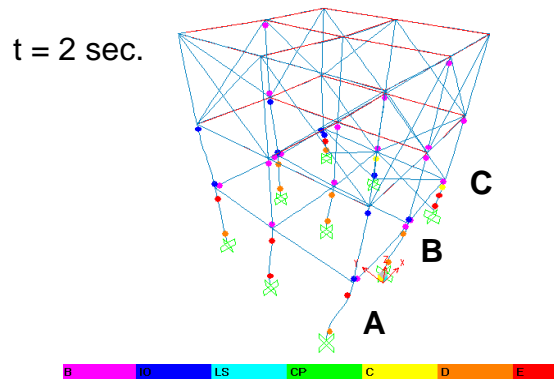


**Figure 6-167.** Hinge Formation for Model 2.1c: San Salvador CIG EQ Y Direction

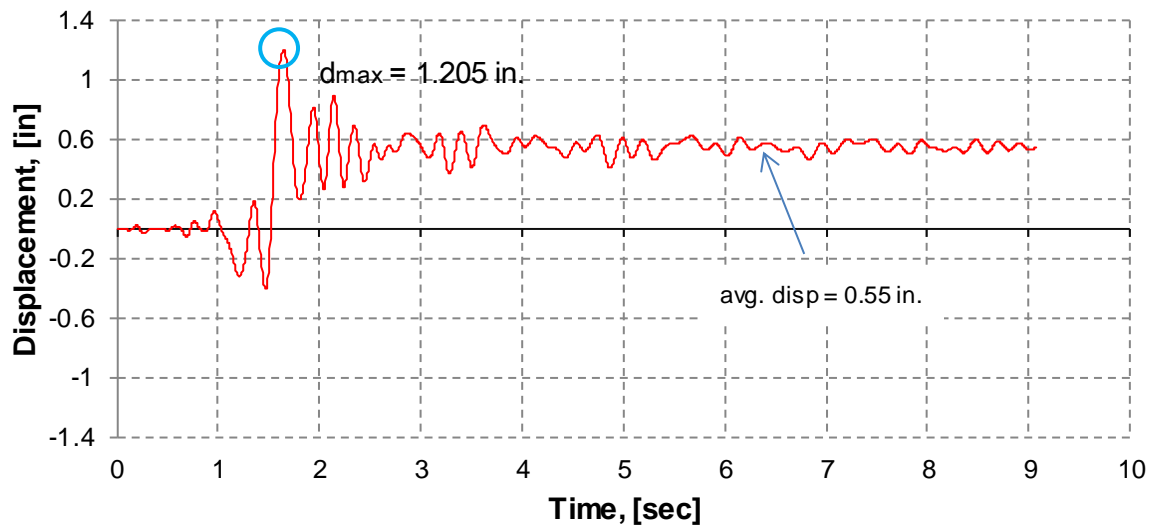
The maximum displacement and base shear in the Y direction for San Salvador CIG earthquake was 4.10 inches and 87 kip respectively. From Figure 6-165 it can be noticed the San Salvador CIG caused large displacements. Figure 6-167 shows that at 2 sec the Model is severely damaged. At frames A and B bottom and top hinges have formed all beyond Collapse limit state.

### 6.3.8 NONLINEAR TIME HISTORY ANALYSIS RESULTS FOR MODEL 1.1.3

For Model 1.1.3 the nonlinear time history analysis was only carried out for the San Salvador CIG record.

#### 6.3.8.1 RESULTS FOR THE SAN SALVADOR CIG EARTHQUAKE: MODEL 1.1.3b

The displacement time history, base shear time history and hinge formation were plotted in Figures 6-168 to 6-173 for the earthquake in the X and Y direction respectively. A discussion of the figures is presented at the end of the section.

**Model 1.1.3b: X direction**

**Figure 6-168.** Displacement Time history of Top Joint for Model 1.1.3b: San Salvador CIG EQ in the X Direction

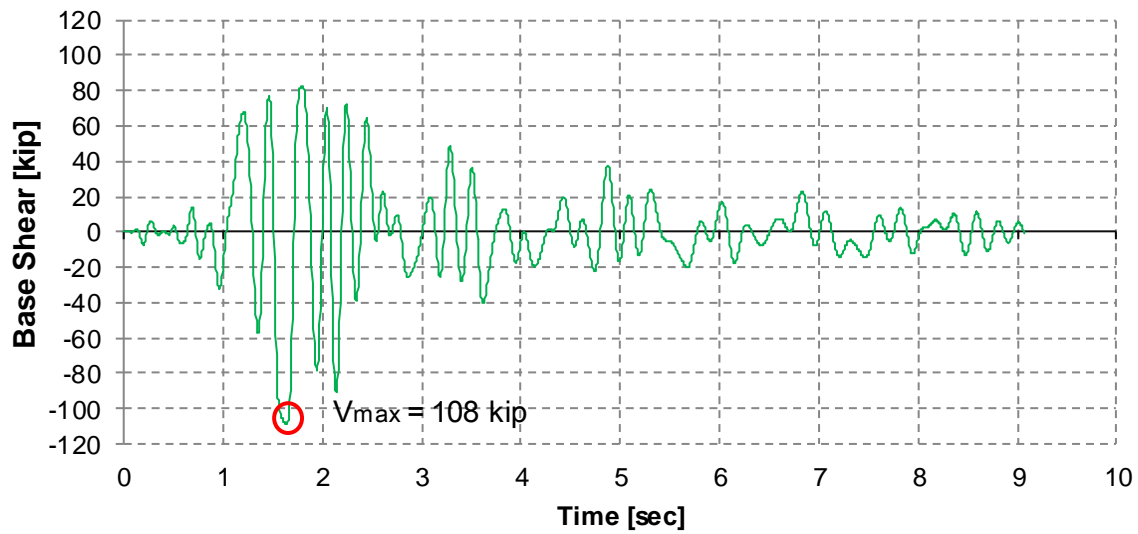


**Figure 6-169.** Base Shear Time History Model 1.1.3b: San Salvador CIG X Direction

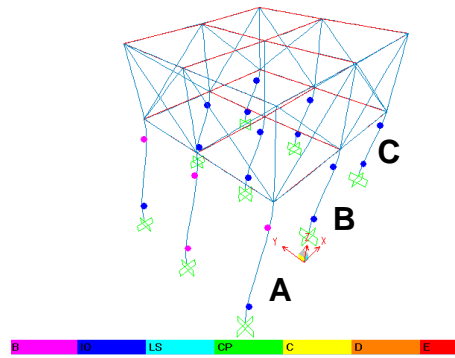


**Figure 6-170.** Hinge Formation for Model 1.1.3b: San Salvador CIG EQ X Direction

**Model 1.1.3b: Y direction**

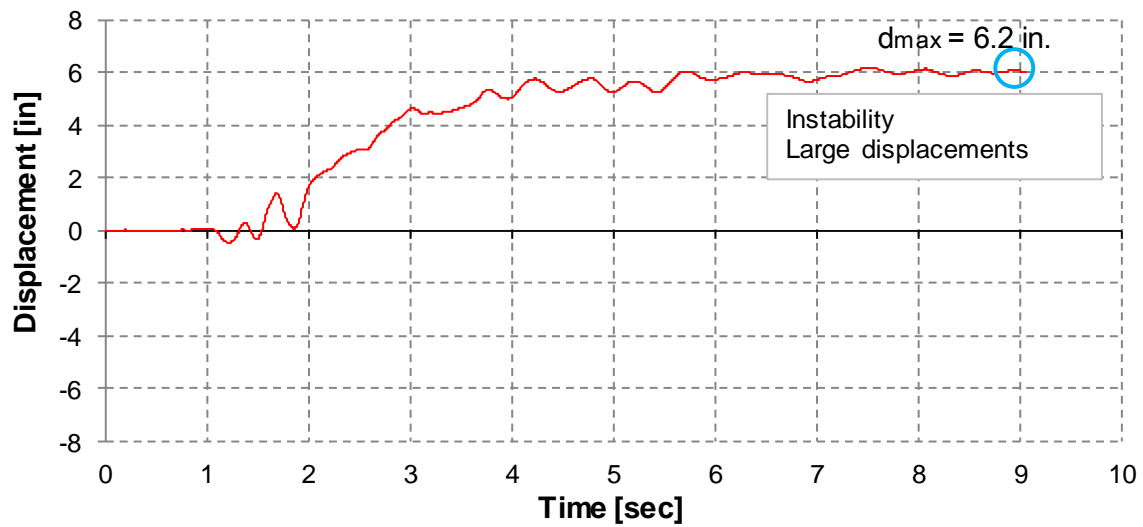


**Figure 6-171.** Displacement Time history of Top Joint for Model 1.1.3b: San Salvador CIG EQ in the Y Direction

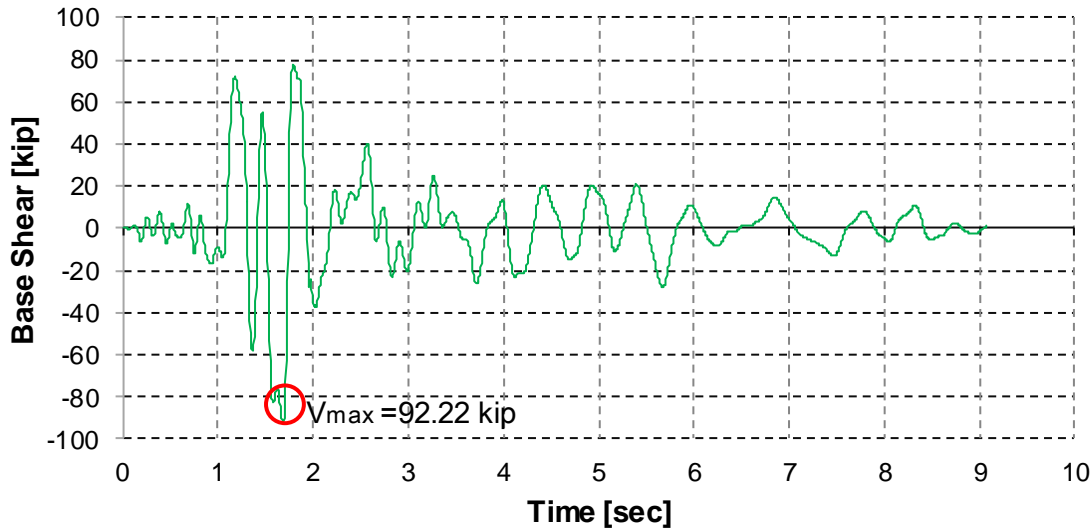


**Figure 6-172.** Base Shear Time History Model 1.1.3b: San Salvador CIG Y Direction

$t = 1.97$  sec.

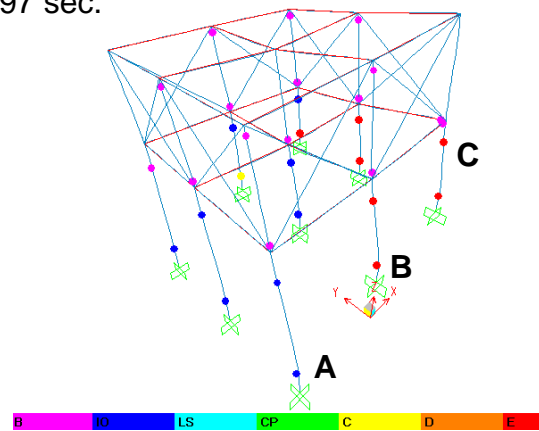


**Figure 6-173.** Hinge Formation for Model 1.1.3b: San Salvador CIG EQ Y Direction

The maximum displacement and base shear in the X direction for San Salvador CIG earthquake was 1.2 inches and 87 kip respectively. From Figure 6-170 it can be noticed the San Salvador CIG record at the end of the analysis all elements are between point B and Immediate Occupancy limit level.

The maximum displacement and base shear in the Y direction for San Salvador CIG earthquake was 6.2 inches and 92 kip respectively. From Figure 6-171 it can be noticed the San Salvador CIG record caused instability issue. Collapse is assumed to occur due



to the large increase in the response. It can be noticed from Figure 6-173 that at 1.97 sec the elements at frame C have failed (E).

### 6.3.8.2 RESULTS FOR THE SAN SALVADOR CIG EARTQUAKE: MODEL 1.1.3c

The displacement time history, base shear time history and hinge formation were plotted in Figures 6-174 to 6-176 for the earthquake in the Y direction. A discussion of the above figures cited before is presented at the end of the section.

#### Model 1.1.3c: Y direction

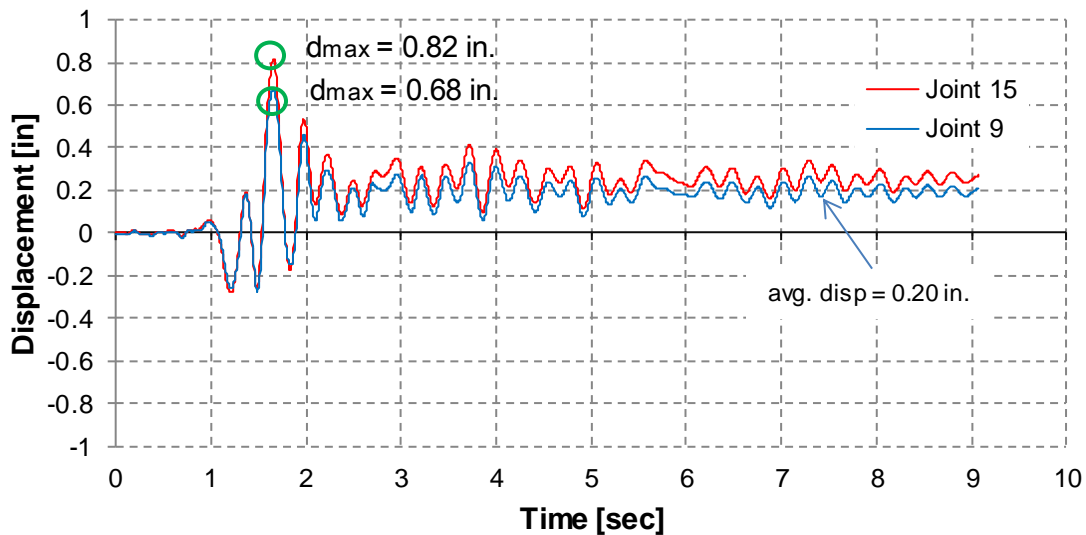


**Figure 6-174.** Displacement Time history of Top Joint for Model 1.1.3c: San Salvador CIG EQ in the Y Direction

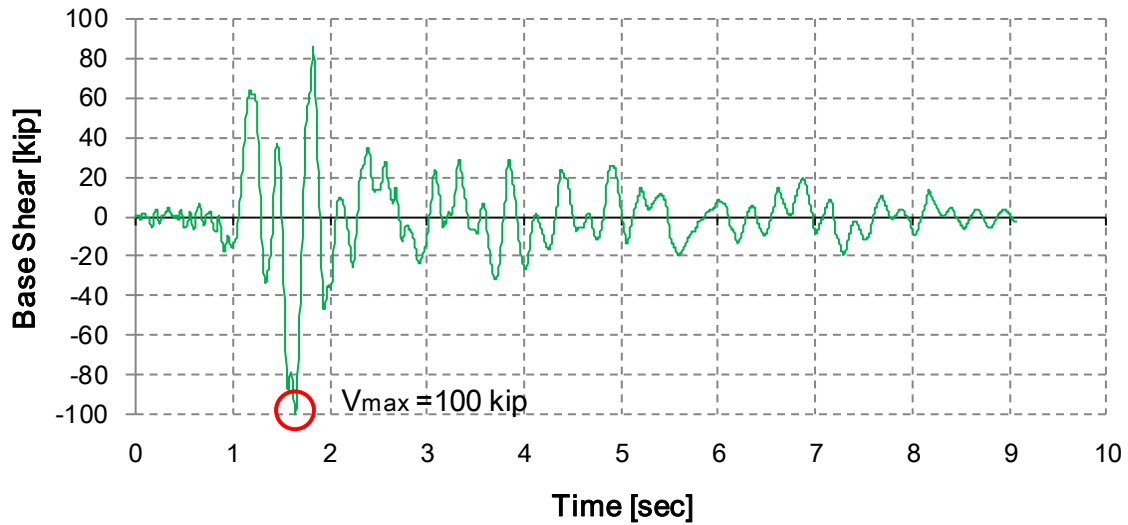


**Figure 6-175.** Base Shear Time History Model 1.1.3c Salvador CIG Y Direction

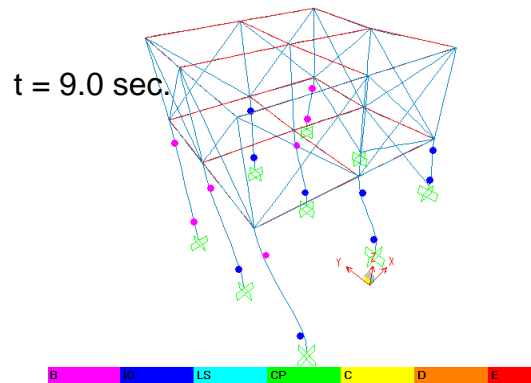


**Figure 6-176.** Hinge Formation for Model 1.1.3c: San Salvador CIG EQ Y Direction

The maximum displacement and base shear in the Y direction for San Salvador CIG earthquake was 0.82 inches and 100 kip, respectively. From Figure 6-176 it can be noticed that at the end of the analysis all elements are between point B and Immediate Occupancy limit level.

### 6.3.9 SUMMARY OF TIME HISTORY ANALYSIS RESULTS

The maximum values of the base shear and lateral displacement obtained from the nonlinear time history analysis for the models analyzed summarized in Tables 6-58. It is important to mention that these values do not occur at the same time in the analyses.

**Table 6-57. Summary Results Nonlinear Time History Analysis**

	V, max (k)	D, max (in)		V, max (k)	D, max (in)
	<b>Model 1.1b - X</b>			<b>Model 1.1b - Y</b>	
Parkfield	72.5	0.32	Parkfield	12.95	0.41
Northridge	23.2	0.08	Northridge	13.18	0.48
San Salvador IGN	83.2	0.30	San Salvador IGN	29.6	
San Salvador CIG	124	0.80	San Salvador CIG	17.24	
	<b>Model 1.4b - X</b>			<b>Model 1.1c - Y</b>	
San Salvador IGN	133.98	1.29	San Salvador IGN	70.81	1.49
San Salvador CIG	214	1.36	San Salvador CIG	79	1.64
	<b>Model 2.1b - X</b>			<b>Model 1.1d - Y</b>	
San Salvador IGN	98.5	0.90	San Salvador CIG	85.44	1.61
San Salvador CIG	152.78			<b>Model 1.4c - Y</b>	
	<b>Model 1.1.3b - X</b>		San Salvador IGN	105	
San Salvador CIG	108	1.21	San Salvador CIG	137	
				<b>Model 2.1c - Y</b>	
			San Salvador CIG	87	
				<b>Model 1.1.3b - Y</b>	
			San Salvador CIG	92.22	
				<b>Model 1.1.3c - Y</b>	
			San Salvador CIG	100	0.82

 Analisis stopped, instability

The following general conclusions for the nonlinear time history analysis are summarized next:

- For Model 1.1 it was observed that the maximum responses occurred for the San Salvador IGN and CIG earthquake records, where lateral load and lateral displacement were higher than those induced by the Parkfield and Northridge earthquake records. This is reasonable because the peak ground acceleration (PGA) for San Salvador's IGN and CIG records was 0.61g and 0.87g, respectively,

while for Parkfield and Northridge records the peak ground acceleration (PGA) was 0.27g and 0.12g, respectively.

- Models type b (bare frame) in the Y direction collapsed.
- Models 1.4b and 2.4b were analyzed with both San Salvador records; it was observed that they experienced more damage than Model 1.1b. For Model 1.4b the bay length increased and for Model 2.4 the bay length and the number of stories increased.
- Models 1.1, 1.4 and 2.4 type c/d (with retaining wall) were only analyzed with the San Salvador CIG and NGI records in the Y direction. It was observed that the analysis did not fail due to instability issues like it was for the case of models type b (without retaining wall), however at the end of the analysis the columns at frames A and B (frames without lateral support) were severely damaged due to the torsion the model experiment results of the unsymmetrical location of the shear wall. It was noticed that several hinges was beyond Collapse limit state, including shear failures. Structural repair for elements with this level of damage is considered not feasible.
- Model 1.1.3b was able to resist the San Salvador CIG record in the X direction, only minor damage was observed. Hinges performance state were within Immediate Occupancy level. In the Y direction the model collapsed.
- Model 1.1.3c was able to resist the San Salvador CIG record in the Y direction, minor damage was observed. Hinges performance state were within Immediate Occupancy level.

## CHAPTER 7. PROPOSED RESIDENCES REHABILITATION

---

### 7.1 INTRODUCTION

To select an appropriate rehabilitation technique, accurate evaluations of the seismic performance of the prototype models were performed. As mentioned before, the Capacity Spectrum Method was used to determine the performance point. The performance point is the graphical intersection of the capacity of the structure with the demands in the structure expressed in terms of a demand spectrum. The coordinates of this points approximate the nonlinear response and help to identify damage states.

Based on this evaluation the analytical models suffered extensive damage when loaded mainly in the Y direction. These structural deficiencies are defined as a condition that will prevent the residences from meeting the designated seismic performance objective. Specifically, the columns in the lower level reached (point C) or exceeded (beyond C) their limit state conditions as the pushover results demonstrated. Pushover analysis results show that no performance point was achieved when the analysis was performed in the Y or X direction, when this matches the weak orientation of the column for models type b (bare frame). The structures are expected to fail under the event or demand represented by the spectrum UBC-97 for Soil type Sd. When the analysis considered a retaining wall in the Y direction (models type c and d) the overall capacity of the model improved. However, due to torsional effects it was observed that locally the columns reached and exceeded their limit state conditions and are severely damaged at the performance point.

The residences also performed very poor while subjected to actual earthquake records. For example, for Model 1.1b in the Y direction, significant damage was observed for a moderate record like Parkfield with a low PGA, 0.27g. Models type c and d also suffered extensive damage when subjected to the San Salvador records.

Most of these residences are at risk of exhibiting poor performance during earthquakes because there was no seismic design code as followed when they were constructed. Most of these residences were constructed before building codes introduced design requirements for ductility behavior; as a result it was shown that they cannot provide the required ductility, lateral stiffness and strength.

Nowadays, most of the strengthening strategies are based on global strengthening and stiffening schemes (Moehle, 2000). In these schemes, global behavior of the system is transformed, the structure is usually retrofit for limiting lateral displacements in order to compensate the low ductility. Common global modifications include the addition of structural walls, steel braces, or base isolators. Another approach is the modification of deficient elements to increase their ductility so that they will not reach their limit state (Moehle, 2000). However, this strategy is more expensive and harder to implement in cases where there are many deficient elements which is the reason that the global strengthening methods have been more popular than element strengthening (Kaplan, 2001).

Among the global strengthening methods, the addition of RC infill (masonry block wall) is a popular option. Researchers have focused on this subject and found that installation of RC infills greatly improve the lateral load capacity and stiffness of the structure (Jirsa & Kreger, 1989). Although the use of masonry block walls increased the strength of the frame, failure is relatively brittle.

Adding concrete shear walls is one of the most common rehabilitation techniques to strengthen existing structures. This approach is effective for controlling global lateral drifts and for reducing damage in frame members. The goal of the strengthening is to generally increase stiffness and reduce member forces in columns. The results demonstrated that the members most damaged were the columns. The distribution of the walls in plan and elevation should achieve a regular structural configuration. The primary purpose of this section is to provide a seismic rehabilitation technique that is practical and effective.

The principal criteria for the rehabilitation analysis was to verify that the RC wall will improve the performance against total collapse or avoid significant member damage that compromise overall structural stability. For example the rehabilitation analysis involves locating only one wall (minimum) in each direction.

## **7.2 PUSHOVER ANALYSIS RESULTS FOR REHABILITATED MODELS**

Considering the previous nonlinear pushover results with the evident deficiencies, retrofit strategy should intend to reduce deformation demands and increase stiffness of the models. The Y direction for Models type b (without retaining wall), were not analyzed. These residences collapsed in the Y direction, therefore for all practical purposes these types of residences should have a wall at both ends of the edge frames in order to prevent collapse when there is no retaining wall or reduce torsion when there is a retaining wall at the edge frame. The analytical model retrofitting scheme will utilize preliminary one shear walls in the X and Y direction (Figure 7-1). The thickness of the wall used was 6 inches. The RC shear wall was analyzed with linear elastic properties using shell elements. It is not necessary to re-analyze all the models with the rehabilitation. It is expected that the implementations of RC shear walls will increase significantly the stiffness of the residences. Assuming that the results with the rehabilitation improve the performance for the worst cases it is assumed that the rehabilitation for models that had better behavior will also improve. Therefore, some models that presented the worst performance based on the pushover analysis results are considered in this section. Models 1.3, 1.4, 2.4 1.1y and 1.1.5 were selected to perform the rehabilitation analysis. The specific criteria for the selection of these models are described below:

- Models 1.3, 1.4 and 2.4 were severely damaged at the performance point with high ductility demands in both the X and Y direction. Model 1.4b and Model 2.4b were analyzed with the rehabilitation in the X direction as shown in Figure 7-1. Model

1.3c, Model 1.4c and Model 2.4c were analyzed with the rehabilitation in the Y direction as shown in Figure 7-1.

- Model 1.1yb collapsed in the X direction due to the change in column orientation.
- Model 1.1.5b collapsed in the X direction due to a reduction in column size from 16 inches to 12 inches. Rehabilitation in the X direction is not necessary as this case is included when the rehabilitation was made for Model 1.1yb in the X direction. For Model 1.1yb the rehabilitation in the X direction is for columns in the X direction of 6 inches, so it is not necessary to repeat the analysis for columns in the X direction of 12 inches. Therefore only Model 1.1.5c were rehabilitated in the Y direction, since it was severely damaged, the Y direction has the same column dimension as Models 1.1, however it was shown that the reduction in column size in the X direction affect the Y direction.

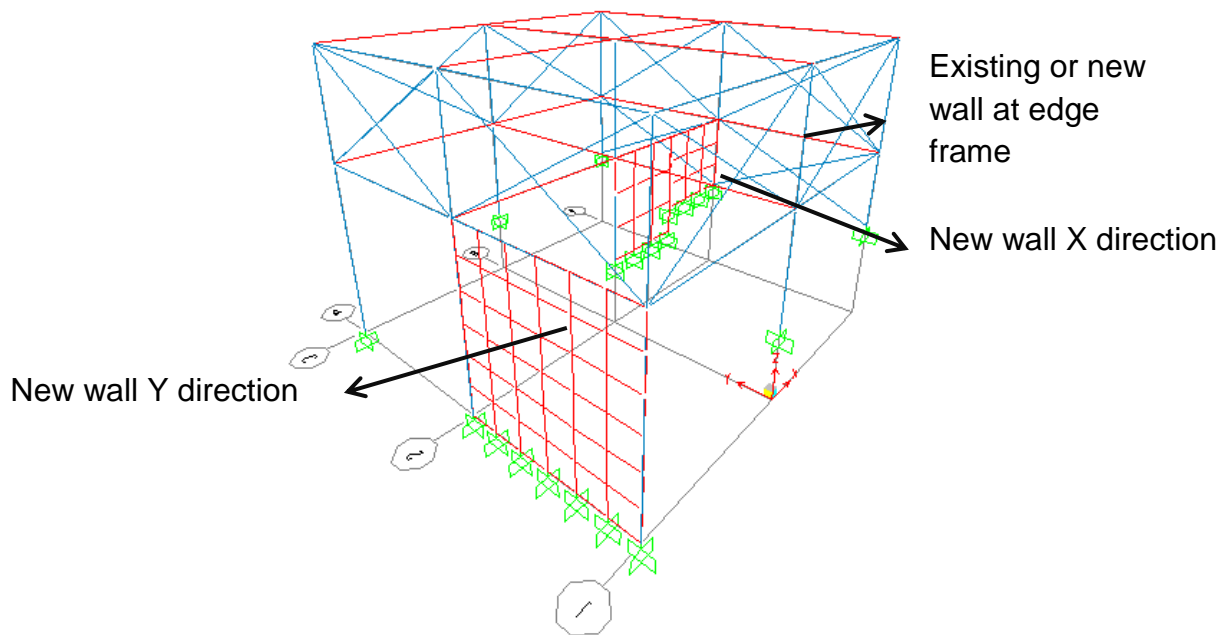


**Figure 7-1.** Analytical Model with RC Shear Walls location.

Table 7-1 to 7-7 includes the tabular data to generate the pushover curves for the retrofitted models. Force displacement plots for the pushover analyses and the plot of



performance point are presented in Figure 7-2 to 7-18. A discussion of the above figures mentioned is presented in the next section (7.2.1). The yield pattern of the hinges is not presented.

### **Model 1.3c: Y direction**

**Table 7-1.** Tabular Data for Pushover Curve for Model 1.3c: Push Y Rehabilitation

PUSH Y Mode			Hinge Sequence								Shear
Step	Disp. (in)	Base Force (Kip)	A to B	B to IO	IO to LS	LS to CP	CP to C	C to D	D to E	E to F	
0	0.00	0.00	102	0	0	0	0	0	0	0	
1	0.10	145.33	101	1	0	0	0	0	0	0	
2	0.35	454.47	95	2	5	0	0	0	0	0	
3	0.47	549.01	83	8	7	0	0	2	1	1	

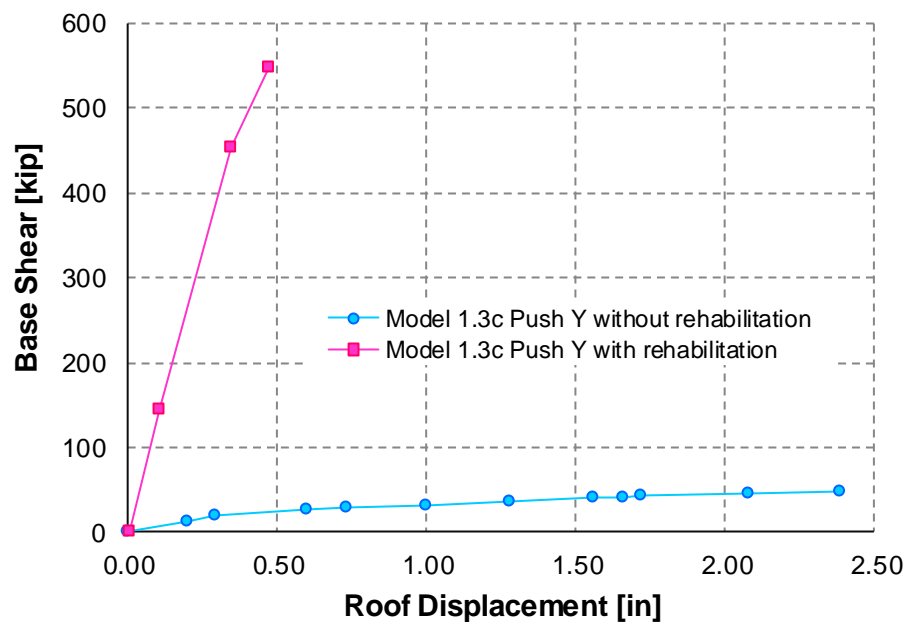


**Figure 7-2.** Comparison Pushover Curves with Rehabilitation for Model 1.3c: Push Y

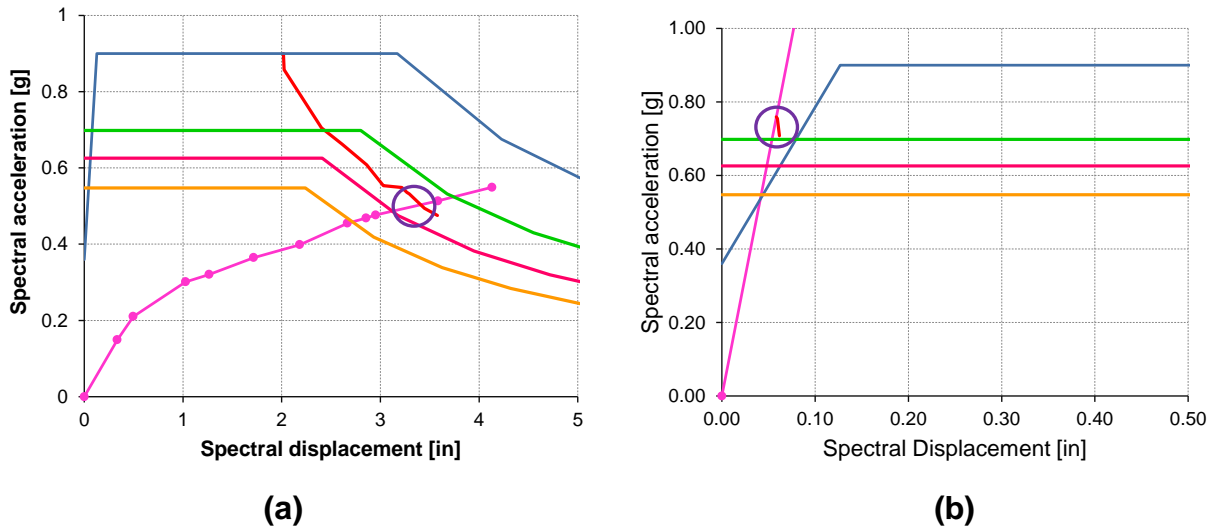
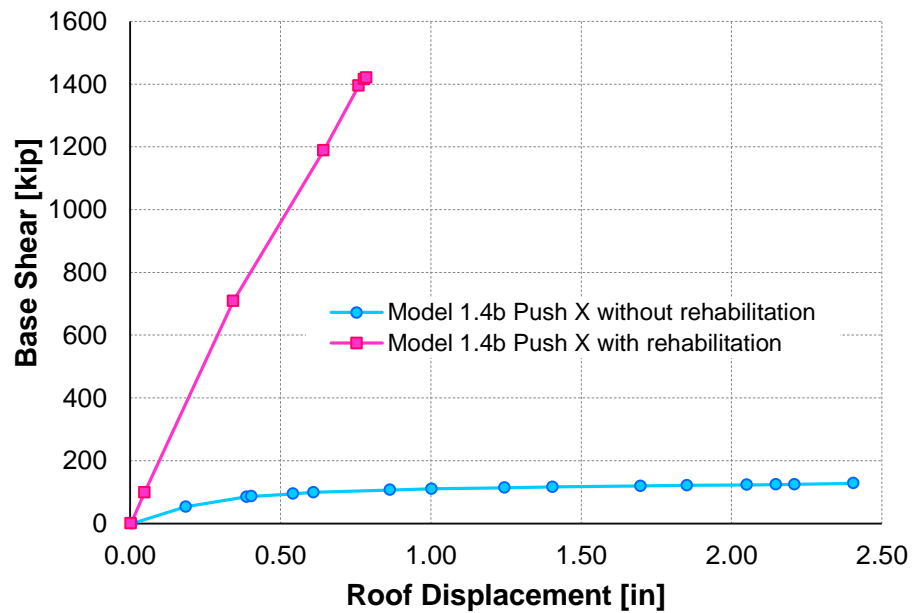


**Figure 7-3.** Comparison Performance Point for Model 1.3c: Push Y. (a) Without Rehabilitation. (b) With Rehabilitation

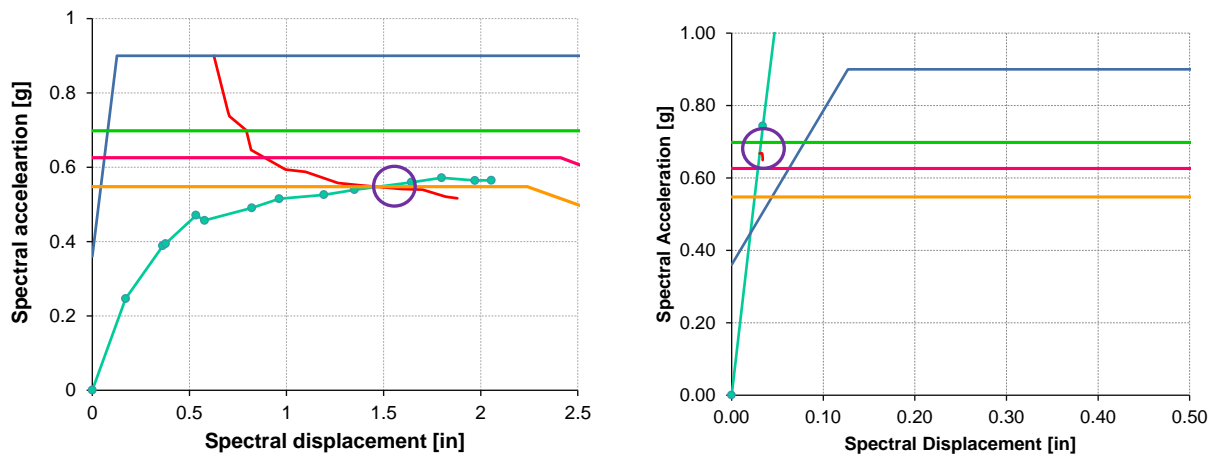
### Model 1.4b: - X direction

**Table 7-2.** Tabular Data for Pushover Curve for Model 1.4b: Push -X Rehabilitation

PUSH -X Mode			Hinge Sequence								
Step	Disp. (in)	Base Force (Kip)	A to B	B to IO	IO to LS	LS to CP	CP to C	C to D	D to E	E to F	Shear
0	0.00	0.00	102	0	0	0	0	0	0	0	
1	-0.05	98.40	102	0	0	0	0	0	0	0	
2	-0.34	709.06	94	4	4	0	0	0	0	0	
3	-0.64	1188.47	86	1	10	0	1	4	0	0	
4	-0.76	1395.12	85	1	12	1	1	1	1	0	
5	-0.78	1415.66	85	1	10	1	1	3	1	0	
6	-0.79	1420.24	85	1	1	1	0	6	8	0	



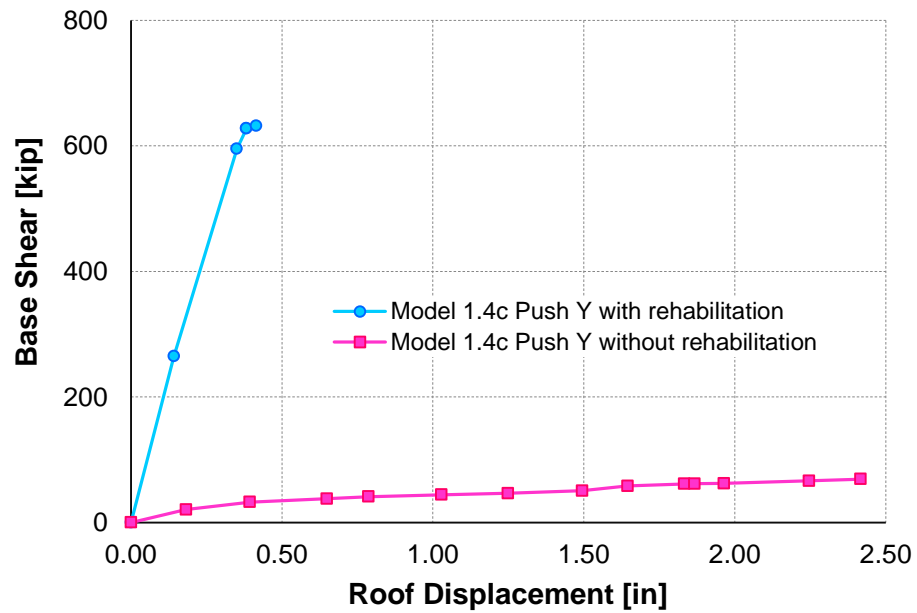
**Figure 7-4.** Comparison Pushover Curves with Rehabilitation for Model 1.4b: Push -X



**Figure 7-5.** Comparison Performance Point for Model 1.4b: Push -X. ((a) Without Rehabilitation. (b) With Rehabilitation

**Model 1.4c: Y direction****Table 7-3.** Tabular Data for Pushover Curve for Model 1.4c: Push Y Rehabilitation

PUSH Y Mode			Hinge Sequence								Shear
Step	Disp. (in)	Base Force (Kip)	A to B	B to IO	IO to LS	LS to CP	CP to C	C to D	D to E	E to F	
0	0.00	0.00	102	0	0	0	0	0	0	0	
1	0.14	264.75	100	2	0	0	0	0	0	0	
2	0.35	595.32	80	4	14	3	0	1	0	0	
3	0.38	627.65	80	3	13	4	0	1	1	0	
4	0.38	627.68	80	2	12	4	0	3	1	0	
5	0.41	631.73	80	2	10	0	0	2	7	1	

**Figure 7-6.** Comparison Pushover Curves with Rehabilitation for Model 1.4c: Push Y

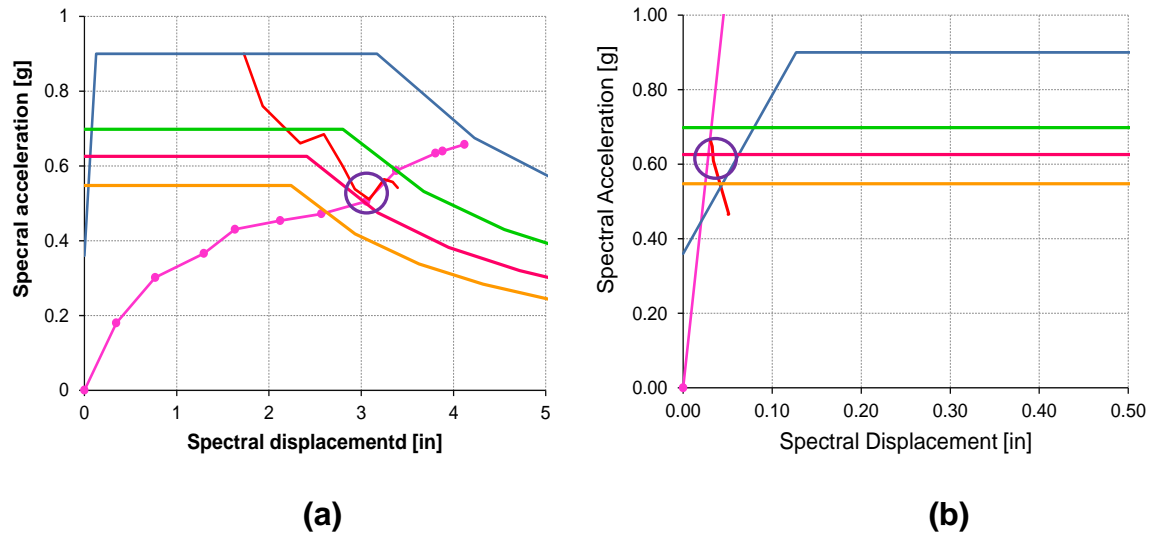
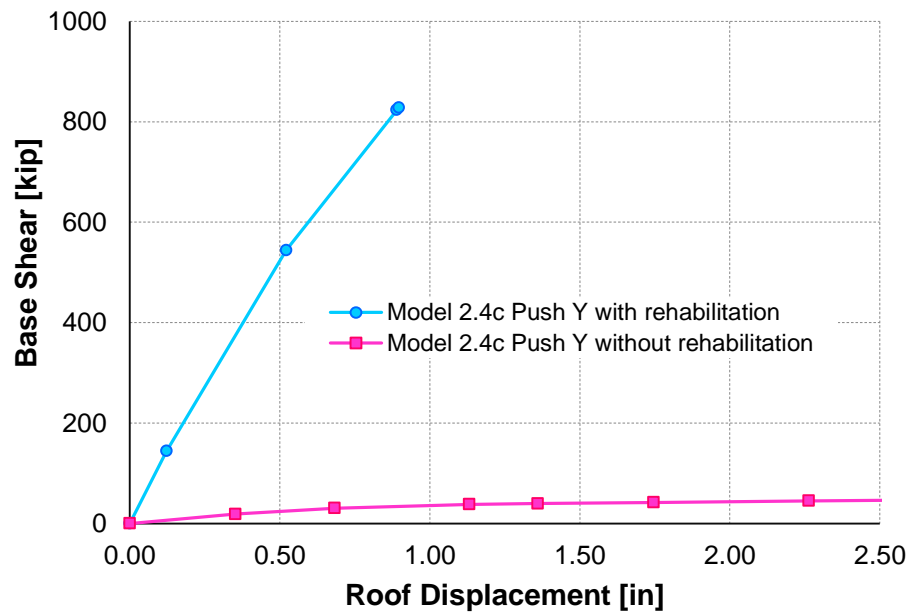


**Figure 7-7.** Comparison Performance Point for Model 1.4c: Push Y. (a) Without Rehabilitation. (b) With Rehabilitation

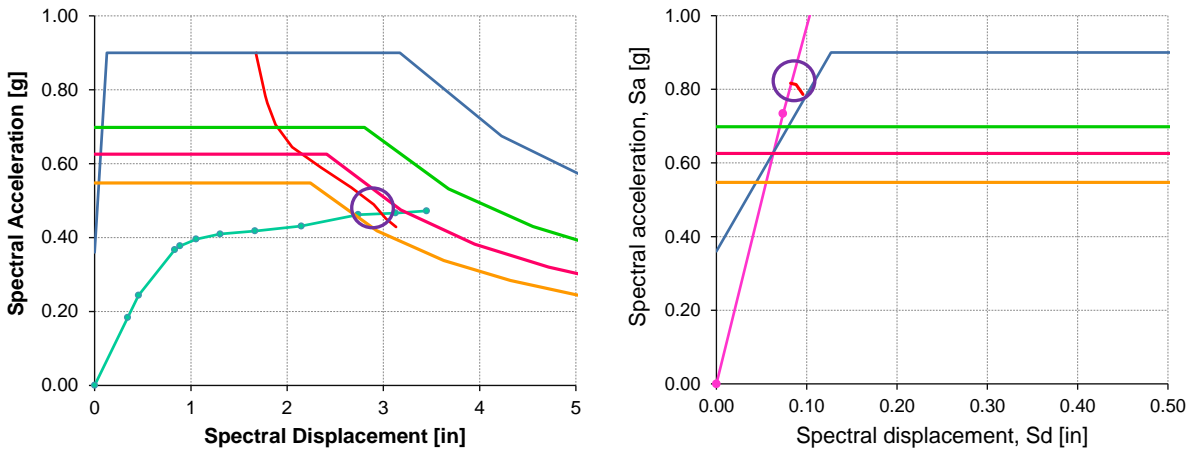
### Model 2.4b: -X direction

**Table 7-4.** Tabular Data for Pushover Curve for Model 2.4b: Push -X Rehabilitation

PUSH X Mode			Hinge Sequence								Shear
Step	Disp. (in)	Base Force (Kip)	A to B	B to IO	IO to LS	LS to CP	CP to C	C to D	D to E	E to F	
0	0.00	0.00	162	0	0	0	0	0	0	0	
1	-0.10	164.56	161	1	0	0	0	0	0	0	
2	-0.49	770.93	145	17	0	0	0	0	0	0	
3	-0.97	1370.64	133	15	7	2	0	2	3	0	
4	-1.04	1453.28	132	16	7	4	0	1	2	0	
5	-1.04	1455.69	132	16	1	0	0	7	6	0	



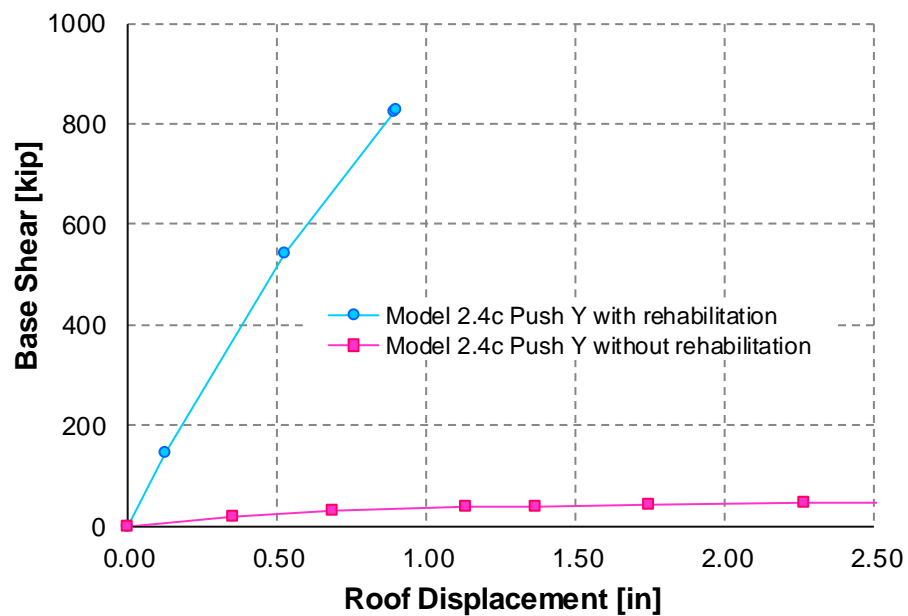
**Figure 7-8.** Comparison Pushover Curves with Rehabilitation for Model 2.4b: Push -X

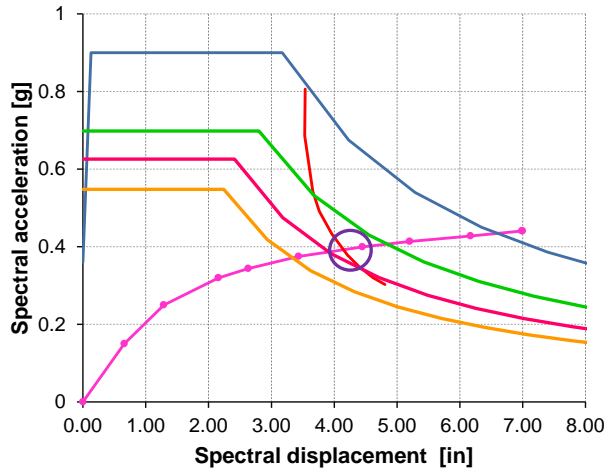


**Figure 7-9.** Comparison Performance Point for Model 2.4b: Push -X. (a) Without Rehabilitation. (b) With Rehabilitation

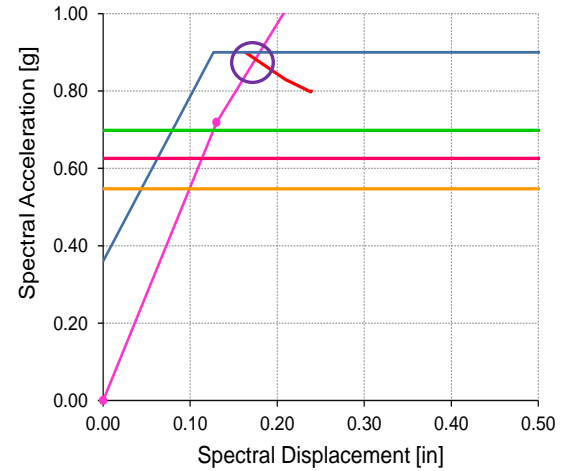
**Model 2.4c: Y direction****Table 7-5.** Tabular Data for Pushover Curve for Model 2.4d: Push Y Rehabilitation

PUSH Y Mode			Hinge Sequence								Shear
Step	Disp. (in)	Base Force (Kip)	A to B	B to IO	IO to LS	LS to CP	CP to C	C to D	D to E	E to F	
0	0.00	0.00	158	0	0	0	0	0	0	0	
1	0.12	144.03	157	1	0	0	0	0	0	0	
2	0.52	544.22	128	4	2	2	8	9	5	0	
3	0.89	823.32	122	7	1	1	2	4	19	2	
4	0.90	827.85	122	7	1	1	2	3	18	4	

**Figure 7-10.** Comparison Pushover Curves with Rehabilitation for Model 2.4c: Push Y



(a)



(b)

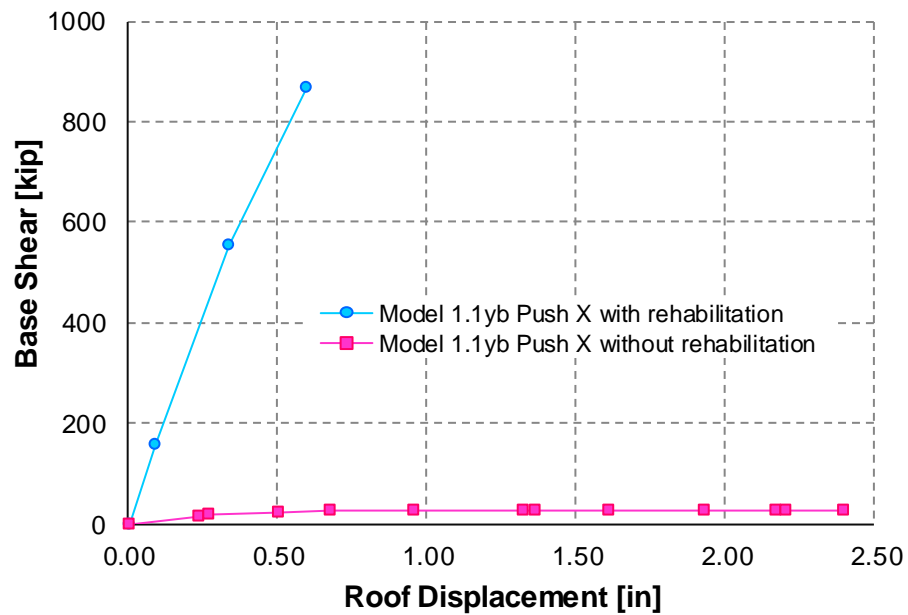
**Figure 7-11.** Comparison Performance Point for Model 2.4c: Push Y. (a) Without Rehabilitation. (b) With Rehabilitation

### Model 1.1.yb : X direction

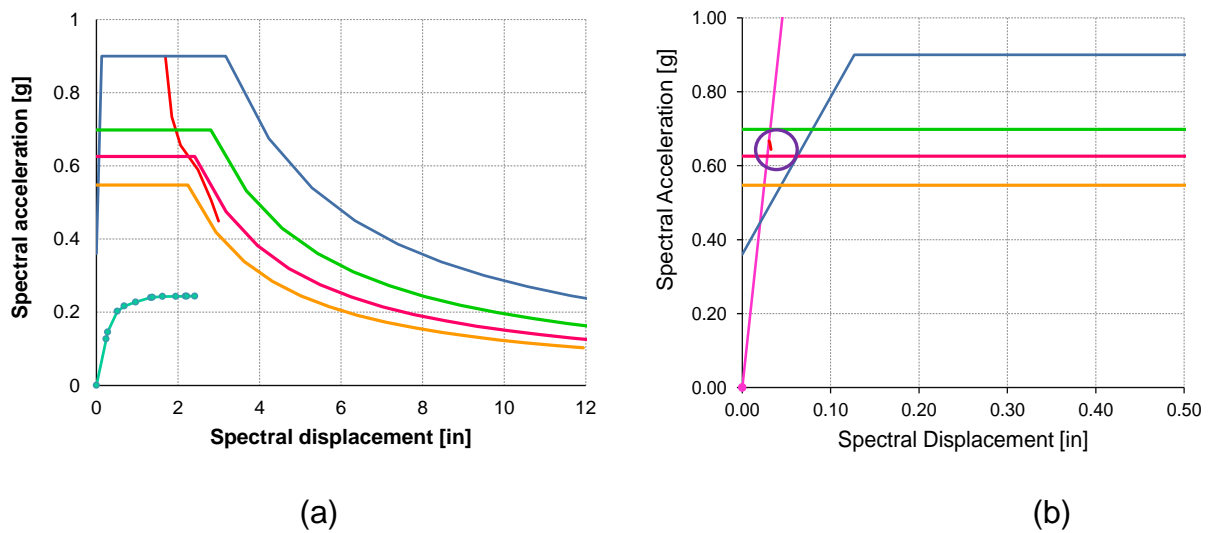
**Table 7-6.** Tabular Data for Pushover Curve for Model 1.1yb: Push –X Rehabilitation

PUSH X Mode			Hinge Sequence								Shear
Step	Disp. (in)	Base Force (Kip)	A to B	B to IO	IO to LS	LS to CP	CP to C	C to D	D to E	E to F	
0	0.00	0.00	102	0	0	0	0	0	0	0	
1	0.09	157.99	102	0	0	0	0	0	0	0	
2	0.34	553.56	92	8	1	0	0	1	0	0	
3	0.59	869.47	87	1	6	0	0	7	0	1	





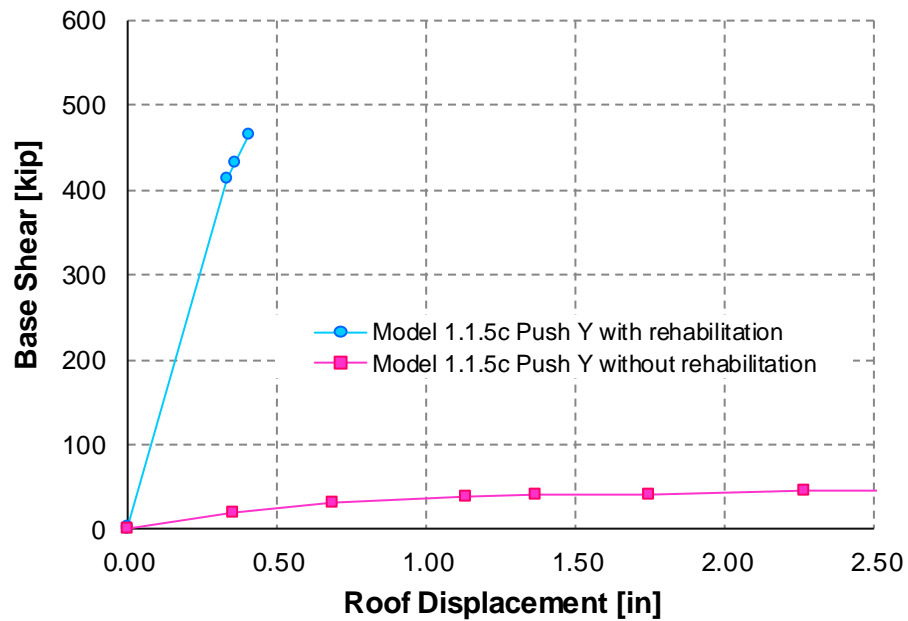
**Figure 7-12.** Comparison Pushover Curves with Rehabilitation for Model 1.1yb: Push -X



**Figure 7-13.** Comparison Performance Point for Model 1.1yb: Push -X. (a) Without Rehabilitation. (b) With Rehabilitation

**Model 1.1.5c : Y direction****Table 7-7.** Tabular Data for Pushover Curve for Model 1.1.5c: Push Y Rehabilitation

PUSH Y Mode			Hinge Sequence								Shear
Step	Disp. (in)	Base Force (Kip)	A to B	B to IO	IO to LS	LS to CP	CP to C	C to D	D to E	E to F	
0	0.00	0.00	102	0	0	0	0	0	0	0	
<b>1</b>	<b>0.00</b>	<b>2.38</b>	<b>102</b>	<b>0</b>	<b>0</b>	<b>0</b>	<b>0</b>	<b>0</b>	<b>0</b>	<b>0</b>	
2	0.33	414.79	90	6	5	0	0	0	1	0	
3	0.36	432.98	89	6	6	0	0	0	1	0	
4	0.41	465.36	85	8	4	0	0	2	2	1	

**Figure 7-14.** Comparison Pushover Curves with Rehabilitation for Model 1.1.5c: Push Y

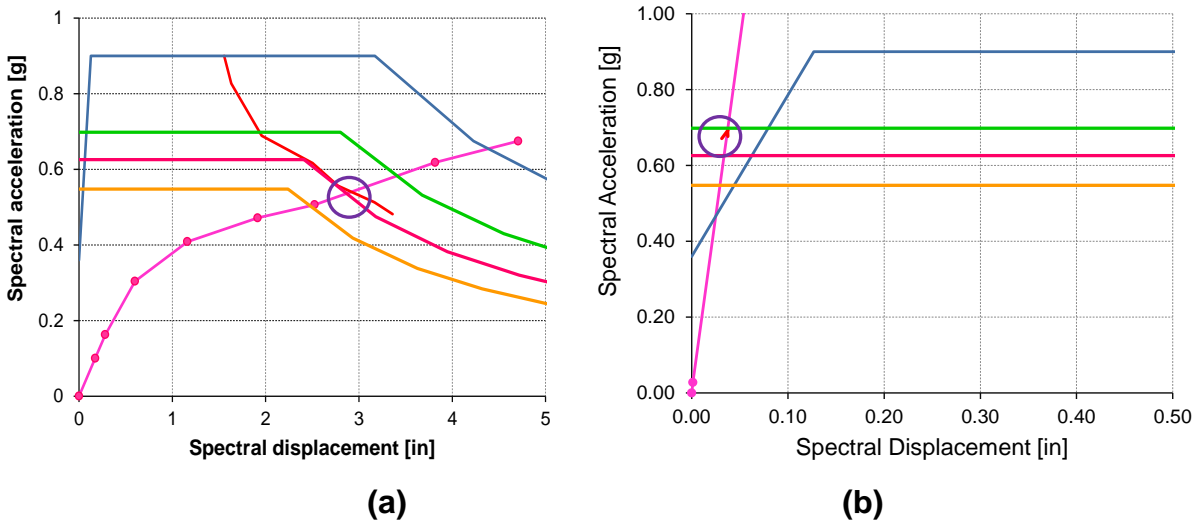


**Figure 7-15.** Comparison Performance Point for Model 1.1.5c: Push Y. (a) Without Rehabilitation. (b) With Rehabilitation

### 7.2.1 DISCUSSION OF RESULTS

Added shear walls, for all the cases presented above, increase the capacity and the stiffness significantly. The initial slope of the pushover curves is extremely steep compared with the models without rehabilitation. The pushover curves showed a very high initial stiffness in the linear range. The performance point occurs before reaching the first step of the pushover analysis showing how much the spectral displacement is reduced. At this stage no hinges have formed. The most important effect of the retrofit is that no damage occurs in the columns. In other word the residences are able to withstand the ground motion in the linear range. From the Tables 7-1 to 7-7 it can be noticed that it is required an extremely high base shear in order to initiate yielding hinge pattern in the elements. Behavior of the structural system transformed completely since the shear wall dominates the behavior of the models. It is though clear that more stiffness reduced the ductility demand and the energy is dissipated through higher base shear and less displacement.

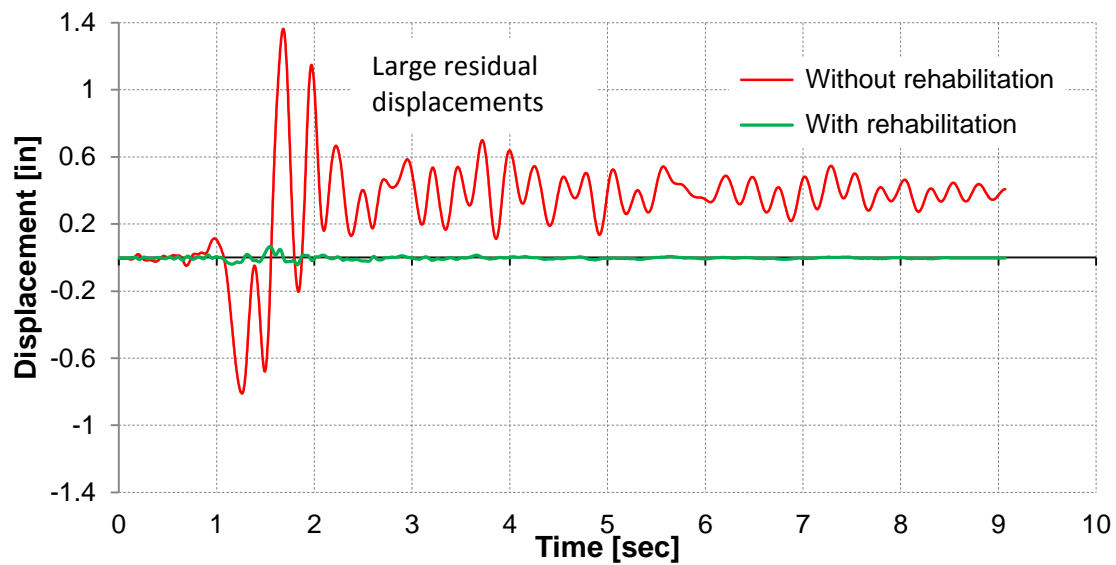
For example, previous to the rehabilitation of Model 1.3c the pushover analysis for this model indicated that as the bay in the X direction was increase the effect was worst in the Y direction due to torsional effects as explained earlier. At the performance point

several hinges were beyond Collapse limit state. After the rehabilitation it was shown no hinge formed at the performance point. The bi-linear approximation of the capacity spectrum occurs far over the plateau of the elastic demand spectrum. The spectral displacement ( $S_d$ ) and spectral acceleration ( $S_a$ ) at the performance point were 3.50 inches and 0.50 g respectively before the rehabilitation. After the rehabilitation the spectral displacement ( $S_d$ ) and spectral acceleration ( $S_a$ ) at the performance point is 0.06 inches and 0.76 g respectively. It can be noticed a significant decrease in the displacement demand. The conclusion above applies for all the cases rehabilitated.

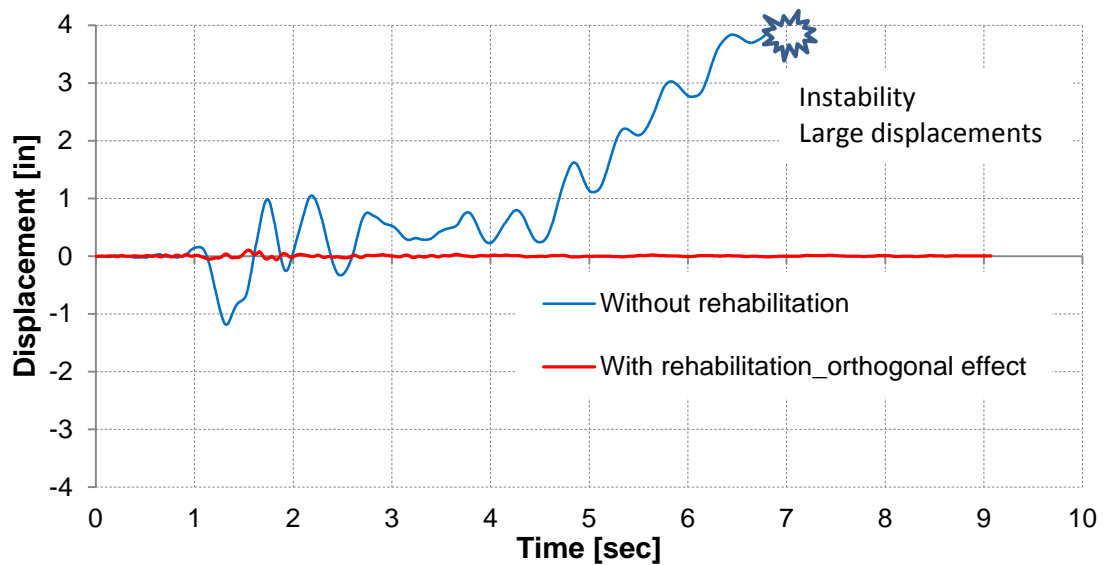
In terms of the dynamic properties, for example for Model 1.3c the effective fundamental periods in the X and Y directions were computed as 0.063 and 0.078 seconds, respectively. These periods were 0.23 and 0.48 seconds before retrofitting with the RC shear walls. Lower periods also reduced the possibility of coincidence with the period of the soil.

## **7.2.2 NONLINEAR TIME HISTORY ANALYSIS REHABILITATED MODELS**

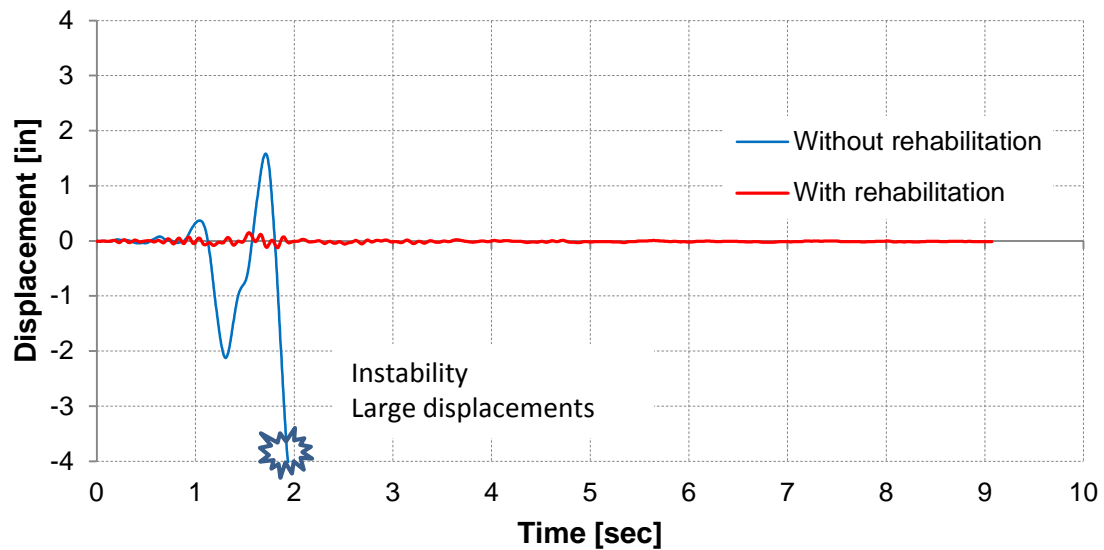
Models 1.4, 2.4 and 1.1y were selected to perform the nonlinear time history analysis with the rehabilitation. As mentioned before not all the cases were re-analyzed with the rehabilitation. Models 1.4 and 2.4 showed poor performance. These models showed large residual displacements in the X direction and instability issues in the Y direction for the San Salvador CIG earthquake. In general the San Salvador CIG record was the most damaging for the models; therefore it was used for the rehabilitation analysis. The displacement time histories were plotted in Figures 7-16 to 7-20 and compared with the model without rehabilitation. The orthogonal effect was included in the analyses. For the analysis in the X direction a 100 percent of the seismic force was applied and a 30 percent of the force acting in the Y direction. For the analysis in the Y direction a 100 percent of the seismic force was applied and a 30 percent of the force acting in the X direction.

**Model 1.4b:-X direction**

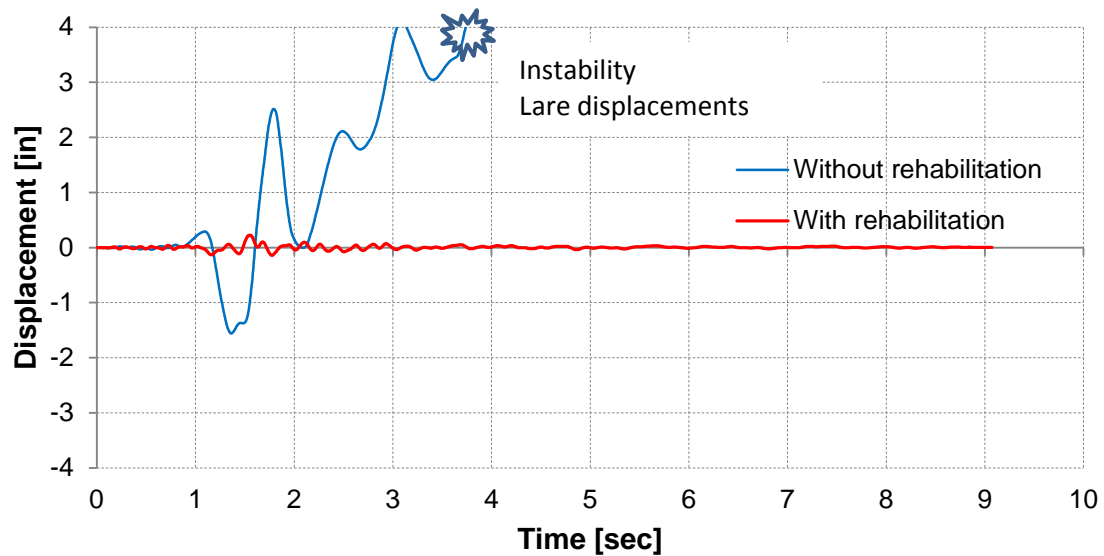
**Figure 7-16.** Displacement Time History of Top Joint for Model 1.4b: San Salvador CIG EQ in the X Direction

**Model 1.4c: Y direction**

**Figure 7-17.** Displacement Time History of Top Joint for Model 1.4c: San Salvador CIG EQ in the Y Direction

**Model 2.4b: X direction**

**Figure 7-18.** Displacement Time History of Top Joint for Model 2.4: San Salvador CIG EQ in the X Direction

**Model 2.4c: Y direction**

**Figure 7-19.** Displacement Time History of Top Joint for Model 1.4c: San Salvador CIG EQ in the Y Direction

### **Model 1.1yb: X direction**

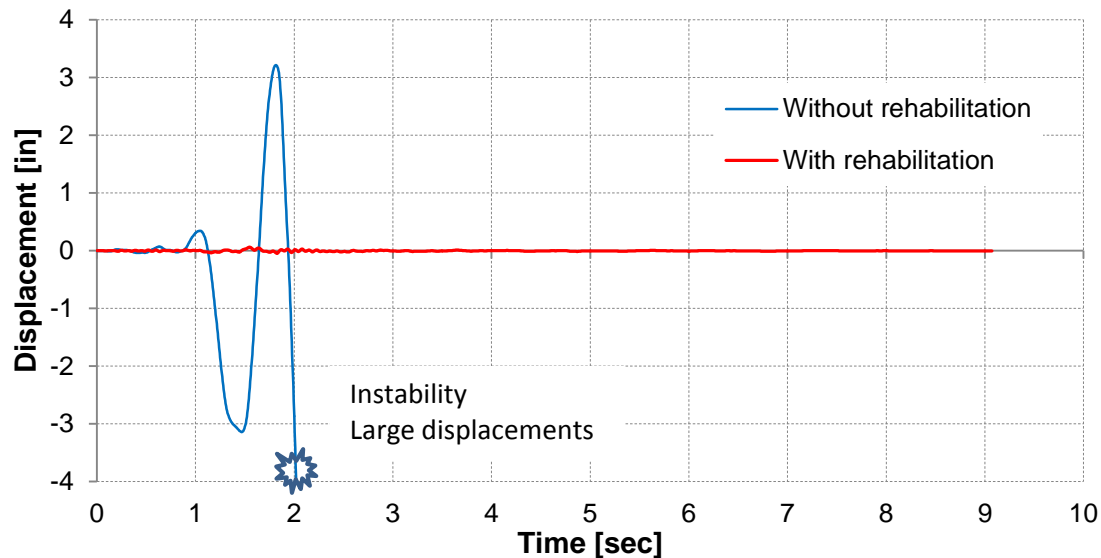


**Figure 7-20.** Displacement Time History of Top Joint for Model 1.1yb: San Salvador CIG EQ in the Y Direction

### **7.2.3 DISCUSSION OF THE RESULTS**

It can be noticed the displacement history is reduced significantly. For Model 1.4b the maximum displacement was 0.07 inch, without the rehabilitation it was 1.38 inch. For Model 1.4c the maximum displacement was 0.08 inch, without the rehabilitation the model presented instability with large displacements (Figure 7-17). No hinges or stability issues occurred formed during the analyses.

## **7.3 STRUCTURAL REHABILITATION WITH RC SHEAR WALL**

For the procedure, structural details, minimum requirements, and material properties for the implementation of the rehabilitation technique with RC shear wall refer to the document “*Rehabilitación Sísmica de Casa en Zancos*.” “*Seismic Rehabilitation for Residences Build Over Gravity Columns*” (Martínez, López and González (2013). This document is a guidance oriented to the general public in Puerto Rico for a quick and

easy understanding to implement the rehabilitation of RC shear walls for residences built over hilly terrain.

### 7.3.1 GENERAL STRUCTURAL CONSIDERATIONS

The analysis with the implementation was performed only verifying that the RC shear wall improved the performance against total collapse, increase stiffness, and decrease significant existing member damage. The design of the new RC shear wall was not performed. The rehabilitation analysis involved locating one wall (minimum) in each direction. The thickness of the wall analyzed was 6 inch. It was verified that the shear capacity of the new RC shear wall for Models 1.4 and 2.4 is greater than the design base shear and the maximum base shear obtained during the San Salvador CIG record as shown in Table 7-8. The shear strength ( $V_n$ ) of the new RC shear wall was calculated according to ACI 318-11 as follows:

$$V_n = A_{cv}(3\sqrt{f'_c} + \rho_n f_y) \quad (7-1)$$

where:

$A_{cv}$  : gross area of wall section bounded by thickness and length of section [in<sup>2</sup>],

$f'_c$  : compressive strength of concrete [psi],

$\rho_n$  : reinforcement ratio = 0.0025, and

$f_y$  : yield strength of reinforcement [psi].

A concrete compressive strength ( $f'_c$ ) of 3,000 psi is required for the new RC shear wall and footing. The minimum reinforcement must be in accordance to ACI 318-11 section 14.3.3 ( $\rho_{\min} = 0.0025$ ).



**Table 7-8.** Shear Strength on New RC Shear Wall

	Vn kip	Design Base Shear kip	V max San Salvador CIG kip
Model 1.4			
RC Wall - X	204.00	55	200
RC Wall - Y	339.00		225
Model 2.4			
RC Wall - X	385.00	60	280
RC Wall - Y	452.00		297

Table 7-9 shows the minimum horizontal and vertical reinforcement requirements and spacing ( $S$ ) for the 6 inch wall. The area of reinforcement required was calculated for a spacing of 12 inch. The area of reinforcement necessary ( $A_{st}$ ) to provide  $\rho_{min}$  is:

$$A_{st} = \rho_{min} t_w s \quad (7-2)$$

where:

$A_{st}$  : area of reinforcement [in<sup>2</sup>],

$\rho_{min}$  : minimum reinforcement ratio,

$t_w$  : thickness of the wall [in], and

$S$  : spacing of vertical and horizontal reinforcement [in].

**Table 7-9.** Reinforcement and Spacing Requirements for 6 inch Wall

thickness wall (in)	rebar	spacing (in)	Ast (in <sup>2</sup> )
6	# 4	12	0.18

The cross section of the new RC shear wall is illustrated in Figure 7-21.

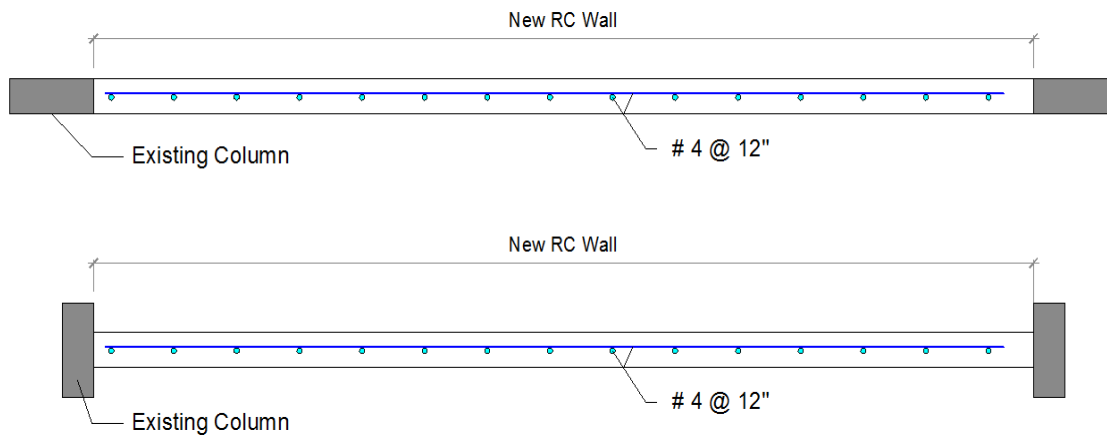


**Figure 7-21.** New RC Shear Wall Structural Detail

An important consideration in the design of RC shear wall rehabilitation is the integration of the new materials with the existing elements. The new RC shear wall must be connected to the existing elements thru the action of dowels. Dowels are used to transfer the shear at the interface between the wall and the frame member. The existing columns act as a boundary element for the new RC shear wall.

### 7.3.2 LIMITATIONS

The new RC shear wall must be designed in accordance to current seismic code requirements. The rehabilitation technique presented in this chapter is limited to a maximum height of twenty (25) feet (from the ground level to the bottom of the residence). A span length up to (15) feet and the maximum number of spans is limited to 4. Only one residence level can stand above the road level, future analysis is required when 2 or more levels over the road exist.

The interactions between the residence and the soil where not considered. As a result, potential problems like land sliding, overturning, uplifting or foundation deficiencies are

not considered. Foundation deficiencies can occur within the foundation element itself, or due to inadequate transfer mechanisms between foundation and soil. Soil conditions need to be verified by a professional geotechnical engineer.

The implementation and design of the shear walls has to be verified by a professional structural engineer.

The construction cost was not considered in this investigation. However, the owner should be aware that the construction cost is always important and it is balanced against other considerations. Other considerations, such as the cost of to be seismically protected and therefore live saving, can be orders of magnitude larger than construction costs, thus lessening its importance.

## CHAPTER 8. CONCLUSIONS

---

### 8.1 SUMMARY

The main purpose of this research work was to study the collapse mechanism and to propose a rehabilitation technique for residences built over hilly terrain in Puerto Rico. Residences built over hilly terrain constitute an important part of the houses in rural Puerto Rico. Three different models have been analyzed to differentiate the effect of retaining walls on lateral resistance. Models type b consisted of a bare frame, models type c had retaining walls considered as masonry block walls and in models type d the retaining walls considered as shear walls.

The residences studied could not satisfy the basic safety requirements of seismic codes because of insufficient material strength, poor detailing, lack of seismic design which eventually lead to brittle response under seismic effects and torsional effects due to asymmetric location of the retaining wall.

The evaluation of the seismic vulnerability was addressed by means a nonlinear pushover analysis followed by a nonlinear time history analysis to the proposed analytical models. Before the pushover analysis was carried out, a linear dynamic analysis was performed in order to obtain the dynamic characteristics of the models. The pushover analysis initially considered both a modal load pattern corresponding to the fundamental mode shape and a uniform load pattern.

The seismic performance evaluation was done as per FEMA 273 and ATC 40 guidelines. Based on the results obtained with the nonlinear pushover and nonlinear time history analyses, the behavior of the analytical models subjected to amplified ground motions was not considered. In general, the models experienced severe damage due to the seismic events without considering amplified loading to account for the site topography. Therefore it was not necessary to go further considering an

amplification factor as the performance of the analytical models has been very adverse without it.

The rehabilitation of the residential houses through retrofitting is a critical issue in reducing seismic risks. Retrofitting of these residences is based on adding new RC shear walls. New walls improve base shear capacity of existing frame system as well as increasing lateral rigidity. Increase in both lateral load capacity and lateral stiffness results in decreasing the deformation demands.

Based on the results obtained during the research, the main conclusions are presented next. The conclusions are subdivided into dynamic analysis results, nonlinear pushover results, nonlinear time history results and rehabilitation. Finally some recommendations for possible future works are presented.

## **8.2 CONCLUSIONS**

### **8.2.1 LINEAR DYNAMIC ANALYSIS RESULTS**

The main conclusions for the linear dynamic analysis are summarized next:

- It was observed that when the span was increased from 10 feet to 15 feet in the Y or X direction the first natural period increased making the structure more flexible.
- When masonry block walls or shear walls (models type c or d) were considered, the natural fundamental period of the analytical models was also reduced.
- In terms of the torsional effects it was observed that all the models that include the retaining wall (models type c/d) the shapes of the vibration modes in the Y direction are affected drastically. In general, these models exhibited high torsional deformations. This phenomenon was expected since the location of the walls is

extremely asymmetric in plan. The center of stiffness of the residences moves away with respect to the center of mass to the wall side causing large eccentricity.

- With the increase in story level (models 2) higher natural periods were obtained when compared to models of group 1.
- When the column orientation was changed (Model 1.1cy), the period increased in the X direction and decreased in the Y direction. This is reasonable because for Model 1.1b the X direction was the strong axis of the column, in contrast for Model 1.1cy where the X direction is now the weak axis of the column. Therefore the period increased as the column became more flexible in this direction.

### **8.2.2 NONLINEAR PUSHOVER ANALYSIS RESULTS**

The main conclusions for the nonlinear pushover analysis are summarized next:

- The elastic limit of the capacity curve does not reach the 5 percent elastic demand spectrum for all the models; therefore, the elastic demand exceeds the elastic capacity and the structure will displace into the inelastic range.
- The capacity predictions obtained with the mode shape load pattern was observed to be the critical case, as the capacity curve leads to less capacity.
- The models are relatively strong at the upper story, since the presence of column hinging was only observed at the lower levels. Plastic hinges formation starts with the frame the shortest columns of the lower story and then propagates to the frames down-hill. Hinges forms at the top and bottom of each column in the lower levels.
- The models are very vulnerable when loaded in their weak direction. It was observed that the capacity of the models in the weak direction of the column is much less than in the strong direction of the column.

- For models without a retaining wall (type b) no performance point was reached in their weak column axis orientation. By the end of the analysis, hinges at the columns in the lower level were beyond the Collapse limit state. These results indicate that failure in the Y direction had occurred or is next to happen. When a hinge state is beyond the Collapse limit level (C to D), it represents the initial failure of the element. It is associated with fracture of longitudinal reinforcement and spalling of concrete. The stage between D to E represents the residual resistance; elements have lost most of their lateral resistance and only are capable of sustaining gravity loads. From a structural repair point of view, elements with this level of damage are not repairable and the structure must be demolished.
- For models that had a retaining wall built either as a masonry block wall or as a concrete wall, the capacity of the residence improved significantly. As expected, it was observed that concrete shear walls had more stiffness and capacity than masonry block walls. The presence of a retaining wall basically provides higher stiffness to the models. However, the retaining wall also caused severe irregularities in stiffness and strength in the residence's elevation and plan. The off-center location of the walls resulted in torsional behavior of the residences. Therefore, even if the capacity of the models increases due to the presence of the walls, the asymmetric location produced torsional problems and this effect is not desirable for the models. It was observed that for this type of models formation of hinges at the lower level went beyond the Collapse limit state. It has been pointed out that repairing the structure with this level of damage is not feasible.
- When the columns weak orientation was changed to the X direction it was observed that the capacity drops drastically due to the change in columns orientation and no performance point was reached. In the Y direction the capacity increased significantly. However, damage was observed at the lower story columns for the pushover analysis in the Y direction. Torsion induced higher forces in the X direction, but now the X direction was the weak axis orientation of the column. As

consequence, columns suffered more damage than for the case when the Y direction was the weak columns orientation.

- For Model 2 (3 stories) It was observed that the middle story is more likely to collapse. Most of the damage was observed at the middle story.
- For square columns (12" x 12"), the overall performance improved in the Y direction.
- For smaller column (12" x 6"), it was observed that the capacity in the X direction for Model 1.1.5b dropped as the column size decreased.
- Overall failure in the models was in flexure. Shear failure was not observed at the performance point.
- Most of the models do not comply with the ductility demand imposed by the response spectrum (UBC 97, soil type Sd)
- Even though many models may not collapse, the damages observed will be beyond repairs.

### **8.2.3 NONLINEAR TIME HISTORY ANALYSIS RESULTS**

The nonlinear time history analysis was carried subjecting the selected models to the earthquakes records described in Chapter 4. For Model 1.1b the analysis was carried out with all four records: Parkfield, Northridge, San Salvador IGN and San Salvador CIG. After evaluating the results it was determined that the most damaging records were both San Salvador records (IGN and CIG). This is reasonable because the peak ground acceleration (PGA) for San Salvador's IGN and CIG records was 0.61 g and 0.87 g, respectively, while for Parkfield and Northridge records the peak ground acceleration (PGA) was 0.27g and 0.12 g, respectively. Therefore it was decided to



analyze the remaining models with Sab Salvador records, which is clearly the critical case scenario.

The main conclusions for the nonlinear time history analysis are summarized next:

### **Model 1.1b**

- For the Parkfield record acting in the X direction the model showed satisfactory behavior: the structural damage state was very limited. The model was capable of withstanding the Parkfield earthquake, local damage was only observed at the bottom columns at frame C within the Immediate Occupancy limit level. On the other hand, the analysis in the Y direction shows significant damage. Plastic hinges were all at or beyond Collapse limit state. Hinges at Collapse limit state were next to experience significant strength degradation and at point D little residual resistance remains, if any. Comparing both X and Y directions, it is evident that the model was more susceptible to extensive damage or collapse in the Y direction, which is the weak column orientation.
- For the Northridge record acting in the X direction, the model was capable of withstanding the earthquake in the elastic range. Similar as it occurred for the Parkfield record, the analysis in the Y direction showed extensive damage. At the end of the analysis, plastic hinges were formed at the bottoms and top of the columns at frame C and B. Plastic hinges at frame C were all at or beyond the collapse limit state.
- For the San Salvador IGN record applied in the X direction, all hinges formed within the Immediate Occupancy limit level. In the Y direction collapse occurred. The program failed to converge at 4.25 seconds, which can be linked to an unstable state of the model. When the analysis was stopped, all hinges in the lower story had failed (E).

- For the San Salvador CIG record acting in the X direction columns at the lower level was severely damaged. Even though the models may not have collapsed the damages could be beyond repairs. In the Y direction collapse occurred.
- In general model type b analyzed in the Y direction collapsed for the San Salvador records. The results were similar to the pushover analysis in terms that it was clearly demonstrated that failure will occur in the Y direction since this is the weak direction of the model and therefore it is more vulnerable. The same behavior is expected when the weak direction of the column is oriented in the X direction (parallel to the road), even worst since this direction normally don't have any lateral support.

#### **Model 1.4b and Model 2.4b**

- Models 1.4b and 2.4b were analyzed with both San Salvador records; it was observed that they experienced more damage than Model 1.1b. For Model 1.4b the bay length was increased and for Model 2.4 the bay length and the number of stories were increased, relative to model 1.1b.

#### **Model 1.1c/d, Model 1.4c and Model 2.1c**

- Models type c/d (with retaining wall) were only analyzed with the San Salvador CIG and NGI records in the Y direction. It was observed that the analysis converge different form results for the case of models type b (without retaining wall). However, at the end of the analysis the columns at frames A and B (frames without lateral support) were severely damaged due to the torsion that the model experienced. It was noticed that several column hinges were at Collapse or beyond Collapse limit state, including shear failures for both records. Structural repair for elements with this level of damage is considered not feasible.

### **Moel 1.1.3b and Model 1.1.3c**

- Model 1.1.3b was able to resist the San Salvador CIG record in the X direction, with only minor damage was observed. Hinges were within the Immediate Occupancy level. In the Y direction the model collapsed.
- Model 1.1.3c was able to resist the San Salvador CIG record in the Y direction, only minor damage was observed. Hinges were within the Immediate Occupancy level.

## **8.2.4 REHABILITATION RESULTS**

The analytical models were rehabilitated with RC shear walls and the effect on the behavior on the models was investigated.

- Adding shear walls, for all the cases presented, increase the stiffness significantly. The performance point occurred before reaching the first step of the pushover analysis. At this stage no hinges have formed. In other words, the residences are able to withstand the ground motion in the linear range.
- The structural rehabilitation improved the seismic performance evaluated by the analytical models and it can prevent the risk of structural collapse

## **8.3 FUTURE WORK**

It is important to study residences with more than one story level above the road level. Also important is to consider disturbance at the lower levels, there are occasions when the underside area is used to make additional housing. It was observed in the field survey that many residences have unfinished construction underside, like masonry block walls elevated to half height of the total story height leading to problems like short column effects. It was also observed changes in stiffness between the stories, like one

story bare frame and other story with masonry block wall on the perimeter leading to vertical irregularities.

This investigation did not consider the effect of the soil structure interaction. It may be important to study the effect of considering this interaction in the seismic behavior of residential models. Slope stability may also be an issue during strong earthquakes.

It is important to instrument several residences of this type around the island to study the dynamic characteristics and compare them with the analytical results.

The rehabilitation with RC shear walls should be studied including the topographic amplification factor.

The effect of including the vertical component of earthquake records in the models can also be investigated. For slender columns vertical acceleration can be serious due to the increase in axial load causing buckling in the column.

## REFERENCES

American Concrete Institute (ACI-318-11) (2011) "Building Code Requirements for Structural Concrete", American Concrete Institute.

Arroyo, M. (2001), "Numerical Study of the Amplification of the Seismic Ground Acceleration Due to Local Topography", MS Thesis, Civil Engineering Department, University of Puerto Rico at Mayagüez.

ASCE SEI/ASCE 7 (2005). "Minimum Design Loads for Buildings and Other Structures", Reston (USA): American Society of Civil Engineers.

ATC (1982). "An Investigation of the Correlation between Earthquake Ground Motion and Building Performance", Report ATC-10, Applied Technology Council, Redwood City, California.

ATC 40 (1996), Seismic Evaluation and Retrofit of Concrete Buildings, Volume 1-2, California.

ATC 19 (1995) "Structural Response Modification Factors", Applied Technology Council, Redwood city, California.

Chandrasekaran, S., Nunziante, L., Serino, G. and Carannante, F. (2010). "Seismic Design Aids for Nonlinear Analysis of Reinforcement Structures", Taylor & Francis Group, U.S.A

Chopra, A.K. and Goel, R.K (2001). "A Modal Pushover Analysis Procedure to Estimate Seismic Demands for Buildings: Theory and Preliminary Evaluation", Pacific Earthquake Engineering Research Center, College of Engineering University of Berkeley: California.

Clinton, J.F., Cua, G., Huérano, V., Von Hillebrandt, C. and Martínez, J.A. (2006) “The Current State of Seismic Monitoring in Puerto Rico”, *Seismological Research Letters* Volume 77, Number 5

FEMA 273 (1997): “NEHRP Guidelines for the Seismic Rehabilitation of Buildings”, developed by the Building Seismic Safety Council for the Federal Emergency Management Agency (Report No. FEMA 273), Washington, D.C.

FEMA 356 (2000), *Prestandard and Commentary for the Rehabilitation of Buildings*,

Frankel, A., C. Mueller, T. Barnhard, D. Perkins, E. Leyendecker, N. Dickman, S. Hanson, and M. Hopper (1996). *National Seismic Hazard Maps: Documentation* June 1996, USGS Open-File Report 96-532, 70 pages.

Frankel, A. D., M.D. Petersen, C.S. Mueller, K.M. Haller, R.L. Wheeler, E.V. Leyendecker, R.L. Wesson, S.C. Harmsen, C.H. Cramer, D.M. Perkins, and K.S.

González, L. (2007), “Retrofitting of R/C Structures on Gravity Columns using Inverted – Y Steel Bracing”, M.S. Thesis, Civil Engineering Department, University of Puerto Rico.

Güner, S. (2007), “Performance Assessment of Shear-Critical Reinforced Concrete Plane Frames”, PhD. Thesis, Civil Engineering Department, University of Toronto, Canada

Irizarry, J. (1999), “Design Earthquake and Design Spectra for Puerto Rico’s Main Cities based on Worldwide Strong Motion Records”, M.S. Thesis, Civil Engineering Department, University of Puerto Rico at Mayagüez.

Jirsa J. and Kreger M. (1989), “Recent Research on Repair and Strengthening of Reinforced Concrete Structures”, *Proceedings of the ASCE Structures Congress*, California, 1: 679–688.

Kaplan H., Yilmazi S., Cetinkaya N., Atimtay E. (2011), “Seismic strengthening of RC structures with exterior shear walls”. *Sadhana* Vol. 36, Part 1, February 2011, pp. 17–34. Indian Academy of Sciences.

King D.J. et al.(1986), “Computer Programs for Concrete Column Designs”, Research Report 86/12, Department of Civil Engineering, University of Canterbury, New Zeland.

Krawinkler H. and Seneviratna G.D.P.K. (1998), “Pros and Cons of a Pushover Analysis of Seismic Performance Evaluation”, *Engineering Structures*, Vol.20, 452-464.

LaForge, R. C., and W. R. McCann (2003). A seismic source model for Puerto Rico, for use in probabilistic ground motion hazard analysis. In *Active Tectonics and Seismic Hazards of Puerto Rico, the Virgin Islands, and Offshore Areas*, ed. P. Mann, Geological Society of America Special Paper 385, 223–248.

Martínez, J. A., López, R.R. and González, Y. (2013) “ Rehabilitación Sísmica de Casas en Zancos”, Puerto Rico Strong Motion Program, University of Puerto Rico, Department of Civil Engineering.

Moehle J, P. (2000). “State of research on seismic retrofit of concrete building structures in the US”. *Proceeding of US-Japan symposium and workshop on seismic retrofit of concrete structures - State of Research and Practice, USA*

Montejo, L.A. and Kowalsky, M.J. (2007) “CUMBIA – Set of Codes for the Analysis of Reinforced Concrete Members”, CFL Technical Report No. IS-07-01. Department of Civil, Construction and Environmental Engineering, North Carolina State University, Raleigh.

Mwafy A.M. and Elnashai A.S. (2001), “Static Pushover versus Dynamic Analysis of R/C Buildings”, *Engineering Structures*, Vol. 23, 407-424.

Mansuri, M. (2009). "Torsional Effects on the Inelastic Seismic Response of Structures", PhD. Thesis, Faculty of the Graduate School University of Southern California, California.

Mueller, C., A. D. Frankel, M. D. Petersen, and E. V. Leyendecker (2003), "Documentation for 2003 USGS Seismic Hazard Maps for Puerto Rico and the U.S. Virgin Islands", U.S. Geological Survey Open-File Report 03-379, [http://earthquake.usgs.gov/hazmaps/products\\_data/Puerto-Rico-VI/prvi2003doc.html](http://earthquake.usgs.gov/hazmaps/products_data/Puerto-Rico-VI/prvi2003doc.html)

Mander, J.B., M.J.N. Priestley, and R. Park (1984), "Theoretical Stress-Strain Model for Confined Concrete", Journal of Structural Engineering. ASCE. 114(3). 1804-1826.

Mondal, A., Gosh, S. and Reddy, G.R. (2013), "Performance-based evaluation of the response reduction factor for ductile RC frames", Engineering Structures, Journal JEST.

National Institute of Building Sciences. (1997). "Earthquake Loss Estimation Methodology HAZUS 97: Technical Manual.", Report prepared for the Federal Emergency Management Agency, Washington, D.C.

National Earthquake Information Center. Earthquake History of Puerto Rico. [http://www.neic.usgs.gov/neis/states/puerto\\_rico/puerto\\_rico\\_history.html](http://www.neic.usgs.gov/neis/states/puerto_rico/puerto_rico_history.html).

SAP2000 (2009). Static and Dynamic Finite Element Analysis for Structures Nonlinear Version 14. Computers and Structures, Inc, Berkeley, California.

Uniform Building Code (1997), International Conference of Building Officials, Whittier, California.



Vázquez, D. (2002). "Seismic Behavior and Retrofitting of Hillside and Hilly Terrain of R/C Houses on Gravity Columns.", Ph.D. Thesis, Department of Civil Engineering, University of Puerto Rico, Mayagüez Campus.

Vélez, E. (2007). "Experimental Cyclic Behaviour of Reinforced Concrete Wall houses. Loaded in their Weak Direction", Ph.D. Thesis, Department of Civil Engineering, University of Puerto Rico, Mayagüez Campus.

Paulay, T. and Priestley, M. J. N. (1992). "Seismic Design of Reinforced Concrete and Masonry Buildings", John Wiley & Sons, Inc., New York, 744 pp.

OpenSeesBerkeley, [http://opensees.berkeley.edu/wiki/index.php/Hilber-Hughes Taylor\\_Method](http://opensees.berkeley.edu/wiki/index.php/Hilber-Hughes_Taylor_Method).

Whittaker A, Hart G, Rojahn C (1999),. "Seismic Response Modification Factors". J Struct Eng, ASCE 1999;125(4):438–44.

Oğuz, S. (2005), "Evaluation of Pushover Analysis Procedures for Frame Structures" M.S Thesis. Engineering. Middle East Technical University.

Themelis, S. (2008), "Pushover Analysis for Seismic Assessment and Design of Structures". Ph.D. Thesis, School of the Built Environment , Heriot Watt University.

Patel, B. and Shah, D. (2010), "Formulation of Response Reduction Factor for RCC Framed Staging of Elevated Water Tank using Static Pushover Analysis", Proceedings of the World Congress on Engineering Vol III, June 30 - July 2, 2010, London, U.K.

Prentice, C. S., and P. Mann (2005). Paleoseismic study of the South Lajas fault: First documentation of an onshore Holocene fault in Puerto Rico. In Active Tectonics and Seismic Hazards of Puerto Rico, the Virgin Islands, and Offshore Areas, ed. P. Mann,

Geological Society of America Special Paper 385, 215–222. PRSN Historical Catalogue, <http://temblor.uprm.edu/~victor/PRSN/history/>

## Appendix A. ATC 40 / FEMA 356 HINGE PROPERTIES

**Table. A-1.** Default hinges properties for Reinforced Concrete Beam (FEMA 356)

Table 6-6 Modeling Parameters and Numerical Acceptance Criteria for Nonlinear Procedures—Reinforced Concrete Beams										
Conditions			Modeling Parameters <sup>3</sup>			Acceptance Criteria <sup>3</sup>				
			Plastic Rotation Angle, radians		Residual Strength Ratio	Plastic Rotation Angle, radians				
						Component Type				
						Primary		Secondary		
						Performance Level				
			a	b	c	IO	LS	CP	LS	CP
i. Beams controlled by flexure <sup>1</sup>										
$\frac{\rho - \rho'}{\rho_{bal}}$	Trans. Reinf. <sup>2</sup>	$\frac{V}{b_w d \sqrt{f'_c}}$								
≤ 0.0	C	≤ 3	0.025	0.05	0.2	0.005	0.02	0.025	0.02	0.05
≤ 0.0	C	≥ 6	0.02	0.04	0.2	0.005	0.01	0.02	0.02	0.04
≥ 0.5	C	≤ 3	0.02	0.03	0.2	0.005	0.01	0.02	0.02	0.03
≥ 0.5	C	≥ 6	0.015	0.02	0.2	0.005	0.005	0.015	0.015	0.02
≤ 0.0	NC	≤ 3	0.02	0.03	0.2	0.005	0.01	0.02	0.02	0.03
≤ 0.0	NC	≥ 6	0.01	0.015	0.2	0.0	0.005	0.01	0.01	0.015
≥ 0.5	NC	≤ 3	0.01	0.015	0.2	0.005	0.01	0.01	0.01	0.015
≥ 0.5	NC	≥ 6	0.005	0.01	0.2	0.0	0.005	0.005	0.005	0.01
ii. Beams controlled by shear <sup>1</sup>										
Stirrup spacing ≤ d/2			0.0	0.02	0.2	0.0	0.0	0.0	0.01	0.02
Stirrup spacing > d/2			0.0	0.01	0.2	0.0	0.0	0.0	0.005	0.01
iii. Beams controlled by inadequate development or splicing along the span <sup>1</sup>										
Stirrup spacing ≤ d/2			0.0	0.02	0.0	0.0	0.0	0.0	0.01	0.02
Stirrup spacing > d/2			0.0	0.01	0.0	0.0	0.0	0.0	0.005	0.01
iv. Beams controlled by inadequate embedment into beam-column joint <sup>1</sup>										
			0.015	0.03	0.2	0.01	0.01	0.015	0.02	0.03

1. When more than one of the conditions i, ii, iii, and iv occurs for a given component, use the minimum appropriate numerical value from the table.
2. Under the heading "Transverse Reinforcement," "C" and "NC" are abbreviations for conforming and nonconforming details, respectively. A component is conforming if, within the flexural plastic region, closed stirrups are spaced at ≤ d/3, and if, for components of moderate and high ductility demand, the strength provided by the stirrups ( $V_s$ ) is at least three-fourths of the design shear. Otherwise, the component is considered nonconforming.
3. Linear interpolation between values listed in the table is permitted.

**Table A-2.** Default hinges properties for Reinforced Concrete Columns (FEMA 356)

Table 6-7 Modeling Parameters and Numerical Acceptance Criteria for Nonlinear Procedures—Reinforced Concrete Columns

Conditions	Modeling Parameters <sup>4</sup>			Acceptance Criteria <sup>4</sup>						
	Plastic Rotation Angle, radians		Residual Strength Ratio	Plastic Rotation Angle, radians						
				Component Type						
				Primary		Secondary				
				Performance Level						
	a	b	c	IO	LS	CP	LS	CP		
i. Columns controlled by flexure <sup>1</sup>										
$\frac{P}{A_g f'_c}$	Trans. Reinf. <sup>2</sup>	$\frac{V}{b_w d \sqrt{f'_c}}$								
≤ 0.1	C	≤ 3	0.02	0.03	0.2	0.005	0.01	0.02	0.015	0.03
≤ 0.1	C	≥ 6	0.015	0.025	0.2	0.005	0.01	0.015	0.01	0.025
≥ 0.4	C	≤ 3	0.015	0.025	0.2	0.0	0.005	0.015	0.010	0.025
≥ 0.4	C	≥ 6	0.01	0.015	0.2	0.0	0.005	0.01	0.01	0.015
≤ 0.1	NC	≤ 3	0.01	0.015	0.2	0.005	0.005	0.01	0.005	0.015
≤ 0.1	NC	≥ 6	0.005	0.005	–	0.005	0.005	0.005	0.005	0.005
≥ 0.4	NC	≤ 3	0.005	0.005	–	0.0	0.0	0.005	0.0	0.005
≥ 0.4	NC	≥ 6	0.0	0.0	–	0.0	0.0	0.0	0.0	0.0
ii. Columns controlled by shear <sup>1,3</sup>										
Hoop spacing ≤ d/2, or $\frac{P}{A_g f'_c} \leq 0.1$			0.0	0.015	0.2	0.0	0.0	0.0	0.01	0.015
Other cases			0.0	0.0	0.0	0.0	0.0	0.0	0.0	0.0
iii. Columns controlled by inadequate development or splicing along the clear height <sup>1,3</sup>										
Hoop spacing ≤ d/2			0.01	0.02	0.4	1	1	1	0.01	0.02
Hoop spacing > d/2			0.0	0.01	0.2	1	1	1	0.005	0.01
iv. Columns with axial loads exceeding 0.70P <sub>e</sub> <sup>1,3</sup>										
Conforming reinforcement over the entire length			0.015	0.025	0.02	0.0	0.005	0.001	0.01	0.02
All other cases			0.0	0.0	0.0	0.0	0.0	0.0	0.0	0.0

1. When more than one of the conditions i, ii, iii, and iv occurs for a given component, use the minimum appropriate numerical value from the table.
2. Under the heading "Transverse Reinforcement," "C" and "NC" are abbreviations for conforming and nonconforming details, respectively. A component is conforming if, within the flexural plastic hinge region, closed hoops are spaced at ≤ d/3, and if, for components of moderate and high ductility demand, the strength provided by the stirrups ( $V_s$ ) is at least three-fourths of the design shear. Otherwise, the component is considered nonconforming.
3. To qualify, hoops must not be lap spliced in the cover concrete, and hoops must have hooks embedded in the core or other details to ensure that hoops will be adequately anchored following spalling of cover concrete.
4. Linear interpolation between values listed in the table is permitted.

## Appendix B. SUPPORTING MATERIAL FOR STEEL CONSTITUTIVE MODELS

The following parameters define rebar stress strain curve, directly taken from SAP2000 technical notes:

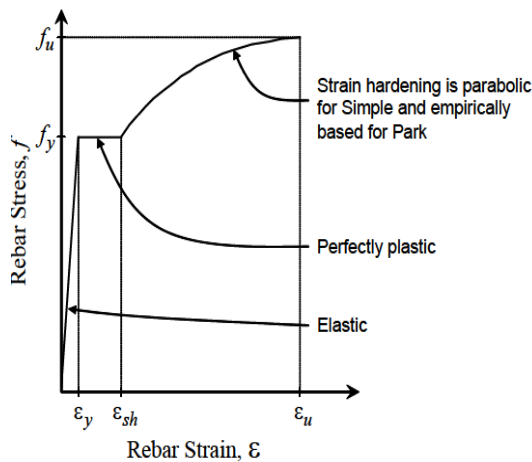


Figure 2 Rebar Parametric Stress-Strain Curve

$\varepsilon$  = Rebar strain

$f$  = Rebar stress

$E$  = Modulus of elasticity

$f_y$  = Rebar yield stress

$f_u$  = Rebar ultimate stress capacity

$\varepsilon_{sh}$  = Strain in rebar at the onset of strain hardening

$\varepsilon_u$  = Rebar ultimate strain capacity

The rebar yield strain,  $\varepsilon_y$ , is determined from  $\varepsilon_y = f_y / E$ .

For  $\varepsilon \leq \varepsilon_y$  (elastic region)

$$f = E\varepsilon$$

For  $\varepsilon_y < \varepsilon \leq \varepsilon_{sh}$  (perfectly plastic region)

$$f = f_y$$

For  $\varepsilon_{sh} < \varepsilon \leq \varepsilon_u$  (strain hardening region)

For Simple parametric curves,

$$f = f_y + (f_u - f_y) \sqrt{\frac{\varepsilon - \varepsilon_{sh}}{\varepsilon_u - \varepsilon_{sh}}}$$

For Park parametric curves,

$$f = f_y \left( \frac{m(\varepsilon - \varepsilon_{sh}) + 2}{60(\varepsilon - \varepsilon_{sh}) + 2} + \frac{(\varepsilon - \varepsilon_{sh})(60 - m)}{2(30r + 1)^2} \right)$$

where,

$$r = \varepsilon_u - \varepsilon_{sh}$$

$$m = \frac{(f_u/f_y)(30r + 1)^2 - 60r - 1}{15r^2}$$

## Appendix C. SUPPORTING MATERIAL FOR CONCRETE CONSTITUTIVE MODELS

The following parameters define the Mander unconfined concrete stress strain curve, directly taken from SAP2000 technical notes:

$\varepsilon$  = Concrete strain

$f$  = Concrete stress

$E$  = Modulus of elasticity

$f'_c$  = Concrete compressive strength

$\varepsilon'_c$  = Concrete strain at  $f'_c$

$\varepsilon_u$  = Ultimate concrete strain capacity

The Mander unconfined concrete stress-strain curve is defined by the following equations:

For  $\varepsilon \leq 2\varepsilon'_c$  (curved portion),

$$f = \frac{f'_c x r}{r - 1 + x^r}$$

where

$$x = \varepsilon / \varepsilon'_c$$

$$r = \frac{E}{E - (f'_c / \varepsilon'_c)}$$

For  $2\varepsilon'_c < \varepsilon \leq \varepsilon_u$  (linear portion),

$$f = \left( \frac{2f'_c r}{r - 1 + 2^r} \right) \left( \frac{\varepsilon_u - \varepsilon}{\varepsilon_u - 2\varepsilon'_c} \right)$$

where  $r$  is as defined previously for the curved portion of the curve.

The tensile yield stress for the Mander unconfined curve is taken at  $7.5\sqrt{f'_c}$  in psi.

The following parameters define the Mander confined concrete stress strain curve, directly taken from SAP2000 technical notes:

$\varepsilon$  = Concrete strain

$f$  = Concrete stress

$E$  = Modulus of elasticity (tangent modulus)

$E_{sec}$  = Secant modulus of elasticity

$f'_c$  = Compressive strength of unconfined concrete

$f'_{cc}$  = Compressive strength of confined concrete; this item is dependent on the confinement steel provided in the section and is explained later

$\varepsilon'_c$  = Concrete strain at  $f'_c$

$\varepsilon_u$  = Ultimate concrete strain capacity for unconfined concrete and concrete spalling strain for confined concrete

$\varepsilon'_{cc}$  = Concrete strain at  $f'_{cc}$

$\varepsilon_{cu}$  = Ultimate concrete strain capacity for confined concrete; this item is dependent on the confined steel provided in the section and is explained later

The Mander confined concrete stress-strain curve is defined by the following equations:

$$f = \frac{f'_{cc} X^r}{r - 1 + X^r}$$

where,

$$\varepsilon'_{cc} = \left\{ 5 \left( \frac{f'_{cc}}{f'_c} - 1 \right) + 1 \right\} \varepsilon'_c$$

$$X = \varepsilon / \varepsilon'_{cc}$$

$$E_{sec} = f'_{cc} / \varepsilon'_{cc}$$

$$r = E / (E - E_{sec})$$

## Mander Confined Concrete Compressive Strength, $f'_{cc}$

The following parameters are used in the explanation of  $f'_{cc}$  :

$A_c$  = Area of concrete core measured from centerline to centerline of confinement steel

$A_{cc}$  = Concrete core area excluding longitudinal bars;  $A_{cc} = A_c (1 - \rho_{cc})$

$A_e$  = Concrete area that is effectively confined

$A_{sc}$  = Area of a circular hoop or spiral confinement bar

$A_{sL}$  = Total area of all longitudinal bars

$A_{sx}$  = Area of rectangular hoop legs extending in the x-direction

$A_{sy}$  = Area of rectangular hoop legs extending in the y-direction

$b_c$  = Centerline to centerline distance between rectangular perimeter hoop legs that extend in the y-direction

$d_c$  = Centerline to centerline distance between rectangular perimeter hoop legs that extend in the x-direction

$d_s$  = Diameter of circular hoops or spirals of confinement steel measured from centerline to centerline of steel

$f'_c$  = Unconfined concrete compressive strength

$f'_L$  = Lateral pressure on confined concrete provided by the confinement steel

$f'_L$  = Effective lateral pressure on confined concrete provided by the confinement steel

$f_{yh}$  = Yield stress of confinement steel

$K_e$  = Coefficient measuring the effectiveness of the confinement steel

$s$  = Centerline to centerline longitudinal distance between hoops or spirals

$s'$  = Clear longitudinal distance between hoops or spirals

$w'$  = Clear transverse distance between adjacent longitudinal bars with cross ties

$\rho_{cc}$  = Longitudinal steel ratio;  $\rho_{cc} = A_{sL}/A_c$

$\rho_s$  = Volumetric ratio of transverse confinement steel to the concrete core

$\rho_x$  = Steel ratio for rectangular hoop legs extending in the x-direction;  $\rho_x = A_{sx}/sd_c$

$\rho_y$  = Steel ratio for rectangular hoop legs extending in the y-direction;  $\rho_y = A_{sy}/sb_c$



For rectangular cores

$$\rho_x = \frac{A_{sx}}{sd_c}$$

$$\rho_y = \frac{A_{sy}}{sb_c}$$

$$f_{Lx} = \rho_x f_{yh}$$

$$f_{Ly} = \rho_y f_{yh}$$

$$A_e = \left( b_c d_c - \sum_{i=1}^n \frac{(w'_i)^2}{6} \right) \left( 1 - \frac{s'}{2b_c} \right) \left( 1 - \frac{s'}{2d_c} \right)$$

$$A_{cc} = b_c d_c$$

$$K_e = \frac{A_e}{A_{cc}}$$

$$f'_{Lx} = K_e f_{Lx}$$

$$f'_{Ly} = K_e f_{Ly}$$

## Mander Confined Concrete Ultimate Strain Capacity,

$\epsilon_{cu}$

The Mander confined concrete ultimate strain capacity,  $\epsilon_{cu}$ , is a function of the confinement steel. The following figure shows the Mander stress-strain curves for confined and unconfined concrete. The difference between the confined and unconfined curves is shown shaded.

The shaded area shown in Figure 9 represents the additional capacity provided by the confinement steel for storing strain energy.

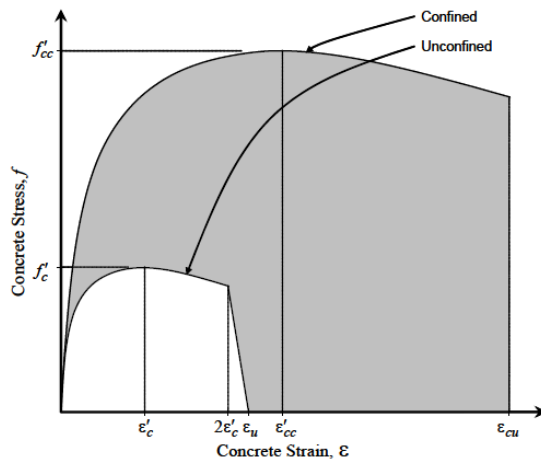


Figure 9 Mander Confined and Unconfined Stress-Strain Curves

This area is limited to the energy capacity available in the area under the confinement steel stress-strain curve up to the ultimate steel strain,  $\epsilon_u$ .

Suppose  $A_1$  is the shaded area between the Mander confined and unconfined curves and  $A_2$  is the area under the confinement steel stress-strain curve. Further suppose  $\rho_s$  is the volumetric ratio of confinement steel to the concrete core. Then, equating energies under the concrete and confinement steel stress-strain curves gives:

$$A_1 = \rho_s A_2$$

The program determines the appropriate value of the confined concrete ultimate straining,  $\epsilon_{cu}$ , by trial and error, equating energies as

described previously. When the  $A_1 = \rho_s A_2$  relationship is satisfied, the correct value of  $\epsilon'_{cu}$  has been found.

The tensile yield stress for the Mander confined curves is taken as  $7.5\sqrt{f'_c}$  in psi.

## Appendix D. AXIAL LOAD CALCULATION

**Table D-1.** Axial Load Calculation Model 1.1

bay X =	10	ft
bay Y =	10	ft
A =	400	ft <sup>2</sup>

	h (in)	b(in)	t(in)
<b>Columns</b>	16	6	-
<b>Beams</b>	16	6	-
<b>Slab</b>	-	-	5

<b>Dead</b>		
w concrete =	0.15	k/ft <sup>3</sup>
w slab =	0.0625	ksf
w partition	0.23	k/ft
w column	0.10	k/ft
w beam =	0.10	k/ft
<b>Live</b>		
Roof =	0.02	ksf
w 20% live load =	0.004	ksf
	0.04	ksf
w 20% live load =	0.008	ksf

<b>Level 1</b>	n =	2
h1 @ A =	15	ft
h1 @ B =	9	ft
h1 @ C =	6.5	ft
h2 =	9	ft

\*\* times multiply slab and beam weight  
 } columns height

tributary area

Col. #	lx (ft)	ly (ft)	W (kip)	lx (ft)	ly (ft)	W (kip)	lx (ft)	ly (ft)	W (kip)
	<b>A</b>			<b>B</b>			<b>C</b>		
1	5	5	10.075	10	5	15.025	5	5	9.225
2	5	10	15.625	10	10	24.000	5	10	14.775
3	5	5	10.075	10	5	15.025	5	5	9.225

<b>Level 2</b>	n =	1
h2 =	9	ft

\*\*times multiply slab and beam weight

Col. #	lx (ft)	ly (ft)	W (kip)	lx (ft)	ly (ft)	W (kip)	lx (ft)	ly (ft)	W (kip)
	<b>A</b>			<b>B</b>			<b>C</b>		
1	5	5	3.563	10	5	5.725	5	5	3.563
2	5	10	5.725	10	10	9.550	5	10	5.725
3	5	5	3.563	10	5	5.725	5	5	3.563

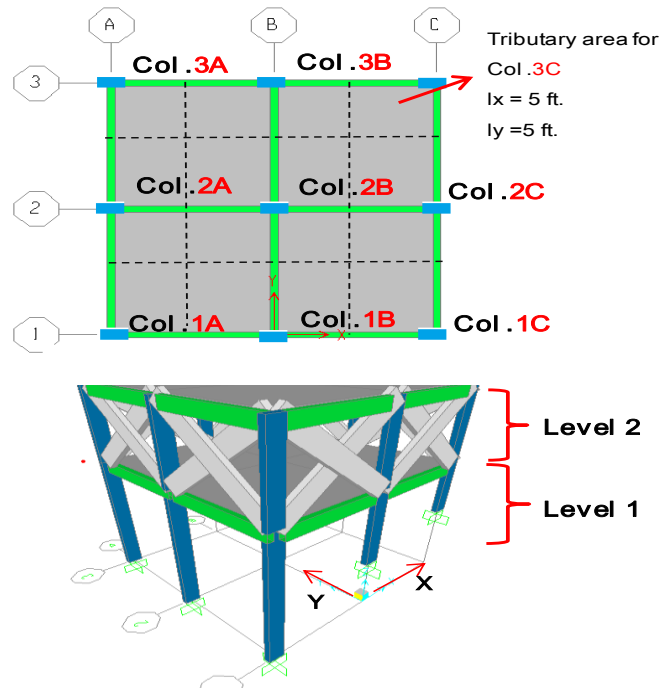


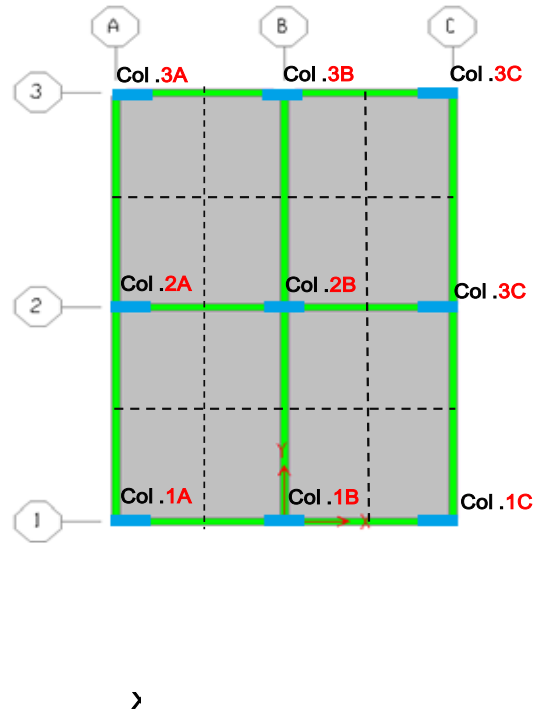
**Table D-2.** Axial Load Calculation Model 1.2

bay X =	10 ft
bay Y =	15 ft
A =	600 ft <sup>2</sup>

	h (in)	b(in)	t(in)
Columns	16	6	-
Beams	16	6	-
Slab	-	-	5

<b>Dead</b>		
w concrete =	0.15	k/ft <sup>3</sup>
w slab =	0.0625	ksf
w block wal =	0.05	ksf
w partition	0.23	k/ft
w column	0.10	k/ft
w beam =	0.10	k/ft

<b>Live</b>		
Roof =	0.02	ksf
w 20% live load =	0.004	ksf
Floor	0.04	ksf
w 20% live load =	0.008	ksf



<b>Level 1</b>	n =	2
h1 @ A =	15	ft
h1 @ B =	9	ft
h1 @ C =	6.5	ft
h2 =	9	ft

\*\* times multiply slab and beam loads

	lx (ft)	ly (ft)	W (kip)	lx (ft)	ly (ft)	W (kip)	lx (ft)	ly (ft)	W (kip)
Col. #	<b>A</b>			<b>B</b>			<b>C</b>		
1	5	7.5	12.850	10	7.5	19.513	5	7.5	12.000
2	5	15	21.175	10	15	32.975	5	15	20.325
3	5	7.5	12.850	10	7.5	19.513	5	7.5	12.000

<b>Level 2</b>	n =	1
h2 =	9	ft

\*\*times multiply slab and beam loads

	lx (ft)	ly (ft)	W (kip)	lx (ft)	ly (ft)	W (kip)	lx (ft)	ly (ft)	W (kip)
Col. #	<b>A</b>			<b>B</b>			<b>C</b>		
1	5	7.5	4.644	10	7.5	7.638	5	7.5	4.644
2	5	15	7.888	10	15	13.375	5	15	7.888
3	5	7.5	4.644	10	7.5	7.638	5	7.5	4.644

**Table D-3.** Axial Load Calculation Model 1.3

bay X =	15 ft
bay Y =	10 ft
A =	600 ft <sup>2</sup>

	h (in)	b(in)	t(in)
<b>Columns</b>	16	6	-
<b>Beams</b>	16	6	-
<b>Slab</b>	-	-	5

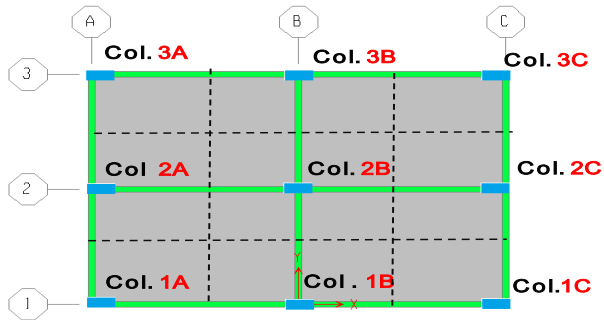
**Dead**

w concrete =	0.15 k/ft <sup>3</sup>
w slab =	0.0625 ksf
w block wal =	0.05 ksf
w partition	0.23 k/ft
w column	0.10 k/ft
w beam =	0.10 k/ft

**Live**

Roof =	0.02 ksf
w 20% live load =	0.004 ksf
Floor	0.04 ksf
w 20% live load =	0.008 ksf

<b>Level 1</b>	n =	2	** times multiply slab and beam loads
h1 @ A =	15 ft		
h1 @ B =	9 ft		
h1 @ C =	6.5 ft		
h2 =	9 ft		



	lx (ft)	ly (ft)	W (kip)	lx (ft)	ly (ft)	W (kip)	lx (ft)	ly (ft)	W (kip)
Col. #	A			B			C		
1	7.5	5	12.850	15	5	20.575	7.5	5	12.000
2	7.5	10	20.113	15	10	32.975	7.5	10	19.263
3	7.5	5	12.850	15	5	20.575	7.5	5	12.000

<b>Level 2</b>	n =	1
h2 =	9 ft	

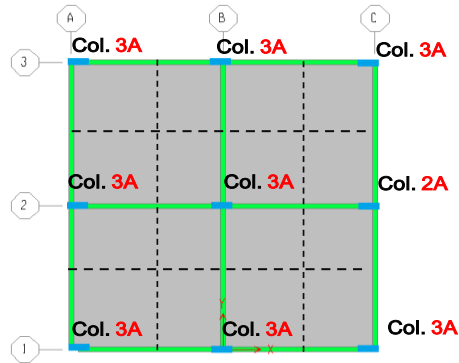
	lx (ft)	ly (ft)	W (kip)	lx (ft)	ly (ft)	W (kip)	lx (ft)	ly (ft)	W (kip)
Col. #	A			B			C		
1	7.5	5	4.644	15	5	7.888	7.5	5	4.644
2	7.5	10	7.638	15	10	13.375	7.5	10	7.638
3	7.5	5	4.644	15	5	7.888	7.5	5	4.644

**Table D-4. Axial Load Calculation Model 1.4**

bay X =	15	ft
bay Y =	15	ft
A =	900	ft <sup>2</sup>

	h (in)	b(in)	t(in)
<b>Columns</b>	16	6	-
<b>Beams</b>	16	6	-
<b>Slab</b>	-	-	5

<b>Dead</b>		
w concrete =	0.15	k/ft <sup>3</sup>
w slab =	0.0625	ksf
w block wal =	0.05	ksf
w partition	0.23	k/ft
w column	0.10	k/ft
w beam =	0.10	k/ft
<b>Live</b>		
Roof =	0.02	ksf
w 20% live load =	0.004	ksf
Floor	0.04	ksf
w 20% live load =	0.008	ksf



<b>Level 1</b>	n =	2
h1 @ A =	15	ft
h1 @ B =	9	ft
h1 @ C =	6.5	ft
h2 =	9	ft

	lx (ft)	ly (ft)	W (kip)	lx (ft)	ly (ft)	W (kip)	lx (ft)	ly (ft)	W (kip)
Col. #	<b>A</b>			<b>B</b>			<b>C</b>		
1	7.5	7.5	16.481	15	7.5	26.775	7.5	7.5	15.631
2	7.5	15	27.375	15	15	45.375	7.5	15	26.525
3	7.5	7.5	16.481	15	7.5	26.775	7.5	7.5	15.631

<b>Level 2</b>	n =	1
h1 @ A =	15	ft
h1 @ B =	9	ft
h1 @ C =	6.5	ft
h2 =	9	ft

\*\*times multiply slab and beam loads

	lx (ft)	ly (ft)	W (kip)	lx (ft)	ly (ft)	W (kip)	lx (ft)	ly (ft)	W (kip)
Col. #	<b>A</b>			<b>B</b>			<b>C</b>		
1	7.5	7.5	6.141	15	7.5	10.631	7.5	7.5	6.141
2	7.5	15	10.631	15	15	18.863	7.5	15	10.631
3	7.5	7.5	6.141	15	7.5	10.631	7.5	7.5	6.141

**Table D-5. Axial Load Calculation Model 2.1**

bay X =	10	ft
bay Y =	10	ft
A =	400	ft <sup>2</sup>

	h (in)	b(in)	t(in)
<b>Columns</b>	16	6	-
<b>Beams</b>	16	6	-
<b>Slab</b>	-	-	5

<b>Dead</b>		
w concrete =	0.15	k/ft <sup>3</sup>
w slab =	0.0625	ksf
w block wal =	0.05	ksf
w partition	0.23	k/ft
w column	0.10	k/ft
w beam =	0.10	k/ft

<b>Live</b>		
Roof =	0.02	ksf
w 20% live load =	0.004	ksf
Floor	0.04	ksf
w 20% live load =	0.008	ksf

<b>Level 1</b>	n=	3
h1 @ A =	10	ft
h1 @ B =	7	ft
h1 @ C =	4	ft
h2 =	9	ft
h3 =	9	ft

	lx (ft)	ly (ft)	W (kip)	lx (ft)	ly (ft)	W (kip)	lx (ft)	ly (ft)	W (kip)
Col. #	<b>A</b>			<b>B</b>			<b>C</b>		
<b>1</b>	5	5	11.475	10	5	17.225	5	5	10.875
<b>2</b>	5	10	16.625	10	10	26.700	5	10	16.925
<b>3</b>	5	5	10.575	10	5	17.225	5	5	10.875

<b>Level 2</b>	n =	2
h2 @ A =	9	ft
h2 @ B =	9	ft
h2 @ C =	9	ft
h3 =	9	ft

	lx (ft)	ly (ft)	W (kip)	lx (ft)	ly (ft)	W (kip)	lx (ft)	ly (ft)	W (kip)
Col. #	<b>A</b>			<b>B</b>			<b>C</b>		
<b>1</b>	5	5	9.475	10	5	15.025	5	5	9.475
<b>2</b>	5	10	15.025	10	10	24.000	5	10	15.025
<b>3</b>	5	5	9.475	10	5	15.025	5	5	9.475

<b>Level 3</b>	n =	1
h3 =	9	ft

	lx (ft)	ly (ft)	W (kip)	lx (ft)	ly (ft)	W (kip)	lx (ft)	ly (ft)	W (kip)
Col. #	<b>A</b>			<b>B</b>			<b>C</b>		
<b>1</b>	5	5	3.563	10	5	5.725	5	5	3.563
<b>2</b>	5	10	5.725	10	10	9.550	5	10	5.725
<b>3</b>	5	5	3.563	10	5	5.725	5	5	3.563

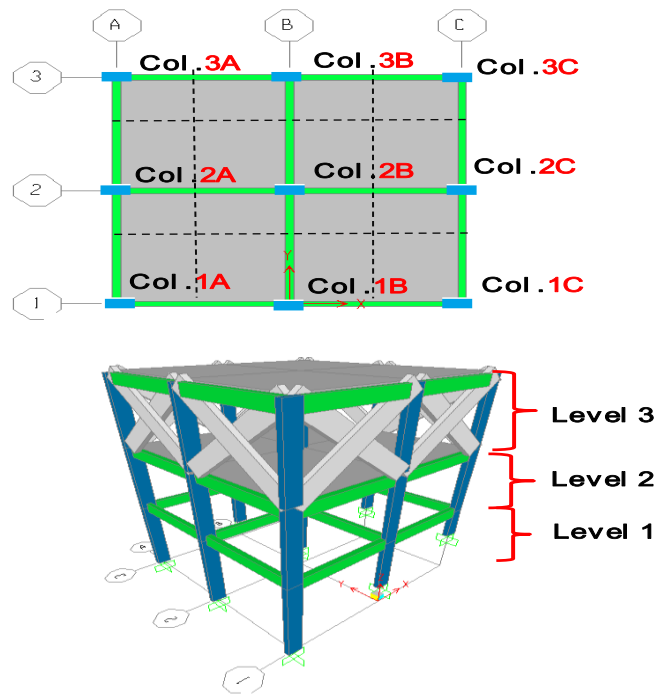


**Table D-6. Axial Load Calculation Model 2.2**

bay X =	10	ft
bay Y =	15	ft
A =	600	ft <sup>2</sup>

	h (in)	b(in)	t(in)
Columns	16	6	-
Beams	16	6	-
Slab	-	-	5

<b>Dead</b>		
w concrete =	0.15	k/ft <sup>3</sup>
w slab =	0.0625	ksf
w block wal =	0.05	ksf
w (40% wall opening)	0.02	ksf
w partition	0.23	k/ft
w column	0.10	k/ft
w beam =	0.10	k/ft
<b>Live</b>		
Roof =	0.02	ksf
w 20% live load =	0.004	ksf
Floor	0.04	ksf
w 20% live load =	0.008	ksf

Level 1	n=	3
h1 @ A =	10	ft
h1 @ B =	7	ft
h1 @ C =	4	ft
h2 =	9	ft
h2 =	9	ft

	lx (ft)	ly (ft)	W (kip)	lx (ft)	ly (ft)	W (kip)	lx (ft)	ly (ft)	W (kip)
Col. #	<b>A</b>			<b>B</b>			<b>C</b>		
1	5	7.5	14.500	10	7.5	21.963	5	7.5	13.900
2	5	15	22.675	10	15	36.175	5	15	22.975
3	5	7.5	13.600	10	7.5	21.963	5	7.5	13.900

Level 2	n =	2	** times multiply slab and beam loads
h1 @ A =	15	ft	
h1 @ B =	9	ft	
h1 @ C =	6.5	ft	
h2 =	9	ft	

	lx (ft)	ly (ft)	W (kip)	lx (ft)	ly (ft)	W (kip)	lx (ft)	ly (ft)	W (kip)
Col. #	<b>A</b>			<b>B</b>			<b>C</b>		
1	5	7.5	12.850	10	7.5	19.513	5	7.5	12.000
2	5	15	21.175	10	15	32.975	5	15	20.325
3	5	7.5	12.850	10	7.5	19.513	5	7.5	12.000

Level 3	n =	1	**times multiply slab and beam loads
h1 @ A =	15	ft	
h1 @ B =	9	ft	
h1 @ C =	6.5	ft	
h2 =	9	ft	

	lx (ft)	ly (ft)	W (kip)	lx (ft)	ly (ft)	W (kip)	lx (ft)	ly (ft)	W (kip)
Col. #	<b>A</b>			<b>B</b>			<b>C</b>		
1	5	7.5	4.644	10	7.5	7.638	5	7.5	4.644
2	5	15	7.888	10	15	13.375	5	15	7.888
3	5	7.5	4.644	10	7.5	7.638	5	7.5	4.644

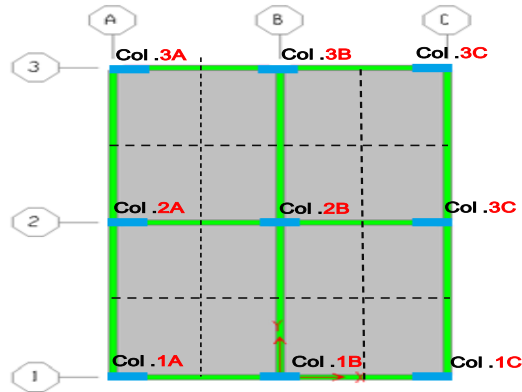


**Table D-7. Axial Load Calculation Model 2.3**



bay X =	15 ft
bay Y =	10 ft
A =	600 ft <sup>2</sup>

	h (in)	b(in)	t(in)
Columns	16	6	-
Beams	16	6	-
Slab	-	-	5

**Dead**

w concrete =	0.15 k/ft <sup>3</sup>
w slab =	0.0625 ksf
w block wal =	0.05 ksf
w partition	0.23 k/ft
w column	0.10 k/ft
w beam =	0.10 k/ft

**Live**

Roof =	0.02 ksf
w 20% live load =	0.004 ksf
Floor	0.04 ksf
w 20% live load =	0.008 ksf

<b>Level 1</b>	n = 3
h1 @ A =	10 ft
h1 @ B =	7 ft
h1 @ C =	4 ft
h2 =	9 ft
h2 =	9 ft

	lx (ft)	ly (ft)	W (kip)	lx (ft)	ly (ft)	W (kip)	lx (ft)	ly (ft)	W (kip)
Col. #	<b>A</b>			<b>B</b>			<b>C</b>		
1	7.5	5	14.500	15	5	23.275	7.5	5	13.900
2	7.5	10	21.363	15	10	36.175	7.5	10	21.663
3	7.5	5	13.600	15	5	23.275	7.5	5	13.900

<b>Level 2</b>	n = 2
h1 @ A =	15 ft
h1 @ B =	9 ft
h1 @ C =	6.5 ft
h2 =	9 ft

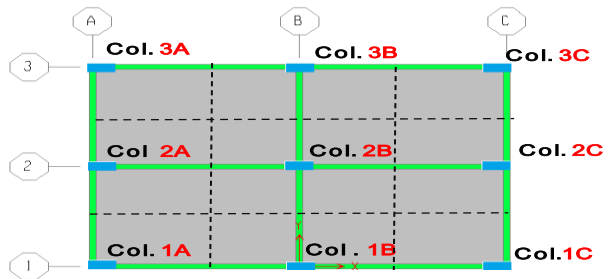
\*\* times multiply slab and beam loads

	lx (ft)	ly (ft)	W (kip)	lx (ft)	ly (ft)	W (kip)	lx (ft)	ly (ft)	W (kip)
Col. #	<b>A</b>			<b>B</b>			<b>C</b>		
1	7.5	5	12.850	15	5	20.575	7.5	5	12.000
2	7.5	10	20.113	15	10	32.975	7.5	10	19.263
3	7.5	5	12.850	15	5	20.575	7.5	5	12.000

<b>Level 3</b>	n = 1
h1 @ A =	15 ft
h1 @ B =	9 ft
h1 @ C =	6.5 ft
h2 =	9 ft

\*\*times multiply slab and beam loads

	lx (ft)	ly (ft)	W (kip)	lx (ft)	ly (ft)	W (kip)	lx (ft)	ly (ft)	W (kip)
Col. #	<b>A</b>			<b>B</b>			<b>C</b>		
1	7.5	5	4.644	15	5	7.888	7.5	5	4.644
2	7.5	10	7.638	15	10	13.375	7.5	10	7.638
3	7.5	5	4.644	15	5	7.888	7.5	5	4.644

**Table D-8.** Axial Load Calculation Model 2.4

bay X =	15 ft
bay Y =	15 ft
A =	900 ft <sup>2</sup>

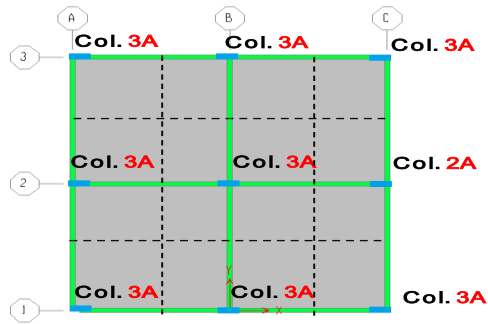
	h (in)	b(in)	t(in)
<b>Columns</b>	16	6	-
<b>Beams</b>	16	6	-
<b>Slab</b>	-	-	5

**Dead**

w concrete =	0.15	k/ft <sup>3</sup>
w slab =	0.0625	ksf
w block wal =	0.05	ksf
w partition	0.23	k/ft
w column	0.10	k/ft
w beam =	0.10	k/ft

**Live**

Roof =	0.02	ksf
w 20% live load =	0.004	ksf
Floor	0.04	ksf
w 20% live load =	0.008	ksf



<b>Level 1</b>	n =	3
h1 @ A =	10	ft
h1 @ B =	7	ft
h1 @ C =	4	ft
h2 =	9	ft
h2 =	9	ft

	lx (ft)	ly (ft)	W (kip)	lx (ft)	ly (ft)	W (kip)	lx (ft)	ly (ft)	W (kip)
Col. #	<b>A</b>			<b>B</b>			<b>C</b>		
<b>1</b>	7.5	7.5	18.381	15	7.5	29.725	7.5	7.5	17.781
<b>2</b>	7.5	15	29.125	15	15	49.075	7.5	15	29.425
<b>3</b>	7.5	7.5	17.481	15	7.5	29.725	7.5	7.5	17.781

<b>Level 2</b>	n =	2
h1 @ A =	15	ft
h1 @ B =	9	ft
h1 @ C =	6.5	ft
h2 =	9	ft

\*\* times multiply slab and beam loads

	lx (ft)	ly (ft)	W (kip)	lx (ft)	ly (ft)	W (kip)	lx (ft)	ly (ft)	W (kip)
Col. #	<b>A</b>			<b>B</b>			<b>C</b>		
<b>1</b>	7.5	7.5	16.481	15	7.5	26.775	7.5	7.5	15.631
<b>2</b>	7.5	15	27.375	15	15	45.375	7.5	15	26.525
<b>3</b>	7.5	7.5	16.481	15	7.5	26.775	7.5	7.5	15.631

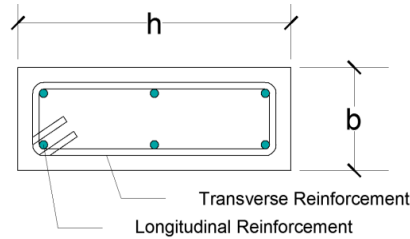
<b>Level 3</b>	n =	1
h1 @ A =	15	ft
h1 @ B =	9	ft
h1 @ C =	6.5	ft
h2 =	9	ft

\*\*times multiply slab and beam loads

	lx (ft)	ly (ft)	W (kip)	lx (ft)	ly (ft)	W (kip)	lx (ft)	ly (ft)	W (kip)
Col. #	<b>A</b>			<b>B</b>			<b>C</b>		
<b>1</b>	7.5	7.5	6.141	15	7.5	10.631	7.5	7.5	6.141
<b>2</b>	7.5	15	10.631	15	15	18.863	7.5	15	10.631
<b>3</b>	7.5	7.5	6.141	15	7.5	10.631	7.5	7.5	6.141

## Appendix E. SHEAR STRENGTH CAPACITY CALCULATION

**Table E-1.** Shear Strength Capacity Calculations: Column 16" X 6"



### Shear Capacity : Strong axis

h =	16	in	
b =	6	in	
s =	12	in	transverse bar spacing
db =	0.5	in	diameter longitudinal bar
dt =	0.375	in	diameter transverse bar
Av =	0.22	in <sup>2</sup>	area shear reinforcement
cc =	1.5	in	distance to longitudinal bar
d =	14.25	in	effective depth
f <sub>c</sub> =	2500	psi	concrete compressive strength

### Summary Shear Capacity

Axial Load (lb)	V <sub>c</sub> (lb)	V <sub>s</sub> (lb)	V <sub>t</sub> (lb)	V <sub>t</sub> (kip)	
6000	8817.2	15738.6	24555.8	24.56	Total shear capacity for different axial loads
12000	9084.4	15738.6	24823.0	24.82	
20000	9440.6	15738.6	25179.3	25.18	
26000	9707.8	15738.6	25446.5	25.45	
32000	9975.0	15738.6	25713.6	25.71	
44000	10509.4	15738.6	26248.0	26.25	

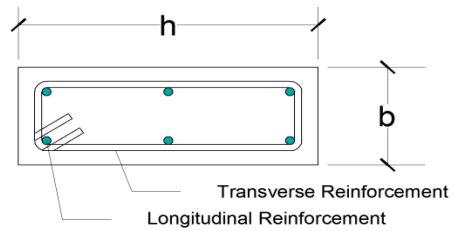
Eqs. 3-1, 3-2 and 3-3

### Shear Capacity : Weak axis

h =	6	in	
b =	16	in	
s =	12	in	
db =	0.5	in	
dt =	0.375	in	
Av =	0.22	in <sup>2</sup>	
cc =	1.5	in	
d =	4.25	in	
f <sub>c</sub> =	2500	psi	

### Summary Shear Capacity

Axial Load (lb)	V <sub>c</sub> (lb)	V <sub>s</sub> (lb)	V <sub>t</sub> (lb)	V <sub>t</sub> (kip)
6000	7012.5	4693.98	11706.5	11.71
12000	7225.0	4693.98	11919.0	11.92
20000	7508.3	4693.98	12202.3	12.20
26000	7720.8	4693.98	12414.8	12.41
32000	7933.3	4693.98	12627.3	12.63
44000	8358.3	4693.98	13052.3	13.05

**Table E-2. Shear Strength Capacity Calculations: Column 16" X 8"****Shear Capacity : Strong axis**

$h =$	16	in	
$b =$	8	in	
$s =$	12	in	transverse bar spacing

$d_b =$	0.50	in	diameter longitudinal bar
$d_t =$	0.38	in	diameter transverse bar
$A_v =$	0.22	in <sup>2</sup>	area shear reinforcement

$c_c =$	1.50	in	distance to longitudinal bar
$d =$	14.25	in	effective depth
$f_c =$	2500	psi	concrete compressive strength

**Summary Shear Capacity**

Axial Load (lb)	$V_c$ (lb)	$V_s$ (lb)	$V_t$ (lb)	$V_t$ (kip)
6000	11667.2	15738.64	27405.8	27.41
15000	12068.0	15738.64	27806.6	27.81
23000	12424.2	15738.64	28162.9	28.16

**Shear Capacity : Weak axis**

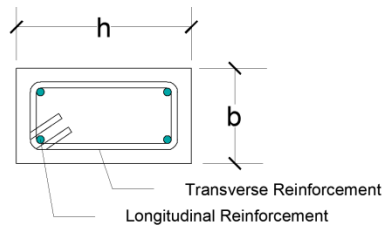
$h =$	8	in	
$b =$	16	in	
$s =$	12	in	

$d_b =$	0.50	in	
$d_t =$	0.38	in	
$A_v =$	0.22	in <sup>2</sup>	

$c_c =$	1.50	in	
$d =$	6.25	in	
$f_c =$	2500	psi	

**Summary Shear Capacity**

Axial Load (lb)	$V_c$ (lb)	$V_s$ (lb)	$V_t$ (lb)	$V_t$ (kip)
6000	10234.4	6902.914	17137.3	17.14
12000	10468.8	6902.914	17371.7	17.37
20000	10781.3	6902.914	17684.2	17.68

**Table E-3. Shear Strength Capacity Calculations: Column 12" X 6"****Shear Capacity : Strong axis**

h =	12	in	
b =	6	in	
s =	12	in	transverse bar spacing

db =	0.50	in	diameter longitudinal bar
dt =	0.38	in	diameter transverse bar
Av =	0.22	in <sup>2</sup>	area shear reinforcement

cc =	1.5	in	distance to longitudinal bar
d =	10.25	in	effective depth
f <sub>c</sub> =	2500	psi	concrete compressive strength

**Summary Shear Capacity**

Axial Load (lb)	V <sub>c</sub> (lb)	V <sub>s</sub> (lb)	V <sub>t</sub> (lb)	V <sub>t</sub> (kip)
6000	6406.3	11320.8	17727.0	17.73
15000	6790.6	11320.8	18111.4	18.11
23000	7132.3	11320.8	18453.1	18.45

**Shear Capacity : Weak axis**

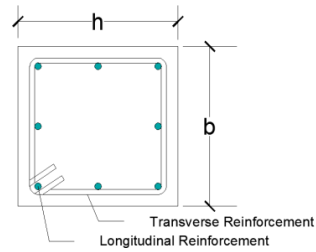
h =	6	in	
b =	12	in	
s =	12	in	

db =	0.50	in	
dt =	0.38	in	
Av =	0.22	in <sup>2</sup>	

cc =	1.50	in	
d =	4.25	in	
f <sub>c</sub> =	2500	psi	

**Summary Shear Capacity**

Axial Load (lb)	V <sub>c</sub> (lb)	V <sub>s</sub> (lb)	V <sub>t</sub> (lb)	V <sub>t</sub> (kip)
6000	5312.5	4693.98	10006.5	10.01
12000	5525.0	4693.98	10219.0	10.22
20000	5808.3	4693.98	10502.3	10.50

**Table E-4. Shear Strength Capacity Calculations: Column 12" X 12"****Shear Capacity**

h =	12	in	
b =	12	in	
s =	12	in	transverse bar spacing

db =	0.5	in	diameter longitudinal bar
dt =	0.375	in	diameter transverse bar
Av =	0.22	in <sup>2</sup>	area shear reinforcement

cc =	1.5	in	distance to longitudinal bar
d =	10.25	in	effective depth
f'c =	2500	psi	concrete compressive strength

**Summary Shear Capacity**

Axial Load (lb)	V <sub>c</sub> (lb)	V <sub>s</sub> (lb)	V <sub>t</sub> (lb)	V <sub>t</sub> (kip)
6000	12556.3	11320.8	23877.0	23.88
15000	12940.6	11320.8	24261.4	24.26
23000	13282.3	11320.8	24603.1	24.60

## Appendix F. STRUCTURAL SYSTEMS

**Table F-1.** Response Modification Factors R proposed by UBC-97

BASIC STRUCTURAL SYSTEM <sup>2</sup>	LATERAL-FORCE-RESISTING SYSTEM DESCRIPTION	R	$\Omega_o$	HEIGHT LIMIT FOR SEISMIC ZONES 3 AND 4 (ft)
				× 304.8 for mm
1. Bearing wall system	1. Light-framed walls with shear panels	5.5	2.8	65
	a. Wood structural panel walls for structures three stories or less	4.5	2.8	65
	b. All other light-framed walls			
	2. Shear walls			
	a. Concrete	4.5	2.8	160
	b. Masonry	4.5	2.8	160
	3. Light steel-framed bearing walls with tension-only bracing	2.8	2.2	65
	4. Braced frames where bracing carries gravity load			
2. Building frame system	a. Steel	4.4	2.2	160
	b. Concrete <sup>3</sup>	2.8	2.2	—
	c. Heavy timber	2.8	2.2	65
	1. Steel eccentrically braced frame (EBF)	7.0	2.8	240
	2. Light-framed walls with shear panels			
	a. Wood structural panel walls for structures three stories or less	6.5	2.8	65
	b. All other light-framed walls	5.0	2.8	65
	3. Shear walls			
	a. Concrete	5.5	2.8	240
	b. Masonry	5.5	2.8	160
	4. Ordinary braced frames			
	a. Steel	5.8	2.2	160
	b. Concrete <sup>3</sup>	5.8	2.2	—
	c. Heavy timber	5.8	2.2	65
3. Moment-resisting frame system	5. Special concentrically braced frames			
	a. Steel	6.4	2.2	240
	1. Special moment-resisting frame (SMRF)			
	a. Steel	8.5	2.8	N.L.
	b. Concrete <sup>4</sup>	8.5	2.8	N.L.
	2. Masonry moment-resisting wall frame (MMRWF)	6.5	2.8	160
	3. Concrete intermediate moment-resisting frame (IMRF) <sup>5</sup>	5.5	2.8	—
	4. Ordinary moment-resisting frame (OMRF)			
4. Dual systems	a. Steel <sup>6</sup>	4.5	2.8	160
	b. Concrete <sup>7</sup>	3.5	2.8	—
	5. Special truss moment frames of steel (STMF)	6.5	2.8	240
	1. Shear walls			
	a. Concrete with SMRF	8.5	2.8	N.L.
	b. Concrete with steel OMRF	4.2	2.8	160
	c. Concrete with concrete IMRF <sup>6</sup>	6.5	2.8	160
	d. Masonry with SMRF	5.5	2.8	160
	e. Masonry with OMRF	4.2	2.8	160
	f. Masonry with IMRF <sup>3</sup>	4.2	2.8	—
	g. Masonry with masonry MMRWF	6.0	2.8	160
	2. Steel EBF			
	a. With steel SMRF	8.5	2.8	N.L.
	b. With steel OMRF	4.2	2.8	160
	3. Ordinary braced frames			
	a. Steel with steel SMRF	6.5	2.8	N.L.
	b. Steel with steel OMRF	4.2	2.8	160
	c. Concrete with concrete SMRF <sup>3</sup>	6.5	2.8	—
	d. Concrete with concrete IMRF <sup>3</sup>	4.2	2.8	—
	4. Special concentrically braced frames			
	a. Steel with steel SMRF	7.5	2.8	N.L.
	b. Steel with steel SMRF	4.2	2.8	160
5. Cantilevered column building systems	1. Cantilevered column elements	2.2	2.0	35 <sup>6</sup>
6. Shear wall-frame interaction systems	1. Concrete <sup>8</sup>	5.5	2.8	160
7. Undefined systems	See Sections 1629.6.7 and 1629.9.2	—	—	—

## Appendix G. DESIGN BASE SHEAR CALCULATION

**Table G-1.** Design Base Shear for Model 1.1

**Base Shear formulas:**

$$V = \frac{2.5 C_a I}{R} W \quad \text{equation (30-5) UBC 97}$$

$$V = \frac{C_v I}{R T} W \quad \text{equation (30-4) UBC 97}$$

$$V_{min} = 0.11 C_a I W \quad \text{equation (30-6) UBC 97}$$

Soil profile = Sd

Seismic Zone = 3      Seismic Zone Factor, table 16-I UBC 97

Zone factor (Z) = 0.3

$C_a = 0.36$       Seismic Coefficient, table 16-Q UBC 97

$C_v = 0.54$       Seismic Coefficient, table 16-R UBC 97

$I = 1$       Seismic Importance Factor, table 16-K UBC 97

$R = 3.5$       Response Modification Factor, table 16-N UBC 97

$T =$  Period, sec

$$T = C_t (h_n)^{3/4}$$

$C_t = 0.030$

$T = 0.325$       sec

**Weight**

$W = 120$       kips      \* total weight of residence

**Base Shear**

$V = 30.86$       kip      equation (30-5) UBC 97

$V = 56.92$       kip      equation (30-4) UBC 97

$V_{min} = 4.75$       kip      equation (30-6) UBC 97

**Table G-2.** Summary Design Base Shear

Model	Vd (kips)
Model 1.1	31.0
Model 1.2	41.0
Model 1.3	41.0
Model 1.4	55.0
Model 2.1	35.0
Model 2.2	45.0
Model 2.3	45.0
Model 2.4	60.0